OXIDATIVE STRESS, ANTIOXIDANTS, TRANSCRIPTION FACTORS, AND ASSIMILATION OF SIGNAL TRANSDUCTION PATHWAYS IN OBESITY-RELATED DISORDERS

EDITED BY: Terry D. Hinds, Jr., David E. Stec and Barbara Wegiel

PUBLISHED IN: Frontiers in Pharmacology

frontiers Research Topics

ISSN 1664-8714
ISBN 978-2-88971-527-5
DOI 10.3389/978-2-88971-527-5

About Frontiers

Frontiers is more than just an open-access publisher of scholarly articles: it is a pioneering approach to the world of academia, radically improving the way scholarly research is managed. The grand vision of Frontiers is a world where all people have an equal opportunity to seek, share and generate knowledge. Frontiers provides immediate and permanent online open access to all its publications, but this alone is not enough to realize our grand goals.

Frontiers Journal Series

The Frontiers Journal Series is a multi-tier and interdisciplinary set of open-access, online journals, promising a paradigm shift from the current review, selection and dissemination processes in academic publishing. All Frontiers journals are driven by researchers for researchers; therefore, they constitute a service to the scholarly community. At the same time, the Frontiers Journal Series operates on a revolutionary invention, the tiered publishing system, initially addressing specific communities of scholars, and gradually climbing up to broader public understanding, thus serving the interests of the lay society, too.

Dedication to Quality

Each Frontiers article is a landmark of the highest quality, thanks to genuinely collaborative interactions between authors and review editors, who include some of the world's best academicians. Research must be certified by peers before entering a stream of knowledge that may eventually reach the public - and shape society; therefore, Frontiers only applies the most rigorous and unbiased reviews.
Frontiers revolutionizes research publishing by freely delivering the most outstanding research, evaluated with no bias from both the academic and social point of view. By applying the most advanced information technologies, Frontiers is catapulting scholarly publishing into a new generation.

What are Frontiers Research Topics?

Frontiers Research Topics are very popular trademarks of the Frontiers Journals Series: they are collections of at least ten articles, all centered on a particular subject. With their unique mix of varied contributions from Original Research to Review Articles, Frontiers Research Topics unify the most influential researchers, the latest key findings and historical advances in a hot research area! Find out more on how to host your own Frontiers Research Topic or contribute to one as an author by contacting the Frontiers Editorial Office: frontiersin.org/about/contact

OXIDATIVE STRESS, ANTIOXIDANTS, TRANSCRIPTION FACTORS, AND ASSIMILATION OF SIGNAL TRANSDUCTION PATHWAYS IN OBESITY-RELATED DISORDERS

Topic Editors:
Terry D. Hinds, Jr., University of Kentucky, United States
David E. Stec, University of Mississippi Medical Center, United States
Barbara Wegiel, Harvard Medical School, United States

Topic Editors Terry Hinds and David Stec have submitted patents related to bilirubin and obesity related disorders. The other Topic Editor declare no potential conflicts of interest with regards to the Research Topic subject.

Citation: Hinds, T. D., Stec, D. E., Wegiel, B., eds. (2021). Oxidative Stress, Antioxidants, Transcription Factors, and Assimilation of Signal Transduction Pathways in Obesity-Related Disorders. Lausanne: Frontiers Media SA.
doi: 10.3389/978-2-88971-527-5

Table of Contents

frontiers in Pharmacology

EDITORIAL
published: 07 September 2021
doi: 10.3389/fphar.2021.759468

Editorial: Oxidative Stress, Antioxidants, Transcription Factors, and Assimilation of Signal Transduction Pathways in Obesity-Related Disorders

David E. Stec[1]*, *Barbara Wegiel*[2] *and Terry D. Hinds Jr*[3]*

[1]Department of Physiology and Biophysics, Cardiorenal and Metabolic Diseases Research Center, University of Mississippi Medical Center, Jackson, MS, United States, [2]Department of Surgery, Division of Surgical Oncology, Cancer Research Institute, Beth Israel Deaconess Medical Center and Harvard Medical School, Boston, MA, United States, [3]Department of Pharmacology and Nutritional Sciences, Barnstable Brown Diabetes Center, Markey Cancer Center, University of Kentucky, Lexington, KY, United States

Keywords: obesity, insulin resistance, therapeutics, bilirubin, reactive oxygen species, inflammation

Editorial on the Research Topic

Oxidative Stress, Antioxidants, Transcription Factors, and Assimilation of Signal Transduction Pathways in Obesity-Related Disorders

OPEN ACCESS

Edited and reviewed by:
Salvatore Salomone, University of Catania, Italy

***Correspondence:**
David E. Stec
dstec@umc.edu
Terry D. Hinds Jr
Terry.Hinds@uky.edu

Specialty section:
This article was submitted to Experimental Pharmacology and Drug Discovery, a section of the journal Frontiers in Pharmacology

Received: *16 August 2021*
Accepted: *23 August 2021*
Published: *07 September 2021*

Citation:
Stec DE, Wegiel B and Hinds Jr TD (2021) Editorial: Oxidative Stress, Antioxidants, Transcription Factors, and Assimilation of Signal Transduction Pathways in Obesity-Related Disorders. Front. Pharmacol. 12:759468. doi: 10.3389/fphar.2021.759468

Obesity and its comorbidities such as fatty liver disease, type II diabetes, and cardiovascular disease can cause an onset of complications, worsened by the accompanying oxidative stress and deleterious signaling mechanisms, leading to irreversible damages. For instance, long-term fat accumulation in the liver may induce oxidative stress, sterile inflammation, and ultimately fibrosis, currently considered as an irreversible event. Oxidative stress occurs with an imbalance of heightened free radicals and reduced antioxidant pool in the body. Reactive oxygen species (ROS) are free oxygen-containing molecules that quickly react with other molecules within the cell leading to tissue damage. This is particularly evident in patients with obesity and metabolic disorders. Nicotinamide adenine dinucleotide phosphate (NADPH) oxidases and the mitochondrial oxidative chain complexes generate the majority of ROS in obesity and the metabolic syndrome, and this can contribute to renal dysfunction [reviewed in (Lee and Jose)]. To combat this complication, antuioxidants are the body's natural defense against ROS. They can be part of an extensive, integrated antioxidant defense system (*i.e.,* glutathione, bilirubin) or derived from vitamins or nutritional sources such as vegetables, fruits, nuts, and seeds. Antioxidants have been proposed as potential therapies for obesity and its associated pathologies. As part of this collection of articles, Tun et al. reviewed the role of oxidative stress and the potential therapeutic role for several antioxidants in obesity and its related comorbidities (Tun et al.).

Adipose tissue is not simply a storage receptacle for excess fats that occur in obesity, but rather it is a complex endocrine organ. Adipose tissue releases hormones such as leptin and adiponectin as well as several cytokines. Hence, these are referred to as adipokines, and some are beneficial for metabolic disease (adiponectin), and others can be disadvantageous and induce inflammation (TNFα). Obesity alters the release of adipokines contributing to metabolic dysfunction and other phenotypes such as altered bone metabolism. Adiponectin levels are lower in the obese patients and may affect cementoblasts' mineralization rate, impacting periodontal tissue homeostasis and orthodontic treatment (Yong et al.). Excessive fructose consumption results in metabolic dysfunction and contributes to insulin resistance, vascular dysfunction, and hypertension. The hydrogen sulfide

(H_2S) system is composed of enzymatic and non-enzymatic pathways capable of scavenging ROS in the cytosol and the mitochondria. Pavlovskiy et al. used H_2S donors to reduce fructose-induced gastric injury and demonstrated that they work in part by decreasing oxidative damage caused by fructose (Pavlovskiy et al.). Retinopathy is a common complication of diabetes. Hyperglycemia-induced ROS and inflammation are contributing factors to this condition. Yang et al. provided evidence that synthetic relaxin-3 (H3 relaxin) attenuated high glucose-induced nod-like receptor protein 3 (NLRP3) inflammasome activation in streptozotocin (STZ)-induced diabetic rats (Yang et al.).

Epigenetic genome modification is a tool for regulating gene expression without changes in the genomic sequence itself. Sirtuin-6 (Sirt6) is a histone deacetylase inhibitor that controls telomere length, DNA repair, and other cellular processes. Raj et al. highlighted the emerging role of Sirt6 in the prevention of metabolic diseases and discussed the potential therapeutic use of Sirt6 modulators (Raj et al.). Histone deacetylase (HDAC) inhibitors improved fatty-acid induced insulin resistance in mice fed high fat and high fructose diets through enhanced fatty acid oxidation and improved mitochondrial function (Lee et al.).

The body produces a potent antioxidant, bilirubin, a product of heme catabolism by the enzyme, heme oxygenase-1 (HO-1), which combats ROS and oxidative stress. Mildly elevated plasma bilirubin levels correlate with reduced risks of cardiovascular and metabolic diseases (Hinds and Stec, 2018; Weaver et al., 2018; Hinds and Stec, 2019). Primary cells (podocytes and aortic endothelial cells) isolated from hyperbilirubinemic Gunn rats exhibited significantly higher viability in response to palmitic acid or angiotensin II treatment (Bianco et al.). Gunn rats also displayed sex-dependent decreases in fat mass, elevated hepatic β-oxidation, and mitochondrial function (Vidimce et al.). These studies were supported by Hana et al., who showed in this series that bilirubin treatment inhibited lipid accumulation in both skeletal muscle and liver cells and that this was dependent upon the glucose level (Hana et al.). While bilirubin is a well-known antioxidant, it might also have a hormonal function as a ligand [reviewed in (Creeden et al., 2020)] for the nuclear receptor peroxisome proliferator-activated receptor-α (PPARα) (Stec et al., 2016; Gordon et al., 2019; Gordon et al., 2020; Gordon et al., 2021). Hinds et al. utilized water-soluble bilirubin nanoparticles to treat obesity and its comorbidity, fatty liver disease. They showed that the bilirubin nanoparticles reduced dietary-induced obesity and hepatic steatosis via the induction of PPARα transactivation, accelerating β-oxidation and the utilization of fat in the liver, raising plasma levels of the ketone β-hydroxybutyrate, a known hepatic fatty acid oxidation marker (Hinds et al.).

Nature antioxidant remedies have been used for centuries in traditional herbal medicines like fenugreek, which treat a wide variety of ailments (Stec and Hinds, 2020). Yang et al. used 4-hydroxyisoleucine, the active component of fenugreek, to prevent dietary-induced obesity inflammatory response via modification of macrophage phenotype in the adipose and liver tissues (Yang et al.). Natural products exhibit antioxidant actions through induction of pathways such as HO-1 or nuclear factor erythroid 2-related factor 2 (Nrf2) (Stec and Hinds, 2020). Kaempferol is a flavonoid compound and antioxidant found in fruits and vegetables. Yao et al. demonstrated that the vascular protective effects of kaempferol are due to its antioxidant actions via induction of Nrf2/HO-1 (Yao et al.). Bauhiniastatin-1, the active component derived from the flowering plant Bauhinia purpurea, decreased high-fat diet-induced weight gain, adiposity, and insulin resistance in rats via modulation of peroxisome proliferator-activated receptor- γ (PPARγ) and AMP-activated protein kinase (AMPK) (Karunakaran et al.).

ROS and inflammation have active roles in obesity and its related pathologies. Antioxidant treatment with scavengers of ROS, cellular and mitochondrial ROS production inhibitors, or natural products that activate endogenous antioxidant pathways are potential therapies to mitigate obesity and metabolic diseases. Contributing articles to this research topic have highlighted how antioxidants may impact specific signaling pathways and transcriptional programs. Either through treatment with natural products or endogenous metabolites and hormones such as bilirubin and relaxin, targeting ROS and its associated transcription factors and signal transduction pathways offers a promise for therapy to combat obesity and its associated metabolic disorders.

AUTHOR CONTRIBUTIONS

All authors listed have made a substantial, direct, and intellectual contribution to the work and approved it for publication.

FUNDING

This work was supported by the National Institutes of Health 1R01DK121797-01A1 (TH) and 1R01DK126884-01A1 (DS), the National Heart, Lung and Blood Institute K01HL-125445 (TH) and P01 HL05197-11 (DS), and the National Institute of General Medical Sciences P20GM104357-02 (DS) and NIDDK R01 DK104714 (BW) and R01 DK125846 (BW). The content is solely the responsibility of the authors and does not necessarily represent the official views of the National Institutes of Health.

REFERENCES

Creeden, J. F., Gordon, D. M., Stec, D. E., and Hinds, T. D., Jr (2020). Bilirubin as a Metabolic Hormone: The Physiological Relevance of Low Levels. *Am. J. Physiol. Endocrinol. Metab.*

Gordon, D. M., Blomquist, T. M., Miruzzi, S. A., McCullumsmith, R., Stec, D. E., and Hinds, T. D., Jr (2019). RNA Sequencing in Human HepG2 Hepatocytes Reveals PPAR-α Mediates Transcriptome Responsiveness of Bilirubin. *Physiol. Genomics* 51 (6), 234–240. doi:10.1152/physiolgenomics.00028.2019

Gordon, D. M., Hong, S. H., Kipp, Z. A., and Hinds, T. D., Jr (2021). Identification of Binding Regions of Bilirubin in the Ligand-Binding Pocket of the Peroxisome Proliferator-Activated Receptor-A (PPARalpha). *Molecules* 26 (10). doi:10.3390/molecules26102975

Gordon, D. M., Neifer, K. L., Hamoud, A. A., Hawk, C. F., Nestor-Kalinoski, A. L., Miruzzi, S. A., et al. (2020). Bilirubin Remodels Murine white

Adipose Tissue by Reshaping Mitochondrial Activity and the Coregulator Profile of Peroxisome Proliferator-Activated Receptor Alpha. *J. Biol. Chem.*

Hinds, T. D., Jr., and Stec, D. E. (2019). Bilirubin Safeguards Cardiorenal and Metabolic Diseases: a Protective Role in Health. *Curr. Hypertens. Rep.* 21 (11), 87. doi:10.1007/s11906-019-0994-z

Hinds, T. D., Jr., and Stec, D. E. (2018). Bilirubin, a Cardiometabolic Signaling Molecule. *Hypertension* 72 (4), 788–795. doi:10.1161/HYPERTENSIONAHA.118.11130

Stec, D. E., and Hinds, T. D., Jr. (2020). Natural Product Heme Oxygenase Inducers as Treatment for Nonalcoholic Fatty Liver Disease. *Int. J. Mol. Sci.* 21 (24). doi:10.3390/ijms21249493

Stec, D. E., John, K., Trabbic, C. J., Luniwal, A., Hankins, M. W., Baum, J., et al. (2016). Bilirubin Binding to PPARα Inhibits Lipid Accumulation. *PLoS One* 11 (4), e0153427. doi:10.1371/journal.pone.0153427

Weaver, L., Hamoud, A. R., Stec, D. E., and Hinds, T. D., Jr (2018). Biliverdin Reductase and Bilirubin in Hepatic Disease. *Am. J. Physiol. Gastrointest. Liver Physiol.* 314 (6), G668–G76. doi:10.1152/ajpgi.00026.2018

Conflict of Interest: DS and TH have submitted patents related to bilirubin and obesity-related disorders.

The remaining author declares that the research was conducted in the absence of any commercial or financial relationships that could be construed as a potential conflict of interest.

Publisher's Note: All claims expressed in this article are solely those of the authors and do not necessarily represent those of their affiliated organizations, or those of the publisher, the editors and the reviewers. Any product that may be evaluated in this article, or claim that may be made by its manufacturer, is not guaranteed or endorsed by the publisher.

frontiers in Pharmacology

ORIGINAL RESEARCH
published: 22 July 2020
doi: 10.3389/fphar.2020.01118

Kaempferol Protects Blood Vessels From Damage Induced by Oxidative Stress and Inflammation in Association With the Nrf2/HO-1 Signaling Pathway

He Yao[1], *Jingyu Sun*[1], *Jie Wei*[1], *Xin Zhang*[1], *Bing Chen*[2]* *and Yajun Lin*[1,3]*

[1] The Key Laboratory of Geriatrics, Beijing Hospital, National Center of Gerontology, Beijing, China, [2] Institute of Basic Theory for Chinese Medicine, China Academy of Chinese Medical Sciences, Beijing, China, [3] The Key Laboratory of Geriatrics, Peking University Fifth School of Clinical Medicine, Beijing, China

OPEN ACCESS

Edited by:
Barbara Wegiel,
Beth Israel Deaconess Medical Center and Harvard Medical School, United States

Reviewed by:
Lars Udo-Bellner, New York Medical College, United States
Andrew Bulmer, Griffith University, Australia

***Correspondence:**
Bing Chen
bingchen1205@163.com
Yajun Lin
linyajun2000@126.com

Specialty section:
This article was submitted to Experimental Pharmacology and Drug Discovery, a section of the journal Frontiers in Pharmacology

Received: 07 May 2020
Accepted: 09 July 2020
Published: 22 July 2020

Citation:
Yao H, Sun J, Wei J, Zhang X, Chen B and Lin Y (2020) Kaempferol Protects Blood Vessels From Damage Induced by Oxidative Stress and Inflammation in Association With the Nrf2/HO-1 Signaling Pathway. Front. Pharmacol. 11:1118. doi: 10.3389/fphar.2020.01118

Over recent years, an increasing number of studies have confirmed that the occurrence and development of vascular pathological changes are closely related to oxidative stress and the inflammatory response of the vascular endothelium. Kaempferol is the most common flavonoid compound found in fruits and vegetables. Our present research identified that kaempferol had the capability to protect the vascular endothelium in a mouse model of vascular injury and explored the specific mechanisms underlying these effects by investigating oxidative stress, the extent of cardiovascular injury, and inflammatory markers such as NF-κB, TNF-α, IL-6, and the Nrf2/HO-1 signaling pathway. Analysis showed that kaempferol reduced oxidative stress and inflammation mediated by H_2O_2 and paraquat, respectively, both *in vitro* and *in vivo*. Furthermore, kaempferol suppressed the levels of TNF-α and IL-6, and the activation of NF-κB, in aortic tissues and human umbilical vein endothelial cells (HUVECs). Finally, we observed that kaempferol corrected the levels of antioxidants and elevated the protein levels of Nrf2 and HO-1 in aortic tissues and HUVECs. Collectively, our findings prove that kaempferol protects blood vessels from damage induced by oxidative stress and inflammation and that the Nrf2/HO-1 signaling pathway plays a key role in mediating these effects.

Keywords: inflammation, kaempferol, Nrf2, oxidative stress, vascular injury

INTRODUCTION

Vascular injury plays an important role in many cardiovascular diseases (Bruder-Nascimento et al., 2019). The dysfunction and activation of endothelial cells induced by various factors leads to the production of pro-inflammatory cytokines and reactive oxygen species; these factors are both important causes of vascular injury (Catapano et al., 2017). A large body of experimental and clinical evidence now indicates that vascular inflammation plays an important role in the

development of endothelial dysfunction. Interactions between the pro-inflammatory and pro-oxidative environments in the vascular system can increase the risk of cardiovascular disease as such interactions work in concert to accelerate the formation of atherosclerotic plaques (Hajjar and Gotto, 2013; Assar et al., 2016).

Flavonoids are a class of compounds widely found in plants. Among the different subclasses of flavonols, the most common compounds are quercetin, myricetin, and kaempferol (Filomeni et al., 2010). Of these, kaempferol (Kae) is well known for its pharmacological ability to reduce oxidative stress and inflammation in various organs and tissues (Kampkotter et al., 2007; Park et al., 2009; Ren et al., 2019). Recent studies have demonstrated the protective effects of Kae on the heart by regulating nuclear factor erythroid-2 related factor (Nrf2) and nuclear factor kappa B (NF-κB) (Suchal et al., 2016; Chen et al., 2018; Zhang et al., 2019). Of these factors, Nrf2, a master transcription factor, is transferred to the nucleus after activation, where it binds to the upstream cis-regulated antioxidant response element (ARE) sequence located in the promoter regions of genes responsible for cell protection (David et al., 2017). Nrf2 subsequently activates a variety of cellular protective enzymes, such as catalase (CAT), superoxide dismutase (SOD), glutathione (GSH-Px), and heme oxygenase-1 (HO-1) (Abdou et al., 2019). There is mounting evidence that the Nrf2 signaling pathway may represent a potential target for fighting oxidative stress-related cardiovascular diseases due to its significant antioxidant properties.

NF-κB is present in the cytoplasm along with IκBα, an inhibitory protein. Previous research has demonstrated that NF-κB is activated by the phosphorylation of IκBα, thereby triggering the expression of genes associated with inflammation (Wang et al., 2020). The activation of NF-κB subsequently induces the expression of proinflammatory cytokines, including nitric oxide synthase (iNOS), COX-2, tumor necrosis factor (TNF-α), interleukin 1 beta (IL-1β), and interleukin-6 (IL-6) (Rojas et al., 2013; Liang et al., 2018). Recent studies have further confirmed that Kae inhibits the activation of NF-κB (Kadioglu et al., 2015). However, the effect of Kae on the oxidative-stress-induced activation of NF-κB in vascular endothelial cells remains unknown.

In brief, although Kae can effectively relieve oxidative damage and inflammation in a variety of organs, only a small number of studies have confirmed its effect on vascular damage. Recent studies have shown that Kae can reduce doxorubicin-induced endothelial toxicity injury, and that this protective effect is related to the inhibition of oxidative stress (Wu et al., 2020). However, it is unclear whether Kae can protect against vascular damage induced by other pro-oxidative factors. To address this outstanding question, we attempted to investigate the anti-inflammatory and anti-oxidant effects of Kae and explore the specific mechanisms underlying such effects. Identification of the specific anti-inflammatory and antioxidant effect of Kae should allow its development as a candidate compound to prevent and treat oxidative damage to blood vessels.

MATERIALS AND METHODS

Reagents and Chemicals

Paraquat, thiazolyl blue tetrazolium bromide (MTT), and dimethyl sulfoxide (DMSO), were purchased from Sigma-Aldrich (Darmstadt, Germany) and kaempferol (98% purity) was purchased from Aladdin Biochemical Technology Co., Ltd. (Shanghai, China). All of the kits used to measure indicators of oxidative stress (including malondialdehyde [MDA], SOD, GSH-Px, total antioxidant capacity [T-AOC] and CAT) were purchased from Nanjing Jiancheng Institute of Biological Engineering (Nanjing, China). We also purchased a DCFH-DA fluorescent probe and an SA-β-gal staining kit from Beyotime Biotechnology (Shanghai, China).

Preparation of Kae Solution and Suspension

Kae solution was used in all *in vitro* experiments. First, we prepared a stock solution of Kae in DMSO. This stock solution was then diluted in culture medium to the required concentration, and DMSO was added to ensure that the concentration of DMSO in each group was consistent at 0.1%. For the control group, 0.1% DMSO was also added to the culture medium. For *in vivo* experiments, we prepared a suspension of Kae with DMSO and normal saline; the final concentration of DMSO was maintained at 1% in each group. The suspension was shaken well prior to administration to experimental mice *via* the intragastric route. The control group was also given 1% DMSO dissolved in normal saline.

Cell Culture

Human umbilical vein cells (HUVECs) were obtained from ScienCell Research Laboratories Inc. (US) and grown in endothelial cell medium (ECM) containing 5% fetal bovine serum (FBS) and 1% penicillin-streptomycin in 5% CO_2 at 37°C.

Cell Viability Assays

Cell viability was evaluated by MTT assays. HUVECs were seeded in 96-well plates (3×10^3 cells/well). The cells were then treated with Kae (2.5, 5, and 10 μmol/l) for 24 h or treated with H_2O_2 (100 μmol/l) plus Kae (2.5, 5, and 10 μmol/l) for 24 h. After 24 h, MTT solution (5 mg/ml; 20 μmol/l) was added and then incubated for 4 h. Finally, the supernatants were removed and 150 μl of DMSO was added to dissolve the formazan crystals. The optical density (OD) was then measured at a wavelength of 570 nm using a microplate reader (Multiskan™ MK3; Thermo Fisher Scientific, Inc., US), and cell viability was calculated.

Determination of Reactive Oxygen Species (ROS)

Intracellular ROS production was assessed by measuring the fluorescence intensity of 2,7-dichlorodi-hydrofluorescein diacetate (DCFH-DA). HUVECs were seeded in 24-well plates (1×10^4 cells/well). Then, the cells were treated with 100 μmol/l H_2O_2 or treated with H_2O_2 (100 μmol/l) plus 5 μmol/l Kae for 24 h. After 24 h, the cells were washed three times in phosphate-

buffered saline (PBS) and then loaded with a DCFH-DA probe (1:1,000, 10 min) at 37°C in a CO_2 incubator. After rinsing in PBS, images were finally acquired by fluorescence microscopy (Olympus, Tokyo, Japan).

Senescence-Associated-β-Galactosidase (SA-β-Gal) Staining Assays

HUVECs were treated with Kae (2.5 and 5 μmol/l) for 24 h or treated with H_2O_2 (100 μmol/l) plus Kae (2.5 and 5 μmol/l) for 24 h. After 24 h, the cell culture medium was removed. Then, the cells were washed once with PBS and fixed at room temperature for 15 min. Following the removal of cell fixative, the cells were washed with PBS three times (for 3 min each time). Next, we added 1 ml of working solution (10 μl of dyeing solution A + 10 μl dyeing solution B + 930 μl dyeing solution C + 50 μl of X-Gal solution) to the plate and incubated for 24 h at 37°C in 5% CO_2. Cell staining was observed by light microscopy. The proportion (%) of positive-stained cells out of the total number of cells was then determined in three random fields by light microscopy at 10× and 20× magnification.

Animals, Groups, and Dosing

In vivo experiments were performed with 8-week-old male C57 BL/6J mice, weighing approximately 23 g. The animals are provided by Sipeifu Biotechnology (Beijing, China). The study was approved by the Animal Ethics Committee of Beijing Hospital. The animals were maintained at a temperature of 22 ± 3°C and a relative humidity of 50 ± 10% with a 12 h dark/light cycle. Experimental animals were provided with standard food and water. The animals were divided into five groups (six mice in each group), as follows: Group 1 (vehicle-treated, control) received 1% DMSO by daily gavage for 10 consecutive days and an intraperitoneal injection of normal saline every 3 days; Group 2 (Kae-treated) received Kae (25 mg/kg body weight) by daily gavage for 10 consecutive days and an intraperitoneal injection of normal saline every 3 days; Group 3 (paraquat-treated) received 1% DMSO by daily gavage for 10 consecutive days and an intraperitoneal injection of paraquat (10 mg/kg body weight) every 3 days; Group 4 (paraquat + Kae-25) received Kae (25 mg/kg body weight) by daily gavage for 10 consecutive days and an intraperitoneal injection of paraquat (10 mg/kg body weight) every 3 days; Group 5 (paraquat + Kae-50) received Kae (50 mg/kg body weight) by daily gavage for 10 consecutive days and an intraperitoneal injection of paraquat (10 mg/kg body weight) every 3 days. At the end of treatment, we recorded body weight, heart weight, and blood was collected from the abdominal aorta according to standard procedures. Blood was centrifuged (3,000 rpm for 15 min) and the serum was stored at −4°C to await analysis. After the mice were sacrificed, the abdominal aorta was removed and cryopreserved at −80°C to await further analysis.

Evaluation of Oxidative Stress

Adherent HUVECs in each group were collected with a scraper and dissolved in 150 μl of PBS. The collected cells were then broken by ultrasound on ice. Then, we determined the levels of various antioxidant indicators, including MDA, SOD, GSH-Px, CAT, and T-AOC, using the above kits in accordance with the manufacturer's guidelines. The concentration of MDA and the relative activities of SOD and GSH-Px in the serum were also analyzed, as described above.

Preparation of Total Protein From Abdominal Aorta Tissues

Abdominal aorta tissues were homogenized in a tissue homogenizer using PBS and the homogenates were centrifuged at 12,000 rpm for 10 min to obtain the supernatants. Next, we used RIPA lysis buffer to extract total protein in accordance with the manufacturer's guidelines. Total protein content was then determined by a protein assay kit (Sigma-Aldrich, US).

Immunoblot Analysis

Total protein extracts were then used in immunoblotting experiments with a variety of antibodies, including GAPDH (1:1,000, CST, US), TNF-α (1:1,000, CST, US), IL-6 (1:1,000, CST, US), NF-κB p65 (1:1,000, CST, US), Nrf2 (1:1,000, Proteintech, US), HO-1(1:1,000, Proteintech, US), and KNDC1 (1:1,000, Sigma-Aldrich, US). The proteins were analyzed using enhanced chemiluminescence western blotting detection reagents (GE Healthcare, US). ImageJ software version 1.0 was then used to quantify the optical density of each protein band normalized to the that of the internal control (GAPDH).

Statistical Analysis

All statistical analysis was conducted using GraphPad Prism 5.0. Data are presented as mean ± standard deviation (SD). One-way analysis of variance (ANOVA) with Tukey's *post-hoc* test was used to determine the statistical significance of multiple comparisons. P values < 0.05 were considered to represent statistically significant results.

RESULTS

The Cytoprotective Effect of Kae on the Senescence of HUVECs Induced by H_2O_2

Observation of the growth of HUVECs in the presence of Kae showed that when the concentration of Kae was 5 μmol/l, the number of cells increased significantly. However, when the concentration of Kae reached 10 μmol/l, the morphology of the cells changed significantly (**Figure 1A**). When HUVECs were treated with 100 μmol/l of H_2O_2 for 24 h, the number of cells that were positive for SA-β-gal staining increased significantly. Observation of cell morphology showed that the cells had undergone significant changes. For example, cells had become spherical, cell volume had increased, the number of connections between cells had decreased, cell growth was slow, and the cell density had decreased. However, after the addition of 2.5 and 5 μmol/l of Kae, along with 100 μmol/l of H_2O_2, we observed that the number of positive cells decreased, the morphology and arrangement of cells were clearly regular, the growth status was significantly improved, and the number of cells was increased (**Figures 1B, C**). Data showed that the application of H_2O_2 at a

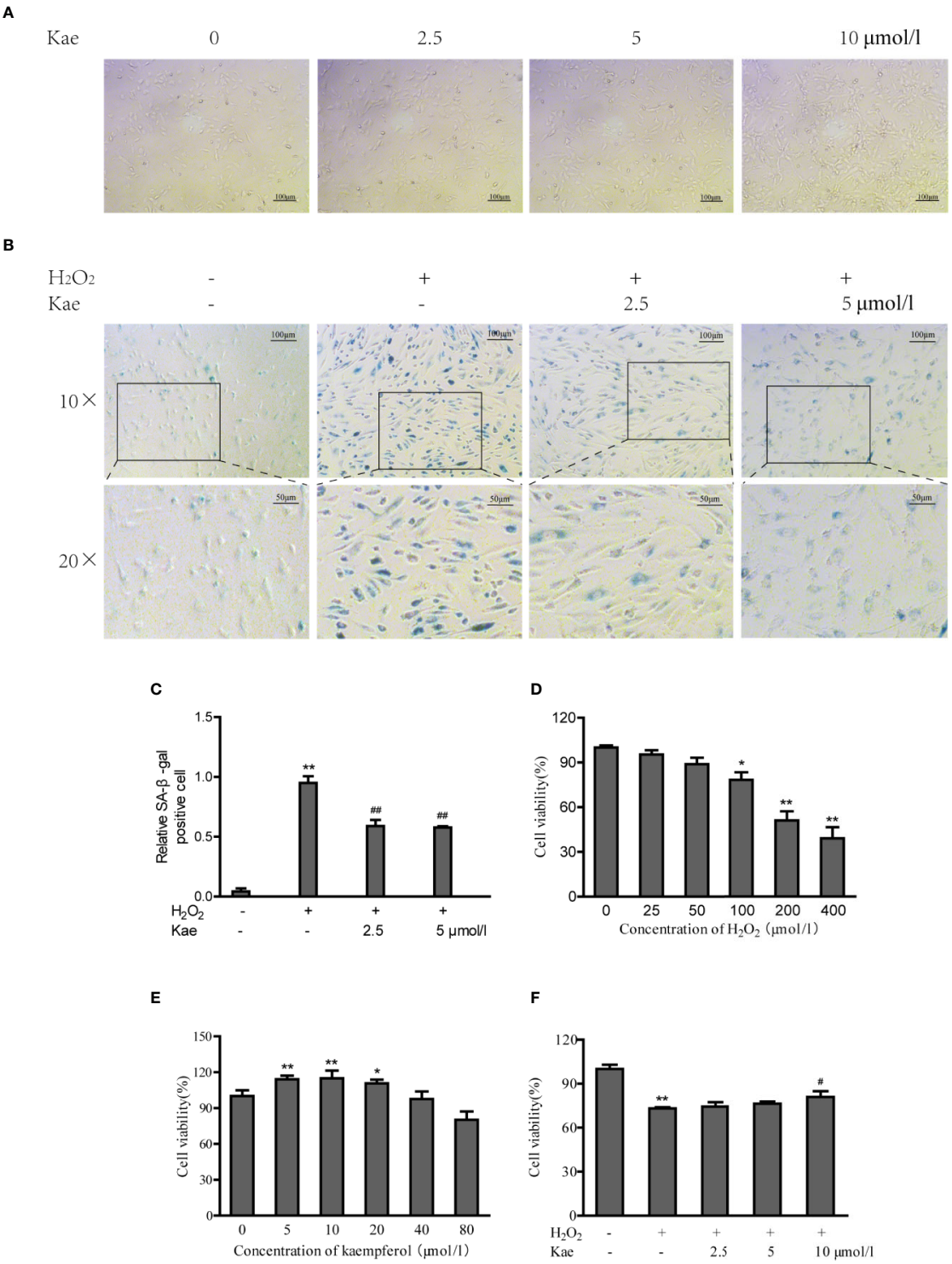

FIGURE 1 | The protective effects of Kae on human umbilical vein endothelial cells (HUVECs). **(A)** Images captured from HUVECs grown in the presence of 0, 2.5, 5, and 10 μmol/l Kae for 24 h (Magnification: 10×). **(B, C)** HUVECs were incubated with 0, 2.5, and 5 μmol/l Kae and 100 μmol/l H_2O_2 for 24 h. Relative levels of senescence were then detected by SA-β-gal staining under light microscopy (Magnification: 10×, 20×). HUVECs were then treated with various concentrations of H_2O_2 **(D)** or Kae **(E)** or both Kae (0, 2.5, 5, and 10 μmol/l) and 100 μmol/l H_2O_2 **(F)** at 37°C for 24 h; viability was then determined by MTT assays (three biological replicates). *P < 0.05 and **P < 0.01, compared with the control group. $^{\#}$P < 0.05 and $^{\#\#}$P < 0.01, compared with the H_2O_2-treated group.

concentration of 100 μmol/l or above could significantly reduce the viability of HUVECs compared with that of the control group (**Figure 1D**). However, compared with the group treated with 100 μmol/l of H_2O_2, the cell viability of the group treated with 10 μmol/l of Kae, and the group treated with 100 μmol/l of H_2O_2, was significantly increased (**Figure 1F**). In addition, concentrations of Kae below10 μmol/l also increased the viability of normal HUVECs. However, when the concentration exceeded 20 μmol/l, this effect began to diminish (**Figure 1E**).

Kae Reduced the Levels of ROS and Increased the Levels of Antioxidant Indicators *In Vitro*

Oxidative stress can lead to the excessive production of ROS, thus leading to an imbalance between the oxidation and antioxidant systems. We measured ROS levels in HUVECs after the addition of H_2O_2 with or without Kae (**Figures 2A, B**). Analysis showed that the addition of H_2O_2 increased the intracellular levels of ROS levels by 10-fold when compared with that in the control group; treatment with 5 μmol/l Kae caused a significant reduction in the upregulated ROS levels induced by H_2O_2. By investigating markers of oxidative stress, we found that H_2O_2 treatment significantly inhibited the antioxidant defense mechanism of the HUVECs. It was also evident that the concentration of MDA increased significantly, whereas the levels or activities of T-AOC and GSH-Px were significantly reduced compared with those of the control group. By treating HUVECs with 5 μmol/l Kae, we were able to significantly reverse this effect and achieve oxidative stress parameters close to the normal range. At a concentration of 5 μmol/l, Kae caused the levels or activities of T-AOC, CAT, and GSH-Px, to increase significantly, whereas the concentration of MDA decreased and the activities of SOD remained unaffected when compared with those of the group treated with H_2O_2. The results also demonstrated the increase of Kae on the antioxidant capacity of normal cells (**Figures 2C–G**).

Kae Ameliorated Cardiovascular Damage and Antioxidant Defense Impairment Induced by Paraquat *In Vivo*

Compared with mice in the control group, the body weights of those receiving three injections of paraquat were significantly reduced ($P < 0.05$). Kae treatment was able to prevent this loss of body weight in a concentration-dependent manner (**Figure 3A**). Although heart weight remained unchanged, the ratio of heart weight to body weight was increased after treatment with paraquat. Kae treatment also inhibited the increase in the ratio

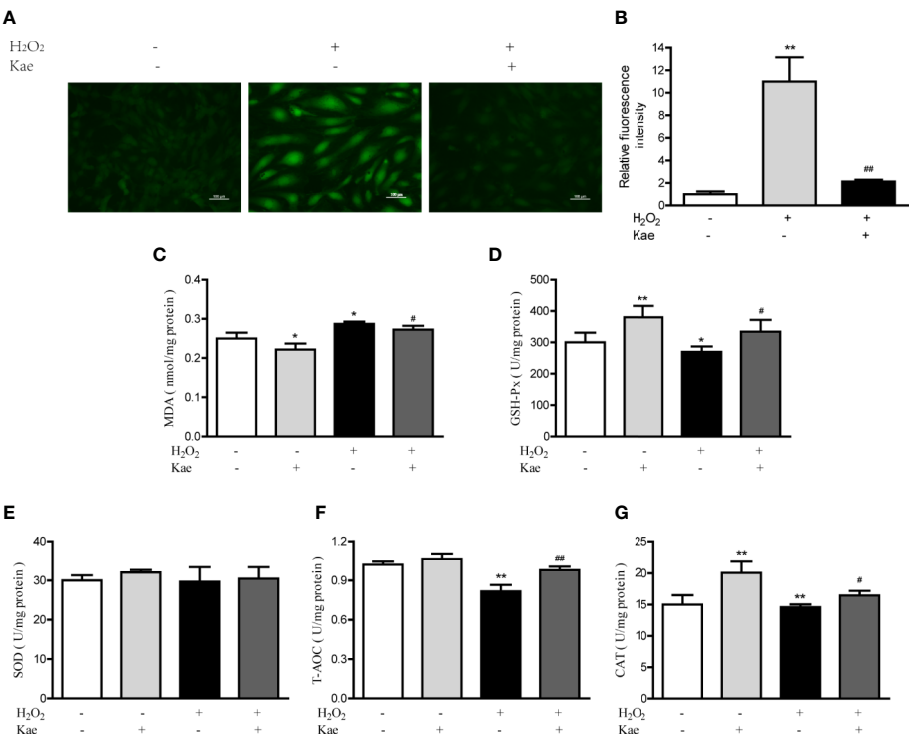

FIGURE 2 | Kae reduced ROS and increased the levels of oxidant indicators *in vitro*. **(A–B)** HUVECs were treated with or without 100 μmol/l H_2O_2 for 24 h with 24 h exposure to 5 μmol/l Kae. The intracellular levels of ROS were then measured by fluorescence microscopy (10×). The concentration of MDA **(C)** and the activities of GSH-Px **(D)**, SOD **(E)**, T-AOC **(F)**, and CAT (G), were then determined using appropriate kits after treating HUVECs for 24 h with 100 μmol/l and 5 μmol/l of H_2O_2 and Kae, respectively. Data are presented as the mean ± standard deviation (SD) of three independent experiments. *$P < 0.05$ and **$P < 0.01$, compared with the control group. #$P < 0.05$ and ##$P < 0.01$, compared with the H_2O_2-treated group.

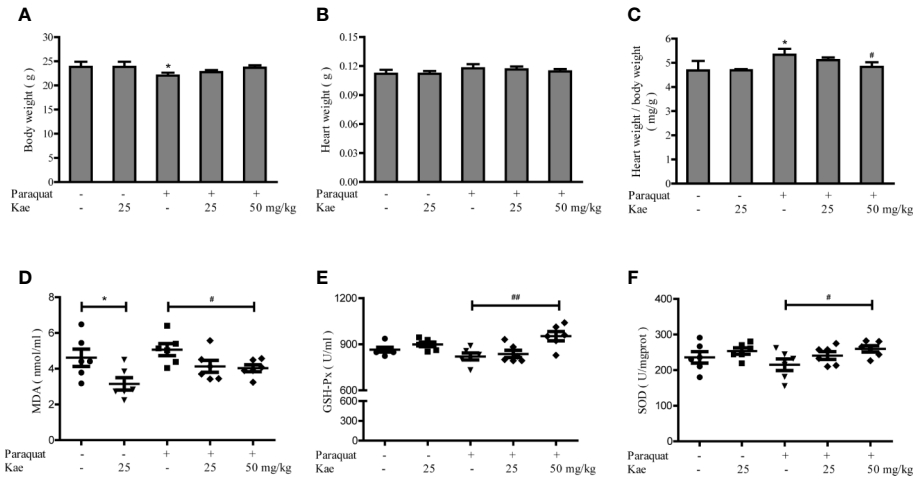

FIGURE 3 | The protective effect of Kae on cardiovascular oxidative stress injury. The effect of Kae on body weight **(A)**, heart weight **(B)**, heart weight/body weight ratio **(C)** treated with or without paraquat. The effect of Kae on the concentration of MDA **(D)** and the activities of GSH-Px **(E)** and SOD **(F)** with or without paraquat. Data are presented as the mean ± standard deviation (SD) of three independent experiments. *P < 0.05, compared with the control group. #P < 0.05 and ##P < 0.01, compared with the paraquat-treated group.

of heart weight to body weight compared with mice that were exposed to paraquat alone (**Figures 3B, C**). There was no significant difference in body weight, or in the absolute and relative weight of the heart, between the group receiving 25 mg/kg of Kae and the control group. In our study, we used paraquat to establish a mouse model of cardiovascular oxidative stress; the ability of paraquat to induce oxidative stress has been previously verified in mice. Analysis showed that, compared with that in the control group, the activities of SOD and GSH-Px were reduced in the serum of the model mice, and that the concentration of MDA was increased. Treatment with Kae was able to reduce this oxidative stress in a concentration-dependent manner. Furthermore, 25 mg/kg of Kae was also able to alleviate oxidative stress in normal mice (**Figures 3D–F**). Collectively, these results indicate that Kae can protect blood vessels from oxidative damage induced by chemicals and play a preventive role in maintaining normal cardiovascular structure and function.

The Effect of Kae on the Levels of Inflammatory Marker Under Normal and Oxidative Stress Conditions *In Vitro* and *In Vivo*

Next, we detected the levels of a series of inflammatory marker (NF-κB p65, TNF-α, and IL-6) by western blotting. Analysis showed that the levels of NF-κB p65, TNF-α, and IL-6, all decreased in a concentration-dependent manner with the application of Kae (**Figures 4A, B**). Furthermore, our results showed that when HUVECs were stimulated with 100 μmol/l of H_2O_2, there was a dramatic increase in the expression of NF-κB p65, TNF-α, and IL-6, compared to the levels in untreated cells. However, Kae markedly inhibited the overexpression of these markers (**Figures 4C, D**). Western-blot analysis was used to evaluate the effect of Kae treatment on the levels of these inflammatory markers *in vivo*. Analysis suggested that the levels of NF-κB p65, TNF-α, and IL-6, were significantly upregulated in the abdominal aortas of mice injected with paraquat alone compared to those injected with the vehicle. Kae treatment also significantly attenuated the expression of NF-κB p65, TNF-α, and IL-6, compared with that in mice treated with paraquat alone. However, although Kae reduced the levels of TNF-α, it had no significant effect on the levels of NF-κB p65 and IL-6 in normal mice over the short-term and when administered at a low dose (**Figures 4E, F**).

The Effect of Kae on the Nrf2/HO-1 Signaling Pathway Under Normal and Oxidative Stress Conditions *In Vitro* and *In Vivo*

In order to investigate whether Kae played a role in the activation of the Nrf2/HO-1 pathway, we evaluated the expression of Nrf2 and HO-1 by western-blotting. We found that the Nrf2/HO-1 signaling pathway showed significant levels of activation following Kae treatment (**Figures 5A, B**). Compared with HUVECs that were stimulated with 100 μmol/l of H_2O_2 alone, Kae significantly reduced the H2O2-induced down-regulation of the Nrf2/HO-1 signaling pathway (**Figures 5C, D**). Furthermore, we observed that the levels of Nrf2 and HO-1 were significantly elevated in total protein extracts prepared from the abdominal aortas of mice receiving a combination of Kae and paraquat compared with those of mice receiving paraquat alone. However, compared with that in the control group, the expression levels of Nrf2 and HO-1 in the total protein extracts of abdominal aortas from mice receiving Kae alone were only slightly increased (**Figures 5E, F**).

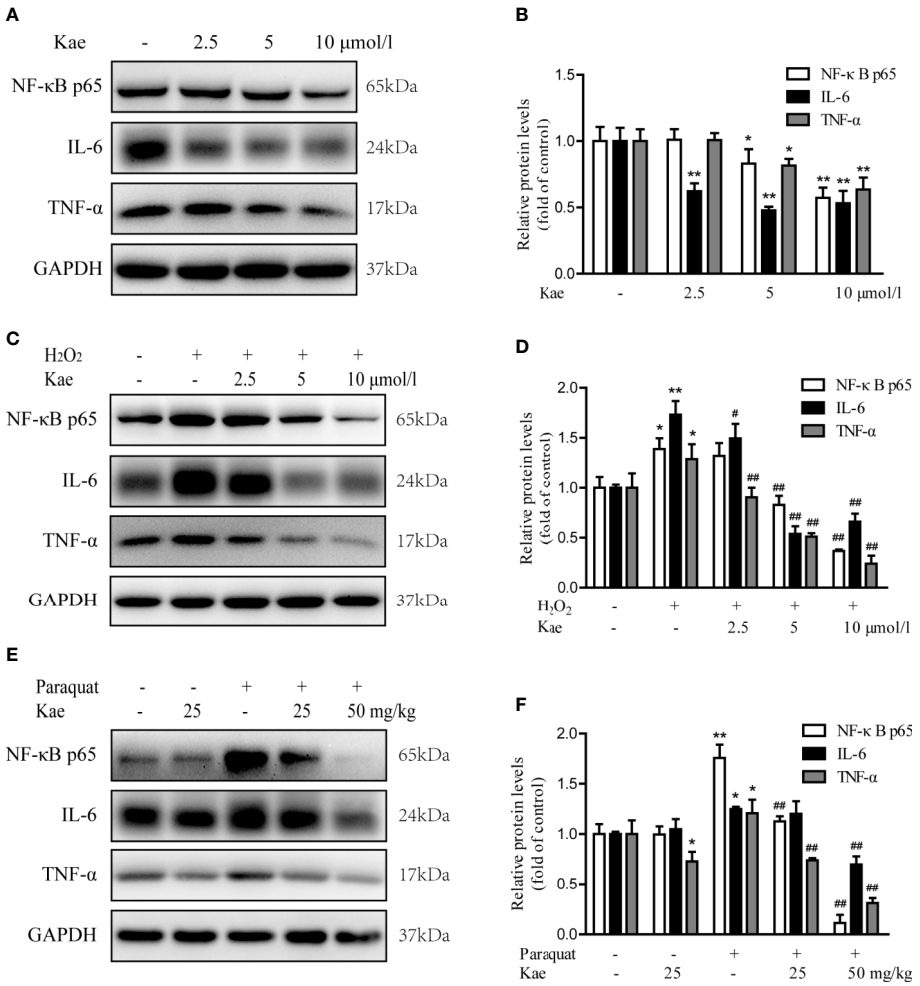

FIGURE 4 | The effect of Kae on the levels of inflammatory markers. **(A, B)** The effect of Kae on the levels of NF-κB p65, IL-6, and TNF-α, in HUVECs. **(C, D)** The effect of Kae and 100 μmol/l H_2O_2 on the levels of NF-κB p65, IL-6, and TNF-α in HUVECs. **(E, F)** The effect of Kae and paraquat on the levels of NF-κB p65, IL-6, and TNF-α, in mice. Data are expressed as the mean ± standard deviation (SD) of three independent experiments. *P < 0.05 and **P < 0.01, compared with the control group. #P < 0.05 and ##P < 0.01, compared with the model group.

DISCUSSION

Cardiovascular disease is a serious threat to human life and health. Oxidative stress, endothelial cell activation, and endothelial dysfunction have been widely recognized as major factors in the pathogenesis of vascular diseases (Mittal et al., 2014). Endothelial cells are monolayer cells that are distributed in the vascular lumen and play an important physiological role in vascular homeostasis. Endothelial cell injury is a complex pathophysiological event, involving increased endothelial cell activation and endothelial dysfunction (Liao, 2013). Cytokine-induced endothelial activation under inflammatory conditions often leads to endothelial dysfunction. By regulating the secretion of cytokines, oxidative stress is closely related to endothelial cell activation and endothelial cell dysfunction (Bulua et al., 2011). Kae is an important flavonoid that is commonly found in medicinal plants and plant-derived foods. Kae can also play a key role in antioxidation, anti-inflammation, and anti-apoptosis in a variety of tissues and organs (Wang et al., 2018). However, the specific role of Kae in relieving the inflammation and oxidative stress caused by vascular endothelial injury, and the mechanisms involved, have yet to be elucidated. In view of this, we investigated whether Kae can improve vascular damage by reducing oxidative damage and inflammation. The results of our study strongly indicated that Kae could protect against vascular damage by alleviating oxidative stress and reducing the levels of inflammatory markers. Furthermore, we found that the mechanism involved is related to activation of the Nrf2/HO-1 signaling pathway. In the present study, we used paraquat to induce vascular damage in mice: we found that an intraperitoneal injection of paraquat at a concentration of 10 mg/kg was sufficient to cause inflammation and oxidative stress in vascular endothelial cells and eventually lead to vascular damage.

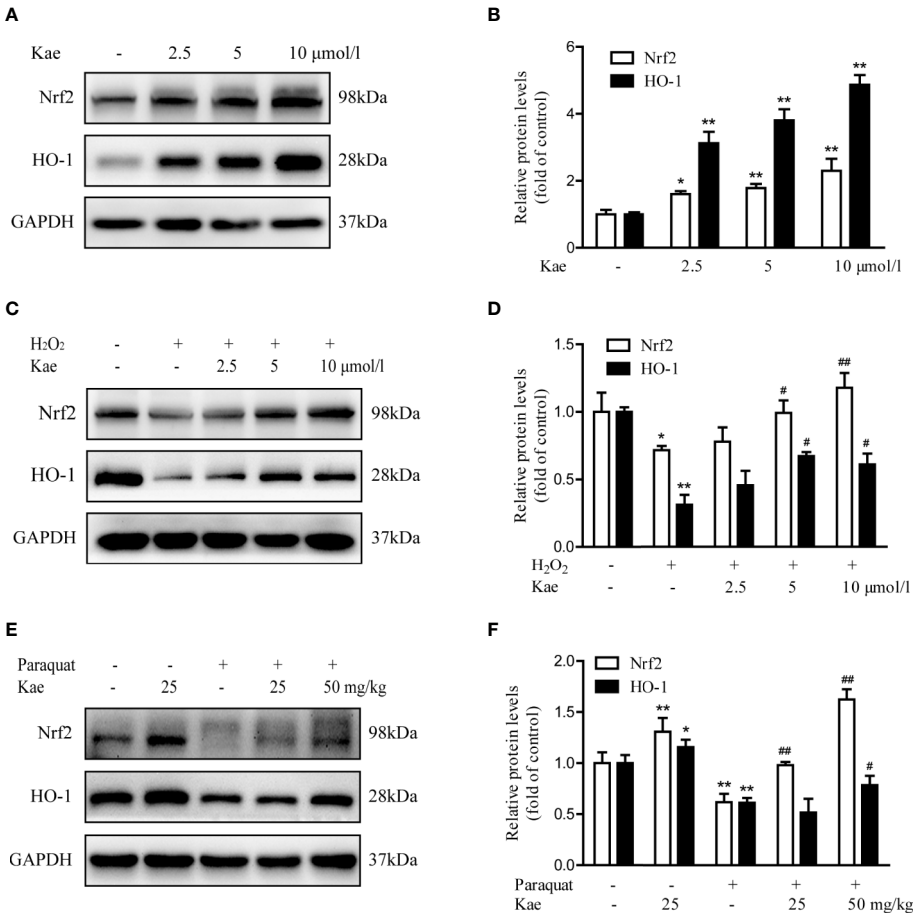

FIGURE 5 | The effect of Kae on the Nrf2/HO-1 signaling pathway. **(A, B)** The effect of Kae on the levels of Nrf2 and HO-1 in HUVECs. **(C, D)** The effect of Kae and 100 μmol/l H_2O_2 on the levels of Nrf2 and HO-1 in HUVECs. **(E, F)** The effect of Kae and paraquat on the levels of Nrf2 and HO-1 in mice. Data are expressed as the mean ± standard deviation of three independent experiments. *P < 0.05 and **P < 0.01, compared with the control group. $^{\#}$P < 0.05 and $^{\#\#}$P < 0.01, compared with the model group.

Most of the current studies on paraquat have focused on lung damage caused by high doses. The increased secretion of proinflammatory factors and proinflammatory mediators in lung tissues that are induced by paraquat have also been reported previously (Amirshahrokhi and Khalili, 2016; Ahmed et al., 2019). Paraquat has also been reported to cause oxidative damage and inflammation in the liver (Amirshahrokhi and Bohlooli, 2013). Recent research suggests that paraquat can induce a phenotype associated with senescence in cardiomyocyte cells by inhibiting the activation of FoxO3, thus leading to cardiac senescence (Chang et al., 2019). In the present study, we demonstrated that paraquat increased the concentration of MDA and reduced the levels of GSH-Px and SOD in the serum of mice. Following treatment with paraquat, mice showed an increase in both the relative and absolute heart weight; these changes were alleviated when paraquat was administered concurrently with Kae. These findings indicate that Kae can alleviate the oxidative stress induced by paraquat in mice, as well as reduce heart weight and the loss in body weight. Consequently, the reduction in paraquat-mediated vascular damage induced by Kae may be related to the up-regulation of antioxidant enzyme activities.

Previous studies have shown that Nrf2 maintains the stability of the intracellular environment by regulating the activity of antioxidant proteins, detoxification enzymes, and other stress response proteins. It has also been established that HO-1 can resist the cytotoxicity of various oxidative stress and inflammatory reactions (Lin et al., 2017; Wu et al., 2017). It is evident that the Nrf2/HO-1 pathway exerts antioxidant and anti-inflammatory effects, reduces mitochondrial damage, regulates cell death and other effects, and ultimately affects the outcome of many diseases. To evaluate the specific involvement of Kae treatment on the levels of Nrf2 in vascular endothelial cells, and its potential role in paraquat-mediated vascular injury, we used immunoblotting to detect the levels of Nrf2 and HO-1. Analysis showed that paraquat caused a significant downregulation of Nrf2 in the abdominal aorta compared with that in vehicle-treated mice. However, the co-administration of paraquat and Kae resulted in a significant increase in the levels of Nrf2 when compared with those in animals treated with only paraquat. These findings are

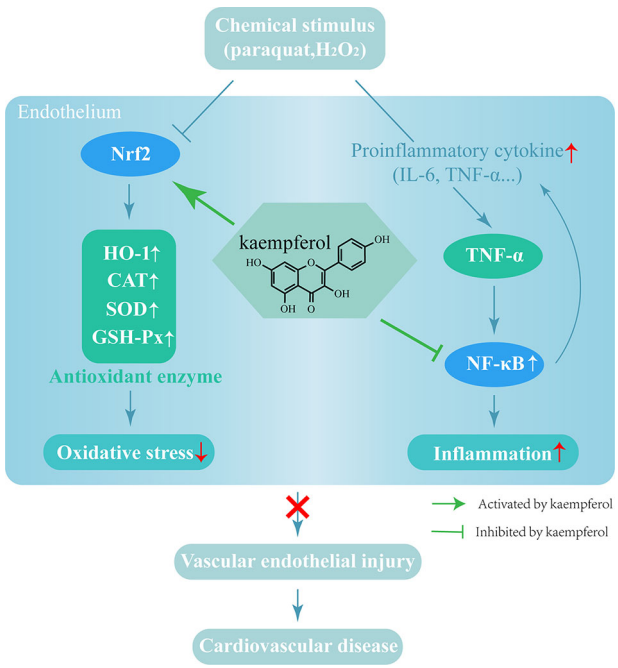

FIGURE 6 | The mechanism by which Kae protects blood vessels from damage.

consistent with the role of Kae in reducing oxidative stress *via* the Nrf2/HO-1 pathway.

Inflammation is believed to be an important causative factor for multiple organ damage. The reduction of inflammation by inhibiting the activation of NF-κB has been shown to be an important mechanism with which to mitigate such damage (Yang et al., 2018). Paraquat, the most commonly used non-selective herbicide, is highly toxic to humans and animals (Baltazar et al., 2013), and is known to increase the expression of TNF-α, IL-1β, IL-6, and NO. These factors are common proinflammatory mediators in blood and organs and can often aggravate damage incurred by the body (Donnelly et al., 1994; Ishida et al., 2006). Inhibiting the expression of these proinflammatory mediators has become an important goal for the treatment of paraquat poisoning (Byrne et al., 2016). The p-p65 subunit of NF-kB can be transferred into the nucleus to induce the release of a large number of inflammatory regulators; it can also enhance the inflammatory response and induce organ damage (Amirshahrokhi and Khalili, 2016). In the present study, we confirmed that paraquat induced the over-expression of TNF-α and IL-6, and the activation of NF-κB in the abdominal aorta. However, we also found that Kae alleviated the inflammatory response induced by paraquat. As reported previously, our present data proved that Kae attenuated inflammation and alleviated the progression of vascular injury. Therefore, Kae could alleviate paraquat-induced vascular injury by reducing inflammation *via* the inactivation of NF-κB.

Oxidative stress is known to induce an inflammatory response that aggravates oxidative stress, thus leading to the excessive production of ROS by a range of cells after stimulation (Elmarakby and Sullivan, 2012). Some researchers have speculated that there may be a circulatory relationship between inflammation and oxidative stress (Yang et al., 2018). It has also been reported that endothelial dysfunction caused by the production of ROS often leads to vascular damage (Incalza et al., 2018). The present results confirm that Kae can reduce the levels of ROS and that Kae may help to improve vascular injury by scavenging reactive oxygen species. However, further research is still required to systematically elucidate the specific mechanisms underlying the effects of Kae on the process of vascular injury.

In summary, the present study used a mouse model to demonstrate that vascular injury led to a significant increase in oxidative damage and the levels of inflammatory factors. Kae was able to alleviate paraquat-induced vascular injury by suppressing inflammation and oxidative stress. Analysis showed that the NF-κB and Nrf2/HO-1 pathways play a key role in these effects. Collectively, our findings demonstrate that Kae is a highly promising candidate for the treatment of acute vascular injury (**Figure 6**).

DATA AVAILABILITY STATEMENT

The raw data supporting the conclusions of this article will be made available by the authors, without undue reservation, to any qualified researcher.

ETHICS STATEMENT

The animal study was reviewed and approved by the Institutional Animal Care and Use Committee of Beijing Hospital.

AUTHOR CONTRIBUTIONS

YL and BC conceived and designed the experiments. HY performed the experiments. JW and XZ were involved in experimental analysis and data acquisition. HY and JS assisted in the western blot analysis and manuscript preparation. YL wrote the manuscript. All authors contributed to the article and approved the submitted version.

FUNDING

This work was supported by grants from CAMS Innovation Fund for Medical Sciences (No. 2018-I2M-1-002), the National Natural Science Foundation of China (No. 81671391), and Beijing Hospital Nova Project (No. BJ-2016-033).

REFERENCES

Abdou, K. H., Moselhy, W. A., Mohamed, H. M., El-Nahass, E. S., and Khalifa, A. G. (2019). Moringa oleifera Leaves Extract Protects Titanium Dioxide Nanoparticles-Induced Nephrotoxicity via Nrf2/HO-1 Signaling and Amelioration of Oxidative Stress. *Biol. Trace element Res.* 187, 181–191. doi: 10.1007/s12011-018-1366-2

Ahmed, M. A. E., El Morsy, E. M., and Ahmed, A. A. E. (2019). Protective effects of febuxostat against paraquat-induced lung toxicity in rats: Impact on RAGE/PI3K/Akt pathway and downstream inflammatory cascades. *Life Sci.* 221, 56–64. doi: 10.1016/j.lfs.2019.02.007

Amirshahrokhi, K., and Bohlooli, S. (2013). Effect of methylsulfonylmethane on paraquat-induced acute lung and liver injury in mice. *Inflammation* 36, 1111–1121. doi: 10.1007/s10753-013-9645-8

Amirshahrokhi, K., and Khalili, A. R. (2016). Carvedilol attenuates paraquat-induced lung injury by inhibition of proinflammatory cytokines, chemokine MCP-1, NF-kappaB activation and oxidative stress mediators. *Cytokine* 88, 144–153. doi: 10.1016/j.cyto.2016.09.004

Assar, M. E., Angulo, J., and Rodriguez-Manas, L. (2016). Diabetes and ageing-induced vascular inflammation. *J. Physiol.* 594, 2125–2146. doi: 10.1113/JP270841

Baltazar, T., Dinis-Oliveira, R. J., Duarte, J. A., de Lourdes Bastos, M., and Carvalho, F. (2013). Paraquat research: do recent advances in limiting its toxicity make its use safer? *Br. J. Pharmacol.* 168, 44–45. doi: 10.1111/j.1476-5381.2012.02017.x

Bruder-Nascimento, T., Callera, G. E., Montezano, A. C., Belin de Chantemele, E. J., Tostes, R. C., and Touyz, R. M. (2019). Atorvastatin inhibits pro-inflammatory actions of aldosterone in vascular smooth muscle cells by reducing oxidative stress. *Life Sci.* 221, 29–34. doi: 10.1016/j.lfs.2019.01.043

Bulua, A. C., Simon, A., Maddipati, R., Pelletier, M., Park, H., Kim, K. Y., et al. (2011). Mitochondrial reactive oxygen species promote production of proinflammatory cytokines and are elevated in TNFR1-associated periodic syndrome (TRAPS). *J. Exp. Med.* 208, 519–533. doi: 10.1084/jem.20102049

Byrne, A. J., Maher, T. M., and Lloyd, C. M. (2016). Pulmonary Macrophages: A New Therapeutic Pathway in Fibrosing Lung Disease? *Trends Mol. Med.* 22, 303–316. doi: 10.1016/j.molmed.2016.02.004

Catapano, A. L., Pirillo, A., and Norata, G. D. (2017). Vascular inflammation and low-density lipoproteins: is cholesterol the link? A lesson from the clinical trials. *Br. J. Pharmacol.* 174, 3973–3985. doi: 10.1111/bph.13805

Chang, Z. S., Xia, J. B., Wu, H. Y., Peng, W. T., Jiang, F. Q., Li, J., et al. (2019). Forkhead box O3 protects the heart against paraquat-induced aging-associated phenotypes by upregulating the expression of antioxidant enzymes. *Aging Cell* 18, e12990. doi: 10.1111/acel.12990

Chen, X., Qian, J., Wang, L., Li, J., Zhao, Y., Han, J., et al. (2018). Kaempferol attenuates hyperglycemia-induced cardiac injuries by inhibiting inflammatory responses and oxidative stress. *Endocrine* 60, 83–94. doi: 10.1007/s12020-018-1525-4

David, J. A., Rifkin, W. J., Rabbani, P. S., and Ceradini, D. J. (2017). The Nrf2/Keap1/ARE Pathway and Oxidative Stress as a Therapeutic Target in Type II Diabetes Mellitus. *J. Diabetes Res.* 2017, 4826724. doi: 10.1155/2017/4826724

Donnelly, T. J., Meade, P., Jagels, M., Cryer, H. G., Law, M. M., Hugli, T. E., et al. (1994). Cytokine, complement, and endotoxin profiles associated with the development of the adult respiratory distress syndrome after severe injury. *Crit. Care Med.* 22, 768–776. doi: 10.1097/00003246-199405000-00010

Elmarakby, A. A., and Sullivan, J. C. (2012). Relationship between oxidative stress and inflammatory cytokines in diabetic nephropathy. *Cardiovasc. Ther.* 30, 49–59. doi: 10.1111/j.1755-5922.2010.00218.x

Filomeni, G., Desideri, E., Cardaci, S., Graziani, I., Piccirillo, S., Rotilio, G., et al. (2010). Carcinoma cells activate AMP-activated protein kinase-dependent autophagy as survival response to kaempferol-mediated energetic impairment. *Autophagy* 6, 202–216. doi: 10.4161/auto.6.2.10971

Hajjar, D. P., and Gotto, A. M.Jr. (2013). Biological relevance of inflammation and oxidative stress in the pathogenesis of arterial diseases. *Am. J. Pathol.* 182, 1474–1481. doi: 10.1016/j.ajpath.2013.01.010

Incalza, M. A., D'Oria, R., Natalicchio, A., Perrini, S., Laviola, L., and Giorgino, F. (2018). Oxidative stress and reactive oxygen species in endothelial dysfunction associated with cardiovascular and metabolic diseases. *Vasc. Pharmacol.* 100, 1–19. doi: 10.1016/j.vph.2017.05.005

Ishida, Y., Takayasu, T., Kimura, A., Hayashi, T., Kakimoto, N., Miyashita, T., et al. (2006). Gene expression of cytokines and growth factors in the lungs after paraquat administration in mice. *Legal Med. (Tokyo Japan)* 8, 102–109. doi: 10.1016/j.legalmed.2005.08.010

Kadioglu, O., Nass, J., Saeed, M. E., Schuler, B., and Efferth, T. (2015). Kaempferol Is an Anti-Inflammatory Compound with Activity towards NF-kappaB Pathway Proteins. *Anticancer Res.* 35, 2645–2650.

Kampkotter, A., Gombitang Nkwonkam, C., Zurawski, R. F., Timpel, C., Chovolou, Y., Watjen, W., et al. (2007). Effects of the flavonoids kaempferol and fisetin on thermotolerance, oxidative stress and FoxO transcription factor DAF-16 in the model organism Caenorhabditis elegans. *Arch. Toxicol.* 81, 849–858. doi: 10.1007/s00204-007-0215-4

Liang, H., Yang, X., Liu, C., Sun, Z., and Wang, X. (2018). Effect of NF-kB signaling pathway on the expression of MIF, TNF-alpha, IL-6 in the regulation of intervertebral disc degeneration. *J. musculoskeletal neuronal Interact.* 18, 551–556.

Liao, J. K. (2013). Linking endothelial dysfunction with endothelial cell activation. *J. Clin. Invest.* 123, 540–541. doi: 10.1172/JCI66843

Lin, W. C., Deng, J. S., Huang, S. S., Wu, S. H., Chen, C. C., Lin, W. R., et al. (2017). Anti-Inflammatory Activity of Sanghuangporus sanghuang Mycelium. *Int. J. Mol. Sci.* 18, 347. doi: 10.3390/ijms18020347

Mittal, M., Siddiqui, M. R., Tran, K., Reddy, S. P., and Malik, A. B. (2014). Reactive oxygen species in inflammation and tissue injury. *Antioxidants Redox Signaling* 20, 1126–1167. doi: 10.1089/ars.2012.5149

Park, M. J., Lee, E. K., Heo, H. S., Kim, M. S., Sung, B., Kim, M. K., et al. (2009). The anti-inflammatory effect of kaempferol in aged kidney tissues: the involvement of nuclear factor-kappaB via nuclear factor-inducing kinase/IkappaB kinase and mitogen-activated protein kinase pathways. *J. medicinal Food* 12, 351–358. doi: 10.1089/jmf.2008.0006

Ren, J., Lu, Y., Qian, Y., Chen, B., Wu, T., and Ji, G. (2019). Recent progress regarding kaempferol for the treatment of various diseases. *Exp. Ther. Med.* 18, 2759–2776. doi: 10.3892/etm.2019.7886

Rojas, A., Delgado-Lopez, F., Gonzalez, I., Perez-Castro, R., Romero, J., and Rojas, I. (2013). The receptor for advanced glycation end-products: a complex signaling scenario for a promiscuous receptor. *Cell. signalling* 25, 609–614. doi: 10.1016/j.cellsig.2012.11.022

Suchal, K., Malik, S., Gamad, N., Malhotra, R. K., Goyal, S. N., Chaudhary, U., et al. (2016). Kaempferol Attenuates Myocardial Ischemic Injury via Inhibition of MAPK Signaling Pathway in Experimental Model of Myocardial Ischemia-Reperfusion Injury. *Oxid. Med. Cell. Longevity* 2016, 7580731. doi: 10.1155/2016/7580731

Wang, J., Fang, X., Ge, L., Cao, F., Zhao, L., Wang, Z., et al. (2018). Antitumor, antioxidant and anti-inflammatory activities of kaempferol and its corresponding glycosides and the enzymatic preparation of kaempferol. *PloS One* 13, e0197563. doi: 10.1371/journal.pone.0197563

Wang, Z., Sun, W., Sun, X., Wang, Y., and Zhou, M. (2020). Kaempferol ameliorates Cisplatin induced nephrotoxicity by modulating oxidative stress, inflammation and apoptosis via ERK and NF-kappaB pathways. *AMB Express* 10, 58. doi: 10.1186/s13568-020-00993-w

Wu, K. C., Huang, S. S., Kuo, Y. H., Ho, Y. L., Yang, C. S., Chang, Y. S., et al. (2017). Ugonin M, a Helminthostachys zeylanica Constituent, Prevents LPS-Induced Acute Lung Injury through TLR4-Mediated MAPK and NF-kappaB Signaling Pathways. *Molecules (Basel Switzerland)* 22, 573. doi: 10.3390/molecules22040573

Wu, W., Yang, B., Qiao, Y., Zhou, Q., He, H., and He, M. (2020). Kaempferol protects mitochondria and alleviates damages against endotheliotoxicity induced by doxorubicin. *Biomedicine pharmacotherapy = Biomedecine pharmacotherapie* 126, 110040. doi: 10.1016/j.biopha.2020.110040

Yang, W., Liu, W., Yu, W., Fei, D., Meng, X., Yang, S., et al. (2018). Angptl2 deficiency attenuates paraquat (PQ)-induced lung injury in mice by altering inflammation, oxidative stress and fibrosis through NF-kappaB pathway. *Biochem. Biophys. Res. Commun.* 503, 94–101. doi: 10.1016/j.bbrc.2018.05.186

Zhang, L., Guo, Z., Wang, Y., Geng, J., and Han, S. (2019). The protective effect of kaempferol on heart via the regulation of Nrf2, NF-kappabeta, and

PI3K/Akt/GSK-3beta signaling pathways in isoproterenol-induced heart failure in diabetic rats. *Drug Dev. Res.* 80, 294–309. doi: 10.1002/ddr.21495

Conflict of Interest: The authors declare that the research was conducted in the absence of any commercial or financial relationships that could be construed as a potential conflict of interest.

frontiers in Pharmacology

ORIGINAL RESEARCH
published: 24 July 2020
doi: 10.3389/fphar.2020.01134

H_2S Donors Reverse Age-Related Gastric Malfunction Impaired Due to Fructose-Induced Injury *via* CBS, CSE, and TST Expression

Yaroslav Pavlovskiy[1], *Antonina Yashchenko*[2] *and Oksana Zayachkivska*[1]*

[1] Physiology Department, Danylo Halytsky Lviv National Medical University, Lviv, Ukraine, [2] Histology, Cytology and Embryology Department, Danylo Halytsky Lviv National Medical University, Lviv, Ukraine

OPEN ACCESS

Edited by:
David Stec,
University of Mississippi Medical Center, United States

Reviewed by:
Patricia Gama,
University of São Paulo, Brazil
Soraia K. P. Costa,
University of São Paulo, Brazil

***Correspondence:**
Oksana Zayachkivska
ozayachkivska@gmail.com

Specialty section:
This article was submitted to Experimental Pharmacology and Drug Discovery, a section of the journal Frontiers in Pharmacology

Received: 01 May 2020
Accepted: 13 July 2020
Published: 24 July 2020

Citation:
Pavlovskiy Y, Yashchenko A and Zayachkivska O (2020) H_2S Donors Reverse Age-Related Gastric Malfunction Impaired Due to Fructose-Induced Injury via CBS, CSE, and TST Expression. Front. Pharmacol. 11:1134. doi: 10.3389/fphar.2020.01134

Objective: Excess of fructose consumption is related to life-treating conditions that affected more than a third of the global population. Therefore, to identify a newer therapeutic strategy for the impact prevention of high fructose injury in age-related malfunctions of the gastric mucosa (GM) in the animal model is important.

Methods: Adult and aged male rats were divided into control groups (standard diet, SD) and high fructose diet (HFD) groups; acute water immersion restraint stress (WIRS) was induced for evaluation of GM adaptive response and effects of testing the therapeutic potential of H_2S-releasing compounds (H_2S donors). Histological examination of gastric damage was done on hematoxylin-eosin stained slides. Cystathionine beta-synthase (CBS), Cystathionine gamma-lyase (CSE), and Thiosulfate-dithiol sulfurtransferase (TST) activities and oxidative index were assessed during exogenous administration of H_2S donors: sodium hydrosulfide (NaHS) and the novel hybrid H_2S-releasing aspirin (ATB-340). The results showed that HFD increased gastric damage in adult and aged rats. HFD-associated malfunction characterized by low activities of H_2S key enzymes, inducing increased oxidation. Pretreatment with NaHS, ATB-340 of aged rats in the models of HFD, and WIRS attenuated gastric damage in contrast to vehicle-treated group ($p < 0.05$). The effect of ATB-340 was characterized by reverse oxidative index and increased CBS, CSE, and TST activities. In conclusion, H_2S donors prevent GM age-related malfunctions by enhancement of CBS, CSE, and TST expression against fructose excess injury though reduction of oxidative damage.

Keywords: hydrogen sulfide, donor, gastric mucosa, aging, fructose, oxidative stress

INTRODUCTION

The World Health Organization defined relation between excess fructose consumption and accelerated aging, which could be a factor for multi-morbidity and has numerous harmful effects (Lyons et al., 2016; Bektas et al., 2018; Miller et al., 2018). Oxidative stress is one of their molecular mechanisms for cellular survival, as well as damage, and accelerated aging that could be the result of the decline of integrated defensive molecular mechanisms (Franceschi et al., 2018a; Franceschi et al., 2018b; Cherkas et al., 2020). Therefore, to search for a novel physiologically based therapeutic strategy that enhances the natural mechanisms of cytoprotection and reverses the influence of aging and high fructose injury is the actual topic in modern pharmacology JL (Wallace et al., 2015; Engevik, 2018). It is known that age-related changes in the gastrointestinal mucosal defense formed increased gastric mucosa (GM) susceptibility to injuries and enhanced low-grade inflammation related to excessive oxidative stress (distress) toxic injury that have systemic character (Schultz et al., 2018; Tarnawski and Ahluwalia, 2018).

Hydrogen sulfide (H_2S) system, the key endogenous signaling mediator that is operated by several enzymatic and non-enzymatic pathways, including catalytic activities of Cystathionine-β-synthase (CBS, EC 4.2.1.22), Cystathionine-γ-lyase (CSE, EC 4.4.1.1) and Thiosulfate-dithiol sulfurtransferase (belong to sulfurtransferase superfamily and rhodanese family, another name—thiosulfate reductase (glutathione-depend), TST, EC 2.8.1.5) is known for more than 15-years study. These key enzymes in H_2S signaling operated in the cytosol (CBS, CSE) and mitochondria (CBS and TST) showed remarkable cytoprotective advances of their multifunctional abilities, as gas neurotransmitters, the mediator of vascular response, platelet adhesion, regulation of glucose metabolism, redox balance, and detoxification of intramitochondrial oxygen free radicals (Wallace et al., 2012; Fu et al., 2012; Szabo et al., 2014; Kanagy et al., 2017; Zhang et al., 2017). Latest studies have concluded that H_2S is the remarkable activator of endothelial vasoactive agents, chemotaxis of immune cells and scavenger of active forms of oxygen species, neutralization of cytokines and autophagy, thus, there is a reason for creation of a pharmacological way to prevent accelerated aging and treat age-related disorders (Sharkey and Mawe, 2014; Pichette and Gagnon, 2016; Wang et al., 2017; Das et al., 2018). Since H_2S is involved in the regulation of intracellular redox status, as well as signaling cascades of phosphorylation, apoptosis, involving mitochondrial K^+ ATP-channels, it is possible to interpret such actions as a powerful antiradical resource (Nakajima, 2015; Mard et al., 2018). TST activity is important for mitochondrial oxidation and could be an effective marker of mitochondrial dysfunction in response to oxidative stress, but its role in the coupling of CBS, CSE expression in the H_2S pathway of age-related changes in gastric cytoprotection against fructose injury is still unknown.

Since the defense reactions of people in advanced age are related with cross-talk of oxidative stress and vascular health, regulated by hypoxia-inducible factor (HIF) that triggered synthesis and release of vascular endothelial growth factor/vascular permeability factor (VEGF/VPF), and as the result of age-related tissue malfunction, which is the first stage of injury, and if not prevented or treated early, the next cellular stage will often induce tissue damage (Donnarumma et al., 2011; Arumugam and Kennedy, 2018). Thus, there is a reason for study of H_2S donors—H_2S-releasing compounds, as agents that could decrease the impact of aging on the susceptibility of GM to high fructose injury in laboratory models by exploring changes in expression of CBS, CSE, and TST.

Present-day animal models of human diseases play an important role in the translational research that helps in identification and testing of compounds for age-related differences in cytoprotection (Verma et al., 2017; Wallace et al., 2018). Studies have shown that exogenous sodium hydrosulfide (NaHS) is the non-organic donor of synthesis of H_2S and enhancer for catalytic activities of CBS and CSE (Wallace et al., 2007; Di Villa Bianca et al., 2011). Recently, it has been found that the synthesis of H_2S from cysteine and cysteine with homocysteine affects glucose regulation and provides protection of vascular endothelium against oxidative stress and correction of hyperhomocysteinemia, which may be a predictor of accelerated aging and H_2S signaling network is the source for reversion of vascular aging (Das et al., 2018; De Cabo and Diaz-Ruiz, 2020). Interestingly, H_2S mediates the activity of arachidonic cycle and production of prostaglandins and recent advances in the creation of the latest hybrid H_2S-releasing drugs, analogs of nonsteroidal anti-inflammatory drugs (NSAIDs, H_2S-NSAIDs) or organic Lawesson's reagent derivative, have shown ability to reverse decrementing side effects that arise from the digestive system, cardiovascular system and systemic reactions (Wallace et al., 2007; Guo et al., 2012; Kang et al., 2017; Zhang et al., 2018; Van Dingenen et al., 2019). Among NSAIDs aspirin is the most widely used drug in the aged population for different reasons. Since 2013, Antibe Therapeutics Inc. is developing H_2S-releasing NSAIDs, in particular ATB-340, which is a novel H_2S-releasing derivate of aspirin (H_2S-aspirin, **Figure 1**) but its effect on age-related changes of gastric mucosal defense system against high fructose injury is unknown. Therefore, in this study, we compare effects of H_2S donors—NaHS, on the CBS, CSE, TST expressions in adult, and aged rats, as well as during treatment by ATB-340 in aged rats exposed to high fructose diet (HFD) during 4 weeks in both aspirin- and stress-related models of gastric injury.

Abbreviations: ASA, Acetylsalicylic acid; ATB-340, H_2S-aspirin; CBS, Cystathionine beta-synthase; COX, Cyclooxygenase; CSE, Cystathionine gamma-lyase; $FeCl_3$, Iron (III) chloride; GM, Gastric mucosa; GPx, Glutathione peroxidase; GSH, Glutathione; GSR, Glutathione-disulfide reductase; H_2S, Hydrogen sulfide; H_2S-NSAIDs, Hybrid H_2S-releasing drugs, analogs of nonsteroidal anti-inflammatory drugs; HCl, Hydrogen chloride; HFD, High fructose diet; K^+ ATP-channels, Adenosine triphosphate-sensitive potassium channels; MPTP, Mitochondrial permeability transition pore; MRPL18, Mitochondrial ribosomal proteins L18; NaHS, Sodium hydrosulfide; NFκB, Nuclear factor kappa-light-chain-enhancer of activated B cells; NO, Nitric oxide; NSAIDs, Nonsteroidal anti-inflammatory drugs; ROS, Reactive oxygen species; SD, Standard diet; SIRT1, Nicotinamide adenine dinucleotide-dependent deacetylase sirtuin-1; TLR4, Toll-like receptor 4; TST, Thiosulfate-dithiol sulfurtransferase; WIRS, Water immersion restraint stress.

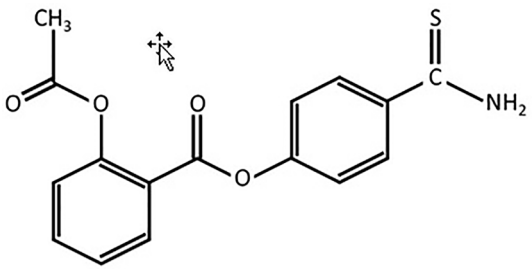

FIGURE 1 | Chemical structure of 4-(5-thioxo-5H-1,2-dithiol-3-yl)phenyl 2-acetoxybenzoate(l)—H_2S-releasing aspirin (ATB-340).

MATERIALS AND METHODS

Animals, Diets, and Treatments

All experiments were carried out on male adult (age = 12-14 weeks) and aged Wistar rats (age = 42-46 weeks) (n = 62) following the norms of animal experiments that guaranteed by ARRIVE guidelines and EU Directive 2010/63/EU for animal experiments and the local animal care committee at the Danylo Halytsky Lviv National Medical University Ethics Committee (protocol № 6 from 29.03.2017). All efforts were made to minimize animal suffering and to reduce the number of animals used.

Experimental Protocol

Animals were maintained under a constant 12-h light and dark cycle and an ambient temperature of 21-23° C with 50 ± 10% relative humidity. All animals were kept in raised mesh-bottom cages to prevent coprophagy and subdivided into groups (n = 5-6). **Figure 2** represents a schematic overview of the experimental protocol. Rats were randomly assigned to nine experimental groups. Rats in the control groups had free access to water and were kept on a standard diet (SD). Animals in the experimental groups received 28 days of fructose-supplemented water (HFD), unrestricted access to a 40% solution of fructose *ad libitum* (Bezpalko et al., 2015). Food deprivation for 12 h before the end of experiments has been performed for all rats. The initial and final body weights in all animals were recorded by an RN 10C13U, 100 g-10 kg, ± 5 g (Vaga, Kyiv, Ukraine).

The rats were deeply anesthetized with an intramuscular injection of ketamine (60 mg/kg; Biovet, Bila Tserkva, Ukraine), sacrificed and after that, the stomachs were resected. Later stomachs were cut open along the lesser curvature and rinsed with saline and were taken for histological examination.

The animals were subdivided into control groups of adult rats and aged rats with SD and vehicle (1.0 ml of saline), and experimental groups receiving 28 days hypercaloric HFD, without and with acute stress. Acute stress was induced on the 29th day of study by the model of Takagi and Okabe, 1968, that involves short-term exposure to water-immersion restraint stress (WIRS) (Takagi and Okabe, 1968). The rats were placed in restraint cages and immersed vertically to the level of the xiphoid process in a water bath of 23° C for 3.5 h. The initial and final body weights were recorded. Blood glucose concentrations were measured daily by glucometer using a blood sample from the tail vein, as described previously (Zayachkivska et al., 2014).

Fasted rats from experimental groups were pre-treated 9-days (from 20th to 28th day of study) intragastrically by: 1) saline, as vehicle (adult); 2) vehicle (aged); 3) NaHS, 5.6 mg/kg/day (adult); 4) NaHS, 5.6 mg/kg/day (aged); 5) vehicle with stress induction (adult); 6) vehicle with stress induction (aged); 7) NaHS, 5.6 mg/kg/day and induction of stress; 8) ASA, 10.0 mg/kg/day and NaHS, 5.6 mg/kg/day and stress induction (aged); 9) ATB-340 17.5 mg/kg/day and induction of stress (aged). The administration of NaHS and ATB-340 was performed in doses tested previously (Zayachkivska et al., 2014; Wallace et al., 2015).

Chemicals and Drugs

Sodium hydrosulfide (NaHS), D, L-homocysteine 3.3 mM, L-cysteine, $Na_2S{\bullet}9H_2O$ were obtained from Sigma-Aldrich (St. Louis, MO, USA). Pyridoxal phosphate 0.67 mM, N,N-Dimethyl-p-phenylenediamine sulfate, 99% was obtained from Acros Organic (New Jersey, USA).

Compound ATB-340 was obtained from Antibe Therapeutics (Toronto, Canada). ASA was purchased from Borshchahivskiy CPP (Kyiv, Ukraine).

All other chemicals used in the experiments were graded by the analytical method that was validated according to the guidelines of the International Conference on Harmonization (ICH).

Morphological Evaluation of Gastric Damage

The stomachs were opened along the lesser curvature. The severity of GM lesions was evaluated by macroscopic inspection and GM damage index using histological double-blind studies of

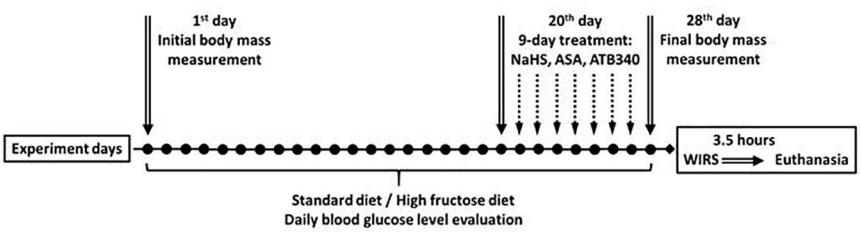

FIGURE 2 | Design of the experiment.

two investigators. Gastric tissues were then fixed in 10% formalin, dehydrated, and embedded in paraffin wax. Paraffin sections of 5 mm were cut and stained with hematoxylin and eosin. Histological changes were checked under a microscope (Leica DM 750/4 and digital camera Leica DFC 420, Germany). The GM lesion, including epithelial cell damage, vasocongestion, hemorrhage, and inflammation, was measured by microscopy investigation, and the total injury in one stomach was assessed by GM damage index scoring that conducted using the criteria in **Table 1** expending four fields of view at 40 × magnification. The mean score was determined for each treatment group and results were expressed as GM damage index.

Biochemical Analysis

Blood glucose concentrations were measured daily by glucometer (Achtung TD-4207, Munich, Germany) using a blood sample from the tail vein.

At the end of the study (on 29th day), after euthanasia animals were sacrificed, the samples from rat gastric mucosa tissue were evaluated for the catalytic activities of CBS, CSE, and TST in H_2S biosynthesis and oxidative stress markers. The stomach was washed with cold 1.15% potassium chloride solution, after which the mucous membrane was separated and homogenized in a medium of 1.15% potassium chloride in a ratio of 1:4. GM homogenates were centrifuged at 600 g and 40° C for 30 min to obtain a post-nuclear fraction.

CBS, CSE, and TST Activities

We evaluated CBS, CSE, and TST activities in gastric tissue (nmol/min*1 mg of protein), using a modified version of the Stipanuk and Beck method (Stipanuk and Beck, 1982). Substrate and cofactor concentrations, pH, and incubation time, which could provide optimal conditions for enzyme activity determination, were selected in advance.

The activity of CBS was determined in the incubation medium containing in final concentrations pyridoxal phosphate 0.67 mM, L-cysteine 3.3 mM, L-homocysteine 3,3 мМ, Tris-HCl buffer 0.08 M (pH 8.5).

The activity of CSE activity was determined in incubation medium containing in final concentrations pyridoxal phosphate 0.67 mM, L-cysteine 3.3 mM, Tris-HCl buffer 0.08 M (pH 8.5).

The activity of the TST was determined in incubation medium containing in the final concentrations: sodium thiosulfate 0.2 mM, 1,4-Dithiothreitol 2.3 mM, Tris-HCl buffer 0.09 M (pH 8.5).

0,1 ml post-nuclear homogenates of the stomach (1:4 w/v in 1,15% Potassium chloride solution) were added to 0.5 ml incubation medium. After 60 min incubation at 37° C in sterile hermetically sealed plastic Eppendorf tubes (to prevent H_2S losses), the reaction was quenched with cooling the tubes on ice and adding of a 0.5 ml 1% zinc acetate solution to bind the produced H_2S.

The control samples were treated similarly, except the studied material was added to the medium after incubation and cooling. The amount of H_2S was estimated with the methylene blue production by a standard method (Van Dingenen et al., 2019). There were added 0.5 ml 20 mM N,N-dimethyl-p-phenylenediamine in 7.2 M HCl, 0.4 ml 30 mM FeCl3 in 1.2 M HCl to the samples and incubated for 20 min at 18-22° C, then added 1 ml 20% TCA and centrifuged for 10 min at 3000 rpm.

The optical density of the supernatant was measured at 670 nm in a cuvette with an optical path of 1.0 cm using the Apel PD-303 spectrophotometer (Japan). Sulfide anion content in the sample was calculated using a calibrated graph (Zaichko et al., 2009).

TABLE 1 | Criteria used for semi-quantitative analysis of gastric mucosa damage.

Criteria	Score
The state of the epithelial layer on the degree of alteration	1—no changes; 2—desquamation of epithelium; 3—destruction of gastric foveoli; 4—hypertrophy and vacuolization of mucosa cells; 5—erosion
The state of subepithelial layer	1—no changes; 2—diffuse swelling of the submucosal basis; 3—pronounced uneven swelling of the submucosal base and insignificant infiltration; 4—severe swelling and disorganization of the submucosal basis; 5—perivascular hemorrhages
The epithelial layer leukocyte infiltration	1—no leukocyte infiltration; 2—moderate leukocyte infiltration; 3—average leukocyte infiltration; 4—severe leukocyte infiltration; 5—multiple leukocyte infiltrates

The measurement of GM damage was determined by protocol-blinded researchers. The number of animals showing these histopathological lesions in each group was compared with that of other groups.

Calculation of the Oxidative Index

For oxidative injury assessment, the oxidative index, as the value of imbalance between pro- and anti-oxidative activity, was calculated using the principle developed by Vassale et al.; Shimomura et al. (Vassalle et al., 2012; Shimomura et al., 2017), as a ratio between the content of lipid peroxidation products and anti-oxidative activity. For biomarker of lipid peroxidation products, the malonic dialdehyde level was detected as demonstrated previously (Pavlovskiy et al., 2018) and for the anti-oxidative activity—the TST colorimetric activity, as reported earlier.

Statistical Analysis

All results were evaluated using Statistical Analysis System and visualization program «Statistica 7.0» (StatSoft, Informer Technologies, Inc.) and expressed as mean ± standard deviation (SD) for a series of experiments. A paired Mann–Whitney U-test was used for comparisons of paired treatments between two groups, and one-way ANOVA using Dunnett's test was performed to compare different experimental groups with control. Statistical significance was set to p values ≤ 0.05.

RESULTS

Effect of 28 Days High Fructose Diet-Induced Injury on Body Weight and Glucose Levels, and Histologic Changes of Gastric Mucosa

Rats consuming drinking water supplemented with fructose for 28 days exhibited a significant elevation of blood glucose levels (from 5.5 ± 0.4 mmol/L to 6.2 ± 0.7 mmol/L—adult rats; from 5.5 ± 0.3 mmol/L to 6.6 mmol/L—aged rats; $p < 0.05$) (**Figure 3A**), and about 10% gain in body weight (339 ± 31 g—adult rats; 499 ± 34 g—aged rats) over that of the control rats with SD (306 ± 21 g—adult rats; 458 ± 28 g—aged rats).

The adult and aged rats fed by SD and treated with vehicle exhibited normal gastric macroscopic appearance. The data in **Figure 3B** shows that the GM damage index of adult control rats on SD was 1.00; in aged rats on both SD and HFD, the GM damage index was 3 times higher, respectively, vs. adult rats ($p < 0.05$). Representative photomicrographs of gastric mucosa in adult and aged rats fed by 28-days of high fructose diet, visualizing surface epithelial cells, foveoli (pits), and glandular cells demonstrated **Figures 3C–L**. The differences of gastric mucosa of aged rats with the glandular cells and hypertrophy of mucous neck cells were observed (**Figures 3E, H**) in comparison to the adult rats (**Figures 3C, D**). Examination of the gastric mucosa of adult rats on HFD revealed an increased

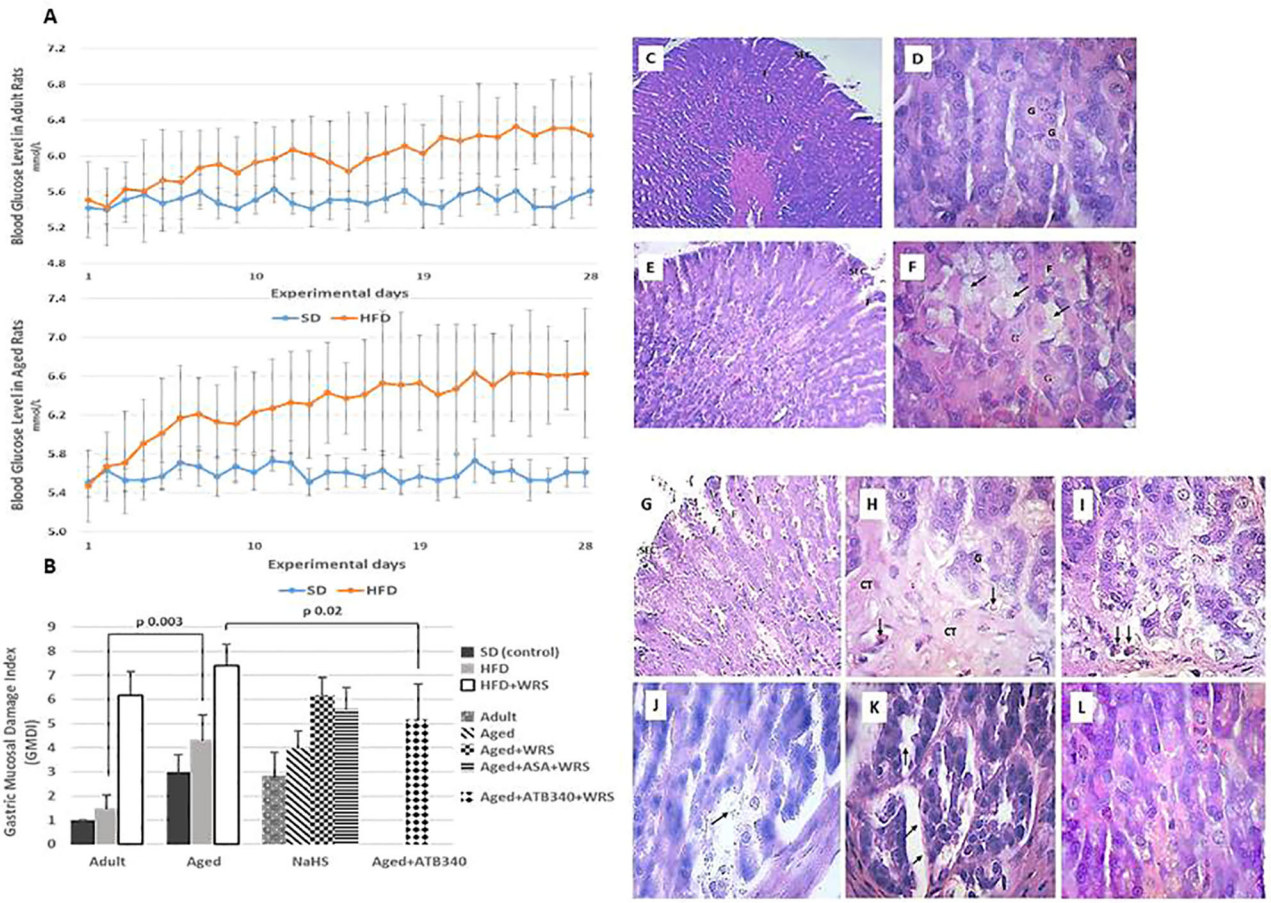

FIGURE 3 | Blood glucose levels in adult (**A**, left graph) and aged (**A**, right graph) rats fed a standard diet (SD) or high fructose diet (HFD) during 28 days. Results are given as mean ± standard deviation (SD) (statistical analysis: one way-ANOVA, n = 5–6/group). Histological characteristic of study groups according to the changes in gastric mucosal damage index **(B)** and representative photomicrographs to illustrate the changes in the gastric mucosa in adult **(C, D)** and aged **(E–L)** rats fed by 28 days of high fructose diet, visualizing surface epithelial cells (SEC), foveoli **(F)**, and glandular cells **(G)**. Hematoxylin and eosin staining at low (C – x 150; E and G – x 200) and higher magnification (**D**, **F**, and **H–L** – x 600). Gastric mucosa of adult and aged rats shows glandular cells (**D**, **F**, respectively), and hypertrophy of mucous neck cells (arrows) **(F)**. In the gastric mucosa of vehicle-treated aged rats exposed to acute stress **(G, H)** and aspirin pretreatment **(I),** there is observed connective tissue (arrows) in basal third of the gastric mucosa, hyperemia in lamina propria (arrows). The gastric mucosa of aged rats exposed to acute stress and pretreated by NaHS **(J)**, a combination of NaHS and aspirin **(K)** shows uneven swelling of the submucosal base in gastric mucosa (arrows) while pretreatment of ATB-340 **(L)** shows diffuse swelling of the submucosal basis of gastric mucosa.

GM damage index in 1.5 times vs. the control group of adult rats ($p > 0.05$).

To assess the adaptive changes of GM defense in aged rats fed by HFD and treated by H_2S donors exposition to WIRS was used. In this experiment, the histological changes of GM in aged rats treated with vehicle without and with exposition to stress were characterized by increased GM damage index in about 4 and 7, respectively, over the adult rats group on HFD treated with vehicle was 1,5 ($p < 0.05$), (**Figure 3B**). In the gastric mucosa of aged rats fed by HFD, vehicle-treated and exposed to acute stress (**Figures 3G, H**), we observed connective tissue in the basal third of the gastric mucosa, hyperemia in lamina propria (arrows) and hypertrophy and vacuolization of glandular cells (arrows). Similar changes of gastric mucosa were observed in the rats with aspirin pretreatment (**Figure 3I).**

In the gastric mucosa of aged rats exposed to acute stress and pretreated by NaHS (**Figure 3J**) and with combination of NaHS and aspirin (**Figure 3K**) we identified uneven swelling of the submucosal base in gastric mucosa (arrows) while pretreatment of ATB-340 (**Figure 3L**) shows diffuse swelling of the submucosal basis of gastric mucosa.

Treatment of ATB-340 attenuated gastric injury and resulted in 1.4 times lower GM damage index compared to rats treated with vehicle ($p < 0.05$). There was also observed decreased susceptibility of GM by lower GM damage index in the ATB-340 treatment group than in the group with co-treatment by the combination of NaHS and ASA group, as well as vehicle group regarding to the difference of GM damage index ($p > 0.05$).

CBS, CSE, TST Activities, and Oxidative Index

To evaluate the role of CBS, CSE, and TST activity in H_2S signaling during HFD-induced GM malfunction in rats, in this study, we examined changes in their activities (**Figures 4A–C**), and oxidative index (**Figure 4D**). In intact adult control rats on SD, the activities of CBS, CSE, TST were reaching 1.01 ± 0.25 nmol/min*1 mg of protein, 1.26 ± 0.08 nmol/min*1 mg of protein and 1.16 ± 0.16 nmol/min*1 mg of protein, respectively. In groups on SD, there were decreased enzyme activities in aged rats compared to adult rats (**Figures 4A–C**). Besides, there was a significant difference in enzyme activities between adult and aged rats on HFD versus SD. Adult rats on HFD had much lower activity of CBS—35%, CSE—48%, and TST—56%, compared to SD group ($p < 0.05$). Aged rats on HDF have lower activities of CBS, CSE, and TST versus aged rats on SD; however, we observed increased activities of all H_2S-related enzymes during induction WIRS (**Figures 4A–C**). We found, that in adult rats exposed to stress on HFD and treatment by NaHS resulted in increased activities of CBS—1.8 times, CSE—1.3 times, and TST by 69% over adult rats with vehicle ($p < 0.05$). Adult rats on HFD with NaHS administration exhibited a higher activity of CBS by 35% than aged rats ($p < 0.05$). However, the

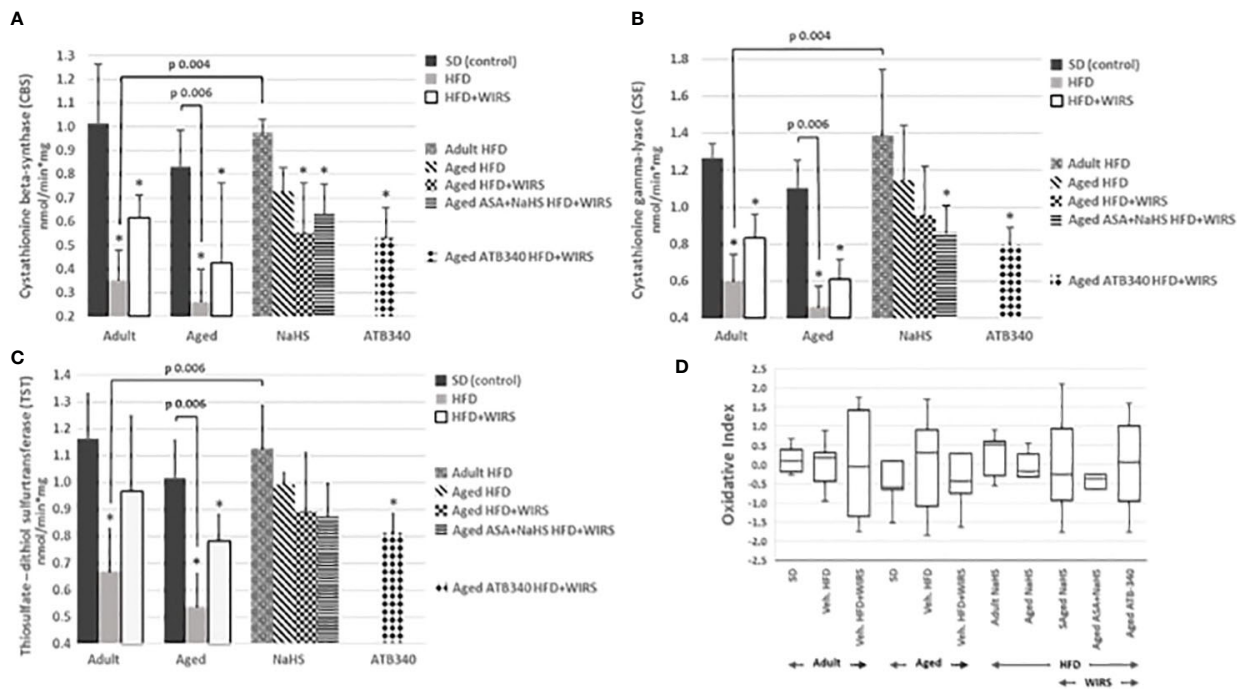

FIGURE 4 | Activities of Cystathionine-β-synthase (CBS) **(A)**, Cystathionine-γ-lyase (CSE) **(B)** and Thiosulfate-dithiol sulfurtransferase (TST) **(C)** and changes of the oxidative index **(D)** in adult and aged rats (n = 5–6) fed with standard diet (SD) or high fructose diet (HFD) without and with H_2S releasing molecule compounds therapy (NaHS, ATB-340) and induction of acute stress (WIRS). Columns with whiskers **(A, B, C)** show mean ± standard deviation (SD). Box plots **(D)** show the median, lower, and upper quartile ranges, and the minimum and maximum values of the oxidative index of all groups; *$p < 0.05$ versus control.

co-treatment of aged rats by NaHS and ASA was alike H_2S–ASA, causing a similar activity of CBS ($p < 0.05$).

Given these results, we determined the oxidative index. We analyzed data of the age-related changes of the oxidative index in **Figure 4D**. It has shown that the oxidative index is increased in aged over adult rats fed by SD or HFD. However, the rats fed by HFD have higher levels of the oxidative index than animals fed by SD. The pretreatment by H_2S donors (NaHS and ATB-340) in aged rats reduced the oxidative index levels and correlate with TST activity, suggesting that treatment demonstrates an anti-oxidant effect.

DISCUSSION

According to the recent data, among the most important risk factors for the increased susceptibility of GM are hyperglycemia and aging which could be triggers for inflammaging and metaflammation—immune-metabolic age-related conditions that contribute to manifestation of cytotoxic injury (Qi et al., 2012; De Cabo and Diaz-Ruiz, 2020). Several animal and human studies suggest that postprandial hyperglycemia related to excessive fructose consumption causes cellular and subcellular oxidative damage, and accelerates the age-related decline in cytoprotection by developing oxidative damage related to a modification in H_2S-NO cross-talk and redox homeostasis (Guan et al., 2012; Cao and Bian, 2018). The process of age-associated increased susceptibility to gastric cytotoxic factors involves several vascular associated molecular signaling pathways, which has a bi-directional detrimental role on the gastric mucosal defense (Yonezawa et al., 2007; Velázquez-Moyado et al., 2018). It has been shown that the key role in gastroprotection at the advanced age belongs to the endothelial dysfunction, reduced mucosal defense, amplified susceptibility to injury by a variety of injurious agents and its dramatic consequences on older patients with hyperglycemia could be expected. ASA is one of the most common drugs among NSAIDs that are commonly reported as gastrotoxic agents, bringing hemorrhagic erosions and bleeding which is seriously threatening human health, especially in older persons. An increasing body of evidence confirms that using new H_2S-releasing compounds, which increase endogenous H_2S content by catalytic activities in H_2S signaling, exert gastrointestinal safety by anti-oxidative, anti-inflammatory, and vasoactive effects (Dombkowski and Russell, 2004; Zhang et al., 2018; Qin et al., 2019; Pereira-Leite et al., 2020). H_2S is important for redox regulation of multiple processes, including regulation of mitochondrial function through its effects as an electrons donor for the electron transport chain and inhibition of mitochondrial permeability transition pore (MPTP) opening, mitochondrial oxidation, and reaction producing thiosulfate (Donnarumma et al., 2011; Zhang et al., 2017; Mys et al., 2018), as well as the proper functioning of the immune system (Wallace et al., 2012; Qin et al., 2019). Therefore, our study was designed to test the hypothesis that linking H_2S-related physiological mechanisms in gastroprotection and H_2S-based therapeutic strategy for reduction of malfunction in gastric mucosal defense in advanced age and chronic nutritional carbohydrate overload. In this study we have used the experimental model of HFD, which mimics the modern "obesogenic" environment on rats and compare age-related effects on the gastric mucosa of 9-day exogenous administration of H_2S donors: the inorganic sulfide salt—NaHS, the commonly used compound as a positive control in animal preclinical studies, which rapidly increases content of plasma H_2S level, co-treatment of NaHS with conventional ASA and novel $NSAID_S$ hybrid ASA-releasing H_2S. To test adaptive changes of gastric mucosa in feature of age-related changes in gastroprotection, we used aged rats fed with HFD and exposed to WIRS. This animal model mimics early signs of the preclinical appearance of gastric ulcerogenesis observed in older patients who use the nutritional overload by unhealthy carbohydrates. Also, we determined the effects of H_2S donors, such as NaHS and ATB-340 on CSE and CBS expression, which play a crucial role in H_2S biogenesis, as well as TST expression which appears exclusively mitochondrial and has co-operative activity with mitochondrial ribosomal proteins L18 (MRPL18) and acts as a mitochondrial important factor for anti-oxidative stress functions and redox regulation, producing thiosulfate and recovering glutathione for defense cellular thiol proteins under oxidative stress (Szabo et al., 2014; Kimura, 2019). We defined that 4 weeks fructose nutritional overload decrease gastric mucosal defense in aged rats in contrast to adult animals and similar up-toward trend for age-associated results was in rats fed with SD and accompanied by increased GM damage index and modulated activities of CBS, CSE, and TST and changes of the oxidative index, reflecting the shift to oxidative damage. In addition, we identified decreased gastric CBS and CSE activities in HFD aged rats over adult rats. During exposure to stress, the activity of H_2S-related enzymes CBS, CSE, and TST increased in contract to animals without stress, as the result of response to acute injury, nonetheless level of the oxidative index also increased in aged rats fed by HFD. These signs of oxidative damage not only negatively affect membranes, but also could initiate the mitochondrial process of apoptosis, which results in cellular damage due to MPTP opening and re-store NO-synthase coupling (Nakajima, 2015; Mys et al., 2018; Kimura, 2019). These results indicate that the H_2S pathway is likely to be an important determinant of gastric mucosa susceptibility to HFD injury in advanced age. Our data of CBS, CSE, and TST activities correlate with histological results that exogenous administration of H_2S donors reverses GM damage that results on H_2S-NO cross-talk (Zhang et al., 2017; Cao and Bian, 2018), sirtuin-1 (SIRT1) activity that has the ability for increasing mitochondrial function, protects against oxidative stress and can promote angiogenesis, as well as H_2S-dependent protein persulfidation (Arumugam and Kennedy, 2018). We analyzed the data during treatment by H_2S donors that characterized by decreased oxidative index and could conclude that in our model of HFD injury the increased CSE, CBS, and TST activities during exposure to stress could be explained by additional involvement of bioavailability of H_2S despite oxidative index changes which exist probably due to the effects of aging and HFD. This is a significant finding because these types of effects could be mechanisms contributing to age-related changes in gastroprotection. This effect was mediated by activation of endogenous H_2S-associated compounds, which have free-radical scavenging activity. Our data could be explained by previous results of several scientific groups that show the role of sulfhydryl

compounds in gastric cytoprotection (Szabo et al., 1981; Wallace et al., 2007). When we compare age-related effect of NaHS on gastroprotection we detected twice lower level of the oxidative index in adult animals over the level of aged rats. Moreover, the NaHS-mediated treatment decreased CBS and CSE activities twice, as well as TST activity by 30% in aged rats over the results of adult rats. A similar trend was obtained during co-administration of NaHS with ASA and resulted in attenuating gastric damage induced by HFD and aging-associated changes in redox balance. Interestingly, the administration of ATB-340 was accompanied by a more intensive decrease of CSE, CBS, and TST activities than during co-treatment with NaHS and convention aspirin. This observation remains in agreement with recent data from several studies during chronic inflammatory conditions when conventional and H_2S-releasing compounds reduced oxidative stress in different tissues decreasing the process of lipid peroxidation, myeloperoxidase activity in a different way, however, only H_2S-$NSAID_S$ showed increased glutathione levels in the tissue and reduced plasma extravasation and gastrointestinal damage and could be promised compounds to decrease susceptibility to oxidative stress (Kang et al., 2017; Ajayi et al., 2018). Thus, data of TST expression, in aged rats with pretreatment by H_2S donors during HFD with WIRS, and GM damage index could be explained by their ability for intracellular antioxidant activity possessing which ameliorates mitochondrial dysfunction that, in turn, improves respiratory electron transport. It helps to explain our obtained results of the gastroprotective effect of ATB-340, as protection against oxidative stress injury of the gastric mucosa resulted in the decreased oxidative index during exposure of aged rats to WIRS.

In conclusion, the H_2S pathway is essential reason of gastric mucosa susceptibility to HFD injury in advanced age and administration of exogenous H_2S donors has demonstrated the efficiency against the reduction of age-associated gastric mucosal defense. Decreased activation of H_2S signaling in the HFD model might be related to the increased mitochondrial malfunctions and oxidative stress that promote excessive TST expression. Gastroprotection during ATB-340 (H_2S-ASA) treatment may be relevant to the increased activity in H_2S signaling by attenuation of oxidative stress.

Translational Perspective

Pharmacological intervention to increase endogenous H_2S levels extends anti-oxidative activity suggesting that H_2S donors could be promising ingredients for the new strategy to treat age-related and HFD-induced malfunctions. Further studies are needed to study the pharmacologically dose-dependent activities of H_2S donors NaHS, and H_2S-ASA and exact molecular mechanisms to explore their anti-oxidative activity. H_2S-ASA has the potential for the target-oriented treatment of gastric malfunction related to HFD and age-associated changes.

DATA AVAILABILITY STATEMENT

The raw data supporting the conclusions of this article will be made available by the authors, without undue reservation.

ETHICS STATEMENT

The animal study was reviewed and approved by animal care committee at the Danylo Halytsky Lviv National Medical University Ethics Committee (protocol № 6 from 29.03.2017).

AUTHOR CONTRIBUTIONS

OZ designed the study. YP performed experiments and data analysis. Gastric histological evaluation was done by YP and AY. YP, AY, and OZ interpreted the findings and prepared and completed the manuscript. All authors contributed to the article and approved the submitted version.

FUNDING

This work has been supported in part by Danylo Halytsky Lviv National Medical University under the project "Role of systemic and local mechanisms in cytoprotection under the extreme influence" (the state registration ID 0116U004510).

ACKNOWLEDGMENTS

Authors would like to thank John Wallace (University of Calgary, Calgary, Canada) for providing ATB-340, Zaichko N. (National Pirogov Memorial Medical University, Vinnytsia, Ukraine) for her expert suggestions, Lutsyk M. (Lviv National Medical University, Lviv, Ukraine) for histological studies.

REFERENCES

Ajayi, O. V., Oluwole, F. S., and Dare, A. (2018). Anti-ulcerogenic, antioxidant and mucogenic effects of L-cysteine in gastric tissue of Wistar rats. *J. Appl. Life Sci. Int.* 14, 1–10. doi: 10.9734/JALSI/2018/45289

Arumugam, T. V., and Kennedy, B. K. (2018). H_2S to Mitigate Vascular Aging: a SIRT1 connection. *Cell* 173 (1), 8–10. doi: 10.1016/j.cell.2018.03.011

Bektas, A., Schurman, S. H., Sen, R., and Ferrucci, L. (2018). Aging, inflammation and the environment. *Exp. Gerontol.* 105, 10–18. doi: 10.1016/j.exger.2017.12.015

Bezpalko, L., Gavrilyuk, O., and Zayachkivska, O. (2015). Inflammatory response in visceral fat tissue and liver is prenatally programmed: experimental research. *J. Physiol. Pharmacol.* 66 (1), 57–64.

Cao, X., and Bian, J. S. (2018). The Signaling Interaction Systems of in NO Biology and H_2S and Medicine. *Gasotransmitters* 12, 145. doi: 10.1039/9781788013000-00145

Cherkas, A., Holota, S., Mdzinarashvili, T., Gabbianelli, R., and Zarkovic, N. (2020). Glucose as a Major Antioxidant: When, What for and Why It Fails? *Antioxidants* 9 (2), 140. doi: 10.3390/antiox9020140

Das, A., Huang, G. X., Bonkowski, M. S., Longchamp, A., Li, C., Schultz, M. B., et al. (2018). Impairment of an endothelial NAD+- H_2S signaling network is a

reversible cause of vascular aging. *Cell* 173 (1), 74–89. doi: 10.1016/j.cell.2018.02.008

De Cabo, R., and Diaz-Ruiz, A. (2020). A central role for the gasotransmitter H_2S in aging. *Cell Metab.* 31 (1), 10–12. doi: 10.1016/j.cmet.2019.11.015

Di Villa Bianca, R. D., Sorrentino, R., Coletta, C., Mitidieri, E., Rossi, A., Vellecco, V., et al. (2011). Hydrogen sulfide-induced dual vascular effect involves arachidonic acid cascade in rat mesenteric arterial bed. *J. Pharmacol. Exp. Ther.* 337 (1), 59–64. doi: 10.1089/ars.2017.7079

Dombkowski, R., and Russell, M. (2004). Hydrogen sulfide as an endogenous regulator of vascular smooth muscle tone in trout. *Am. J. Physiol. Regul. Integr. Comp. Physiol.* 286, 678–685. doi: 10.1152/ajpregu.00419.2003

Donnarumma, E., Trivedi, R. K., and Lefer, D. J. (2011). Protective actions of H_2S in acute myocardial infarction and heart failure. *Compr. Physiol.* 7 (2), 583–602. doi: 10.1002/cphy.c160023

Engevik, A. C. (2018). The Age of Angiogenesis: A Novel Role of NGF in Gastric Repair. *Cell. Mol. Gastroenterol. Hepatol.* 6 (2), 227. doi: 10.1016/j.jcmgh.2018.06.001

Franceschi, C., Capri, M., Garagnani, P., Ostan, R., Santoro, A., Monti, D., et al. (2018a). *Inflammaging. Handbook of immunosenescence: Basic understanding and clinical implications*. (Cham: Springer), 1–31. doi: 10.1007/978-3-319-64597-1_45-1

Franceschi, C., Garagnani, P., Parini, P., Giuliani, C., and Santoro, A. (2018b). Inflammaging: a new immune–metabolic viewpoint for age-related diseases. *Nat. Rev. Endocrinol.* 14 (10), 576–590. doi: 10.1038/s41574-018-0059-4

Fu, M., Zhang, W., Wu, L., Yang, G., Li, H., and Wang, R. (2012). Hydrogen sulfide (H_2S) metabolism in mitochondria and its regulatory role in energy production. *Proc. Natl. Acad. Sci.* 109 (8), 2943–2948. doi: 10.1073/pnas.1115634109

Guan, Q., Zhang, Y., Yu, C., Liu, Y., Gao, L., and Zhao, J. (2012). Hydrogen sulfide protects against high-glucose–induced apoptosis in endothelial cells. *J. Cardiovasc. Pharmacol.* 59 (2), 188–193. doi: 10.1097/FJC.0b013e31823b4915

Guo, S., Gao, Q., Jiao, Q., Hao, W., Gao, X., and Cao, J. M. (2012). Gastric mucosal damage in water immersion stress: mechanism and prevention with GHRP-6. *World J. Gastroenterol.: WJG* 18 (24), 3145. doi: 10.3748/wjg.v18.i24.3145

Kanagy, N. L., Szabo, C., and Papapetropoulos, A. (2017). Vascular biology of hydrogen sulfide. *Am. J. Physiol. Cell Physiol.* 312 (5), 537–549. doi: 10.1152/ajpcell.00329.2016

Kang, J., Neill, D. L., and Xian, M. (2017). Phosphonothioate-based hydrogen sulfide releasing reagents: chemistry and biological applications. *Front. Pharmacol.* 8, 457. doi: 10.3389/fphar.2017.00457

Kimura, H. (2019). Signaling by hydrogen sulfide (H_2S) and polysulfides (H_2S_n) in the central nervous system. *Neurochem. Int.* 126, 118–125. doi: 10.1016/j.neuint.2019.01.027

Lyons, C., Kennedy, E., and Roche, H. (2016). Metabolic inflammation-differential modulation by dietary constituents. *Nutrients* 8 (5), 247. doi: 10.3390/nu8050247

Mard, S. A., Dehkohneh, K. A., and Ahangarpour, A. (2018). Decreased mRNA expression of cystathionine gamma lyase and H_2S concentration in gastric mucosal tissue in diabetic rats. *Braz. Arch. Biol. Technol.* 61, e18160308. doi: 10.1590/1678-4324-2018160308

Miller, C. O., Yang, X., Lu, K., Cao, J., Herath, K., Rosahl, T. W., et al. (2018). Ketohexokinase knockout mice, a model for essential fructosuria, exhibit altered fructose metabolism and are protected from diet-induced metabolic defects. *Am. J. Physiol. Endocrinol. Metab.* 315 (3), 386–393. doi: 10.1152/ajpendo.00027.2018

Mys, L. A., Strutynska, N. A., Strutynskyi, V. R., and Sagach, V. F. (2018). Activation of Endogenous Hydrogen Sulfide synthesis inhibits mitochondrial permeability transition pore opening and restores constitutive NO-synthase coupling in old rat heart. *Int. J. Physiol. Pathophysiol.* 9 (1), 59–67. doi: 10.1615/IntJPhysPathophys.v9.i1.70

Nakajima, T. (2015). Roles of sulfur metabolism and rhodanese in detoxification and anti-oxidative stress functions in the liver: Responses to radiation exposure. *Med. Sci. Monitor: Int. Med. J. Exp. Clin. Res.* 21, 1721–1725. doi: 10.12659/MSM.893234

Pavlovskiy, Y., Lutsyk, M., Yashchenko, A., Zaichko, N., Wallace, J., and Zayachkivska, O. (2018). ATB 340, a modulator of Sulfite Oxidase activity, reduces oxidative stress in hyperglycemia and stress exposed gastric mucosa in old rats. Proceeding of the Shevchenko Scientific Society. *Med. Sci.* 54 (2), 33–41. doi: 10.25040/ntsh2018.02.033

Pereira-Leite, C., Jamal, S. K., Almeida, J. P., Coutinho, A., Prieto, M., Cuccovia, I. M., et al. (2020). Neutral diclofenac causes remarkable changes in phosphatidylcholine bilayers: relevance for gastric toxicity mechanisms. *Mol. Pharmacol.* 97 (4), 295–303. doi: 10.1124/mol.119.118299

Pichette, J., and Gagnon, J. (2016). Implications of hydrogen sulfide in glucose regulation: how H_2S can alter glucose homeostasis through metabolic hormones. *Oxid. Med. Cell. Longev.* 2016, 3285074. doi: 10.1155/2016/3285074

Qi, H. N., Cui, J., Liu, L., Lu, F. F., Song, C. J., Shi, Y., et al. (2012). Exogenous hydrogen sulfide delays the senescence of human umbilical vein endothelial cells by lessening oxidative stress. *Acta Physiol. Sinica* 64 (4), 425–432.

Qin, M., Long, F., Wu, W., Yang, D., Huang, M., Xiao, C., et al. (2019). Hydrogen sulfide protects against DSS-induced colitis by inhibiting NLRP3 inflammasome. *Free Radical Biol. Med.* 137, 99–109. doi: 10.1016/j.freeradbiomed.2019.04.025

Schultz, M. B., Bochaton, T., Bonkowski, M., Li, J., Lokitiyakul, D., Colville, A., et al. (2018). NAD+ Depletion as a cause of inflammaging. *Innovation Aging* 2 (1), 746. doi: 10.1093/geroni/igy023.2751

Sharkey, K. A., and Mawe, G. M. (2014). Neurohormonal signalling in the gastrointestinal tract: new frontiers. *J. Physiol.* 592 (14), 2923–2925. doi: 10.1113/jphysiol.2014.275487

Shimomura, Y., Takaki, A., Wada, N., Yasunaka, T., Ikeda, F., Maruyama, T., et al. (2017). The serum oxidative/anti-oxidative stress balance becomes dysregulated in patients with non-alcoholic steatohepatitis associated with hepatocellular carcinoma. *Internal Med.* 56 (3), 243–251. doi: 10.2169/internalmedicine.56.7002

Stipanuk, M. H., and Beck, P. W. (1982). Characterization of the enzymic capacity for cysteine desulphhydration in liver and kidney of the rat. *Biochem. J.* 206 (2), 267–277. doi: 10.1042/bj2060267

Szabo, S., Trier, J. S., and Frankel, P. W. (1981). Sulfhydryl compounds may mediate gastric cytoprotection. *Science* 214 (4517), 200–202. doi: 10.1126/science.7280691

Szabo, C., Ransy, C., Mydis, K., Andriamihaja, M., Murghes, B., Coletta, C., et al. (2014). Regulation of mitochondrial bioenergetic function by hydrogen sulfide. Part I. Biochemical and physiological mechanisms. *Br. J. Pharmacol.* 171 (8), 2099–2122. doi: 10.1111/bph.12369

Takagi, K., and Okabe, S. (1968). The effects of drugs on the production and recovery processes of the stress ulcer. *Japan J. Pharmacol.* 18 (1), 9–18. doi: 10.1254/jjp.18.9

Tarnawski, A., and Ahluwalia, A. (2018). Increased susceptibility of aging gastric mucosa to injury and delayed healing: clinical implications. *World J. Gastroenterol.* 24 (42), 4721. doi: 10.3748/wjg.v24.i42.4721

Van Dingenen, J., Pieters, L., Vral, A., and Lefebvre, R. A. (2019). The H_2S-releasing naproxen derivative ATB-346 and the slow-release H_2S donor GYY4137 reduce intestinal inflammation and restore transit in postoperative ileus. *Front. Pharmacol.* 10, 116. doi: 10.3389/fphar.2019.00116

Vassalle, C., Sciarrino, R., Bianchi, S., Battaglia, D., Mercuri, A., and Maffei, S. (2012). Sex-related differences in association of oxidative stress status with coronary artery disease. *Fertility Sterility* 97 (2), 414–419. doi: 10.1016/j.fertnstert.2011.11.045

Velázquez-Moyado, J. A., Balderas-López, J. L., Pineda-Peña, E. A., Sánchez-Ortiz, B. L., Tavares-Carvalho, J. C., and Navarrete, A. (2018). Diligustilide releases H_2S and stabilizes S-nitrosothiols in ethanol-induced lesions on rat gastric mucosa. *Inflammopharmacology* 26 (2), 611–619. doi: 10.1007/s10787-017-0392-6

Verma, R., Akhtar, Y., and Singh, S. (2017). A review of patents on therapeutic potential and delivery of hydrogen sulfide. *Recent Patents Drug Deliv. Formulation.* 11 (2), 114–123. doi: 10.2174/1872211311666170911160914

Wallace, J. L., Dicay, M., McKnight, W., and Martin, G. R. (2007). Hydrogen sulfide enhances ulcer healing in rats. *FASEB J.* 21 (14), 4070–4076. doi: 10.1096/fj.07-8669com

Wallace, J. L., Ferraz, J. G., and Muscara, M. N. (2012). Hydrogen sulfide: an endogenous mediator of resolution of inflammation and injury. *Antioxid. Redox Signaling* 17 (1), 58–67. doi: 10.1089/ars.2011.4351

Wallace, J. L., Blackler, R. W., Chan, M. V., Da Silva, G. J., Elsheikh, W., Flannigan, K. L., et al. (2015). Anti-inflammatory and cytoprotective actions of hydrogen sulfide: translation to therapeutics. *Antioxid. Redox Signal.* 22, 398–410. doi: 10.1089/ars.2014.5901

Wallace, J., Pshyk-Titko, I., Muscara, M. N., Bula, N., Pavlovsky, Y., Gavriluk, E., et al. (2015). Influence of Hydrogen Sulfide-releasing aspirin on mucosal

integrity of esophageal and gastric mucosa. *Proceed. Shevchenko Sci. Soc. Med. Sci.* 43 (27), 63–74.

Wallace, J. L., Vaughan, D., Dicay, M., MacNaughton, W. K., and de Nucci, G. (2018). Hydrogen sulfide-releasing therapeutics: translation to the clinic. *Antioxid. Redox Signaling* 28 (16), 1533–1540. doi: 10.1089/ars.2017.7068

Wang, M., Tang, W., and Zhu, Y. Z. (2017). An update on AMPK in hydrogen sulfide pharmacology. *Front. Pharmacol.* 8, 810. doi: 10.3389/fphar.2017.00810

Yonezawa, D., Sekiguchi, F., Miyamoto, M., Taniguchi, E., Honjo, M., Masuko, T., et al. (2007). A protective role of hydrogen sulfide against oxidative stress in rat gastric mucosal epithelium. *Toxicology* 241 (1–2), 11–18. doi: 10.1016/j.tox.2007.07.020

Zaichko, N., Pentyuk, N., and Melnik, A. (2009). The formation of hydrogen sulfide in the organs of rats. *Med. Chem.* 11 (4), 7–13.

Zayachkivska, O., Havryluk, O., Hrycevych, N., Bula, N., Grushka, O., and Wallace, J. L. (2014). Cytoprotective effects of hydrogen sulfide in novel rat models of non-erosive esophagitis. *PloS One* 9 (10), e110688. doi: 10.1371/journal.pone.0110688

Zhang, D., Du, J., Tang, C., Huang, Y., and Jin, H. (2017). H_2S-Induced Sulfhydration: Biological Function and Detection Methodology. *Front. Pharmacol.* 8, 608. doi: 10.3389/fphar.2017.00608

Zhang, L., Wang, Y., Li, Y., Li, L., Xu, S., Feng, X., et al. (2018). Hydrogen sulfide (H2S)-releasing compounds: therapeutic potential in cardiovascular diseases. *Front. Pharmacol.* 9, 1066. doi: 10.3389/fphar.2018.01066

Conflict of Interest: The authors declare that the research was conducted in the absence of any commercial or financial relationships that could be construed as a potential conflict of interest.

frontiers in Pharmacology

REVIEW
published: 13 August 2020
doi: 10.3389/fphar.2020.01234

Therapeutic Efficacy of Antioxidants in Ameliorating Obesity Phenotype and Associated Comorbidities

Steven Tun[†], *Caleb James Spainhower*[†], *Cameron Lee Cottrill*[†], *Hari Vishal Lakhani*, *Sneha S. Pillai*, *Anum Dilip*, *Hibba Chaudhry*, *Joseph I. Shapiro* and *Komal Sodhi*[*]

Departments of Medicine, Surgery and Biomedical Sciences, Marshall University Joan C. Edwards School of Medicine, Huntington, WV, United States

OPEN ACCESS

Edited by:
Terry D. Hinds, Jr., University of Toledo, United States

Reviewed by:
Darren Mikael Gordon, University of Toledo Medical Center, United States
Luca Vanella, University of Catania, Italy

***Correspondence:**
Komal Sodhi
sodhi@marshall.edu

[†]*These authors have contributed equally to this work*

Specialty section:
This article was submitted to Experimental Pharmacology and Drug Discovery, a section of the journal Frontiers in Pharmacology

Received: *07 July 2020*
Accepted: *28 July 2020*
Published: *13 August 2020*

Citation:
Tun S, Spainhower CJ, Cottrill CL, Lakhani HV, Pillai SS, Dilip A, Chaudhry H, Shapiro JI and Sodhi K (2020) Therapeutic Efficacy of Antioxidants in Ameliorating Obesity Phenotype and Associated Comorbidities. Front. Pharmacol. 11:1234. doi: 10.3389/fphar.2020.01234

Obesity has been a worldwide epidemic for decades. Despite the abundant increase in knowledge regarding the etiology and pathogenesis of obesity, the prevalence continues to rise with estimates predicting considerably higher numbers by the year 2030. Obesity is characterized by an abnormal lipid accumulation, however, the physiological consequences of obesity are far more concerning. The development of the obesity phenotype constitutes dramatic alterations in adipocytes, along with several other cellular mechanisms which causes substantial increase in systemic oxidative stress mediated by reactive oxygen species (ROS). These alterations promote a chronic state of inflammation in the body caused by the redox imbalance. Together, the systemic oxidative stress and chronic inflammation plays a vital role in maintaining the obese state and exacerbating onset of cardiovascular complications, Type II diabetes mellitus, dyslipidemia, non-alcoholic steatohepatitis, and other conditions where obesity has been linked as a significant risk factor. Because of the apparent role of oxidative stress in the pathogenesis of obesity, there has been a growing interest in attenuating the pro-oxidant state in obesity. Hence, this review aims to highlight the therapeutic role of antioxidants, agents that negate pro-oxidant state of cells, in ameliorating obesity and associated comorbidities. More specifically, this review will explore how various antioxidants target unique and diverse pathways to exhibit an antioxidant defense mechanism.

Keywords: obesity, oxidative stress, antioxidants, adipocytes, cardiovascular disease, diabetes

INTRODUCTION

Chronic state of obesity is an ever-growing health concern burdening millions of individuals worldwide. Characterized physiologically as the accumulation of excess body fat, a substantial difficulty that comes with determining treatment and prevention of the disease is the multifactorial origin of the etiology (Hruby and Hu, 2015). The complexity of the etiology has led to obesity being one of the most uncontrollable disease epidemics of the last four decades. Since 1980, the prevalence

of worldwide obesity has doubled with approximately 39% of people being overweight and 13% obese in 2014, according the World Health Organization. Further estimations indicate that by 2030, the worldwide obesity could reach 20% (Hruby and Hu, 2015; Mohammed et al., 2018). What is more worrisome is the increase of early onset obesity in children where obesity and potential comorbidities persist into adulthood in approximately 50% of cases versus 10% for children without obesity (Fruh, 2017). The stark incline of prevalence across all age groups is exceedingly concerning when considering the mortality associated with obesity. Across all age groups, according to compiled data of 19 cohort studies and 1.46 million participating individuals, mortality rate generally increased significantly in association with increased body mass index (BMI) (Berrington de Gonzalez et al., 2010). On average, obesity can lead to as much as a 5–10 year decrease on life expectancy (Kuk et al., 2011; Fruh, 2017).

Obesity has been known to be a cause of wide range of complications due to several underlying pathophysiological processes. Comorbidities of obesity are diverse and can occur in many bodily systems including cardiovascular complications, type 2 diabetes mellitus (T2DM), non-alcoholic steatohepatitis (NASH), metabolic syndrome, and several other lesser known morbidities (Sodhi et al., 2015; Srikanthan et al., 2016; Fruh, 2017; Lakhani et al., 2018; Lauby-Secretan et al., 2019). The trigger for obesity and associated comorbidities is intricately linked with an increase in reactive oxygen species (ROS) and subsequent oxidative stress. Several primary sources of endogenous intracellular ROS have been implicated including cellular mitochondria, endoplasmic reticulum (ER) stress, activation of oxidative stress pathways and upregulated activity of NADPH oxidase (NOX) (Bhatti et al., 2017). This causes a state of redox imbalance, where the pro-oxidants are excessively produced and the antioxidant defense mechanisms are diminished, facilitating a state of chronic inflammation (Fonseca-Alaniz et al., 2007; Wensveen et al., 2015). The interlinking relation between systemic redox imbalance and release of inflammatory mediators creates an inflammatory milieu affecting the regulation of metabolic pathways, consequences of which can lead to impaired physiological functions in obesity and associated comorbidities.

Due to the modulation of redox mechanisms in obesity, evidence suggests that a multimodal approach to treatment including diet changes, exercise, and medical treatments may be successful in curbing oxidant stress (Thompson et al., 2007; Achkasov et al., 2016). One such considerable approach against obesity is to counter the cellular pro-oxidant state by ameliorate the excessive production of ROS and subsequent oxidative stress. Antioxidants may present a viable therapeutic target to help ameliorate the negative effects of obesity and oxidative stress on the physiological systems of the body. The cumulative line of evidence suggests that antioxidants may modulate dynamic cellular targets and processes to improve the redox imbalance in obesity. The mechanisms involved in the regulation of cellular redox present increasing importance of unraveling the potential of endogenous and exogenous antioxidants in ameliorating obesity associated phenotype. Hence, this review aims to independently uncover the potential of several antioxidants in ameliorating obesity phenotype and associated comorbidities. Specifically, this review presents evidence from past literature in elucidating the role of antioxidants in improving antioxidant defense mechanism by manipulating localized redox signaling pathways in an obese state.

OXIDATIVE STRESS IN OBESITY AND ASSOCIATED COMORBIDITIES

The complex relationship between obesity and the associated comorbidities involves, first, the dysregulation of the vital communication system that adipocytes have within the body. Compared to the smaller, healthy adipocytes, the influence of obesity is drastic causing a transition to a subset of large, dysfunctional adipocytes (Lakhani et al., 2018). These larger adipocytes suffer from poor regulation mechanisms that disrupt the normal signaling functions that adipocytes play (Haczeyni et al., 2018). There are over 50 known adipokines that are released as signaling molecules from adipocytes including leptin, adiponectin, multiple interleukins, and TNF-α to name a few (Stolarczyk, 2017). In the obese model, the balance of these signaling adipokines are significantly disrupted. Pro-inflammatory adipokines (IL-6, TNF-α, MCP-1) and leptin, associated with the maintenance of the obese state, are elevated during the obese state whereas adiponectin, which plays an important role in insulin sensitivity, is decreased, connecting its role to insulin resistance and T2DM (Friedman and Halaas, 1998; Sirico et al., 2018). The increased levels of these pro-inflammatory adipokines place the body into a perpetual state of inflammation, or chronic inflammation. During the onset of obesity, this added inflammatory burden and subsequent adipocyte turnover/remodel to account for the increased fat accumulation is destructive to the cellular environment. Macrophages, which are recruited to aid in the adipocyte turnover, have also been implicated with obesity to potentiate the subsequent negative effects (Kuroda and Sakaue, 2017).

Following the stark transition to the state of chronic inflammation, the physiological environment quickly becomes burdened with oxidative stress in the form of increased ROS and oxidative radicals. One particular cellular component of concern following initial increase in ROS is at the mitochondrial level. Mitochondria, when functioning healthily, is already well-known as a major generator of ROS in the body (Oyewole and Birch-Machin, 2015). Invasion of macrophages to remodeling adipose tissue breaks down older adipocytes which leads to release of lipid components, inflammatory signals, and ROS (Lee et al., 2010). The continued release of inflammatory signals and ROS from this cycle of apoptosis and remodeling has a harmful effect on the mitochondria to exacerbate the inflammation and oxidative stress (Dela Cruz and Kang, 2018). ROS plays an imperative role in facilitating transition of healthy mitochondria to dysfunctional mitochondria. These dysfunctional mitochondria

and increased ROS impair the Krebs cycle and respiratory chain (de Mello et al., 2018). The dysfunctional mitochondria produce abnormally high amounts of ROS that create a vicious positive feedback effect on the functional status of the mitochondria (Wang et al., 2013; de Mello et al., 2018). Although the chronic inflammation induces the state of oxidative stress, dysfunctional mitochondria are vital for maintaining the diseased state. Furthermore, brown adipose tissue (BAT) is a mitochondria rich tissue with high oxidative capacity which have been implicated in the process of adaptive thermogenesis (Lettieri-Barbato, 2019). The production of mitochondrial ROS under thermogenesis is important to maintain the bodily homeostasis, and this process is finely controlled through feedback mechanism. However, in a diseased metabolic condition, there is a shift in the redox state causing more oxidative stress during thermogenesis. This shift leads to altered expression of markers associated with thermogenesis causing an alteration in the adipocyte phenotype (Lettieri-Barbato, 2019). Studies have demonstrated a causal relationship between mitochondrial ROS and thermogenesis using the mitochondria-targeted antioxidant MitoQ, which efficiently ameliorates lipid peroxides and superoxides *in vivo* (Rodriguez-Cuenca et al., 2010). It is important to note that the redox changes occurring in BAT upon thermogenesis are dynamic, reversible and adapted to by antioxidant pathways (Chouchani et al., 2017).

This perpetual state of oxidative stress and inflammation is what links obesity to its associated comorbidities. The detrimental role that this diseased state plays on the cardiovascular system is substantial. Chronic inflammation has a negative effect on cardiovascular tissue contributing to the associated cardiovascular disease (CVD) and arteriosclerosis (Libby, 2006). With respect to obesity, the chronic, low-grade inflammation and oxidative from obesity places the cardiovascular system at an increased risk for developing plaques in blood vessels and cardiac remodeling (Kachur et al., 2017). Two studies, one done clinically with patients and the other in mice on high-fat diet, have shown that increased pressure in the heart stimulated an increase in function of NADPH oxidase 4 (NOX4), primarily located in the mitochondria of cardiac myocytes (Kuroda et al., 2010; Munzel et al., 2017). Under states of stress, NOX4 produces superoxide (O_2^-) to exacerbate the oxidative stress of the cardiovascular system (Kuroda et al., 2010). The inflammatory signals released by adipocytes also contribute to altering the physiology of the heart in obesity. Adiponectin, downregulated in obesity, plays a protective role in the heart by stimulating endothelial nitric oxide synthase (eNOS) to maintain healthy vascular tone. Conversely, the rising leptin levels in the heart positively correlate with coronary artery disease, left ventricular hypertrophy, stroke, and myocardial infarction (Soderberg et al., 1999; Wallace et al., 2001; Chait and den Hartigh, 2020). Along with pro-inflammatory circulating signals, a transcription factor, NF-κB, is a product of chronic inflammation in cardiovascular tissue and is a useful clinical indicator for obesity-related inflammation (de Almeida et al., 2020).

Insulin resistance and T2DM are also example of diseases extensively linked as a comorbidity of obesity. A few of the prominent inflammatory adipokines associated with decreasing insulin sensitivity in tissues are IL-6 and TNF-α (Stolarczyk, 2017). In addition, IL-10 and adiponectin, two adipokines that promote insulin sensitivity are decreased in the obese state (Stolarczyk, 2017). Meanwhile, oxidative stress promotes a diabetic state by disrupting certain metabolic pathways such as inhibiting G-3-P dehydrogenase, stimulating buildup of G-3-P, and up-regulating glycolytic, hexosamine, advanced glycation end-product (AGE), protein kinase C, and polyl pathways (Ighodaro, 2018). Despite the specific mechanisms not being completely understood, the primary method by which obesity links to T2DM is through insulin resistance (Burhans et al., 2018). One proposed mechanism observed over multiple studies (but not all) is that as adipogenesis takes place, the adipocytes become dysregulated and release a larger amount of free fatty acids (FFA) into circulation (Mittendorfer et al., 2009). The FFA-mediated insulin resistance involves the products of oxidation of FFA in tissues which exacerbates already impaired glucose metabolism (Randle et al., 1965). Several *in vitro* studies have revealed a secondary mechanism linking the adipokine, TNF-α, to insulin resistance by regulating ceramide synthesis (Grigsby and Dobrowsky, 2001; Hernandez-Corbacho et al., 2015). Oxidative stress and inflammation resulting from obesity is a systemic problem impacting several regions of the body through similar mechanisms as seen in T2DM and cardiovascular complications (**Figure 1**).

ANTIOXIDANTS IN AMELIORATING OBESITY AND ASSOCIATED COMORBIDITIES

Peroxiredoxin

Peroxiredoxins (Prxs) are a family of peroxidase enzymes that have a highly conserved function to reduce hazardous peroxides in the body. There are a few different subtypes within the Prx family, but the mechanism of action of the class as a whole is mediated through a highly conserved peroxidatic cysteine residue (C_P) (Hall et al., 2009). Despite the fact that the catalytic function of all Prxs is conserved involving oxidation of the C_P by the peroxide substrate to sulfenic acid, the recycling of the sulfenic acid back to thiol is the defining feature of the three classes of Prxs: typical 2-Cys, atypical 2-Cys, and 1-Cys Prxs (Wood et al., 2003; Rhee, 2016). In the mammalian system, there are six known peroxiredoxin subtypes including PrxI-IV (typical 2-Cys), PrxV (atypical 2-Cys), and PrxVI (1-Cys) (Perkins et al., 2015).

Prxs are widespread across the body, and the subtypes are localized to several different cellular compartments to play a universal role against oxidative stress. PrxI and PrxII are both found predominantly in the cytosol or nuclei of cells with PrxII playing a vital role in protecting erythrocytes (Rhee et al., 2012). PrxIII (typical 2-Cys) and PrxV (atypical 2-Cys) are both found in the mitochondria where they are the primary antioxidant defense mechanism against the most abundant producer of ROS. PrxV, however, has also been found in peroxisomes and cytosol

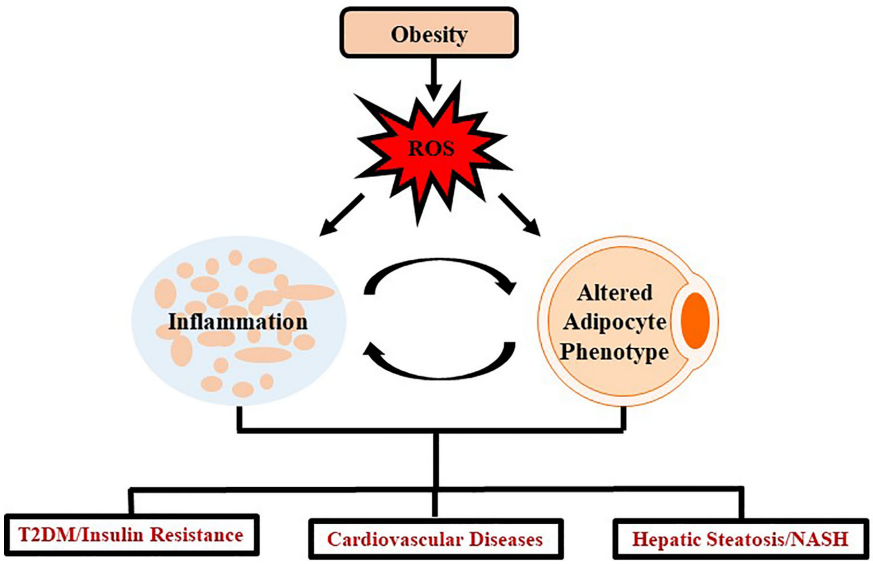

FIGURE 1 | Schematic representation demonstrating impact of oxidative stress in obesity. Obesity mediates excessive production of ROS which leads to chronic inflammation and altered adipocyte phenotype which further induces several systemic changes causing oxidative stress. Such oxidative stress leads to the development and progression of chronic diseases such as T2DM, cardiovascular diseases and/or NASH.

(Perkins et al., 2015). PrxIV is the only subtype to be identified in the endoplasmic reticulum, which is vital for its antioxidant role governing protein processing protection (Rhee et al., 2012; Yamada and Guo, 2018). The only 1-Cys structural subtype is PrxVI, and this enzyme resides in the cytosolic and lysosomal compartments in cells (Fisher, 2018).

Because of the highly conserved antioxidant function in reducing peroxide agents, the extensive bodily coverage of Prxs allows them to play a significant role in obesity-induced oxidative stress and complications. In mice with PrxV knockout on high-fat diet, progression to obesity and enhanced adipogenesis was far more likely than mice without the gene knockout. Mice with PrxV treatment saw decreased levels of PPARγ and C/EBPα, two markers that indicate an adipogenic state (Kim et al., 2018; Hammarstedt et al., 2018). Another study induced hepatic steatosis in a HepG2 cell line with treatment of FFA to simulate an obese state *in vitro*. Inducing PrxV overexpression ameliorated hepatic steatosis progression by inhibiting lipogenesis associated protein, SREBP-1 and RAS, and FFA-induced mitochondrial ROS generation (Kim et al., 2020). A follow-up study in mice revealed that the mechanism of PrxV in achieving this role appears to be through phosphorylation of AMPK pathway (Kim et al., 2020). Two separate studies have also implicated PrxIV and PrxVI in having a protective role against steatosis by targeting mitochondrial ROS generation (Yamada and Guo, 2018; Lee et al., 2019).

Another study found that PrxIII was expressed at high levels in 3T3-L1 mature adipocytes (Huh et al., 2012). Subsequently, PrxIII knockout (KO) in mice produced a substantial increase in adipocyte hypertrophy and fat mass compared to wild-type mice. The PrxIII KO mice were observed to have increased levels of mitochondrial ROS generation, adipogenic markers, aP2, CCAAT/enhancer binding proteins (C/EBPα), and peroxisomal proliferator activated receptor γ (PPARγ), and protein carbonylation. The study also demonstrated decreased levels of adiponectin, alteration of mitochondrial biogenesis, and other antioxidant enzymes in mitochondria. The PrxIII KO mice were identified to have impaired glucose metabolism and insulin resistance (Huh et al., 2012). Although the mechanism to how PrxIII regulates adipocyte function has yet to be established, this study provides ample data to strongly suggest therapeutic implications for PrxIII in obesity.

Similarly, recent study also identified PrxVI as a vital component leading to an early stage of T2DM with diabetic dyslipidemia in PrxVI KO mice (Pacifici et al., 2014). In the KO mice, elevated levels of triglycerides and VLDLs were identified; a hallmark indicator of adipocyte dysregulation in obesity (Makhoul et al., 2011). Similarly, the PrxVI KO mice exhibited increased levels of pro-inflammatory cytokines, TNFα, IL-1β, IL-10, and IL-6, from adipose tissue. Altogether, this study exemplifies PrxVI in protecting against progression to T2DM with diabetic dyslipidemia (Pacifici et al., 2014). PrxIV is another subtype implicated in its protective role against diabetes due to stimulation of enhanced insulin secretion (Mehmeti et al., 2014). Overall, the mechanisms responsible for mediating the antioxidant actions of Prxs against obesity are somewhat undiscovered or undefined due to the relative recency of many studies involving Prx. However, there is growing evidence linking some Prx subtypes as key protective mechanisms against obesity-induced inflammation and comorbidities.

N-Acetylcysteine (NAC)

N-Acetylcysteine (NAC) is an antioxidant that serves to reduce ROS through both direct and indirect effects (Mokhtari et al.,

2017). The direct effects revolve around its' ability to react with hydroxyls, nitrogen dioxide and carbonate (Samuni et al., 2013). The indirect effects arise from NAC being derived from a conditionally essential amino acid, L-cysteine and subsequently provides the cysteine for the formation of glutathione, a well-established potent physiological antioxidant (Kerksick and Willoughby, 2005). However, the oral bioavailability of glutathione is controversial (Allen and Bradley, 2011; Richie et al., 2015). Therefore, NAC is marketed as an over-the-counter oral antioxidant supplement while being utilized in many treatment protocols and clinical studies with relatively low adverse effects (Schmitt et al., 2015).

The role of NAC in obesity has yielded promising results across countless studies. Given that obesity is characterized by elevated levels of oxidative stress and inflammation has made NAC a profound target for research to minimize the progression of obesity and associated co-morbidities (Manna and Jain, 2015; McMurray et al., 2016). Recent *in vitro* studies have been able to demonstrate a beneficial role in attenuating biomarkers associated with adipocyte differentiation pathways such as PPARγ and C/EBPβ in 3T3-L1 preadipocyte cells (Calzadilla et al., 2011). The reduction in these biomarkers was shown to be equal to glutathione level elevation through NAC supplementation, reducing ROS, that upregulate the activity of PPARγ and C/EBPβ (Lee et al., 2009; Calzadilla et al., 2011; Pratt et al., 2019). This allows for speculation that supplementation of NAC during the progression of obesity could reduce adipogenesis through elevation of glutathione level content. Furthermore, *in vivo* studies revealed that supplementation of NAC in murine models that were fed a high fat diet to induce obesity, reduced triglyceride and cholesterol content within the liver by reducing PPARγ levels amongst other genes involved in hepatic storage and metabolism of lipids (Ma et al., 2016). Studies have given promising evidence that NAC may normalize levels of hepatic malondialdehyde and superoxide dismutase (SOD) providing further insight that there could be a role in preventing obesity associated co-morbidities of the liver including NASH (Thong-Ngam et al., 2007; Korou et al., 2014).

A major factor revolving around obesity is the oxidative stress associated inflammation present across various metabolic tissues that has shown to be linked to insulin resistance, atherosclerosis, and ischemic strokes (Manna and Jain, 2015; Assari and Bazargan, 2019). The plausible efficacy of NAC in counteracting obesity associated inflammation and apoptosis that contributes to progression of metabolic disorders is attributed to NAC's ability to reduce inflammatory cytokines and apoptotic factors while increasing antioxidant components (Samuni et al., 2013; de Andrade et al., 2015). These anti-apoptotic effects are elicited by the increased levels of SOD, catalase, glutathione peroxidase and activity of peroxynitrate which serve to reduce ROS (Zaragoza et al., 2000; de Andrade et al., 2015). *In vitro* studies uncovered further contributions to the reduction of inflammation and apoptosis by NAC reducing levels of vascular cell adhesion molecule 1 (VCAM-1), TNF-α, IL-6, IL-8, Ikβ kinase and subsequent activation of NF-κB, which have roles in multiple inflammatory cascades (Samuni et al., 2013; de Andrade et al., 2015; Sun et al., 2019). The capability of NAC to reduce inflammatory pathways and ROS generation may allow for improvement in insulin sensitivity in obese individuals that begin to progress to the development of T2DM (Fulghesu et al., 2002; Lasram et al., 2015; Shen et al., 2018). This was evidenced by recent studies that revealed treatment with NAC improved plasma insulin levels, increased insulin sensitivity across multiple tissues and increased motor activity in murine models of obesity (Lasram et al., 2015; Shen et al., 2018). The increase in motor activity could be attributed to NAC's ability to improve insulin sensitivity in skeletal muscle tissues as well as possibly preventing the decline of skeletal muscle sodium potassium adenosine triphosphatase (Na^+/K^+ ATPase) activity allowing for slowed muscle fatigue (McKenna et al., 2006). Both of these contributions could indicate a theoretical route of research to determine if any correlation exists between NAC and increased total daily energy expenditure in obese individuals which may be combined with proper diet, decreasing the total degree of inflammation by reducing adiposity and fat mass. Furthermore, NAC was shown to improve insulin sensitivity and glucose utilization in hyperglycemia induced mice *via* high sucrose diet as well as in human volunteers during a hyperglycemic clamp (Ammon et al., 1992; Diniz et al., 2006). These studies reinforce the plausible link between NAC and improving insulin sensitivity to glucose which may provide insight into improvement of glucose utilization within obese individuals that have progressed to developing T2DM (Straub et al., 2019).

The current cumulative line of evidence strongly suggests that NAC may have a role in being utilized as a cardioprotective agent by reducing hyperglycemia induced oxidative damage to cardiac myocytes and cardiac remodeling (Chen et al., 1985; Dludla et al., 2017). This reduction in oxidative stress attenuates a progressive loss in cardiac efficiency and cardiac fibrosis that would have progressed to more severe clinical outcomes prior to intervention (Seddon et al., 2007; Talasaz et al., 2013). Data from multiple studies indicated that NAC elevated levels of SOD and glutathione in cardiac myocytes, while reducing levels of TGF-β, lipid hydroperoxides and various biomarkers for oxidative stress (Haleagrahara et al., 2011; Talasaz et al., 2013; Dludla et al., 2017). Obesity and T2DM both exhibit a characteristic feature of hypercoagulable states through chronic inflammation associated with obesity and dysregulation of platelet aggregation (Anderson and Weitz, 2010; Blokhin and Lentz, 2013; Widjaja et al., 2019). Studies have uncovered that NAC may have a potential role in reducing the likelihood of thrombus generation through elevation of platelet glutathione levels and nitric oxide (Girouard et al., 2003; Martinez de Lizarrondo et al., 2017; Craver et al., 2020). The elevation in platelet glutathione ameliorated platelet ROS preventing oxidative constituents to induce coagulation cascades (Wang et al., 2016). It was also indicated that NAC may exert antagonistic effects toward Von Willebrand factor, a necessary component of coagulation cascades, reducing the risk of thrombosis and stroke (Wang et al., 2016; Martinez de Lizarrondo et al., 2017). Through elevating levels of nitric oxide, NAC may have a possible role

in regulation of high blood pressure in obese individuals *via* nitric oxide mediated vasodilation (Zicha et al., 2006; Gibson et al., 2011). NAC's cardioprotective abilities also correlate to its ability to reduce the expression of malic enzyme, fatty acid synthase and other enzymes involved in biosynthesis of triglyceride and cholesterol biosynthesis pathways (Lin and Yin, 2008; Korou et al., 2010; Korou et al., 2014; Ma et al., 2016). This cardioprotective ability may indicate that NAC may play a role in prevention of atherosclerosis.

Vitamin E

Vitamin E (VitE) primarily describes a group of eight compounds known as tocopherols and tocotrienols where each group consists of α, β, γ, and δ tocopherol/tocotrienol compounds (Colombo and vitamin, 2010; Rizvi et al., 2014). Each of the eight compounds, has shown to elicit some degree of antioxidant properties. However, of all the compounds the constituent α-tocopherol (αT) possesses the highest physiological concentrations (Baxter et al., 2012). It has been shown extensively that αT acts as an antioxidant through its chromanol ring, allowing it to scavenge and remove ROS preventing oxidative damage (Ahsan et al., 2015). Through their lipophilic characteristics, αT serves to protect polyunsaturated fatty acids present in membrane phospholipids and lipoproteins to stabilize cellular membranes (Kuznetsov et al., 1993; Wallert et al., 2014; Galmes et al., 2018). Many studies have suggested a positive correlation between αT and attenuating inflammation, clinical disorders and promoting immune system functionality (Galmes et al., 2018; Lewis et al., 2019). This research along with VitE being widely available, obtained solely from the diet particularly from vegetable oils, has peaked interest into incorporating αT supplementation into many treatment protocols of various clinical disorders including metabolic syndrome where individuals are shown to have lower levels of αT (Montonen et al., 2004; Mehmetoglu et al., 2011). This may indicate that the development and progression of obesity related metabolic syndrome could in part be attributed to reduced levels of αT (Lira et al., 2011).

Recent *in vivo* studies in models of obesity and human studies have indicated that αT supplementation was capable of attenuating inflammatory processes by reducing the expression of IL-6, TNF-α, malondialdehyde and C reactive protein while increasing antioxidant constituents (Patrick and Uzick, 2001; Wong et al., 2017). Furthermore, αT may also act to inhibit pathways that are activated by ROS such as p38 MAPK (Schett et al., 2008; Thalhamer et al., 2008; Wang et al., 2011; Wong et al., 2017). These pathways tend to be elevated in obese individuals, various inflammatory pathologies and are diminished with αT supplementation (Wong et al., 2017; Donohoe et al., 2020). Administration of αT in obese individual induces differentiation of macrophages toward an M2 phenotype that exhibits anti-inflammatory effects (Alcala et al., 2015; Ray et al., 2016). Thus, αT may have a plausible role in reducing inflammation mediated by ROS-induced oxidative damage and exert effects on immune system functionality (Lee and Han, 2018).

The ability of αT to reduce total cholesterol and triglycerides has yielded promising results in metabolic syndrome patients and in prevention of obesity associated atherosclerosis (Upston et al., 2003; Wong et al., 2017). These beneficial effects elicited by αT are mediated through the reduction of low density lipoprotein (LDL), high density lipoprotein (HDL) and total cholesterol levels (Upston et al., 2003; Kirmizis and Chatzidimitriou, 2009; Wong et al., 2017). In murine models of diet induced obesity, αT diminished the degree of hepatic steatosis and circulating triglycerides indicating a plausible role in the prevention of atherosclerosis and NASH, associated with obesity (Kawanaka et al., 2013; Alcala et al., 2015). Cumulative evidence across diabetic individuals, and various animal models indicate that αT is able to reduce lipid peroxidation within cellular membranes and reduce overall lipid content in circulation (Kuznetsov et al., 1993; Wiseman et al., 1995; Eder et al., 2004). This same reduction of lipids can also be seen within adipocytes as αT may serve a role in shifting the metabolic profile of obese individuals toward normalcy. These deviations within adipocytes in obese individuals compared to non-obese individuals includes an elevation of matrix metalloproteinase activity and collagen deposition (Sun et al., 2013; Lauhio et al., 2016). The accumulation of collagen prevents adipocyte expansion and may contribute to the phenotype and inflammation seen in obesity (Unal et al., 2010; Jaoude and Koh, 2016; Lin et al., 2016; Wong et al., 2017). However, supplementation with αT promoted adipocyte differentiation and expansion indicating that αT may play a role in downregulating pathways associated with collagen accumulation and abnormal adipocyte growth to attenuate the pathogenic obesity phenotype (Kim et al., 2007).

Cumulative studies have indicated that αT supplementation reduces biomarkers of lipid peroxidation in T2DM patients and improve insulin sensitivity (Wu et al., 2007; Thalhamer et al., 2008; Murer et al., 2014; Niki, 2015). The elevation in insulin sensitivity may be attributed to the anti-inflammatory action of αT in visceral adipose tissue, by reducing the level of p38 phosphorylation, which is associated with many inflammatory responses and insulin resistance (Wu et al., 2007; Wong et al., 2017). Through scavenging of ROS, αT may serve to ameliorate the impact that persistent hyperglycemic conditions have on promoting ROS production and inflammatory cascade activation (Alcala et al., 2015; Wong et al., 2017). Thus, there may be a role linking αT's effects on inflammatory cascades that may lead to the attenuation of the diabetic phenotype (Lee et al., 1999).

The actions of αT have shown to attenuate production of ROS and activity of protein kinase C (PKC) pathways associated with cellular cascades that promote proliferation and differentiation (Martin-Nizard et al., 1998). These cascades have shown to be affected by αT through increasing the expression of biological compounds that inhibit PKC resulting in the downregulation of a multitude of cascades (Engin, 2009). Among these cascades, αT exhibits an inhibitory effect on the proliferation of vascular smooth muscle cells that may contribute to CVD diseases such as atherosclerosis (Nakashima et al., 1998), indicating that αT may have a plausible role in cardio protection (Engin, 2009; Rizvi et al., 2014). Evidence has highlighted that αT serves a role in cardioprotective mechanisms through prevention of retinal vascular disease in hyperglycemic states associated with T2DM patients by inhibition of these PKC mediated pathways (Engin, 2009). αT may also serve to attenuate platelet

aggregation, stimulate prostacyclin release, and elevate nitric oxide synthase (Rizvi et al., 2014). Moreover, αT reduced the systolic blood pressure through increasing nitric oxide synthase activity in murine models of hypertension (Tran and Chan, 1990; Rizvi et al., 2014). Thus, the elevation of prostacyclin and nitric oxide synthase uncovers a plausible cardioprotective mechanism against hypertension as both are potent vasodilators (Moncada and Vane, 1979; Ahmad et al., 2018). Evidence accumulated across *in vitro* studies suggest that αT may lower the levels of TNF-α induced stimulation of intracellular cell adhesion molecule (ICAM-1) and VCAM-1 (Kirmizis and Chatzidimitriou, 2009; Cook-Mills et al., 2013; Cook-Mills, 2013; Rizvi et al., 2014). This downregulation may indicate diminished platelet aggregation and plausible reduction in the risk for atherosclerosis and thrombosis (Nakashima et al., 1998; Rizvi et al., 2014).

Heme Oxygenase-1

Heme oxygenase-1 (HO-1) has been established as a stress-inducible enzyme that possesses cytoprotective, anti-inflammatory and antioxidant properties (Nath, 2006; Araujo et al., 2012). Other functions include its role in the rate limiting step for heme degradation as it exerts an indirect antioxidant effect in this manner through the degradation products (Nath, 2006). Heme is a potent pro-oxidant that serves to increase production of ROS seen in many pathological states (Wu et al., 2019). HO-1 degrades heme through a series of catabolic steps that yield products including biliverdin, carbon monoxide (CO) and free iron (Gozzelino et al., 2010). These effects have sparked interest into multitudes of studies for incorporation into therapeutic regimens for a plausible impediment of disease progression in various inflammatory diseases, CVD and metabolic dysregulation associated with obesity (Durante, 2003; Pae and Chung, 2009; Bereczki et al., 2018).

The importance of functioning HO-1 has been shown by *in vivo* HMOX1 gene KO murine models (Poss and Tonegawa, 1997; Chan et al., 2011; Ayer et al., 2016). Studies have shown that induced deficiency of HO-1 results in chronic inflammatory states with elevated levels of pro-inflammatory cytokines that are similar to the levels in various inflammatory diseases (Poss and Tonegawa, 1997; Chan et al., 2011; Lenoir et al., 2017). The anti-inflammatory effects elicited by HO-1 under normal conditions can be attributed to its ability to degrade free heme. In excess, free heme has the capability to contribute to the pathology of various inflammatory diseases through destabilizing cellular membranes, damaging organelles and DNA (Kumar and Bandyopadhyay, 2005; Sparkenbaugh et al., 2015). Biliverdin, CO and free iron produced from degradation of heme have been shown to elicit anti-inflammatory actions through a variety of different cascades (Peterson et al., 2020). CO is able to reduce pro-inflammatory cytokines attributing to the toxicity of free heme including TNF-α, IL-1β and IL-2 through its actions on MAPK and NF-kβ pathways (Kruger et al., 2006; Wang et al., 2009; Burgess et al., 2010; Paine et al., 2010; Chan et al., 2011). This reduction in IL-2 may contribute to most of the anti-proliferative actions associated with CO signaling (Pae et al., 2004; Pae and Chung, 2009). Biliverdin may also regulate its anti-inflammatory actions through multiple mechanisms that involve the inhibition of NF-kβ and enhancing production of anti-inflammatory constituents (Pae and Chung, 2009). The free iron that is released from heme degradation possess inflammatory and cytotoxic characteristics (Dutra and Bozza, 2014). However, to compensate for the elevation in free iron from heme degradation, HO-1 upregulates ferritin synthesis that is capable of storing free iron preventing possible initiation of otherwise harmful inflammatory cascades (Balla et al., 1992; Pae and Chung, 2009). Through the suppression of pro-inflammatory mediators and antioxidant actions, HO-1 and the products of heme degradation are able to reduce inflammation and possibly diminish the phenotypic expression associated with obesity.

Through the reduction in proinflammatory mediators directly and indirectly, HO-1 may contribute to improving insulin sensitivity in diabetics, reducing adipogenesis and the probability of CVD development. Recent studies indicate that the reduced adipogenesis and adipocyte dysfunction may be attributed to the regulation of HO-1 mediated Wnt/β-catenin pathways that act to reduce expression of PPARγ and C/EBPα (Siersbaek et al., 2010; Cao et al., 2012; Khitan et al., 2014). Biliverdin, produced *via* HO-1 degradation of heme, may contribute to normalizing adipocyte function by exerting regulatory effects on PKC pathways (Wegiel and Otterbein, 2012; Khitan et al., 2014). By limiting adipogenesis, adipocyte proliferation and differentiation, HO-1 is able to reduce the inflammatory response within adipocytes promoting a more stable microenvironment (Cao et al., 2012; Wagner et al., 2017). This is due to smaller adipocytes being more responsive to insulin and release higher concentrations of adiponectin compared to larger adipocytes (Peterson et al., 2019). The improvement of insulin action can be attributed to the effects of HO-1 attenuating the expression of insulin resistance mediators including TNF-α, IL-1β and increasing the levels of adiponectin (Kim et al., 2008; Burgess et al., 2010; Cao et al., 2012). Adiponectin is a hormone that is released from adipocytes, that possesses anti-inflammatory characteristics and confers insulin sensitivity (Li et al., 2008). The actions of adiponectin resemble those of HO-1, that decreases the expression of TNF-α, IL-1β, NF-kβ signaling as well as other inflammatory mediators to subvert this pathological phenotype (Kim et al., 2008; Burgess et al., 2010; Aprahamian and Sam, 2011). Furthermore, adiponectin and HO-1 both serve to act on inhibiting AMPK pathway, which is profound in obesity associated inflammation (Hosick and Stec, 2012; Sodhi et al., 2015; Smith et al., 2016; Achari and Jain, 2017). By inducing adiponectin upregulation, HO-1 is able to work in concert with adiponectin involving AMPK cascades to improve insulin sensitivity, attenuate adipogenesis and progression of NASH (Burgess et al., 2010; Hwang et al., 2013; Sodhi et al., 2015; Smith et al., 2016; Peterson et al., 2019).

Further elucidating the importance of HO-1 in CVD associated with obesity is the therapeutic use of statins that have been shown to promote the induction of HO-1 to prevent

atherosclerosis (Heeba et al., 2009). The ability of HO-1 to reduce ROS and pro-oxidant constituents diminishes the risk for oxidation of LDL providing cardioprotective mechanisms against generation of atherosclerotic plaques (Cheng et al., 2009). These plaques elicit higher levels of HO-1 induction that can likely be attributed to physiological response to prevent plaque progression, thrombus generation and activation of inflammatory cascades in vascular endothelium (Cheng et al., 2009; Durante, 2011). Moreover, HO-1 may attenuate vascular inflammation by reducing VCAM levels, apoptotic factors, release of inflammatory mediators from mast cells and upregulating anti-apoptotic factors (Takamiya et al., 2002; Kruger et al., 2006; Chan et al., 2011). The cardioprotective mechanisms provided through induction of HO-1 may be attributed to not only the direct actions of HO-1 but also the indirect actions mediated through heme degradation products CO and biliverdin (Chan et al., 2011; Hosick and Stec, 2012; Ayer et al., 2016). CO may activate soluble guanylyl cyclase cascades leading to vascular relaxation and diminishing platelet aggregation to prevent subsequent thrombus formation (Furchgott and Jothianandan, 1991; Cheng et al., 2009; Hosick and Stec, 2012; Ayer et al., 2016). The actions of CO and biliverdin also seem to mediate pathways acting on vascular smooth muscle cell proliferation in response to injury associated from the pathological microenvironment produced from obesity mediated inflammatory responses (Ollinger et al., 2005; Beck et al., 2010). Through the actions of CO and biliverdin, HO-1 inhibitory effect may attenuate the development and progression of multiple vascular diseases associated with metabolic syndrome and obesity (Frismantiene et al., 2018). The plausible contribution of HO-1 in prevention of CVD, NASH, insulin resistance, inflammation, apoptosis, oxidation and adipogenesis provide insight into the importance of utilizing HO-1 and associated pathways in therapeutic regimens to reduce the morbidity and mortality associated with obesity phenotypes.

Polyphenols

Polyphenols are a type of antioxidants that are commonly found in diets such as cranberries, red wine, green teas, and many others (Fraga et al., 2019). Although the direct mechanism of action of polyphenols is not well understood, many studies have shown that polyphenols attenuates the obesity phenotype and related comorbidities. Polyphenols has been shown to affect the gut microbiota and stimulate signaling pathways that promote fatty acid β-oxidation, mobilization of adipose tissue through lipolysis, lowering of body weight and fat mass by increasing fat use and energy expenditure through thermogenesis induction, adipose apoptosis, satiety, and an increase in basal metabolic rate (Castro-Barquero et al., 2018). Polyphenol's inhibitory actions include the downregulation of adipose differentiation and adipogenesis, buildup of triglyceride, and chronic obesity-related inflammation.

Cumulative lines of evidence have demonstrated the beneficial role of polyphenol, found in cranberry extract, to improve diet induced obese phenotype in murine model. The study comparing a diet with high fat/high sucrose and high fat/high sucrose with cranberry extract revealed that polyphenols lowers total weight gain, visceral adipose tissue weight, hepatic triglyceride accumulation, and plasma cholesterol levels (Anhe et al., 2015). Also, mice given cranberry extract had similar fasting glycaemia but with lower fasting insulinaemia, which implies that polyphenols accentuate insulin sensitivity (Anhe et al., 2015). In addition to cranberry extract, the polyphenols present in pomegranate extracts have also been reported to prevent and treat obesity. Previous studies have reported that the pomegranate extract could decrease the level of lipids in the blood with significant anti-inflammatory activities. Recent *in vitro* study has also demonstrated that the polyphenols contained in pomegranate extracts in combination with probiotics induces synergistic effects that substantially reduces the triglyceride levels and intracellular lipid increase (Sorrenti et al., 2019). The study showed that *in vitro* treatment with pomegranate extract and probiotics improved the expression of fatty acid synthase, adiponectin, adipogenic markers, PPARγ and SREBP, as well as inflammatory cytokine, IL-6.

Parallel to the availability of cranberry polyphenols, resveratrol is found in red wine and it undergoes rapid metabolism in the small intestine and by the gut microbiota, leading to low plasma bioavailability and complex outcomes (Galiniak et al., 2019). Resveratrol has been shown to increase endurance during exercise by expanding air capacity and oxygen consumption and also increase insulin sensitivity of visceral white adipose tissue in mice (Springer and Moco, 2019). Consumption of resveratrol alters the composition of gut microbiota by increasing symbiotic bacteria like *Bacteroidetes* and decreasing opportunistic pathogens like *Escherichia coli*. The favorable stimulation of *Bacteroidetes* by resveratrol decreases the levels of trimethylamine-*N*-oxide (TMAO), which is associated with chronic diseases like obesity (Schugar et al., 2017). A fecal transplant of resveratrol-fed mice to obese mice improved their glucose homeostasis. Another study demonstrated that resveratrol's protein interaction stimulates mitochondrial biogenesis and increases the use of lipids while decreasing glycolysis in the muscle and liver by the deacetylation of PGC1α, leading to an increase in energy expenditure (Lagouge et al., 2006). Concomitantly with protein interactions, resveratrol increases lipolysis and decreases adipogenesis by the inhibition of PPARγ and SIRT1 (Houtkooper et al., 2012). Resveratrol's function as an antioxidant in redox cycling leads to the activation of Nuclear factor-erythroid 2-related factor-2 (Nrf2), increase in SOD, and reduction in BMI, blood pressure and body weight (Springer and Moco, 2019).

Recent advances have suggested the beneficial role of curcumin, a polyphenol antioxidant, in ameliorating obesity phenotype. In vitro evidence suggests the ability of curcumin in the browning of white adipocytes by increasing the protein levels of hormone-sensitive lipase and p-acyl-CoA carboxylase, augmenting lipolysis (Lone et al., 2016). Curcumin has been largely implicated in attenuating insulin resistance, hyperglycemia, hyperlipidemia and comorbidities associated with obesity (Aggarwal, 2010). The cumulative line of evidence suggest that curcumin can modulate various targets involved in obesity and

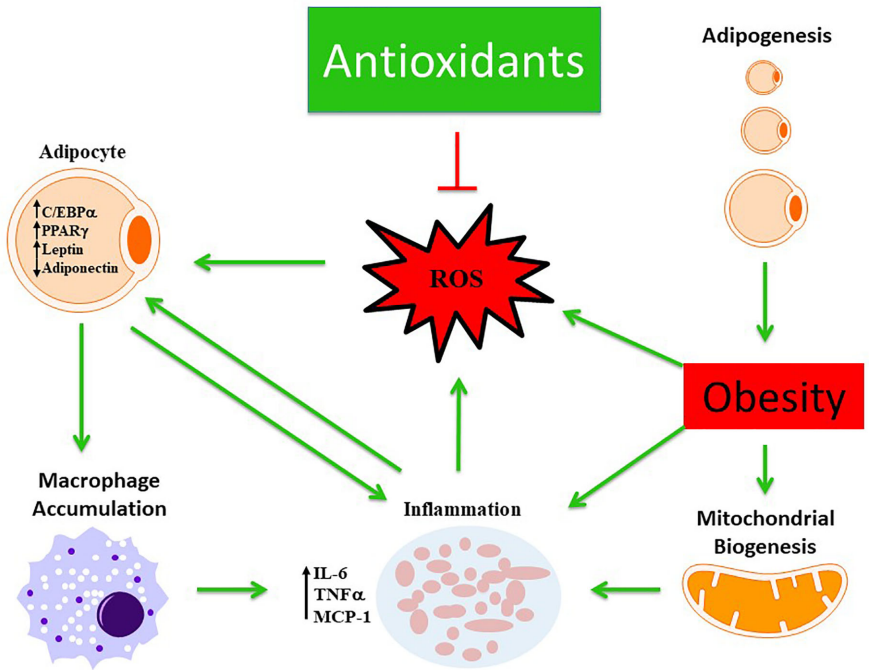

FIGURE 2 | Schematic representation demonstrating the beneficial role of antioxidants in modulating obesity phenotype. Obesity mediates excessive ROS production and inflammation which is further exacerbated by altered mitochondrial biogenesis and activation of macrophages from dysfunctional adipocytes. The antioxidant defense mechanism scavenges ROS and ameliorates obesity phenotype.

metabolic diseases including, suppression of NF-κB and its regulation inflammatory cytokines (Singh and Aggarwal, 1995), IKK (Aggarwal et al., 2006), JNK (Wang et al., 2009). Studies in murine models also demonstrated the effectiveness of dietary curcumin in lowering triglycerides, cholesterol and phospholipid levels (Rao et al., 1970; Babu and Srinivasan, 1997). Apart from that, bergamot has also been shown to illicit antioxidant properties and ameliorate obesity and associated comorbidities. Bergamot is rich with flavonoids and phenolic compounds that have been shown to improve dyslipidemia and systemic inflammation in patients with metabolic syndrome (Musolino et al., 2019). The mechanistic action of bergamot is mediated by its compounds, bruteridin and melitidin, which bind the catalytic site of HMG-CoA reductase causing inhibition of cholesterol synthesis by replacing its endogenous substrate HMG-CoA (Leopoldini et al., 2010). The antioxidant property of bergamot also stimulates the growth of beneficial gut microbiota. Studies have provided preclinical proof of concept that induction of bergamot may improve the phenotypical and morphological features of NASH along with reduction in adipose tissue inflammation and inflammatory cytokines, IL-6 and TNFα, hypoadiponectinemia, insulin resistance and dyslipidemia (Musolino et al., 2020).

Epigallocatechin-3-gallate (EGCG) found in green tea is the most dominantly studied catechin. Although EGCG is known for its anti-cancer effects, studies have demonstrated a significant role in ameliorating diabetes. In the context of T2DM, EGCG promotes glucose homeostasis and inhibits lipogenesis and gluconeogenesis in the liver in murine models (Li et al., 2018). EGCG further attenuates the diabetic phenotype by improving the wound healing process through lowering of macrophage accumulation and inflammation (Zhang et al., 2018). When treated with EGCG, insulin resistance along with adipose differentiation is also lowered (Khan and Mukhtar, 2018). In the context of lipid metabolism, EGCG stimulates β-oxidation and lipolysis and downregulates lipogenic enzymes and lipid emulsification (Huang et al., 2014).

Carotenoids

Carotenoids are 40-carbon molecules found in red, yellow, and orange fruits and vegetables and are subdivided into carotenes and xanthophylls (Langi et al., 2018). Carotenes differ in structure from xanthophylls by the absence of oxygen groups, while xanthophylls may have multiple oxygen groups and are more soluble in water (Moran et al., 2018). The complexity of their actions on lipid membranes is due to its unique action of each carotenoid to various compositions of membranes (Johnson et al., 2018). In the small intestine, carotenoids are emulsified into micelles and their absorptions are facilitated by cell surface proteins (Bohn et al., 2017). After absorption, carotenoids are packaged into chylomicrons for transport to the liver and then released into blood. Carotenes are usually packaged into LDL, while xanthophylls are typically packaged into HDL (Wang et al., 2007). Both types of carotenoids are known for their functions in vision, but growing evidence suggests their anti-obesity activities (Coronel et al., 2019).

TABLE 1 | Summary of mechanistic action of antioxidants in ameliorating obesity phenotype and associated comorbidities.

Antioxidant	Source	Pathway/Mechanism	Anti-Obesity Phenotype and Related Comorbidities	References
Peroxiredoxin	Endogenous Enzyme	Inhibition of PPARγ and C/EBPα	↑Adiponectin ↑Insulin sensitivity ↓Adipogenesis ↓Protein carbonylation	(Huh et al., 2012; Mehmeti et al., 2014; Pacifici et al., 2014; Hammarstedt et al., 2018; Kim et al., 2018; Yamada and Guo, 2018; Lee et al., 2019; Kim et al., 2020)
		Phosphorylation of AMPK	↑Fatty acid oxidation ↓SREBP-1 ↓FAS ↓Lipid accumulation	
		Inhibition of IL-6, IL-10, and TNFα	↑Insulin secretion ↓Diabetes ↓Dyslipidemia	
N-Acetylcysteine	Over-the-counter oral supplement	Inhibition of PPARγ and C/EBPβ	↑Lipolysis ↓Adipogenesis ↓NAFLD/NASH	(Girouard et al., 2003; McKenna et al., 2006; Carlsen et al., 2009; Calzadilla et al., 2011; Haleagrahara et al., 2011; Schmitt et al., 2015; Ma et al., 2016; Pratt et al., 2019; Sun et al., 2019)
		Inhibition of NFkB	↑ Insulin sensitivity ↓ Inflammatory cascades	
		Promotes skeletal muscle Na^+/K^+ ATPase activity	↑ Motor activity	
		Activates cardiac Superoxide dismutase and glutathione	↑ Cardiac efficiency ↓ Cardiac fibrosis	
		Upregulates platelet glutathione and Nitric Oxide	↑ Vasodilation ↓ Thrombogenicity	
		Downregulates malic enzyme and fatty acid synthase	↓ Lipogenesis ↓ Cholesterologenesis	
		Destabilizes Von Willebrand Factor	↓ Thrombogenicity	
Vitamin E	Vegetable oils, wheatgerm, sunflower, soybean, walnut, over-the-counter oral supplement	Downregulates IL-6, TNF-α, malondialdehyde and c-reactive protein	↑ Insulin sensitivity ↓ Inflammatory cascades	(Boscoboinik et al., 1991; Cook-Mills, 2013; Alcala et al., 2015; Lin et al., 2016; Wong et al., 2017; Lee and Han, 2018)
		Inhibition of p38 MAPK pathways	↑ Insulin sensitivity ↑ Adipogenesis ↓ Inflammatory cascades ↓ Oxidative cascades ↓ Collagen deposition and fibrosis	
		Upregulates M2 macrophage phenotype	↓ Inflammatory response	
		Inhibition of PKC pathways	↓ Vascular disease ↓ Thrombogenicity ↓ Inflammatory cascades	
		Upregulates nitric oxide synthase and prostacyclins	↑ Vasodilation	
		Downregulates LDL, HDL and cholesterologenesis	↑Lipid Mobilization ↓ Vascular disease	

(Continued)

TABLE 1 | Continued

Antioxidant	Source	Pathway/Mechanism	Anti-Obesity Phenotype and Related Comorbidities	References
			↓ Hepatic steatosis	
		Downregulates ICAM-1 and VCAM-1	↓ Vascular disease ↓ Thrombogenicity	
		Downregulates Matrix Metalloproteinases	↑Adipocyte expansion ↑ Insulin sensitivity ↓ Inflammatory response	
Heme Oxygenase–1	Endogenous enzyme	Degrades free heme	↑ Liberation of CO and Biliverdin ↓ Inflammatory response ↓ Oxidative cascades	(Burgess et al., 2010; Gozzelino et al., 2010; Chan et al., 2011; Cao et al., 2012; Sodhi et al., 2015; Peterson et al., 2020)
		Inhibits MAPK, NF-kβ, PKC	↑ Vasodilation ↓ Inflammatory response ↓Adipogenesis ↓ Thrombogenicity	
		Upregulates ferritin synthesis	↓ Inflammatory response	
		Inhibition of PPARγ and C/EBPα	↑Lipolysis ↓Adipogenesis	
		Downregulates TNF-α, IL-1β, IL-2	↑ Insulin sensitivity ↓ Inflammatory response	
		Upregulates adiponectin	↑ Insulin sensitivity ↓ Inflammatory response ↓ Adipogenesis	
		Reduces oxidized LDL, VCAM-1, mast cell degranulation	↓ Vascular disease ↓ Inflammatory response	
		Upregulates AMPK cascades	↑Lipid Mobilization ↑ Insulin sensitivity ↓ Vascular disease ↓ Hepatic steatosis ↓ Lipogenesis	
		Activates soluble guanylyl cyclase	↑ Vasodilation ↓ Thrombogenicity	
Polyphenol	Cranberry, red wine, green tea, pomegranate extract, curcumin, bergamot	Deacetylation of PGC1α	↑Mitochondrial Biogenesis ↑Lipid Mobilization ↑Energy expenditure	(Lagouge et al., 2006; Houtkooper et al., 2012; Fraga et al., 2019; Springer and Moco, 2019)
		Inhibition of PPARγ and SIRT1	↑Lipolysis ↓Adipogenesis	
		Activation of Nuclear factor-erythroid 2-related factor-2 (Nrf2)	↑Superoxide dismutase ↓Body Mass Index ↓Blood pressure ↓Weight	

(Continued)

TABLE 1 | Continued

Antioxidant	Source	Pathway/Mechanism	Anti-Obesity Phenotype and Related Comorbidities	References
Carotenoids	Red, yellow, and orange fruits and vegetables	Inhibition of PPARγ Upregulates uncoupling protein-1 (UCP-1) and β3-adrenergic receptor (Adrb3)	↓Adipogenesis ↑Thermogenesis ↑Lipid Mobilization ↑Energy expenditure ↑Weight loss	(Schwarz et al., 1997; Maeda et al., 2005; Langi et al., 2018)
Superoxide Dismutase	Endogenous Enzyme	Inhibition of PPARγ, PPARα, FIAF Decreases levels of Carnitine Palmitoyl Transferase and Fatty Acid Synthase Inhibition of ERK1/2 and NF-κB	↑Lipolysis ↓Adipogenesis ↓ Lipogenesis ↓ Inflammatory cascades	(Hennig et al., 2006; Samuni et al., 2010; Perriotte-Olson et al., 2016)

This table summarizes the source of each antioxidant along with the mechanism that is modulated with the supplementation of each antioxidant. The mechanistic action of each antioxidant results in amelioration of obesity phenotype and characteristics associated with it. The green arrow (↑) represents upregulation and red arrow (↓) represents downregulation of phenotypical characteristics of obesity in response to antioxidants.

Studies have demonstrated the roles β-carotene play in adipose differentiation as a vitamin A precursor. β-carotene is cleaved by β-carotene oxygenase 1 (BCO1) into retinal and then rapidly metabolized to transcriptionally active retinoic acid, which is a type of vitamin A (von Lintig, 2012). In cell culture models, retinoic acid inhibits the expression of adipogenic transcription factors like PPARγ, leading to a decrease in adipogenesis (Schwarz et al., 1997). A rat study demonstrated that vitamin A reduce obesity, but only when supplemented to rats with mature adipocytes. When vitamin A was administrated in newborns, adipocyte proliferation was promoted, while supplementation to mature adipocyte led to loss of weight (Coronel et al., 2019). Relatedly, a human study with 29,000 participants revealed that elevated serum β-carotene levels are associated with lower cardiovascular and heart disease (Huang et al., 2018). Other human studies have demonstrated that higher β-carotene is associated with lower incidence of metabolic syndrome (Beydoun et al., 2019) and lower body weight (Berry et al., 2012) (PMID: 22396202). An analogous study showed that higher serum levels of β-carotene are related to lower BMI and subcutaneous adipose tissue in children (Canas et al., 2017).

Similar to carotenes, xanthophylls like fucoxanthin found in seaweed elicit physiological effects against the obesity phenotype and related diseases. Fucoxanthin is processed into fucoxanthinol in the gastrointestinal tract and then amarouciaxanthin A in the liver (Asai et al., 2004). The proportion of the metabolites of fucoxanthin differ in that more fucoxanthiol is found in the visceral organs like the lungs, heart, and kidneys, while amarouciaxanthin A is more preferentially found in adipose white tissue (Hashimoto et al., 2009). *In vivo* study with fucoxanthin and its metabolite's actions against the characteristics associated with obesity, demonstrated reduction of serum and hepatic levels of triglycerides and inflammatory cytokines like PGE_2, nitric oxide, IL-1, and TNF-α (Sakai et al., 2009; Hu et al., 2012). The study also demonstrated an increase in HDL levels, while LDL receptor levels decreased (Beppu et al., 2012). Furthermore, the administration of fucoxanthin led to decrease in both mRNA expression of fatty acid synthase and blood leptin levels (Beppu et al., 2013). Further studies have shown that fucoxanthin upregulates uncoupling protein-1 (UCP-1) in white adipose tissue and β3-adrenergic receptor (Adrb3), leading to increased thermogenesis, fatty acid oxidation, energy expenditure, and weight loss (Maeda et al., 2005). Fucoxanthinol and amarouciaxanthin accentuates these anti-obesity actions of fucoxanthin in later stages of adipocyte differentiation by suppressing PPARγ expression and glucose uptake (Kang et al., 2011).

Superoxide Dismutase

Various forms of mammalian SOD are characterized by where the enzyme is found and what metal it is catalyzed by. SOD1 and SOD3 are associated with copper and zinc, while SOD2 requires manganese (Zelko et al., 2002; Fukai and Ushio-Fukai, 2011). Despite the differing compartmentalization of each forms of SOD in the mitochondria, cytoplasm and extracellular matrix, they all share the function of neutralizing ROS (Miao and St Clair, 2009). Since all SODs are endogenous enzymes, SOD murine trials are conducted through mimetics like 4-Hydroxy-2,2,6,6-tetramethylpiperidine-N-oxyl (tempol), nanoformulated SOD (NanoSOD), and hydrodynamic injections of SOD3 plasmids. Although SODs are known for their essential role in handling oxidative stress, recent studies suggest a crucial role in ameliorating the obesity phenotype.

Mimetics of SOD have been shown to attenuate the obesity phenotype. Recent *in vivo* study demonstrated that mice supplemented with tempol in their diet weighed less than control mice (Samuni et al., 2010). In parallel, a recent study demonstrated that *in vivo* treatment of NanoSOD in high fat diet fed mice improved the levels of plasma triglyceride, liver triglyceride, and hepatic lipid accumulation (Perriotte-Olson et al., 2016). The anti-obesity effects of SOD were demonstrated

when mice received hydrodynamic injections of SOD3 plasmids (Cui et al., 2014). The mice induced with SOD3 showed improvement in body weight which was similar to mice fed a regular chow, as compared to high fat diet fed mice (Cui et al., 2014). Concomitantly, the administration of SOD3 led to smaller epididymal, inguinal, and perirenal white adipose tissues in comparison to the same diet without SOD3 (Cui et al., 2014). Furthermore, the study showed that mice fed a high fat diet with adenoviral SOD3 vectors had lower liver weight, levels of triglycerides, cholesterol by weight, and quantity of non-esterified fatty acids, compared to mice fed a high fat diet (Cui et al., 2014). The study provided a conclusive evidence that the induction of SOD3 improved glucose tolerance and insulin resistance in high fat diet fed mice (Cui et al., 2014).

Several studies have demonstrated that SOD analogs have anti-obesity effects in the molecular level by influencing metabolic pathways and related enzymes. In a cell culture of adipocytes, tempol lowered the cellular level of PPARγ and PPARα, and this led to the downregulation of fasting-induced adipose factor (FIAF) (Samuni et al., 2010). PPARγ and PPARα positively regulate FIAF in the liver and skeletal muscle during the fasted state and can lead to adipogenic outcomes (Dutton and Trayhurn, 2008). In a similar study, mice administered with NanoSOD had markedly decreased levels of fatty acid metabolic enzyme Carnitine Palmitoyl Transferase and a lipogenic *de novo* enzyme fatty acid synthase (Perriotte-Olson et al., 2016). This study also revealed the downregulation of the ERK1/2 signaling pathway by NanoSOD. The ERK1/2 pathway can lead to obesity-linked inflammation by the activation of NF-κB (Hennig et al., 2006). In conjunction, the levels of CPT1α, CPT1β, PGC1α, PGC1β, and UCP2, which are mRNA genes associated with energy expenditure and lipolysis, were higher when mice were given SOD3 (Cui et al., 2014).

Inflammation by itself or caused by excess macrophage is intricately linked with obesity, and the induction of SODs alleviates these outcomes. Studies have shown that mice fed a high fat diet and administered NanoSOD, showed improvement in obesity-related macrophage accumulation levels and inflammatory markers like TNFα, MCP1, and MMP12 improved (Perriotte-Olson et al., 2016). In a related study, mice that were fed a high fat diet had crown-like signs of macrophage infiltrations, while mice that were given a high fat diet and injected with SOD3 had minimal signs of infiltrate (Cui et al., 2014). Activated $F4/80^{+}$/$CD11c^{+}$ macrophages form these crown-like structures and leads to the remodeling and expansion of adipose tissue (Sun et al., 2011). The mRNA levels of obesity-related inflammation genes like F4/80, TNFα, CD11c, MCP1 and IL6 were lower in these SOD3-administered mice and hepatic *de novo* lipogenesis genes like SREBP1c, fatty acid synthase and Scd1 were higher in mice that were just given a high fat diet (Cui et al., 2014).

CONCLUSION

This review aims to highlight the therapeutic potential of seven antioxidants and their mechanistic actions in ameliorating the obese phenotype and associated comorbidities including cardiovascular diseases, NAFLD/NASH and T2DM. We demonstrate that obesity propagates cellular oxidative stress and the activation of a multitude of inflammatory signaling cascades that exacerbate the pathophysiological condition. Obesity mediated induction of oxidative stress promotes a shift from physiological homeostasis to favor physical profiles associated with metabolic syndrome. This shift leads to perturbations that include alterations within the phenotypic expression of adipocytes, cardiovascular damage, insulin resistance and abnormal accumulation of triglycerides playing key roles in the morbidity and mortality associated with obesity. Such pathological modifications promote disequilibrium within the redox state disturbing the functionality of antioxidant defense mechanisms. These alterations allow for the generation and sustained action of oxidative free radicals leading to cytotoxic, inflammatory, and apoptotic cascades to be continually initiated. The typical non-obese phenotype allows for scavenging of the oxidative radicals reducing the overall potential for damage. However, the loss of this defense contributes to developing the chronic inflammatory state associated with obesity. Therefore, the roles of various antioxidants were addressed for plausible therapeutic applications to improve clinical outcomes.

The contribution of antioxidants was investigated to determine their efficacy in attenuating the dysfunctional phenotype. Given the ease of availability of these antioxidants as dietary constituents and over-the-counter supplements enables individuals to reap the benefits at minimal cost. This offers an optimal potential therapy for the obese population to slow the development of the obese phenotype. Not surprisingly, the expression of these antioxidants seems to be reduced across *in vitro* or *in vivo* models and in obese individuals. This provides speculation that widespread oxidative free radicals may be a major contributor to the progression of the pathophysiology associated with obesity and the potential need for antioxidant supplementation in the obese population.

The actions of these antioxidants have a hallmark trait of being able to scavenge ROS reducing oxidative stress (**Figure 2**). Each individual antioxidant has its own characteristic mechanism to counteract the pathological environment based on their physical and chemical properties. For instance, the lipophilicity of αT and carotenoids enable them to elicit more beneficial effects within lipid membranes and lipoproteins compared to others. Some of these antioxidants were able to act through indirect and direct mechanisms allowing for the potential to act across various pathways such as HO-1, NAC, various polyphenols and carotenoids. Although there is a long list of endogenous and exogenous antioxidants that have been investigated previously to scavenge free radicals, however, the mechanistic action of each antioxidant is distinct in terms of the pathways they inhibit or stimulate. The specific properties of each antioxidant, listed in this review, provides insight into uncovering a link between which obesity induced metabolic dysfunction they are individually able to respond to optimally, hence these antioxidants were chosen for review. In the case of

hypertension, it could be argued that many of the antioxidants may serve a cardioprotective role that is equivalent to each other. However, for hypertension and hyperglycemic conditions one may benefit more from antioxidants that promote insulin sensitivity and lowered blood pressure such as HO-1. Furthermore, many of the antioxidants may serve a role working in concert with one another promoting a synergistic effect across multiple signaling and inflammatory cascades that may attenuate obese phenotypes more-so than one individual antioxidant.

Primarily, the mechanistic actions of each individual antioxidant favored normalization within the inflammatory responses encouraging the progression toward non-obese phenotypes. By acting through inflammatory cascades such as PKC and NF-kβ, these antioxidants serve to reduce the levels of various inflammatory mediators including TNF-α, IL-1 β, VCAM-1, and IL-6 (Carlsen et al., 2009; Kirmizis and Chatzidimitriou, 2009; Burgess et al., 2010; Rizvi et al., 2014; Lee and Han, 2018). Furthermore, antioxidants restore the shift in redox state during altered thermogenesis under diseased metabolic conditions (Wood Dos Santos et al., 2018). The antioxidants, like polyphenols and carotenoids, through induction of thermogenesis, improves the expression of thermogenic markers like UCP1, hence improving the overall mitochondrial function and redox imbalance (Wood Dos Santos et al., 2018). In addition, the activity of proliferative and differentiative cascades within adipocytes were improved leading to ameliorated expressions of PPARγ and C/EBPα (Schwarz et al., 1997; Calzadilla et al., 2011; Cao et al., 2012; Khitan et al., 2014; Springer and Moco, 2019). These effects resulted in a multitude of improvements including enhanced insulin sensitivity, adipocyte functionality, reduced circulating triglycerides, adipogenesis and fat mass (as summarized in **Table 1**). This infers that each antioxidant has the capability to attenuate the development and progression of associated comorbidities through their own mechanisms. Thus, indicating that there may be a strong relationship between antioxidant action and alleviating obesity induced oxidative damage and metabolic dysfunction. The various roles that antioxidants possess may provide a key to unlocking the optimal therapy for the pathophysiology of obesity. More research is required to determine the efficacy of antioxidants working in concert with one another and with current pharmacotherapy in preventing/reverting associated comorbidities of obesity.

AUTHOR CONTRIBUTIONS

Conceptualization: HL and KS. Validation: KS. Writing—original draft preparation: ST, CS, CC, AD, SP, and HC. Writing—review and editing: HL. Supervision: KS and JS. Project administration: KS. Funding: JS. All authors contributed to the article and approved the submitted version.

FUNDING

This research was supported by the BrickStreet Foundation and the Huntington Foundation. This research was also supported by National Institute of Health Grant R15 1R15HL150721 (to K.S.).

REFERENCES

Achari, A. E., and Jain, S. K. (2017). Adiponectin, a Therapeutic Target for Obesity,Diabetes, and Endothelial Dysfunction. *Int. J. Mol. Sci.* 18 (6). doi: 10.3390/ijms18061321

Achkasov, E. E., Razina, A. O., and Runenko, S. D. (2016). Pathogenetically targeted method for conservative treatment of obesity and overweight correction. *Klin. Med. (Mosk)* 94 (7), 509–517.

Aggarwal, B. B., Shishodia, S., Sandur, S. K., Pandey, M. K., and Sethi, G. (2006). Inflammation and cancer: how hot is thelink? *Biochem. Pharmacol.* 72 (11),1605–1621. doi: 10.1016/j.bcp.2006.06.029

Aggarwal, B. B. (2010). Targeting inflammation-induced obesity and metabolic diseases by curcumin and other nutraceuticals. *Annu. Rev. Nutr.* 30, 173–199. doi: 10.1146/annurev.nutr.012809.104755

Ahmad, A., Dempsey, S. K., Daneva, Z., Azam, M., Li, N., Li, P. L., et al. (2018). Role of Nitric Oxide in the Cardiovascular and Renal Systems. *Int. J. Mol. Sci.* 19 (9). doi: 10.3390/ijms19092605

Ahsan, H., Ahad, A., and Siddiqui, W. A. (2015). A review of characterization of tocotrienols from plant oils and foods. *J. Chem. Biol.* 8 (2), 45–59. doi: 10.1007/s12154-014-0127-8

Alcala, M., Sanchez-Vera, I., Sevillano, J., Herrero, L., Serra, D., Ramos, M. P., et al. (2015). Vitamin E reduces adipose tissue fibrosis, inflammation, and oxidative stress and improves metabolic profile in obesity. *Obes. (Silver Spring)* 23 (8), 1598–1606. doi: 10.1002/oby.21135

Allen, J., and Bradley, R. D. (2011). Effects of oral glutathione supplementation on systemic oxidative stress biomarkers in human volunteers. *J. Altern. Complement Med.* 17 (9), 827–833. doi: 10.1089/acm.2010.0716

Ammon, H. P., Muller, P. H., Eggstein, M., Wintermantel, C., Aigner, B., Safayhi, H., et al. (1992). Increase in glucose consumption by acetylcysteine during hyperglycemic clamp. A study with healthy volunteers. *Arzneimittelforschung* 42 (5), 642–645.

Anderson, J. A., and Weitz, J. I. (2010). Hypercoagulable states. *Clin. Chest Med.* 31 (4), 659–673. doi: 10.1016/j.ccm.2010.07.004

Anhe, F. F., Roy, D., Pilon, G., Dudonne, S., Matamoros, S., Varin, T. V., et al. (2015). A polyphenol-rich cranberry extract protectsfrom diet-induced obesity, insulin resistance and intestinal inflammation in association withincreased Akkermansia spp. population in the gut microbiota of mice. *Gut* 64 (6), 872–883. doi: 10.1136/gutjnl-2014-307142

Aprahamian, T. R., and Sam, F. (2011). Adiponectin in cardiovascular inflammation and obesity. *Int. J. Inflam.* 2011, 376909. doi: 10.4061/2011/376909

Araujo, J. A., Zhang, M., and Yin, F. (2012). Heme oxygenase-1, oxidation, inflammation, and atherosclerosis. *Front. Pharmacol.* 3, 119. doi: 10.3389/fphar.2012.00119

Asai, A., Sugawara, T., Ono, H., and Nagao, A. (2004). Biotransformation of fucoxanthinol into amarouciaxanthin A in mice and HepG2 cells: formation and cytotoxicity of fucoxanthin metabolites. *Drug Metab. Dispos.* 32 (2), 205–211. doi: 10.1124/dmd.32.2.205

Assari, S., and Bazargan, M. (2019). Baseline Obesity Increases 25-Year Risk of Mortality due to Cerebrovascular Disease: Role of Race. *Int. J. Environ. Res. Public Health* 16 (19). doi: 10.3390/ijerph16193705

Ayer, A., Zarjou, A., Agarwal, A., and Stocker, R. (2016). Heme Oxygenases in Cardiovascular Health and Disease. *Physiol. Rev.* 96 (4), 1449–1508. doi: 10.1152/physrev.00003.2016

Babu, P. S., and Srinivasan, K. (1997). Hypolipidemic action of curcumin, the active principle of turmeric (Curcuma longa) in streptozotocin induced diabetic rats. *Mol. Cell Biochem.* 166 (1-2), 169–175. doi: 10.1023/A:1006819605211

Balla, G., Jacob, H. S., Balla, J., Rosenberg, M., Nath, K., Apple, F., et al. (1992). Ferritin: a cytoprotective antioxidant strategem of endothelium. *J. Biol. Chem.* 267 (25), 18148–18153.

Baxter, L. L., Marugan, J. J., Xiao, J., Incao, A., McKew, J. C., Zheng, W., et al. (2012). Plasma and tissue concentrations of alpha-tocopherol and delta-tocopherol following high dose dietary supplementation in mice. *Nutrients* 4 (6), 467–490. doi: 10.3390/nu4060467

Beck, K., Wu, B. J., Ni, J., Santiago, F. S., Malabanan, K. P., Li, C., et al. (2010). Interplay between heme oxygenase-1 and the multifunctional transcription factor yin yang 1 in the inhibition of intimal hyperplasia. *Circ. Res.* 107 (12), 1490–1497. doi: 10.1161/CIRCRESAHA.110.231985

Beppu, F., Hosokawa, M., Niwano, Y., and Miyashita, K. (2012). Effects of dietary fucoxanthin on cholesterol metabolism in diabetic/obese KK-A(y) mice. *Lipids Health Dis.* 11, 112. doi: 10.1186/1476-511X-11-112

Beppu, F., Hosokawa, M., Yim, M. J., Shinoda, T., and Miyashita, K. (2013). Down-regulation of hepatic stearoyl-CoA desaturase-1 expression by fucoxanthin via leptin signaling in diabetic/obese KK-A(y) mice. *Lipids* 48 (5), 449–455. doi: 10.1007/s11745-013-3784-4

Bereczki, D.Jr., Balla, J., and Bereczki, D. (2018). Heme Oxygenase-1: Clinical Relevance in Ischemic Stroke. *Curr. Pharm. Des.* 24 (20), 2229–2235. doi: 10.2174/1381612824666180717101104

Berrington de Gonzalez, A., Hartge, P., Cerhan, J. R., Flint, A. J., Hannan, L., MacInnis, R. J., et al. (2010). Body-mass index and mortality among 1.46million white adults. *N. Engl. J. Med.* 363 (23), 2211–2219. doi: 10.1056/NEJMoa1000367

Berry, D. C., DeSantis, D., Soltanian, H., Croniger, C. M., and Noy, N. (2012). Retinoic acid upregulates preadipocyte genes to block adipogenesis and suppress diet-induced obesity. *Diabetes* 61 (5), 1112–1121. doi: 10.2337/db11-1620

Beydoun, M. A., Chen, X., Jha, K., Beydoun, H. A., Zonderman, A. B., Canas, J. A., et al. (2019). Carotenoids, vitamin A, and their association with the metabolic syndrome: a systematic review and meta-analysis. *Nutr. Rev.* 77 (1), 32–45. doi: 10.1093/nutrit/nuy044

Bhatti, J. S., Bhatti, G. K., and Reddy, P. H. (2017). Mitochondrial dysfunction and oxidative stress in metabolic disorders - A step towards mitochondria based therapeutic strategies. *Biochim. Biophys. Acta Mol. Basis Dis.* 1863 (5), 1066–1077. doi: 10.1016/j.bbadis.2016.11.010

Blokhin, I. O., and Lentz, S. R. (2013). Mechanisms of thrombosis in obesity. *Curr. Opin. Hematol.* 20 (5), 437–444. doi: 10.1097/MOH.0b013e3283634443

Bohn, T., Desmarchelier, C., Dragsted, L. O., Nielsen, C. S., Stahl, W., Ruhl, R., et al. (2017). Host-related factors explaining interindividual variability of carotenoid bioavailability and tissue concentrations in humans. *Mol. Nutr. Food Res.* 61 (6). doi: 10.1002/mnfr.201600685

Boscoboinik, D., Szewczyk, A., Hensey, C., and Azzi, A. (1991). Inhibition of cell proliferation by alpha-tocopherol. Role of protein kinase C. *J. Biol. Chem.* 266 (10), 6188–6194.

Burgess, A., Li, M., Vanella, L., Kim, D. H., Rezzani, R., Rodella, L., et al. (2010). Adipocyte heme oxygenase-1 induction attenuates metabolic syndrome in both male and female obese mice. *Hypertension* 56 (6), 1124–1130. doi: 10.1161/HYPERTENSIONAHA.110.151423

Burhans, M. S., Hagman, D. K., Kuzma, J. N., Schmidt, K. A., and Kratz, M. (2018). Contribution of Adipose Tissue Inflammation to the Development of Type 2 Diabetes Mellitus. *Compr. Physiol.* 9 (1), 1–58. doi: 10.1002/cphy.c170040

Calzadilla, P., Sapochnik, D., Cosentino, S., Diz, V., Dicelio, L., Calvo, J. C., et al. (2011). N-acetylcysteine reduces markers of differentiation in 3T3-L1 adipocytes. *Int. J. Mol. Sci.* 12 (10), 6936–6951. doi: 10.3390/ijms12106936

Canas, J. A., Lochrie, A., McGowan, A. G., Hossain, J., Schettino, C., and Balagopal, P. B. (2017). Effects of Mixed Carotenoids on Adipokines and Abdominal Adiposity in Children: A Pilot Study. *J. Clin. Endocrinol. Metab.* 102 (6), 1983–1990. doi: 10.1210/jc.2017-00185

Cao, J., Peterson, S. J., Sodhi, K., Vanella, L., Barbagallo, I., Rodella, L. F., et al. (2012). Heme oxygenase gene targeting to adipocytes attenuates adiposity and vascular dysfunction in mice fed a high-fat diet. *Hypertension* 60 (2), 467–475. doi: 10.1161/HYPERTENSIONAHA.112.193805

Carlsen, H., Haugen, F., Zadelaar, S., Kleemann, R., Kooistra, T., Drevon, C. A., et al. (2009). Diet-induced obesity increases NF-kappaB signaling in reporter mice. *Genes Nutr.* 4 (3), 215–222. doi: 10.1007/s12263-009-0133-6

Castro-Barquero, S., Lamuela-Raventos, R. M., Domenech, M., and Estruch, R. (2018). Relationship between Mediterranean Dietary Polyphenol Intake and Obesity. *Nutrients* 10 (10). doi: 10.3390/nu10101523

Chait, A., and den Hartigh, L. J. (2020). Adipose Tissue Distribution, Inflammation and Its Metabolic Consequences, Including Diabetes and Cardiovascular Disease. *Front. Cardiovasc. Med.* 7, 22. doi: 10.3389/fcvm.2020.00022

Chan, K. H., Ng, M. K., and Stocker, R. (2011). Haem oxygenase-1 and cardiovascular disease: mechanisms and therapeutic potential. *Clin. Sci. (Lond)* 120 (12), 493–504. doi: 10.1042/CS20100508

Chen, F., Hadfield, J. M., Berzingi, C., Hollander, J. M., Miller, D. B., Nichols, C. E., et al. (1985). N-acetylcysteine reverses cardiac myocytedysfunction in a rodent model of behavioral stress. *J. Appl. Physiol.* 2013. 115 (4), 514–524. doi: 10.1152/japplphysiol.01471.2012

Cheng, C., Noordeloos, A. M., Jeney, V., Soares, M. P., Moll, F., Pasterkamp, G., et al. (2009). Heme oxygenase 1 determines atherosclerotic lesion progression into a vulnerable plaque. *Circulation* 119 (23), 3017–3027. doi: 10.1161/CIRCULATIONAHA.108.808618

Chouchani, E. T., Kazak, L., and Spiegelman, B. M. (2017). Mitochondrial reactive oxygen species and adipose tissue thermogenesis: Bridging physiology and mechanisms. *J. Biol. Chem.* 292 (41), 16810–16816. doi: 10.1074/jbc.R117.789628

Colombo, M. L., and vitamin, E. (2010). tocopherol and tocotrienol-perspectives. *Molecules* 15 (4), 2103–2113. doi: 10.3390/molecules15042103

Cook-Mills, J. M., Abdala-Valencia, H., and Hartert, T. (2013). Two faces of vitamin E in the lung. *Am. J. Respir. Crit. Care Med.* 188 (3), 279–284. doi: 10.1164/rccm.201303-0503ED

Cook-Mills, J. M. (2013). Isoforms of Vitamin E Differentially Regulate PKC alpha and Inflammation: A Review. *J. Clin. Cell Immunol.* 4 (137). doi: 10.4172/2155-9899.1000137

Coronel, J., Pinos, I., and Amengual, J. (2019). beta-carotene in Obesity Research: Technical Considerations and Current Status of the Field. *Nutrients* 11 (4). doi: 10.3390/nu11040842

Craver, B. M., Ramanathan, G., Hoang, S., Chang, X., Mendez Luque, L. F., Brooks, S., et al. (2020). N-acetylcysteine inhibits thrombosis in a murine model of myeloproliferative neoplasm. *Blood Adv.* 4 (2), 312–321. doi: 10.1182/bloodadvances.2019000967

Cui, R., Gao, M., Qu, S., and Liu, D. (2014). Overexpression of superoxide dismutase 3 gene blocks high-fat diet-induced obesity, fatty liver and insulin resistance. *Gene Ther.* 21 (9), 840–848. doi: 10.1038/gt.2014.64

de Almeida, A., de Almeida Rezende, M. S., Dantas, S. H., de Lima Silva, S., de Oliveira, J., de Lourdes Assuncao Araujo de Azevedo, F., et al. (2020). Unveiling the Role of Inflammation and Oxidative Stress on Age-Related Cardiovascular Diseases. *Oxid. Med. Cell Longev.* 2020, 1954398. doi: 10.1155/2020/1954398

de Andrade, K. Q., Moura, F. A., dos Santos, J. M., de Araujo, O. R., de Farias Santos, J. C., Goulart, M. O., et al. (2015). Oxidative Stress and Inflammation in Hepatic Diseases: Therapeutic Possibilities of N-Acetylcysteine. *Int. J. Mol. Sci.* 16 (12), 30269–30308. doi: 10.3390/ijms161226225

de Mello, A. H., Costa, A. B., Engel, J. D. G., and Rezin, G. T. (2018). Mitochondrial dysfunction in obesity. *Life Sci.* 192, 26–32. doi: 10.1016/j.lfs.2017.11.019

Dela Cruz, C. S., and Kang, M. J. (2018). Mitochondrial dysfunction and damage associated molecular patterns (DAMPs) in chronic inflammatory diseases. *Mitochondrion* 41, 37–44. doi: 10.1016/j.mito.2017.12.001

Diniz, Y. S., Rocha, K. K., Souza, G. A., Galhardi, C. M., Ebaid, G. M., Rodrigues, H. G., et al. (2006). Effects of N-acetylcysteine on sucrose-rich diet-induced hyperglycaemia, dyslipidemia and oxidative stress in rats. *Eur. J. Pharmacol.* 543 (1-3), 151–157. doi: 10.1016/j.ejphar.2006.05.039

Dludla, P. V., Nkambule, B. B., Dias, S. C., and Johnson, R. (2017). Cardioprotective potential of N-acetyl cysteine against hyperglycaemia-induced oxidative damage: a protocol for a systematic review. *Syst. Rev.* 6 (1), 96. doi: 10.1186/s13643-017-0493-8

Donohoe, F., Wilkinson, M., Baxter, E., and Brennan, D. J. (2020). Mitogen-Activated Protein Kinase (MAPK) and Obesity-Related Cancer. *Int. J. Mol. Sci.* 21 (4). doi: 10.3390/ijms21041241

Durante, W. (2003). Heme oxygenase-1 in growth control and its clinical application to vascular disease. *J. Cell Physiol.* 195 (3), 373–382. doi: 10.1002/jcp.10274

Durante, W. (2011). Protective role of heme oxygenase-1 against inflammation in atherosclerosis. *Front. Biosci. (Landmark Ed)* 16, 2372–2388. doi: 10.2741/3860

Dutra, F. F., and Bozza, M. T. (2014). Heme on innate immunity and inflammation. *Front. Pharmacol.* 5:115. doi: 10.3389/fphar.2014.00115

Dutton, S., and Trayhurn, P. (2008). Regulation of angiopoietin-like protein 4/fasting-induced adipose factor (Angptl4/FIAF) expression in mouse white adipose tissue and 3T3-L1 adipocytes. *Br. J. Nutr.* 100 (1), 18–26. doi: 10.1017/S0007114507882961

Eder, K., Keller, U., and Brandsch, C. (2004). Effects of a dietary oxidized fat on cholesterol in plasma and lipoproteins and the susceptibility of low-density lipoproteins to lipid peroxidation in guinea pigs fed diets with different concentrations of vitamins E and C. *Int. J. Vitam Nutr. Res.* 74 (1), 11–20. doi: 10.1024/0300-9831.74.1.11

Engin, K. N. (2009). Alpha-tocopherol: looking beyond an antioxidant. *Mol. Vis.* 15, 855–860.

Fisher, A. B. (2018). The phospholipase A2 activity of peroxiredoxin 6. *J. Lipid Res.* 59 (7), 1132–1147. doi: 10.1194/jlr.R082578

Fonseca-Alaniz, M. H., et al. (2007). Adipose tissue as an endocrine organ: from theory to practice. *J. Pediatr. (Rio J)* 83 (5 Suppl), S192–S203. doi: 10.2223/JPED.1709

Fraga, C. G., Croft, K. D., Kennedye, D. O., and Tomás-Barberán, F. A. (2019). The effects of polyphenols and other bioactives on human health. *Food Funct.* 10 (2), 514–528. doi: 10.1039/C8FO01997E

Friedman, J. M., and Halaas, J. L. (1998). Leptin and the regulation of body weight inmammals. *Nature* 395 (6704), 763–770. doi: 10.1038/27376

Frismantiene, A., Philippova, M., Erne, P., and Resink, T. J. (2018). Smooth muscle cell-driven vascular diseases and molecular mechanisms of VSMC plasticity. *Cell Signal* 52, 48–64. doi: 10.1016/j.cellsig.2018.08.019

Fruh, S. M. (2017). Obesity: Risk factors, complications, and strategies for sustainable long-term weight management. *J. Am. Assoc. Nurse Pract.* 29 (S1), S3–S14. doi: 10.1002/2327-6924.12510

Fukai, T., and Ushio-Fukai, M. (2011). Superoxide dismutases: role in redox signaling, vascular function, and diseases. *Antioxid. Redox Signal* 15 (6), 1583–1606. doi: 10.1089/ars.2011.3999

Fulghesu, A. M., Ciampelli, M., Muzj, G., Belosi, C., Selvaggi, L., Ayala, G. F., et al. (2002). N-acetyl-cysteine treatment improves insulin sensitivity in women with polycystic ovary syndrome. *Fertil. Steril.* 77 (6), 1128–1135. doi: 10.1016/S0015-0282(02)03133-3

Furchgott, R. F., and Jothianandan, D. (1991). Endothelium-dependent and -independent vasodilation involving cyclic GMP: relaxation induced by nitric oxide, carbon monoxide and light. *Blood Vessels* 28 (1-3), 52–61. doi: 10.1159/000158843

Galiniak, S., Aebisher, D., and Bartusik-Aebisher, D. (2019). Health benefits of resveratrol administration. *Acta Biochim. Pol.* 66 (1), 13–21. doi: 10.18388/abp.2018_2749

Galmes, S., Serra, F., and Palou, A. (2018). Vitamin E Metabolic Effects and Genetic Variants: A Challenge for Precision Nutrition in Obesity and Associated Disturbances. *Nutrients* 10 (12). doi: 10.3390/nu10121919

Gibson, K. R., Winterburn, T. J., Barrett, F., Sharma, S., MacRury, S. M., and Megson, I. L. (2011). Therapeutic potential of N-acetylcysteine as an antiplatelet agent in patients with type-2 diabetes. *Cardiovasc. Diabetol.* 10, 43. doi: 10.1186/1475-2840-10-43

Girouard, H., Chulak, C., Wu, L., Lejossec, M., and de Champlain, J. (2003). N-acetylcysteine improves nitric oxide and alpha-adrenergic pathways in mesenteric beds of spontaneously hypertensive rats. *Am. J. Hypertens.* 16 (7), 577–584. doi: 10.1016/S0895-7061(03)00863-X

Gozzelino, R., Jeney, V., and Soares, M. P. (2010). Mechanisms of cell protection by heme oxygenase-1. *Annu. Rev. Pharmacol. Toxicol.* 50, 323–354. doi: 10.1146/annurev.pharmtox.010909.105600

Grigsby, R. J., and Dobrowsky, R. T. (2001). Inhibition of ceramide production reverses TNF-induced insulin resistance. *Biochem. Biophys. Res. Commun.* 287 (5), 1121–1124. doi: 10.1006/bbrc.2001.5694

Haczeyni, F., Bell-Anderson, K. S., and Farrell, G. C. (2018). Causes and mechanisms of adipocyte enlargement and adipose expansion. *Obes. Rev.* 19 (3), 406–420. doi: 10.1111/obr.12646

Haleagrahara, N., Julian, V., and Chakravarthi, S. (2011). N-acetylcysteine offers cardioprotection by decreasing cardiac lipid hydroperoxides and 8-isoprostane level in isoproterenol-induced cardiotoxicity in rats. *Cardiovasc. Toxicol.* 11 (4), 373–381. doi: 10.1007/s12012-011-9132-0

Hall, A., Karplus, P. A., and Poole, L. B. (2009). Typical 2-Cys peroxiredoxins–structures, mechanisms and functions. *FEBS J.* 276 (9), 2469–2477. doi: 10.1111/j.1742-4658.2009.06985.x

Hammarstedt, A., Gogg, S., Hedjazifar, S., Nerstedt, A., and Smith, U. (2018). Impaired Adipogenesis and Dysfunctional Adipose Tissue in Human Hypertrophic Obesity. *Physiol. Rev.* 98 (4), 1911–1941. doi: 10.1152/physrev.00034.2017

Hashimoto, T., Ozaki, Y., Taminato, M., Das, S. K., Mizuno, M., Yoshimura, K., et al. (2009). The distribution and accumulation of fucoxanthin and its metabolites after oral administration in mice. *Br. J. Nutr.* 102 (2), 242–248. doi: 10.1017/S0007114508199007

Heeba, G., Moselhy, M. E., Hassan, M., Khalifa, M., Gryglewski, R., and Malinski, T. (2009). Anti-atherogenic effect of statins: role of nitric oxide, peroxynitrite and haem oxygenase-1. *Br. J. Pharmacol.* 156 (8), 1256–1266. doi: 10.1111/j.1476-5381.2009.00125.x

Hennig, B., Lei, W., Arzuaga, X., Ghosh, D. D., Saraswathi, V., and Toborek, M. (2006). Linoleic acid induces proinflammatory events in vascular endothelial cells via activation of PI3K/Akt and ERK1/2 signaling. *J. Nutr. Biochem.* 17 (11), 766–772. doi: 10.1016/j.jnutbio.2006.01.005

Hernandez-Corbacho, M. J., Canals, D., Adada, M. M., Liu, M., Senkal, C. E., Yi, J. K., et al. (2015). Tumor Necrosis Factor-alpha (TNFalpha)-induced Ceramide Generation via Ceramide Synthases Regulates Loss of Focal Adhesion Kinase (FAK) and Programmed Cell Death. *J. Biol. Chem.* 290 (42), 25356–25373. doi: 10.1074/jbc.M115.658658

Hosick, P. A., and Stec, D. E. (2012). Heme oxygenase, a novel target for the treatmentof hypertension and obesity? *Am. J. Physiol. Regul. Integr. Comp. Physiol.* 302 (2), R207–R214. doi: 10.1152/ajpregu.00517.2011

Houtkooper, R. H., Pirinen, E., and Auwerx, J. (2012). Sirtuins as regulators of metabolism and healthspan. *Nat. Rev. Mol. Cell Biol.* 13 (4), 225–238. doi: 10.1038/nrm3293

Hruby, A., and Hu, F. B. (2015). The Epidemiology of Obesity: A Big Picture. *Pharmacoeconomics* 33 (7), 673–689. doi: 10.1007/s40273-014-0243-x

Hu, X., Li, Y., Li, C., Fu, Y., Cai, F., Chen, Q., et al. (2012). Combination of fucoxanthin and conjugated linoleic acid attenuates body weight gain and improves lipid metabolism in high-fat diet-induced obese rats. *Arch. Biochem. Biophys.* 519 (1), 59–65. doi: 10.1016/j.abb.2012.01.011

Huang, J., Wang, Y., Xie, Z., Zhou, Y., Zhang, Y., and Wan, X. (2014). The anti-obesity effects of green tea in human intervention and basic molecular studies. *Eur. J. Clin. Nutr.* 68 (10), 1075–1087. doi: 10.1038/ejcn.2014.143

Huang, J., Weinstein, S. J, Yu, K., Mannisto, S., and Albanes, D. (2018). Serum Beta Carotene and Overall and Cause-Specific Mortality. *Circ. Res.* 123 (12), 1339–1349. doi: 10.1161/CIRCRESAHA.118.313409

Huh, J. Y., Kim, Y., Jeong, J., Park, J., Kim, I., Huh, K. H., et al. (2012). Peroxiredoxin 3 is a key molecule regulating adipocyte oxidative stress, mitochondrial biogenesis, and adipokine expression. *Antioxid. Redox Signal* 16 (3), 229–243. doi: 10.1089/ars.2010.3766

Hwang, S. L., Jeong, Y. T., Li, X., Kim, Y. D., Lu, Y., Chang, Y. C., et al. (2013). Inhibitory cross-talk between the AMPK and ERK pathways mediates endoplasmic reticulum stress-induced insulin resistance in skeletal muscle. *Br. J. Pharmacol.* 169 (1), 69–81. doi: 10.1111/bph.12124

Ighodaro, O. M. (2018). Molecular pathways associated with oxidative stress in diabetes mellitus. *BioMed. Pharmacother.* 108, 656–662. doi: 10.1016/j.biopha.2018.09.058

Jaoude, J., and Koh, Y. (2016). Matrix metalloproteinases in exercise and obesity. *Vasc. Health Risk Manag.* 12, 287–295. doi: 10.2147/VHRM.S103877

Johnson, Q. R., Mostofian, B., Fuente Gomez, G., Smith, J. C., Cheng, X., Johnson, Q. R., et al. (2018). Effects of carotenoids on lipid bilayers. *Phys. Chem. Chem. Phys.* 20 (5), 3795–3804. doi: 10.1039/C7CP07126D

Kachur, S., Lavie, C. J., de Schutter, A., Milani, R. V., and Ventura, H. O. (2017). Obesity and cardiovasculardiseases. *Minerva Med.* 108 (3), 212–228. doi: 10.23736/S0026-4806.17.05022-4

Kang, S. I., Ko, H. C., Shin, H. S., Kim, H. M., Hong, Y. S., Lee, N. H., et al. (2011). Fucoxanthin exerts differing effects on 3T3-L1 cells according to differentiation stage and inhibits glucose uptake in mature adipocytes. *Biochem. Biophys. Res. Commun.* 409 (4), 769–774. doi: 10.1016/j.bbrc.2011.05.086

Kawanaka, M., Nishino, K., Nakamura, J., Suehiro, M., Goto, D., Urata, N., et al. (2013). Treatment of nonalcoholic steatohepatitis with vitamins E and C: a pilot study. *Hepat. Med.* 5, 11–16. doi: 10.2147/HMER.S41258

Kerksick, C., and Willoughby, D. (2005). The antioxidant role of glutathione and N-acetyl-cysteine supplements and exercise-induced oxidative stress. *J. Int. Soc. Sports Nutr.* 2, 38–44. doi: 10.1186/1550-2783-2-2-38

Khan, N., and Mukhtar, H. (2018). Tea Polyphenols in Promotion of Human Health. *Nutrients* 11 (1). doi: 10.3390/nu11010039

Khitan, Z., Harsh, M., Sodhi, K., Shapiro, J. I., and Abraham, N. G. (2014). HO-1 Upregulation Attenuates Adipocyte Dysfunction, Obesity, and Isoprostane Levels in Mice Fed High Fructose Diets. *J. Nutr. Metab.* 2014, 980547. doi: 10.1155/2014/980547

Kim, J. Y., van de Wall, E., Laplante, M., Azzara, A., Trujillo, M. E., Hofmann, S. M., et al. (2007). Obesity-associated improvements in metabolic profile through expansion of adipose tissue. *J. Clin. Invest.* 117 (9), 2621–2637. doi: 10.1172/JCI31021

Kim, D. H., Burgess, A. P., Li, M., Tsenovoy, P. L., Addabbo, F., McClung, J. A., et al. (2008). Heme oxygenase-mediated increases in adiponectin decrease fat content and inflammatory cytokines tumor necrosis factor-alpha and interleukin-6 in Zucker rats and reduce adipogenesis in human mesenchymal stem cells. *J. Pharmacol. Exp. Ther.* 325 (3), 833–840. doi: 10.1124/jpet.107.135285

Kim, M. H., Park, S. J., Kim, J. H., Seong, J. B., Kim, K. M., Woo, H. A., et al. (2018). Peroxiredoxin 5 regulates adipogenesis-attenuating oxidative stress in obese mouse models induced by a high-fat diet. *Free Radic. Biol. Med.* 123, 27–38. doi: 10.1016/j.freeradbiomed.2018.05.061

Kim, M. H., Seong, J. B., Huh, J. W., Bae, Y. C., Lee, H. S., Lee, D. S., et al. (2020). Peroxiredoxin 5 ameliorates obesity-induced non-alcoholic fatty liver disease through the regulation of oxidative stress and AMP-activated protein kinase signaling. *Redox Biol.* 28, 101315. doi: 10.1016/j.redox.2019.101315

Kirmizis, D., and Chatzidimitriou, D. (2009). Antiatherogenic effects of vitamin E: the search for the Holy Grail. *Vasc. Health Risk Manag.* 5, 767–774. doi: 10.2147/VHRM.S5532

Korou, L. M., Agrogiannis, G., Pantopoulou, A., Vlachos, I. S., Iliopoulos, D., Karatzas, T., et al. (2010). Comparative antilipidemic effect of N-acetylcysteine and sesame oil administration in diet-induced hypercholesterolemic mice. *Lipids Health Dis.* 9, 23. doi: 10.1186/1476-511X-9-23

Korou, L. M., Agrogiannis, G., Koros, C., Kitraki, E., Vlachos, I. S., Tzanetakou, I., et al. (2014). Impact of N-acetylcysteine and sesame oil on lipid metabolism and hypothalamic-pituitary-adrenal axis homeostasis in middle-aged hypercholesterolemic mice. *Sci. Rep.* 4, 6806. doi: 10.1038/srep06806

Kruger, A. L., Peterson, S. J., Schwartzman, M. L., Fusco, H., McClung, J. A., Weiss, M., et al. (2006). Up-regulation of heme oxygenase provides vascular protection in an animal model of diabetes through its antioxidant and antiapoptotic effects. *J. Pharmacol. Exp. Ther.* 319 (3), 1144–1152. doi: 10.1124/jpet.106.107482

Kuk, J. L., Ardern, C.II, Church, T. S., Sharma, A. M., Padwal, R., Sui, X., et al. (2011). Edmonton Obesity Staging System: association with weight history and mortality risk. *Appl. Physiol. Nutr. Metab.* 36 (4), 570–576. doi: 10.1139/h11-058

Kumar, S., and Bandyopadhyay, U. (2005). Free heme toxicity and its detoxification systems in human. *Toxicol. Lett.* 157 (3), 175–188. doi: 10.1016/j.toxlet.2005.03.004

Kuroda, M., and Sakaue, H. (2017). Adipocyte Death and Chronic Inflammation in Obesity. *J. Med. Invest.* 64 (3.4), 193–196. doi: 10.2152/jmi.64.193

Kuroda, J., Ago, T., Matsushima, S., Zhai, P., Schneider, M. D., and Sadoshima, J. (2010). NADPH oxidase 4 (Nox4) is a major source of oxidative stress in the failing heart. *Proc. Natl. Acad. Sci. U.S.A.* 107 (35), 15565–15570. doi: 10.1073/pnas.1002178107

Kuznetsov, N. S., Abulela, A. M., and Neskoromnyi, V. N. (1993). [The use of antioxidants (alpha-tocopherol acetate) in the treatment of diabetes mellitus]. *Probl. Endokrinol. (Mosk)* 39 (2), 9–11. doi: 10.14341/probl11942

Lagouge, M., Argmann, C., Gerhart-Hines, Z., Meziane, H., Lerin, C., Daussin, F., et al. (2006). Resveratrol improves mitochondrial function and protects against metabolic disease by activating SIRT1 and PGC-1alpha. *Cell* 127 (6), 1109–1122. doi: 10.1016/j.cell.2006.11.013

Lakhani, H. V., Sharma, D., Dodrill, M. W., Nawab, A., Sharma, N., Cottrill, C. L., et al. (2018). Phenotypic Alteration of Hepatocytes in Non-Alcoholic Fatty Liver Disease. *Int. J. Med. Sci.* 15 (14), 1591–1599. doi: 10.7150/ijms.27953

Langi, P., Kiokias, S., Varzakas, T., and Proestos, C. (2018). Carotenoids: From Plants to Food and Feed Industries. *Methods Mol. Biol.* 1852, 57–71. doi: 10.1007/978-1-4939-8742-9_3

Lasram, M. M., Dhouib, I. B., Annabi, A., El Fazaa, S., and Gharbi, N. (2015). A review on the possible molecular mechanism of action of N-acetylcysteine against insulin resistance and type-2 diabetes development. *Clin. Biochem.* 48 (16-17), 1200–1208. doi: 10.1016/j.clinbiochem.2015.04.017

Lauby-Secretan, B., Dossus, L., Marant-Micallef, C., and His, M. (2019). [Obesity and Cancer]. *Bull. Cancer* 106 (7-8), 635–646. doi: 10.1016/j.bulcan.2019.04.008

Lauhio, A., Farkkila, E., Pietilainen, K. H., Astrom, P., Winkelmann, A., Tervahartiala, T., et al. (2016). Association of MMP-8 with obesity, smoking and insulin resistance. *Eur. J. Clin. Invest.* 46 (9), 757–765. doi: 10.1111/eci.12649

Lee, G. Y., and Han, S. N. (2018). The Role of Vitamin E in Immunity. *Nutrients* 10 (11). doi: 10.3390/nu10111614

Lee, I. K., Koya, D., Ishi, H., Kanoh, H., and King, G. L. (1999). d-Alpha-tocopherol prevents the hyperglycemia induced activation of diacylglycerol (DAG)-protein kinase C (PKC) pathway in vascular smooth muscle cell by an increase of DAG kinase activity. *Diabetes Res. Clin. Pract.* 45 (2-3), 183–190. doi: 10.1016/S0168-8227(99)00048-0

Lee, H., Lee, Y. J., Choi, H., Ko, E. H., and Kim, J. W. (2009). Reactive oxygen species facilitate adipocyte differentiation by accelerating mitotic clonal expansion. *J. Biol. Chem.* 284 (16), 10601–10609. doi: 10.1074/jbc.M808742200

Lee, M. J., Wu, Y., and Fried, S. K. (2010). Adipose tissue remodeling in pathophysiology of obesity. *Curr. Opin. Clin. Nutr. Metab. Care* 13 (4), 371–376. doi: 10.1097/MCO.0b013e32833aabef

Lee, D. H., Jung, Y. Y., Park, M. H., Jo, M. R., Han, S. B., Yoon, D. Y., et al. (2019). Peroxiredoxin 6 Confers Protection Against Nonalcoholic Fatty Liver Disease Through Maintaining Mitochondrial Function. *Antioxid. Redox Signal* 31 (5), 387–402. doi: 10.1089/ars.2018.7544

Lenoir, O., Gaillard, F., Lazareth, H., Robin, B., and Tharaux, P. L. (2017). Hmox1 Deficiency Sensitizes Mice to Peroxynitrite Formation and Diabetic Glomerular Microvascular Injuries. *J. Diabetes Res.* 2017, 9603924. doi: 10.1155/2017/9603924

Leopoldini, M., Malaj, N., Toscano, M., Sindona, G., and Russo, N. (2010). On the inhibitor effects of bergamot juice flavonoids binding to the 3-hydroxy-3-methylglutaryl-CoA reductase (HMGR) enzyme. *J. Agric. Food Chem.* 58 (19), 10768–10773. doi: 10.1021/jf102576j

Lettieri-Barbato, D. (2019). Redox control of non-shivering thermogenesis. *Mol. Metab.* 25, 11–19. doi: 10.1016/j.molmet.2019.04.002

Lewis, E. D., Meydani, S. N., and Wu, D. (2019). Regulatory role of vitamin E in the immune system and inflammation. *IUBMB Life* 71 (4), 487–494. doi: 10.1002/iub.1976

Li, M., Kim, D. H., Tsenovoy, P. L., Peterson, S. J., Rezzani, R., Rodella, L. F., et al. (2008). Treatment of obese diabetic mice with a heme oxygenase inducer reduces visceral and subcutaneous adiposity, increases adiponectin levels, and improves insulin sensitivity and glucose tolerance. *Diabetes* 57 (6), 1526–1535. doi: 10.2337/db07-1764

Li, X., Li, S., Chen, M., Wang, J., Xie, B., and Sun, Z. (2018). (-)-Epigallocatechin-3-gallate (EGCG) inhibits starch digestion and improves glucose homeostasis through direct or indirect activation of PXR/CAR-mediated phase II metabolism in diabetic mice. *Food Funct.* 9 (9), 4651–4663. doi: 10.1039/C8FO01293H

Libby, P. (2006). Inflammation and cardiovascular disease mechanisms. *Am. J. Clin. Nutr.* 83 (2), 456S–460S. doi: 10.1093/ajcn/83.2.456S

Lin, C. C., and Yin, M. C. (2008). Effects of cysteine-containing compounds on biosynthesis of triacylglycerol and cholesterol and anti-oxidative protection in liver from mice consuming a high-fat diet. *Br. J. Nutr.* 99 (1), 37–43. doi: 10.1017/S0007114507793881

Lin, T. H., Chun,, and Kang, L. (2016). Adipose extracellular matrix remodelling in obesity and insulin resistance. *Biochem. Pharmacol.* 119, 8–16. doi: 10.1016/j.bcp.2016.05.005

Lira, F. S., Rosa, J. C., Cunha, C. A., Ribeiro, E. B., do Nascimento, C. O., Oyama, L. M., et al. (2011). Supplementing alpha-tocopherol (vitamin E) and vitamin D3 in high fat diet decrease IL-6 production in murine epididymal adipose tissue and 3T3-L1 adipocytes following LPS stimulation. *Lipids Health Dis.* 10, 37. doi: 10.1186/1476-511X-10-37

Lone, J., Choi, J. H., Kim, S. W., and Yun, J. W. (2016). Curcumin induces brown fat-like phenotype in 3T3-L1 and primary white adipocytes. *J. Nutr. Biochem.* 27, 193–202. doi: 10.1016/j.jnutbio.2015.09.006

Ma, Y., Gao, M., and Liu, D. (2016). N-acetylcysteine Protects Mice from High Fat Diet-induced Metabolic Disorders. *Pharm. Res.* 33 (8), 2033–2042. doi: 10.1007/s11095-016-1941-1

Maeda, H., Hosokawa, M., Sashima, T., Funayama, K., and Miyashita, K. (2005). Fucoxanthin from edible seaweed, Undaria pinnatifida, shows antiobesity effect

through UCP1 expression in white adipose tissues. *Biochem. Biophys. Res. Commun.* 332 (2), 392–397. doi: 10.1016/j.bbrc.2005.05.002

Makhoul, Z., Kristal, A. R., Gulati, R., Luick, B., Bersamin, A., O'Brien, D., et al. (2011). Associations of obesity with triglycerides and C-reactive protein are attenuated in adults with high red blood cell eicosapentaenoic and docosahexaenoic acids. *Eur. J. Clin. Nutr.* 65 (7), 808–817. doi: 10.1038/ejcn.2011.39

Manna, P., and Jain, S. K. (2015). Obesity, Oxidative Stress, Adipose Tissue Dysfunction, and the Associated Health Risks: Causes and Therapeutic Strategies. *Metab. Syndr. Relat. Disord.* 13 (10), 423–444. doi: 10.1089/met.2015.0095

Martinez de Lizarrondo, S., Gakuba, C., Herbig, B. A., Repesse, Y., Ali, C., Denis, C. V., et al. (2017). Potent Thrombolytic Effect of N-Acetylcysteine on Arterial Thrombi. *Circulation* 136 (7), 646–660. doi: 10.1161/CIRCULATIONAHA.117.027290

Martin-Nizard, F., Boullier, A., Fruchart, J. C., and Duriez P. (1998). Alpha-tocopherol but not beta-tocopherol inhibits thrombin-induced PKC activation and endothelin secretion in endothelial cells. *J. Cardiovasc. Risk* 5 (5-6), 339–345. doi: 10.1177/174182679800500510

McKenna, M. J., Medved, I., Goodman, C. A., Brown, M. J., Bjorksten, A. R., Murphy, K. T., et al. (2006). N-acetylcysteine attenuates the decline in muscle Na+,K+-pump activity and delays fatigue during prolonged exercise in humans. *J. Physiol.* 576 (Pt 1), 279–288. doi: 10.1113/jphysiol.2006.115352

McMurray, F., Patten, D. A., and Harper, M. E. (2016). Reactive Oxygen Species and Oxidative Stress in Obesity-Recent Findings and Empirical Approaches. *Obes. (Silver Spring)* 24 (11), 2301–2310. doi: 10.1002/oby.21654

Mehmeti, I., Lortz, S., Elsner, M., and Lenzen, S. (2014). Peroxiredoxin 4 improves insulin biosynthesis and glucose-induced insulin secretion in insulin-secreting INS-1E cells. *J. Biol. Chem.* 289 (39), 26904–26913. doi: 10.1074/jbc.M114.568329

Mehmetoglu, I., Yerlikaya, F. H., and Kurban, S. (2011). Correlation between vitamin A, E, coenzyme Q(10) and degree of insulin resistance in obese and non-obese subjects. *J. Clin. Biochem. Nutr.* 49 (3), 159–163. doi: 10.3164/jcbn.11-08

Miao, L., and St Clair, D. K. (2009). Regulation of superoxide dismutase genes: implications in disease. *Free Radic. Biol. Med.* 47 (4), 344–356. doi: 10.1016/j.freeradbiomed.2009.05.018

Mittendorfer, B., Magkos, F., Fabbrini, E., Mohammed, B. S., and Klein, S. (2009). Relationship between body fat mass and free fatty acid kinetics in men and women. *Obes. (Silver Spring)* 17 (10), 1872–1877. doi: 10.1038/oby.2009.224

Mohammed, M. S., Sendra, S., Lloret, J., and Bosch, I. (2018). Systems and WBANs for Controlling Obesity. *J. Healthc. Eng.* 2018, 1564748. doi: 10.1155/2018/1564748

Mokhtari, V., Afsharian, P., Shahhoseini, M., Kalantar, S. M., and Moini, A. (2017). A Review on Various Uses of N-Acetyl Cysteine. *Cell J.* 19 (1), 11–17. doi: 10.22074/cellj.2016.4872

Moncada, S., and Vane, J. R. (1979). The role of prostacyclin in vascular tissue. *Fed. Proc.* 38 (1), 66–71.

Montonen, J., Knekt, P., Jarvinen, R., and Reunanen, A. (2004). Dietary antioxidant intake and risk of type 2 diabetes. *Diabetes Care* 27 (2), 362–366. doi: 10.2337/diacare.27.2.362

Moran, N. E., Mohn, E. S., Hason, N., Erdman, J. W.Jr., and Johnson, E. J. (2018). Intrinsic and Extrinsic Factors Impacting Absorption, Metabolism, and Health Effects of Dietary Carotenoids. *Adv. Nutr.* 9 (4), 465–492. doi: 10.1093/advances/nmy025

Munzel, T., Camici, G. G., Maack, C., Bonetti, N. R., Fuster, V., and Kovacic, J. C. (2017). Impact of Oxidative Stress on the Heart and Vasculature: Part 2 of a 3-Part Series. *J. Am. Coll. Cardiol.* 70 (2), 212–229. doi: 10.1016/j.jacc.2017.05.035

Murer, S. B., Aeberli, I., Braegger, C. P., Gittermann, M., Hersberger, M., Leonard, S. W., et al. (2014). Antioxidant supplements reduced oxidative stress and stabilized liver function tests but did not reduce inflammation in a randomized controlled trial in obese children and adolescents. *J. Nutr.* 144 (2), 193–201. doi: 10.3945/jn.113.185561

Musolino, V., Gliozzi, M., Nucera, S., Carresi, C., Maiuolo, J., Mollace, R., et al. (2019). The effect of bergamot polyphenolic fraction on lipid transfer protein system and vascular oxidative stress in a rat model of hyperlipemia. *Lipids Health Dis.* 18 (1), 115. doi: 10.1186/s12944-019-1061-0

Musolino, V., Gliozzi, M., Scarano, F., Bosco, F., Scicchitano, M., Nucera, S., et al. (2020). Bergamot Polyphenols Improve Dyslipidemia and Pathophysiological Features in a Mouse Model of Non-Alcoholic Fatty Liver Disease. *Sci. Rep.* 10 (1), 2565. doi: 10.1038/s41598-020-59485-3

Nakashima, Y., Raines, E. W., Plump, A. S., Breslow, J. L., and Ross, R. (1998). Upregulation of VCAM-1 and ICAM-1 at atherosclerosis-prone sites on the endothelium in the ApoE-deficient mouse. *Arterioscler. Thromb. Vasc. Biol.* 18 (5), 842–851. doi: 10.1161/01.ATV.18.5.842

Nath, K. A. (2006). Heme oxygenase-1: a provenance for cytoprotective pathways in the kidney and other tissues. *Kidney Int.* 70 (3), 432–443. doi: 10.1038/sj.ki.5001565

Niki, E. (2015). Evidence for beneficial effects of vitamin E. *Korean J. Intern Med.* 30 (5), 571–579. doi: 10.3904/kjim.2015.30.5.571

Ollinger, R., Bilban, M., Erat, A., Froio, A., McDaid, J., Tyagi, S., et al. (2005). Bilirubin: a natural inhibitor of vascular smooth muscle cell proliferation. *Circulation* 112 (7), 1030–1039. doi: 10.1161/CIRCULATIONAHA.104.528802

Oyewole, A. O., and Birch-Machin, M. A. (2015). Mitochondria-targeted antioxidants. *FASEB J.* 29 (12), 4766–4771. doi: 10.1096/fj.15-275404

Pacifici, F., Arriga, R., Sorice, G. P., Capuani, B., Scioli, M. G., Pastore, D., et al. (2014). Peroxiredoxin 6, a novel player in the pathogenesis of diabetes. *Diabetes* 63 (10), 3210–3220. doi: 10.2337/db14-0144

Pae, H. O., and Chung, H. T. (2009). Heme oxygenase-1: its therapeutic roles in inflammatory diseases. *Immune Netw.* 9 (1), 12–19. doi: 10.4110/in.2009.9.1.12

Pae, H. O., Oh, G. S., Choi, B. M., Chae, S. C., Kim, Y. M., Chung, K. R., et al. (2004). Carbon monoxide produced by heme oxygenase-1 suppresses T cell proliferation via inhibition of IL-2 production. *J. Immunol.* 172 (8), 4744–4751. doi: 10.4049/jimmunol.172.8.4744

Paine, A., Eiz-Vesper, B., Blasczyk, R., and Immenschuh, S. (2010). Signaling to heme oxygenase-1 and its anti-inflammatory therapeutic potential. *Biochem. Pharmacol.* 80 (12), 1895–1903. doi: 10.1016/j.bcp.2010.07.014

Patrick, L., and Uzick, M. (2001). Cardiovascular disease: C-reactive protein and the inflammatory disease paradigm: HMG-CoA reductase inhibitors, alpha-tocopherol, red yeast rice, and olive oil polyphenols. *A. Rev. Literature Altern. Med. Rev.* 6 (3), 248–271.

Perkins, A., Nelson, K. J., Parsonage, D., Poole, L. B., and Karplus, P. A. (2015). Peroxiredoxins: guardians against oxidative stress and modulators of peroxide signaling. *Trends Biochem. Sci.* 40 (8), 435–445. doi: 10.1016/j.tibs.2015.05.001

Perriotte-Olson, C., Adi, N., Manickam, D. S., Westwood, R. A., Desouza, C. V., Natarajan, G., et al. (2016). Nanoformulated copper/zinc superoxide dismutase reduces adipose inflammation in obesity. *Obes. (Silver Spring)* 24 (1), 148–156. doi: 10.1002/oby.21348

Peterson, S. J., Rubinstein, R., Faroqui, M., Raza, A., Boumaza, I., Zhang, Y., et al. (2019). Positive Effects of Heme Oxygenase Upregulation on Adiposity and Vascular Dysfunction: Gene Targeting vs. Pharmacologic Therapy. *Int. J. Mol. Sci.* 20 (10). doi: 10.3390/ijms20102514

Peterson, S. J., Dave, N., and Kothari, J. (2020). The Effects of Heme Oxygenase Upregulation on Obesity and the Metabolic Syndrome. *Antioxid. Redox Signal* 32 (14), 1061–1070. doi: 10.1089/ars.2019.7954

Poss, K. D., and Tonegawa, S. (1997). Heme oxygenase 1 is required for mammalian iron reutilization. *Proc. Natl. Acad. Sci. U.S.A.* 94 (20), 10919–10924. doi: 10.1073/pnas.94.20.10919

Pratt, R., Lakhani, H. V., Zehra, M., Desauguste, R., Pillai, S. S., and Sodhi, K. (2019). Mechanistic Insight of Na/K-ATPase Signaling and HO-1 into Models of Obesity and Nonalcoholic Steatohepatitis. *Int. J. Mol. Sci.* 21 (1). doi: 10.3390/ijms21010087

Randle, P. J., Garland, P. B., Newsholme, E. A., and Hales, C. N. (1965). The glucose fatty acid cycle in obesity and maturity onset diabetes mellitus. *Ann. N. Y. Acad. Sci.* 131 (1), 324–333. doi: 10.1111/j.1749-6632.1965.tb34800.x

Rao, D. S., Sekhara, N. C., Satyanarayana, M. N., and Srinivasan, M. (1970). Effect of curcumin on serum and liver cholesterol levels in the rat. *J. Nutr.* 100 (11), 1307–1315. doi: 10.1093/jn/100.11.1307

Ray, I., Mahata, S. K., and De, R. K. (2016). Obesity: An Immunometabolic Perspective. *Front. Endocrinol. (Lausanne)* 7:157. doi: 10.3389/fendo.2016.00157

Rhee, S. G., Woo, H. A., Kil, I. S., and Bae, S. H. (2012). Peroxiredoxin functions as a peroxidase and a regulator and sensor of local peroxides. *J. Biol. Chem.* 287 (7), 4403–4410. doi: 10.1074/jbc.R111.283432

Rhee, S. G. (2016). Overview on Peroxiredoxin. *Mol. Cells* 39 (1), 1–5. doi: 10.14348/molcells.2016.2368

Richie, J. P. Jr., Nichenametla, S., Neidig, W., Calcagnotto, A., Haley, J. S., Schell, T. D., et al. (2015). Randomized controlled trial of oral glutathione supplementation on body stores of glutathione. *Eur. J. Nutr.* 54 (2), 251–263. doi: 10.1007/s00394-014-0706-z

Rizvi, S., Raza, S. T., Ahmed, F., Ahmad, A., Abbas, S., and Mahdi, F. (2014). The role of vitamin e in human health and some diseases. *Sultan Qaboos Univ. Med. J.* 14 (2), e157–e165.

Rodriguez-Cuenca, S., Cocheme, H. M., Logan, A., Abakumova, I., Prime, T. A., Rose, C., et al. (2010). Consequences of long-term oral administration of the mitochondria-targeted antioxidant MitoQ to wild-type mice. *Free Radic. Biol. Med.* 48 (1), 161–172. doi: 10.1016/j.freeradbiomed.2009.10.039

Sakai, S., Sugawara, T., Matsubara, K., and Hirata, T. (2009). Inhibitory effect of carotenoids on the degranulation of mast cells via suppression of antigen-induced aggregation of high affinity IgE receptors. *J. Biol. Chem.* 284 (41), 28172–28179. doi: 10.1074/jbc.M109.001099

Samuni, Y., Cook, J. A., Choudhuri, R., Degraff, W., Sowers, A. L., Krishna, M. C., et al. (2010). Inhibition of adipogenesis by Tempol in 3T3-L1 cells. *Free Radic. Biol. Med.* 49 (4), 667–673. doi: 10.1016/j.freeradbiomed.2010.05.028

Samuni, Y., Goldstein, S., Dean, O. M., and Berk, M. (2013). The chemistry and biological activities of N-acetylcysteine. *Biochim. Biophys. Acta* 1830 (8), 4117–4129. doi: 10.1016/j.bbagen.2013.04.016

Schett, G., Zwerina, J., and Firestein, G. (2008). The p38 mitogen-activated protein kinase (MAPK) pathway in rheumatoid arthritis. *Ann. Rheum. Dis.* 67 (7), 909–916. doi: 10.1136/ard.2007.074278

Schmitt, B., Vicenzi, M., Garrel, C., and Denis, F. M. (2015). Effects of N-acetylcysteine, oral glutathione (GSH) and a novel sublingual form of GSH on oxidative stress markers: A comparative crossover study. *Redox Biol.* 6, 198–205. doi: 10.1016/j.redox.2015.07.012

Schugar, R. C., Shih, D. M., Warrier, M., Helsley, R. N., Burrows, A., Ferguson, D., et al. (2017). The TMAO-Producing Enzyme Flavin-Containing Monooxygenase 3 Regulates Obesity and the Beiging of White Adipose Tissue. *Cell Rep.* 19 (12), 2451–2461. doi: 10.1016/j.celrep.2017.05.077

Schwarz, E. J., Reginato, M. J., Shao, D., Krakow, S. L., and Lazar, M. A. (1997). Retinoic acid blocks adipogenesis by inhibiting C/EBPbeta-mediated transcription. *Mol. Cell Biol.* 17 (3), 1552–1561. doi: 10.1128/MCB.17.3.1552

Seddon, M., Looi, Y. H., and Shah, A. M. (2007). Oxidative stress and redox signalling in cardiac hypertrophy and heart failure. *Heart* 93 (8), 903–907. doi: 10.1136/hrt.2005.068270

Shen, F. C., Weng, S. W., Tsao, C. F., Lin, H. Y., Chang, C. S., Lin, C. Y., et al. (2018). Early intervention of N-acetylcysteine better improves insulin resistance in diet-induced obesity mice. *Free Radic. Res.* 52 (11-12), 1296–1310. doi: 10.1080/10715762.2018.1447670

Siersbaek, R., Nielsen, R., and Mandrup, S. (2010). PPARgamma in adipocyte differentiation and metabolism–novel insights from genome-wide studies. *FEBS Lett.* 584 (15), 3242–3249. doi: 10.1016/j.febslet.2010.06.010

Singh, S., and Aggarwal, B. B. (1995). Activation of transcription factor NF-kappa B is suppressed by curcumin (diferuloylmethane) [corrected]. *J. Biol. Chem.* 270 (42), 24995–25000. doi: 10.1074/jbc.270.42.24995

Sirico, F., Bianco, A., D'Alicandro, G., Castaldo, C., Montagnani, S., Spera, R., et al. (2018). Effects of Physical Exercise on Adiponectin, Leptin, and Inflammatory Markers in Childhood Obesity: Systematic Review and Meta-Analysis. *Child Obes.* 14 (4), 207–217. doi: 10.1089/chi.2017.0269

Smith, B. K., Marcinko, K., Desjardins, E. M., Lally, J. S., Ford, R. J., and Steinberg, G. R. (2016). Treatment of nonalcoholic fatty liver disease: role of AMPK. *Am. J. Physiol. Endocrinol. Metab.* 311 (4), E730–E740. doi: 10.1152/ajpendo.00225.2016

Soderberg, S., Ahren, B., Jansson, J. H., Johnson, O., Hallmans, G., Asplund, K., et al. (1999). Leptin is associated with increased risk of myocardial infarction. *J. Intern Med.* 246 (4), 409–418. doi: 10.1046/j.1365-2796.1999.00571.x

Sodhi, K., Maxwell, K., Yan, Y., Liu, J., Chaudhry, M. A., Getty, M., et al. (2015). pNaKtide inhibits Na/K-ATPase reactive oxygen species amplification and attenuates adipogenesis. *Sci. Adv.* 1 (9), e1500781.

Sodhi, K., Puri, N., Favero, G., Stevens, S., Meadows, C., Abraham, N. G., et al. (2015). Fructose Mediated Non-Alcoholic Fatty Liver Is Attenuated by HO-1-SIRT1 Module in Murine Hepatocytes and Mice Fed a High Fructose Diet. *PloS One* 10 (6), e0128648. doi: 10.1371/journal.pone.0128648

Sorrenti, V., Randazzo, C. L., Caggia, C., Ballistreri, G., Romeo, F. V., Fabroni, S., et al. (2019). Beneficial Effects of Pomegranate Peel Extract and Probiotics on Pre-adipocyte Differentiation. *Front. Microbiol.* 10:660. doi: 10.3389/fmicb.2019.00660

Sparkenbaugh, E. M., Chantrathammachart, P., Wang, S., Jonas, W., Kirchhofer, D., Gailani, D., et al. (2015). Excess of heme induces tissue factor-dependent activation of coagulation in mice. *Haematologica* 100 (3), 308–314. doi: 10.3324/haematol.2014.114728

Springer, M., and Moco, S. (2019). Resveratrol and Its Human Metabolites-Effects on Metabolic Health and Obesity. *Nutrients* 11 (1). doi: 10.3390/nu11010143

Srikanthan, K., Feyh, A., Visweshwar, H., Shapiro, J.II, and Sodhi, K. (2016). Systematic Review of Metabolic Syndrome Biomarkers: A Panel for Early Detection, Management, and Risk Stratification in the West Virginian Population. *Int. J. Med. Sci.* 13 (1), 25–38. doi: 10.7150/ijms.13800

Stolarczyk, E. (2017). Adipose tissue inflammation in obesity: a metabolic or immune response? *Curr. Opin. Pharmacol.* 37, 35–40. doi: 10.1016/j.coph.2017.08.006

Straub, L. G., Efthymiou, V., Grandl, G., Balaz, M., Challa, T. D., Truscello, L., et al. (2019). Antioxidants protect against diabetes by improving glucose homeostasis in mouse models of inducible insulin resistance and obesity. *Diabetologia* 62 (11), 2094–2105. doi: 10.1007/s00125-019-4937-7

Sun, K., Kusminski, C. M., and Scherer, P. E. (2011). Adipose tissue remodeling and obesity. *J. Clin. Invest.* 121 (6), 2094–2101. doi: 10.1172/JCI45887

Sun, K., et al. (2013). Fibrosis and adipose tissue dysfunction. *Cell Metab.* 18 (4), 470–477. doi: 10.1016/j.cmet.2013.06.016

Sun, J., Song, P., Wang, Y., and Chen, Y. (2019). Clinical efficacy of acetylcysteine combined with tetrandrine tablets in the treatment of silicosis and the effect on serum IL-6 and TNF-alpha. *Exp. Ther. Med.* 18 (5), 3383–3388. doi: 10.3892/etm.2019.7966

Takamiya, R., Murakami, M., Kajimura, M., Goda, N., Makino, N., Takamiya, Y., et al. (2002). Stabilization of mast cells by heme oxygenase-1: an anti-inflammatory role. *Am. J. Physiol. Heart Circ. Physiol.* 283 (3), H861–H870. doi: 10.1152/ajpheart.00740.2001

Talasaz, A. H., Khalili, H., Jenab, Y., Salarifar, M., Broumand, M. A., and Darabi, F. (2013). N-Acetylcysteine effects on transforming growth factor-beta and tumor necrosis factor-alpha serum levels as pro-fibrotic and inflammatory biomarkers in patients following ST-segment elevation myocardial infarction. *Drugs R. D.* 13 (3), 199–205. doi: 10.1007/s40268-013-0025-5

Thalhamer, T., McGrath, M. A., and Harnett, M. M. (2008). MAPKs and their relevance to arthritis and inflammation. *Rheumatol. (Oxford)* 47 (4), 409–414.

Thompson, W. G., Cook, D. A., Clark, M. M., Bardia, A., and Levine, J. A. (2007). Treatment of obesity. *Mayo Clin. Proc.* 82 (1), 93–101. quiz 101-2. doi: 10.1016/S0025-6196(11)60971-3

Thong-Ngam, D., Samuhasaneeto, S., Kulaputana, O., and Klaikeaw, N. (2007). N-acetylcysteine attenuates oxidative stress and liver pathology in rats with non-alcoholic steatohepatitis. *World J. Gastroenterol.* 13 (38), 5127–5132. doi: 10.3748/wjg.v13.i38.5127

Tran, K., and Chan, A. C. (1990). R,R,R-alpha-tocopherol potentiates prostacyclin release in human endothelial cells. Evidence for structural specificity of the tocopherol molecule. *Biochim. Biophys. Acta* 1043 (2), 189–197. doi: 10.1016/0005-2760(90)90295-9

Unal, R., Yao-Borengasser, A., Varma, V., Rasouli, N., Labbate, C., Kern, P. A., et al. (2010). Matrix metalloproteinase-9 is increased in obese subjects and decreases in response to pioglitazone. *J. Clin. Endocrinol. Metab.* 95 (6), 2993–3001. doi: 10.1210/jc.2009-2623

Upston, J. M., Kritharides, L., and Stocker, R. (2003). The role of vitamin E in atherosclerosis. *Prog. Lipid Res.* 42 (5), 405–422. doi: 10.1016/S0163-7827(03)00024-9

von Lintig, J. (2012). Provitamin A metabolism and functions in mammalian biology. *Am. J. Clin. Nutr.* 96 (5), 1234S–1244S. doi: 10.3945/ajcn.112.034629

Wagner, G., Lindroos-Christensen, J., Einwallner, E., Husa, J., Zapf, T. C., Lipp, K., et al. (2017). HO-1 inhibits preadipocyte proliferation and differentiation at the onset of obesity via ROS dependent activation of Akt2. *Sci. Rep.* 7, 40881. doi: 10.1038/srep40881

Wallace, A. M., McMahon, A. D., Packard, C. J., Kelly, A., Shepherd, J., Gaw, A., et al. (2001). Plasma leptin and the risk of cardiovascular disease in the west of Scotland coronary prevention study (WOSCOPS). *Circulation* 104 (25), 3052–3056. doi: 10.1161/hc5001.101061

Wallert, M., Schmolz, L., Galli, F., Birringer, M., and Lorkowski, S. (2014). Regulatory metabolites of vitamin E and their putative relevance for atherogenesis. *Redox Biol.* 2, 495–503. doi: 10.1016/j.redox.2014.02.002

Wang, W., Connor, S. L., Johnson, E. J., Klein, M. L., Hughes, S., and Connor, W. E. (2007). Effect of dietary lutein and zeaxanthin on plasma carotenoids and their transport in lipoproteins in age-related macular degeneration. *Am. J. Clin. Nutr.* 85 (3), 762–769. doi: 10.1093/ajcn/85.3.762

Wang, X. M., Kim, H. P., Nakahira, K., Ryter, S. W., and Choi, A. M. (2009). The heme oxygenase-1/carbon monoxide pathway suppresses TLR4 signaling by regulating the interaction of TLR4 with caveolin-1. *J. Immunol.* 182 (6), 3809–3818. doi: 10.4049/jimmunol.0712437

Wang, S. L., Li, Y., Wen, Y., Chen, Y. F., Na, L. X., Li, S. T., et al. (2009). Curcumin, a potential inhibitor of up-regulation of TNF-alpha and IL-6 induced by palmitate in 3T3-L1 adipocytes through NF-kappaB and JNK pathway. *BioMed. Environ. Sci.* 22 (1), 32–39. doi: 10.1016/S0895-3988(09)60019-2

Wang, X., Liu, J. Z., Hu, J. X., Wu, H., Li, Y. L., Chen, H. L., et al. (2011). ROS-activated p38 MAPK/ERK-Akt cascade plays a central role in palmitic acid-stimulated hepatocyte proliferation. *Free Radic. Biol. Med.* 51 (2), 539–551. doi: 10.1016/j.freeradbiomed.2011.04.019

Wang, C. H., Wu, S. B., Wu, Y. T., and Wei, Y. H. (2013). Oxidative stress response elicited by mitochondrial dysfunction: implication in the pathophysiology of aging. *Exp. Biol. Med. (Maywood)* 238 (5), 450–460. doi: 10.1177/1535370213493069

Wang, B., Aw, T. Y., and Stokes, K. Y. (2016). The protection conferred against ischemia-reperfusion injury in the diabetic brain by N-acetylcysteine is associated with decreased dicarbonyl stress. *Free Radic. Biol. Med.* 96, 89–98. doi: 10.1016/j.freeradbiomed.2016.03.038

Wegiel, B., and Otterbein, L. E. (2012). Go green: the anti-inflammatory effects of biliverdin reductase. *Front. Pharmacol.* 3, 47. doi: 10.3389/fphar.2012.00047

Wensveen, F. M., Valentic, S., Sestan, M., Turk Wensveen, T., and Polic, B. (2015). The "Big Bang" in obese fat: Events initiating obesity-induced adipose tissue inflammation. *Eur. J. Immunol.* 45 (9), 2446–2456. doi: 10.1002/eji.201545502

Widjaja, S. S., Syahputra, M. O. K., and Ginting, A. (2019). Hypercoagulable State and Glycemic Control in Diabetic Patients with Malignancy. *Open Access Maced J. Med. Sci.* 7 (23), 4066–4068. doi: 10.3889/oamjms.2019.860

Wiseman, S. A., Van den Boom, M. A., De Fouw, N. J., Wassink, M. G., Op den Kamp, J. A., and Tijburg, L. B. (1995). Comparison of the effects of dietary vitamin E on in vivo and in vitro parameters of lipid peroxidation in the rabbit. *Free Radic. Biol. Med.* 19 (5), 617–626. doi: 10.1016/0891-5849(95)00078-C

Wong, S. K., Chin, K. Y., Suhaimi, F. H., Ahmad, F., and Ima-Nirwana, S. (2017). Vitamin E As a Potential Interventional Treatment for Metabolic Syndrome: Evidence from Animal and Human Studies. *Front. Pharmacol.* 8, 444. doi: 10.3389/fphar.2017.00444

Wood Dos Santos, T., Cristina Pereira, Q., Teixeira, L., Gambero, A. J. A. V., and Lima Ribeiro, M. (2018). Effects of Polyphenols on Thermogenesis and Mitochondrial Biogenesis. *Int. J. Mol. Sci.* 19 (9). doi: 10.3390/ijms19092757

Wood, Z. A., Schroder, E., Robin Harris, J., and Poole, L. B. (2003). Structure, mechanism and regulation of peroxiredoxins. *Trends Biochem. Sci.* 28 (1), 32–40. doi: 10.1016/S0968-0004(02)00003-8

Wu, J. H., Ward, N. C., Indrawan, A. P., Almeida, C. A., Hodgson, J. M., Proudfoot, J. M., et al. (2007). Effects of alpha-tocopherol and mixed tocopherol supplementation on markers of oxidative stress and inflammation in type 2 diabetes. *Clin. Chem.* 53 (3), 511–519. doi: 10.1373/clinchem.2006.076992

Wu, B., Wu, Y., and Tang, W. (2019). Heme Catabolic Pathway in Inflammation and Immune Disorders. *Front. Pharmacol.* 10:825. doi: 10.3389/fphar.2019.00825

Yamada, S., and Guo, X. (2018). Peroxiredoxin 4 (PRDX4): Its critical in vivo roles in animal models of metabolic syndrome ranging from atherosclerosis to nonalcoholic fatty liver disease. *Pathol. Int.* 68 (2), 91–101. doi: 10.1111/pin.12634

Zaragoza, A., Diez-Fernandez, C., Alvarez, A. M., Andres, D., and Cascales, M. (2000). Effect of N-acetylcysteine and deferoxamine on endogenous antioxidant defense system gene expression in a rat hepatocyte model of cocaine cytotoxicity. *Biochim. Biophys. Acta* 1496 (2-3), 183–195. doi: 10.1016/S0167-4889(00)00036-7

Zelko, I. N., Mariani, T. J., and Folz, R. J. (2002). Superoxide dismutase multigene family: a comparison of the CuZn-SOD (SOD1), Mn-SOD (SOD2), and EC-SOD (SOD3) gene structures, evolution, and expression. *Free Radic. Biol. Med.* 33 (3), 337–349. doi: 10.1016/S0891-5849(02)00905-X

Zhang, Q., Yuan, H., Zhang, C., Guan, Y., Wu, Y., Ling, F., et al. (2018). Epigallocatechin gallate improves insulin resistance in HepG2 cells through alleviating inflammation and lipotoxicity. *Diabetes Res. Clin. Pract.* 142, 363–373. doi: 10.1016/j.diabres.2018.06.017

Zicha, J., Dobesova, Z., and Kunes, J. (2006). Antihypertensive mechanisms of chronic captopril or N-acetylcysteine treatment in L-NAME hypertensive rats. *Hypertens. Res.* 29 (12), 1021–1027. doi: 10.1291/hypres.29.1021

Conflict of Interest: The authors declare that the research was conducted in the absence of any commercial or financial relationships that could be construed as a potential conflict of interest.

frontiers in Pharmacology

REVIEW
published: 07 December 2020
doi: 10.3389/fphar.2020.598326

Sirt6 Deacetylase: A Potential Key Regulator in the Prevention of Obesity, Diabetes and Neurodegenerative Disease

Swapnil Raj[1†], *Liston Augustine Dsouza*[1†], *Shailendra Pratap Singh*[2*] and *Abhinav Kanwal*[1,3*]

[1]Department of Pharmacology, Manipal College of Pharmaceutical Sciences, Manipal Academy of Higher Education, Manipal, India, [2]Department of Biomedical Engineering, School of Engineering and Technology, Central University of Rajasthan, Kishangarh, India, [3]Department of Pharmacology, All India Institute of Medical Sciences (AIIMS), Bathinda, India

Sirtuins, NAD + dependent proteins belonging to class III histone deacetylases, are involved in regulating numerous cellular processes including cellular stress, insulin resistance, inflammation, mitochondrial biogenesis, chromatin silencing, cell cycle regulation, transcription, and apoptosis. Of the seven mammalian sirtuins present in humans, Sirt6 is an essential nuclear sirtuin. Until recently, Sirt6 was thought to regulate chromatin silencing, but new research indicates its role in aging, diabetes, cardiovascular disease, lipid metabolism, neurodegenerative diseases, and cancer. Various murine models demonstrate that Sirt6 activation is beneficial in alleviating many disease conditions and increasing lifespan, showing that Sirt6 is a critical therapeutic target in the treatment of various disease conditions in humans. Sirt6 also regulates the pathogenesis of multiple diseases by acting on histone proteins and non-histone proteins. Endogenous and non-endogenous modulators regulate both activation and inhibition of Sirt6. Few Sirt6 specific non-endogenous modulators have been identified. Hence the identification of Sirt6 specific modulators may have potential therapeutic roles in the diseases described above. In this review, we describe the development of Sirt6, the role it plays in the human condition, the functional role and therapeutic importance in disease processes, and specific modulators and molecular mechanism of Sirt6 in the regulation of metabolic homeostasis, cardiovascular disease, aging, and neurodegenerative disease.

Keywords: drug discovery, epigenetics, diseases, modulators, Sirt6, sirtuins

OPEN ACCESS

Edited by:
Terry D. Hinds Jr.,
University of Toledo, United States

Reviewed by:
Dante Rotili,
Sapienza University of Rome, Italy
Pedro Gomes,
University of Coimbra, Portugal

***Correspondence:**
Abhinav Kanwal
abhinavkanwal@gmail.com
Shailendra Pratap Singh
spsingh@curaj.ac.in

[†]*These authors have contributed equally to this work*

Specialty section:
This article was submitted to Experimental Pharmacology and Drug Discovery, a section of the journal Frontiers in Pharmacology

Received: *24 August 2020*
Accepted: *27 October 2020*
Published: *07 December 2020*

Citation:
Raj S, Dsouza LA, Singh SP and Kanwal A (2020) Sirt6 Deacetylase: A Potential Key Regulator in the Prevention of Obesity, Diabetes and Neurodegenerative Disease. Front. Pharmacol. 11:598326. doi: 10.3389/fphar.2020.598326

INTRODUCTION

Sirtuins are energy linked NAD + dependent proteins that are activated during calorie restriction (Corbi et al., 2012; Rack et al., 2015; Bheda et al., 2016; Yu et al., 2018), mainly altering the acetylation/deacetylation status of histones, thus regulating chromatin silencing. Proteomic studies suggest that human cells possess histones with various lysine acyl modifications and these sirtuins have specific deacetylating activities that remove acyl moieties from lysine, thus modulating gene expression, without altering the gene sequence itself (Kupis et al., 2016). This unique property of sirtuins and their ability to bind to various substrates and other moieties bearing acyl modifications

allow us to examine different mechanisms involved in multiple diseases, thus showing the importance of sirtuins (Carafa et al., 2012). Sirtuins are epigenetic regulators, belonging to class III Histone Deacetylases (HDACs) (Rack et al., 2015) which are known to affect multiple pathways involved in various disease conditions including cancer, diabetes, cardiac failure, hypertrophy, cachexia, pulmonary fibrosis, aging etc. (Dryden et al., 2003; Vassilopoulos et al., 2011; Lee and Goldberg, 2013; Lee and Gu, 2013; Bheda et al., 2016; Kupis et al., 2016; Graham et al., 2018; Kanwal and Dsouza, 2019) These energy linked proteins were first discovered in the yeast cells, as silencing information regulator-2 (Sir-2) (Haigis and Sinclair, 2010; Grabowska et al., 2017; Graham et al., 2018; Rajabi et al., 2018). Orthologues of Sir-2 in mammals are known as sirtuins (Polito et al., 2010). In humans, sirtuins are divided into seven types (**Figure 1**, Mammalian sirtuins and their functions) (Sirt1-Sirt7), localized in different cellular components, that has crucial role in various cellular processes (Kobayashi et al., 2005; Haigis and Sinclair, 2010; Vassilopoulos et al., 2011; Hoffmann et al., 2014; Wu et al., 2015; Tang, 2016; Dai et al., 2018; Graham et al., 2018; Wang et al., 2018; Kanwal, 2018). Significant differences exist between sirtuin homologues in their variable N and C terminal extensions with conserved C-terminal extensions. Among the 7 types of sirtuins, Sirt6 is an essential sirtuin in humans that is localized in the nucleus. Like other sirtuins, Sirt6 is also a stress responsive protein deacetylase, but unlike other sirtuins, in addition to its deacetylase activity, it also transfers ADP ribosyl via mono-ADP ribosyltransferase enzyme. In humans, Sirt6 has a plethora of functions, including DNA repair, telomerase function, genomic stability, cellular senescence, and metabolic homeostasis (**Figure 2**: Clinical significance of Sirt6 in various diseases) (Michishita et al., 2008; Watroba and Szukiewicz, 2016). Until recently, Sirt6 was mainly known for chromatin signaling. Recent data indicate that Sirt6 is involved in various disease conditions mentioned above (Khan R. I. et al., 2018); due to their action on multiple substrates and catalytic sites (Tasselli et al., 2017). Studies indicate that they control activities of p53, FOXO proteins, NF-KB, PGC-1α, PARP1, TNFα, GCN5, HIF1α, which are involved in the pathogenesis of various diseases (Kawahara et al., 2009; Dominy et al., 2012; Zwaans and Lombard, 2014). This review focuses on Sirt6, its mechanism(s) in multiple disease states, its significance in human health, and as a therapeutic target in drug discovery.

SIRT6: IMPORTANCE AND RECENT DEVELOPMENT

Sirt6 is a NAD^+ dependent nuclear histone deacetylase, having deacetylase, deacylase and mono-ADP ribosyltransferase activity. In the past 5 years, the development of Sirt6 suggests a crucial role in a broad spectrum of metabolic processes. Sirt6 has a significant role in maintaining genetic stability and DNA repair, by activating several DNA-repair genes (Mao et al., 2011; Khan R. I. et al., 2018). It was identified as a suppressor of genomic instability due to its association with chromatin through its ability to modulate base excision-pair repair and double strand break repair (Kugel and Mostoslavsky, 2014). In addition to maintaining genetic stability, it also plays a crucial role in intermediary metabolism including glucose metabolism, lipid metabolism, circadian metabolism, etc. (Watroba and Szukiewicz, 2016; Tasselli et al., 2017). Studies in the recent past have also shown implications of Sirt6 in various diseases including dyslipidemia, diabetes, heart disease, cancer, neurodegenerative diseases, brain aging etc. (Roichman et al., 2016; Xiwen et al., 2016; D'Onofrio et al., 2017). Sirt6 is a longevity protein; various studies have demonstrated its involvement in increasing life expectancy (Schumacher, 2011; Kanfi et al., 2012; Giblin and Lombard, 2016; Schumacher, 2017). Overexpression of Sirt6 in transgenic mice resulted in significantly longer half-life compared to wild-types, and that IGF-1 plays a crucial role in regulating lifespan (Kanfi et al., 2012). Sirt6 blocks the action of IGF-1, which is responsible for increasing lifespan (Sundaresan et al., 2012). There are two main theories that postulate how Sirt6 regulates longevity, they are: maintenance of genetic stability and regulation of metabolism, and various studies show that either of these theories contribute to Sirt6's function in longevity (Mostoslavsky et al., 2006; Michishita et al., 2008; Kanfi et al., 2012). Sirt6 knockout mice died within a month of birth due to the development of significant metabolic abnormalities due to deficiency of IGF-1 (Watroba and Szukiewicz, 2016). Lack of IGF-1 was correlated with a decrease in adipose tissue, lordokyphosis, and severe hypoglycemia (Lombard et al., 2008; Peshti et al., 2017; Ferrer et al., 2018). Another study reveals the role of Sirt6 in longevity by the maintenance of genetic stability (Tian et al., 2019). The mechanism involved is double-strand break repair of DNA; an activity controlled by Sirt6 resulted in an increase in lifespan in animal models (Mostoslavsky et al., 2006; Lombard et al., 2008; Tian et al., 2019). Macaque monkeys that lacked the gene for Sirt6 died a few hours after the birth and exhibited prenatal developmental retardation (Zhang W. et al., 2018). In this study, it was observed that the brain was underdeveloped, suggesting low levels of Sirt6 can lead to neurodegenerative diseases and brain aging (Zhang W. et al., 2018; Naiman and Cohen, 2018; Niu, 2019). Sirt6 is necessary in human development as shown by a study that the deletion of Sirt6 in humans can cause perinatal lethality (Ferrer et al., 2018). Several other studies have highlighted telomeres' role in aging and its association with Sirt6 (Aubert and Lansdorp, 2008; Tennen et al., 2011). With aging, the length of the telomere declines, but Sirt6 by its deacetylation activity, maintain the length of telomeres, thus preventing telomere sequence loss (Aubert and Lansdorp, 2008; Cacchione et al., 2019; Cao et al., 2019). Cells lacking Sirt6 had malformed telomere structure and also replication associated sequence loss of telomeres (Aubert and Lansdorp, 2008). Apart from telomeres, mammalian aging and aging related disorders are also associated with abnormal IGF-Akt signaling, which in turn is controlled by Sirt6 (Pillai et al., 2014). Heart failure is one of the age-related disorder in mammals, where the IGF-Akt on sustained activation promotes hypertrophy and heart failure (Wang et al., 2015; D'Onofrio et al., 2017; Lee and Kim, 2018), whereas Sirt6 impedes IGF-Akt signaling via c-Jun by

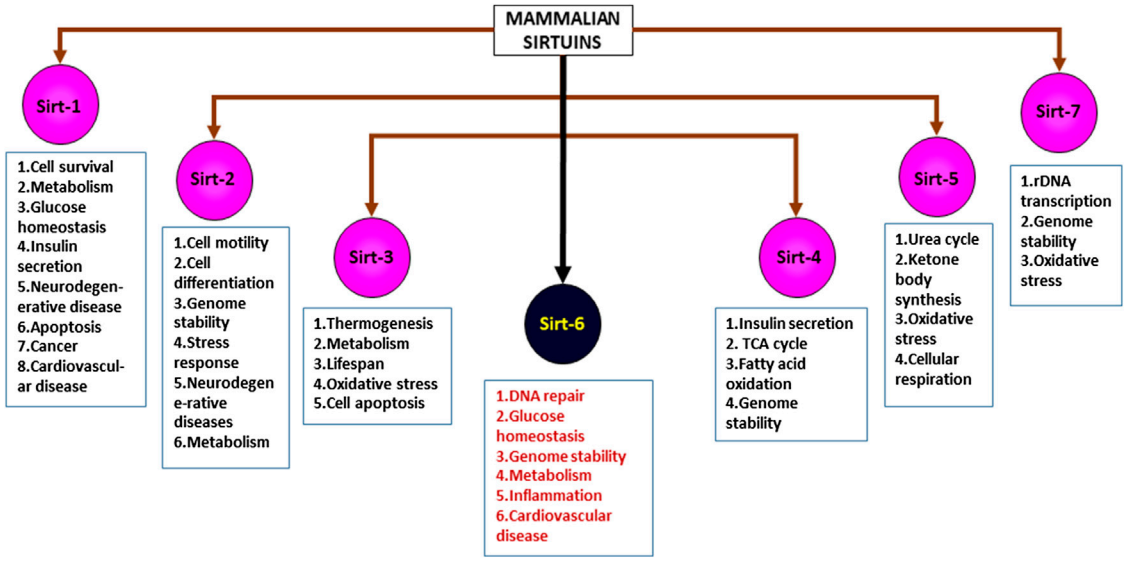

FIGURE 1 | Mammalian sirtuins and their functions.

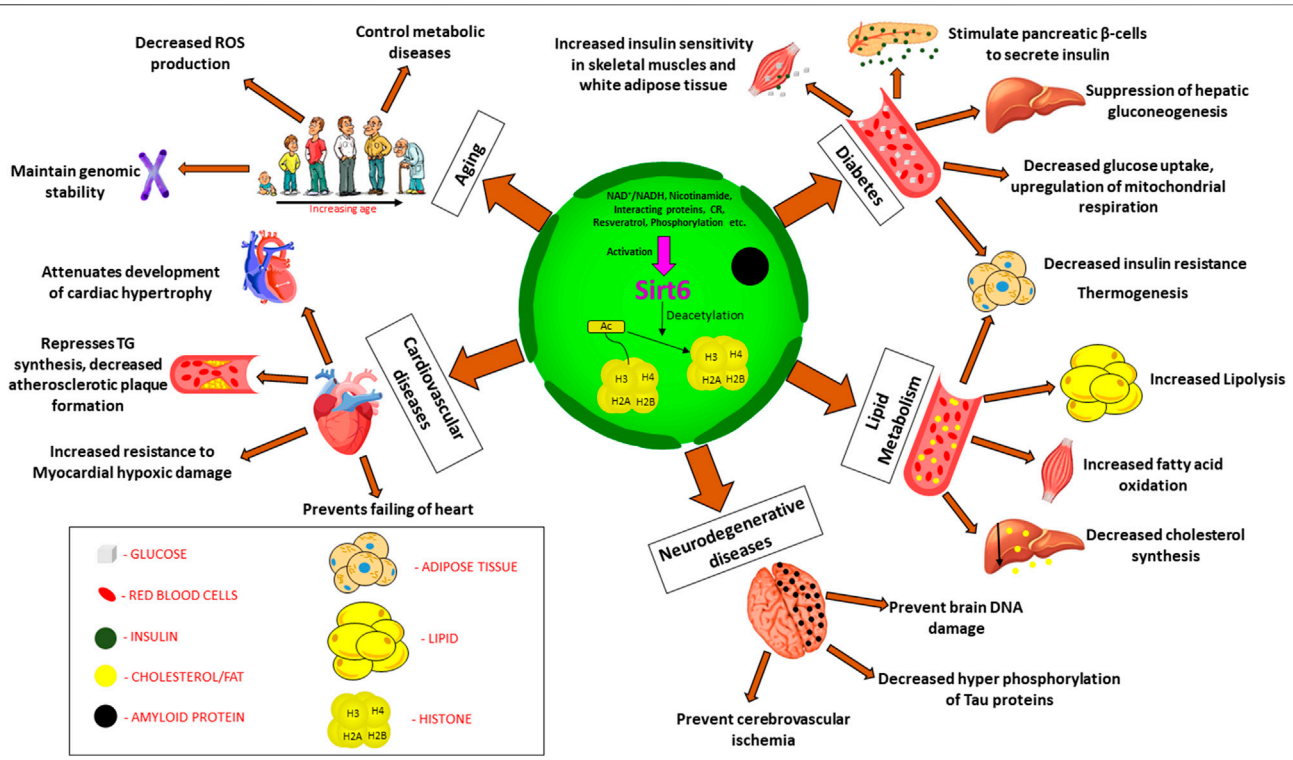

FIGURE 2 | Clinical significance of Sirt6 in various diseases. Sirt6 is a nuclear sirtuin activated by CR, NAD+, resveratrol etc., promoting deacetylation of histone which plays a major role in (a) Diabetes: increased insulin sensitivity, insulin secretion, suppress gluconeogenesis, decrease glucose uptake. (b) Lipid metabolism: increased lipolysis, increased fatty acid oxidation, decreased cholesterol synthesis. (c) Neurodegenerative diseases: decreased phosphorylation of Tau proteins, prevent cerebrovascular ischemia and brain DNA damage (d) Cardiovascular diseases: decrease TG synthesis, attenuates cardiac hypertrophy, prevents failing of heart, resistance to hypoxic damage (e) Aging: decreased ROS production, maintain genomic stability, control metabolic diseases. Abbreviation: Ac, Acetylated; CR, calorie restriction; TG, triglycerides; ROS, reactive oxygen species.

deacetylation of H3K9 (Sundaresan et al., 2012). Few studies found that failing hearts of humans and mice showed decreased levels of Sirt6, suggesting that low levels of Sirt6 increase the activity of IGF-Akt, leading to initiation and progression of cardiac hypertrophy and heart failure (Sundaresan et al., 2012; Zhang D. et al., 2018). Osteoporosis is yet another age-related disorder in mammals, and recent studies have found that Sirt6 prevents osteoporosis, but the mechanism remains unclear. Sirt6 knockout mice suffering from osteopenia, exhibited more significant bone loss than the non-mutant mice (Zhang D. et al., 2018), indicating that Sirt6 was involved in decreased osteoclast activation (Zhang D. et al., 2018; Wang and Mbalaviele, 2019).

SUBSTRATES FOR SIRT6

Sirt6 functions are diversified (Pan et al., 2011; Kuang et al., 2018). They include different molecular pathways associated with glycolysis, DNA repair, gluconeogenesis, cardiac hypertrophic responses, neurodegeneration, and tumorigenesis due to its activity on varied number of substrates, which include PARP1, TNFα, GCN5, HIF1α, etc. (Liu et al., 2012; Sundaresan et al., 2012; Li et al., 2017; Kuang et al., 2018; Khan R. I. et al., 2018; Yang H. et al., 2019). HIFs are transcription factors that are expressed as regulators of genes during cellular deprivation of oxygen. Overexpression of HIFs is implicated with tumor growth and metastasis, and is involved in initiating angiogenesis (Jun et al., 2017; Pezzuto and Carico, 2018). Sirt6 can inhibit these activities of HIF. Thus activation of Sirt6 controls tumor growth and metastasis by regulating the overexpression of HIF1α (Zhong et al., 2010; Zwaans and Lombard, 2014; Yang Z. et al., 2019).

TNF-α, a Sirt6 substrate, is a proinflammatory cytokine that is involved in various inflammatory pathological processes (Ravussin and Smith, 2016; Josephs et al., 2018), and increased expression of Sirt6 inhibits TNF-α (He et al., 2017). Although Sirt6 is essential in the deacetylation process, the de-fatty acylation, specifically the hydrolysis of lysine units at the 19 and 20 positions of H3 histone, regulates TNF-α secretion (Jiang et al., 2016). Catalysis of fatty acyl lysine hydrolysis by Sirt6 is more efficient when compared to deacetylation (Jiang et al., 2013). Sirt6 has a significant role in chronic inflammation due to its association with TNF-α. Cells treated with TNF-α had decreased levels of Sirt6 in a dose dependent manner, identifying a symbiotic relationship between TNF-α and Sirt6 (Yeo et al., 2017). In addition to the above, Sirt6 attenuates inflammatory response through inhibition of NF-κB signaling (Li Z. et al., 2018; Santos-Barriopedro et al., 2018; Santos-Barriopedro and Vaquero, 2018).

Sirt6 binds to and activates GCN5, thereby inhibiting the acetylation of PGC-1α (Peroxisome Proliferator activated Receptor coactivator one alpha) and decreasing gluconeogenic gene expression (Giblin and Lombard, 2016; D'Onofrio et al., 2017; Kuang et al., 2018; De Céu Teixeira et al., 2019). This correlation between Sirt6 levels and glucose metabolism is a key in understanding involvement of Sirt6 in the pathogenesis in diabetes mellitus and a potential therapeutic target in the management of the disease (Dominy et al., 2012; D'Onofrio et al., 2017; Kuang et al., 2018).

Sirt6 deacetylase, along with FoxO3a, can reduce LDL-cholesterol levels by regulating the expression of PCSK9 (Proprotein Convertase Subtilisin/Kexin Type 9) (Chaudhary et al., 2017). PCSK9 is a gene that regulates LDL receptors, which in turn is involved in decreased LDL clearance from the circulation in the hepatocytes (Spolitu et al., 2019). FoxO3 recruits NAD^+ -dependent Sirt6 deacetylase, to the promoter region of the PCSK9 gene for the deacetylating histone H3 at lysine 9 and 56, which resulted in suppression of the expression of PCSK9 gene, thereby promoting LDL receptors and subsequent hepatic clearance of pathogenic LDL (Tao et al., 2013a; Gao et al., 2018). Activation of Sirt6 inhibited PCSK9, thus positively regulating hypercholesterolemia. Therefore Sirt6 could be a potential target in the treatment of dyslipidemia (Tao et al., 2013a; Chaudhary et al., 2017; Glerup et al., 2017; Handelsman and Lepor Norman, 2018; Spolitu et al., 2019).

The activity of Poly (ADP-ribose) polymerase 1 (PARP1) is increased when acted upon by Sirt6 where it undergoes mono (ADP-ribosylation). This enzyme is involved in the modification of nuclear proteins, responsible for DNA repair and proliferation, differentiation and tumor transformation (Xu et al., 2015; Rizzo et al., 2016; Van Meter et al., 2016; Tang, 2017; Fujimoto et al., 2017; Yang et al., 2018). PARP-1 is also an essential regulator of Apoptosis Inducing Factor (AIF) mediated cell death (Song Y. et al., 2016). The expression levels of this protein were low under Sirt6 deficient conditions. Levels of PARP-1 were reduced faster under Sirt6 defective conditions (Zhang Q. et al., 2019).

Recently attention has been focused on the role of Thioredoxin-interacting protein (TXNIP), as overexpression of this protein is negatively associated with the insulin secretion by β-cells of the pancreas (Alhawiti et al., 2017; Nagaraj et al., 2018). Sirt6 influences the expression of TXNIP i.e. overexpression of Sirt6 inhibits TXNIP, thus making it an important therapeutic target (Kuang et al., 2018; Qin et al., 2018). In addition to the above, Sirt6 has been reported to act on various other substrates that could potentially be implicated in multiple other diseases for which a better understanding of the molecular mechanism is required (Tasselli et al., 2017; Khan R. I. et al., 2018; Gertman et al., 2018).

SIRT6 AND DISEASES

As we delve into the cellular level, Sirt6 deprivation leads to several changes in sensitivity to reactive oxygen species, glucose metabolism, and genomic stability (Mostoslavsky et al., 2006; Kanfi et al., 2012; Li et al., 2017; Peshti et al., 2017; Xu et al., 2019; Yepuri and Ramasamy, 2019). Mice placed on caloric restriction or Sirt6 activators overexpress Sirt6, improving cancer, and age-related disorders in animal models (Zhang et al., 2016a; Kuang et al., 2018; Iachettini et al., 2018; Rahnasto-Rilla et al., 2018), on the contrary, lower Sirt6 levels in mice showed shorter life expectancy, cancer occurrence, diabetes and other metabolic disorders increased. The animals also exhibited other

complications such as curved spines, decreased subcutaneous fat, hypoglycemia, and lowered levels of IGF-1 (Peshti et al., 2017; Khan R. I. et al., 2018; Ghosh et al., 2018; Simon et al., 2019). This suggests that Sirt6 is a therapeutic target in aging, cardiac disorders, neurodegenerative disorders, and metabolic disorders (Rodgers and Puigserver, 2006; Serravallo et al., 2013; Demir et al., 2017; Harlan et al., 2019). **Table 1**.

SIRT6 IN AGING

Aging is a complex, multifactorial process resulting in the accumulation of diverse harmful changes in the cell, increasing risk of disease and death. Multiple theories can explain the aging process but none can be considered absolute (Tosato et al., 2007; Jin, 2010; Sergiev et al., 2015). These include evolutionary theory, Free radical theory, Mitochondrial theory, Gene regulation theory, Telomere theory, Inflammation hypothesis, Immunity theory, Neuroendocrine theory, Neuroendocrine- immune method theory, and Caloric restriction (Wei et al., 2001; Gavrilov and Gavrilova, 2002; Tosato et al., 2007; López-Lluch and Navas, 2016). In addition to these theories, sirtuins too contribute to aging. Initially, sirtuins were first identified in yeast, which led them to discover its life prolonging activity. Studies in the worm flies confirmed the link between sirtuins and aging (Finkel et al., 2007; Guarente, 2007). Of the seven mammalian sirtuins, Sirt6 is pivotal in regulating lifespan (Kanfi et al., 2012; Hirvonen et al., 2017; Peshti et al., 2017). It promotes chromatin changes essential for DNA repair and maintenance of telomere structure, preventing genomic instability, and cellular senescence (Tasselli et al., 2017). The DNA repair mechanism in longevity is Double-Strand Break repair, where Sirt6 performs this function more efficiently (Tian et al., 2019). Sirt6 is thought to have a protective action on telomeres, as deficiency of Sirt6 causes a loss of telomere sequence associated with replication, leading to genomic instability and early cell death (Watroba and Szukiewicz, 2016; Naiman and Cohen, 2018). Furthermore, Sirt6 maintains redox homeostasis in mesenchymal stem cells, thus suggesting that it regulates longevity (Liao and Kennedy, 2016; Pan et al., 2016). IGF-1 is yet another factor that is related to aging. Lower levels of IGF-1 delayed the process of aging. Transgenic mice models that overexpressed the Sirt6 gene had low levels of IGF-1, slowing the aging process in mice (Kanfi et al., 2012; Ravi et al., 2019). Thus, Sirt6 can be targeted for therapeutic interventions in aging and aging related diseases (Khan R. I. et al., 2018).

Table 1 | Sirt6: action on various targets in diseases.

DISEASE	TARGET	EFFECT	References
Aging	H3K9ac	Telomere stability, DNA damage response	(Khan R. I. et al., 2018)
	H3K56ac	Telomere stability, DNA damage response	(Khan R. I. et al., 2018)
	H3K18ac	Heterochromatin silencing	(Khan R. I. et al., 2018)
	IGF-1	Reduction in somatotropic axis	(Mao et al., 2018)
Cardiac disorder	PDK4	Improve cardiac glucose metabolism	(Khan D. et al., 2018)
	IL1, NF-⊠B	Inhibit activation of pro-inflammatory cytokines responsible for atherosclerosis; Prevent endothelial damage	(Vitiello et al., 2017)
	ICAM-1, PAI-1	Protect endothelial damage	(Guo et al., 2019) (D'Onofrio et al., 2017)
	IGF	Prevent heart failure and cardiac hypertrophy	(Sundaresan et al., 2012)
	Nmnat-II	Activates Nmnat-II, prevent cardiac hypertrophy	(Cai et al., 2012)
Neurodegenerative	WRN	Maintains genomic stability and telomeric length	(Khan R. I. et al., 2018)
disease	GSK3α/β	Decreased tau protein activation	(Tang, 2017)
	Aβ42	Prevents DNA damage	(Jung et al., 2016)
Lipid metabolism	SREBP	Suppresses LDL- cholesterol synthesis	(Kuang et al., 2018) (Tao et al., 2013b)
	CK2	Facilitates adipogenesis	(Kuang et al., 2018) (Chen et al., 2017)
	PGC1α	Increased Brown adipose tissue thermogenesis and expression of thermogenesis genes	(Kuang et al., 2018) (Yao et al., 2017)
	PCSK9	Decreased LDL cholesterol levels	(Kuang et al., 2018) (Tao et al., 2013a)
Diabetes	TXNIP	Increased glucose stimulated insulin secretion	(Qin et al., 2018)
	FOXO1	Reduces expression of gluconeogenic genes	(Kuang et al., 2018)
	GLUT1, LDH & PDK1	Promote glycolysis	(Hu et al., 2006) (Zhong et al., 2010)
	GCN5 & PGC1α	suppress hepatic gluconeogenesis	(Dominy et al., 2012)

H3K9/56/18ac- acetylated histone 3 at lysine position 9, 56, 18 respectively; IGF- insulin like growth factor-1; PDK4- pyruvate dehydrogenase kinase 4; IL1- Interleukin 1; NF-KB- Nuclear factor kappa B; ICAM1- Intercellular adhesion molecule 1; PAI1- Plasminogen activator inhibitor 1; Nmnat2- Nicotinamide mononucleotide adenylyl transferase; WRN- WRN gene that encodes for Werner protein; GSK3α/β- Glycogen synthase kinase 3α/β; Aβ42- Plasma amyloid β peptide 42; SREBP- Sterol regulatory element binding protein; CK2- Casein kinase 2; PGC1α- Peroxisome proliferator activated receptor gamma coactivator 1 alpha; PCSK9- proprotein convertase subtilisin/kexin type 9; TXNIP- Thioredoxin interacting protein; FOXO1- Forkhead box 1; GLUT1- Glucose transporter 1; LDH- lactic acid dehydrogenase; GCN5- General control non depressible 5

SIRT6 IN CARDIAC DISORDERS

Congestive heart failure and coronary artery diseases are the two most common types of cardiac complications associated with Sirt6 activity (Bindu et al., 2016; D'Onofrio et al., 2017; Li et al., 2017; Guo et al., 2019; Yepuri and Ramasamy, 2019). Deficiency of Sirt6 in cardiomyocytes results in the accumulation of lactate due to impaired glucose oxidation, leading to various comorbidities relating to the heart, including heart failure (Khan D. et al., 2018). Sirt6 heterozygous mice were used to show lactic acid accumulation in mice hearts. Sirt6 deficiency increased FOXO1 localization in heart, upregulating PDK4, reducing oxygen consumption and ATP production, thereby demonstrating the protective role of Sirt6 in maintaining cardiac homeostasis (Khan D. et al., 2018). Another factor involved in the development of cardiac disorders is the formation of atherosclerotic plaque. No evidence suggests a direct link between Sirt6 and atherosclerotic plaque formation (Zi et al., 2019). However, Sirt6 deficiency enhances the expression of pro-inflammatory cytokines like Interleukin-1 and transcriptional signaling of NF-KB (Lappas, 2012; Yu et al., 2013), which are indirectly linked to the pathogenesis of atherosclerosis (Xu et al., 2016). In addition, Sirt6 depletion increased expression of ICAM-1 and PAI-1 and upregulation of p21 gene and reduction of eNOS (**Figure 3**, Schematic representation of molecular mechanism of Sirt6 in various diseases) further leading to atherosclerotic vascular

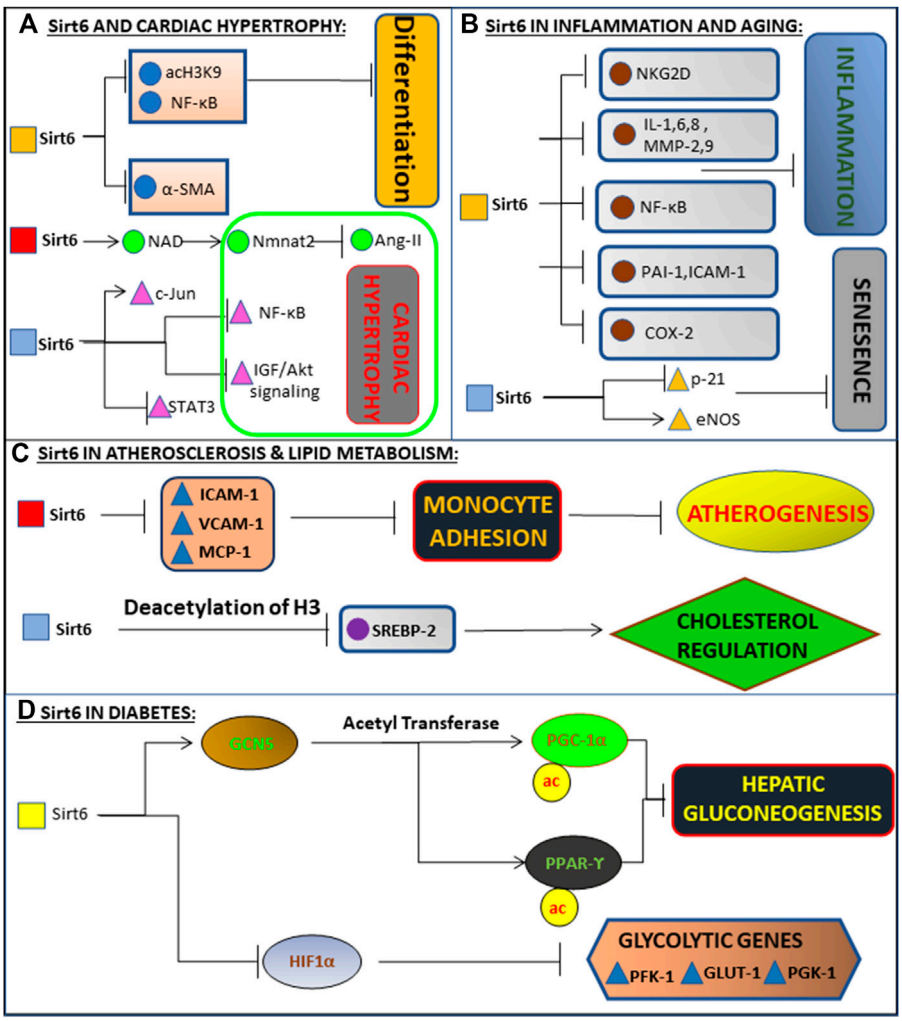

FIGURE 3 | Schematic representation of molecular mechanism of Sirt6 in various diseases. **(A)** Deacetylates H3K9, inhibiting NF-kB and differentiation of cardiac cells into myofibroblasts. Also binds to c-Jun, promoting deacetylation of H3K9, inhibiting the expression of NF-kB and IGF-Akt signalling. Inhibits activation of Ang 2 and STAT3 via Nmnat1 and NAD, together preventing Cardiac Hypertrophy and subsequently Heart Failure. **(B)** Exerts anti-inflammatory action in the endothelial cells via blockade of NF-kB, cytokines (i.e., IL-1, IL-6, IL-8), metalloproteinases (MMP-2, MMP-9), PAI-1, ICAM-1, and COX-2. Delays senescence by inhibiting p21 signalling and maintaining high levels of eNOS. **(C)** Prevents monocyte adhesion and Atherogenesis by inhibiting pro inflammatory mediators (ICAM-1, VCAM-1, MCP-1). Regulates Cholesterol levels by deacetylating H3K9 and inhibiting SREBP gene. **(D)** Enhances activity of GCN5, leading to down-regulation of gluconeogenesis-related enzymes and inhibiting gluconeogenesis via acetylation of PGC-1α and activation of PPARγ. It inhibits glycolysis by inhibiting glycolytic genes (PFK-1, GLUT-1, PGK-1) via inhibition of HIF-1α.

disease (Yepuri and Ramasamy, 2019; Zi et al., 2019). Sirt6 is also involved in the pathogenesis of cardiomyocyte hypertrophy (Yu et al., 2013; Lu et al., 2016; Ravi et al., 2019; Kanwal et al., 2019b), which includes angiotensin-II induced and IGF-Akt signaling induced cardiac hypertrophy (Li et al., 2017). Increased expression of Sirt6 in cardiomyocytes decreased angiotensin-II action on cardiomyocytes (Yu et al., 2013; Zhang et al., 2017; Eguchi et al., 2018; Ianni et al., 2018). Angiotensin-II induced cardiac hypertrophy is blocked by over-expression of nicotinamide mononucleotide adenylyltransferase-II (Nmnat-II) that is responsible for activation of Sirt6 (Vitiello et al., 2017). Another pathway involved in cardiac hypertrophy is mediated through increased activation of IGF-Akt pathway (Yan et al., 2019) (**Figure 3**: Schematic representation of molecular mechanism of Sirt6 in various diseases), which was shown in Sirt6 deficient mice (Sundaresan et al., 2012; Vitiello et al., 2017).

SIRT6 IN NEURODEGENERATIVE DISEASES AND BRAIN AGING

Alzheimer's disease (AD) is involved in neurodegeneration, and characterized by dementia. AD is pathologically characterized by formation of beta amyloid plaques and neurofibrillary tangles known as tau proteins (Kocahan and Doğan, 2017; Takahashi et al., 2017). Oxidative stress, cell senescence, and aging are the major risk factors for the progression of this disease (Markesbery, 1999; Huang et al., 2016; Kerchner and Wyss-Coray, 2016; Xia X. et al., 2018; Butterfield and Boyd-Kimball, 2018; Trevisan et al., 2019). During the pathogenesis of AD, telomere length has a causal role. As cells divide, telomere length shortens, and this shortening is associated with cognitive impairment, amyloid plaque deposition and hyper-phosphorylation of tau protein that are characteristics of AD (Cai et al., 2013; Forero et al., 2016; Liu et al., 2016). Oxidative stress affects telomeres as they contain guanine, which undergoes oxidation to produce 8-oxo-7,8-dihydro-2-deoxyguanosine (8-oxodG) (Kawanishi and Oikawa, 2004; Cai et al., 2013). Sirt6 maintains telomere function as it prevents telomere dysfunction through WRN protein stabilization at telomeric chromatin (Mohamad Nasir et al., 2018). In addition to telomere maintenance, Sirt6 regulates tau protein stabilization during AD oxidative stress. Activation of Sirt6 maintains both genomic stability in the brain and leads to loss of tau protein stability via inhibition of GSK3α/β (Kaluski et al., 2017; Stein and Toiber, 2017; Kim H. et al., 2018). Sirt6 reduction alters DNA repair in the brain of an AD mouse model, and Sirt6 overexpression prevents Amyloid beta protein (Aβ42) induced DNA damage, thereby proving the beneficial effects of Sirt6 in AD (Jung et al., 2016; Tang, 2017). This is confirmed by the fact that the levels of Sirt6 are reduced in the brains of both AD containing mice as well as AD patients. In addition, Aβ42 decreased Sirt6 levels (Kaluski et al., 2017; Cacabelos et al., 2019). Sirt6 is associated with age related disorders. Activation of Sirt6 is protective in AD and other neurodegenerative disorders involving brain aging, thus proving to be an essential therapeutic target in the treatment of neurodegenerative disorders (Naiman and Cohen, 2018).

SIRT6 IN LIPID METABOLISM

Lipid metabolism disorders are pervasive and play a vital role in the pathogenesis of atherosclerosis, leading to cardiovascular diseases (Parhofer, 2016; Schofield et al., 2016). Recently Sirt6 has been shown to have a critical role in lipid metabolism (Ye et al., 2017; Assadi-Porter et al., 2018; Kuang et al., 2018) as it is involved in the regulation of fatty acid synthesis, triglyceride synthesis, cholesterol synthesis, fatty acid beta oxidation, lipolysis, adipogenesis and thermogenesis (Liu et al., 2012; Elhanati et al., 2013; Tao et al., 2013a; Tao et al., 2013b; Chen et al., 2017; Yao et al., 2017; Kuang et al., 2018; Gao et al., 2019). Lipid homeostasis and cholesterol biosynthesis are regulated by a transcription factor called Sterol regulatory binding proteins (SREBP), and the expression of SREBP is controlled by Sirt6 (Eberle et al., 2004). SREBP activation is also implicated in inflammation, autophagy, endoplasmic reticulum stress (Shimano and Sato, 2017). Sirt6 inhibits the expression of SREBP, which is indirectly linked with cholesterol biosynthesis, hence regulating Cholesterol homeostasis (Tao et al., 2013b; Ye et al., 2017). Sirt6 negatively regulates cholesterol biosynthesis by various pathways involving SREBP. It causes downregulation of SREBP by reducing mRNA expression (Kuang et al., 2018). Sirt6 is also recruited to the *Srebp* gene promoter (**Figure 3**: Schematic representation of molecular mechanism of Sirt6 in various diseases) by FOXO3, where it deacetylates H3K9 and H3K56 in the promoter regions of *Srebp* and suppresses the transcription levels of *Srebp* and its target genes (Tao et al., 2013b; Elhanati et al., 2013; Kugel and Mostoslavsky, 2014). It also inhibits SREBP's subsequent conversion into active forms (Elhanati et al., 2013; Kugel and Mostoslavsky, 2014) and activates AMPK, leading to the phosphorylation and inactivation of SREBP (Kugel and Mostoslavsky, 2014; Kuang et al., 2018). The absence of Sirt6 leads to increased production of Triglycerides due to increased expression of genes involved in Triglyceride synthesis (Ye et al., 2017). The genes responsible for Fatty acid metabolism by beta oxidation is downregulated (Ye et al., 2017; Kuang et al., 2018). Sirt6 also regulates adipogenesis and thermogenesis, it is an essential factor in adipogenesis, by enhancing casein kinase 2 (CK2) activity (Chen et al., 2017; Kuang et al., 2017; Kuang et al., 2018). Similarly, expression of PGC-1α is a central regulator in thermogenesis. Overexpression of PGC-1α causes mitochondrial oxidative phosphorylation and expression of thermogenic genes. Sirt6 controls expression of PGC-1α, as depletion of Sirt6 decreases the appearance of PGC-1α, thus resulting in decreased thermogenesis (Yao et al., 2017; Kuang et al., 2018; Singh et al., 2020).

SIRT6 AND DIABETES

The prevalence of Type 2 Diabetes Mellitus (T2DM) is increasing at an alarming rate worldwide. With an increased understanding of the pathogenesis of T2DM various new therapeutic approaches are being developed to target the fundamental cause of T2DM, Sirt6 being one among them (Kitada et al., 2013; Bae, 2017;

Chellappan et al., 2018). The pathophysiology of T2DM is characterized by many causes (Mahler and Adler, 1999). The primary cause of T2DM is decreased sensitivity of beta cell functioning to the levels of glucose, but recent studies have proven the crucial role Sirt6 in glucose stimulated insulin secretion (GSIS), enhancing the release of insulin (Mahler and Adler, 1999; Song M. Y. et al., 2016; Xiwen et al., 2016) (**Figure 3**: Schematic representation of molecular mechanism of Sirt6 in various diseases). Various studies show different mechanisms of how Sirt6 is involved in increasing beta cell function. One such pathway is Sirt6 suppresses expression of the thioredoxin-interacting protein (TXNIP), which is engaged in β-cell apoptosis (Shalev, 2014; Qin et al., 2018). Thus, Sirt6 maintains the functioning of beta cells. Another pathway where Sirt6 supports GSIS functioning of beta cells is via regulation of FOXO1 expression. Sirt6 inhibits FOXO1, maintaining the glucose-sensing ability of pancreatic β-cell and systemic glucose tolerance (Song M. Y. et al., 2016). Hence Sirt6 has proven to be a chief regulator in glucose homeostasis (Zhong et al., 2010; Gertman et al., 2018). Studies done on mice have been conclusive in showing that knockdown of Sirt6 can lead to complications, namely severe hypoglycemia leading to death (Lee et al., 2017; Kuang et al., 2018). The primary reason for this were increased uptake from the muscle and adipose tissue rather than intestinal uptake of glucose or increased secretion from the kidneys (Kuang et al., 2018). There is both *in vitro* and *in vivo* evidence, showing that increased glucose uptake may be due to deficiency of Sirt6 (Zhong et al., 2010; Zhong and Mostoslavsky, 2010). Sirt6 suppresses HIF1α (hypoxia inducible factor-1α), which is responsible for suppressing several genes like GLUT-1, LDH, and PDK-1, which coordinate various processes involving glucose metabolism such as glycolysis (Kim et al., 2006; Zhong et al., 2010; Laemmle et al., 2012; Khan D. et al., 2018; Kuang et al., 2018). Growth hormone and IGF-1 signaling alter the metabolism of glucose (Sundaresan et al., 2012; Takasaka et al., 2014). Sirt6 controls gluconeogenesis by the receptor PGC-1α and p53/FOXO1 signaling. Inhibition of PGC-1α activity by Sirt6 occurs via deacetylation of GCN5, increasing its acetyltransferase activity, which is a form of histone acetylation and thereby increases the acetylation of PGC-1α which leads to inhibition of hepatic gluconeogenesis and thereby hyperglycemia (**Figure 3**: Schematic representation of molecular mechanism of Sirt6 in various diseases) (Jeninga et al., 2010; Satoh and Imai, 2014; Sharabi et al., 2017; Kanwal and Dsouza, 2019; Singh et al., 2019).

SIRT6 MODULATORS

Sirt6 has a plethora of biological activities, making it a vital molecule, allowing researchers to identify Sirt6 modulators (**Figure 4**, Modulators of Sirt6) in developing effective therapeutic approaches to a broad spectrum of diseases. Some endogenous activators of Sirt6 include Lamin A and long chain free fatty acids (Feldman et al., 2013; Rahnasto-Rilla et al., 2016; Ghosh, 2019). Lamin A increases the deacetylation activity of Sirt6 and Sirt1 by directly interacting with the deacetylating proteins (Ghosh et al., 2013; Ghosh et al., 2015). Free fatty acids were also seen to increase the deacetylate ing activity of Sirt6. Free fatty acids stimulated Sirt6 deacetylase activity, where acyl group binding pocket binds to free fatty acids, splaying Sirt6 subdomains, thus stimulating deacetylase activity (Feldman et al., 2013). In addition to the above endogenous activators, Sirt6 is activated by CR (Caloric restriction), c-Fos protein, p53 and increased intracellular levels of NAD^+ (Kugel and Mostoslavsky, 2014; Zhang et al., 2014; Zhang et al., 2016b; Li M. et al., 2018; Khan R. I. et al., 2018; Kuang et al., 2018; De Céu Teixeira et al., 2019).

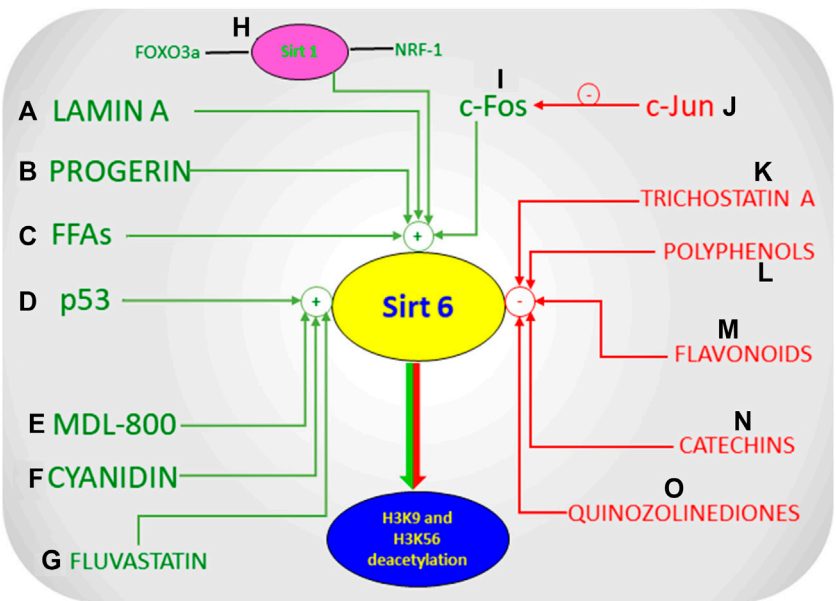

FIGURE 4 | Modulators of Sirt6.

Although CR and NAD + activates all isoforms of sirtuins, free-fatty acids and c-Fos protein selectively activates Sirt6. Furthermore, other endogenous activators that indirectly activate Sirt6 include increased Sirt1, FoxO3a, and Nrf-1 (Tosato et al., 2007; D'Onofrio et al., 2017). Pyrrolo (1,2-α) quinoxaline derivatives are among the first discovered Sirt6 activators (Hassanieh and Mostoslavsky, 2018). UBCS039 is another activator of Sirt6 which is one of the first synthetic and specific activators of the same. It has been known to cause Sirt6 specific Histone H3 deacetylation and accentuate autophagy in various types of cancer cells thereby showing its tumor suppressor effects (Iachettini et al., 2018). Another novel Sirt6 activator, CL5D also regulates the process of Histone deacetylation but its exact mechanism and clinical relevance has not yet been clearly elucidated (Klein et al., 2020).

Polyphenols, such as quercetin and luteolin at higher concentrations activate Sirt6, whereas inhibit at lower levels. Thus polyphenols modulate Sirt6 activity in a concentration dependent manner (Rahnasto-Rilla et al., 2016; Rahnasto-Rilla et al., 2018; Heger et al., 2019). Cyanidin, another polyphenol, is a potent activator of Sirt6 producing 5–15 folds increase in Sirt6 activity compared to other polyphenols (Rahnasto-Rilla et al., 2018). These compounds are non-specific modulators of Sirt6, and are able to modulate the activities of other sirtuin isoforms. Selective small molecule activators of Sirt6 like MDL-800 bind to the allosteric site, increasing Sirt6's deacetylase activity (Klein et al., 2017; You et al., 2017; Huang et al., 2018). This binding led to a significant and overall increase in deacetylation of H3K9ac and H3K56ac in HCC (human-hepatocellular-carcinoma cells) which prevented the proliferation and differentiation of HCC cells through cell cycle arrest thus proving that the activation of Sirt6 is crucial in the treatment of Hepatocellular Carcinoma (Huang et al., 2018). Fluvastatin, which competitively inhibits HMG CoA reductase, reduces cholesterol synthesis and is yet another activator of Sirt6 (Kim J. H. et al., 2018). Exposure of fluvastatin to HepG2 cells increased Sirt6 expression (Kim J. H. et al., 2018; Zhang C. et al., 2019). The mechanism underlying cholesterol regulation when fluvastatin increased Sirt6 expression was via phosphorylation of AMPKα and SREBP-1 pathway (Kim J. H. et al., 2018). Apart from activators, many small molecule Sirt6 inhibitors have been developed over time that directly acts on Sirt6 (Liu and Zheng, 2016). 2,4-dioxo-*N*-(4-(pyridin-3-yloxy) phenyl)-1,2,3,4-tetrahydroquinazoline-6-sulfonamide, a Sirt6 inhibitor, improved glucose tolerance in mice, and reduced insulin, triglycerides, and cholesterol levels indicating that a Sirt6 inhibitor could improve glycemic control in T2DM (Sociali et al., 2017; Khan R. I. et al., 2018). Trichostatin A (TSA) is an inhibitor of Sirt6 that selectively inhibits Sirt6 and no other mammalian sirtuins (Parenti et al., 2014; Wood et al., 2018; You and Steegborn, 2018). A study showed that TSA inhibited Sirt6 thus inhibiting deacetylation of p53 at lysine 382 (Wood et al., 2018), thus providing a lead compound in development of Sirt6 specific inhibitors in regulating apoptosis and stress resistance (Zhao et al., 2019). In addition to the above inhibitors, specific peptides and pseudo peptides including SDK (thioAc)TM^{21}, HKK(thioAc)LM^{21}, AKK(thioAc)LM^{21} were also studied for their ability to inhibit Sirt6 activity (Kokkonen et al., 2012; Rahnasto-Rilla et al., 2018). Derivatives of Quinazolinedione were recently discovered to inhibit Sirt6 activity, and these compounds were seen to sensitise the tumour cells to chemotherapeutic agents (Sociali et al., 2015; Rahnasto-Rilla et al., 2018). Their activity of inhibition of Sirt6 would have represented a potential therapeutic approach in the treatment of cancer, but this is not entirely true because Sirt6 acts as a double-edged sword in cancer, as activation of Sirt6 has shown to act as a tumor suppressor in many forms of cancer such as Colon, Ovarian, Prostate, Breast Cancer etc. (Lerrer et al., 2015; Lee et al., 2016; Xia Y. Q. et al., 2018) Although various Sirt6 modulators show a promising therapeutic intervention, Sirt6 under certain circumstances seems to play contradictory roles, the reason for this discrepancy is unknown, hence making it difficult to develop Sirt6 modulators (Gomes, Leal et al. 2019).

CONCLUSION

In an era where the sheer number of cases of metabolic and cardiovascular diseases is progressively escalating, resulting in a significant health challenge. Scientists are on a continuous search to discover novel molecular targets. One such target is Sirt6, an NAD + dependent histone deacetylase that regulates the expression of several essential genes. As a regulator of gene expression, Sirt6 has been implicated in cancer, neurodegenerative diseases, heart diseases, diabetes, and aging-related processes. Popularly known as "longevity protein," Sirt6 plays a critical role in aging by controlling cellular processes including genomic stability, DNA-repair, maintenance of telomere length, thereby increasing lifespan. Sirt6 involvement in increasing lifespan requires a better understanding of the molecular mechanisms of Sirt6 in humans relating to aging. In cardiovascular diseases, Sirt6 is involved in regulating the heart's multiple pathophysiological conditions, including hypertrophy, atherosclerotic vascular disease, coronary artery disease, and heart failure. Abnormal lipid metabolism also plays a crucial role in the pathogenesis of heart disease. Sirt6 activation is beneficial in alleviating various factors involved in heart disease. The ubiquity of neurodegenerative diseases is increasing, and decreased levels of Sirt6 in degenerative disease animal models have given a clear understanding of its role, especially in AD. The purpose of Sirt6 in T2DM has been extensively studied, as it improves major pathophysiological defects in pancreatic β-cells, skeletal muscle, and tissues impaired during T2DM. Therefore, Sirt6 plays a crucial role in metabolic diseases and neurodegenerative diseases; future studies should be directed in developing genetic and pharmacologic activation of Sirt6. Various activators and inhibitors that directly and indirectly modulate the activity of Sirt6 have been discovered. Further studies on these Sirt6 modulators may generate potential therapeutic targets that may enhance therapy. Sirt6 has the potential to be a critical therapeutic target in clinical approaches to treating a broad spectrum of disease states. Due to the diversified effects of Sirt6, it poses both a challenge as well as a ray of hope for extensive studies to

understand its precise mechanism and functioning, further as a potential therapeutic target, it can enhance or even substitute existing lines of therapy. Apart from the development of new modulators, extensive research must be done in concluding the roles of Sirt6 in various other diseases.

AUTHOR CONTRIBUTIONS

AK and SPS has designed, edited, and revised the manuscript. SR and LAD have written the manuscript. Final proof reading is done by by SPS and AK. All the authors have agreed the ultimate version.

ACKNOWLEDGMENTS

All authors have read and agree with the manuscript as written. We thank Professor Nader G. Abraham (1R56HL139561 NA) Departments of Internal medicine and Pharmacology from New York Medical College New York, United States, for his editorial assistance and suggestions for preparing the manuscript.

REFERENCES

Alhawiti, N. M., Al Mahri, S., Aziz, M. A., Malik, S. S., and Mohammad, S. (2017). TXNIP in metabolic regulation: physiological role and therapeutic outlook. *Curr. Drug Targets* 18, 1095–1103. doi:10.2174/1389450118666170130145514

Assadi-Porter, M. F., Reiland, H., Sabatini, M., Lorenzini, L., Carnicelli, V., Rogowski, M., et al. (2018). Metabolic reprogramming by 3-iodothyronamine (T1AM): a new perspective to reverse obesity through Co-regulation of sirtuin 4 and 6 expression. *Int. J. Mol. Sci.* 19 (5), 1535. doi:10.3390/ijms19051535

Aubert, G. and Lansdorp, P. M. (2008). Telomeres and aging. *Physiol. Rev.* 88, 557–579. doi:10.1152/physrev.00026.2007

Bae, E. J. (2017). Sirtuin 6, a possible therapeutic target for type 2 diabetes. *Arch. Pharm. Res.* 40, 1380–1389. doi:10.1007/s12272-017-0989-8

Bheda, P., Jing, H., Wolberger, C., and Lin, H. (2016). The substrate specificity of sirtuins. *Annu. Rev. Biochem.* 85, 405–429. doi:10.1146/annurev-biochem-060815-014537

Bindu, S., Pillai, V. B., and Gupta, M. P. (2016). Role of sirtuins in regulating pathophysiology of the heart. *Trends Endocrinol. Metab.* 27, 563–573. doi:10.1016/j.tem.2016.04.015

Butterfield, D. A. and Boyd-Kimball, D. (2018). Oxidative stress, amyloid-β peptide, and altered key molecular pathways in the pathogenesis and progression of alzheimer's disease. *J. Alzheimers Dis.* 62, 1345–1367. doi:10.3233/JAD-170543

Cacabelos, R., Carril, J. C., Cacabelos, N., Kazantsev, A. G., Vostrov, A. V., Corzo, L., et al. (2019). Sirtuins in alzheimer's disease: SIRT2-related GenoPhenotypes and implications for PharmacoEpiGenetics. *Int. J. Mol. Sci.* 20, 1249. doi:10.3390/ijms20051249

Cacchione, S., Biroccio, A., and Rizzo, A. (2019). Emerging roles of telomeric chromatin alterations in cancer. *J. Exp. Clin. Cancer Res.* 38, 21. doi:10.1186/s13046-019-1030-5

Cai, Y., Yu, S. S., Chen, S. R., Pi, R. B., Gao, S., Li, H., et al. (2012). Nmnat2 protects cardiomyocytes from hypertrophy via activation of SIRT6. *FEBS Lett.* 586, 866–874. doi:10.1016/j.febslet.2012.02.014

Cai, Z., Yan, L. J., and Ratka, A. (2013). Telomere shortening and Alzheimer's disease. *Neuromolecular Med.* 15, 25–48. doi:10.1007/s12017-012-8207-9

Cao, D., Zhao, J., Nguyan, L. N., Nguyen, L. N. T., Khanal, S., Dang, X., et al. (2019). Disruption of telomere integrity and DNA repair machineries by KML001 induces T cell senescence, apoptosis, and cellular dysfunctions. *Front. Immunol.* 10, 1152. doi:10.3389/fimmu.2019.01152

Carafa, V., Nebbioso, A., and Altucci, L. (2012). Sirtuins and disease: the road ahead. *Front. Pharmacol.* 3, 4. doi:10.3389/fphar.2012.00004

Chaudhary, R., Garg, J., Shah, N., and Sumner, A. (2017). PCSK9 inhibitors: a new era of lipid lowering therapy. *World J. Cardiol.* 9, 76–91. doi:10.4330/wjc.v9.i2.76

Chellappan, D. K., Yap, W. S., Bt Ahmad Suhaimi, N. A., Gupta, G., and Dua, K. (2018). Current therapies and targets for type 2 diabetes mellitus. *Panminerva Med.* 60, 117–131. doi:10.23736/S0031-0808.18.03455-9

Chen, Q., Hao, W., Xiao, C., Wang, R., Xu, X., Lu, H., et al. (2017). SIRT6 is essential for adipocyte differentiation by regulating mitotic clonal expansion. *Cell Rep.* 18, 3155–3166. doi:10.1016/j.celrep.2017.03.006

Corbi, G., Conti, V., Scapagnini, G., Filippelli, A., and Ferrara, N. (2012). Role of sirtuins, calorie restriction and physical activity in aging. *Front. Biosci. (Elite Ed.)* 4, 768–778. doi:10.2741/417

D'onofrio, N., Servillo, L., and Balestrieri, M. L. (2017). SIRT1 and SIRT6 signaling pathways in cardiovascular disease protection. *Antioxid. Redox Signal.* 28, 711–732. doi:10.1089/ars.2017.7178

Dai, H., Sinclair, D. A., Ellis, J. L., and Steegborn, C. (2018). Sirtuin activators and inhibitors: promises, achievements, and challenges. *Pharmacol. Ther.* 188, 140–154. doi:10.1016/j.pharmthera.2018.03.004

De Céu Teixeira, M., Sanchez-Lopez, E., Espina, M., Garcia, M. L., Durazzo, A., Lucarini, M., et al. (2019). Sirtuins and SIRT6 in carcinogenesis and in diet. *Int. J. Mol. Sci.* 20, 4945. doi:10.3390/ijms20194945

Demir, I. E., Ceyhan, G. O., and Friess, H. (2017). Epigenomic therapies: the potential of targeting SIRT6 for the treatment of pancreatic cancer. *Expert Opin. Ther. Targets* 21, 1–3. doi:10.1080/14728222.2017.1265507

Dominy, J. E., Jr., Lee, Y., Jedrychowski, M. P., Chim, H., Jurczak, M. J., Camporez, J. P., et al. (2012). The deacetylase Sirt6 activates the acetyltransferase GCN5 and suppresses hepatic gluconeogenesis. *Mol. Cell* 48, 900–913. doi:10.1016/j.molcel.2012.09.030

Dryden, S. C., Nahhas, F. A., Nowak, J. E., Goustin, A. S., and Tainsky, M. A. (2003). Role for human SIRT2 NAD-dependent deacetylase activity in control of mitotic exit in the cell cycle. *Mol. Cell Biol.* 23, 3173–3185. doi:10.1128/mcb.23.9.3173-3185.2003

Eberle, D., Hegarty, B., Bossard, P., Ferré, P., and Foufelle, F. (2004). SREBP transcription factors: master regulators of lipid homeostasis. *Biochimie* 86, 839–848. doi:10.1016/j.biochi.2004.09.018

Eguchi, S., Kawai, T., Scalia, R., and Rizzo, V. (2018). Understanding angiotensin II type 1 receptor signaling in vascular pathophysiology. *Hypertension* 71, 804–810. doi:10.1161/HYPERTENSIONAHA.118.10266

Elhanati, S., Kanfi, Y., Varvak, A., Roichman, A., Barth, S., Gibor, G., et al. (2013). Carmel-gross, I.multiple regulatory layers of SREBP1/2 by SIRT6. *Cell Rep.* 4, 905–912. doi:10.1016/j.celrep.2013.08.006

Feldman, J. L., Baeza, J., and Denu, J. M. (2013). Activation of the protein deacetylase SIRT6 by long-chain fatty acids and widespread deacylation by mammalian sirtuins. *J. Biol. Chem.* 288, 31350–31356. doi:10.1074/jbc.C113.511261

Ferrer, C. M., Alders, M., Postma, A. V., Park, S., Klein, M. A., Cetinbas, M., et al. (2018). An inactivating mutation in the histone deacetylase SIRT6 causes human perinatal lethality. *Genes Dev.* 32, 373–388. doi:10.1101/gad.307330.117

Finkel, T., Serrano, M., and Blasco, M. A. (2007). The common biology of cancer and ageing. *Nature* 448, 767–774. doi:10.1038/nature05985

Forero, D. A., González-Giraldo, Y., López-Quintero, C., Castro-Vega, L. J., Barreto, G. E., and Perry, G. (2016). Meta-analysis of telomere length in alzheimer's disease. *J. Gerontol. A Biol. Sci. Med. Sci.* 71, 1069–1073. doi:10.1093/gerona/glw053

Fujimoto, M., Takii, R., Takaki, E., Katiyar, A., Nakato, R., Shirahige, K., et al. (2017). The HSF1-PARP13-PARP1 complex facilitates DNA repair and promotes mammary tumorigenesis, *Nat. Commun.* 8, 1638. doi:10.1038/s41467-017-01807-7

Gao, T., Li, M., Mu, G., Hou, T., Zhu, W.-G., and Yang, Y. (2019). PKCζ phosphorylates SIRT6 to mediate fatty acid β-oxidation in colon cancer cells. *Neoplasia* 21, 61–73. doi:10.1016/j.neo.2018.11.008

Gao, W. Y., Chen, P. Y., Chen, S. F., and Wu, M. J. (2018). Pinostrobin inhibits proprotein convertase subtilisin/kexin-type 9 (PCSK9) gene expression through the modulation of FoxO3a protein in HepG2 cells, *J. Agric. Food Chem.* 66, 6083–6093. doi:10.1021/acs.jafc.8b02559

Gavrilov, L. A. and Gavrilova, N. S. (2002). Evolutionary theories of aging and longevity. *ScientificWorldJournal* 2, 339–356. doi:10.1100/tsw.2002.96

Gertman, O., Omer, D., Hendler, A., Stein, D., Onn, L., Khukhin, Y., et al. (2018). Directed evolution of SIRT6 for improved deacylation and glucose homeostasis maintenance. *Sci. Rep.* 8, 3538. doi:10.1038/s41598-018-21887-9

Ghosh, S., Liu, B., and Zhou, Z. (2013). Resveratrol activates SIRT1 in a Lamin A-dependent manner.*Cell Cycle* 12 (6), 872–876. doi:10.4161/cc.24061

Ghosh, S., Liu, B., Wang, Y., Hao, Q., and Zhou, Z. (2015). Lamin A is an endogenous SIRT6 activator and promotes SIRT6-mediated DNA repair. *Cell Rep.* 13, 1396–1406. doi:10.1016/j.celrep.2015.10.006

Ghosh, S. (2019). "Results-I. Lamin A is an endogenous activator of SIRT6 in DNA damage repair process," in *SIRT6 activities in DNA damage repair and premature aging: functions of SIRT6*. Editor S. Ghosh (Singapore: Springer Singapore), 73–95.

Ghosh, S., Wong, S. K., Jiang, Z., and Liu, B. (2018). Haploinsufficiency of Trp53 dramatically extends the lifespan of Sirt6-deficient mice. *Elife* 7, e32127. doi:10.7554/eLife.32127

Giblin, W. and Lombard, D. B. (2016). "Chapter 3 - sirtuins, healthspan, and longevity in mammals," in *Handbook of the biology of aging*. 8th Edn, Editors M.R. Kaeberlein and G.M. Martin (San Diego: Academic Press), 83–132.

Glerup, S., Schulz, R., Laufs, U., and Schlüter, K. D. (2017). Physiological and therapeutic regulation of PCSK9 activity in cardiovascular disease. *Basic Res. Cardiol.* 112, 32. doi:10.1007/s00395-017-0619-0

Gomes, P., Leal, H., Mendes, A. F., Reis, F., and Cavadas, C. (2019). Dichotomous sirtuins: implications for drug discovery in neurodegenerative and cardiometabolic diseases. *Trends Pharmacol. Sci.* 40 (12), 1021–1039. doi:10.1016/j.tips.2019.09.003

Grabowska, W., Sikora, E., and Bielak-Zmijewska, A. (2017). Sirtuins, a promising target in slowing down the ageing process, *Biogerontology* 18, 447–476. doi:10.1007/s10522-017-9685-9

Graham, E., Rymarchyk, S., Wood, M., and Cen, Y. (2018). Development of activity-based chemical probes for human sirtuins, *ACS Chem. Biol.* 13, 782–792. doi:10.1021/acschembio.7b00754

Guarente, L. (2007). Sirtuins in aging and disease. *Cold Spring Harb. Symp. Quant. Biol.* 72, 483–488. doi:10.1101/sqb.2007.72.024

Guo, J., Wang, Z., Wu, J., Liu, M., Li, M., Sun, Y., et al. (2019). Endothelial SIRT6 is vital to prevent hypertension and associated cardiorenal injury through targeting nkx3.2-GATA5 signaling. *Circ. Res.* 124, 1448–1461. doi:10.1161/CIRCRESAHA.118.314032

Haigis, M. C. and Sinclair, D. A. (2010). Mammalian sirtuins: biological insights and disease relevance. *Annu. Rev. Pathol.* 5, 253–295. doi:10.1146/annurev.pathol.4.110807.092250

Handelsman, Y. and Lepor Norman, E. (2018). PCSK9 inhibitors in lipid management of patients with diabetes mellitus and high cardiovascular risk: a review. *J. Am. Heart Assoc.* 7, e008953. doi:10.1161/JAHA.118.008953

Harlan, B. A., Pehar, M., Killoy, K. M., and Vargas, M. R. (2019). Enhanced SIRT6 activity abrogates the neurotoxic phenotype of astrocytes expressing ALS-linked mutant SOD1. *FASEB J.* 33, 7084–7091. doi:10.1096/fj.201802752R

Hassanieh, S. and Mostoslavsky, R. (2018). "Chapter 9 - multitasking roles of the mammalian deacetylase SIRT6," in *Introductory review on sirtuins in biology, aging, and disease*. Editors L. Guarente, R. Mostoslavsky, and A. Kazantsev (Cambridge, MA: Academic Press), 117–130.

He, Y., Xiao, Y., Yang, X., Li, Y., Wang, B., Yao, F., et al. (2017). SIRT6 inhibits TNF-α-induced inflammation of vascular adventitial fibroblasts through ROS and Akt signaling pathway. *Exp. Cell Res.* 357, 88–97. doi:10.1016/j.yexcr.2017.05.001

Heger, V., Tyni, J., Hunyadi, A., Horáková, L., Lahtela-Kakkonen, M., and Rahnasto-Rilla, M. (2019). Quercetin based derivatives as sirtuin inhibitors. *Biomed. Pharmacother.* 111, 1326–1333. doi:10.1016/j.biopha.2019.01.035

Hirvonen, K., Laivuori, H., Lahti, J., Strandberg, T., Eriksson, J. G., and Hackman, P. (2017). SIRT6 polymorphism rs117385980 is associated with longevity and healthy aging in Finnish men. *BMC Med. Genet.* 18, 41. doi:10.1186/s12881-017-0401-z

Hoffmann, G., Breitenbucher, F., Schuler, M., and Ehrenhofer-Murray, A. E. (2014). A novel sirtuin 2 (SIRT2) inhibitor with p53-dependent pro-apoptotic activity in non-small cell lung cancer. *J. Biol. Chem.* 289, 5208–5216. doi:10.1074/jbc.M113.487736

Hu, C. J., Iyer, S., Sataur, A., Covello, K. L., Chodosh, L. A., and Simon, M. C. (2006). Differential regulation of the transcriptional activities of hypoxia-inducible factor 1 alpha (HIF-1alpha) and HIF-2alpha in stem cells. *Mol. Cell Biol.* 26, 3514–3526. doi:10.1128/MCB.26.9.3514-3526.2006

Huang, W. J., Zhang, X., and Chen, W. W. (2016). Role of oxidative stress in Alzheimer's disease. *Biomed. Rep.* 4, 519–522. doi:10.3892/br.2016.630

Huang, Z., Zhao, J., Deng, W., Chen, Y., Shang, J., Song, K., et al. (2018). Identification of a cellularly active SIRT6 allosteric activator, *Nat. Chem. Biol.* 14, 1118–1126. doi:10.1038/s41589-018-0150-0

Ianni, A., Yuan, X., Bober, E., and Braun, T. (2018). Sirtuins in the cardiovascular system: potential targets in pediatric cardiology. *Pediatr. Cardiol.* 39, 983–992. doi:10.1007/s00246-018-1848-1

Jeninga, E. H., Schoonjans, K., and Auwerx, J. (2010). Reversible acetylation of PGC-1: connecting energy sensors and effectors to guarantee metabolic flexibility. *Oncogene* 29, 4617–4624. doi:10.1038/onc.2010.206

Jiang, H., Khan, S., Wang, Y., Charron, G., He, B., Sebastian, C., et al. (2013). SIRT6 regulates TNF-α secretion through hydrolysis of long-chain fatty acyl lysine. *Nature* 496**,** 110–113. doi:10.1038/nature12038

Jiang, H., Zhang, X., and Lin, H. (2016). Lysine fatty acylation promotes lysosomal targeting of TNF-α. *Sci. Rep.* 6, 24371. doi:10.1038/srep24371

Jin, K. (2010). Modern biological theories of aging. *Aging Dis.* 1, 72–74.

Josephs, S. F., Ichim, T. E., Prince, S. M., Kesari, S., Marincola, F. M., Escobedo, A. R., et al. (2018). Unleashing endogenous TNF-alpha as a cancer immunotherapeutic. *J. Transl. Med.* 16, 242. doi:10.1186/s12967-018-1611-7

Jun, J. C., Rathore, A., Younas, H., Gilkes, D., and Polotsky, V. Y. (2017). Hypoxia-inducible factors and cancer. *Curr. Sleep Med. Rep.* 3, 1–10. doi:10.1007/s40675-017-0062-7

Jung, E. S., Choi, H., Song, H., Hwang, Y. J., Kim, A., Ryu, H., et al. (2016). p53-dependent SIRT6 expression protects Aβ42-induced DNA damage. *Sci. Rep.* 6, 25628. doi:10.1038/srep25628

Kaluski, S., Portillo, M., Besnard, A., Stein, D., Einav, M., Zhong, L., et al. (2017). Neuroprotective functions for the histone deacetylase SIRT6. *Cell Rep.* 18, 3052–3062. doi:10.1016/j.celrep.2017.03.008

Kanfi, Y., Naiman, S., Amir, G., Peshti, V., Zinman, G., Nahum, L., et al. (2012). The sirtuin SIRT6 regulates lifespan in male mice. *Nature* 483, 218–221. doi:10.1038/nature10815

Kanwal, A. (2018). Functional and therapeutic potential of mitochondrial SIRT3 deacetylase in disease conditions. *Expert Rev. Clin. Pharmacol.* 11, 1151–1155. doi:10.1080/17512433.2018.1546119

Kanwal, A., Pillai, V. B., Samant, S., Gupta, M., and Gupta, M. P. (2019b). The nuclear and mitochondrial sirtuins, Sirt6 and Sirt3, regulate each other's activity and protect the heart from developing obesity-mediated diabetic cardiomyopathy. *FASEB J.* 33, 10872–10888. doi:10.1096/fj.201900767R

Kanwal, A. and Dsouza, L. A. (2019). Sirtuins and diabetes: optimizing the sweetness in the blood. *Transl. Med. Commun.* 4, 3. doi:10.1186/s41231-019-0034-7

Kawahara, T. L., Michishita, E., Adler, A. S., Damian, M., Berber, E., Lin, M., et al. (2009). SIRT6 links histone H3 lysine 9 deacetylation to NF-kappaB-dependent gene expression and organismal life span. *Cell* 136, 62–74. doi:10.1016/j.cell.2008.10.052

Kawanishi, S. and Oikawa, S. (2004). Mechanism of telomere shortening by oxidative stress. *Ann. N. Y. Acad. Sci.* 1019, 278–284. doi:10.1196/annals.1297.047

Kerchner, G. A. and Wyss-Coray, T. (2016). "The role of aging in alzheimer's disease," in *Advances in geroscience*. Editors F. Sierra and R. Kohanski (Cham: Springer International Publishing), 197–227.

Khan, D., Sarikhani, M., Dasgupta, S., Maniyadath, B., Pandit, A. S., Mishra, S., et al. (2018). SIRT6 deacetylase transcriptionally regulates glucose metabolism in heart, *J. Cell. Physiol.* 233, 5478–5489. doi:10.1002/jcp.26434

Khan, R. I., Nirzhor, S. S. R., and Akter, R. (2018). A review of the recent advances made with SIRT6 and its implications on aging related processes, major human

diseases, and possible therapeutic targets. *Biomolecules* 8, 44. doi:10.3390/biom8030044

Kim, H., Kim, H.-S., and Kaang, B.-K. (2018). Elevated contextual fear memory by SIRT6 depletion in excitatory neurons of mouse forebrain. *Mol. Brain* 11, 49. doi:10.1186/s13041-018-0391-6

Kim, J. H., Lee, J. M., Kim, J. H., and Kim, K. R. (2018). Fluvastatin activates sirtuin 6 to regulate sterol regulatory element-binding proteins and AMP-activated protein kinase in HepG2 cells. *Biochem. Biophys. Res. Commun.* 503, 1415–1421. doi:10.1016/j.bbrc.2018.07.057

Kim, J. W., Tchernyshyov, I., Semenza, G. L., and Dang, C. V. (2006). HIF-1-mediated expression of pyruvate dehydrogenase kinase: a metabolic switch required for cellular adaptation to hypoxia. *Cell Metab.* 3, 177–185. doi:10.1016/j.cmet.2006.02.002

Kitada, M., Kume, S., Kanasaki, K., Takeda-Watanabe, A., and Koya, D. (2013). Sirtuins as possible drug targets in type 2 diabetes. *Curr. Drug Targets* 14, 622–636. doi:10.2174/1389450111314060002

Klein, M. A., Liu, C., Kuznetsov, V. I., Feltenberger, J. B., Tang, W., and Denu, J. M. (2020). Mechanism of activation for the sirtuin 6 protein deacylase. *J. Biol. Chem.* 295 (5), 1385–1399. doi:10.1074/jbc.RA119.011285

Klein, M., Liu, C., Camacho, B., Tang, W., and Denu, J. M. (2017). Development and mechanism of small-molecule SIRT6 activators. *FAESB J.* 31, 921.9. doi:10.1096/fasebj.31.1_supplement.921.9

Kobayashi, Y., Furukawa-Hibi, Y., Chen, C., Horio, Y., Isobe, K., Ikeda, K., et al. (2005). SIRT1 is critical regulator of FOXO-mediated transcription in response to oxidative stress. *Int. J. Mol. Med.* 16, 237–243. doi:10.3892/ijmm.16.2.237

Kocahan, S. and Doğan, Z. (2017). Mechanisms of alzheimer's disease pathogenesis and prevention: the brain, neural pathology, N-methyl-D-aspartate receptors, tau protein and other risk factors. *Clin. Psychopharmacol. Neurosci.* 15, 1–8. doi:10.9758/cpn.2017.15.1.1

Kokkonen, P., Rahnasto-Rilla, M., Kiviranta, P. H., Huhtiniemi, T., Laitinen, T., Poso, A., et al. (2012). Peptides and pseudopeptides as SIRT6 deacetylation inhibitors. *ACS Med. Chem. Lett.* 3, 969–974. doi:10.1021/ml300139n

Kuang, J., Zhang, Y., Liu, Q., Shen, J., Pu, S., Cheng, S., et al. (2017). Fat-specific Sirt6 ablation sensitizes mice to high-fat diet-induced obesity and insulin resistance by inhibiting lipolysis. *Diabetes* 66, 1159. doi:10.2337/db16-1225

Kuang, J., Chen, L., Tang, Q., Zhang, J., Li, Y., and He, J. (2018). The role of Sirt6 in obesity and diabetes. *Front. Physiol.* 9, 135. doi:10.3389/fphys.2018.00135

Kugel, S. and Mostoslavsky, R. (2014). Chromatin and beyond: the multitasking roles for SIRT6. *Trends Biochem. Sci.* 39, 72–81. doi:10.1016/j.tibs.2013.12.002

Kupis, W., Pałyga, J., Tomal, E., and Niewiadomska, E. (2016). The role of sirtuins in cellular homeostasis. *J. Physiol. Biochem.* 72, 371–380. doi:10.1007/s13105-016-0492-6

Laemmle, A., Lechleiter, A., Roh, V., Schwarz, C., Portmann, S., Furer, C., et al. (2012). Inhibition of SIRT1 impairs the accumulation and transcriptional activity of HIF-1α protein under hypoxic conditions. *PLoS One* 7, e33433. doi:10.1371/journal.pone.0033433

Lappas, M. (2012). Anti-inflammatory properties of sirtuin 6 in human umbilical vein endothelial cells. *Mediators Inflamm.* 2012, 597514. doi:10.1155/2012/597514

Lee, D. and Goldberg, A. L. (2013). SIRT1 protein, by blocking the activities of transcription factors FoxO1 and FoxO3, inhibits muscle atrophy and promotes muscle growth. *J. Biol. Chem.* 288, 30515–30526. doi:10.1074/jbc.M113.489716

Lee, J. T. and Gu, W. (2013). SIRT1: regulator of p53 deacetylation. *Genes Cancer* 4, 112–117. doi:10.1177/1947601913484496

Lee, N., Ryu, H. G., Kwon, J. H., Kim, D. K., Kim, S. R., Wang, H. J., et al. (2016). SIRT6 depletion suppresses tumor growth by promoting cellular senescence induced by DNA damage in HCC. *PLoS One* 11, e0165835. doi:10.1371/journal.pone.0165835

Lee, W.-S. and Kim, J. (2018). Insulin-like growth factor-1 signaling in cardiac aging. *Biochim. Biophys. Acta Mol. Basis Dis.* 1864, 1931–1938. doi:10.1016/j.bbadis.2017.08.029

Lee, Y., Ka, S. O., Cha, H. N., Chae, Y. N., Kim, M. K., Park, S. Y., et al. (2017). Myeloid sirtuin 6 deficiency causes insulin resistance in high-fat diet-fed mice by eliciting macrophage polarization toward an M1 phenotype, *Diabetes* 66, 2659–2668. doi:10.2337/db16-1446

Lerrer, B., Gertler, A. A., and Cohen, H. Y. (2015). The complex role of SIRT6 in carcinogenesis. *Carcinogenesis* 37, 108–118. doi:10.1093/carcin/bgv167

Li, M., Hou, T., Gao, T., Lu, X., Yang, Q., Zhu, Q., et al. (2018). p53 cooperates with SIRT6 to regulate cardiolipin de novo biosynthesis. *Cell Death Dis.* 9, 941. doi:10.1038/s41419-018-0984-0

Li, Z., Xu, K., Zhang, N., Amador, G., Wang, Y., Zhao, S., et al. (2018). Overexpressed SIRT6 attenuates cisplatin-induced acute kidney injury by inhibiting ERK1/2 signaling. *Kidney Int.* 93, 881–892. doi:10.1016/j.kint.2017.10.021

Li, Y., Meng, X., Wang, W., Liu, F., Hao, Z., Yang, Y., et al. (2017). Cardioprotective effects of SIRT6 in a mouse model of transverse aortic constriction-induced heart failure. *Front. Physiol.* 8, 394. doi:10.3389/fphys.2017.00394

Liao, C. Y. and Kennedy, B. K. (2016). SIRT6, oxidative stress, and aging. *Cell Res.* 26, 143–144. doi:10.1038/cr.2016.8

Liu, J. and Zheng, W. (2016). Cyclic peptide-based potent human SIRT6 inhibitors. *Org. Biomol. Chem.* 14, 5928–5935. doi:10.1039/c5ob02339d

Liu, M., Huo, Y. R., Wang, J., Wang, C., Liu, S., Liu, S., et al. (2016). Telomere shortening in alzheimer's disease patients. *Ann. Clin. Lab. Sci.* 46, 260–265

Liu, T. F., Vachharajani, V. T., Yoza, B. K., and Mccall, C. E. (2012). NAD+-dependent sirtuin 1 and 6 proteins coordinate a switch from glucose to fatty acid oxidation during the acute inflammatory response. *J. Biol. Chem.* 287, 25758–25769. doi:10.1074/jbc.M112.362343

Lombard, D. B., Schwer, B., Alt, F. W., and Mostoslavsky, R. (2008). SIRT6 in DNA repair, metabolism and ageing. *J. Intern. Med.* 263, 128–141. doi:10.1111/j.1365-2796.2007.01902.x

López-Lluch, G. and Navas, P. (2016). Calorie restriction as an intervention in ageing. *J. Physiol.* 594, 2043–2060. doi:10.1113/JP270543

Lu, J., Sun, D., Liu, Z., Li, M., Hong, H., Liu, C., et al. (2016). SIRT6 suppresses isoproterenol-induced cardiac hypertrophy through activation of autophagy. *Transl. Res.* 172, 96. doi:10.1016/j.trsl.2016.03.002

Mahler, R. J. and Adler, M. L. (1999). Clinical review 102: type 2 diabetes mellitus: update on diagnosis, pathophysiology, and treatment. *J. Clin. Endocrinol. Metab.* 84, 1165–1171. doi:10.1210/jcem.84.4.5612

Mao, K., Quipildor, G. F., Tabrizian, T., Novaj, A., Guan, F., Walters, R. O., et al. (2018). Late-life targeting of the IGF-1 receptor improves healthspan and lifespan in female mice. *Nat. Commun.* 9, 2394. doi:10.1038/s41467-018-04805-5

Mao, Z., Hine, C., Tian, X., Van Meter, M., Au, M., Vaidya, A., et al. (2011). SIRT6 promotes DNA repair under stress by activating PARP1. *Science* 332, 1443–1446. doi:10.1126/science.1202723

Markesbery, W. R. (1999). The role of oxidative stress in alzheimer disease. *Arch. Neurol.* 56, 1449–1452. doi:10.1001/archneur.56.12.1449

Michishita, E., Mccord, R. A., Berber, E., Kioi, M., Padilla-Nash, H., Damian, M., et al. (2008). SIRT6 is a histone H3 lysine 9 deacetylase that modulates telomeric chromatin. *Nature* 452, 492–496. doi:10.1038/nature06736

Mohamad Nasir, N. F., Zainuddin, A., and Shamsuddin, S. (2018). Emerging roles of sirtuin 6 in alzheimer's disease. *J. Mol. Neurosci.* 64, 157–161. doi:10.1007/s12031-017-1005-y

Mostoslavsky, R., Chua, K. F., Lombard, D. B., Pang, W. W., Fischer, M. R., Gellon, L., et al. (2006). Genomic instability and aging-like phenotype in the absence of mammalian SIRT6. *Cell* 124, 315–329. doi:10.1016/j.cell.2005.11.044

Nagaraj, K., Lapkina-Gendler, L., Sarfstein, R., Gurwitz, D., Pasmanik-Chor, M., Laron, Z., et al. (2018). Identification of thioredoxin-interacting protein (TXNIP) as a downstream target for IGF1 action. *Proc. Natl. Acad. Sci. U.S.A.* 115, 1045. doi:10.1073/pnas.1715930115

Naiman, S. and Cohen, H. Y. (2018). Role for the longevity protein SIRT6 in primate development. *Nature* 560, 559–560. doi:10.1038/d41586-018-05970-9

Niu, Y. (2019). Genetic monkeys reveal a new role for a longevity protein in embryonic development. *Natl. Sci. Rev.* 6, 392. doi:10.1093/nsr/nwz051

Pan, H., Guan, D., Liu, X., Li, J., Wang, L., Wu, J., et al. (2016). SIRT6 safeguards human mesenchymal stem cells from oxidative stress by coactivating NRF2. *Cell Res.* 26, 190–205. doi:10.1038/cr.2016.4

Pan, P. W., Feldman, J. L., Devries, M. K., Dong, A., Edwards, A. M., and Denu, J. M. (2011). Structure and biochemical functions of SIRT6. *J. Biol. Chem.* 286, 14575–14587. doi:10.1074/jbc.M111.218990

Parenti, M. D., Grozio, A., Bauer, I., Galeno, L., Damonte, P., Millo, E., et al. (2014). Discovery of novel and selective SIRT6 inhibitors. *J. Med. Chem.* 57, 4796–4804. doi:10.1021/jm500487d

Parhofer, K. G. (2016). The treatment of disorders of lipid metabolism. *Dtsch. Arztebl. Int.* 113, 261–268. doi:10.3238/arztebl.2016.0261

Peshti, V., Obolensky, A., Nahum, L., Kanfi, Y., Rathaus, M., Avraham, M., et al. (2017). Characterization of physiological defects in adult SIRT6-/- mice. *PLoS One* 12, e0176371. doi:10.1371/journal.pone.0176371

Pezzuto, A. and Carico, E. (2018). Role of HIF-1 in cancer progression: novel insights. A review. *Curr. Mol. Med.* 18, 343–351. doi:10.2174/1566524018666181109121849

Pillai, V. B., Sundaresan, N. R., and Gupta, M. P. (2014). Regulation of Akt signaling by sirtuins: its implication in cardiac hypertrophy and aging. *Circ. Res.* 114, 368–378. doi:10.1161/CIRCRESAHA.113.300536

Polito, L., Kehoe, P. G., Forloni, G., and Albani, D. (2010). The molecular genetics of sirtuins: association with human longevity and age-related diseases. *Int. J. Mol. Epidemiol. Genet.* 1, 214–225

Qin, K., Zhang, N., Zhang, Z., Nipper, M., Zhu, Z., Leighton, J., et al. (2018). SIRT6-mediated transcriptional suppression of Txnip is critical for pancreatic beta cell function and survival in mice. *Diabetologia* 61, 906–918. doi:10.1007/s00125-017-4542-6

Rack, J. G., Morra, R., Barkauskaite, E., Kraehenbuehl, R., Ariza, A., Qu, Y., et al. (2015). Identification of a class of protein ADP-ribosylating sirtuins in microbial pathogens. *Mol. Cell* 59, 309–320. doi:10.1016/j.molcel.2015.06.013

Rahnasto-Rilla, M., Kokkola, T., Jarho, E., Lahtela-Kakkonen, M., and Moaddel, R. (2016). N-acylethanolamines bind to SIRT6. *Chembiochem* 17, 77–81. doi:10.1002/cbic.201500482

Rahnasto-Rilla, M., Tyni, J., Huovinen, M., Jarho, E., Kulikowicz, T., Ravichandran, S., et al. (2018). Natural polyphenols as sirtuin 6 modulators. *Sci. Rep.* 8, 4163. doi:10.1038/s41598-018-22388-5

Rajabi, N., Galleano, I., Madsen, A. S., and Olsen, C. A. (2018). Targeting sirtuins: substrate specificity and inhibitor design. *Prog. Mol. Biol. Transl. Sci.* 154, 25–69. doi:10.1016/bs.pmbts.2017.11.003

Ravi, V., Jain, A., Khan, D., Ahamed, F., Mishra, S., Giri, M., et al. (2019). SIRT6 transcriptionally regulates global protein synthesis through transcription factor Sp1 independent of its deacetylase activity. *Nucleic Acids Res.* 47, 9115–9131. doi:10.1093/nar/gkz648

Ravussin, E. and Smith, S. R. (2016). "Chapter 36 - role of the adipocyte in metabolism and endocrine function," in *Endocrinology: adult and pediatric*. 7th Edn, Editors J. L. Jameson, L. J. De Groot, D. M. De Kretser, L. C. Giudice, A. B. Grossman, S. Melmed, et al. (Philadelphia: W.B. Saunders), 627–647.e629.

Rizzo, A., Iachettini, S., Salvati, E., Zizza, P., Maresca, C., D'angelo, C., et al. (2016). SIRT6 interacts with TRF2 and promotes its degradation in response to DNA damage. *Nucleic Acids Res.* 45, 1820–1834. doi:10.1093/nar/gkw1202

Rodgers, J. T. and Puigserver, P. (2006). Certainly can't live without this: SIRT6. *Cell Metab.* 3, 77–78. doi:10.1016/j.cmet.2006.01.009

Roichman, A., Kanfi, Y., Glazz, R., Naiman, S., Amit, U., Landa, N., et al. (2016). SIRT6 overexpression improves various aspects of mouse healthspan. *J. Gerontol. A Biol. Sci. Med. Sci.* 72, 603–615. doi:10.1093/gerona/glw152

Santos-Barriopedro, I., Bosch-Presegué, L., Marazuela-Duque, A., De La Torre, C., Colomer, C., Vazquez, B. N., et al. (2018). SIRT6-dependent cysteine monoubiquitination in the PRE-SET domain of Suv39h1 regulates the NF-κB pathway. *Nat. Commun.* 9, 101. doi:10.1038/s41467-017-02586-x

Santos-Barriopedro, I. and Vaquero, A. (2018). Complex role of SIRT6 in NF-κB pathway regulation. *Mol. Cell. Oncol.* 5, e1445942. doi:10.1080/23723556.2018.1445942

Satoh, A. and Imai, S. (2014). Systemic regulation of mammalian ageing and longevity by brain sirtuins. *Nat. Commun.* 5, 4211. doi:10.1038/ncomms5211

Schofield, J. D., Liu, Y., Rao-Balakrishna, P., Malik, R. A., and Soran, H. (2016). Diabetes dyslipidemia. *Diabetes Ther.* 7, 203–219. doi:10.1007/s13300-016-0167-x

Schumacher, A. (2011). "Chapter 25 - aging epigenetics," in *Handbook of epigenetics*. Editor T. Tollefsbol (San Diego: Academic Press), 405–422.

Schumacher, A. (2017). "Chapter 25–aging epigenetics," in *Handbook of epigenetics*. 2nd Edn, Editor T. O. Tollefsbol (Academic Press), 371–388.

Sergiev, P. V., Dontsova, O. A., and Berezkin, G. V. (2015). Theories of aging: an ever-evolving field. *Acta Naturae* 7, 9–18. doi:10.32607/20758251-2015-7-1-9-18

Serravallo, M., Jagdeo, J., Glick, S., Siegel, D., and Brody, N. (2013). Sirtuins in dermatology: applications for future research and therapeutics. *Arch. Dermatol. Res.* 305, 269. doi:10.1007/s00403-013-1320-2

Shalev, A. (2014). Minireview: thioredoxin-interacting protein: regulation and function in the pancreatic β-cell. *Mol. Endocrinol.* 28, 1211–1220. doi:10.1210/me.2014-1095

Sharabi, K., Lin, H., Tavares, C. D., Dominy, J. E., Camporez, J. P., Perry, R. J., et al. (2017). Selective chemical inhibition of PGC-1α gluconeogenic activity ameliorates type 2 diabetes. *Cell* 169, 148–e15. doi:10.1016/j.cell.2017.03.001

Shimano, H. and Sato, R. (2017). SREBP-regulated lipid metabolism: convergent physiology - divergent pathophysiology. *Nat. Rev. Endocrinol.* 13, 710. doi:10.1038/nrendo.2017.91

Simon, M., Van Meter, M., Ablaeva, J., Ke, Z., Gonzalez, R. S., Taguchi, T., et al. (2019). LINE1 derepression in aged wild-type and SIRT6-deficient mice drives inflammation. *Cell Metab.* 29, 871–e875. doi:10.1016/j.cmet.2019.02.014

Singh, S. P., Mcclung, J. A., Thompson, E., Glick, Y., Greenberg, M., Acosta-Baez, G., et al. (2019). Cardioprotective heme oxygenase-1-pgc1α signaling in epicardial fat attenuates cardiovascular risk in humans as in obese mice. *Obesity (Silver Spring)* 27, 1634–1643. doi:10.1002/oby.22608

Singh, S. P., Greenberg, M., Glick, Y., Bellner, L., Favero, G., Rezzani, R., et al. (2020). Adipocyte specific HO-1 gene therapy is effective in antioxidant treatment of insulin resistance and vascular function in an obese mice model. *Antioxidants (Basel)* 9, 40. doi:10.3390/antiox9010040

Sociali, G., Galeno, L., Parenti, M. D., Grozio, A., Bauer, I., Passalacqua, M., et al. (2015). Quinazolinedione SIRT6 inhibitors sensitize cancer cells to chemotherapeutics. *Eur. J. Med. Chem.* 102, 530–539. doi:10.1016/j.ejmech.2015.08.024

Sociali, G., Magnone, M., Ravera, S., Damonte, P., Vigliarolo, T., Von Holtey, M., et al. (2017). Pharmacological Sirt6 inhibition improves glucose tolerance in a type 2 diabetes mouse model. *FASEB J.* 31, 3138–3149. doi:10.1096/fj.201601294R

Song, M. Y., Wang, J., Ka, S. O., Bae, E. J., and Park, B. H. (2016). Insulin secretion impairment in Sirt6 knockout pancreatic β cells is mediated by suppression of the FoxO1-Pdx1-Glut2 pathway. *Sci. Rep.* 6, 30321. doi:10.1038/srep30321

Song, Y., Fan, Z., Bai, X., Liu, W., Han, Y., Xu, L., et al. (2016). PARP-1-modulated AIF translocation is involved in streptomycin-induced cochlear hair cell death. *Acta Otolaryngol.* 136, 545–550. doi:10.3109/00016489.2016.1143968

Spolitu, S., Okamoto, H., Dai, W., Zadroga John, A., Wittchen Erika, S., Gromada, J., et al. (2019). Hepatic glucagon signaling regulates PCSK9 and low-density lipoprotein cholesterol. *Circ. Res.* 124, 38–51. doi:10.1161/CIRCRESAHA.118.313648

Stein, D. and Toiber, D. (2017). DNA damage and neurodegeneration: the unusual suspect. *Neural Regen. Res.* 12, 1441–1442. doi:10.4103/1673-5374.215254

Sundaresan, N. R., Vasudevan, P., Zhong, L., Kim, G., Samant, S., Parekh, V., et al. (2012). The sirtuin SIRT6 blocks IGF-Akt signaling and development of cardiac hypertrophy by targeting c-Jun. *Nat. Med.* 18, 1643–1650. doi:10.1038/nm.2961

Takahashi, R. H., Nagao, T., and Gouras, G. K. (2017). Plaque formation and the intraneuronal accumulation of β-amyloid in Alzheimer's disease. *Pathol. Int.* 67, 185–193. doi:10.1111/pin.12520

Takasaka, N., Araya, J., Hara, H., Ito, S., Kobayashi, K., Kurita, Y., et al. (2014). Autophagy induction by SIRT6 through attenuation of insulin-like growth factor signaling is involved in the regulation of human bronchial epithelial cell senescence. *J. Immunol.* 192, 958. doi:10.4049/jimmunol.1302341

Tang, B. L. (2016). Sirt1 and the mitochondria. *Mol. Cells* 39, 87–95. doi:10.14348/molcells.2016.2318

Tang, B. L. (2017). Is SIRT6 activity neuroprotective and how does it differ from SIRT1 in this regard? *Front. Cell. Neurosci.* 11, 165. doi:10.3389/fncel.2017.00165

Tao, R., Xiong, X., Depinho, R. A., Deng, C. X., and Dong, X. C. (2013a). FoxO3 transcription factor and Sirt6 deacetylase regulate low density lipoprotein (LDL)-cholesterol homeostasis via control of the proprotein convertase subtilisin/kexin type 9 (Pcsk9) gene expression. *J. Biol. Chem.* 288, 29252–29259. doi:10.1074/jbc.M113.481473

Tao, R., Xiong, X., Depinho, R. A., Deng, C. X., and Dong, X. C. (2013b). Hepatic SREBP-2 and cholesterol biosynthesis are regulated by FoxO3 and Sirt6. *J. Lipid Res.* 54, 2745–2753. doi:10.1194/jlr.M039339

Tasselli, L., Zheng, W., and Chua, K. F. (2017). SIRT6: novel mechanisms and links to aging and disease. *Trends Endocrinol. Metab.* 28, 168–185. doi:10.1016/j.tem.2016.10.002

Tennen, R. I., Bua, D. J., Wright, W. E., and Chua, K. F. (2011). SIRT6 is required for maintenance of telomere position effect in human cells. *Nat. Commun.* 2, 433. doi:10.1038/ncomms1443

Tian, X., Firsanov, D., Zhang, Z., Cheng, Y., Luo, L., Tombline, G., et al. (2019). SIRT6 is responsible for more efficient DNA double-strand break repair in long-lived species. *Cell* 177, 622–e22. doi:10.1016/j.cell.2019.03.043

Tosato, M., Zamboni, V., Ferrini, A., and Cesari, M. (2007). The aging process and potential interventions to extend life expectancy. *Clin. Interv. Aging* 2, 401–412

Trevisan, K., Cristina-Pereira, R., Silva-Amaral, D., and Aversi-Ferreira, T. A. (2019). Theories of aging and the prevalence of alzheimer's disease. *BioMed. Res. Int.* 2019, 9171424. doi:10.1155/2019/9171424

Van meter, M., Simon, M., Tombline, G., May, A., Morello, T. D., Hubbard, B. P., et al. (2016). JNK phosphorylates SIRT6 to stimulate DNA double-strand break repair in response to oxidative stress by recruiting PARP1 to DNA breaks. *Cell Rep.* 16, 2641–2650. doi:10.1016/j.celrep.2016.08.006

Vassilopoulos, A., Fritz, K. S., Petersen, D. R., and Gius, D. (2011). The human sirtuin family: evolutionary divergences and functions. *Hum. Genomics.* 5, 485–496. doi:10.1186/1479-7364-5-5-485

Vitiello, M., Zullo, A., Servillo, L., Mancini, F. P., Borriello, A., Giovane, A., et al. (2017). Multiple pathways of SIRT6 at the crossroads in the control of longevity, cancer, and cardiovascular diseases. *Ageing Res. Rev.* 35, 301–311. doi:10.1016/j.arr.2016.10.008

Wang, C. and Mbalaviele, G. (2019). Role of APD-ribosylation in bone health and disease. *Cells* 8, 1201. doi:10.3390/cells8101201

Wang, G., Meyer, J. G., Cai, W., Li, M. E., Softic, S., and Kahn, C. R. (2018). Sirt5 plays a critical role in mitochondrial protein acylation and mitochondrial metabolic homeostasis in brown fat. *Diabetes* 67, 274. doi:10.2337/db18- 274-OR

Wang, K. C., Tosh, D. N., Zhang, S., Mcmillen, I. C., Duffield, J. A., Brooks, D. A., et al. (2015). IGF-2R-Gαq signaling and cardiac hypertrophy in the low-birth-weight lamb. *Am. J. Physiol. Regul. Integr. Comp. Physiol.* 308, R627–R635. doi:10.1152/ajpregu.00346.2014

Watroba, M. and Szukiewicz, D. (2016). The role of sirtuins in aging and age-related diseases. *Adv. Med. Sci.* 61, 52–62. doi:10.1016/j.advms.2015.09.003

Wei, Y. H., Ma, Y. S., Lee, H. C., Lee, C. F., and Lu, C. Y. (2001). Mitochondrial theory of aging matures–roles of mtDNA mutation and oxidative stress in human aging. *Zhonghua Yixue Zazhi (Taipei)* 64, 259–270

Wood, M., Rymarchyk, S., Zheng, S., and Cen, Y. (2018). Trichostatin A inhibits deacetylation of histone H3 and p53 by SIRT6. *Arch. Biochem. Biophys.* 638, 8–17. doi:10.1016/j.abb.2017.12.009

Wu, Y., Chen, L., Wang, Y., Li, W., Lin, Y., Yu, D., et al. (2015). Overexpression of Sirtuin 6 suppresses cellular senescence and NF-κB mediated inflammatory responses in osteoarthritis development. *Sci. Rep.* 5, 17602. doi:10.1038/srep17602

Xia, X., Jiang, Q., Mcdermott, J., and Han, J. J. (2018). Aging and Alzheimer's disease: comparison and associations from molecular to system level. *Aging Cell* 17, e12802. doi:10.1111/acel.12802

Xia, Y. Q., Hua, R. J., Juan, C., Zhong, Z. H., Tao, C. S., Fang, R., et al. (2018). SIRT6 depletion sensitizes human hepatoma cells to chemotherapeutics by downregulating MDR1 expression. *Front. Pharmacol.* 9, 194. doi:10.3389/fphar.2018.00194

Xiwen, X., Xupeng, S., Qingzhi, W., Xinlai, Q., Yang, Z., Xiaoyan, P., et al. (2016). SIRT6 protects against palmitate-induced pancreatic β-cell dysfunction and apoptosis. *J. Endocrinol.* 231, 159–165. doi:10.1530/JOE-16-0317

Xu, P., Wang, T.-T., Liu, X.-Z., Wang, N.-Y., Sun, L.-H., Zhang, Z.-Q., et al. (2019). Sirt6 regulates efficiency of mouse somatic reprogramming and maintenance of pluripotency. *Stem Cell Res. Ther.* 10, 9. doi:10.1186/s13287-018-1109-5

Xu, S., Yin, M., Koroleva, M., Mastrangelo, M. A., Zhang, W., Bai, P., et al. (2016). SIRT6 protects against endothelial dysfunction and atherosclerosis in mice. *Aging (Albany NY)* 8, 1064–1082. doi:10.18632/aging.100975

Xu, Z., Zhang, L., Zhang, W., Meng, D., Zhang, H., Jiang, Y., et al. (2015). SIRT6 rescues the age related decline in base excision repair in a PARP1-dependent manner. *Cell Cycle* 14, 269–276. doi:10.4161/15384101.2014.980641

Yan, K., Wang, K., and Li, P. (2019). The role of post-translational modifications in cardiac hypertrophy. *J. Cell Mol. Med.* 23, 3795–3807. doi:10.1111/jcmm.14330

Yang, G., Liu, C., Chen, S. H., Kassab, M. A., Hoff, J. D., Walter, N. G., et al. (2018). Super-resolution imaging identifies PARP1 and the Ku complex acting as DNA double-strand break sensors. *Nucleic Acids Res.* 46, 3446–3457. doi:10.1093/nar/gky088

Yang, H., Zhu, R., Zhao, X., Liu, L., Zhou, Z., Zhao, L., et al. (2019). Sirtuin-mediated deacetylation of hnRNP A1 suppresses glycolysis and growth in hepatocellular carcinoma. *Oncogene* 38, 4915–4931. doi:10.1038/s41388-019-0764-z

Yang, Z., Yu, W., Huang, R., Ye, M., and Min, Z. (2019). SIRT6/HIF-1α axis promotes papillary thyroid cancer progression by inducing epithelial–mesenchymal transition. *Cancer Cell Int.* 19, 17. doi:10.1186/s12935-019-0730-4

Yao, L., Cui, X., Chen, Q., Yang, X., Fang, F., Zhang, J., et al. (2017). Cold-inducible SIRT6 regulates thermogenesis of Brown and beige fat. *Cell Rep.* 20, 641–654. doi:10.1016/j.celrep.2017.06.069

Ye, X., Li, M., Hou, T., Gao, T., Zhu, W. G., and Yang, Y. (2017). Sirtuins in glucose and lipid metabolism. *Oncotarget* 8, 1845–1859. doi:10.18632/oncotarget.12157

Yeo, D., Kang, C., and Ji, L. (2017). Overexpression of SIRT6 suppresses TNFα-induced muscle cell atrophy via NFκB inhibition. *FASEB J.* 31, doi:1022.10161022.1016

Yepuri, G. and Ramasamy, R. (2019). Significance and mechanistic relevance of SIRT6-mediated endothelial dysfunction in cardiovascular disease progression. *Circ. Res.* 124, 1408–1410. doi:10.1161/CIRCRESAHA.119.315098

You, W., Rotili, D., Li, T. M., Kambach, C., Meleshin, M., Schutkowski, M., et al. (2017). Structural basis of sirtuin 6 activation by synthetic small molecules. *Angew Chem. Int. Ed. Engl.* 56, 1007–1011. doi:10.1002/anie.201610082

You, W. and Steegborn, C. (2018). Structural basis of sirtuin 6 inhibition by the hydroxamate trichostatin A: implications for protein deacylase drug development *J. Med. Chem.* 61, 10922–10928. doi:10.1021/acs.jmedchem.8b01455

Yu, S. S., Cai, Y., Ye, J. T., Pi, R. B., Chen, S. R., Liu, P. Q., et al. (2013). Sirtuin 6 protects cardiomyocytes from hypertrophy *in vitro* via inhibition of NF-κB-dependent transcriptional activity. *Br. J. Pharmacol.* 168, 117–128. doi:10.1111/j.1476-5381.2012.01903.x

Yu, W., Qin, J., Chen, C., Fu, Y., and Wang, W. (2018). Moderate calorie restriction attenuates age-associated alterations and improves cardiac function by increasing SIRT1 and SIRT3 expression. *Mol. Med. Rep.* 18, 4087–4094. doi:10.3892/mmr.2018.9390

Zhang, C., Yu, Y., Huang, Q., and Tang, K. (2019). SIRT6 regulates the proliferation and apoptosis of hepatocellular carcinoma via the ERK1/2 signaling pathway. *Mol. Med. Rep.* 20, 1575–1582. doi:10.3892/mmr.2019.10398

Zhang, Q., Tu, W., Tian, K., Han, L., Wang, Q., Chen, P., et al. (2019). Sirtuin 6 inhibits myofibroblast differentiation via inactivating transforming growth factor-beta1/Smad2 and nuclear factor-kappaB signaling pathways in human fetal lung fibroblasts. *J. Cell Biochem.* 120, 93–104. doi:10.1002/jcb.27128

Zhang, D., Jing, J., Lou, F., Li, R., Ping, Y., Yu, F., et al. (2018). Evidence for excessive osteoclast activation in SIRT6 null mice. *Sci. Rep.* 8, 10992. doi:10.1038/s41598-018-28716-z

Zhang, W., Wan, H., Feng, G., Qu, J., Wang, J., Jing, Y., et al. (2018). SIRT6 deficiency results in developmental retardation in cynomolgus monkeys. *Nature* 560, 661–665. doi:10.1038/s41586-018-0437-z

Zhang, N., Li, Z., Mu, W., Li, L., Liang, Y., Lu, M., et al. (2016a). Calorie restriction-induced SIRT6 activation delays aging by suppressing NF-κB signaling. *Cell Cycle* 15, 1009–1018. doi:10.1080/15384101.2016.1152427

Zhang, N., Li, Z., Mu, W., Li, L., Liang, Y., Lu, M., et al. (2016b). Calorie restriction-induced SIRT6 activation delays aging by suppressing NF-κB signaling. *Cell Cycle* 15, 1009–1018. doi:10.1080/15384101.2016.1152427

Zhang, P., Tu, B., Wang, H., Cao, Z., Tang, M., Zhang, C., et al. (2014). Tumor suppressor p53 cooperates with SIRT6 to regulate gluconeogenesis by promoting FoxO1 nuclear exclusion. *Proc. Natl. Acad. Sci. U.S.A.* 111, 10684–10689. doi:10.1073/pnas.1411026111

Iachettini, S., Trisciuoglio, D., Rotili, D., Lucidi, A., Salvati, E., Zizza, P., et al. (2018). Pharmacological activation of SIRT6 triggers lethal autophagy in human cancer cells. *Cell Death Dis.* 9, 996. doi:10.1038/s41419-018-1065-0

Zhang, Z. Z., Cheng, Y. W., Jin, H. Y., Chang, Q., Shang, Q. H., Xu, Y. L., et al. (2017). The sirtuin 6 prevents angiotensin II-mediated myocardial fibrosis and

injury by targeting AMPK-ACE2 signaling. *Oncotarget* 8, 72302–72314. doi:10.18632/oncotarget.20305

Zhao, J., Wozniak, A., Adams, A., Cox, J., Vittal, A., Voss, J., et al. (2019). SIRT7 regulates hepatocellular carcinoma response to therapy by altering the p53-dependent cell death pathway. *J. Exp. Clin. Cancer Res.* 38, 252. doi:10.1186/s13046-019-1246-4

Zhong, L., D'urso, A., Toiber, D., Sebastian, C., Henry, R. E., Vadysirisack, D. D., et al. (2010). The histone deacetylase Sirt6 regulates glucose homeostasis via Hif1alpha. *Cell* 140, 280–293. doi:10.1016/j.cell.2009.12.041

Zhong, L. and Mostoslavsky, R. (2010). SIRT6: a master epigenetic gatekeeper of glucose metabolism. *Transcription* 1, 17–21. doi:10.4161/trns.1.1.12143

Zi, Y., Yi-An, Y., Bing, J., Yan, L., Jing, T., Chun-Yu, G., et al. (2019). Sirt6-induced autophagy restricted TREM-1-mediated pyroptosis in ox-LDL-treated endothelial cells: relevance to prognostication of patients with acute myocardial infarction. *Cell Death Discov.* 5, 88. doi:10.1038/s41420-019-0168-4

Zwaans, B. M. and Lombard, D. B. (2014). Interplay between sirtuins, MYC and hypoxia-inducible factor in cancer-associated metabolic reprogramming. *Dis. Model. Mech.* 7, 1023–1032. doi:10.1242/dmm.016287

Conflict of Interest: The authors declare that the research was conducted in the absence of any commercial or financial relationships that could be construed as a potential conflict of interest.

frontiers in Pharmacology

ORIGINAL RESEARCH
published: 10 December 2020
doi: 10.3389/fphar.2020.601448

A Class I Histone Deacetylase Inhibitor Attenuates Insulin Resistance and Inflammation in Palmitate-Treated C2C12 Myotubes and Muscle of HF/HFr Diet Mice

Soo Jin Lee[1†], Sung-E Choi[2†], Han Byeol Lee[1,3], Min-Woo Song[1,3], Young Ha Kim[4], Jae Yeop Jeong[1], Yup Kang[2], Hae Jin Kim[1], Tae Ho Kim[5], Ja Young Jeon[1] and Kwan Woo Lee[1*]*

[1]Department of Endocrinology and Metabolism, Ajou University School of Medicine, Suwon, South Korea, [2]Department of Physiology, Ajou University School of Medicine, Suwon, South Korea, [3]Department of Biomedical Science, The Graduate School, Ajou University, Suwon, South Korea, [4]Division of Cosmetics and Biotechnology, Hoseo University, Asan-si, South Korea, [5]Division of Endocrinology and Metabolism, Department of Internal Medicine, Seoul Medical Center, Seoul, South Korea

OPEN ACCESS

Edited by:
Barbara Wegiel,
Harvard Medical School,
United States

Reviewed by:
Aleksander M. Grabiec,
Jagiellonian University, Poland
Wei Chen,
Beijing Institute of Pharmacology and Toxicology, China

***Correspondence:**
Kwan Woo Lee
lkw65@ajou.ac.kr
Ja Young Jeon
twinstwins@hanmail.net

[†]These authors have contributed equally to this work

Specialty section:
This article was submitted to Experimental Pharmacology and Drug Discovery, a section of the journal Frontiers in Pharmacology

Received: 01 September 2020
Accepted: 09 November 2020
Published: 10 December 2020

Citation:
Lee SJ, Choi S-E, Lee HB, Song M-W, Kim YH, Jeong JY, Kang Y, Kim HJ, Kim TH, Jeon JY and Lee KW (2020) A Class I Histone Deacetylase Inhibitor Attenuates Insulin Resistance and Inflammation in Palmitate-Treated C2C12 Myotubes and Muscle of HF/HFr Diet Mice. Front. Pharmacol. 11:601448. doi: 10.3389/fphar.2020.601448

Histone deacetylase (HDAC) inhibitors, which regulate gene expression by inhibiting the deacetylation of histones and nonhistone proteins, have been shown to exert a wide array of biological effects; these include anti-cancer, anti-obesity, and anti-diabetes effects, as well as cardiovascular-protective activity. However, the effects of class I HDAC inhibition on lipotoxicity in C2C12 myotubes and skeletal muscle tissue remain poorly understood. In this study, we investigated the molecular mechanism underlying the protective effect of class I HDAC inhibition under lipotoxic conditions, i.e., in palmitate (PA)-treated C2C12 myotubes and skeletal muscle tissue in high fat (HF)/high fructose (HFr) diet mice. PA treatment of C2C12 myotubes increased HDAC3 protein expression and impaired mitochondrial oxidation, resulting in increased mitochondrial ROS generation and an accumulation of intracellular triglycerides (TG). Prolonged exposure led to increased inflammatory cytokine expression and insulin resistance. In contrast, MS-275, a class I HDAC inhibitor, dramatically attenuated lipotoxicity, preventing PA-induced insulin resistance and inflammatory cytokine expression. Similar beneficial effects were also seen following HDAC3 knockdown. In addition, MS-275 increased the mRNA expression of peroxisome proliferator activator receptor γ-coactivator 1α (PGC1α) and mitochondrial transcription factor A (TFAM), which serve as transcriptional coactivators in the context of mitochondrial metabolism and biogenesis, and restored expression of peroxisome proliferator-activated receptor alpha (PPARα), medium-chain acyl-coenzyme A dehydrogenase (MCAD), enoyl-CoA hydratase, and 3-hydroxyacyl CoA dehydrogenase (EHHADH). *In vivo,* treatment of HF/HFr-fed mice with MS-275 ameliorated hyperglycemia, insulin resistance, stress signals, and TNF-α expression in skeletal muscle. Taken together, these results suggest that HDAC3 inhibition rather than HDAC1/2 inhibition by MS-275 protects against lipotoxicity in C2C12 myotubes and skeletal muscle, and may be effective for the treatment of obesity and insulin resistance.

Keywords: Histone deacetylase inhibitor, MS-275, Insulin resistance, Inflammation, C2C12, Lipotoxicity

1. INTRODUCTION

Obesity is a rapidly growing global epidemic, and an important comorbidity of numerous metabolic diseases including diabetes, dyslipidemia, hypertension, and cardiovascular disease (Eckel et al., 2005; Poirier et al., 2006). The link between obesity and insulin resistance is well known. As the primary organ for whole-body glucose absorption and disposal, skeletal muscle accounts for ~70% of the body's glucose consumption (Smith and Muscat, 2005). Therefore, any abnormality in glucose metabolism in muscle tissue may induce lipotoxicity, resulting in systemic lipid accumulation and insulin resistance (Petersen et al., 2007; Petersen and Shulman, 2002; DeFronzo and Tripathy, 2009). A tightly regulated balance between fatty acid intake, synthesis, and oxidation is critical for proper lipid metabolism, with prolonged disruption of this balance resulting in lipid accumulation and insulin resistance (Tumova et al., 2016). Ectopic lipid accumulation in muscle tissue produces lipid intermediates such as ceramides, diacylglycerol, and lysophosphatidic acid, which cause oxidative stress, iron dysregulation, and endoplasmic reticulum (ER) stress (Daemen et al., 2018). Fatty acids and various cytokines secreted from intermuscular adipose tissue and peri-muscular adipose tissue have also been shown to activate inflammatory signals (Sachs et al., 2019). This combination of lipid intermediaries and inflammatory signals stimulates serine kinases such as phospho-C-JUN-N-terminal kinase (p-JNK), IkB kinase (IKK), and protein kinase C θ (PKC θ), leading to insulin resistance (Glass and Olefsky, 2012; Wu and Ballantyne, 2017).

Recently, epigenetic dysregulation has been proposed as a key contributor to the development of obesity and diabetes (Ling and Ronn, 2019; Loh et al., 2019), with regulation of these events being a potential treatment target for these conditions (Ling and Ronn, 2019). Previous studies have demonstrated the efficacy of histone deacetylase (HDAC) inhibitors for the treatment of various metabolic diseases, such as obesity, type 1 and type 2 diabetes mellitus (DM), non-alcoholic fatty liver disease (NAFLD), and even chronic kidney disease (CKD) (Zhang et al., 2019; Christensen et al., 2011; Meier and Wagner, 2014). Ferrari *et al.* demonstrated that MS-275, a class 1-specific HDAC inhibitor, dramatically reduced fat mass and adipocyte size in a mouse model of diet-induced obesity (DIO) by increasing the rate of lipolysis and fatty acid β-oxidation, resulting in improved glucose tolerance and attenuation of fatty liver disease. Similar effects were seen in db/db mice (Galmozzi et al., 2013). In primary hepatocytes, MS-275 stimulated hepatic expression and secretion of FGF21, which serves as the master regulator of fat oxidation and ketogenesis, via H3K18ac-mediated CREBH signaling (Christensen et al., 2011). MS-275 was also shown to protect human islet cells and MIN6 murine cells against palmitate (PA)-induced cells death via the attenuation of activating transcription factor 3 (Atf3) and C/EBP homologous protein (CHOP) expression (Meier and Wagner, 2014). Finally, MS-275 was shown to attenuate DIO via the induction of white fat browning in mice (Galmozzi et al., 2013). However, the effects of class I HDAC inhibition on free fatty acid-induced insulin resistance and inflammation in the C2C12 myotubes and skeletal muscle of high fat (HF)/high fructose (HFr) diet mice is not known. In this study, we investigated the effects of MS-275 on PA-induced lipotoxicity in C2C12 myotubes and HF/HFr diet mice, and whether these effects were mediated by specific HDAC inhibition.

We found that MS-275 treatment of differentiated C2C12 myotubes improved PA-induced insulin resistance and inflammatory cytokine expression via the inhibition of JNK and nuclear factor-kappa B (NK-κB). Enhanced fatty acid oxidation and mitochondrial function were also observed following attenuation of lipotoxicity by MS-275. Similar beneficial effects were also seen following HDAC3 knockdown. In addition, *in vivo* treatment of HF/HFr-fed mice with MS-275 ameliorated insulin resistance, stress signals, and tumor necrosis factor (TNF)-α expression in skeletal muscle. Together, these results showed that MS-275 improved inflammation and insulin resistance in skeletal muscle, principally by inhibiting HDAC3, and may thus be a promising candidate treatment for obesity and diabetes-related insulin resistance.

2. METHODS

2.1. Cell Culture and Differentiation

Mouse myoblast C2C12 cells were maintained in Dulbecco's modified Eagle's medium (DMEM) supplemented with 10% fetal bovine serum (FBS) and antibiotics (10 μg/ml streptomycin and 100 IU/ml penicillin) at 37°C in a 5% CO_2 atmosphere. C2C12 myoblasts were differentiated in DMEM supplemented with 2% horse serum, with medium changes every 3–5 days. Differentiation states were determined based on morphological changes and the expression of differentiation marker genes.

2.2. Reagents

Entinostat (MS-275) was purchased from MedChemExpress (Monmouth Junction, NJ, United States). Other chemicals, including bovine serum albumin (BSA; 2207008), PA (P5585), and insuli n (I9278) were purchased from Sigma-Aldrich (Burlington, MA, United States). 2-(N-(7-nitrobenz-2-oxa-1,3-diazol-4-yl)-amino)-2-deoxyglucose (2-NBDG; N13195), 4,4-difluoro-1,3,5,7,8-pentamethyl-4-bora-3a,4a-diaza-s-indacene (BODIPY$_{TM}$ 493/503; D3922), and MitoSOX Red mitochondrial superoxide indicator (M36008) were obtained from Thermo Fisher Scientific (Waltham, MA, United States). Anti-histone deacetylase 1 (HDAC1) (34589), anti-HDAC2 (57156), anti-HDAC3 (85057), anti-phospho-AKT (9271), anti-AKT (9272), anti-phospho-GSK3 α/β (9331), anti-GSK3β (9315), anti-phospho-JNK (9251), anti-JNK (9252), anti-phospho-NF-kB (3033), and anti-NF-kB (3034) antibodies were obtained from Cell Signaling Technology (Beverly, MA, United States). Anti-β-actin (A300-491A) antibody was purchased from Bethyl Laboratories (Montgomery, TX, United States). Anti-α-tubulin (sc-5286) antibody was purchased from Santa Cruz biotechnology (Dallas, TX, United States).

2.3. Preparation of PA

Prior to use, 0.01 M NaOH was added to a 20 mM PA solution and incubated at 70°C for 30 min. The resulting fatty acid soap was mixed with 5% BSA in phosphate-buffered saline at a 1:3 volume ratio. BSA/PA conjugates consisting of 3.75% BSA and 5 mM PA were then used to treat differentiated C2C12 cells at the indicated concentrations.

2.4. Uptake of 2-NBDG

C2C12 myotubes were pretreated with or without 300 or 400 μM PA for 16 h and starved for 4 h. Cells were then incubated in Krebs-Ringer bicarbonate buffer (pH 7.4) containing 2% BSA at 37°C for 30 min, and then treated with 500 μM 2-NBDG with or without 100 nM insulin at 37°C for 2 h. Collected cells were lyzed with lysis buffer and centrifuged at 12,000 rpm for 30 min. The fluorescence intensity of 2-NBDG in the separated supernatant was measured (excitation: 475 nM; emission: 550 nM) using a SpectraMax iD3 microplate reader (Molecular Devices, Sunnyvale, CA, United States).

2.5. Western Blot Analysis

C2C12 myotubes and mouse gastrocnemius muscles were lyzed with RIPA buffer [150 mM NaCl, 1% NP-40, 0.5% deoxycholate, 0.1% sodium dodecyl sulfate (SDS), and 50 mM Tris-Hcl (pH7.5)] supplemented with a protease inhibitor cocktail. Equal concentrations of proteins were diluted in SDS sample buffer (50 mM Tris-Cl at pH 6.8, 2% SDS, 100 mM DL-dithiothreitol (DTT), 10% glycerol), separated on 8–12% polyacrylamide, and transferred to a poly (vinylidene fluoride) (PVDF) membrane sheet. After blocking the membrane in 5% skim milk for 30 min, the target antigen was reacted with the primary antibody at RT for 2 h. The membrane was then incubated with the secondary antibody (horseradish peroxidase-conjugated anti-mouse IgG or anti-rabbit IgG antibodies) at RT for 1 h, after which an immunoreactive band was detected using an enhanced chemiluminescence system (Pierce ECL Western Blotting Substrate; Thermo, Rockford, IL, United States). Band intensity was measured using Quantity One 1D image analysis software (Bio-Rad, Hercules, CA, United States).

2.6. Reverse Transcriptase-Polymerase Chain Reaction (RT-PCR)

Total RNA from cells and mouse gastrocnemius muscles was extracted with RNAiso Plus reagent (Takara Bio, Shiga, Japan). cDNA was synthesized using the AMV reverse transcriptase and random 9-mers supplied with the TaKaRa RNA PCR Kit (version 3.0; TaKaRa Bio, Shiga, Japan). The primer sets for PCR amplification are listed in **Supplementary Table S1**. Quantitative real-time PCR was performed with SYBR Green (TaKaRa Bio) using a TaKaRa TP-815 instrument. Relative quantities of amplified DNA were analyzed using the software bundled with the TP-815 instrument and normalized to mouse 36B4 mRNA levels.

2.7. Oxygen Consumption Rate (OCR)

C2C12 myotubes were plated onto XF24 cell culture microplates and differentiated for 3 days in differentiation medium, after which the C2C12 myotubes were either treated or not treated with drugs, depending on the experimental condition. Following treatment, the C2C12 myotubes were pre-washed with Krebs-Ringer bicarbonate (KRB) buffer and equilibrated with XF assay medium supplemented with 2.5 mM glucose/50 mM carnitine/0.2 mM PA (for PA OCR) at 37°C in a CO_2-free incubator for 1 h. The OCR of PA as a carbon substrate was measured using a XF24 extracellular analyzer (Seahorse Bioscience, North Billerica, MA, United States).

2.8. Transfection of Small Interfering RNA (siRNA)

Small interfering RNA duplexes were designed and synthesized by Bioneer Corporation (Daejeon, Korea). The sequences were as follows: green fluorescent protein (GFP) (GenBank: GU983383), sense-GUU CAG CGU GUC CGG CGA, antisense- CUC GGC GGA CAC GCU GAA C; mouse HDAC1 (GenBank: NM_008228.2), sense-GAG GUU GAU AGC CUA GCU U, antisense-AAG CUA GGC UAU CAA CCU C; mouse HDAC2 (GenBank:NM_008229.2), sense-UCA GAC AAA CGG AUA GCU U, antisense-AAG CUA UCC GUU UGU CUG A; mouse histone deacetylase 3 (HDAC3) (GenBank: NM_010411.2), sense-CAC AGA GAC UGU UAG AGA U, antisense-AUC UCU AAC AGU CUC UGU G. C2C12 cells were transfected with siRNA duplex using a Neon™ electro-transfection system (Invitrogen, Carlsbad, CA, United States). siRNA duplexes were suspended in R buffer supplied in the Neon™ electro-transfection system and transfected into C2C12 myoblasts under a pulse voltage of 1,005 V, with a pulse width of 35 ms and pulse number of 2. Transfected C2C12 myoblasts were then seeded into growth plates and incubated for 16 h, and then differentiated in differentiation medium for 3 days followed by treatment with 300 or 400 μM PA (or no treatment) for 12 h.

2.9. Animal Studies

All animal experiments were approved by the Animal Ethics Committee of Ajou University (Permission number: 2018–0030). Six-week-old male C57BL/6J mice were purchased from GEM Pharmatechnology (Nanjing, China). The mice were housed in a temperature-controlled room at 22 ± 2°C with a light/dark cycle of 12 h and fed *ad libitum*. After 2 weeks of adaptation, 8-week-old mice were randomly divided into three groups: 1) DMSO-injected control diet group (CD/DMSO) (n = 5); 2) DMSO-injected high fat (HF)/high fructose (HFr) diet group (HF/HFr/DMSO) (n = 5); and 3) MS-275-injected HF/HFr diet group (HF/HFr/MS-275) (n = 5). The CD mice were fed normal chow diet containing 10% fat (D12450B; Research Diets Inc., New Brunswick, NJ, United States) and water. HF/HFr mice were fed a diet containing 60% fat (D12492; Research Diets Inc.) and drinking water including 30% fructose. Mice were injected intraperitoneally every other day with DMSO or 10 mg/kg MS-275 for 11 weeks. Insulin tolerance test (ITT) and glucose tolerance test (GTT) were performed during week 10 of the

diet. Mice were fasted for 6 h and insulin (0.7 U/kg) or glucose (1 g/kg) was injected intraperitoneally. Blood was collected from the tail at the indicated time points (0, 15, 30, 60, and 90 min), with glucose levels measured using an Accu-Chek device (Roche Diagnostics, Mannheim, Germany).

2.10. Intracellular Triglyceride Staining

Intracellular triglyceride (TG) levels were determined by measuring relative fluorescence intensity in cells after treatment with BODIPY. Briefly, C2C12 myotubes were pretreated with MS-275 for 16 h in a dose-dependent manner. Cells were then treated with 500 uM PA for 3 h, washed with PBS buffer (137 mM NaCl, 2.7 mM KCl, 10 mM Na_2HPO_4, 1.8 mM KH_2PO_4), and incubated in 100 μL of 2.0 μM BODIPY at 37°C for 30 min. Fluorescence intensity was measured at 430 and 510 nm (exciting and emitting wavelengths, respectively) using a SpectraMax iD3 microplate reader (Molecular Devices).

2.11. Mitochondrial Superoxide Staining

After treatment with MitoSOX Red, mitochondrial superoxide levels were determined by measuring relative the fluorescence intensity in C2C12 myotubes. Mitochondrial superoxide in C2C12 myotubes was measured using the same protocol as for intracellular TG. Fluorescence intensity was measured by fluorescence spectrophotometry at 510 and 580 nm (exciting and emitting wavelengths, respectively).

2.12. Insulin Measurement

Plasma insulin levels were measured using the Shibayagi Mouse Insulin ELISA kit (Cunma, Japan). Briefly, blood obtained from the mouse tail vein was immediately centrifuged at 3,000 × *g* for 10 min at 37°C. The supernatant plasma was collected and stored at -80°C. A biotinylated-anti-insulin antibody solution (100 μL) was added to each well of a 96-well plate coated with an anti-insulin antibody and mixed with 10 μL of plasma. After 2 h incubation at room temperature, the solution containing the insulin/biotinylated-anti-insulin antibody complex was removed. Biotinylated-anti-insulin antibody bound to insulin coated onto the plate was incubated with 100 μL of horse radish peroxidase (HRP)-streptavidin solution (one of the kit components) for 30 min at room temperature. After removal of unbound HRP-streptavidin, the HRP-streptavidin bound to the plate was reacted with 3, 3', 5, 5'–tetramethylbenzidine (TMB) in 100 μL of the chromogen solution. After the reaction was stopped with 100 μL 1 M sulfuric acid, absorbance at 450 nm was measured using a microplate reader (Bio-Rad, Hercules, CA, United States). The plasma insulin levels were calculated using an insulin standard curve. The homeostasis model for insulin resistance (HOMA-IR) was calculated as the fasting blood glucose level (mg/dl) × the fasting plasma insulin level (μU/ml) divided by 405.

2.13. Statistical Analysis

All experiments were repeated at least three times. All data are expressed as the mean ± SE and were analyzed using GraphPad Prism 6.0 (GraphPad Software Inc., San Diego, CA, United States). One-way analysis of variance (ANOVA) with the Bonferroni post hoc test was used. p values < 0.05 were considered statistically significant.

3. RESULTS

3.1. PA Induces Mitochondrial Dysfunction and Lipotoxicity in C2C12 Myotubes

An increasing body of evidence suggests an association between mitochondrial dysfunction and lipotoxicity, which is implicated in insulin resistance and inflammation. To detect mitochondrial failure in PA-treated C2C12 myotubes, we measured PA oxidation using the Seahorse Extracellular Flux (XF) Analyzer (Agilent, Santa Clara, CA, United States). Mitochondrial OCR was reduced in PA-treated C2C12 myotubes compared to BSA-treated myotubes (**Figure 1A**).

Next, we confirmed lipotoxicity induction in C2C12 myotubes following treatment with PA. The addition of 300 or 400 μM PA for 12 h was shown to induce insulin resistance and impair insulin-stimulated glucose uptake. 2-NBDG uptake increased in response to insulin stimulation compared to the unstimulated myotubes, while 2-NBDG uptake in PA-treated myotubes remained unchanged (**Figure 1B**). Levels of various insulin signaling molecules, including phospho-protein kinase B (p-AKT) and phospho-glycogen synthase kinase three *ß* (p-GSK3β) were reduced by PA treatment in a dose-dependent manner (**Figure 1C**). The expression levels of inflammatory cytokines, such as TNF-α, interleukin (IL)-1β, and IL-6 were increased by PA treatment (**Figure 1D**). Furthermore, PA increased the expression of stress and inflammatory markers, such as p-JNK and p-NF-κB, in C2C12 myotubes (**Figure 1E**). Together, these results suggested that PA induced mitochondrial dysfunction and lipotoxicity in C2C12 myotubes, leading to significant increases in insulin resistance and inflammation.

3.2. MS-275 Attenuated PA-Induced Insulin Resistance and Inflammation

To explore whether inhibition of class I HDACs via treatment with MS-275 could protect against lipotoxicity, such as that seen in PA-treated C2C12 myotubes, we added PA with or without MS-275. MS-275 treatment significantly restored the expression of insulin signaling markers, including p-AKT and p-GSK3β, which were reduced by PA (**Figure 2A**). The expression levels of inflammatory cytokine genes, such as TNF-α, IL-1β, and IL-6, were also increased by PA treatment but this was attenuated by MS-275 treatment (**Figure 2B**). MS-275 treatment of C2C12 myotubes was also shown to reduce levels of inflammatory markers, such as p-JNK and p-NF-κB, which were increased by PA (**Figure 2C**). Together, these data demonstrated that MS-275 had a protective effect against lipotoxicity, preventing PA-induced insulin resistance and inflammation in C2C12 myotubes.

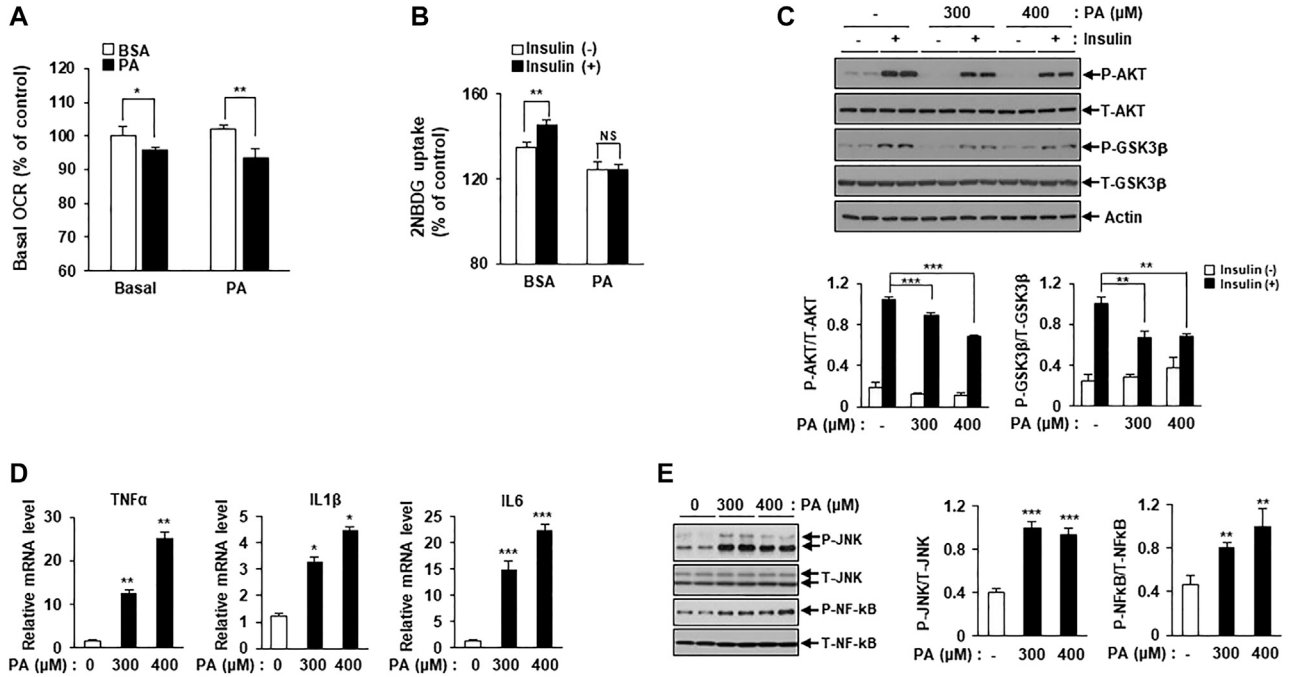

FIGURE 1 | PA induces mitochondrial dysfunction and lipotoxicity. **(A)** Differentiated C2C12 myotubes were treated with or without 400 μM PA for 12 h. The OCR of PA was measured using the Seahorse XF Analyzer (Agilent). *$p < 0.05$; **$p < 0.01$ vs. PA-untreated cells. **(B)** C2C12 myotubes were treated with 400 μM PA for 12 h, and then stimulated with insulin at 100 nM for 3 h. 2-NBDG uptake was measured using a SpectraMax iD3 microplate reader (excitation: 475 nM; emission: 550 nM). **$p < 0.01$ vs. 2-NBDG uptake after insulin treatment. **(C)** After treatment with 300 or 400 μM PA, insulin resistance in C2C12 myotubes was determined by measuring p-AKT and p-GSK3β by Western blot. **$p < 0.01$; ***$p < 0.001$ vs. insulin-stimulated and PA-untreated cells. **(D)** C2C12 myotubes were incubated with 300 or 400 μM PA for 12 h, after which inflammatory cytokine gene expression was measured by real-time PCR. *$p < 0.05$; ***$p < 0.001$ vs. PA-untreated cells. **(E)** The expression levels of the inflammatory protein markers p-JNK and p-NF-kB were measured by Western blot. **$p < 0.01$; ***$p < 0.001$ vs. PA-untreated cells.

3.3. HDAC3 Protein Levels, but Not Those of HDAC1 or HDAC2, Were Significantly Increased in PA-Treated C2C12 Myotubes

To detect changes in the levels of class I HDAC family members, C2C12 myotubes were treated with PA, followed by assessment of HDAC1, HDAC2, and HDAC3 protein levels via immunoblotting. HDAC3 protein expression was significantly increased in PA-treated myotubes compared to untreated myotubes, but HDAC1 and HDAC2 protein levels did not increase (**Figure 3**). The increase in HDAC3 protein expression may play a role in the PA-induced lipotoxicity evident in C2C12 myotubes.

3.4. Inhibition of HDAC3 Prevented PA-Induced Insulin Resistance and Inflammation

Figure 2 showed that MS-275 exhibited strong protective effects against PA-induced lipotoxicity, including insulin resistance and inflammation. Since MS-275 inhibits HDAC1, HDAC2, and HDAC3, we aimed to determine which HDAC was involved in this protective effect. To identify the main effector protein, C2C12 myotubes were transfected with HDAC1, HDAC2, or HDAC3 small interfering RNAs (siRNAs), and cytokine expression and inflammatory signaling were assessed. Class I HDAC knockdown was confirmed by real-time PCR and immunoblotting. The expression levels of HDAC1, HDAC2, and HDAC3 were significantly reduced (**Figure 4A**). The PA-induced increases in the expression levels of TNF-α, IL-1β, and IL-6 were significantly reduced on transfection of HDAC3 siRNA. HDAC1 knockdown slightly reduced only the TNF-α level, and HDAC2 knockdown only that of IL6 (**Figure 4B**). Similarly, the level of the inflammatory marker p-JNK was attenuated by HDAC3 siRNA only (**Figure 4C**). Next, we investigated the role of insulin signaling, with or without insulin treatment, via Western blot. After insulin stimulation, the levels of p-AKT and p-GSK3β were significantly increased in HDAC3 knockdown myotubes compared to siGFP-transfected C2C12 myotubes. Moreover, this reduction in insulin signaling following PA treatment was restored in HDAC3 knockdown myotubes (**Supplementary Figure S1**). Together, the data suggest that HDAC3 inhibition of MS-275 protected against PA-induced lipotoxicity.

3.5. MS-275 Reduced Intracellular TG via Induction of Mitochondrial Fatty Acid Oxidation

To investigate the mechanisms underlying the protective effect of MS-275 on PA-induced insulin resistance and inflammation, PA-

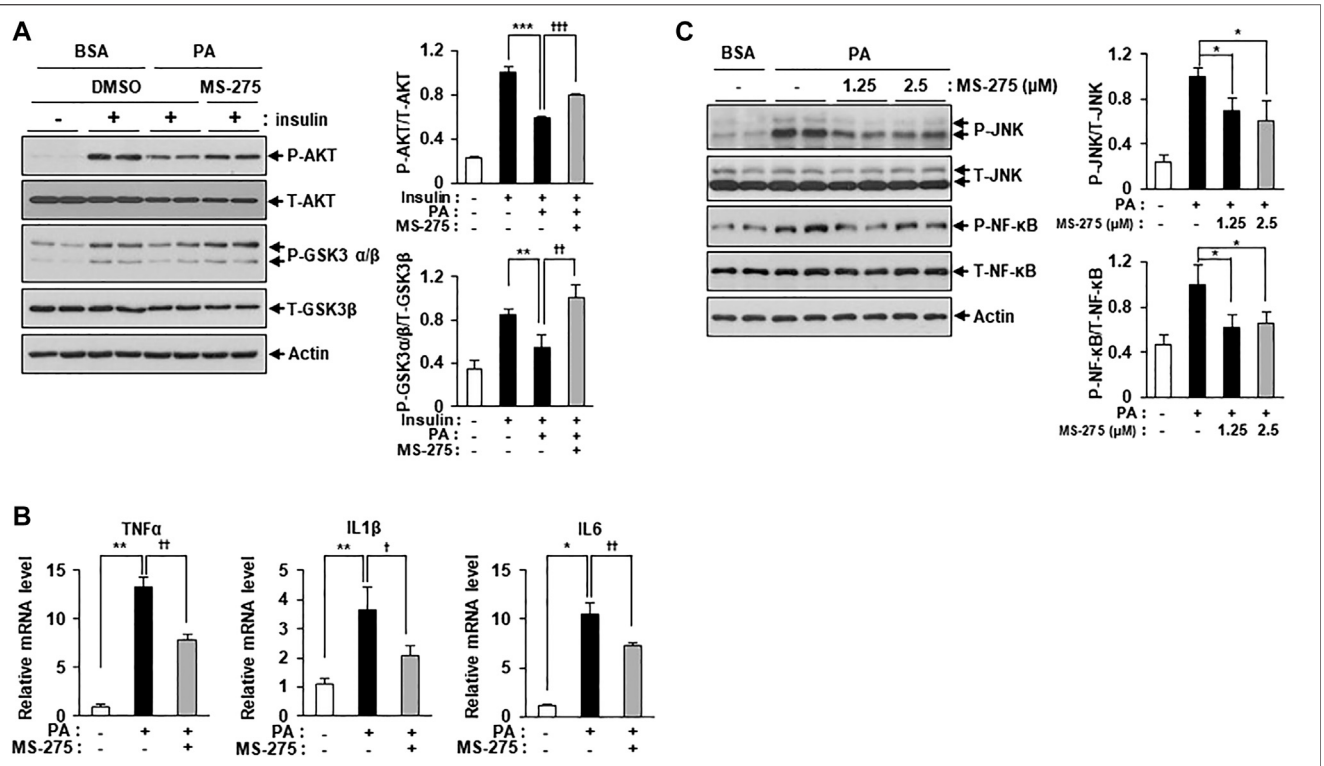

FIGURE 2 | MS-275 restored PA-induced insulin resistance and inflammation in C2C12 myotubes. **(A)** C2C12 myotubes were treated with 2.5 μM MS-275 in the presence of 300 μM PA for 12 h, and then stimulated with 100 nM insulin for 20 min. Cells were then harvested and analyzed by Western blot. The levels of insulin signaling-related proteins (p-AKT and p-GSK3β) were detected by Western blot; $^{**}p < 0.01$; $^{***}p < 0.001$ vs. insulin-stimulated and PA-untreated cells, $^{\dagger\dagger}p < 0.01$; $^{\dagger\dagger\dagger}p < 0.001$ vs. insulin-stimulated and PA-treated cells. **(B)** After treatment with 300 μM PA with or without 2.5 μM MS-275 for 12 h, the expression of inflammatory genes (TNF-α, IL-1β, and IL-6) was quantified by real-time PCR. $^{*}p < 0.05$; $^{**}p < 0.01$ vs. PA-untreated cells, $^{\dagger}p < 0.05$; $^{\dagger\dagger}p < 0.01$ vs. PA-treated cells. **(C)** C2C12 myotubes were treated with the indicated dosage of MS-275 in the presence of 300 μM PA for 12 h. The levels of stress/inflammation-related proteins were analyzed by Western blot using antibodies against p-JNK and p-NF-κB. $^{*}p < 0.05$ vs. PA-treated cells.

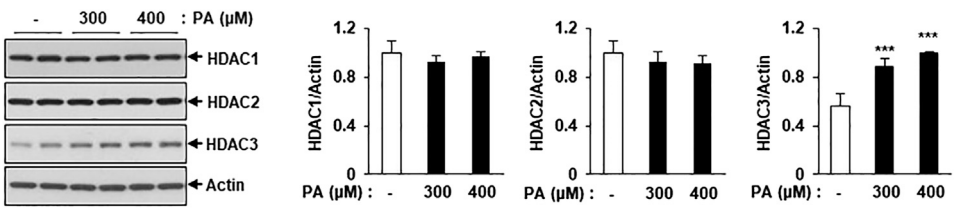

FIGURE 3 | Treatment of PA increased the class I HDACs protein level in C2C12 myotubes. C2C12 myotubes were incubated with 300 or 400 μM PA for 12 h and class1 HDAC protein levels were detected by Western blot. $^{***}p < 0.001$ vs. PA-untreated cells.

induced fat accumulation was investigated via staining of intracellular TGs using BODIPY dyes. Treatment with MS-275 was shown to reduce PA-induced TG accumulation in a dose-dependent manner (**Figure 5A**). After adding PA as a carbon substrate in C2C12 myotubes, fatty acid oxidation was measured as a function of OCR using the XF Analyzer. Pretreatment of MS-275 for 16 h increased OCR in C2C12 myotubes compared to untreated controls (**Figure 5B**). Next, we investigated gene expression in relation to fatty acid oxidation and lipid synthesis. Treatment of PA decreased the expression levels of fatty acid oxidation-related genes, such as proliferator-activated receptor alpha (PPARα) and medium-chain acyl-coenzyme A dehydrogenase (MCAD). In contrast, MS-275 treatment significantly rescued the expression of fatty acid oxidation-related genes and stearoyl-CoA desaturase 1 (SCD1). Sterol regulatory element-binding protein 1 (SREBP1) and diglyceride acyltransferase (DGAT) were significantly reduced following PA treatment, but were unchanged by MS-275 (**Figure 5C**). Furthermore, MS-275 treatment in C2C12 without PA was found to increase the expression of PPARα,

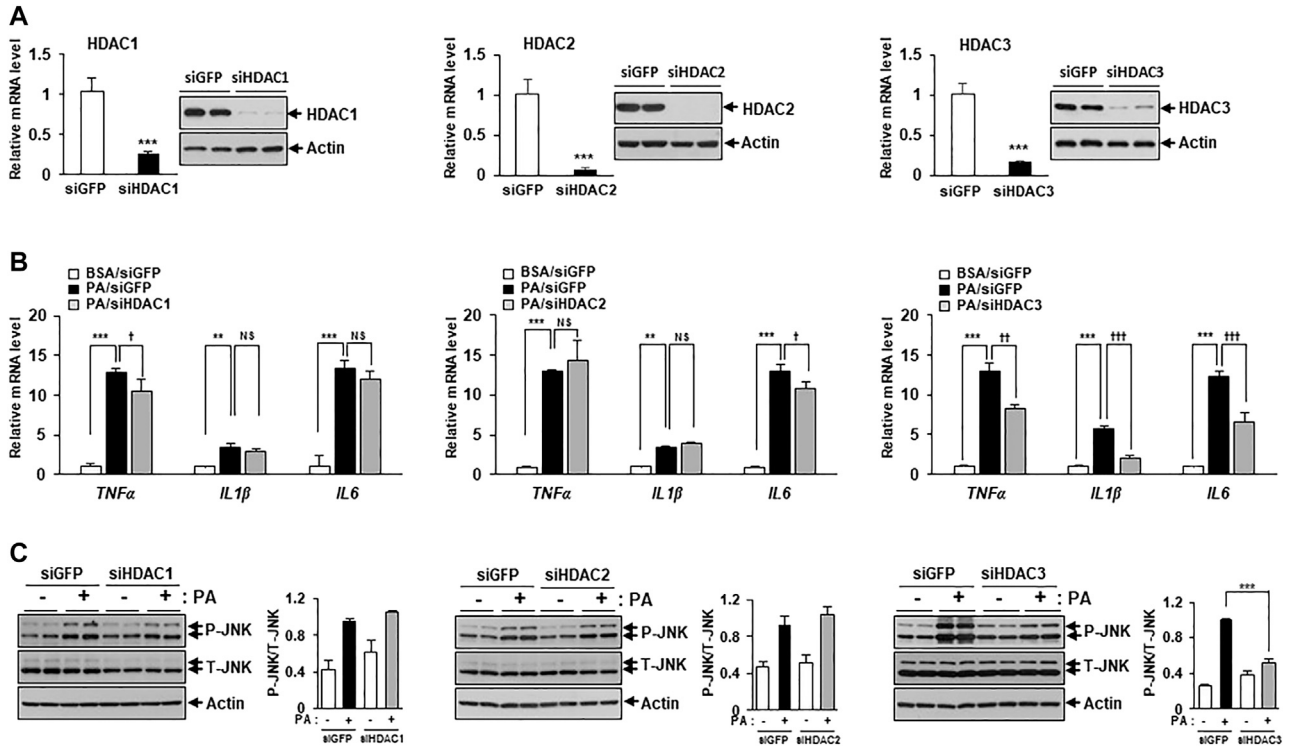

FIGURE 4 | HDAC3 knockdown improved PA-induced inflammation. **(A)** C2C12 myotubes were transfected with HDAC1, HDAC2, HDAC3, or GFP (control) siRNAs. After incubation in differentiation media for 48 h, knockdown of HDAC1, HDAC2 or HDAC3 was determined by real-time PCR and Western blot. ***$p < 0.001$ vs. GFP-transfected cells. Transfected C2C12 myotubes were treated with 300 μM PA for 12 h. The induction of inflammatory genes (TNF-α, IL-1β, and IL-6) was determined by real-time PCR **(B)** and stress/inflammatory signal activation was determined by measuring the levels of p-JNK by Western blot **(C)**. ***$p < 0.001$ vs. GFP-transfected cells, $^{††}p < 0.01$; $^{†††}p < 0.001$ vs. GFP-transfected and PA-treated cells.

MCAD, and EHHADH (**Figure 5D**). In addition, MS-275 increased the expression of PGC1α and mitochondrial transcription factor A (TFAM) genes. PGC1α and TFAM are used as markers of transcriptional coactivation in the context of mitochondrial metabolism and biogenesis (**Figure 5E**). In addition, MS-275 decreased PA-stimulated MitoSOX Red staining, which is used as a marker of mitochondrial reactive oxygen species (ROS) generation (**Figure 5F**). To investigate the mechanisms underlying the protective effect of HDAC3 knockdown on PA-induced insulin resistance and inflammation, we performed an experiment similar to that described above. PA treatment decreased PPARα, MCAD, SREBP1, DGAT, and SCD1 levels. As was also true of MS-275, HDAC3 knockdown significantly rescued the PA-induced decreases in PPARα, MCAD, EHHADH, and SCD1 gene expression (**Figure 5G**). In addition, HDAC3 knockdown in C2C12 cells (in the absence of PA) increased the expression of PPARα, EHHADH, PGC1α, and TFAM (**Figures 5H,I**). Furthermore, PA-stimulated mitochondrial ROS generation reduced on transfection of HDAC3 siRNA compared to transfection of green fluorescent protein (GFP) siRNA (**Figure 5J**). Song et al. published similar results (Song et al., 2019). Together, the data suggest that MS-275 treatment and HDAC3 knockdown increased the expression of fat oxidation-related genes, reduced mitochondrial ROS production, and restored mitochondrial function. Thus, MS-275 and HDAC3 knockdown promoted fatty acid oxidation by improving mitochondrial metabolism and biogenesis.

3.6. MS-275 ameliorated HF/HFr-Induced Insulin Resistance and Inflammation in Skeletal Muscle

Increased HF intake and HFr consumption have previously been shown to contribute to insulin resistance in mice (Han et al., 2016). As MS-275 was found to confer a strong protective effect against PA-induced lipotoxicity in C2C12 myotubes, we further investigated the protective effect of MS-275 in the muscle of HF/HFr diet mice. C57BL/6J mice were randomly divided into three groups: a standard CD group, an HF/HFr diet group, and an HF/HFr group treated with MS-275 (HF/HFr/MS-275). All HF/HFr mice were fed a diet consisting of 60% fat along with 30% fructose water (HF/HFr) for 11 weeks. Each group was intraperitoneally administered either dimethyl sulfoxide (DMSO) or MS-275 (10 mg/kg) every other day for 11 weeks (**Supplementary Figure S2**). As shown in **Figure 6A**, the intraperitoneal glucose tolerance test (IPGTT) was performed during week 10

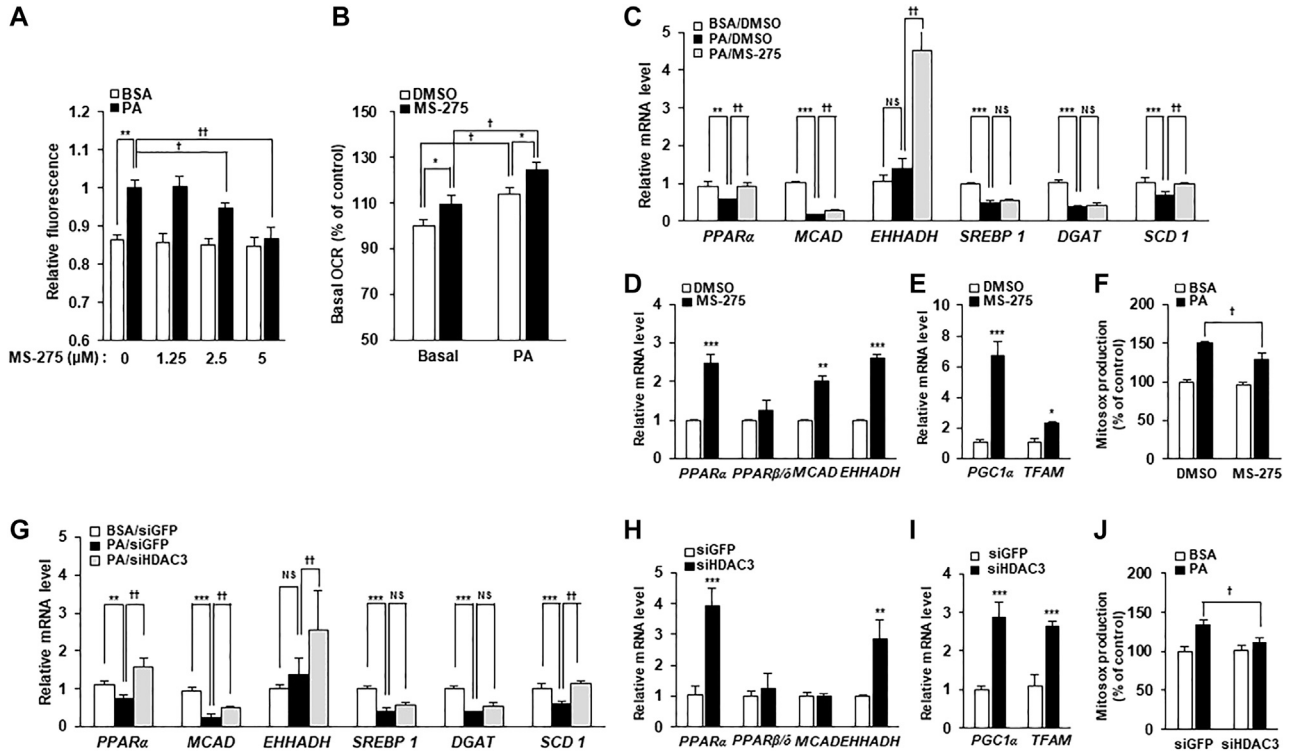

FIGURE 5 | Inhibition of HDAC3 by MS-275 or siRNA increased mitochondrial fatty acid oxidation and related gene expression. **(A)** C2C12 myotubes were pretreated with various concentrations of MS-275 for 16 h and then treated with 300 μM PA for 6 h. The intracellular TG content was determined by measuring the fluorescence of BODIPY. $^{**}p < 0.01$ vs. PA-untreated cells, $^{\dagger}p < 0.05$; $^{\dagger\dagger}p < 0.01$ vs. PA-treated cells. **(B)** The OCR of PA when used as the sole carbon substrate was measured using the Seahorse XF Analyzer (Agilent). $^{*}p < 0.05$ vs. MS-275-untreated cells, $\dagger p < 0.05$ vs. PA-untreated cells. **(C)** C2C12 myotubes were treated with or without 2.5 μM MS-275 in the presence of 300 μM PA for 12 h. The expression of fatty acid metabolism-related genes was determined by real-time PCR. $^{***}p < 0.001$ vs. PA-untreated cells, $^{\dagger\dagger}p < 0.01$ vs. PA-treated cells. **(D)** After treatment of 2.5 μM MS-275 for 16 h, the expression of fatty acid oxidation-related genes was measured by real-time PCR. $^{**}p < 0.01$; $^{***}p < 0.00$ vs. MS-275-untreated cells. **(E)** C2C12 myotubes were treated with 2.5 μM MS-275 for 16 h, and mitochondrial metabolism/biogenesis related gene expression was then measured using real-time PCR. $^{*}p < 0.05$; $^{**}p < 0.01$; $^{***}p < 0.00$ vs. MS-275-untreated cells. **(F)** C2C12 myotubes were pretreated with 2.5 μM MS-275 for 16 h and then treated with 300 μM PA for 4 h. Mitochondrial superoxide was determined by measuring the fluorescence of MitoSOX Red. $^{**}p < 0.01$ vs. PA-untreated cells, $^{\dagger}p < 0.05$; $^{\dagger\dagger}p < 0.01$ vs. PA-treated cells. **(G)** C2C12 myotubes were transfected with HDAC3 siRNA and then 300 μM PA was treated for 12 h. The expression of fatty acid metabolism-related genes was determined by real-time PCR. $^{***}p < 0.001$ vs. PA-untreated cells, $^{\dagger\dagger}p < 0.01$ vs. PA-treated cells. **(H and I)** After transfection with HDAC3 siRNA, C2C12 myotubes were differentiated for 3 days, and then the expression of fatty acid oxidation-related genes or mitochondrial metabolism/biogenesis related genes, respectively were measured by real-time PCR. $^{**}p < 0.01$; $^{***}p < 0.00$ vs. GFP-transfected cells. **(J)** After transfection with HDAC3 siRNA, C2C12 myotubes were differentiated for 3 days, and then treated with 300 μM PA for 4 h. Mitochondrial superoxide was determined by measuring the fluorescence of MitoSOX Red. $^{**}p < 0.01$ vs. PA-untreated cells and GFP-transfected cells, $^{\dagger}p < 0.05$; $^{\dagger\dagger}p < 0.01$ vs. PA-treated cells and GFP-transfected cells.

of the dietary regime. The blood glucose level at this time, and the area under the curve (AUC) value of mice on the HF/HFr diet, were increased compared to those of mice on the control diet. However, MS-275-treated mice exhibited significant reductions in these parameters (**Figure 6A**). The intraperitoneal insulin tolerance test (IPITT) was also performed during week 10 of the dietary regime. The blood glucose level at this, time and the AUC in MS-275-treated mice, were significantly lower compared to those of mice on the HF/HFr diet. The basal glucose levels at this time are shown in **Figure 6B** right panel. The fasting glucose and insulin levels increased in HF/HFr-diet mice, as did the HOMA-IR. However, MS-275-treated mice exhibited significantly lower fasting glucose and insulin levels, and a lower HOMA-IR, compared to HF/HFr-diet mice (**Figure 6B**). The TNF-α expression level was reduced in the MS-275-treated gastrocnemius and soleus muscles of HF/HFr-diet mice (**Figure 6C**). The phospho-AKT and phospho-GSK-3α/β levels in mice on the HF/HFr diet decreased compared to those of insulin-stimulated CD mice. However, the p-AKT and p-GSK-3α/β levels of the gastrocnemius and soleus muscles of HF/HFr/MS-275-diet mice were increased compared to those of insulin-stimulated mice on the HF/HFr diet (**Figure 6D**). In addition, levels of markers such as p-JNK and p-NF-κB were decreased by MS-275 treatment (**Figure 6E**). These data suggested that treatment of HF/HFr-diet mice with MS-275 significantly attenuated hyperglycemia, insulin resistance, and inflammation in skeletal muscle both *in vivo* and *in vitro*.

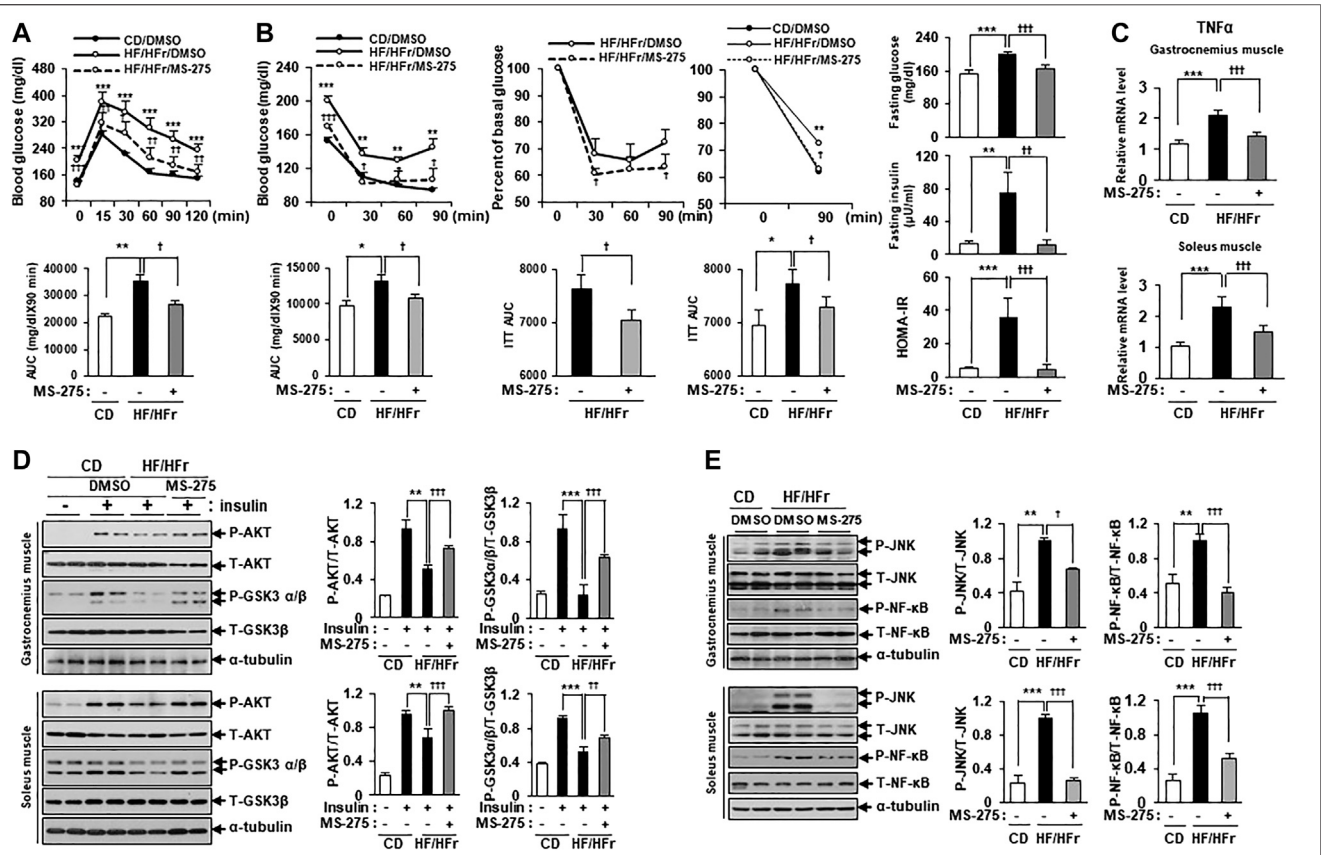

FIGURE 6 | MS-275 ameliorated HF/HFr-induced insulin resistance and inflammation in skeletal muscle from C57BL/6J mice. **(A)** To assess blood glucose levels, mice were fasted for 6 h and then intraperitoneally injected with glucose (1 g/kg). Blood glucose levels were measured at the indicated times using an Accu-Chek glucometer (Roche Diagnostics). The area under the curve (AUC) was obtained from an intraperitoneal glucose tolerance test (IPGTT). $^{**}p < 0.01$; $^{***}p < 0.001$ vs. CD mice, $^{\dagger}p < 0.05$; $^{\dagger\dagger}p < 0.005$; $^{\dagger\dagger\dagger}p < 0.001$ vs. HF/HFr mice. **(B)** Mice were fasted for 6 h and then intraperitoneally injected with insulin (0.7 U/kg) and then Blood glucose level were analyzed by ACCU-CHEK during IPITT. AUC was obtained from an intraperitoneal insulin tolerance test (IPITT). $^{*}p < 0.05$; $^{**}p < 0.01$; $^{***}p < 0.001$ vs. CD mice, $^{\dagger}p < 0.05$; $^{\dagger\dagger\dagger}p < 0.001$ vs. HF/HFr mice. Percent of basal glucose level and the inverse integrated area under the glucose curve during IPITT. $^{*}p < 0.05$; $^{**}p < 0.01$ vs. CD mice, $^{\dagger}p < 0.05$ vs. HF/HFr mice. To assess fasting glucose and insulin levels, after serum sample collection, plasma insulin concentration was analyzed by ELISA described in Methods. HOMA-IR was calculated as described in Methods. $^{**}p < 0.01$; $^{***}p < 0.001$ vs. CD mice, $^{\dagger\dagger}p < 0.01$; $^{\dagger\dagger\dagger}p < 0.001$ vs. HF/HFr mice. **(C)** The relative expression of TNFα gene related to inflammation in gastrocnemius muscle or soleus muscle, respectively was determined by real-time PCR. $^{***}p < 0.001$ vs. CD mice, $^{\dagger\dagger\dagger}p < 0.001$ vs. HF/HFr mice. **(D)** Levels of insulin signaling molecules after insulin stimulation in gastrocnemius muscle or soleus muscle, respectively were analyzed by Western blot using anti-p-AKT and anti-p-GSK3β antibodies. $^{**}p < 0.01$; $^{***}p < 0.001$ vs. insulin-stimulated CD mice, $^{\dagger\dagger}p < 0.01$; $^{\dagger\dagger\dagger}p < 0.001$ vs. insulin-stimulated HF/HFr mice. **(E)** The levels of stress/inflammation signaling molecules in gastrocnemius muscle or soleus muscle, respectively were analyzed by Western blot using anti-p-JNK and anti-p-NF-κB antibodies. $^{**}p < 0.01$; $^{***}p < 0.001$ vs. CD mice, $^{\dagger}p < 0.05$; $^{\dagger\dagger\dagger}p < 0.001$ vs. HF/HFr mice.

4. DISCUSSION

Obesity and systemic lipid overflow are strongly associated with insulin resistance (Samuel and Shulman, 2016). Skeletal muscle, which is the main target site of insulin, plays an important role in the development of insulin resistance (Samuel and Shulman, 2016). Impaired fatty acid oxidation and increased fatty acid content in skeletal muscle results in an accumulation of intracellular fat in skeletal muscle and chronic low-grade inflammation (van der Kolk et al., 2016; Meex et al., 2019). This accumulation of excess fat in skeletal muscle leads to mitochondrial dysfunction and inflammation, which is associated with insulin resistance (Hoeks and Schrauwen, 2012; Meex et al., 2019). Previous studies showed that TSA and sodium butyrate, which function as pan-HDAC inhibitors, improved insulin signaling in mouse skeletal muscle (Sun and Zhou, 2008; Chriett et al., 2019). Here, we assess the effects of MS-275, a class I-specific HDAC inhibitor, on insulin resistance and inflammatory signaling in skeletal muscle. The data presented here provide strong evidence that MS-275 prevented PA-induced insulin resistance and reduced the expression of inflammatory cytokines in differentiated C2C12, by increasing mitochondrial oxidation and lipid oxidation-related gene expression. Over time, MS-275 was shown to reduce PA-induced accumulation of cellular TGs, attenuated mitochondrial ROS, and restored mitochondrial biogenesis. PA treatment of C2C12 myotubes significantly increased HDAC3 protein levels, but not those of HDAC1 or HDAC2. Knockdown of HDAC3 exhibited similar

beneficial effects. In addition, MS-275 treatment of HF/HFr-fed mice ameliorated insulin resistance, stress-related signaling, and TNF-α expression in skeletal muscle. The data presented here suggest that treatment with MS-275 may help restore lipotoxicity-induced insulin resistance and inflammation in skeletal muscle via the inhibition of HDAC3, rather than HDAC1/2.

While the beneficial metabolic effects of MS-275 have been demonstrated in several animal models (Galmozzi et al., 2013; Ferrari et al., 2017), the effects of MS-275 appear to differ depending on the animal model and experimental design. Galmozzi *et al.* suggested that HDAC inhibitors enhanced energy metabolism in skeletal muscle and adipose tissue, resulting in reduced body weight in db/db mice. Ferrari reported MS-275 improved glucose tolerance by acting on adipose tissue, but not liver or muscle. They found no improvement in insulin-tolerance in DIO mice. Here, we injected MS-275 intraperitoneally in HF/HFr diet mice every other day for 11 weeks, and found that treatment with MS-275 reduced body weight and improved both glucose tolerance and insulin sensitivity. Moreover, MS-275 restored the levels of major insulin signals such as p-AKT and p-GSK. Possible explanations for these differences include differences in diet (HF vs. HF/HFr diet), and in the initiation, timing, and duration of MS-275 treatment (every other day for 22 days after induction of obesity in Ferrari study vs. every other day for 11 weeks before induction of obesity in this study). Based on this experiment, MS-275 may be expected to have a better metabolic and preventive effect when administered to high-risk groups before obesity induction.

Histological experiments showed that fatty liver was dramatically improved in MS-275-treated mice compared to HF/HFr-diet mice (data not shown). Although we focused on the effects of MS-275 on skeletal muscle, improvement of glucose tolerance and insulin tolerance by MS-275 *in vivo* suggests a diverse activity profile, with improvements in disease-related conditions in skeletal muscle as well as liver.

A recent study reported transcriptional effects of butyrate, a pan-HDAC inhibitor, on PA-induced insulin resistance in L6 rat muscle cells (Chriett et al., 2019). In this study, we also used PA to induce insulin resistance and found that MS-275 was able to protect against lipotoxicity in C2C12 myotubes. Increased concentrations of free fatty acids in plasma suggests a metabolic link between obesity and insulin resistance (Boden et al., 1994). PA, as a saturated fatty acid, is one of the most abundant fatty acids in the blood and is produced via result of lipolysis or lipogenesis (Nolan and Prentki, 2008). PA treatment is thought to mimic the lipotoxicity associated with obesity. In our study, PA induced the expression of various markers of stress and inflammation. Treatment with MS-275 reduced mitochondrial reactive oxygen species (ROS) generation and the activation of JNK and NK-κB by PA in C2C12 myotubes. These results suggest that MS-275 prevented PA-induced insulin resistance via regulation of the mitochondrial ROS/JNK axis. The effect of MS-275 on PA-induced lipotoxicity is consistent with that seen in beta cells, and is mediated by reduced Atf3 and CHOP expression (Plaisance et al., 2014).

We found that MS-275 exerted anti-inflammatory effects on skeletal muscles, associated with suppression of NF-κB and JNK activity. The effects of HDAC inhibitors, including MS-275, on the NF-κB and MAP signaling pathways are complex and may vary among cell types (Leus et al., 2017; Dai et al., 2005). HDAC inhibitors affected these signaling pathways in immune cells such as macrophages, but not in synovial or gingival fibroblasts (Lagosz et al., 2019; Grabiec et al., 2011; Dai et al., 2005). Previous studies reported the effects of HDAC inhibitors on NF-κB or MAP signaling in the context of insulin resistance and skeletal muscle atrophy (Chriett et al., 2017; To et al., 2017). HDAC inhibitors, such as MS-275, are thought to affect NF-kb and JNK signaling in skeletal muscle as in macrophages.

MS-275, as a class 1-specific HDAC inhibitor, has been shown to primarily inhibit HDACs 1, 2 and 3 (Ye, 2013). In our study, the effect of MS-275 on PA-induced lipotoxicity in C2C12 myotubes appears to be mediated by inhibition of HDAC3 rather than HDAC1 or HDAC2, as evidenced by the enhancement of only the HDAC3 protein level by PA, the restoration of insulin-signaling, reduction in inflammatory cytokine production, and recovery of the expression of fatty acid oxidation-related genes in HDAC3 knockdown myotubes. These results are broadly consistent with previous studies (Galmozzi et al., 2013). One study reported that a 70% reduction in HDAC3 expression is sufficient to mimic the effect of class I HDAC inhibitors on PGC1α, glucose transporter 4, TFAM, and isocitrate dehydrogenase 3α (IDH3α) expression, while silencing of HDAC1 had no effect on the expression of these genes in C2C12 (Galmozzi et al., 2013). MS-275 treatment was also shown to enhance mitochondrial activation and oxidative metabolism in skeletal muscle and adipose tissue, and improved obesity and diabetes in db/db mice (Galmozzi et al., 2013). Depletion of HDAC3 in knockout mice models restored normal metabolic activity, as reflected in improved systemic insulin sensitivity in Hdac3-/Osx1+, enhancement of oxidative metabolism in skeletal muscle-specific HDAC3-depleted mice, and prevention of DIO in intestinal epithelial cells (Hong et al., 2017; McGee-Lawrence et al., 2018; Whitt et al., 2018). In addition, patients with type 2 diabetes showed higher HDAC3 expression in peripheral blood mononuclear cells, along with simultaneous activation of pro-inflammatory markers and insulin resistance (Sathishkumar et al., 2016).

In conclusion, our study showed that MS-275 treatment of PA-induced C2C12 myotubes prevented insulin resistance and attenuated inflammatory signaling and cytokine production by restoring mitochondrial biogenesis and lipid oxidation. These effects were shown to be mediated by the inhibition of HDAC3 rather than HDAC1 and HDAC2. Similar results were seen *in vivo*, with MS-275 treatment of HF/HFr-fed mice ameliorating insulin resistance and reducing the expression of stress markers and TNF-α in skeletal muscle. Our study showed that HDAC inhibition is a promising therapeutic target for various metabolic diseases related to insulin resistance.

CONTRIBUTION TO THE FIELD STATEMENT

Recently, epigenetic dysregulation has been proposed as a key contributor to the development of obesity and diabetes, with regulation of these events being a potential treatment target for these conditions. Previous studies have demonstrated the efficacy of histone deacetylase (HDAC) inhibitors for the treatment of various metabolic diseases, such as obesity, type 1 and type 2 diabetes mellitus, non-alcoholic fatty liver disease, and even chronic kidney disease. However, the effects of HDAC3 inhibition on free fatty acid-induced insulin resistance and inflammation in the C2C12 myotubes and skeletal muscle of high fat (HF)/high fructose (HFr) diet mice is not known. We found that MS-275 treatment of differentiated C2C12 myotubes improved PA-induced insulin resistance and decreased stress signals and inflammatory cytokine expression via the inhibition of JNK and NK-κB. Enhanced fatty acid oxidation and mitochondrial function were also observed following attenuation of lipotoxicity by MS-275. Similar beneficial effects were also seen following HDAC3 knockdown. In addition, *in vivo* treatment of HF/HFr-fed mice with MS-275 ameliorated insulin resistance, stress signals, and tumor necrosis factor-α expression in gastrocnemius muscle. Together, these results showed that MS-275 induced HDAC3 inhibition in skeletal muscle and may represent a promising candidate treatment for obesity and diabetes-related insulin resistance.

DATA AVAILABILITY STATEMENT

All data analyzed in this work will be made available by corresponding authors at the request of qualified researchers.

ETHICS STATEMENT

All experiments were performed in accordance with the Ajou University Safety and Ethics guidelines. In particular, animal experiments were carried out according to the animal experiment procedure approved by the Animal Ethics Committee of Ajou University.

AUTHOR CONTRIBUTIONS

SJL, SEC, JYJ, and KWL contributed to the conception and design of the study. HBL, MWS, YK, HJK, THK, and JYJ were involved in data acquisition. YK, JYJ, and KWL contributed to data interpretation. All authors approved the paper for submission.

FUNDING

This work was supported by Grant Nos NRF-2019R1A2C1003489 and NRF-2016R1D1A1B03930214 to KW Lee, NRF-2020M3A9E8024904 and NRF-2020R1I1A1A01075337 to JY Jeon from the National Research Foundation of Korea.

SUPPLEMENTARY MATERIAL

The Supplementary Material for this article can be found online at: https://www.frontiersin.org/articles/10.3389/fphar.2020.601448/full#supplementary-material

REFERENCES

Boden, G., Chen, X., Ruiz, J., White, J. V., and Rossetti, L. (1994). Mechanisms of fatty acid-induced inhibition of glucose uptake. *J. Clin. Invest.* 93, 2438–2446. doi:10.1172/JCI117252

Chriett, S., Dąbek, A., Wojtala, M., Vidal, H., Balcerczyk, A., and Pirola, L. (2019). Prominent action of butyrate over β-hydroxybutyrate as histone deacetylase inhibitor, transcriptional modulator and anti-inflammatory molecule. *Sci. Rep.* 9, 742. doi:10.1038/s41598-018-36941-9

Chriett, S., Zerzaihi, O., Vidal, H., and Pirola, L. (2017). The histone deacetylase inhibitor sodium butyrate improves insulin signalling in palmitate-induced insulin resistance in L6 rat muscle cells through epigenetically-mediated up-regulation of Irs1. *Mol. Cell. Endocrinol.* 439, 224–232. doi:10.1016/j.mce.2016.09.006

Christensen, D. P., Dahllöf, M., Lundh, M., Rasmussen, D. N., Nielsen, M. D., Billestrup, N., et al. (2011). Histone deacetylase (HDAC) inhibition as a novel treatment for diabetes mellitus. *Mol. Med.* 17, 378–390. doi:10.2119/molmed.2011.00021

Daemen, S., van Polanen, N., and Hesselink, M. K. C. (2018). The effect of diet and exercise on lipid droplet dynamics in human muscle tissue. *J. Exp. Biol.* 221 (1), 167015. doi:10.1242/jeb.167015

Dai, Y., Rahmani, M., Dent, P., and Grant, S. (2005). Blockade of histone deacetylase inhibitor-induced RelA/p65 acetylation and NF-κB activation potentiates apoptosis in leukemia cells through a process mediated by oxidative damage, XIAP downregulation, and c-jun N-terminal kinase 1 activation. *Mol. Cell. Biol.* 25, 5429–5444. doi:10.1128/mcb.25.13.5429-5444.2005

DeFronzo, R. A. and Tripathy, D. (2009). Skeletal muscle insulin resistance is the primary defect in type 2 diabetes. *Diabetes Care* 32 (2), S157–S163. doi:10.2337/dc09-S302

Eckel, R. H., Grundy, S. M., and Zimmet, P. Z. (2005). The metabolic syndrome. *Lancet* 365, 1415–1428. doi:10.1016/S0140-6736(05)66378-7

Ferrari, A., Fiorino, E., Longo, R., Barilla, S., Mitro, N., Cermenati, G., et al. (2017). Attenuation of diet-induced obesity and induction of white fat browning with a chemical inhibitor of histone deacetylases. *Int. J. Obes.* 41, 289–298. doi:10.1038/ijo.2016.191

Galmozzi, A., Mitro, N., Ferrari, A., Gers, E., Gilardi, F., Godio, C., et al. (2013). Inhibition of class I histone deacetylases unveils a mitochondrial signature and enhances oxidative metabolism in skeletal muscle and adipose tissue. *Diabetes* 62, 732–742. doi:10.2337/db12-0548

Glass, C. K., and Olefsky, J. M. (2012). Inflammation and lipid signaling in the etiology of insulin resistance. *Cell Metab.* 15, 635–645. doi:10.1016/j.cmet.2012.04.001

Grabiec, A. M., Korchynskyi, O., Tak, P. P., and Reedquist, K. A. (2011). Histone deacetylase inhibitors suppress rheumatoid arthritis fibroblast-like synoviocyte and macrophage IL-6 production by accelerating mRNA decay. *Ann. Rheum. Dis.* 71, 424–431. doi:10.1136/ard.2011.154211

Han, S. J., Choi, S. E., Yi, S. A., Jung, J. G., Jung, I. R., Shin, M., et al. (2016). Glutamate dehydrogenase activator BCH stimulating reductive amination prevents high fat/high fructose diet-induced steatohepatitis and hyperglycemia in C57BL/6J mice. *Sci. Rep.* 5, 37468.

Hoeks, J. and Schrauwen, P. (2012). Muscle mitochondria and insulin resistance: a human perspective. *Trends Endocrinol. Metab.* 23, 444–450. doi:10.1016/j.tem.2012.05.007

Hong, S., Zhou, W., Fang, B., Lu, W., Loro, E., Damle, M., et al. (2017). Dissociation of muscle insulin sensitivity from exercise endurance in mice by HDAC3 depletion. *Nat. Med.* 23, 223–234. doi:10.1038/nm.4245

Lagosz, K. B., Bysiek, A., Macina, J. M., Bereta, G. P., Kantorowicz, M., Lipska, W., et al. (2019). HDAC3 regulates gingival fibroblast inflammatory responses in periodontitis. *J. Dent. Res.* 99, 98–106. doi:10.1177/0022034519885088

Leus, N. G. J., van den Bosch, T., van der Wouden, P. E., Krist, K., Ourailidou, M. E., Eleftheriadis, N., et al. (2017). HDAC1-3 inhibitor MS-275 enhances IL10 expression in RAW264.7 macrophages and reduces cigarette smoke-induced airway inflammation in mice. *Sci. Rep.* 7, 45047. doi:10.1038/srep45047

Ling, C. and Rönn, T. (2019). Epigenetics in human obesity and type 2 diabetes. *Cell Metab.* 29, 1028–1044. doi:10.1016/j.cmet.2019.03.009

Loh, M., Zhou, L., Ng, H. K., and Chambers, J. C. (2019). Epigenetic disturbances in obesity and diabetes: epidemiological and functional insights. *Mol. Metab.* 27, S33–S41. doi:10.1016/j.molmet.2019.06.011

McGee-Lawrence, M. E., Pierce, J. L., Yu, K., Culpepper, N. R., Bradley, E. W., and Westendorf, J. J. (2018). Loss of Hdac3 in osteoprogenitors increases bone expression of osteoprotegerin, improving systemic insulin sensitivity. *J. Cell. Physiol.* 233, 2671–2680. doi:10.1002/jcp.26148

Meex, R. C. R., Blaak, E. E., and Loon, L. J. C. (2019). Lipotoxicity plays a key role in the development of both insulin resistance and muscle atrophy in patients with type 2 diabetes. *Obes. Rev.* 20, 1205–1217. doi:10.1111/obr.12862

Meier, B. C. and Wagner, B. K. (2014). Inhibition of HDAC3 as a strategy for developing novel diabetes therapeutics. *Epigenomics* 6, 209–214. doi:10.2217/epi.14.11

Nolan, C. J. and Prentki, M. (2008). The islet β-cell: fuel responsive and vulnerable. *Trends Endocrinol. Metabol.* 19, 285–291. doi:10.1016/j.tem.2008.07.006

Petersen, K. F., Dufour, S., Savage, D. B., Bilz, S., Solomon, G., Yonemitsu, S., et al. (2007). The role of skeletal muscle insulin resistance in the pathogenesis of the metabolic syndrome. *Proc. Natl. Acad. Sci. Unit. States Am.* 104, 12587–12594. doi:10.1073/pnas.0705408104

Petersen, K. F. and Shulman, G. I. (2002). Pathogenesis of skeletal muscle insulin resistance in type 2 diabetes mellitus. *Am. J. Cardiol.* 90, 11–18. doi:10.1016/s0002-9149(02)02554-7

Plaisance, V., Rolland, L., Gmyr, V., Annicotte, J.-S., Kerr-Conte, J., Pattou, F., et al. (2014). The class I histone deacetylase inhibitor MS-275 prevents pancreatic beta cell death induced by palmitate. *J. Diabetes Res.* 2014, 1. doi:10.1155/2014/195739

Poirier, P., Giles, T. D., Bray, G. A., Hong, Y., Stern, J. S., Pi-Sunyer, F. X., et al. (2006). Obesity and cardiovascular disease: pathophysiology, evaluation, and effect of weight loss. *Arterioscler. Thromb. Vasc. Biol.* 26, 968–976. doi:10.1161/01.ATV.0000216787.85457.f3

Sachs, S., Zarini, S., Kahn, D. E., Harrison, K. A., Perreault, L., Phang, T., et al. (2019). Intermuscular adipose tissue directly modulates skeletal muscle insulin sensitivity in humans. *Am. J. Physiol. Endocrinol. Metabol.* 316, E866–E879. doi:10.1152/ajpendo.00243.2018

Samuel, V. T. and Shulman, G. I. (2016). The pathogenesis of insulin resistance: integrating signaling pathways and substrate flux. *J. Clin. Invest.* 126, 12–22. doi:10.1172/JCI77812

Sathishkumar, C., Prabu, P., Balakumar, M., Lenin, R., Prabhu, D., Anjana, R. M., et al. (2016). Augmentation of histone deacetylase 3 (HDAC3) epigenetic signature at the interface of proinflammation and insulin resistance in patients with type 2 diabetes. *Clin. Epigenet.* 8, 125. doi:10.1186/s13148-016-0293-3

Smith, A. G. and Muscat, G. E. O. (2005). Skeletal muscle and nuclear hormone receptors: implications for cardiovascular and metabolic disease. *Int. J. Biochem. Cell Biol.* 37, 2047–2063. doi:10.1016/j.biocel.2005.03.002

Song, S., Wen, Y., Tong, H., Loro, E., Gong, Y., Liu, J., et al. (2019). The HDAC3 enzymatic activity regulates skeletal muscle fuel metabolism. *J. Mol. Cell Biol.* 11, 133–143. doi:10.1093/jmcb/mjy066

Sun, C. and Zhou, J. (2008). Trichostatin A improves insulin stimulated glucose utilization and insulin signaling transduction through the repression of HDAC2. *Biochem. Pharmacol.* 76, 120–127. doi:10.1016/j.bcp.2008.04.004

To, M., Swallow, E. B., Akashi, K., Haruki, K., Natanek, S. A., Polkey, M. I., et al. (2017). Reduced HDAC2 in skeletal muscle of COPD patients. *Respir. Res.* 18, 99. doi:10.1186/s12931-017-0588-8

Tumova, J., Andel, M., and Trnka, J. (2016). Excess of free fatty acids as a cause of metabolic dysfunction in skeletal muscle. *Physiol. Res.* 65, 193–207. doi:10.33549/physiolres.932993

van der Kolk, B. W., Goossens, G. H., Jocken, J. W., and Blaak, E. E. (2016). Altered skeletal muscle fatty acid handling is associated with the degree of insulin resistance in overweight and obese humans. *Diabetologia* 59 (12), 2686–2696. doi:10.1007/s00125-016-4104-3

Whitt, J., Woo, V., Lee, P., Moncivaiz, J., Haberman, Y., Denson, L., et al. (2018). Disruption of epithelial HDAC3 in intestine prevents diet-induced obesity in mice. *Gastroenterology* 155, 501–513. doi:10.1053/j.gastro.2018.04.017

Wu, H. and Ballantyne, C. M. (2017). Skeletal muscle inflammation and insulin resistance in obesity. *J. Clin. Invest.* 127, 43–54. doi:10.1172/JCI88880

Ye, J. (2013). Improving insulin sensitivity with HDAC inhibitor. *Diabetes* 62 (3), 685–687. doi:10.2337/db12-1354

Zhang, Q., Zhu, Q., Deng, R., Zhou, F., Zhang, L., Wang, S., et al. (2019). MS-275 induces hepatic FGF21 expression via H3K18ac-mediated CREBH signal. *J. Mol. Endocrinol.* 62, 187–196. doi:10.1530/JME-18-0259

Conflict of Interest: The authors declare that the research was conducted in the absence of any commercial or financial relationships that could be construed as a potential conflict of interest.

Glossary

HDAC3 Histone deacetylase 3

HDAC2 Histone deacetylase 2

HDAC1 Histone deacetylase 1

PA Palmitate

TG triglyceride

ER Endoplasmic reticulum

p-JNK Phospho-C-JUN-N-terminal kinase

P-NK-κB Phospho-nuclear factor-kappaB

DIO Diet induced obesity

CHOP C/EBP homologous protein

TFAM mitochondrial transcription factor A

HF High fat

HFr High fructose

2-NBDG 2-(N-(7-Nitrobenz-2-oxa-1,3-diazol-4-yl)Amino)-2-Deoxyglucos

TNF-α Tumor necrosis factor-α

IL-1β Interleukin-1β

IL-6 Interleukin-6

OCR oxygen consumption rate

PGC1α peroxisome proliferator activator receptor γ-coactivator 1α

PPARα peroxisome proliferator-activated receptor alpha

MCAD Medium-chain acyl-coenzyme A dehydrogenase

EHHADH Enoyl-CoA Hydratase And 3-Hydroxyacyl CoA Dehydrogenase

SREBP1 Sterol regulatory element-binding protein 1

DGAT Diglyceride acyltransferase

p-AKT Phospho-protein kinase B

p-GSK3β Phospho-glycogen synthase kinase 3 β

frontiers in Pharmacology

ORIGINAL RESEARCH
published: 16 December 2020
doi: 10.3389/fphar.2020.603689

H3 Relaxin Alleviates Migration, Apoptosis and Pyroptosis Through P2X7R-Mediated Nucleotide Binding Oligomerization Domain-Like Receptor Protein 3 Inflammasome Activation in Retinopathy Induced by Hyperglycemia

*Kelaier Yang[1], Jiannan Liu[2], Xiaohui Zhang[3], Ziqi Ren[3], Lei Gao[3], Ying Wang[3], Wenjian Lin[1], Xuefei Ma[1], Ming Hao[1] and Hongyu Kuang[1]**

[1]The Department of Endocrinology, The First Affiliated Hospital of Harbin Medical University, Harbin, China, [2]The Department of Urology, The First Affiliated Hospital of Harbin Medical University, Harbin, China, [3]The Department of Cardiology, The First Affiliated Hospital of Harbin Medical University, Harbin, China

OPEN ACCESS

Edited by:
Terry D. Hinds,
University of Toledo, United States

Reviewed by:
Claudio Bucolo,
University of Catania, Italy
Simonetta Falzoni,
University of Ferrara, Italy

***Correspondence:**
Hongyu Kuang
ydyneifenmi@163.com

Specialty section:
This article was submitted to Experimental Pharmacology and Drug Discovery, a section of the journal Frontiers in Pharmacology

Received: 07 September 2020
Accepted: 16 October 2020
Published: 16 December 2020

Citation:
Yang K, Liu J, Zhang X, Ren Z, Gao L, Wang Y, Lin W, Ma X, Hao M and Kuang H (2020) H3 Relaxin Alleviates Migration, Apoptosis and Pyroptosis Through P2X7R-Mediated Nucleotide Binding Oligomerization Domain-Like Receptor Protein 3 Inflammasome Activation in Retinopathy Induced by Hyperglycemia. Front. Pharmacol. 11:603689. doi: 10.3389/fphar.2020.603689

Introduction: P2X7R excitation-interrelated NLRP3 inflammasome activation induced by high glucose contributes to the pathogenesis of diabetic retinopathy (DR). Relaxin-3 is a bioactive peptide with a structure similar to insulin, which has been reported to be effective in diabetic cardiomyopathy models *in vivo* and *in vitro*. However, it is not known whether relaxin-3 has a beneficial impact on DR, and the underlying mechanisms of the effect are also remain unknown.

Methods and Results: The retinas of male streptozotocin (STZ)-induced diabetic Sprague-Dawley (SD) rats were characterized. Human retinal microvascular endothelial cells (HRMECs) were used to evaluate the anti-inflammatory, antiapoptotic, antipyroptotic and anti-migration effects of H3 relaxin by transmission electron microscopy, wound-healing assay, transwell assay, flow cytometry, cytokine assays and western-blot analysis. After H3 relaxin treatment, changes of the ultrastructure and expression of NLRP3 inflammasome related proteins in the retinas of rats were compared with those in the diabetic group. *In vitro*, H3 relaxin played a beneficial role that decreased cell inflammation, apoptosis, pyroptosis and migration stimulated by advanced glycation end products (AGEs). Moreover, inhibition of P2X7R and NLRP3 inflammasome activation decreased NLRP3 inflammasome-mediated injury that similar to the effects of H3 relaxin. H3 relaxin suppressed the stimulation of apoptosis, pyroptosis and migration of HRMECs in response to AGEs mediated by P2X7R activation of the NLRP3 inflammasome.

Conclusion: Our findings provide new insights into the mechanisms of the inhibitory effect of H3 relaxin on AGE-induced retinal injury, including migration, apoptosis and pyroptosis, mediated by P2X7R-dependent activation of the NLRP3 inflammasome in HRMECs.

Keywords: relaxin, NLRP3 inflammasome, diabetic retinopathy, P2X7, diabetes

INTRODUCTION

Diabetic retinopathy (DR) is a predominant comorbidity caused by uncontrolled hyperglycemia that leads to severe visual impairment and blindness (The Diabetes Control and Complications Trial Research Group, 1993; Yau et al., 2012). Sustained hyperglycemia, which impacts the homeostasis of the retinal vasculature and the integrity of the blood-retinal barrier (BRB), is regarded as the dominant promoter of DR development (Perrone et al., 2014; Simó and Hernández, 2014; Kowluru et al., 2015). Retinal microvessels are the pervasive targets of diabetic damage, which is characterized by inflammation, neovascularization, and abnormal permeability of the BRB. During hyperglycemia, dysfunction of retinal microvascular endothelial celsl (RMECs) is considered to be the initiator of a multifactorial etiology and pathogenesis, which are manifested as close relationships with cell migration and apoptosis upon exposure of cells to the cellular advanced glycation end products (AGEs) and are regulated by a variety of inflammatory and apoptotic factors (Mizutani et al., 1996; Stitt et al., 2016). Identification of innovative approaches for the prevention and treatment of DR is essential for neutralization of the negative consequence of vision loss related to hyperglycemia.

Nucleotide binding oligomerization domain-like receptor protein 3 (NLRP3) inflammasome, a kind of intracellular supramolecular protein complex composed of the core sensor protein NLRP3, the adaptor apoptosis-associated speck-like protein containing a CARD (ASC) and effector caspase-1 (Duncan et al., 2007). Upon stimulation, ASC interacts with the upstream NLRP3 protein and recruits the downstream target caspase-1. Caspase-1 is activated by autoproteolysis to form the active p10 and p20 subunits. Active caspase-1 mainly acts on interleukin (IL)-1 family substrates, promoting the release of IL-1β and IL-18 (Schmidt et al., 2016; Willingham et al., 2009; von Moltke et al., 2013). Several models of NLRP3 inflammasome activation have been developed, including an ion redistribution model, a lysosomal disruption model, a mitochondrial dysfunction model, a metabolic changes model and a trans-Golgi disassembly model. The ion redistribution model mainly includes potassium ion (K^+) efflux, calcium ion (Ca^{2+}) flux and chloride ion (Cl^-) efflux. The K^+ ionophore and ATP-mediated purinergic ligand-gated ion channel seven receptor (P2X7R), a ligand-gated ion channel in the purinergic receptor family, promote the secretion of IL-1β and IL-18 via K^+ efflux and Ca^{2+} influx (Surprenant et al., 1996; Samways et al., 2014). P2X7R and the NLRP3 inflammasome always intimately interact and colocalize at discrete spots in the subplasmalemmal area in the resting and active states. The NLRP3 inflammasome is the primary transducer that translates a decrease in cytoplasmic K^+ induced by P2X7R receptor activation into pro-inflammatory signals (Franceschini et al., 2015). P2X7R has various polymorphic variants with variable abilities to increase cytosolic Ca^{2+} levels upon induction by ATP. Treatment with P2X7R antagonists and data obtained from $P2X7^{-/-}$ mice demonstrates that suppression of P2X7R attenuates inflammatory processes, indicating that P2X7R plays the role of a trigger that decreases intracellular K^+, and is an essential ATP-sensing receiver of NLRP3 inflammasome signaling (Karmakar et al., 2016). Therefore, inhibition of P2X7R expression indirectly reduces the activation of the NLRP3 inflammasome.

P2X7R is considered as a potential pharmacological target in several ocular diseases (Kerur et al., 2013; Beckel et al., 2014; Sanderson et al., 2014). Validated selective P2X7R antagonists are currently being evaluated in Phase I/II clinical trials (Clapp et al., 2019). P2X7R plays an important role in BRB integrity by regulating trans-endothelial electrical resistance (TEER) and the cell junction morphology (Platania et al., 2019). P2X7R antagonists protect against alterations of mitochondrial function and changes in cell permeability, which are caused by enhanced vulnerability to P2X7R activation in retinal microvessels; these properties of P2X7R antagonists suggest their potential use in the treatment of DR (Platania et al., 2017). Active P2X7R signaling induces vasotoxicity mediated by the activation of K^+ and Ca^{2+} channels, as well as ROS accumulation in retinal pericytes and capillaries to potentially amplify the inflammatory reaction induced by high glucose (Shibata et al., 2018).

Relaxin is a multipotent peptide hormone of the insulin superfamily that was discovered in the circulating blood of pregnant women in 1926 (Bathgate et al., 2002). Relaxin plays an anti-inflammatory role in inflammatory response by enhancing the synthesis of endogenous nitric oxide and inhibiting the production of inflammatory mediators such as IL-1, IL-6 and tumor necrosis factor-α (TNF-α) (Masini et al., 2004; Bani, 2012). It should be noted that relaxin can improve insulin resistance, enhance pancreatic beta cell function, restore vascular endothelial dysfunction and promote the remediation of injured tissue under diabetic conditions (Szepietowska et al., 2008). Previous studies on the relaxin family have mainly focused on relaxin-2, the biological role of relaxin-3 is similar to that of relaxin-2. Relaxin-3 is present in the brain and participates in the regulation of feeding, learning, memory and physiological stress (Bathgate et al., 2002). It has been confirmed that H3 relaxin (synthetic relaxin-3) inhibits the apoptosis and fibrosis in ventricular myocytes induced by high glucose through regulating both external and internal pathways (Zhang et al., 2005). Similarly, our previous studies have shown that H3 relaxin can alleviate inflammation and fibrosis in the kidneys of diabetic rats, however, it is not known whether H3 relaxin is effective against diabetic retinopathy, which belongs to the group of microvascular complications of diabetes along with diabetic nephropathy, is still unknown.

Our study aimed to evaluate the anti-inflammatory, antiapoptotic and anti-cell migration effects of H3 relaxin and to determine whether H3 relaxin inhibits cell migration and apoptosis through the regulation of P2X7R-mediated activation of the NLRP3 inflammasome.

MATERIALS AND METHODS

Experimental Animals and Groups

A total of 110 adult male Sprague-Dawley (SD) rats (weighing 200–250 g) were obtained from the Experimental Animal Centre at the Second Affiliated Hospital of Harbin Medical University. The rats were randomly divided into control (Group C, n = 30) and diabetic groups after stable feeding. The animals in the

diabetic group was established by intraperitoneal injection of 65 mg/kg STZ (Sigma, St. Louis, MO, USA; diluted in 0.1% mol/L citrate buffer, pH = 4.5). After successful development of the diabetic model, the diabetic group was randomly divided into three subgroups containing approximately equal number of animals (n = 26–29): a high-dose H3 relaxin group (2 μg/kg/d, Group A), a low-dose H3 relaxin group (0.2 μg/kg/d, Group B) and a diabetic group treated with the same dose of normal saline (Group D). Synthetic H3 relaxin (Cat#035–36A, Phoenix Pharmaceuticals, USA; diluted in sterile water for injection) was injected into Group A and Group B rats for 14 consecutive days during the last 2 weeks before the end of the experiment. The retinas and plasma were obtained after 4 and 8 weeks of STZ treatment, and the samples were fixed or stored at specific temperature for subsequent imaging or biochemical analyses.

The study was approved by the Ethics Committee of The First Affiliated Hospital of Harbin Medical University. All animal studies and experimental protocols were carried out in accordance with the Animal Management Rule of the Ministry of Health in the People's Republic of China (Document No. 55, 2001) and the Guide for the Care and Use of Laboratory Animals published by the US National Institutes of Health (NIH Publication No. 85-23, revised 1996).

Human Retinal Microvascular Endothelial Cell Culture

Human retinal microvascular endothelial cells (hRMECs) were obtained from the Ophthalmology Laboratory of Harbin Medical University and cultured in endothelial cell medium (ECM; Sciencell, San Diego, CA, United States) supplemented with 5% fetal bovine serum (Sciencell, San Diego, CA, United States), 100 U/ml penicillin and 100 μg/ml streptomycin in a humidified atmosphere of 5% CO2 at 37°C. hRMECs were used in the experiments at passages 3–6. The cell experiments involved three stages. In the first phase, the cells were pretreated with H3 relaxin (100 ng/ml), insulin (50 nmol/L, Novo Nordisk), both or physiological saline for 30 min with exposure to AGE-BSA (100 μg/ml, Cat#2221-10, BioVision, San Francisco, CA, USA) or control-BSA (100 μg/ml, BioVision, San Francisco, CA, USA) for 48 h. In the second phase, the cells were treated with H3 relaxin (100 ng/ml), MCC950 (1 μmol/L, Cat#PZ0280, Sigma-Aldrich, St. Louis, MO, USA), both or physiological saline with exposure to AGE-BSA (100 μg/ml) or control-BSA (100 μg/ml) for 48 h. In the third phase, cells were treated with control-BSA (100 μg/ml), AGE-BSA (100 μg/ml), AGE-BSA+H3 relaxin (100 ng/ml), AGE-BSA+BzATP (100 μmol/L, Cat#B6396, Sigma-Aldrich, St. Louis, MO, United States), AGE-BSA+A438079 (10 μmol/L, Cat#A9736, Sigma-Aldrich, St. Louis, MO, United States), or AGE-BSA + BzATP (100 μmol/L)+ H3 relaxin (100 ng/ml) for 48 h.

Observation of the Ultrastructure by Transmission Electron Microscopy

To prepare retinal samples, after anesthetizing and sacrificing the rats, the whole eyeball was immediately extracted and cutted into hemisles by the optic nerve, then fixed the samples in 2.5% pre-cooling glutaraldehyde. To prepare hRMECs samples for the observation of apoptosis and pyroptosis, cells were treated according to experimental requirements, digested with the enzyme trypsin, centrifuged at 3,000 rpm for 15 min and fixed in 2.5% pre-cooling glutaraldehyde.

After at least 2 h of fixation under the condition of 4°C, the samples were further fixed with 2% cacodylate-buffered 2% osmium tetroxide, followed by dehydrating in an ascending alcohol procedure and embedding in Epon 812. Then, ultrathin sections which are about 50 nm thick were cutted and loaded on the copper net. After staining the sections with uranyl acetate and lead citrate, the samples were observed under a transmission electron microscope (JEM 1210; JEOL, Ltd., Japan).

Measurement of Inflammatory Factor Levels in the Plasma

After anesthetization, plasma samples were obtained from the abdominal aorta of rats and then were centrifuged at 1,000 rpm for 10 min. The plasma samples were used to detect IL-18, IL-1β, vascular endothelial growth factor (VEGF) and TNF-α concentrations with a Cytokine/Chemokine Magnetic Bead Panel kit (Cat#RECYTMAG-65K, EMD Millipore, Germany).

Detection of Cytokines in the Culture Medium

Culture medium was extracted by centrifuging at 1,000 g for 10 min, and IL-18 (Cat#EK0864, Bosterbio, Wuhan, China) and IL-1β (Cat#EK0392, Bosterbio, Wuhan, China) concentrations were measured by enzyme-linked immunosorbent assay.

Western Blot Analysis

Protein was harvested from rat retinal tissue and hRMECs using RIPA buffer with protease inhibitors, and the protein concentration was determined by the BCA protein assay (Beyotime, China). Protein samples were separated with 10% and 12% SDS–PAGE in a running buffer and transferred to PVDF membranes with a transfer buffer. After blocking in 5% skim milk, the membranes were incubated with the primary antibodies anti-NLRP3 (1:1,000, Cat#ab214185, Abcam), anti-ASC (1:500, Cat#sc-514414, Santa Cruz Biotech), anti-cleaved caspase-1 (1:1,000, Cat#4199, Cell Signaling Technology; 1:1,000, Cat#ab179515, Abcam), anti-IL-1β (1:500, Cat#sc-515598, Santa Cruz Biotech), anti-IL-18 (1:1,000, Cat#ab191152, Abcam; 1:500, Cat#bs-0529R, Bioss), anti-MMP-2 (1:1,000, Cat#ab92536, Abcam), anti-MMP-9 (1:1,000, Cat#ab76003, Abcam), anti-VE-cadherin (1:1,000, Cat#ab119785, Abcam), anti-ZO-1 (1:1,000, Cat#ab96587, Abcam; 1:2000, Cat#21773-1-AP, ProteinTech), anti-occludin (1:1,000, Cat#ab216327, Abcam), anti-cleaved caspase-3 (1:1,000, Cat#9661, Cell Signaling Technology), anti-cleaved caspase-9 (1:1,000, Cat#9508, Cell Signaling Technology; 1:1,000, Cat#ab2324, Abcam), anti-cleaved caspase-8 (1:1,000, Cat#13423-1-AP, ProteinTech), anti-P2X7R (1:1,000, Cat#ab48871, Abcam), anti-gasdermin D (1:1,000, Cat#39754, Cell Signaling Technology) and anti-β-actin (1:1,000, Cat#TA-09, ZSJQ-BIO), followed by incubation with

peroxidase-conjugated secondary antibodies (1:1,000, Cat#zb-2305&zb-2301, ZSGB-BIO). The immunoreactive complexes were analyzed using Bio-Rad Image Lab software for quantification. All experiments were repeated at least three times.

Wound-Healing Assay

After growing to complete confluency, hRMECs were treated with 10 μg/ml mitomycin C for 2 h. Wounds were created by scratching with a pipette tip, and then the cells were incubated according to experimental requirements for 24 h. Images of the wound areas were obtained at 0 and 24 h using a microscope to analyze cell movement. ImageJ software (National Institutes of Health, USA) was used to analyze the extent of migration. Each assay was repeated more than three times. The extent of wound healing was calculated as a percentage according to the following equation: [1−(empty area 24 h/empty area 0 h)]×100%.

Transwell Assay

The migration of hRMECs was assessed with transwell chambers (Corning, United States). Pretreated cells were suspended in serum-free medium and then seeded in the upper compartment of the transwell chambers. The lower compartment was filled with medium containing 20% FBS. After a 24-h incubation, migrated cells were fixed with 4% paraformaldehyde and stained with 0.5% crystal violet. The degree of migration was analyzed under a light microscope, and the average number of migrating cells was calculated based on three replicate experiments.

Flow Cytometry Analysis of Cell Apoptosis

FITC-conjugated Annexin V (Annexin V-FITC)/propidium iodide (PI) Apoptosis Detection kit was purchased from Beyotime Biotechnology (Shanghai, China). After treatment and centrifugation at 2000 rpm for 5 min under the condition of 4°C, hRMECs were harvested and added with binding buffer to re-suspend, followed by staining in the dark with Annexin V-FITC and PI for 15 min. A FACSCalibur flow cytometer (BD Biosciences, Franklin Lakes, NJ, United States) was employed to detect and analyze the apoptosis of hRMECs. The experiments were repeated three times.

Statistical Analyses

Data are expressed as the mean ± SD, SPSS 22.0 was used to analyze the results. One-way ANOVA followed by the Newman-Keuls multiple-comparison test was used for statistical analysis of more than two groups. $p < 0.05$ was considered statistically significant.

RESULTS

H3 Relaxin Improved the Ultrastructure of Rat Retinas Under High-Glucose Conditions

Transmission electron microscope was used to observe the layered structure of the retina in rats after 4 or 8 weeks of treatment. At 8 weeks, the retinal layers of the control group were intact and clear. After STZ treatment, disorganized membrane discs were observed, mitochondria in several layers were degenerated, and the numbers of synapses and synaptic vesicles in the inner plexiform layer and outer plexiform layer were decreased. The ganglion cell layer showed ganglion nuclei swelling and endoplasmic reticulum expansion. After administration of a high dose of H3 relaxin, the membrane discs were substantially clearer, the numbers of synapses in the outer and inner plexiform layers were increased in H3 relaxin-treated rats compared with the diabetic rats, and the morphology of the ganglion cells was normal; however, the improvement was less pronounced in the low-dose treatment group (**Supplementary Figure S1**). The degree of injury at 4 weeks was weaker than that at 8 weeks, however, the trends in each group were similar.

H3 Relaxin Alleviated Inflammatory Activity in Diabetic Rat Retinas

To investigate whether inflammation is induced by hyperglycemia, the expression of the NLRP3 inflammasome and inflammatory cytokines IL-18 and IL-1β were assayed by western blot analysis. After STZ treatment, the levels of NLRP3, ASC, cleaved caspase-1, IL-18 and IL-1β were significantly increased at both 4 and 8 weeks. At 8 weeks, the expression levels of these components were higher than at 4 weeks (**Figure 1E** and **Supplementary Figure SF2A,B**). After administration of H3 relaxin, the expression of all the tested proteins decreased in the high-dose group compared with those in the low-dose group. Similar patterns were detected at the two time points at 4 and 8 weeks. Moreover, according to the cytokine kit analysis, the VEGF, TNF-α, IL-18 and IL-1β levels in rat plasma demonstrated similar trends, which also supported that H3 relaxin lessened the inflammatory activity induced by hyperglycemia (**Figures 1A–D**).

H3 Relaxin Suppressed Apoptosis in the Rat Retina Under Diabetic Conditions

Western blot analysis was performed to evaluate the induction of apoptosis by hyperglycemia, including the death receptor and mitochondrial pathways characterized by the expression of caspase-8 and caspase-9, respectively, which were evaluated as well as the downstream executor caspase-3. The results indicated that the expression of cleaved caspase-3, cleaved caspase-8 and cleaved caspase-9 was enhanced in the high-glucose environment and that the levels of these proteins at 8 weeks were higher than those at 4 weeks. H3 relaxin reduced the expression of all of these proteins, and the high-dose treatment had a preferable protective effect than the low-dose treatment (**Figure 1F** and **Supplementary Figure S2C,D**).

H3 Relaxin Weakened AGE-Induced NLRP3 Inflammasome Expression in hRMECs

The expression of the NLRP3 inflammasome and relevant cytokines IL-18 and IL-1β was assayed in hRMECs. Compared with the con-BSA group, the AGE-BSA group showed heightened expression of NLRP3, ASC, cleaved caspase-1, IL-18 and IL-1β. Additionally, we observed protection by treatment with H3 relaxin, insulin, or both. H3 relaxin and insulin produced similar anti-inflammatory effects, and the combination therapy exerted a more

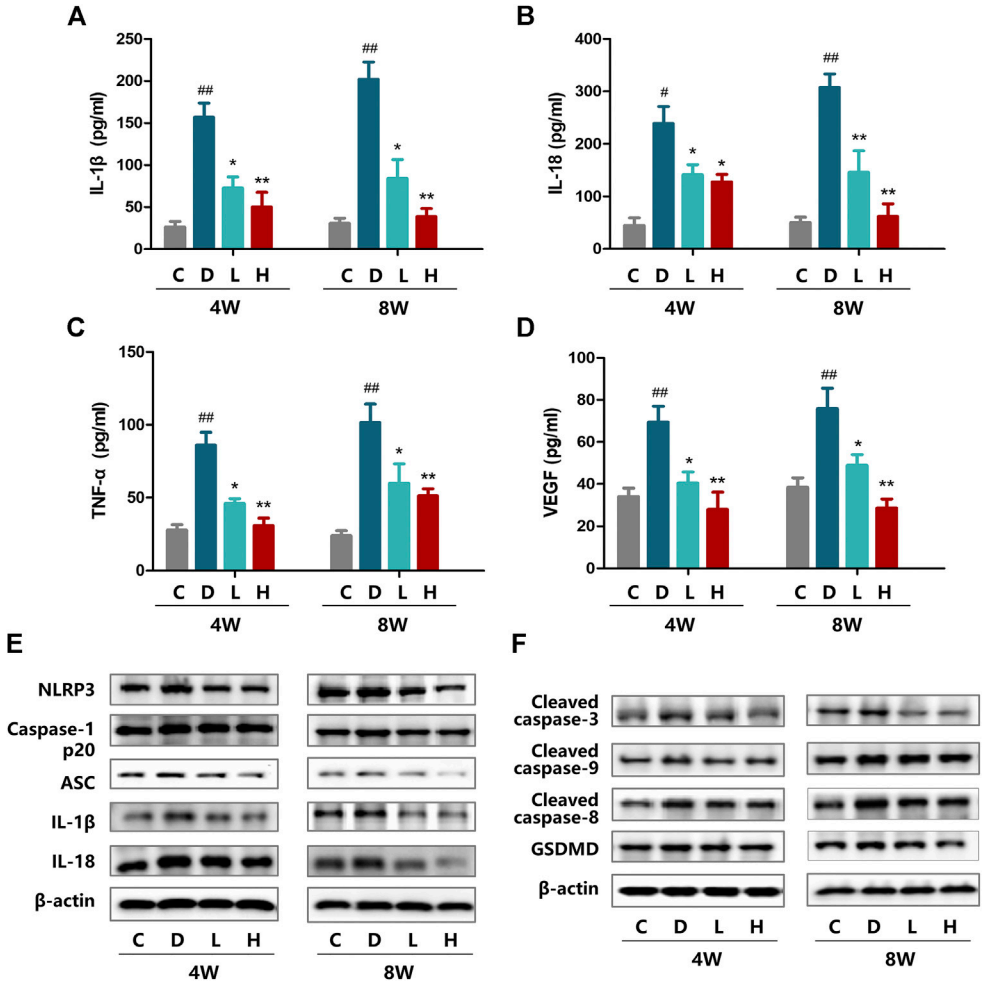

FIGURE 1 | Effect of H3 relaxin treatment on inflammation and apoptosis in retinas of diabetic rats. **(A)** The expression of IL-1β at 4 and 8 weeks in the plasma of diabetic rats. **(B)** The expression of IL-18 at 4 and 8 weeks in the plasma of diabetic rats. **(C)** The expression of TNF-α at 4 and 8 weeks in the plasma of diabetic rats. **(D)** The expression of VEGF at 4 and 8 weeks in the plasma of diabetic rats. **(E)** The protein expression of NLRP3 inflammasome and inflammatory cytolines at 4 and 8 weeks were evaluated by western blot. **(F)** The expression of apoptosis-related protein at 4 and 8 weeks were evaluated by western blot. Data are the means ± SD, and each measurement was repeated six times. $^{\#}p < 0.05$ vs. Control group, $^{\#\#}p < 0.01$ vs. Control group, $^{*}p < 0.05$ vs. Diabetic group, $^{**}p < 0.01$ vs. Diabetic group.

obvious impact than the either single therapy (**Figure 2B** and **Supplementary Figure S3A**). Moreover, IL-18 and IL-1β in the culture medium were detected by ELISA, which also showed increased concentrations induced by AGE-BSA and decreased concentrations induced by H3 relaxin or/and insulin (**Figure 2A**). These results indicated that H3 relaxin weakened the process of NLRP3 inflammasome activity in AGE-BSA-treated hRMECs, and these effects were similar to that of insulin.

H3 Relaxin Suppressed AGE-Induced Apoptosis and Pyroptosis in hRMECs

Transmission electron microscopy was used to observe the ultrastructure of hRMECs to evaluate apoptosis and pyroptosis. We noticed complete cell membranes and nuclear membranes, a rich cytoplasm and well-organized organelles in hRMECs treated with con-BSA. In the AGE-BSA group, a variety of cells in late-stage apoptosis demonstrated a loss of the cytoplasm and reduced cell protuberance. Notably, a few cells exhibited cellular swelling and karyopyknosis, which are the signature features of pyroptosis. After treatment with H3 relaxin, similar to insulin treatment, the cellular morphology was improved with reduced apoptosis, and many cells were in the early or middle stage of apoptosis. hRMECs treated with the combination therapy demonstrated pronounced improvement, and pyroptosis was not observed (**Figure 2E**). Consistently, western blot analysis showed a decrease in the expression levels of the apoptosis-related proteins, including cleaved caspase-3, cleaved caspase-8 and cleaved caspase-9, and pyroptosis-related proteins, including GSDMD and cleaved caspase-1, in hRMECs treated with H3 relaxin and/or insulin (**Figures 2C,F,G** and **Supplementary Figure SF3B**). These results suggested that H3 relaxin played a protective role against apoptosis and pyroptosis in AGE-BSA-induced

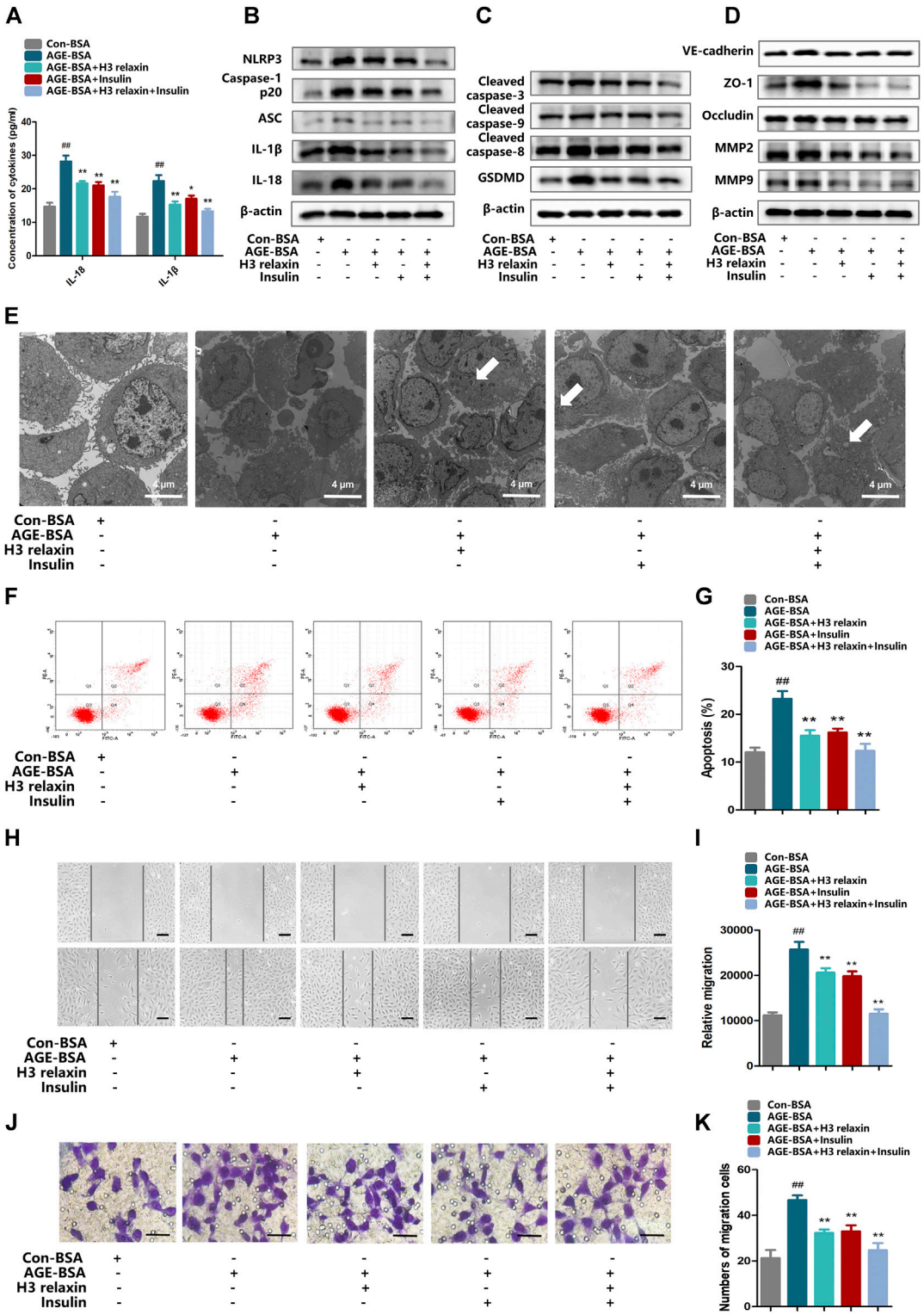

FIGURE 2 | H3 relaxin alleviated NLRP3 inflammasome activation, apoptosis, pyroptosis and migration in hRMECs. **(A)** The protein levels of IL-1β and IL-18 in cell culture media. **(B)** The protein expression of NLRP3 inflammasome and inflammatory cytolines were evaluated by western blot. **(C)** The protein expression of cleaved caspase-3, cleaved caspase-9, cleaved caspase-8 and GSDMD were evaluated by western blot. **(D)** The protein expression of VE-cadherin, ZO-1, occludin, MMP2 and MMP9 were evaluated by western blot. **(E)** The apoptosis in hRMECs were observed by transmission electron microscopy. (original magnification, ×5,000). Ultrastructural evaluation was performed: The majority of hRMECs treated by AGE-BSA showed apoptosis in early and middle phase. After H3 relaxin or/and insulin treatment, hRMECs were noticed improvement in early phase of apoptosis. Medullary corpuscles (arrow) can be noticed. **(F,G)** Cell apoptosis was measured by flow cytometry. **(H,I)** Wound-healing assay of hRMECs (Scale bar = 200 μm). **(J,K)** Transwell assay of hRMECs (Scale bar = 200 μm). Data are the means ± SD, and each measurement was repeated six times. $^{\#\#}p < 0.01$ vs. Control group, $^{*}p < 0.05$ vs. Diabetic group, $^{**}p < 0.01$ vs. Diabetic group.

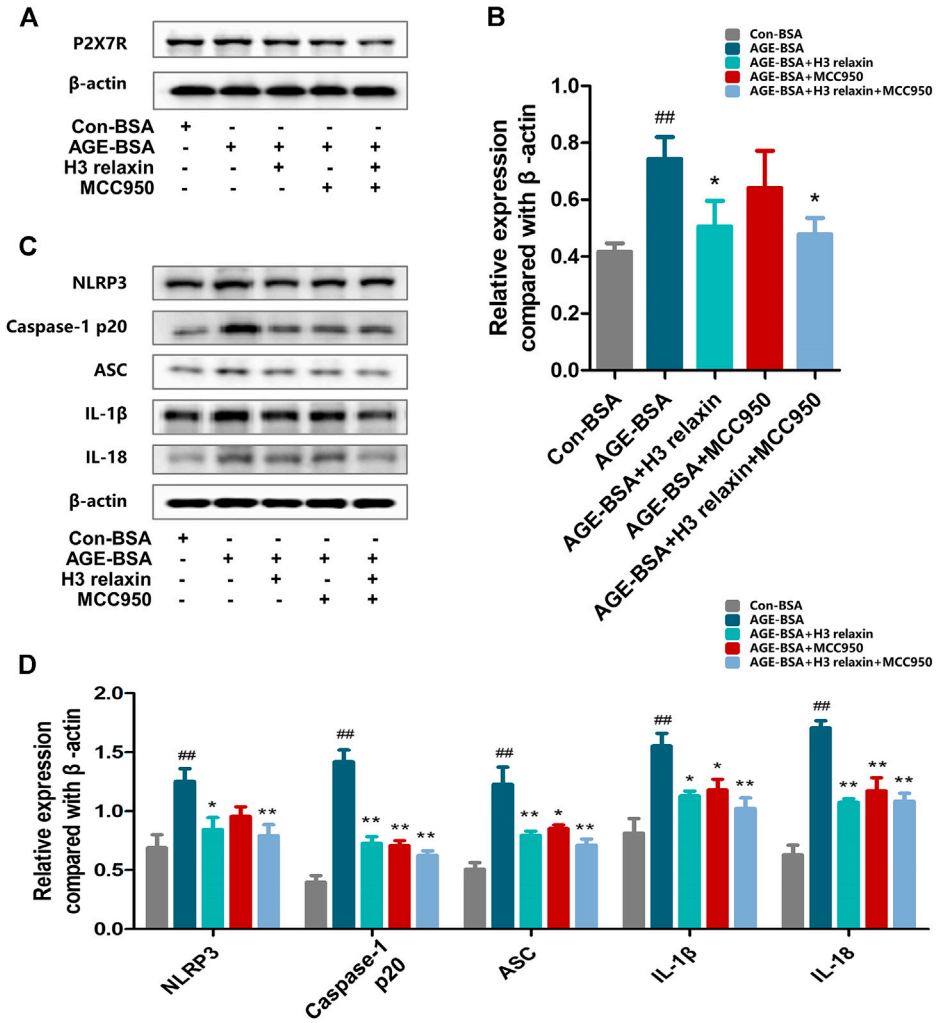

FIGURE 3 | MCC950 and H3 relaxin inhibited AGE-induced inflammatory reaction in hRMECs. **(A,B)** The expression of P2X7R protein were analysed by Western blot. **(C)** The protein expression of NLRP3 inflammasome and inflammatory cytolines were evaluated by western blot after H3 relaxin or/and MCC950 treatment. **(D)** The protein levels of NLRP3 inflammasome and inflammatory cytolines were normalized to β-actin. Data are the means ± SD, and each measurement was repeated six times. $^{\#\#}p < 0.01$ vs. Control group, $^{*}p < 0.05$ vs. Diabetic group, $^{**}p < 0.01$ vs. Diabetic group.

hRMECs and that the effect of H3 relaxin was similar to that of insulin.

H3 Relaxin Reduced the AGE-Induced Migration of hRMECs

To determine whether the migration of hRMECs can be induced by AGE-BSA and influenced by H3 relaxin or insulin, the expression of β-actin and the migration markers VE-cadherin, ZO-1, occludin, MMP2 and MMP9 were measured. The western blot analysis results revealed that the expression levels of VE-cadherin, ZO-1, occludin, MMP2 and MMP9 were enhanced by AGE-BSA after hRMECs were cultured in the presence of H3 relaxin or insulin, the levels of these proteins were downregulated, and the combination treatment provided stronger protection than that induced by the single treatments (**Figure 2D** and **Supplementary Figure S3C**). Wound-healing assays were further used to determine the migration of hRMECs. The data indicated that hRMECs migration was enhanced after stimulation by AGE-BSA, whereas H3 relaxin, insulin or their combination suppressed hRMEC migration (**Figures 2H,I**). Moreover, the transwell assay results also indicated a decrease in the migration of H3 relaxin- or insulin-treated hRMECs stimulated by AGE-BSA (**Figures 2J,K**). These data indicated that H3 relaxin prevented the migration of AGE-BSA-stimulated hRMECs, and this protection was similar to that of insulin.

H3 Relaxin Weakened AGE-Induced Apoptosis and Pyroptosis by Attenuating NLRP3 Inflammasome Activation

To determine whether the effect of H3 relaxin on apoptosis and pyroptosis are mediated by the NLRP3 inflammasome, MCC950 was used to decrease the activation of the NLRP3 inflammasome.

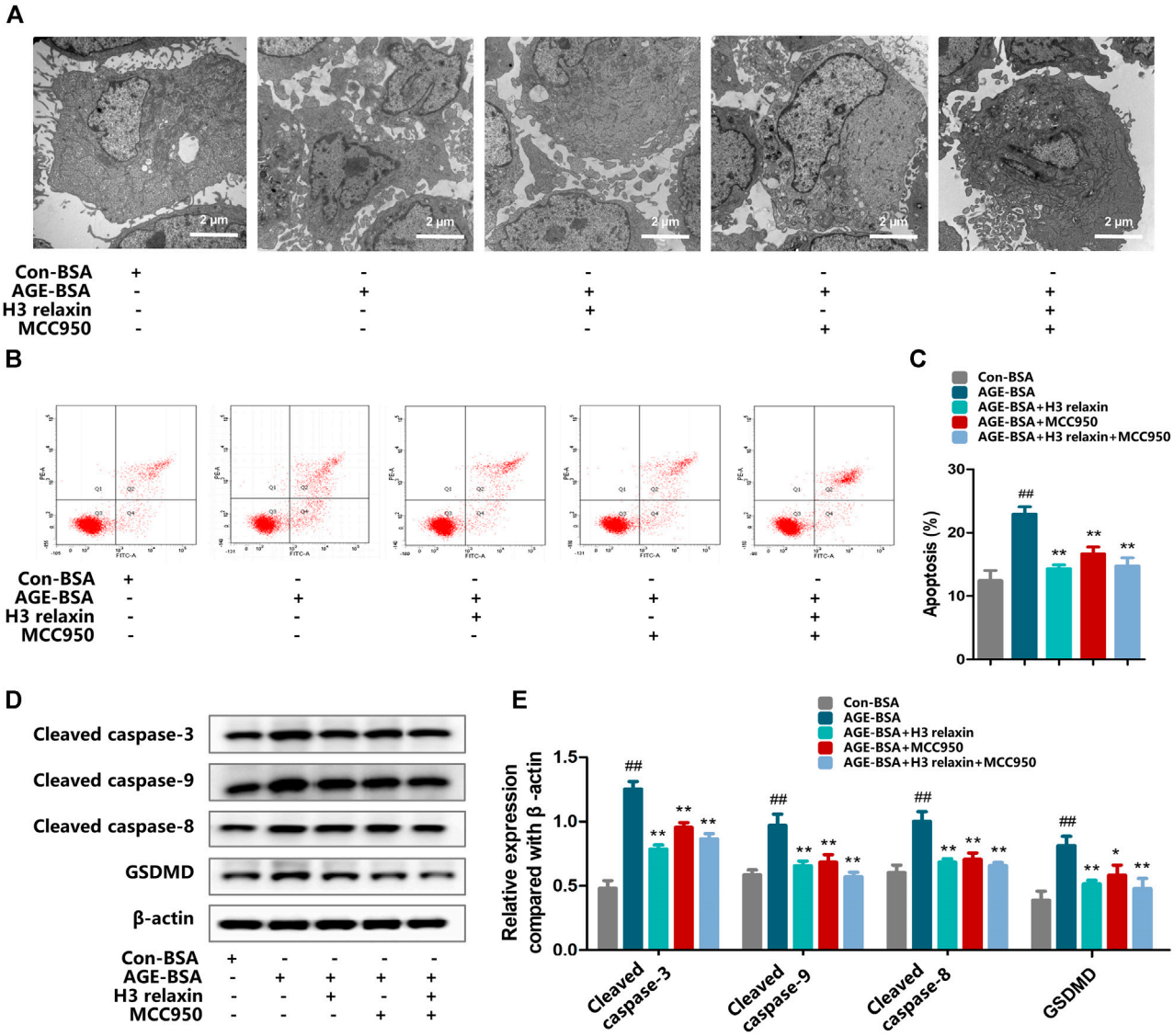

FIGURE 4 | H3 relaxin alleviated AGE-induced apoptosis and pyroptosis in hRMECs by attenuating the activation of NLRP3 inflammasome. **(A)** The apoptosis in hRMECs were observed by transmission electron microscopy (original magnification, ×10,000). Ultrastructural evaluation was performed: After H3 relaxin or/and MCC950 treatment, hRMECs were noticed improvement in apoptosis compared with AGE-BSA group. **(B,C)** Cell apoptosis was measured by flow cytometry. **(D)** The protein expression of cleaved caspase-3, cleaved caspase-9, cleaved caspase-8 and GSDMD were evaluated by western blot. **(E)** The protein levels of cleaved caspase-3, cleaved caspase-9, cleaved caspase-8 and GSDMD were normalized to β-actin. Data are the means ± SD, and each measurement was repeated six times. $^{\#\#}p < 0.01$ vs. Control group, $^{*}p < 0.05$ vs. Diabetic group, $^{**}p < 0.01$ vs. Diabetic group.

In the presence of MCC950, the expression levels of cleaved caspase-1, IL-18 and IL-1β were suppressed, whereas the protein levels of NLRP3 and P2X7R were not observably influenced (**Figures 3A–D**). Proteins related to apoptosis and pyroptosis were detected by western blot analysis, including cleaved caspase-3, cleaved caspase-8, cleaved caspase-9 and GSDMD, the data indicated that the levels of all of these proteins were attenuated by MCC950. In addition, the effect of MCC950 was compared with that of H3 relaxin, and the results indicated that H3 relaxin were somewhat weaker than those of MCC950. Treatment of hRMECs with the combination of H3 relaxin and MCC950 reduced apoptosis and pyroptosis compared with those in hRMECs treated with AGE-BSA, however, the reduction was incomplete (**Figures 4A–E**). These results indicated that H3 relaxin alleviated AGE-induced apoptosis and pyroptosis and the roles involved in these improvements might be partially mediated by the NLRP3 inflammasome.

H3 Relaxin Subdued AGE-Induced Migration by Alleviating NLRP3 Inflammasome Activation

We further evaluated the effect of H3 relaxin on migration by inhibiting the NLRP3 inflammasome. The expression levels of

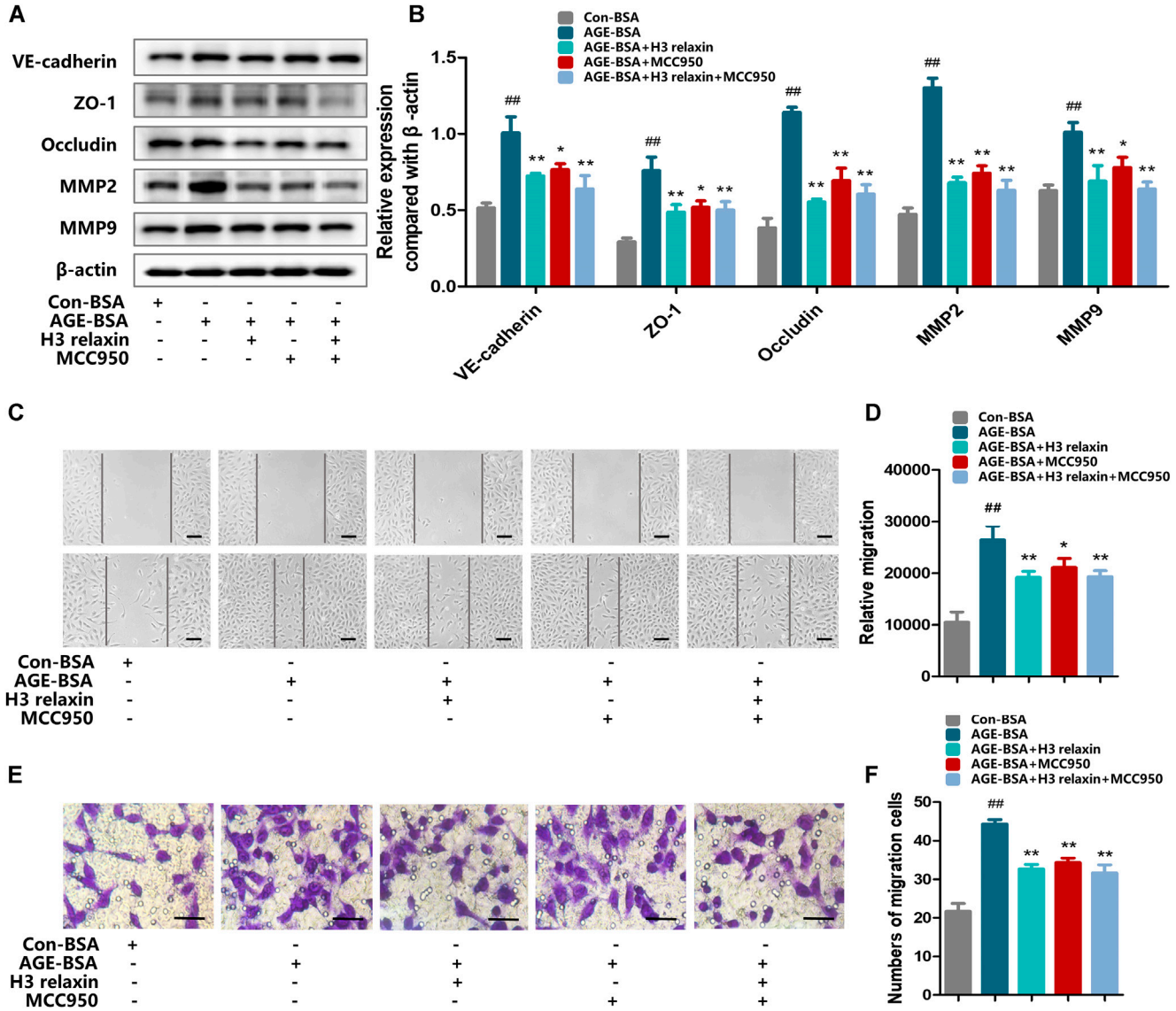

FIGURE 5 | H3 relaxin alleviated AGE-induced migration in hRMECs by attenuating the activation of NLRP3 inflammasome. **(A)** The protein expression of VE-cadherin, ZO-1, occludin, MMP2 and MMP9 were evaluated by western blot. **(B)** The protein levels of VE-cadherin, ZO-1, occludin, MMP2 and MMP9 were normalized to *β*-actin. **(C,D)** Wound-healing assay of hRMECs (Scale bar = 200 μm). **(E,F)** Transwell assay of hRMECs (Scale bar = 200 μm). Data are the means ± SD, and each measurement was repeated six times. $^{\#\#}p < 0.01$ vs. Control group, $^{*}p < 0.05$ vs. Diabetic group, $^{**}p < 0.01$ vs. Diabetic group.

proteins related to migration, including VE-cadherin, ZO-1, occludin, MMP2 and MMP9 were assayed. The results showed that hRMECs treated with MCC950 manifested a decrease in the levels of VE-cadherin, ZO-1, occludin, MMP2 and MMP9, accompanied by reduced expression levels of cleaved caspase-1, IL-18 and IL-1β. hRMECs treated with H3 relaxin also exhibited improvements in VE-cadherin, ZO-1, occludin, MMP2 and MMP9; unlike the MCC950 group, the H3 relaxin group showed improvements in all components of the NLRP3 inflammasome. Treatment with MCC950 and H3 relaxin decreased the levels of proteins related to the migration and NLRP3 inflammasome compared with those in cells treated with AGE-BSA (**Figures 5A,B**). The wound-healing and transwell assays showed a similar trend in migration (**Figures 5C–F**). These data suggested that activation of the NLRP3 inflammasome may contribute to H3 relaxin-induced suppression of AGE-stimulated migration.

H3 Relaxin Suppressed AGE-Induced Retinal Apoptosis and Pyroptosis by Attenuating P2X7R-Mediated NLRP3 Inflammasome Activation

ATP-mediated K+ efflux through P2X7R is an upstream signal essential for the activation of the NLRP3 inflammasome, which increases the secretion of IL-1β and IL-18 (Surprenant et al.,

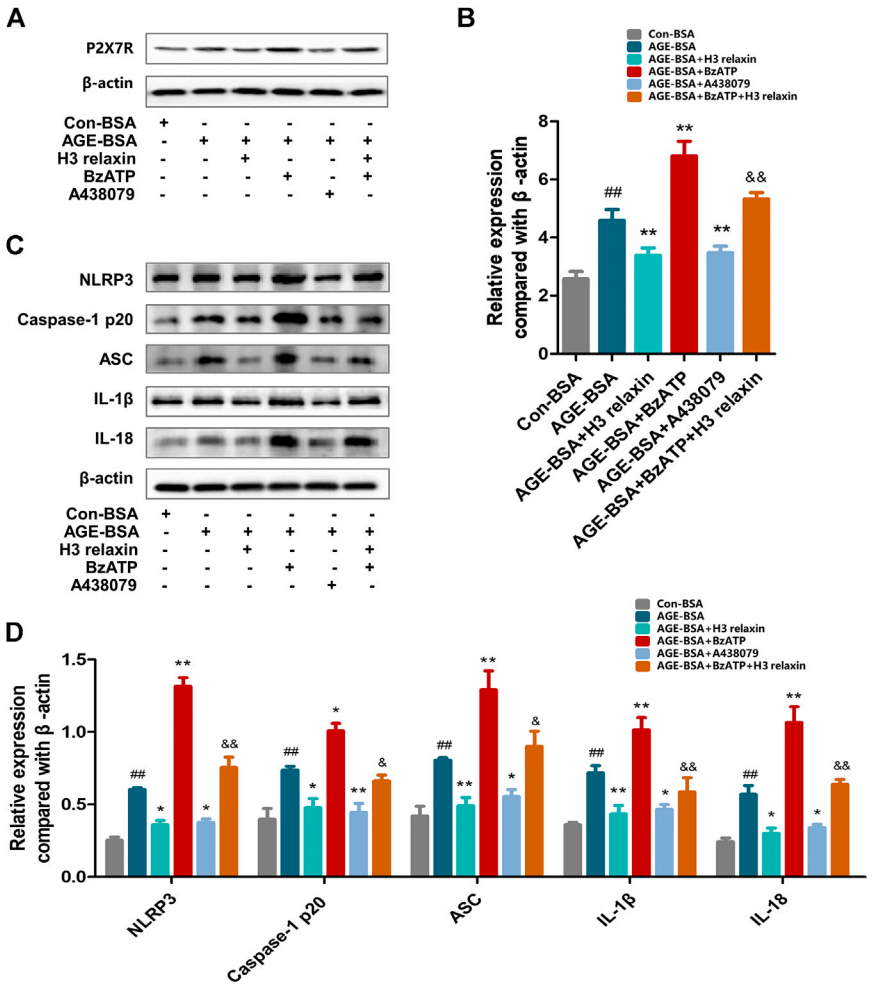

FIGURE 6 | The regulation of P2X7R changed the inflammatory reaction induced by AGE-BSA in hRMECs. **(A,B)** The expression of P2X7R protein were analysed by Western blot. **(C)** The protein expression of NLRP3 inflammasome and inflammatory cytolines were evaluated by western blot after P2X7R agonist or inhibitor treatment. **(D)** The protein levels of NLRP3 inflammasome and inflammatory cytolines were normalized to *β*-actin. Data are the means ± SD, and each measurement was repeated six times. ##$p < 0.01$ vs. Control group, *$p < 0.05$ vs. Diabetic group, **$p < 0.01$ vs. Diabetic group. $^{\&}p < 0.05$ vs. AGE-BSA+BzATP group, $^{\&\&}p < 0.01$ vs. AGE-BSA+BzATP group.

1996). Our team found that H3 relaxin reduced the expression of P2X7R induced by AGE-BSA (**Figure 6A–D**). Then, the potential mechanism of the H3 relaxin-dependent reduction in AGE-induced apoptosis and pyroptosis via P2X7R-mediated activation of the NLRP3 inflammasome was investigated. Initially, hRMECs were treated with AGE-BSA and the P2X7R agonist BzATP or the P2X7R inhibitor A438079. The BzATP treatment enhanced the expression of the NLRP3 inflammasome and proteins related to apoptosis and pyroptosis, including cleaved caspase-3, cleaved caspase-8 and cleaved caspase-9 and GSDMD, whereas the treatment with A438079 weakened the expression levels of these proteins, similar to the results obtained in the H3 relaxin treatment group. Treatment with a combination of H3 relaxin and BzATP decreased the levels of these proteins compared with those in cells treated with BzATP alone. The IL-18 and IL-1β levels in the culture medium followed a similar trend (**Figures 7A–E**). These data indicated that H3 relaxin might play roles in AGE-induced apoptosis and pyroptosis, which are at least partially mediated by P2X7R-dependent activation of the NLRP3 inflammasome.

H3 Relaxin Mitigated AGE-Induced Retinal Cell Migration by Alleviating P2X7R-Mediated NLRP3 Inflammasome Activation

We further investigated whether H3 relaxin reduces AGE-induced migration via P2X7R-mediated NLRP3 inflammasome activation. Compared with con-BSA, H3 relaxin and A438079 both reduced the expression of proteins related to migration, and BzATP increased the migration of hRMECs induced by AGE-BSA, which was consistent with the trend for NLRP3-mediated inflammation (**Figures 8A,B**). This observation was further supported by wound-healing and transwell assays (**Figures**

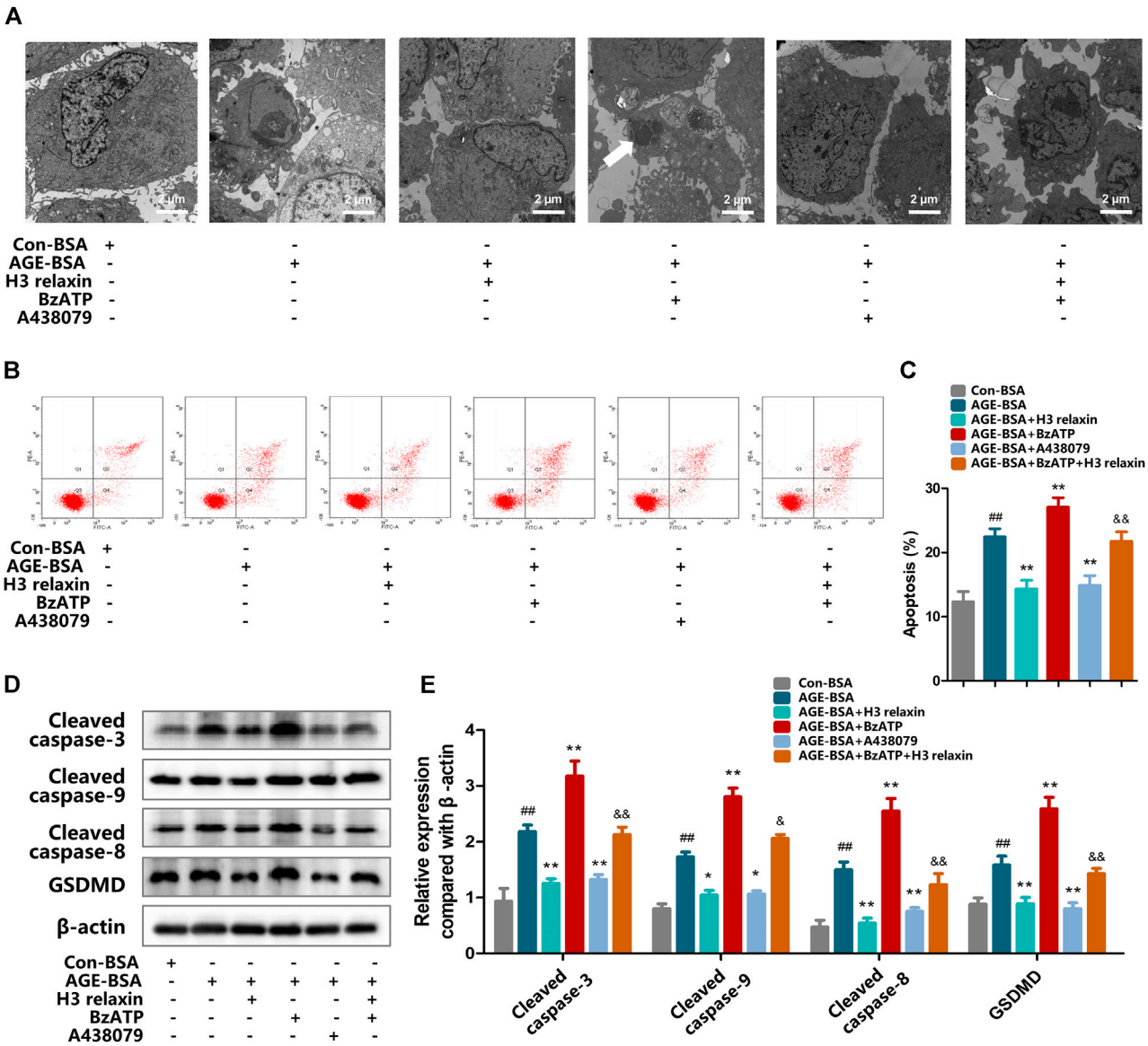

FIGURE 7 | The regulation of P2X7R changed apoptosis and pyroptosis induced by AGE-BSA in hRMECs. **(A)** The apoptosis in hRMECs were observed by transmission electron microscopy. (original magnification, ×10,000). Ultrastructural evaluation was performed: After H3 relaxin or/and A438079 treatment, hRMECs were noticed improvement in apoptosis compared with AGE-BSA group. BzATP enhanced cell injury into late phase of apoptosis and a phagosome can be noticed (arrow). **(B,C)** Cell apoptosis was measured by flow cytometry. **(D)** The protein expression of cleaved caspase-3, cleaved caspase-9, cleaved caspase-8 and GSDMD were evaluated by western blot. **(E)** The protein levels of cleaved caspase-3, cleaved caspase-9, cleaved caspase-8 and GSDMD were normalized to *β*-actin. Data are the means ± SD, and each measurement was repeated six times. $^{\#\#}p < 0.01$ vs. Control group, $^{*}p < 0.05$ vs. Diabetic group, $^{**}p < 0.01$ vs. Diabetic group. $^{\&}p < 0.05$ vs. AGE-BSA+BzATP group, $^{\&\&}p < 0.01$ vs. AGE-BSA+BzATP group.

8C–F). These data indicated that H3 relaxin might attenuate AGE-induced migration, which at least played a protective role partially through P2X7R-mediated NLRP3 inflammasome activation.

DISCUSSION

Studies have shown that the levels of caspase-1 and the inflammatory cytokine IL-18 are increased in patients with proliferative diabetic retinopathy (PDR) and the level of NLRP3 in the optic disc in the eyes of patients with PDR is higher than that in the eyes of patients with inactive neovascularization (Qi et al., 2014). Inhibition of the NLRP3 inflammasome enhances insulin sensitivity and glucose tolerance compared with no treatment (Vandanmagsar et al., 2011). Here, we observed that high glucose increased the expression of the NLRP3 inflammasome in the rat retina. In AGE-BSA-induced hRMECs, the levels of the NLRP3 inflammasome and its effector cytokines were also significantly increased. The detection of IL-18 and IL-1β in rat plasma and culture medium supported the conclusion. Recently, a

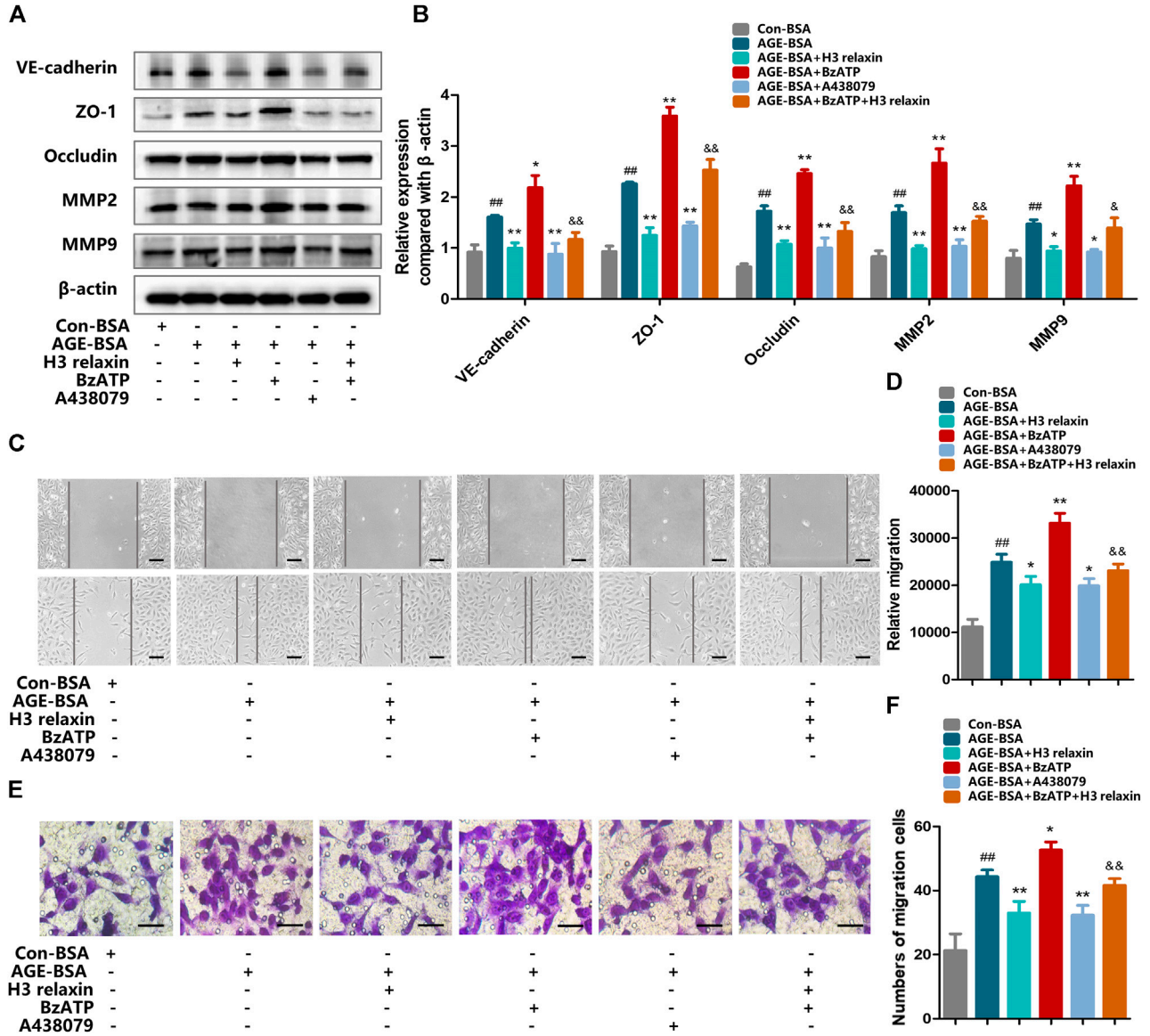

FIGURE 8 | The regulation of P2X7R changed migration induced by AGE-BSA in hRMECs. **(A)** The protein expression of VE-cadherin, ZO-1, occludin, MMP2 and MMP9 were evaluated by western blot. **(B)** The protein levels of VE-cadherin, ZO-1, occludin, MMP2 and MMP9 were normalized to *β*-actin. **(C,D)** Wound-healing assay of hRMECs (Scale bar = 200 μm). **(E,F)** Transwell assay of hRMECs (Scale bar = 200 μm). Data are the means ± SD, and each measurement was repeated six times. $^{\#\#}p < 0.01$ vs. Control group, $^{*}p < 0.05$ vs. Diabetic group, $^{**}p < 0.01$ vs. Diabetic group. $^{\&}p < 0.05$ vs. AGE-BSA+BzATP group, $^{\&\&}p < 0.01$ vs. AGE-BSA+BzATP group.

diaryl sulfonylurea compound, MCC550, was reported to be a highly specific inhibitor of NLRP3-mediated inflammation, and this compound was initially identified the most effective inhibitor of the IL-1β-releasing enzyme (Perregaux et al., 2001). Our results showed that MCC950 controlled the activation of the NLRP3 inflammasome by inhibiting cleaved caspase-1 and decreasing the levels of the downstream cytokines IL-1β and IL-18, thus reducing the migration, apoptosis and pyroptosis of hRMECs by inhibiting the production of cleaved caspase-1 and inflammatory cytokines. However, MCC950 did not influence the expression of NLRP3 or caspase-1 precursors. MCC950 played an anti-inflammatory role in the pathogenesis of glucose-mediated retinopathy, and our data are consistent with the results of previous reports.

P2X7R is an oxidative stress and metabolic sensor that contributes to the activation of the NLRP3 inflammasome as an activator. In the retinas of murine and primates, P2X7R is present in the retinal microvascular system, neural cells and macrophages. On the condition of low extracellular ATP production, phagocytosis contributes to cleaning cell debris, when the concentrations of ATP are high, neuroinflammation enhanced instead of phagocytosis (Ho et al., 2016). After binding with ATP, P2X7R forms a nonselective cation channel on the cell

surface (Kahlenberg and Dubyak, 2004). It is worth noting that the intimate relationship between P2X7R and NLRP3 inflammasome shows significant contribution to the activation of inflammasome. Firstly, P2X7R can assist NLRP3 to precisely focus on the position of K^+ efflux and Ca^{2+} influx. Moreover, P2X7R recruitment also amplifies proinflammatory signals by regulating the expression levels of NLRP3 (Franceschini et al., 2015). Previous studies have demonstrated that a deficiency in P2X7R can provide resistance to the induction of diabetes and have suggested that P2X7R-targeted therapy of clinical diabetes may be feasible. P2X7R mediates the accumulation of the NLRP3 inflammasome and is involved the development of diabetic cardiomyopathy (Zhang et al., 2018). Our findings are consistent with previous studies that have demonstrated that enhancement of P2X7R signaling by the agonist BzATP can significantly activate the NLRP3 inflammasome stimulated by AGE-BSA and that the inhibitor A438079 attenuates the inflammatory response. Our data indicate that P2X7R indirectly affected AGE-induced hRMECs via the NLRP3 inflammasome. An increase in the expression of P2X7R changed the interendothelial cell junctions composed of protein complexes, including tight junctions and adherens junctions which contain Vascular endothelial (VE)-cadherin and zonula occludens (ZO)-1 respectively. In addition, upregulation of the expression of highly conserved MMPs, which are involved in extracellular matrix remodeling, angiogenesis, cell migration and proliferation, enhanced hRMECs migration and influenced the steady state of retinal microvessels (Firth et al., 1983). Moreover, our data indicated an increase in pyroptosis in hRMECs, which was consistent with the occurrence of apoptosis. Activation of the NLRP3 inflammasome in multiple pathological states can be induced by the recruitment of pro-IL-1β and pro-IL-18, which are cleaved by caspase-1, leading to pore formation, osmotic swelling, early loss of membrane integrity and eventual rapid inflammatory lytic death (Miao et al., 2011). Studies have proven that cell apoptosis and migration are closely related. Endothelial cell apoptosis plays an indispensable role in the development and angiogenesis of the vascular system and is strictly regulated by the expression of proapoptotic and antiapoptotic factors. Recently, knockout of bcl-2 was reported to influence the proliferation, adhesion, migration and capillary morphogenesis of hRMECs, which destroyed the relationship between cell survival and angiogenesis-promoting signals, prevented the formation of capillary morphology, decreased the branching and formation of retinal vessels, and reduced the numbers of endothelial cells and pericytes. (Kondo et al., 2008).

Relaxin is a peptide hormone composed of 57 amino acids with a structure similar to that of insulin (Bathgate et al., 2006). Bitto and colleagues noticed that relaxin significantly improved the wound-healing process in obese diabetic mice and effectively induced vascular regeneration by improving the expression of damaged endothelial growth factor (Bonner et al., 2013). A Russian study suggested that relaxin may act as a substitute when insulin is less effective as the receptors of relaxin are expressed in the pancreas, liver and muscle, which is consistent with the distribution of target organs of insulin action (Whittaker et al., 2003; Halls et al., 2007). Previous studies have shown that H3 relaxin plays an important role in diabetic vascular complications. The antifibrotic effect of H3 relaxin in diabetic cardiomyopathy has been confirmed, as has its beneficial effect on diabetic nephropathy (Zhang et al., 2018). Our results focus on another type of diabetic microvascular complication, diabetic retinopathy. In animal models, 14 days of continuous treatment with H3 relaxin significantly reduced retinal inflammation and apoptosis, attenuated the thickening of the basement membrane of the retinal capillary wall, weakened the swelling of endothelial cells and pericytes, and improved the morphology of cellular organelles. The photoreceptors on retinas are sensitive to high concentration of glucose, and the structural modifications precede the vasculopathy in the retinas. (Maisto et al., 2020) In our study, we noticed denatured mitochondria especially in the outer segments of the photoreceptors, as well as at the periphery of cone and rod bodies in the retinas of diabetic mice, and after H3 relaxin or/and treatment, the structural modifications of mitochondria were mildly but not totally improved. It is also reported that the mitochondria were the worst victims among organelles due to the changes in the mitochondrial fusion fission and transport proteins In the retina of diabetic mice (Zhong & Kowluru, 2011; Platania et al., 2019). *In vitro* experiments demonstrated that H3 relaxin attenuated the expression of the NLRP3 inflammasome in hRMECs stimulated by AGE-BSA and also inhibited the migration, apoptosis and pyroptosis of cells. AGE-BSA at a concentration of 100 μg/ml has little impact on the viability of hRMECs but influences the expression of proteins related to apoptosis and pyroptosis. Images acquired by electron microscopy also showed that the majority of AGE-BSA-induced hRMECs were in the middle stage of apoptosis, with some cells in the late stage of apoptosis. After H3 relaxin treatment, the majority of hRMECs were in the early stage of apoptosis, and pyroptosis was not observed.

MCC950 treatment of hRMECs alleviated the expression of NLRP3 inflammasome, and the migration, apoptosis and pyroptosis were synchronously suppressed. Treatment of hRMECs with a combination of MCC950 and H3 relaxin mildly reduced the expression of proteins related to migration, apoptosis and pyroptosis compared with those in cells treated with the agents separately, however, the mitigation was not complete. This phenomenon may be due to the intermediate role of the NLRP3 inflammasome in the antiapoptotic and antimigratory effects of H3 relaxin; when the NLRP3 inflammasome is partially inhibited, the beneficial effects of H3 relaxin are partially affected and are not completely eliminated. Therefore, treatment with a combination of MCC950 and H3 relaxin did not produce enough synergistic effects.

Our subsequent experiments focused on P2X7R, the upstream signal of the NLRP3 inflammasome. Studies have showed different opinions on how P2X7R contribute to retinal microvascular damage induced by high glucose through inflammatory signals. It is likely supposed that the protective mechanism of P2X7R antagonist are attributed to the inhibition of both infammatory cytokine and VEGF release, resulting in enhanced angiogenesis and vascular permeability, which trigger

to the invasion of DR (Clapp et al., 2019). Sugiyama et al. suggested that the activation of P2X7R can increase the vulnerability of retinal microvessels by formating large nonselective transmembrane pores to drive cation fluxes and intensive cell apoptosis in retinal microvascular cells (Sugiyama et al., 2004). However, in subsequent studies, the authors suggested an alternative mechanism. ATP-P2X7R may kill the cells via voltage-dependent Ca^{2+} channels (VDCC) because pore formation may be decreased by ATP activation of P2Y4R, which still need further discuss (Sugiyama et al., 2005). Our results indicated that AGE-BSA triggered the activation of P2X7R, followed by the activation of the NLRP3 inflammasome in hRMECs. H3 relaxin inhibited the activation of P2X7R induced by AGE-BSA, suggesting that H3 relaxin regulated the activation of the NLRP3 inflammasome through P2X7R under AGE-BSA-stimulated conditions. We found that the inhibition of P2X7R significantly reduced the expression and activation of the NLRP3 inflammasome induced by AGE-BSA, indicating that the initiation of NLRP3 inflammasome activation is dependent on the activation of P2X7R mediated by AGE-BSA. AGE-BSA promoted NLRP3 inflammasome-dependent migration, apoptosis and pyroptosis in hRMECs via the P2X7R pathway. Therefore, we elucidated a novel mechanism of inhibition of P2X7R-mediated activation of the NLRP3 inflammasome by H3 relaxin in the pathogenesis of diabetic retinopathy.

CONCLUSION

In summary, our results illustrated a new mechanism of H3 relaxin-dependent inhibition of retinal injury induced by AGE-BSA via P2X7R-mediated activation of the NLRP3 inflammasome in hRMECs. Therefore, our findings provide new insights into the mechanisms involved in the migration, apoptosis and pyroptosis of hRMECs and demonstrate that H3 relaxin is a potential therapeutic agent for ameliorating the activation of the NLRP3 inflammasome associated with high glucose, especially that in AGE-BSA-induced diabetic retinopathy.

DATA AVAILABILITY STATEMENT

The original contributions presented in the study are included in the article/**Supplementary Material**, further inquiries can be directed to the corresponding author.

ETHICS STATEMENT

The animal study was reviewed and approved by the Ethics Committee of The First Affiliated Hospital of Harbin Medical University.

AUTHOR CONTRIBUTIONS

KY, JL, XZ, and HK designed the study. KY, JL, and XZ refined the process. KY, JL, XZ, and ZR participated in rats section. KY, JL, ZR, LG, and YW participated *in vitro* experiment. KY and JL performed most of the experiments. ZR, LG, YW, WL, XM, and MH performed some of the experiments. KY, WL, XM, and MH analyzed the data. KY wrote the manuscript. HK supervised the study and the manuscript. All authors reviewed and approved the final draft.

FUNDING

This work was supported by the National Natural Science Foundation of China (No. 81670739) and the Research innovation foundation of Harbin medical university (No. YJSKYCX2019-34HYD).

SUPPLEMENTARY MATERIAL

The Supplementary Material for this article can be found online at: https://www.frontiersin.org/articles/10.3389/fphar.2020.603689/full#supplementary-material

REFERENCES

Bani, D. (2012). Cellular retrograde cardiomyoplasty and relaxin therapy for postischemic myocardial repair in a rat model. *Tex. Heart Inst. J.*, 39 (4), 488–499.

Bathgate, R. A. D., Samuel, C. S., Burazin, T. C. D., Layfield, S., Claasz, A. A., Reytomas, I. G. T., et al. (2002). Human relaxin gene 3 (H3) and the equivalent mouse relaxin (M3) gene. *J. Biol. Chem.* 277 (2), 1148–1157. doi:10.1074/jbc.m107882200

Bathgate, R., Ivell, R., Sanborn, B. M., Sherwood, O. D., and Summers, R. J. (2006). International Union of Pharmacology LVII: recommendations for the nomenclature of receptors for relaxin family peptides. *Pharmacol. Rev.* 58 (1), 7–31. doi:10.1124/pr.58.1.9

Beckel, J. M., Argall, A. J., Lim, J. C., Xia, J., Lu, W., Coffey, E. E., et al. (2014). Mechanosensitive release of adenosine 5′-triphosphate through pannexin channels and mechanosensitive upregulation of pannexin channels in optic nerve head astrocytes: a mechanism for purinergic involvement in chronic strain. *Glia* 62 (9), 1486–1501. doi:10.1002/glia.22695

Bonner, J. S., Lantier, L., Hocking, K. M., Kang, L., Owolabi, M., James, F. D., et al. (2013). Relaxin treatment reverses insulin resistance in mice fed a high-fat diet. *Diabetes* 62 (9), 3251–3260. doi:10.2337/db13-0033

Clapp, C., Diaz-Lezama, N., Adan-Castro, E., Ramirez-Hernandez, G., Moreno-Carranza, B., Sarti, A. C., et al. (2019). Pharmacological blockade of the P2X7 receptor reverses retinal damage in a rat model of type 1 diabetes. *Acta Diabetol.* 56 (9), 1031–1036. doi:10.1007/s00592-019-01343-4

Duncan, J. A., Bergstralh, D. T., Wang, Y., Willingham, S. B., Ye, Z., Zimmermann, A. G., et al. (2007). Cryopyrin/NALP3 binds ATP/dATP, is an ATPase, and requires ATP binding to mediate inflammatory signaling. *Proc. Natl. Acad. Sci. Unit. States Am.* 104 (19), 8041–8046. doi:10.1073/pnas.0611496104

Firth, J. A., Bauman, K. F., and Sibley, C. P. (1983). The intercellular junctions of Guinea-pig placental capillaries: a possible structural basis for endothelial solute permeability. *J. Ultra. Res.* 85 (1), 45–57. doi:10.1016/s0022-5320(83)90115-6

Franceschini, A., Capece, M., Chiozzi, P., Falzoni, S., Sanz, J. M., Sarti, A. C., et al. (2015). The P2X7 receptor directly interacts with the NLRP3 inflammasome scaffold protein. *Faseb. J.* 29 (6), 2450–2461. doi:10.1096/fj.14-268714

Halls, M. L., van der Westhuizen, E. T., Bathgate, R. A. D., and Summers, R. J. (2007). Relaxin Family Peptide Receptors - former orphans reunite with their

parent ligands to activate multiple signalling pathways. *Br. J. Pharmacol.* 150 (6), 677–691. doi:10.1038/sj.bjp.0707140

Ho, T., Aplin, F. P., Jobling, A. I., Phipps, J. A., de Iongh, R. U., Greferath, U., et al. (2016). Localization and possible function of P2X receptors in normal and diseased retinae. *J. Ocul. Pharmacol. Therapeut.* 32, 509–517. doi:10.1089/jop.2015.0158

Kahlenberg, J. M, and Dubyak, G. R. (2004). Mechanisms of caspase-1 activation by P2X7 receptor-mediated K+ release. *Am. J. Physiol. Cell Physiol.* 286 (5), 1100–1108. doi:10.1152/ajpcell.00494.2003

Karmakar, M., Katsnelson, M. A., Dubyak, G. R., and Pearlman, E. (2016). Neutrophil P2X7 receptors mediate NLRP3 inflflammasome-dependent IL-1b secretion in response to ATP. *Nat. Commun.* 7, 10555. doi:10.1038/ncomms10555

Kerur, N., Hirano, Y., Tarallo, V., Fowler, B. J., Bastos-Carvalho, A., Yasuma, T., et al. (2013). TLR-independent and P2X7-dependent signaling MediateAluRNA-induced NLRP3 inflammasome activation in geographic atrophy. *Invest. Ophthalmol. Vis. Sci.* 54 (12), 7395–7401. doi:10.1167/iovs.13-12500

Kondo, S., Tang, Y., Scheef, E. A., Sheibani, N., and Sorenson, C. M. (2008). Attenuation of retinal endothelial cell migration and capillary morphogenesis in the absence of bcl-2. *Am. J. Physiol. Cell Physiol.* 294 6, 1521–1530. doi:10.1152/ajpcell.90633.2007

Kowluru, R. A., Kowluru, A., Mishra, M., and Kumar, B. (2015). Oxidative stress and epigenetic modifications in the pathogenesis of diabetic retinopathy. *Prog. Retin. Eye Res.* 48, 40–61. doi:10.1016/j.preteyeres.2015.05.001

Maisto, R., Trotta, M. C., Petrillo, F., et al. (2020). Resolvin D1 modulates the intracellular VEGF-related miRNAs of retinal photoreceptors challenged with high glucose. *Front. Pharmacol.* 11, 235. doi:10.3389/fphar.2020.00871

Masini, E., Nistri, S., Vannacci, A., Sacchi, T. B., Novelli, A., and Bani, D. (2004). Relaxin inhibits the activation of human neutrophils: involvement of the nitric oxide pathway. *Endocrinology*, 145 (3), 1106–1112. doi:10.1210/en.2003-0833

Miao, E. A., Rajan, J. V., and Aderem, A. (2011). Caspase-1-induced pyroptotic cell death. *Immunol. Rev.* 243 (1), 206–214. doi:10.1111/j.1600-065x.2011.01044.x

Mizutani, M., Kern, T. S., and Lorenzi, M. (1996). Accelerated death of retinal microvascular cells in human and experimental diabetic retinopathy. *J. Clin. Invest.* 97 (12), 2883–2890. doi:10.1172/jci118746

Perregaux, D. G., McNiff, P., Laliberte, R., Hawryluk, N., Peurano, H., Stam, E., et al. (2001). Identification and characterization of a novel class of interleukin-1 post-translational processing inhibitors. *J. Pharmacol. Exp. Therapeut.* 299 (1), 187–197.

Perrone, L., Matrone, C., and Singh, L. P. (2014). Epigenetic modifications and potential new treatment targets in diabetic retinopathy. *J Ophthalmol* 2014, 789120. doi:10.1155/2014/789120

Platania, C. B. M., Maisto, R., Trotta, M. C., D'Amico, M., Rossi, S., Gesualdo, C., et al. (2019). Retinal and circulating miRNA expression patterns in diabetic retinopathy: an in silico and *in vivo* approach. *Br. J. Pharmacol.* 176 (13), 2179–2194. doi:10.1111/bph.14665

Platania, C. B. M., Giurdanella, G., Di Paola, L., Leggio, G. M., Drago, F., Salomone, S., et al. (2017). P2X7 receptor antagonism: implications in diabetic retinopathy. *Biochem. Pharmacol.* 138, 130–139. doi:10.1016/j.bcp.2017.05.001

Platania, C. B. M., Lazzara, F., Fidilio, A., Fresta, C. G., Conti, F., Giurdanella, G., et al. (2019). Blood-retinal barrier protection against high glucose damage: the role of P2X7 receptor. *Biochem. Pharmacol.* 168, 249–258. doi:10.1016/j.bcp.2019.07.010

Qi, Y., Zhao, M., Bai, Y., Huang, L., Yu, W., Bian, Z., et al. (2014). Retinal ischemia/reperfusion injury is mediated by toll-like receptor 4 activation of NLRP3 inflammasomes. *Invest. Ophthalmol. Vis. Sci.* 55 (9), 5466–5475. doi:10.1167/iovs.14-14380

Samways, D. S., Li, Z., and Egan, T. M. (2014). Principles and properties of ion flow in P2X receptors. *Front. Cell. Neurosci.* 8, 6. doi:10.3389/fncel.2014.00006

Sanderson, J., Dartt, D. A., Trinkaus-Randall, V., Pintor, J., Civan, M. M., Delamere, N. A., et al. (2014). Purines in the eye: recent evidence for the physiological and pathological role of purines in the RPE, retinal neurons, astrocytes, Müller cells, lens, trabecular meshwork, cornea and lacrimal gland. *Exp. Eye Res.* 127, 270–279. doi:10.1016/j.exer.2014.08.009

Schmidt, F. I., Lu, A., Chen, J. W., Ruan, J., Tang, C., Wu, H., et al. (2016). A single domain antibody fragment that recognizes the adaptor ASC defines the role of ASC domains in inflammasome assembly. *J. Exp. Med.* 213 (5), 771–790. doi:10.1084/jem.20151790

Shibata, M., Ishizaki, E., Zhang, T., Fukumoto, M., Barajas-Espinosa, A., Li, T., et al. (2018). Purinergic vasotoxicity: role of the pore/oxidant/KATP channel/Ca2+ pathway in P2X7-induced cell death in retinal capillaries. *Vision* 2 (3), 25. doi:10.3390/vision2030025

Simó, R. and Hernández, C. (2014). Neurodegeneration in the diabetic eye: new insights and therapeutic perspectives. *Trends Endocrinol. Metabol.* 25 (1), 23–33. doi:10.1016/j.tem.2013.09.005

Stitt, A. W., Curtis, T. M., Chen, M., Medina, R. J., McKay, G. J., Jenkins, A., et al. (2016). The progress in understanding and treatment of diabetic retinopathy. *Prog. Retin. Eye Res.* 51, 156–186. doi:10.1016/j.preteyeres.2015.08.001

Sugiyama, T., Kawamura, H., Yamanishi, S., Kobayashi, M., Katsumura, K., and Puro, D. G. (2005). Regulation of P2X7-induced pore formation and cell death in pericyte containing retinal microvessels. *Am. J. Physiol. Cell Physiol.* 288 (3), 568–576. doi:10.1152/ajpcell.00380.2004

Sugiyama, T., Kobayashi, M., Kawamura, H., Li, Q., and Puro, D. G. (2004). Enhancement of P2X7-induced pore formation and apoptosis: an early effect of diabetes on the retinal microvasculature. *Invest. Ophthalmol. Vis. Sci.* 45 (3), 1026–1032. doi:10.1167/iovs.03-1062

Surprenant, A., Rassendren, F., Kawashima, E., North, R. A., and Buell, G. (1996). The cytolytic P2Z receptor for extracellular ATP identified as a P2X receptor (P2X7). *Science* 272 (5262), 735–738. doi:10.1126/science.272.5262.735

Szepietowska, B., Gorskaa, M., and Szelachowskaa, M. (2008). Plasma relaxin concentration is related to beta -cell function and insulin sensitivity in women with type 2 diabetes mellitus. *Diabetes Res. Clin. Pract.* 79 (3), 1–3. doi:10.1016/j.diabres.2007.10.017

The Diabetes Control and Complications Trial Research Group (1993). The effect of intensive treatment of diabetes on the development and progression of long-term complications in insulin-dependent diabetes mellitus. *N. Engl. J. Med.* 329 (14), 977–986. doi:10.1056/NEJM199309303291401

Vandanmagsar, B., Youm, Y.-H., Ravussin, A., Galgani, J. E., Stadler, K., Mynatt, R. L., et al. (2011). The NLRP3 inflammasome instigates obesity-induced inflammation and insulin resistance. *Nat. Med.* 17 (2), 179–188. doi:10.1038/nm.2279

von Moltke, J., Trinidad, N. J., Moayeri, M., et al. (2013). Rapid induction of inflammatory lipid mediators by the inflammasome *in vivo*. *Nature* 490 (7418), 107–111. doi:10.1038/nature11351

Whittaker, P. G., Edwards, J. R. G., Randolph, C., Büllesbach, E. E., Schwabe, C., and Steinetz, B. G. (2003). Abnormal relaxin secretion during pregnancy in women with type 1 Diabetes1," *Exp. Biol. Med.*, 228 1, 33–40. doi:10.1177/153537020322800104

Willingham, S. B., Allen, I. C., Bergstralh, D. T., Brickey, W. J., Huang, M. T.-H., Taxman, D. J., et al. (2009). NLRP3 (NALP3, Cryopyrin) facilitates *in vivo* caspase-1 activation, necrosis, and HMGB1 release via inflammasome-dependent and -independent pathways. *J. Immunol.* 183 (3), 2008–2015. doi:10.4049/jimmunol.0900138

Yau, J. W. Y., Rogers, S. L., Kawasaki, R., Lamoureux, E. L., Kowalski, J. W., Bek, T., et al. (2012). Global prevalence and major risk factors of diabetic retinopathy. *Diabetes Care*, 35 (3), 556–564. doi:10.2337/dc11-1909

Zhang, J., Qi, Y.-F., Geng, B., Pan, C.-S., Zhao, J., Chen, L., et al. (2005). Effect of relaxin on myocardial ischemia injury induced by isoproterenol. *Peptides* 26 (9), 1632–1639. doi:10.1016/j.peptides.2005.02.008

Zhang, X., Fu, Y., Li, H., Shen, L., Chang, Q., Pan, L., et al. (2018). H3 relaxin inhibits the collagen synthesis via ROS- and P2X7R-mediated NLRP3 inflammasome activation in cardiac fibroblasts under high glucose. *J. Cell. Mol. Med.* 22 (3), 1816–1825. doi:10.1111/jcmm.13464

Zhong, Q. and Kowluru, R. A. Diabetic retinopathy and damage to mitochondrial structure and transport machinery. (2011). *Invest. Ophthalmol. Vis. Sci.* 52 (12), 8739–8746. doi:10.1167/iovs.11-8045

Conflict of Interest: The authors declare that the research was conducted in the absence of any commercial or financial relationships that could be construed as a potential conflict of interest.

frontiers in Pharmacology

ORIGINAL RESEARCH
published: 18 December 2020
doi: 10.3389/fphar.2020.594574

Bilirubin Nanoparticles Reduce Diet-Induced Hepatic Steatosis, Improve Fat Utilization, and Increase Plasma β-Hydroxybutyrate

Terry D. Hinds Jr.[1]*, *Justin F. Creeden*[2], *Darren M. Gordon*[2], *Donald F. Stec*[3], *Matthew C. Donald*[4] *and David E. Stec*[4]*

[1]Department of Pharmacology and Nutritional Sciences, University of Kentucky College of Medicine, Lexington, KY, United States, [2]Department of Neurosciences, University of Toledo College of Medicine, Toledo, OH, United States, [3]Small Molecule NMR Facility Core, Vanderbilt Institute of Chemical Biology, Vanderbilt University, Nashville, TN, United States, [4]Department of Physiology and Biophysics, Cardiorenal and Metabolic Diseases Research Center, University of Mississippi Medical Center, Jackson, MS, United States

OPEN ACCESS

Edited by:
Gaetano Cairo,
University of Milan, Italy

Reviewed by:
Vincenzo Ronca,
University of Birmingham, United Kingdom
Ivo Pieter Van De Peppel,
University Medical Center Groningen, Netherlands

***Correspondence:**
Terry D. Hinds
terry.hinds@uky.edu
David E. Stec
dstec@umc.edu

Specialty section:
This article was submitted to Experimental Pharmacology and Drug Discovery, a section of the journal Frontiers in Pharmacology

Received: 13 August 2020
Accepted: 13 November 2020
Published: 18 December 2020

Citation:
Hinds TD, Creeden JF, Gordon DM, Stec DF, Donald MC and Stec DE (2020) Bilirubin Nanoparticles Reduce Diet-Induced Hepatic Steatosis, Improve Fat Utilization, and Increase Plasma β-Hydroxybutyrate. Front. Pharmacol. 11:594574. doi: 10.3389/fphar.2020.594574

The inverse relationship of plasma bilirubin levels with liver fat accumulation has prompted the possibility of bilirubin as a therapeutic for non-alcoholic fatty liver disease. Here, we used diet-induced obese mice with non-alcoholic fatty liver disease treated with pegylated bilirubin (bilirubin nanoparticles) or vehicle control to determine the impact on hepatic lipid accumulation. The bilirubin nanoparticles significantly reduced hepatic fat, triglyceride accumulation, *de novo* lipogenesis, and serum levels of liver dysfunction marker aspartate transaminase and ApoB100 containing very-low-density lipoprotein. The bilirubin nanoparticles improved liver function and activated the hepatic β-oxidation pathway by increasing PPARα and acyl-coenzyme A oxidase 1. The bilirubin nanoparticles also significantly elevated plasma levels of the ketone β-hydroxybutyrate and lowered liver fat accumulation. This study demonstrates that bilirubin nanoparticles induce hepatic fat utilization, raise plasma ketones, and reduce hepatic steatosis, opening new therapeutic avenues for NAFLD.

Keywords: obesity, non-alcoholic fatty liver disease, ketone, ketosis, apolipoprotein, heme oxygenase, HO-1

INTRODUCTION

Obesity is at an all-time high, and this is prevalent worldwide. The tissue overload from lipids in the obese may cause other comorbidities such as non-alcoholic fatty liver disease (NAFLD), insulin-resistant diabetes, cardiovascular disease, and some cancers (John et al., 2016; Lega and Lipscombe, 2020). Therapeutic inventions for reducing obesity are limited, and most increase blood pressure and may further complicate the cardiovascular outcomes. We and others have previously shown that the heme metabolite, bilirubin, reduce fat accumulation and blood glucose levels in obese mice (Dong et al., 2014; Hinds et al., 2014; Liu et al., 2015; Gordon et al., 2016; Hinds et al., 2016; Stec et al., 2016; Hinds et al., 2017; Takei et al., 2019; Stec et al., 2020). Bilirubin offers a promising therapeutic approach as it benefits the cardiovascular system (Hinds and Stec, 2018; Hinds and Stec, 2019) by preventing hypertension (Vera et al., 2009) and improving blood flow (Vera and Stec, 2010). Bilirubin's actions to reduce lipid accumulation have been attributed to the recent findings that it has a hormonal function by binding directly to the nuclear receptor

peroxisome proliferator-activated receptor α (PPARα), which induces gene transcription that promotes fat burning (Gordon et al., 2016; Stec et al., 2016; Gordon et al., 2019).

Not surprisingly, mice with a hepatocyte-specific deletion of PPARα develop hepatic steatosis and NAFLD that is worsened on a high-fat diet (Stec et al., 2019). PPARα induces genes for β-oxidation and fat utilization, which reduces hepatic fat and NAFLD (Burri et al., 2010; Grabacka et al., 2016). During this process, PPARα regulates processes that mediate ketone body production from fatty acid oxidation that increases serum levels of the ketone β-hydroxybutyrate (BOHB) (Kersten et al., 1999; Grabacka et al., 2016). The BOHB is excreted by the liver to the blood and serves as a fuel source for the body other than glucose (Newman and Verdin, 2014a; Newman and Verdin, 2014b). Fat accumulation in the liver suppresses β-oxidation and reduces ketone production lowering plasma BOHB. Mey et al. found that BOHB levels are reduced in humans with obesity-related NAFLD (Mey et al., 2020). While it was not a major conclusion in the paper, they also found that bilirubin levels were lower in patients with NAFLD. Others have shown that plasma bilirubin levels are negatively associated with NAFLD (Hjelkrem et al., 2012; Puri et al., 2013; Salomone et al., 2013). While patients exhibiting mildly elevated bilirubin levels had significantly less NAFLD indicating an inverse relationship (Kwak et al., 2012). These studies suggest that bilirubin and BOHB may be positively correlated; however, no studies have shown that when bilirubin is elevated that BOHB is also higher.

While large-scale population studies have associated the protective effects of plasma bilirubin levels on NAFLD development, translating these findings into therapies to patients has been complicated. One of the main reasons for this difficulty is the lack of formulations of bilirubin that could be administered to human patient populations. Bilirubin is a very hydrophobic molecule and does not dissolve in aqueous solutions easily. This property limits its use in patients because solvents are customarily required to get bilirubin into solutions such as saline and others used. One resolution to this problem is to covalently attach a polyethylene glycol compound to bilirubin to form pegylated bilirubin (PEG-BR) and promote the formation of highly water-soluble bilirubin nanoparticles (Zheng et al., 2019). PEG-BR has been an effective anti-inflammatory and anti-oxidant in several *in vivo* models (Lee et al., 2016; Kim M. J. et al., 2017). However, its effectiveness as a potential therapeutic for NAFLD has not been evaluated.

Here, we wanted to determine bilirubin's functionality on obesity-induced hepatic steatosis and NAFLD and determine whether it activates β-oxidation, fat utilization, and BOHB production using bilirubin nanoparticles. We found that hepatic PPARα induced and liver fat content was lower, which correlated with higher plasma BOHB levels and lower serum triglycerides. Our results demonstrate a possible role for bilirubin nanoparticles in the protection against obesity-induced fatty liver disease.

MATERIALS AND METHODS

Animals. The experimental procedures and protocols of this study conformed to the National Institutes of Health Guide for the Care and Use of Laboratory Animals and approved by the Institutional Animal Care and Use Committee of the University of Mississippi Medical Center. C57BL/6J mice were purchased from Jackson Labs (Bar Harbor, ME, United States) and placed on a 60% high-fat diet (diet #D12492, Research Diets, Inc., New Brunswick, NJ, United States) for 24 weeks with full access to tap water. After this time, mice were randomly assigned to either a treatment group consisting of pegylated bilirubin nanoparticles (30 mg/kg every other day, i.p.) or vehicle (saline) for 4 weeks while continuing on the high-fat diet.

Pegylated bilirubin synthesis. The synthesis of PEG-BR was done at the Research Institute of Pharmaceutical Sciences at the University of Mississippi (Oxford, MS, United States). The PEG-BR was prepared from bilirubin-IX-alpha (Frontier Scientific, Logan, UT, United States) and mPEG2000-NH2 (Sigma-Aldrich, St. Louis, MO, United States) as previously described (Gordon et al., 2016; Lee et al., 2016; Kim M. J. et al., 2017). The size and morphology of PEG-BR were analyzed by transmission electron microscopy (TEM) using a model JEM-2100 (JEOL Ltd., Tokyo, Japan). Purity of the PEG-BR was found to be 95%. PEG-BR was resuspended in saline with slight sonication to dissolve and stored at −20°C in the dark.

Liver composition. Liver composition was measured at the end of the study using magnetic resonance imaging (EchoMRI-900TM, Echo Medical System, Houston, TX, United States). MRI measurements were performed on whole livers placed in a thin-walled plastic cylinder. Liver fat and lean mass were obtained and expressed as a percent of total liver weight.

Liver triglyceride measurement. Triglycrides were measured from 100 mg of liver tissue homogenized in 1 ml of 5% NP-40 in water. Homogenized tissues were then heated to 95°C for 5 min and then centrifuged (13,000 × *g*) for 2 min. Tissue triglyceride levels were measured using a colorimetric assay kit according to manufactures' guidelines (Triglyceride Quantification Colorimetric/Fluorometric Kit, BioVision, Milpitas, CA, United States). Tissue triglyceride are expressed as mM. Samples from individual mice were run in duplicate and averaged, and the averages used to obtain group averages.

Liver histology. To determine hepatic differences of the pegylated bilirubin and vehicle treated mice, livers were mounted and frozen in Tissue-Tek O.C.T and sectioned at 10 μm. Hematoxylin and Eosin (H&E) staining were performed as previously described (Hinds et al., 2016; Hinds et al., 2017; Stec et al., 2019). The Oil Red O (CAS Number 1320-06-5, Sigma-Aldrich, St. Louis, MI, United States) staining was performed on 10 μm thick formalin-fixed livers. The livers were stained with freshly prepared Oil Red O working solution 15 min, rinsed with 60% isopropanol, and nuclei stained with alum hematoxylin. Then, slides were rinsed with distilled water and mounted in aqueous mountant and prepared for imaging. The degree of Oil Red O staining was determined at 20× magnification using a color video camera attached to an Olympus VS120 slide scanning microscope (Olympus Corporation, Center Valley, PA, United States). Images

were analyzed using the Olympus OlyVIA software. Image J (NIH) was used to quantitate the lipid droplets. Data are presented as the ±SEM of the Oil Red O staining for each group.

AST/ALT measurements. Plasma alanine transaminase (ALT) and aspartate transaminase (AST) were measured using a Vet Axcel serum chemistry analyzer (AlfaWassermann, West Caldwell, NJ, United States) from 30 μL of plasma. Samples were measured in duplicate with standards supplied by the manufacturer. Data are presented as Units (U)/L.

Quantitative Real-Time PCR Analysis. Total RNA was harvested from the animals by lysing livers using a Qiagen Tissue Lyser LT (Qiagen Inc., Germantown, MD, United States) and then extraction by 5-Prime PerfectPure RNA Tissue Kit (Thermo Fisher Scientific, Wilmington, DE, United States). Total RNA was read on a NanoDrop 2,000 spectrophotometer (Thermo Fisher Scientific, Wilmington, DE, United States) and cDNA was synthesized using High Capacity cDNA Reverse Transcription Kit (Applied Biosystems, Foster City, CA, United States). PCR amplification of the cDNA was performed by quantitative real-time PCR using TrueAmp SYBR Green qPCR SuperMix (Alkali Scientific, Fort Lauderdale, FL, United States) for gene-specific primers as previously described (Hinds et al., 2011; Hinds et al., 2014; Hinds et al., 2016; Marino et al., 2016; Stec et al., 2016; Hinds et al., 2017). The thermocycling protocol consisted of 5 min at 95°C, 40 cycles of 15 s at 95°C, and 30 s at 60°C, finished with a melting curve ranging from 60 to 95°C to allow distinction of specific products. Normalization was performed in separate reactions with primers to GAPDH.

Gel Electrophoresis and Western Blotting—Mouse tissues were flash frozen in liquid nitrogen during harvesting and stored at −80°C. For gel electrophoresis, 50–100 mg of cut tissue was then resuspended in three volumes of CelLytic Buffer (Sigma-Aldrich, St. Louis, MO, United States, Cat No. C3228) plus 10% protease inhibitor cocktail (Sigma-Aldrich, St. Louis, MO, United States, Cat No. P2714-1BTL) and Halt phosphatase inhibitor cocktail (Thermo Fisher Scientific, Wilmington, DE, United States, Cat No. PI78420), and then incubated on ice for 30 min. The livers were lyzed using a Qiagen Tissue Lyser LT (Qiagen Inc., Germantown, MD, United States) and then centrifuged at 100,000 × *g* at 4°C. Protein samples were resolved by SDS polyacrylamide gel electrophoresis and electrophoretically transferred to Immobilon-FL membranes. Membranes were blocked at room temperature for 2 h in TBS (10 mM Tris-HCl (pH 7.4) and 150 mM NaCl) containing 3% BSA. Subsequently, the membranes were incubated overnight at 4°C with the following antibodies: ACOX1 (Santa Cruz Biotechnology, Santa Cruz, CA, sc-98499), fatty acid synthase (FAS) (Cell Signaling Technology, Danvers, MA, United States, Cat No. 3180S), SCD1(Cell Signaling Technology, Danvers, MA, United States, Cat No. 2794S), or heat shock protein 90 (HSP90) (Santa Cruz, sc-13119). After three washes in TBS + 0.1% Tween 20, the membrane was incubated with an infrared anti-rabbit (IRDye 800, green) or anti-mouse (IRDye 680, red) secondary antibody labeled with IRDye infrared dye (LI-COR Biosciences) (1:10,000 dilution in TBS) for 2 h at 4°C. Immunoreactivity was visualized and quantified by infrared scanning in the Odyssey system (LI-COR Biosciences).

Analysis of plasma lipids and metabolites. Plasma lipids and metabolites were measured in mice following an 8 h fast by nuclear magnetic resonance (NMR) spectroscopy as part of the Bruker IVDr platform (Bruker Scientific LLC, Billerica, MA, United States), as previously described (Stec et al., 2019). Plasma samples (50 μL) were combined with 150 μL of buffer supplied by Bruker Biospin specifically for the IVDr protocol and were analyzed according to the Bruker *In-Vitro* Diagnostics research (IVDr) protocol. Lipoprotein subclass analysis was performed using regression analysis of the NMR data as previously described (Stec et al., 2019).

Statistics. All bar graph data are presented as mean ± S.E.M. Box and whisker plots display whiskers from the minimum or maximum, with a vertical line in the box to indicate the median. Differences between treatment groups were determined using student t-test or one-way analysis of variance with a post hoc test (Dunnett's). A $p < 0.05$ was considered to be significant. All analyses were performed with GraphPad Prism eight software (GraphPad Software, Inc., San Diego, CA).

RESULTS

Bilirubin has almost exclusively been correlated with liver dysfunction. The recent findings that bilirubin is inversely associated with NAFLD (Jang, 2012; Kwak et al., 2012) and that a mouse model of Gilbert's syndrome with hyperbilirubinemia were resistant to hepatic steatosis (Hinds et al., 2017), has provided new insights into its function. We wanted to determine if bilirubin nanoparticles (pegylated bilirubin) that we and others have recently described (Gordon et al., 2016; Lee et al., 2016; Kim et al., 2017a; Kim M. J. et al., 2017; Lee et al., 2019) could improve hepatic steatosis in an obese mouse model. As previously described (Gordon et al., 2016), we put mice on a high-fat diet (HFD) for 24 weeks and then treated for 4-weeks with PEG-BR or vehicle while maintaining them on a HFD. The obese mice's body weights at the 24-weeks point were comparable, with the starting weight of the mice over 50 g for each group (55.7 ± 4.1 g Vehicle vs. 53.4 ± 2.6 PEG-BR treated) ($p = 0.2823$). After the 4-weeks treatment, the plasma bilirubin levels were increased in the PEG-BR treated (0.45 ± 0.08 mg/dl) compared to the vehicle (0.13 ± 0.05 mg/dl) ($p < 0.0001$). After the 4-weeks PEG-BR and vehicle treatments, the percent body weight change was greater in the vehicle but not the PEG-BR (103.4% ± 2.5 for vehicle and 96.3% ± 2.7 for PEG-BR) ($p = 0.0058$). The PEG-BR group had a 7% reduction in body weight gain compared to the vehicle treated animals. There was no difference between the groups for the liver weight (**Figure 1A**). The liver to body weight ratio was 0.056 ± 0.004 vs. 0.055 ± 0.004 g/g Vehicle vs. PEG-BR treated. However, percent liver fat measured by echoMRI, liver triglycerides, and lipid Oil Red O staining all showed less fat accumulation in the PEG-BR treated animals compared to vehicle (**Figures 1B–D**).

To better understand how the bilirubin nanoparticles impact hepatic function, the livers from both groups of mice were analyzed by hematoxylin and eosin (H&E) staining for

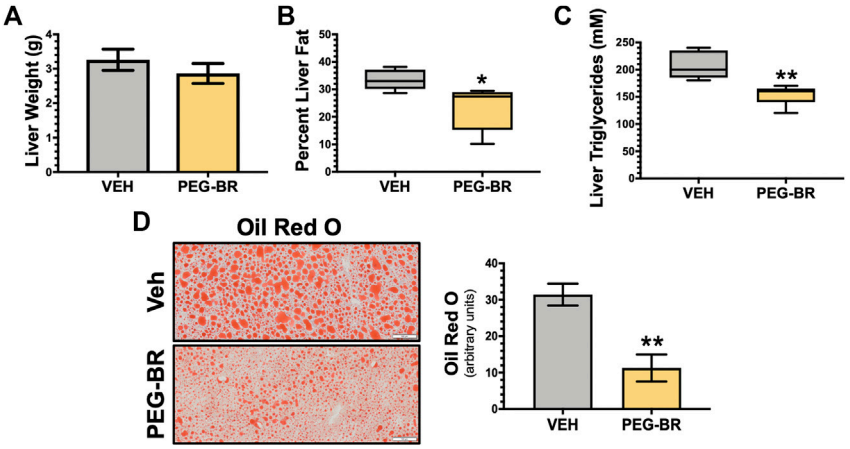

FIGURE 1 | Bilirubin nanoparticles reduce hepatic fat content. Liver weight (*g*) **(A)**, percent liver fat as determined by EchoMRI **(B)**, hepatic triglycerides (mM) **(C)**, and hepatic Oil Red O staining **(D)** in vehicle (VEH) and pegylated bilirubin (PEG-BR) treated mice. White scale bar = 100 μm. * = $p < 0.05$ vs. VEH; ** = $p < 0.01$ vs. VEH; (VEH, $n = 5$ and PEG-BR, $n = 6$).

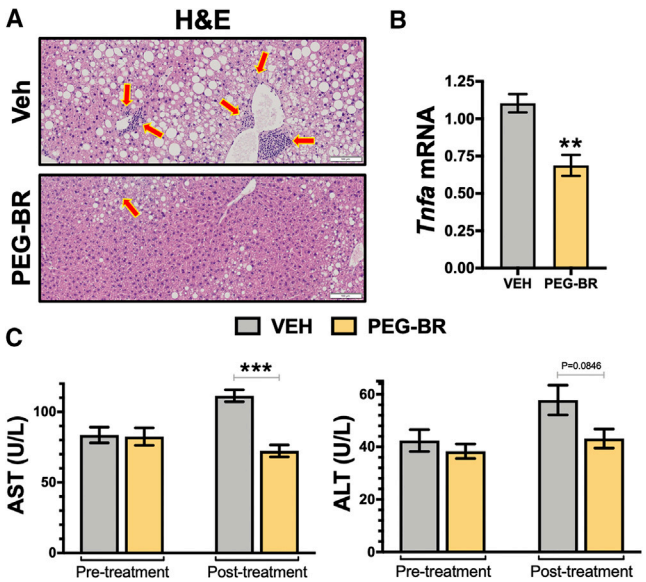

FIGURE 2 | Bilirubin nanoparticles improve hepatic function and inflammation in obese mice. Hematoxylin and eosin (H&E) staining in vehicle (VEH) and pegylated bilirubin (PEG-BR) treated mice **(A)**. Real-time PCR expression of hepatic tumor necrosis factor alpha (*Tnfa*) **(B)**; ** = $p < 0.001$ vs. VEH; (VEH, $n = 4$ and PEG-BR, $n = 4$). Liver dysfunction markers alanine transaminase (ALT) and aspartate transaminase (AST) plasma levels were measured at the beginning (pre-treatment) of the study and after the 4-weeks treatment was completed (post-treatment); ** = $p < 0.01$ vs. VEH; (VEH, $n = 5$ and PEG-BR, $n = 6$).

observable differences in treated animals and hepatic dysfunction biomarkers. The H&E staining revealed that the VEH treated animals possibly had inflammation, which were found to be lower in the PEG-BR treated group (**Figure 2A**). This was paralleled with pro-inflammatory gene *Tnfa*, in that PEG-BR significantly ($p < 0.01$) reduced expression compared to VEH (**Figure 2B**). We measured plasma levels of hepatic dysfunction markers alanine transaminase (ALT) and aspartate transaminase (AST) before (pre-treatment) treatment and after the study was completed (post-treatment). There were no differences in AST or ALT levels at the beginning of the study (**Figure 2C**). However, post-treatment, the AST levels were significantly ($p < 0.001$) reduced with PEG-BR compared to VEH groups. The ALT level was also reduced with PEG-BR was not reduced but showed a trend toward reduction that did not reach statistical significance. Overall, these data demonstrate that PEG-BR improved hepatic function and reduced inflammation.

Next, we determined how PEG-BR treatments affect plasma metabolites of amino acids by NMR spectroscopy using the Bruker IVDr platform. We found no significant differences in

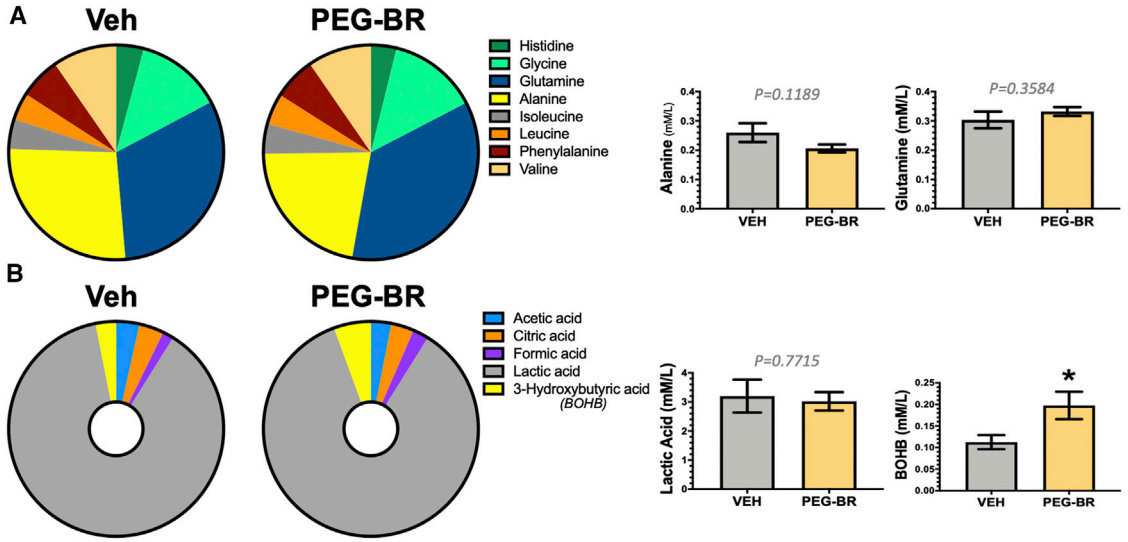

FIGURE 3 | Plasma metabolites in bilirubin nanoparticles and vehicle treated obese mice. Pie chart and bar graphs of plasma amino acids in vehicle and pegylated bilirubin treated mice **(A)**. Pie chart and bar graphs of plasma carboxylic and keto acids in vehicle and pegylated bilirubin treated mice **(B)**. * = $p < 0.05$ vs. VEH; (VEH, $n = 3$ and PEG-BR, n = 4–5).

amino acids measured in the plasma of the PEG-BR or vehicle-treated groups (**Figure 3A**). Exercise and fat burning metabolites lactic acid, acetic acid, formic acid, and β-hydroxybutyrate (3-hydroxybutyric acid) were measured in the two groups. Analysis showed that only elevated plasma BOHB levels had a significant ($p < 0.05$) difference for PEG-BR treated compared to the vehicle groups (**Figure 3B**). There were no differences between the lactic acid, formic acid, citric acid, and acetic acid between the groups. The PEG-BR reduces hepatic lipids possibly by inducing β-oxidation, which provide metabolites for ketone production. Therefore, we measured known mediators that regulate fatty acid β-oxidation, such as PPARα and target genes. PPARα (*Ppara*) mRNA expression was increased in the PEG-BR treated animals compared to the vehicle group (**Figure 4A**). Huang *et al.* showed that sustained activation of PPARα by endogenous ligands in obese mice increases the rate-limiting mediator of β-oxidation, *Acox1* (Vluggens et al., 2010), and p450 *Cyp4a* pathways (Hirai et al., 2007; Huang et al., 2012). Here, we also found that *Acox1* and cytochrome P450 *Cyp4a12* (**Figures 4B,C**) were significantly ($p < 0.05$) higher in the PEG-BR compared to vehicle-treated animals. Also, the PPARα-target genes for long-chain fatty acid transporters FATP1 (gene *Slc27a1*) and FATP2 (gene *Slc27a2*) (Hirai et al., 2007), were significantly increased in the PEG-BR treated mice compared to vehicle (**Figures 4D,E**). The lipogenesis gene, *Scd1*, was significantly ($p < 0.01$) reduced with PEG-BR (**Figure 4F**). Immunoblotting of ACOX1 showed that the protein was significantly ($p = 0.0137$) higher in the PEG-BR treated animals compared to the vehicle (**Figure 4G**). The *de novo* lipogenesis proteins fatty acid synthase (FAS) and stearoyl-Coenzyme A desaturase 1 (SCD1) were significantly ($p < 0.05$ and $p < 0.0001$, respectively) reduced with PEG-BR compared to vehicle treatments. These indicate that PEG-BR enhances fatty acid uptake and lipid utilization for hepatic β-oxidation increasing plasma BOHB and inhibits *de novo* lipogenesis, improving fatty liver.

We have previously shown that mice with a hepatocyte-specific deletion of PPARα ($Ppara^{HepKO}$) had worsened hepatic steatosis on a HFD that also caused significantly higher plasma triglycerides and ApoB100 levels (Stec et al., 2019). PEG-BR did not change in plasma total ApoB100 levels (**Figure 5A**). However, PEG-BR significantly reduced the ApoB100 containing very-low-density lipoproteins (VLDL) but not ApoB100 containing low-density lipoproteins (LDL) particles (**Figures 5B,C**). We had shown in the $Ppara^{HepKO}$ on HFD that had higher ApoB100 in plasma than floxed control, and that this was also correlated with reduced hepatic microsomal triglyceride transfer protein (*Mttp*) expression (Stec et al., 2019). ApoB100 and the *Mttp* are essential for excretion of the VLDL molecule from the liver (Chen et al., 2008). Here, we found that PEG-BR induced *Mttp* expression but not *ApoB* (**Figure 5D**). The serum ApoB-VLDL, triglycerides, and VLDL cholesterol were significantly ($p < 0.05$) lower in the PEG-BR compared to vehicle treated animals (**Figures 6A,B**). The triglyceride distribution panel for VLTG, IDTG, LDTG, and HDTG showed no sigificant differences, and this was also observed for the VLDL, LDL, and HDL triglyceride subfractions (**Supplementary Figure S1**). There was no change in total cholesterol, HDL cholesterol, or LDL cholesterol levels (**Figures 6C–E**). This was also observed in the cholesterol and free cholesterol distribution and HDL, LDL, and VLDL cholesterol subfractions (**Supplementary Figures S2, S3**). Also, lipoproteins ApoA1 and ApoA2 that remove cholesterol from peripheral tissues had no difference between the treated groups (**Figures 7A,B**). This was also observed in the ApoA1 and ApoA2 distribution profiles (**Supplementary Figure S4**). Overall, treatment of PEG-BR in obese mice improved the hepatic steatosis potentially by utilizing fat for β-oxidation, increasing fatty acid uptake, reducing plasma ApoB-VLDL and triglycerides (**Figure 8**).

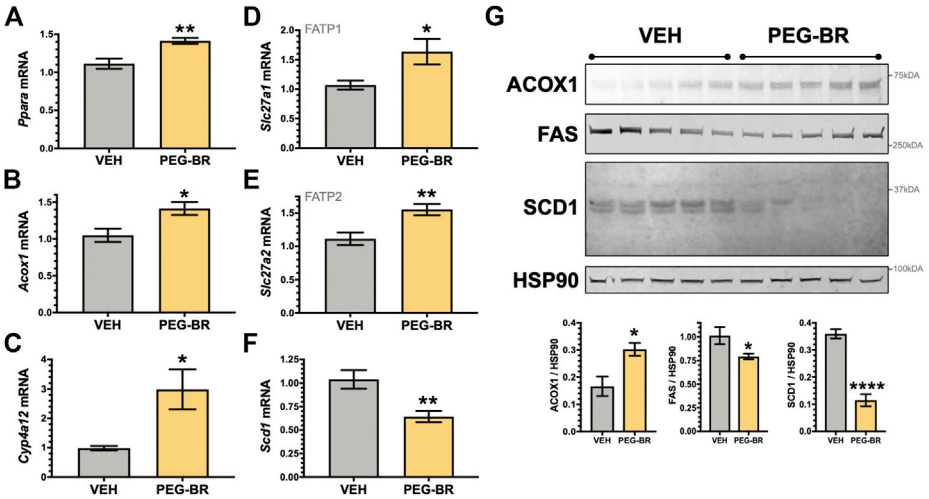

FIGURE 4 | Hepatic PPARα and target gene expression in bilirubin nanoparticle and vehicle treated obese mice. Real-time PCR expression of hepatic PPARα (*Ppara*) **(A)** and target genes, acyl-Coenzyme A oxidase 1 (*Acox1*) **(B)**; cytochrome P450, family 4, subfamily a, polypeptide 12a (*Cyp4a12*) **(C)**; FATP1, solute carrier family 27 member 1 (*Slc27a1*) **(D)**; and, FATP2, solute carrier family 27 member 2 (*Slc27a2*) **(E)**; stearoyl-Coenzyme A desaturase 1 (*Scd1*) **(F)** in vehicle and pegylated bilirubin treated mice. * = $p < 0.05$ vs. VEH; ** = $p < 0.001$ vs. VEH. (VEH, $n = 5$ and PEG-BR, $n = 6$). **(G)** Immunoblotting of acyl-Coenzyme A oxidase 1 (ACOX1), fatty acid synthase (FAS), stearoyl-Coenzyme A desaturase 1 (SCD1), and heat shock protein 90 (HSP90) in vehicle and pegylated bilirubin treated mice. * = $p < 0.05$; ****=<0.0001 vs. VEH; (VEH, $n = 5$ and PEG-BR, $n = 5$).

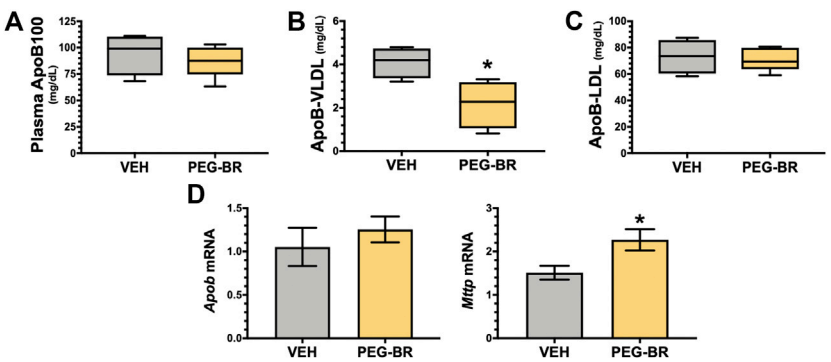

FIGURE 5 | Apolipoprotein B levels in bilirubin nanoparticle and vehicle treated obese mice. Plasma apolipoprotein B levels in vehicle and pegylated bilirubin treated mice **(A)**. Plasma apolipoprotein B-Very-low-density lipoprotein (ApoB-VLDL) **(B)**. Plasma apolipoprotein B-low-density lipoprotein (ApoB-LDL) **(C)**; * = $p < 0.05$ vs. VEH; (VEH, $n = 4$ and PEG-BR, $n = 5$). **(D)** Real time PCR of hepatic apolipoprotein B (*Apob*) and Microsomal Triglyceride Transfer Protein (Mttp) mRNA in vehicle and pegylated bilirubin treated mice. * = $p < 0.05$; **=<0.01 vs. VEH; (VEH, $n = 5$ and PEG-BR, $n = 6$).

DISCUSSION

The novel finding in our studies is that PEG-BR (bilirubin nanoparticles) improved NAFLD, which is potentially due to fat-burning mechanisms, as demonstrated by reduced hepatic triglyceride content, changes in gene expression in line with increased fat utilization and β-oxidation, and increased plasma levels of BHOB. Based on our current data and previous studies clearly demonstrating the induction of PPARα by bilirubin and bilirubin nanoparticles, it is likely that the effects on hepatic steatosis are at least in part mediated via PPARα regulated mechanisms. These are the first findings that PEG-BR increases plasma concentrations of BHOB. We have previously shown that bilirubin binds directly to PPARα (Gordon et al., 2016; Stec et al., 2016; Gordon et al., 2019), which is a known regulator of fatty acid β-oxidation (Hirai et al., 2007; Huang et al., 2012; Stec et al., 2019) that supplies the substrates for BOHB production (Kersten et al., 1999; Grabacka et al., 2016). Patients with NAFLD have lower plasma levels of BHOB (Mey et al., 2020), which is likely due to the activation of lipogenic pathways such as FAS or *Scd1* that transcribes the stearoyl-CoA desaturase-1 (SCD1) enzyme that forms fatty acids and lipid synthesis (Sampath et al., 2007; Flowers and Ntambi, 2009). A deficiency in SCD1 in mice protects against weight gain and adiposity (Ntambi et al., 2002). Activation of these pathways induces *de novo* lipogenesis for the synthesis of fat, causing the accumulation of lipids shutting down the β-oxidation fat burning mechanisms.

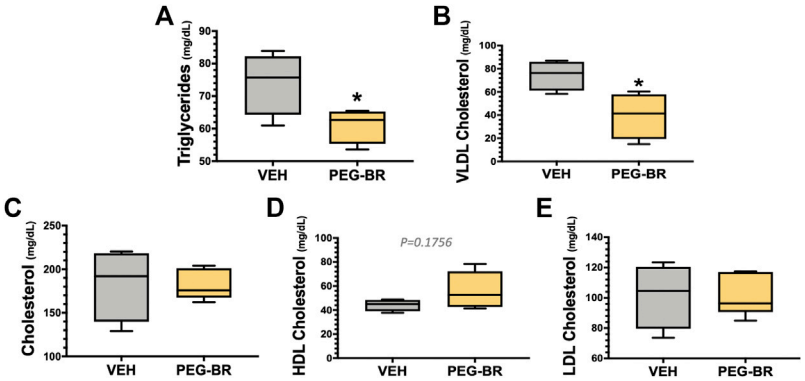

FIGURE 6 | Plasma triglyceride and cholesterol levels in bilirubin nanoparticle and vehicle treated obese mice. Plasma triglycerides **(A)**, very-low-density lipoprotein (VLDL) cholesterol **(B)**, total cholesterol **(C)**, high-density lipoprotein (HDL) cholesterol **(D)**, low-density lipoprotein (LDL) cholesterol **(E)** in vehicle and pegylated bilirubin treated mice. * = $p < 0.05$ vs. VEH; (VEH, $n = 4$ and PEG-BR, $n = 5$).

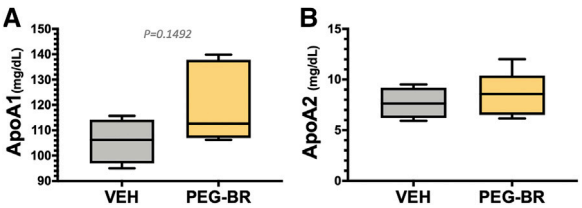

FIGURE 7 | Apolipoprotein A levels in bilirubin nanoparticle and vehicle treated obese mice. Plasma apolipoprotein A1 (ApoA1) **(A)** and apolipoprotein A2 (ApoA2) **(B)** levels in vehicle and pegylated bilirubin treated mice. (VEH, $n = 4$ and PEG-BR, $n = 5$).

We had previously shown that mice with the Gilbert's mutation UGT1A1*28 and hyperbilirubinemia were resistant to high-fat diet-induced hepatic steatosis by inhibiting *de novo* lipogenesis and activation of β-oxidation (Hinds et al., 2017). We have also shown that exercise elevated plasma bilirubin by suppressing hepatic UGT1A1 and increasing biliverdin reductase-A (BVRA) (Hinds et al., 2020), the enzyme that generates bilirubin (Adeosun et al., 2018; O'Brien et al., 2015), which improved hepatic glycogen storage and PPARα target genes (Hinds et al., 2020). Here, we found that PEG-BR reduced SCD1 and FAS while activating PPARα and ACOX1, improving hepatic steatosis in obese mice. We have also previously demonstrated that mice with a hepatocyte-specific loss of BVRA had worsened hepatic steatosis on a HFD compared to floxed control due to lower hepatic bilirubin levels (Hinds et al., 2016). We found that these mice had higher hepatic *de novo* lipogenesis and reduced β-oxidation via lessor bilirubin-PPARα activity. Later, a similar observation was made using murine hepatocyte cell culture with CRISPR/Cas9 deletion of BVRA (Gordon et al., 2019). Mildly elevated plasma bilirubin in obese patients may improve fatty liver and related adverse metabolic parameters such as high cholesterol or triglycerides. In line with a study by Wallner *et al.* that found humans with hyperbilirubinemia due to Gilbert syndrome have reduced serum cholesterol and triglycerides, we also showed that PEG-BR reduced VLDL cholesterol but not triglycerides (Wallner et al., 2013).

Weight gain and obesity are associated with increased plasma ApoB100 and triglyceride levels partly due to an greater in hepatic VLDL release (Chen et al., 2008; Fabbrini et al., 2016; Vine et al., 2017). PEG-BR treatment in the obese mice reduced plasma triglycerides and VLDL cholesterol, but no effect on total cholesterol levels or HDL and LDL was observed. However, the total cholesterol was slightly lower and HDL higher. The PEG-BR had a similar impact on ApoA-1 and ApoA-2 plasma levels with no changes, but a trend to increase ApoA-1 was observed. We previously showed that mice with a hepatocyte-specific deletion of PPARα ($Ppara^{HepKO}$) on a HFD had no changes in serum cholesterol, HDL, LDL, or ApoA proteins (Stec et al., 2019). However, the $Ppara^{HepKO}$ mice on a HFD did have higher plasma triglycerides and ApoB100 levels compared to floxed animals (Stec et al., 2019). The PEG-BR activation of PPARα in obese mice reduced ApoB100 containing VLDL particles in serum, but no effect was observed on *Apob* mRNA expression in the liver. We showed that PPARα in the liver had no impact on *Apob* expression as the hepatic loss in the $Ppara^{HepKO}$ mice on normal chow diet (NFD) or HFD showed no differences (Stec et al., 2019). The hepatic microsomal triglyceride transfer protein (*Mttp*) assists ApoB100 for excretion of the VLDL molecule from the liver (Chen et al., 2008). PEG-BR treated animals had higher *Mttp* levels compared to control. We also found that Mttp levels were low in $Ppara^{HepKO}$ mice, suggesting that Mttp is regulated via PPARα (Stec et al., 2019).

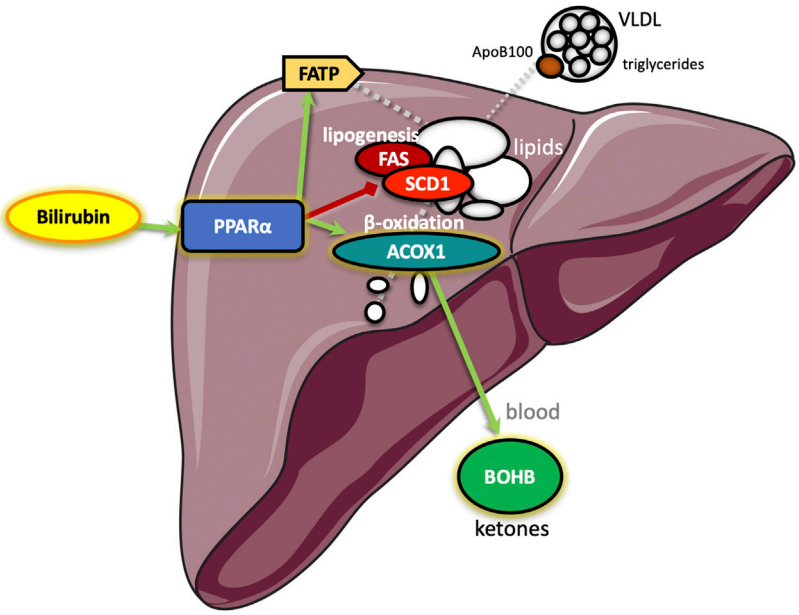

FIGURE 8 | Schematic diagram of the proposed pathway by which bilirubin reduces hepatic steatosis. Bilirubin serves as a ligand to the peroxisome proliferator-activated receptor-alpha (PPARα), which increases transcription of genes for β-oxidation of fatty acids (acyl-Coenzyme A oxidase 1, ACOX1) resulting in metabolites that elevate hepatic production of the ketone β-hydroxybutyrate (BOHB), which is secreted to blood increasing levels. Bilirubin activated PPARα also stimulates hepatic fatty acid transport protein (FATP) that imports lipids to reduce blood levels and inhibits stearoyl-Coenzyme A desaturase 1 (SCD1) and fatty acid synthase (FAS) to inhibit *de novo* lipogenesis. Together, the bilirubin-PPARα controlled pathways decrease the hepatic secretion of apolipoprotein B100 (ApoB100) containing very-low-density lipoproteins (VLDL) that increase blood triglyceride levels.

Previous studies have shown a negative correlation between serum total bilirubin levels and blood triglyceride levels (Zhong et al., 2017; Petelin et al., 2020). Interestingly, in obese patients with low serum total bilirubin and higher triglycerides than lean control with bariatric surgery increased plasma bilirubin by two-fold and reduced triglycerides by 50% (Bawahab et al., 2017), illustrating the potential role of bilirubin in triglyceride metabolism. However, these are yet to be tested. Ligands for PPARα effectively reduce plasma triglyceride levels (Srivastava et al., 2006), and plasma ApoB100 containing VLDL (Linden et al., 2002). The bilirubin nanoparticles may be a useful therapy for patients with hypertriglyceridemia. Part of the action of the PEG-BR may be in the reduction of SCD1, which is important for *de novo* production of saturated fatty acids that are contained in ApoB100 VLDL particles (Miyazaki et al., 2000; Flowers and Ntambi, 2009). ApoB100 is a critical component of the VLDL particle that is essential for excretion from the liver (Chen et al., 2008), which carries mostly triglycerides and some cholesterol out of the liver to the blood. The PEG-BR decreased *de novo* lipogenesis and increased fat-burning β-oxidation, the latter which provides metabolites for ketone production and secretion of BOHB (Newman and Verdin, 2014b). These findings show a possible role of the bilirubin-PPARα interaction in ketosis, but this has yet to be determined. We have previously used the obesity-induced model with PEG-BR treatments and observed effects on whole-body metabolism (lower plasma glucose and percent fat mass), which could be interrelated to the effects observed in the liver (Gordon et al., 2016).

There is an intriguing accord for BOHB, PPARα, and bilirubin, as they seem to have a metabolic axis that works in concert to control hepatic fat accumulation. The finding that bilirubin may induce the PPARα pathway and increase BHOB production to control hepatic steatosis needs validated by clinical studies. Also, the bilirubin nanoparticles should be used in PPARα knockout mice, preferably tissue-specific KOs, to further validate their mechanisms. Bilirubin is a well-known and highly studied molecule that has been known for centuries as a toxic bile substance, as observed in cases with extremely elevated plasma bilirubin, especially in its unconjugated form, such as that seen with Crigler-Najjar syndrome. Our investigation here posits that bilirubin and the PEG-BR nanoparticle may improve metabolic action and liver function, primarily by reducing liver fat accumulation and NAFLD. We have previously shown that PEG-BR reduced white adipocyte size in obese mice by stimulating PPARα transcriptional activity via regulating its' coregulator protein interaction (Gordon et al., 2016). Others have shown that the bilirubin nanoparticles protect against hepatic ischemia-reperfusion injury (Kim et al., 2017a), inflammatory lung disease (Kim D. E. et al., 2017), colitis and gut microbiome (Lee et al., 2019), and pancreatic islet xenotransplantation (Kim M. J. et al., 2017). There is promise in bilirubin nanoparticles as a therapeutic, and bilirubin is protective of the cardiovascular system (Hinds and Stec, 2018; Hinds and Stec, 2019) by improving blood pressure (Vera et al., 2009) and renal blood flow (Vera and Stec, 2010). Total bilirubin serum levels were negatively associated with cerebral atherosclerosis, and higher levels had less incidence of extracranial arterial stenosis (ECAS) and intracranial arterial stenosis (ICAS) (Kim et al., 2017b). The protective action of bilirubin may be related to its ability to lower plasma triglycerides, increase fat utilization, promote liver

function, and enhance the production of ketones. More studies are required to fully understand the use of bilirubin and bilirubin nanoparticles as a therapeutic for NAFLD and metabolic and cardiovascular disorders.

DATA AVAILABILITY STATEMENT

The raw data supporting the conclusions of this article will be made available by the authors, without undue reservation.

ETHICS STATEMENT

The animal study was reviewed and approved by Institutional Animal Care and Use Committee of the University of Mississippi Medical Center.

AUTHOR CONTRIBUTIONS

TH and DS designed and funded the experiments for the study. JC, DG, DS, and MD performed experiments and obtained the data. TH and DS wrote the manuscript. All authors edited and approved the final version of the manuscript.

FUNDING

This work was supported by the National Institutes of Health 1R01DK121797-01A1 (TH) and 1R01DK126884-01 (DS), the National Heart, Lung and Blood Institute K01HL-125445 (TH) and P01 HL05197-11 (DS), and the National Institute of General Medical Sciences P20GM104357-02 (DS). This project was partially supported by Grant Number P30GM122733 (Chemistry and DMPK Core Faculty)-funded by the National Institute of General Medical Sciences (NIGMS) a component of the National Institutes of Health (NIH) as one of its Centers of Biomedical Research Excellence (COBRE). The content is solely the responsibility of the authors and does not necessarily represent the official views of the National Institutes of Health.

ACKNOWLEDGMENTS

We would like to thank John M. Rimoldi, Rama S. Gadepalli, and the Research Institute of Pharmaceutical Sciences at the University of Mississippi (Oxford, MS) for their synthesis of pegylated bilirubin used in the studies. The authors would also like to thank the Analytical and Assay Core Laboratory in the Department of Physiology and Biophysics at the University of Mississippi Medical Center.

SUPPLEMENTARY MATERIAL

The Supplementary Material for this article can be found online at: https://www.frontiersin.org/articles/10.3389/fphar.2020.594574/full#supplementary-material.

REFERENCES

Adeosun, S. O., Moore, K. H., Lang, D. M., Nwaneri, A. C., Hinds, T. D., and Stec, D. E. (2018). A novel fluorescence-based assay for the measurement of biliverdin reductase activity. *React. Oxygen Species* 5 (13), 35–45. doi:10.20455/ros.2018.809

Bawahab, M. A., Assiri, A. S., Maksoud, W. A., Patel, A., Kadoumi, O., Zaman, G. S., et al. (2017). Effects of weight reduction after sleeve gastrectomy on metabolic variables in Saudi obese subjects in aseer province of kingdom of Saudi arabia. *Obes. Surg.* 27 (8), 2005–2014. doi:10.1007/s11695-017-2579-8

Burri, L., Thoresen, G. H., and Berge, R. K. (2010). The role of PPARα activation in liver and muscle. *PPAR Res.* 2010, 542359. doi:10.1155/2010/542359

Chen, Z., Newberry, E. P., Norris, J. Y., Xie, Y., Luo, J., Kennedy, S. M., et al. (2008). ApoB100 is required for increased VLDL-triglyceride secretion by microsomal triglyceride transfer protein in ob/ob mice. *J. Lipid Res.* 49 (9), 2013–2022. doi:10.1194/jlr.M800240-JLR200

Dong, H., Huang, H., Yun, X., Kim, D. S., Yue, Y., Wu, H., et al. (2014). Bilirubin increases insulin sensitivity in leptin-receptor deficient and diet-induced obese mice through suppression of ER stress and chronic inflammation. *Endocrinology* 155 (3), 818–828. doi:10.1210/en.2013-1667

Fabbrini, E., Tiemann Luecking, C., Love-Gregory, L., Okunade, A. L., Yoshino, M., Fraterrigo, G., et al. (2016). Physiological mechanisms of weight gain-induced steatosis in people with obesity. *Gastroenterology* 150 (1), 79–81. doi:10.1053/j.gastro.2015.09.003

Flowers, M. T., and Ntambi, J. M. (2009). Stearoyl-CoA desaturase and its relation to high-carbohydrate diets and obesity. *Biochim. Biophys. Acta* 1791 (2), 85–91. doi:10.1016/j.bbalip.2008.12.011

Gordon, D. M., Adeosun, S. O., Ngwudike, S. I., Anderson, C. D., Hall, J. E., Hinds, T. D., et al. (2019). CRISPR Cas9-mediated deletion of biliverdin reductase A (BVRA) in mouse liver cells induces oxidative stress and lipid accumulation. *Arch. Biochem. Biophys.* 672, 108072. doi:10.1016/j.abb.2019.108072

Gordon, D. M., Neifer, K. L., Hamoud, A.-R. A., Hawk, C. F., Nestor-Kalinoski, A. L., Miruzzi, S. A., et al. (2020). Bilirubin remodels murine white adipose tissue by reshaping mitochondrial activity and the coregulator profile of peroxisome proliferator-activated receptor alpha. *J. Biol. Chem.* 295, 9804–9822. doi:10.1074/jbc.RA120.013700

Gordon, D. M., Blomquist, T. M., Miruzzi, S. A., McCullumsmith, R., Stec, D. E., and Hinds, T. D. (2019). RNA-sequencing in human HepG2 hepatocytes reveals PPARα mediates transcriptome responsiveness of bilirubin. *Physiol. Genom.* 51 (6), 234–240. doi:10.1152/physiolgenomics.00028.2019

Grabacka, M., Pierzchalska, M., Dean, M., and Reiss, K. (2016). Regulation of ketone body metabolism and the role of PPARα. *Int. J. Mol. Sci.* 17 (12), 2093. doi:10.3390/ijms17122093

Hinds, T. D., Creeden, J. F., Gordon, D. M., Spegele, A. C., Britton, S. L., Koch, L. G., et al. (2020). Rats genetically selected for high aerobic exercise capacity have elevated plasma bilirubin by upregulation of hepatic biliverdin reductase-A (BVRA) and suppression of UGT1A1. *Antioxidants* 9 (9), 889. doi:10.3390/antiox9090889

Hinds, T. D., Jr., Burns, K. A., Hosick, P. A., McBeth, L., Nestor-Kalinoski, A., Drummond, H. A., et al. (2016). Biliverdin reductase A attenuates hepatic steatosis by inhibition of glycogen synthase kinase (gsk) 3β phosphorylation of serine 73 of peroxisome proliferator-activated receptor (PPAR) α. *J. Biol. Chem.* 291 (48), 25179–25191. doi:10.1074/jbc.M116.731703

Hinds, T. D., Jr., Hosick, P. A., Chen, S., Tukey, R. H., Hankins, M. W., Nestor-Kalinoski, A., et al. (2017). Mice with hyperbilirubinemia due to Gilbert's

syndrome polymorphism are resistant to hepatic steatosis by decreased serine 73 phosphorylation of PPARα. *Am. J. Physiol. Endocrinol. Metab.*, 312 (4), E244–E252. doi:10.1152/ajpendo.00396.2016

Hinds, T. D., Jr., Sodhi, K., Meadows, C., Fedorova, L., Puri, N., Kim, D. H., et al. (2014). Increased HO-1 levels ameliorate fatty liver development through a reduction of heme and recruitment of FGF21. *Obesity* 22 (3), 705–712. doi:10.1002/oby.20559

Hinds, T. D., Jr., and Stec, D. E. (2019). Bilirubin safeguards cardiorenal and metabolic diseases: a protective role in Health. *Curr. Hypertens. Rep.* 21 (11), 87. doi:10.1007/s11906-019-0994-z

Hinds, T. D., Jr., and Stec, D. E. (2018). Bilirubin, a cardiometabolic signaling molecule. *Hypertension* 72 (4), 788–795. doi:10.1161/HYPERTENSIONAHA.118.11130

Hinds, T. D., Jr., Stechschulte, L. A., Cash, H. A., Whisler, D., Banerjee, A., Yong, W., et al. (2011). Protein phosphatase 5 mediates lipid metabolism through reciprocal control of glucocorticoid receptor and peroxisome proliferator-activated receptor-γ (PPARγ). *J. Biol. Chem.* 286 (50), 42911–42922. doi:10.1074/jbc.M111.311662

Hinds, T. D., Jr., Burns, K. A., Hosick, P. A., McBeth, L., Nestor-Kalinoski, A., Drummond, H. A., et al. (2016). Biliverdin reductase A attenuates hepatic steatosis by inhibition of glycogen synthase kinase (GSK) 3beta phosphorylation of serine 73 of peroxisome proliferator-activated receptor (PPAR) alpha. *J. Biol. Chem.* 291 (48), 25179–25191. doi:10.1074/jbc.M116.731703

Hirai, T., Fukui, Y., and Motojima, K. (2007). PPARα agonists positively and negatively regulate the expression of several nutrient/drug transporters in mouse small intestine. *Biol. Pharm. Bull.* 30 (11), 2185–2190. doi:10.1248/bpb.30.2185

Hjelkrem, M., Morales, A., Williams, C. D., and Harrison, S. A. (2012). Unconjugated hyperbilirubinemia is inversely associated with non-alcoholic steatohepatitis (NASH). *Aliment. Pharmacol. Ther.* 35 (12), 1416–1423. doi:10.1111/j.1365-2036.2012.05114.x

Huang, J., Jia, Y., Fu, T., Viswakarma, N., Bai, L., Rao, M. S., et al. (2012). Sustained activation of PPARα by endogenous ligands increases hepatic fatty acid oxidation and prevents obesity in ob/ob mice. *Faseb. J.* 26 (2), 628–638. doi:10.1096/fj.11-194019

Jang, B. K. (2012). Elevated serum bilirubin levels are inversely associated with nonalcoholic fatty liver disease. *Clin. Mol. Hepatol.* 18 (4), 357–359. doi:10.3350/cmh.2012.18.4.357

John, K., Marino, J. S., Sanchez, E. R., and Hinds, T. D. (2016). The glucocorticoid receptor: cause of or cure for obesity? *Am. J. Physiol. Endocrinol. Metab.* 310 (4), E249–E257. doi:10.1152/ajpendo.00478.2015

Kersten, S., Seydoux, J., Peters, J. M., Gonzalez, F. J., Desvergne, B., and Wahli, W. (1999). Peroxisome proliferator-activated receptor alpha mediates the adaptive response to fasting. *J. Clin. Invest.* 103 (11), 1489–1498. doi:10.1172/JCI6223

Kim, D. E., Lee, Y., Kim, M., Lee, S., Jon, S., and Lee, S. H. (2017). Bilirubin nanoparticles ameliorate allergic lung inflammation in a mouse model of asthma. *Biomaterials* 140, 37–44. doi:10.1016/j.biomaterials.2017.06.014

Kim, J. Y., Lee, D. Y., Kang, S., Miao, W., Kim, H., Lee, Y., et al. (2017a). Bilirubin nanoparticle preconditioning protects against hepatic ischemia-reperfusion injury. *Biomaterials* 133, 1–10. doi:10.1016/j.biomaterials.2017.04.011

Kim, J. Y., Yoon, S. J., Woo, M. H., Kim, S. H., Kim, N. K., Kim, J., et al. (2017b). Differential impact of serum total bilirubin level on cerebral atherosclerosis and cerebral small vessel disease. *PloS One* 12 (3), e0173736. doi:10.1371/journal.pone.0173736

Kim, M. J., Lee, Y., Jon, S., and Lee, D. Y. (2017). PEGylated bilirubin nanoparticle as an anti-oxidative and anti-inflammatory demulcent in pancreatic islet xenotransplantation. *Biomaterials* 133, 242–252. doi:10.1016/j.biomaterials.2017.04.029

Kwak, M. S., Kim, D., Chung, G. E., Kang, S. J., Park, M. J., Kim, Y. J., et al. (2012). Serum bilirubin levels are inversely associated with nonalcoholic fatty liver disease. *Clin. Mol. Hepatol.* 18 (4), 383–390. doi:10.3350/cmh.2012.18.4.383

Lee, Y., Kim, H., Kang, S., Lee, J., Park, J., and Jon, S. (2016). Bilirubin nanoparticles as a nanomedicine for anti-inflammation therapy. *Angew Chem. Int. Ed. Engl.* 55 (26), 7460–7463. doi:10.1002/anie.201602525

Lee, Y., Sugihara, K., Gillilland, M. G., Jon, S., Kamada, N., and Moon, J. J. (2019). Hyaluronic acid-bilirubin nanomedicine for targeted modulation of dysregulated intestinal barrier, microbiome and immune responses in colitis. *Nat. Mater.* 19, 118–126. doi:10.1038/s41563-019-0462-9

Lega, I. C., and Lipscombe, L. L. (2020). Review: diabetes, obesity, and cancer-pathophysiology and clinical implications. *Endocr. Rev.* 41 (1), 33–52. doi:10.1210/endrev/bnz014

Lindén, D., Lindberg, K., Oscarsson, J., Claesson, C., Asp, L., Li, L., et al. (2002). Influence of peroxisome proliferator-activated receptor alpha agonists on the intracellular turnover and secretion of apolipoprotein (Apo) B-100 and ApoB-48. *J. Biol. Chem.* 277 (25), 23044–23053. doi:10.1074/jbc.M110416200

Liu, J., Dong, H., Zhang, Y., Cao, M., Song, L., Pan, Q., et al. (2015). Bilirubin increases insulin sensitivity by regulating cholesterol metabolism, adipokines and PPARγ levels. *Sci. Rep.* 5, 9886. doi:10.1038/srep09886

Marino, J. S., Stechschulte, L. A., Stec, D. E., Nestor-Kalinoski, A., Coleman, S., and Hinds, T. D. (2016). Glucocorticoid receptor beta induces hepatic steatosis by augmenting inflammation and inhibition of the peroxisome proliferator-activated receptor (PPAR) alpha. *J. Biol. Chem.* 291 (50), 25776–25788. doi:10.1074/jbc.M116.752311

Mey, J. T., Erickson, M. L., Axelrod, C. L., King, W. T., Flask, C. A., McCullough, A. J., et al. (2020). β-Hydroxybutyrate is reduced in humans with obesity-related NAFLD and displays a dose-dependent effect on skeletal muscle mitochondrial respiration *in vitro*. *Am. J. Physiol. Endocrinol. Metab.* 319 (1), E187–E195. doi:10.1152/ajpendo.00058.2020

Miyazaki, M., Kim, Y. C., Gray-Keller, M. P., Attie, A. D., and Ntambi, J. M. (2000). The biosynthesis of hepatic cholesterol esters and triglycerides is impaired in mice with a disruption of the gene for stearoyl-CoA desaturase 1. *J. Biol. Chem.* 275 (39), 30132–30138. doi:10.1074/jbc.M005488200

Newman, J. C., and Verdin, E. (2014a). β-hydroxybutyrate: much more than a metabolite. *Diabetes Res. Clin. Pract.* 106 (2), 173–181. doi:10.1016/j.diabres.2014.08.009

Newman, J. C., and Verdin, E. (2014b). Ketone bodies as signaling metabolites. *Trends Endocrinol. Metabol.* 25 (1), 42–52. doi:10.1016/j.tem.2013.09.002

Ntambi, J. M., Miyazaki, M., Stoehr, J. P., Lan, H., Kendziorski, C. M., Yandell, B. S., et al. (2002). Loss of stearoyl-CoA desaturase-1 function protects mice against adiposity. *Proc. Natl. Acad. Sci. U.S.A.* 99 (17), 11482–11486. doi:10.1073/pnas.132384699

O'Brien, L., Hosick, P. A., John, K., Stec, D. E., and Hinds, T. D. (2015). Biliverdin reductase isozymes in metabolism. *Trends Endocrinol. Metabol.* 26 (4), 212–220. doi:10.1016/j.tem.2015.02.001

Petelin, A., Jurdana, M., Pražnikar, Z. K., and Žiberna, L. (2020). Serum bilirubin correlates with serum adipokines in normal weight and overweight asymptomatic adults. *Acta Clin. Croat.* 59 (1), 19–29. doi:10.20471/acc.2020.59.01.03

Puri, K., Nobili, V., Melville, K., Corte, C. D., Sartorelli, M. R., Lopez, R., et al. (2013). Serum bilirubin level is inversely associated with nonalcoholic steatohepatitis in children. *J. Pediatr. Gastroenterol. Nutr.* 57 (1), 114–118. doi:10.1097/MPG.0b013e318291fefe

Salomone, F., Li Volti, G., Rosso, C., Grosso, G., and Bugianesi, E. (2013). Unconjugated bilirubin, a potent endogenous antioxidant, is decreased in patients with non-alcoholic steatohepatitis and advanced fibrosis. *J. Gastroenterol. Hepatol.* 28 (7), 1202–1208. doi:10.1111/jgh.12155

Sampath, H., Miyazaki, M., Dobrzyn, A., and Ntambi, J. M. (2007). Stearoyl-CoA desaturase-1 mediates the pro-lipogenic effects of dietary saturated fat. *J. Biol. Chem.* 282 (4), 2483–2493. doi:10.1074/jbc.M610158200

Srivastava, R. A., Jahagirdar, R., Azhar, S., Sharma, S., and Bisgaier, C. L. (2006). Peroxisome proliferator-activated receptor-alpha selective ligand reduces adiposity, improves insulin sensitivity and inhibits atherosclerosis in LDL receptor-deficient mice. *Mol. Cell. Biochem.* 285 (1-2), 35–50. doi:10.1007/s11010-005-9053-y

Stec, D. E., Gordon, D. M., Hipp, J. A., Hong, S., Mitchell, Z. L., Franco, N. R., et al. (2019). Loss of hepatic PPARα promotes inflammation and serum hyperlipidemia in diet-induced obesity. *Am. J. Physiol. Regul. Integr. Comp. Physiol.* 317 (5), R733–R745. doi:10.1152/ajpregu.00153.2019

Stec, D. E., Gordon, D. M., Nestor-Kalinoski, A. L., Donald, M. C., Mitchell, Z. L., Creeden, J. F., et al. (2020). Biliverdin reductase A (BVRA) knockout in adipocytes induces hypertrophy and reduces mitochondria in white fat of obese mice. *Biomolecules* 10 (3), 387. doi:10.3390/biom10030387

Stec, D. E., John, K., Trabbic, C. J., Luniwal, A., Hankins, M. W., Baum, J., et al. (2016). Bilirubin binding to PPARα inhibits lipid accumulation. *PloS One* 11 (4), e0153427. doi:10.1371/journal.pone.0153427

Takei, R., Inoue, T., Sonoda, N., Kohjima, M., Okamoto, M., Sakamoto, R., et al. (2019). Bilirubin reduces visceral obesity and insulin resistance by suppression of inflammatory cytokines. *PloS One* 14 (10), e0223302. doi:10.1371/journal.pone.0223302

Vera, T., Granger, J. P., and Stec, D. E. (2009). Inhibition of bilirubin metabolism induces moderate hyperbilirubinemia and attenuates ANG II-dependent hypertension in mice. *Am. J. Physiol. Regul. Integr. Comp. Physiol.* 297 (3), R738–R743. doi:10.1152/ajpregu.90889.2008

Vera, T., and Stec, D. E. (2010). Moderate hyperbilirubinemia improves renal hemodynamics in ANG II-dependent hypertension. *Am. J. Physiol. Regul. Integr. Comp. Physiol.* 299 (4), R1044–R1049. doi:10.1152/ajpregu.00316.2010

Vine, D. F., Wang, Y., Jetha, M. M., Ball, G. D., and Proctor, S. D. (2017). Impaired ApoB-lipoprotein and triglyceride metabolism in obese adolescents with polycystic ovary syndrome. *J. Clin. Endocrinol. Metab.* 102 (3), 970–982. doi:10.1210/jc.2016-2854

Vluggens, A., Andreoletti, P., Viswakarma, N., Jia, Y., Matsumoto, K., Kulik, W., et al. (2010). Reversal of mouse Acyl-CoA oxidase 1 (ACOX1) null phenotype by human ACOX1b isoform [corrected]. *Lab. Invest.* 90 (5), 696–708. doi:10.1038/labinvest.2010.46

Wallner, M., Marculescu, R., Doberer, D., Wolzt, M., Wagner, O., Vitek, L., et al. (2013). Protection from age-related increase in lipid biomarkers and inflammation contributes to cardiovascular protection in Gilbert's syndrome. *Clin. Sci.* 125 (5), 257–264. doi:10.1042/CS20120661

Zheng, J. D., He, Y., Yu, H. Y., Liu, Y. L., Ge, Y. X., Li, X. T., et al. (2019). Unconjugated bilirubin alleviates experimental ulcerative colitis by regulating intestinal barrier function and immune inflammation. *World J. Gastroenterol.* 25 (15), 1865–1878. doi:10.3748/wjg.v25.i15.1865

Zhong, P., Sun, D. M., Wu, D. H., Li, T. M., Liu, X. Y., and Liu, H. Y. (2017). Serum total bilirubin levels are negatively correlated with metabolic syndrome in aged Chinese women: a community-based study. *Braz. J. Med. Biol. Res.* 50 (2), e5252. doi:10.1590/1414-431X20165252

Conflict of Interest: TH and DS have submitted patents on bilirubin and obesity related disorders.

The remaining authors declare that the research was conducted in the absence of any commercial or financial relationships that could be construed as a potential conflict of interest.

frontiers in Pharmacology

ORIGINAL RESEARCH
published: 22 December 2020
doi: 10.3389/fphar.2020.585346

Adiponectin Interacts *In-Vitro* With Cementoblasts Influencing Cell Migration, Proliferation and Cementogenesis Partly Through the MAPK Signaling Pathway

Jiawen Yong, Julia von Bremen, Gisela Ruiz-Heiland and Sabine Ruf**

Department of Orthodontics, Faculty of Medicine, Justus Liebig University Giessen, Giessen, Germany

Current clinical evidences suggest that circulating Adipokines such as Adiponectin can influence the ratio of orthodontic tooth movement. We aimed to investigate the effect that Adiponectin has on cementoblasts (OCCM-30) and on the intracellular signaling molecules of Mitogen-activated protein kinase (MAPK). We demonstrated that OCCM-30 cells express AdipoR1 and AdipoR2. Alizarin Red S staining revealed that Adiponectin increases mineralized nodule formation and quantitative AP activity in a dose-dependent manner. Adiponectin up-regulates the mRNA levels of *AP*, *BSP*, *OCN*, *OPG*, *Runx-2* as well as *F-Spondin*. Adiponectin also increases the migration and proliferation of OCCM-30 cells. Moreover, Adiponectin induces a transient activation of JNK, P38, ERK1/2 and promotes the phosphorylation of STAT1 and STAT3. The activation of Adiponectin-mediated migration and proliferation was attenuated after pharmacological inhibition of P38, ERK1/2 and JNK in different degrees, whereas mineralization was facilitated by MAPK inhibition in varying degrees. Based on our results, Adiponectin favorably affect OCCM-30 cell migration, proliferation as well as cementogenesis. One of the underlying mechanisms is the activation of MAPK signaling pathway.

Keywords: adiponectin, cementoblasts, migration, proliferation, cementogenesis, MAPK

OPEN ACCESS

Edited by:
David E. Stec, University of Mississippi Medical Center, United States

Reviewed by:
Takashi Muramatsu, Tokyo Dental College, Japan
Higinio Arzate, National Autonomous University of Mexico, Mexico

****Correspondence:***
Jiawen Yong
Jiawen.Yong@dentist.med.uni-giessen.de

Specialty section:
This article was submitted to Experimental Pharmacology and Drug Discovery, a section of the journal Frontiers in Pharmacology

Received: *20 July 2020*
Accepted: *23 November 2020*
Published: *22 December 2020*

Citation:
Yong J, von Bremen J, Ruiz-Heiland G and Ruf S (2020) Adiponectin Interacts In-Vitro With Cementoblasts Influencing Cell Migration, Proliferation and Cementogenesis Partly Through the MAPK Signaling Pathway. Front. Pharmacol. 11:585346. doi: 10.3389/fphar.2020.585346

INTRODUCTION

The periodontium consists of the gingiva, periodontal ligament, root cementum and alveolar bone (Park et al., 2017). Cementum, a heterogeneous mineralized layer covering the entire root dentin surface, anchors fibrous connective tissues on tooth-root surfaces (Caverzasio and Manen, 2007). As a special mineralized tissue, cementum has a similar composition to bone, consisting of approximately 61% mineralized as well as 27% organic matrix and 12% water (Nanci and Bosshardt, 2006).

Cementoblasts are highly differentiated mesenchymal cells of the periodontal ligament (PDL) with the capacity to build up cementum (Arzate et al., 2015). The cementum matrix is composed of collagenous proteins and non-collagenous proteins such as Bone Sialoprotein (BSP), Osteopontin (OPN), Osteocalcin (OCN), Osteoprotegerin (OPG), Fibronectin, Osteonectin and several growth factors (Saygin et al., 2000).

It has been demonstrated that Adipocytokines, which are mainly secreted by adipose tissue, can influence bone metabolism (Funahashi et al., 1999). Adiponectin, which is produced by adipocytes but also by salivary gland epithelial cells, has been shown to modulate metabolic and immune functions of salivary gland epithelial cell (Katsiougiannis et al., 2006).

Two Adiponectin receptor (AdipoRs) subtypes (Adiponectin receptor 1 and 2 (AdipoR1 and AdipoR2)), expressed on various tissues and cells such as human gingival fibroblasts and PDL cells (Yamauchi et al., 2003a) mediate the biological effects of Adiponectin. Yamaguchi et al. (2012) showed that the AdipoRs were ubiquitously expressed in the oral tissues of mice such as gingiva, tongue, buccal mucosa and labial mucosa, as well as in RAW24 cells (Yamauchi et al., 2012). Both AdipoRs exert similar effects but have individual signaling preferences. Whereas phosphorylation of Extracellular Regulated Kinase 1/2 (ERK1/2) may depend on both receptors, AdipoR1 is more prominent in AMP-activated protein kinase (AMPK) phosphorylation, and AdipoR2 is involved in PPAR-α activation in muscle cells (Buechler et al., 2010). AdipoR1 and AdipoR2 have been identified in the plasma membrane (Yamauchi et al., 2003b) as well as in the cytoplasm (cytoplasmic puncta) (Ding et al., 2009).

In-vivo, Adiponectin secretion is regulated by the degree of obesity (Carbone et al., 2012). Its secretion is inversely proportional to the amount of adipose tissue (Swarbrick and Havel, 2008; Benedix et al., 2011; de Carvalho et al., 2017). It has been shown that patients with type 2 diabetes and obesity have lower serum Adiponectin levels than normal weight individuals (Cao et al., 2015). Furthermore, clinical studies have analyzed the relationship between the body mass index (BMI) and salivary Adiponectin levels (Mamali et al., 2012; Nigro et al., 2015) and found a trend toward slightly higher expression of salivary Adiponectin in obese patients than in controls, however they could not show a statistic significance between groups, whereas they previously reported that Adiponectin serum levels are reduced in obese patients compared to healthy controls. Also, patients with severe periodontitis had lower Adiponectin- and AdipoRs-levels than healthy subjects (Saito et al., 2008; Yamaguchi et al., 2010).

Recent studies revealed that local submucosal injection of Adiponectin prevented experimental orthodontic tooth movement in rats (Haugen et al., 2017). The data suggested that Adiponectin is involved in the homeostasis of periodontal tissues and thus might influence orthodontic treatment.

It has been demonstrated that Adiponectin and its receptors are also expressed in bone marrow-derived osteoblasts and adipocytes (Seo et al., 2004), suggesting that Adiponectin may play a role in bone metabolism (Chen et al., 2013). Considering the multifunctional role of Adiponectin, it seems possible that it may have functional characteristics in cementoblasts similar to that in other mineralized tissue-forming cells such as osteoblasts (Seo et al., 2004).

Since fat mass may impact peripheral bone formation, it may be one of the critical factors for orthodontic tooth movement rate and orthodontically-induced tooth root resorption. Adipocyte-derived hormones such as Adiponectin may contribute to this relationship. To date, the physiological effect of Adiponectin on cementoblasts has not been elucidated. The decreased levels of Adiponectin, as found in obese individuals, might be a critical pathomechanistic link. Therefore, the present study was undertaken to investigate the effect of Adiponectin on OCCM-30 cells *in vitro*.

MATERIALS AND METHODS

Cell Culture and Reagents

The OCCM-30 cementoblast cell line was kindly provided by Prof. M. Somerman (NIH, NIDCR, Bethesda, MA) and cultured as previously described (D'Errico et al., 2000). Briefly, cells were maintained in α-MEM (11095-080, Gibco) containing 10% Fetal Bovine Serum (FBS) (10270-106, Gibco) and 1% Penicillin/Streptomycin (15140-122, Gibco) and incubated in a humidified atmosphere of 5% CO_2 at 37°C. The cells were seeded into 6-well plates (657160, Greiner Bio-one) at a density of 3×10^4 cells/well until confluence. The cells used were between passages 3 and 7. To induce cementogenesis, the cell culture medium was supplemented with 10 mM β-Glycerophosphate (#35675, Calbiochem) and 50 μg/ml Ascorbic Acid (6288.1, Roth).

Cells were stimulated using different concentrations of mouse Adiponectin/Acrp30/ADIPOQ protein (His Tag) from Sino Biological Inc. (Cat. No: 50636-M08H). Purity > 95% (Determined by SDS-PAGE). Endotoxin < 1.0 EU/μg (Determined by the LAL method). Protein construction: The DNA sequence encoding mouse ADIPOQ (NP_033735.3) (Met 1-Asn 247) was expressed with a C-terminal polyhistidine tag. Expression Host: HEK 293 cells. Formulation: Lyophilized from sterile PBS, pH 7.4, 5% Trehalose, 5% Mannitol, 0.01% Tween-80. The protein was reconstituted following manufacturer indications to a stock solution of 0.25 mg/ml in sterile water and stored at −20°C. The MAPK inhibitor for P38 (SB203580) (#tlrl-sb20, InvivoGen), the ERK1/2 inhibitor (FR180204) (#328007, Calbiochem) and the JNK inhibitor (SP600125) (#tlrl-sp60, InvivoGen) were used.

Quantitative Real-Time Reverse Transcriptase-Polymerase Chain Reaction

Cells were kept overnight in starvation medium (α-MEM (11095-080, Gibco) containing 0.5% FBS (10270-106, Gibco) and 1% Penicillin/Streptomycin (15140-122, Gibco)). Further, 100 ng/ml Adiponectin (50636-M08H, Sino Biological Inc.) were added for indicated time periods: 0, 45 min, 1.5 and 3 h. Then, total RNA was isolated using the NucleoSpin® RNA Kit (740955.50, MACHEREY-NAGEL). RNA concentrations were measured at 260 nm using a spectrophotometer (Nanodrop2000, Thermo Scientific). cDNA was synthesized from 1.0 μg of total RNA using the InnuSCRIPT Reverse Transcriptase kit (845-RT-6000100, Analytik Jena) and performed on CFX96™ System Cycler (Bio-Rad).

The SsoAdvanced™ Universal SYBR® Green Supermix (1723271, Bio-Rad) was used in each reaction setup. The primers employed were: Mouse AdipoR1&2 (qMmuCID0023619, qMmuCID0010157), AP (qMmuCED0003797), BSP (qMmuCID0006396), OCN (qMmuCED0041364), OPG (qMmuCID0005205), Runx-2 (qMmuCID0005205) and F-Spondin (qMmuCED0049433) all from Bio-Rad. GAPDH (qMmuCED0027497, Bio-Rad) was used as housekeeping gene. Results were analyzed using the Bio-Rad CFX Manager 3.1 software.

Protein Extraction and Western Blot Analysis

RIPA buffer (89901, Thermo Scientific) supplied with 3% protease inhibitor (78442, Thermo Scientific) was used for protein extraction. Protein concentrations were measured using Pierce™ BCA Protein Assay Kit (23225, Thermo Scientific) on direct reading Spectrophotometer (DR/2000, HACH). Further, 20 µg protein samples were separated using 10% SDS-PAGE gel by electrophoresis and transferred to a nitrocellulose membrane (1704271, Bio-Rad). The membranes were blocked with 5% non-fat milk (T145.1, ROTH) for 1 h and incubated with the primary antibodies for Adiponectin Receptor 1 (ab70362, Abcam); Adiponectin Receptor 2 (ab77612, Abcam); ERK1/2 (MBS8241746, BIOZOL); phospho-ERK1/2 (44-680G, Thermo-Fisher); P54/P46 JNK (#9252, Cell Signaling Technology), phospho-JNK (07-175, Thermo-Fisher); P38 MAPK (#9212, Cell Signaling Technology); phospho-P38 MAPK Alpha (#4511, Cell Signaling Technology), STAT1 (AHP2527, Bio-Rad); phospho-STAT1 Tyr701 (05-1064, Thermo-Fisher); phospho-STAT1 S727 (ab109461, Abcam); STAT3 (PA1-86605, Thermo-Fisher); phospho-STAT3 S727 (OPA1-03007, Thermo-Fisher), and β-actin (ab8227, Abcam) at a concentration of 1:1,000. The secondary antibodies employed were: Polyclonal Goat Anti-Rabbit (P0448, Dako); Rabbit Anti-Goat (P0160, Dako) and Polyclonal Goat Anti-Mouse (P0447, Dako) at a concentration of 1:2000. The band signals were detected with X-ray Amersham Hyperfilm (28906836, GE Healthcare) utilizing Amersham ECL Western Blotting Detection Reagents (9838243, GE Healthcare) and visualized using OPTIMAX X-Ray Film Processor (11701-9806-3716, PROTEC GmbH).

Immunofluorescence Staining

OCCM-30 cells were cultured overnight on sterile Falcon™ Chambered Cell Culture Slides (354108, Fisher Scientific) and further fixed with 4% paraformaldehyde (30525-89-4, Sigma-Aldrich) for 10 min at room temperature. Cells were permeabilized with 0.5% Triton™ X-100 Surfact-Amps™ Detergent Solution (28313, Thermo-Fisher) for 20 min. Then, cells were incubated in blocking buffer containing 10% goat serum, 0.3 M glycine, 1% BSA (071M8410, Sigma) and 0.1% Tween-20 (P1379, Sigma-Aldrich) for 30 min at room temperature and further incubated with primary antibodies AdipoR1 (ab70362, Abcam) (dilution 1:250) or AdipoR2 (ab77612, Abcam) (dilution 1:250) at 4°C overnight. The secondary antibodies DyLight 488 polyclonal goat anti-rabbit (ab96899, Abcam) (dilution 1:500) or donkey anti-goat Alexa Fluor 647 (ab150131, Abcam) (dilution 1:500) conjugated to fluorescein isothiocyanate were used. After washing with 1× phosphate-buffered saline (PBS) (10010023, Thermo-Fisher), samples were mounted using a fluorescent Mounting Medium with DAPI (ab104139, Abcam). Staining was analyzed using a high-resolution fluorescence microscope (Leica Microsystems, Wetzlar, Germany) and photographed.

Cell Migration Assay

OCCM-30 cells were plated at a density of 8×10^3 cells/well in 6-well plates (657160, Greiner Bio-one), in α-MEM (11095-080, Gibco) containing 10% FBS (10270-106, Gibco) and 1% Penicillin/Streptomycin (15140-122, Gibco) and cultured until confluence. Cells were preincubated for 12 h in starvation medium and wounded by scratching using a 100 µL tip. Through this, a cell-free area was created in the center of the cell layer. Afterwards, all non-adherent cells were washed with 1× PBS (10010023, Thermo-Fisher). The wounded cell monolayers were incubated in the presence and absence of different concentration of Adiponectin (50636-M08H, Sino Biological Inc.) for 24 h. Wounded-area images were taken immediately after wounding and 24 h after scratching. The wounded cell layers were photographed at ×10 magnification (Leica Microsystems, Wetzlar, Germany) and the percentages of wound closure area between cell layer borders were analyzed and calculated over time using the Image J software (National Institutes of Health and University of Wisconsin, United States).

For the MAPK inhibition experiment, OCCM-30 cells were pretreated with the P38 inhibitor SB203580 (InvivoGen), the ERK1/2 inhibitor FR180204 (Calbiochem) or the JNK inhibitor SP600125 (InvivoGen) at a concentration of 1.0 µg/mL as well as with DimethyIsulfoxide (DMSO) (D8418-50ML, Sigma-Aldrich) at 0.1% (v/v) (Control group) for 1 h before Adiponectin addition. Afterward, the pretreated OCCM-30 cells were wounded and cultivated in the presence or absence of 1.0 µg/ml Adiponectin (50636-M08H, Sino Biological Inc.).

Cell Proliferation Assay

Cell viability and proliferation was examined using 3-(4,5-dimethylthiazol-2-yl)-5-(3-carboxymethoxyphenyl)-2-(4-sulfophenyl)-2H-tetrazolium (MTS) assay (CellTiter 96® Aqueous One Solution Cell Proliferation Assay, Promega) according to manufacturer's instructions. Briefly, OCCM-30 cells at a passage three to five were seeded at a density of 5×10^3 cells/well in a 96-well plate (655180, Greiner Bio-one). Cells were cultured in α-MEM containing 5% FBS overnight to allow adherence. Then, cells were washed twice with 1× PBS (10010023, Thermo-Fisher) and treated with various concentrations of Adiponectin (50636-M08H, Sino Biological Inc.) in α-MEM containing 0.5% FBS over a period of 24 h. To assess involvement of the MAP kinase cascade in Adiponectin-induced proliferation, cells were pretreated 1 h with the inhibitors: SB203580 (InvivoGen), FR180204 (Calbiochem) and SP600125 (InvivoGen) at a concentration of 1.0 µg/mL as well as with DMSO (D8418-50ML, Sigma-Aldrich) at 0.1% (v/v), respectively. Thereafter, 20 µL of the MTS reagent was added into each well and the

cells were incubated during 2 h at 37°C in a 5% CO_2 atmosphere. Plates were read by 490 nm using a 96-well micro-plate reader (BioTek, Winooski, VT, United States) to measure the amount of formazan by cellular reduction of MTS.

Alizarin Red S Staining

OCCM-30 cells at passages five to seven were seeded to 6-well plates (657160, Greiner Bio-one) at a density of 3×10^4 cells/well using α-MEM (11095-080, Gibco) containing 10% FBS (10270-106, Gibco) and 1% Penicillin/Streptomycin (15140-122, Gibco). Upon confluence, the culture medium was supplemented with 50 μg/ml Ascorbic Acid and 10 mM β-Glycerophosphate disodium salt hydrate with different concentrations of Adiponectin (50636-M08H, Sino Biological Inc.). Mineralization of extracellular matrix was determined on days 7 and 14 by Alizarin Red S staining. Briefly, mineralized monolayer cell cultures were washed with 1× PBS (10010023, Thermo-Fisher) three times and stained using 1% Alizarin Red S solution (A5533, Sigma-Aldrich) during 5 min at room temperature after being fixed with 70% Ethanol (64-17-5, Sigma-Aldrich) for 1 h at 4°C. Mineralized nodule formation was assessed by inverted phase contrast microscopy (Leica Microsystems, Wetzlar, Germany) using the LASV4.8 software (Leica).

To quantify the degree of calcium accumulation in the mineralized extracellular matrix, Alizarin Red S stained cultures were dissolved using 100 mM Cetylpyridinium chloride (6004-24-6, Sigma-Aldrich) for 1 h to release calcium-bound dye into the solution. The absorbance of the released dye was measured at 570 nm using a spectrophotometer (xMarkTM, Microplate Absorbance Spectrophotometer, 1681150 BioRad).

To measure the effect of MAP kinase in Adiponectin-induced cementogenesis, cells were incubated with the inhibitors: SB203580 (InvivoGen), FR180204 (Calbiochem) and SP600125 (InvivoGen) at a concentration of 1.0 μg/mL as well as with DMSO (D8418-50 ML, Sigma-Aldrich) at 0.1% (v/v) for 7 and 14 days, respectively.

Alkaline Phosphatase Enzymatic Activity Assay

After cementogenesis induction during 14 days, OCCM-30 cells were lysed in distilled deionized water and sonicated for 15 s (SONIFIER 150, BRANSON, G. HEIHEMANA). The lysate was incubated at 37°C for 30 min with p-Nitrophenyl phosphate (p-NPP; Alkaline phosphatase Substrate, Sigma) in an alkaline phosphatase buffer solution (1.5 mM). The reaction was stopped by adding NaOH, and absorbance was read at 405 nm (xMarkTM, Microplate Absorbance Spectrophotometer, 1681150 BioRad).

Statistical Analysis

Statistical analyses were performed using GraphPad Prism 6.0 software (GraphPad software). All values are expressed as means ± standard deviation (SD) and analyzed using one-way *t*-test for unpaired samples to determine the statistically significant differences between groups. Differences were considered statistically significant at a p value of < 0.05. Data distribution was analyzed using the Kolmogorov-Smirnov and the Shapiro-Wilk test and visually using QQ plots. All experiments were repeated successfully at least three times.

RESULTS

Cementoblasts Express Adiponectin Receptor 1 and 2

First, we aimed to verify if OCCM-30 cementoblasts express Adiponectin receptors. By Western blot analysis, we could establish that AdipoR1 as well as AdipoR2 are expressed on this cell line (**Figure 1A**). The mRNA expression of Adiponectin receptors was also demonstrated by RT-PCR analysis (**Figure 1B**). Immunofluorescence staining show that AdipoR1 are mostly expressed in the cytoplasm, cytomembrane and nucleus, while AdipoR2 are expressed around the nucleus (**Figure 1C**).

Adiponectin Promotes In-Vitro Cementoblast Mineralization

Second, we analyzed the possible effect that exogenous Adiponectin exerts during cementogenesis. Alizarin Red S staining was used to visualize and quantify the biological effect of Adiponectin on OCCM-30 cell mineralization. This method revealed that Adiponectin significantly increased mineralized nodule formation in a dose-dependent manner over a period of 14 days (**Figure 2A**). Colorimetric analysis revealed that Adiponectin-stimulated OCCM-30 cells had higher levels of mineralized matrix production in comparison to unstimulated cells ($p < 0.01$) (**Figures 2B,C**).

The analysis of the Alkaline Phosphatase enzymatic activity (AP) over a period of 48 h of cells stimulated with different concentrations of Adiponectin, showed increased AP activity time and dose-dependently, reaching statistical significance ($p < 0.01$) after 24 h in the group stimulated with 80 ng/ml Adiponectin (**Figure 2D**).

Cells cultivated for a period of 7 days in a mineralization-inducing medium, were afterwards stimulated over a period of 3 h with Adiponectin (100 ng/ml). The kinetic analysis of the relative mRNA expression of *AP*, *Runx-2*, *BSP*, *OPG*, *OCN* and *F-Spondin* increased notably, reaching statistical significance after 45 min of stimulation with Adiponectin (100 ng/ml) in comparison to timepoint 0 min. These stimulatory effects were sustained over the entire period of 3 h ($p < 0.05$) (**Figure 2E**).

Elevated Levels of Adiponectin Facilitate Cell Migration and Proliferation

Next, we analyze the effect that Adiponectin exerts on cell proliferation and migration. Cells were grown to 100% confluency and then were scratched using a 100 μL pipet tip. Immediately thereafter, cells were stimulated with different concentrations of Adiponectin (0, 0.1, 0.5, 1, and 2 μg/ml)

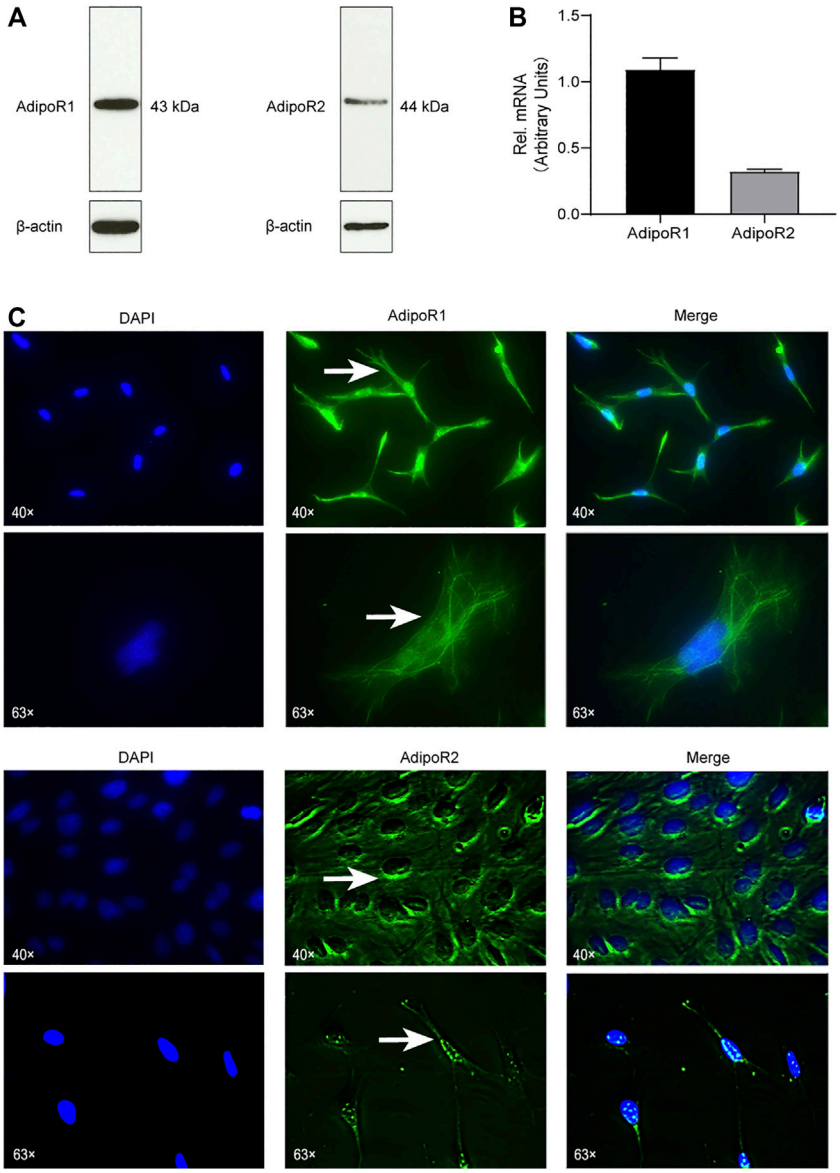

FIGURE 1 | Cementoblasts express Adiponectin receptors. **(A)** The expression of Adiponectin receptors (AdipoR1 and AdipoR2) in OCCM-30 mouse cementoblasts was examined by WB. β-actin is shown as internal control protein. **(B)** RT-PCR analysis show the mRNA expression of AdipoR1 and AdipoR2. Values are expressed as means ± SD. **(C)** Adiponectin receptors in OCCM-30 cells were visualized by immunofluorescence staining (Green color). DAPI staining was used for nuclei detection. Arrows show cellular receptor localization. AdipoR1 are located in the cytoplasm, cytomembrane and nucleus, while AdipoR2 are distributed mostly around the nucleus.

during 24 h. The cell migration ability was visualized and measured using microscopic photography (**Figure 3A**). The analysis of the recovered data indicates that Adiponectin at concentrations of 1 and 2 μg/ml significantly promotes wound closure (24.35 ± 2.38 and 30.3 ± 2.68%, respectively) (**Figure 3B**). Furthermore, we observed that cells stimulated with Adiponectin over a period of 24 h have increased mitogenic activity. The groups stimulated with 0.4, 0.8 and 1.6 μg/ml adipokine showed a significantly increased proliferation rate ($p < 0.05$) in comparison to unstimulated cells (**Figure 3C**).

Adiponectin Promotes P38, ERK1/2 and JNK Phosphorylation in OCCM-30 Cells

In order to elucidate if Adiponectin can activate the MAPK pathway, we performed a kinetic analysis of P38, ERK1/2 and JNK protein phosphorylation (**Figure 4A**).

Western blots revealed that P38 phosphorylation occurs 5 min after Adiponectin (20 ng/ml) stimulation. The phosphorylated-state of P38 was sustained over a period of 4 h, reaching a peak at time point 10 min ($p < 0.001$). The phosphorylation of ERK1/2 as well as P54/P46 JNK reached a peak after 5 min Adiponectin

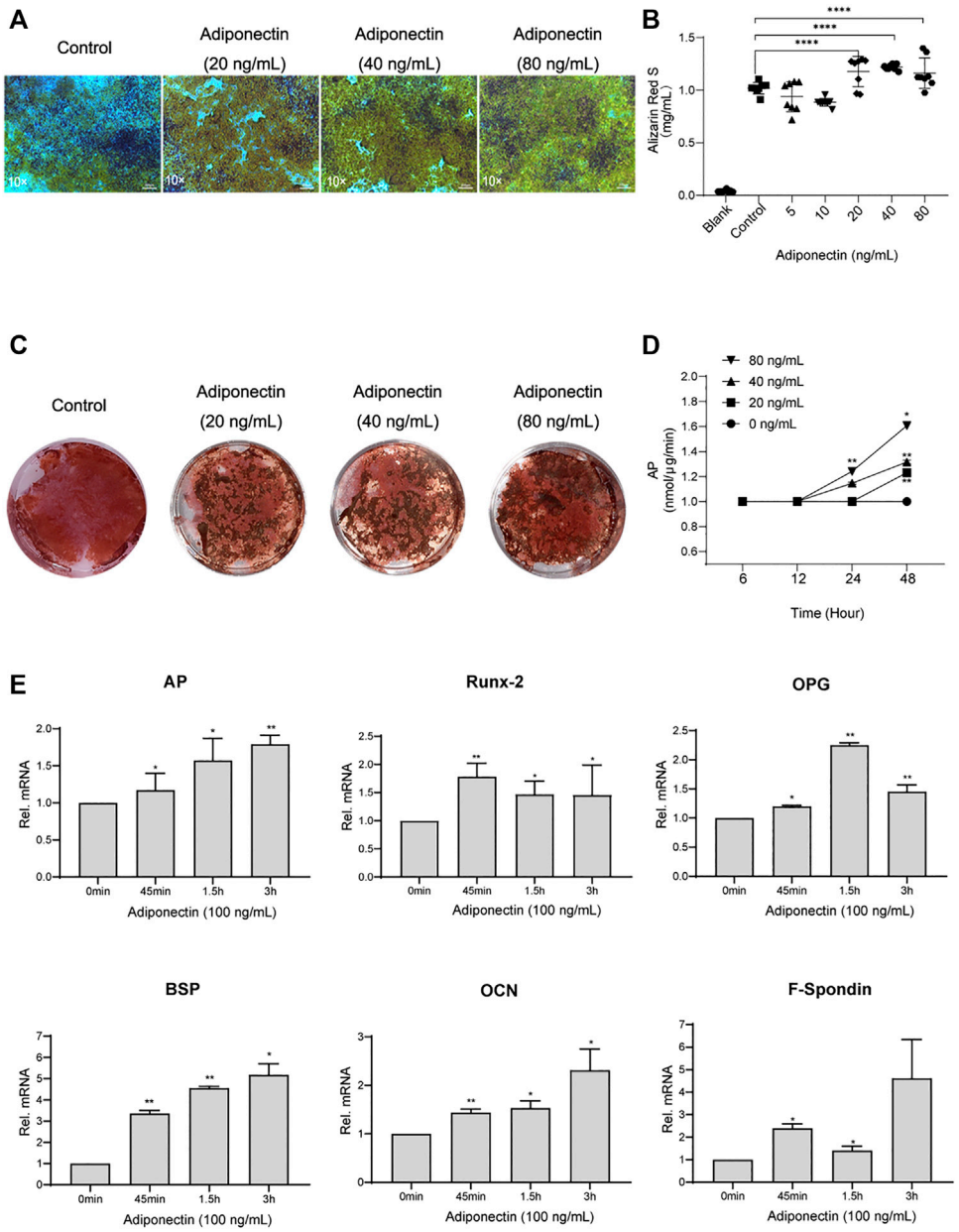

FIGURE 2 | Adiponectin promotes cementogenesis *in vitro*. **(A)** Microscopic view of OCCM-30 cells after 14 days of stimulation with different concentrations of Adiponectin (Staining: Alizarin Red S). **(B,C)** Cells were cultivated with 0 (Control), 20, 40, and 80 ng/ml Adiponectin during 14 days. Mineralization grade was visualized and quantified using Alizarin Red S staining and by further dilution with Cetylpiridiumchlorid. Results are expressed as mg/ml Alizarin Red S (Mean ± SD of three independent results). **(D)** Adiponectin added to OCCM-30 cells increases the Alkaline Phosphatase (AP) enzymatic activity dose-dependently, reaching statistical significance after 24 h in comparison to the untreated group (Data are normalized to 1, $*p < 0.05$; $**p < 0.01$). **(E)** Kinetic analysis of relative mRNA expression of Alkaline Phosphatase (*AP*), Bone Sialoprotein (*BSP*), Osteoprotegerin (*OPG*), Osteocalcin (*OCN*), *Runx-2* and *F-Spondin* on cementoblasts after Adiponectin (100 ng/ml) stimulation. Data are normalized to 1. GAPDH was used as housekeeping Gene. Values are expressed as means ± SD: Ns (not significant); $*p < 0.05$; $**p < 0.01$; $***p < 0.001$ and $****p < 0.0001$.

addition, being the WB's bands detectable during 30 min in both cases (**Figure 4B**). The WB analysis revealed that cementoblasts express STAT1 and STAT3 being these proteins target of Adiponectin stimulation. The phosphorylation of STAT1 and STAT3 occurred likewise after 5 min and was detectable over a period of 30 min (**Figures 4C,D**).

Blockade of MAPK Attenuates Adiponectin-Induced Cementoblast Migration and Proliferation

To evaluate whether activation of P38, ERK1/2 or JNK are essential for Adiponectin-stimulated cell migration and

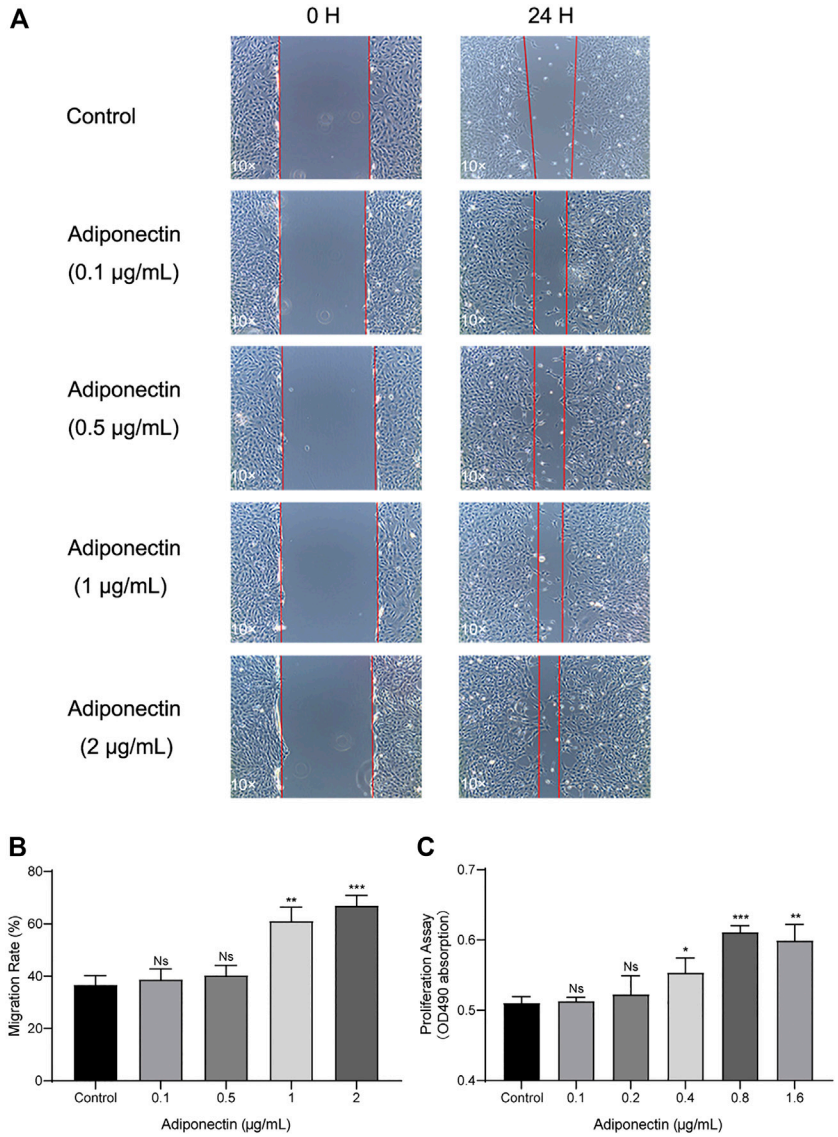

FIGURE 3 | Increased migration and proliferation rates of OCCM-30 cells treated with Adiponectin. **(A,B)** Images show the migration effect that different concentrations of Adiponectin exert on OCCM-30 cells wounded monolayers at 0 and 24 h after standard scratching using a 100 µL pipet tip. The red lines indicate the wound edge at the beginning and at the end of the experiment. The migration rates were measured over a period of 24 h by ImageJ software. Data are presented as percentage of wound recovery. **(C)** The MTS assay showed that Adiponectin-treated cells during 24 h have an increased proliferation rate in comparison to untreated cells. This effect occurred dose-dependently, reaching statistical significance at a concentration of 0.4, 0.8, and 1.6 µg/ml Adiponectin. Values are expressed as means ± SD: ns (not significant); *$p < 0.05$; **$p < 0.01$; ***$p < 0.001$.

proliferation, OCCM-30 cementoblasts were preincubated with the pharmacological inhibitors: SB203580 (InvivoGen), FR180204 (Calbiochem) and SP600125 (InvivoGen) as well as with DimethyIsulfoxide (Sigma-Aldrich) (Control group) for 1 h and afterwards stimulated with Adiponectin.

The MTS assay indicated that MAPK blockade reduced the cell proliferation in unstimulated and stimulated cells. However, this effect was partially counteracted by Adiponectin (100 ng/ml) (**Figures 5A,B**).

As shown in the pictures, the scratched areas were measured after 24 h, which is represented by a front-end yellow edge line (**Figure 5C**). The migratory capacity of OCCM-30 cells treated with MAPK inhibitors was examined in the presence or absence of Adiponectin (100 ng/ml). As results, the migration rate of cells was significantly attenuated after ERK1/2 as well as JNK blockade despite Adiponectin (100 ng/ml) co-stimulation, whereas this effect was not observed in the group pretreated with the P38 inhibitor (**Figure 5C**).

Inhibition of MAP Kinases Alter Adiponectin-Induced Cementogenesis

The colorimetric analysis performed after dilution of Alizarin Red S staining for a period of 7 days mineralization induction, did not show significant differences among groups despite Adiponectin treatment (**Figures 6A,B**). Cells treated with P38 and ERK1/2 inhibitors during

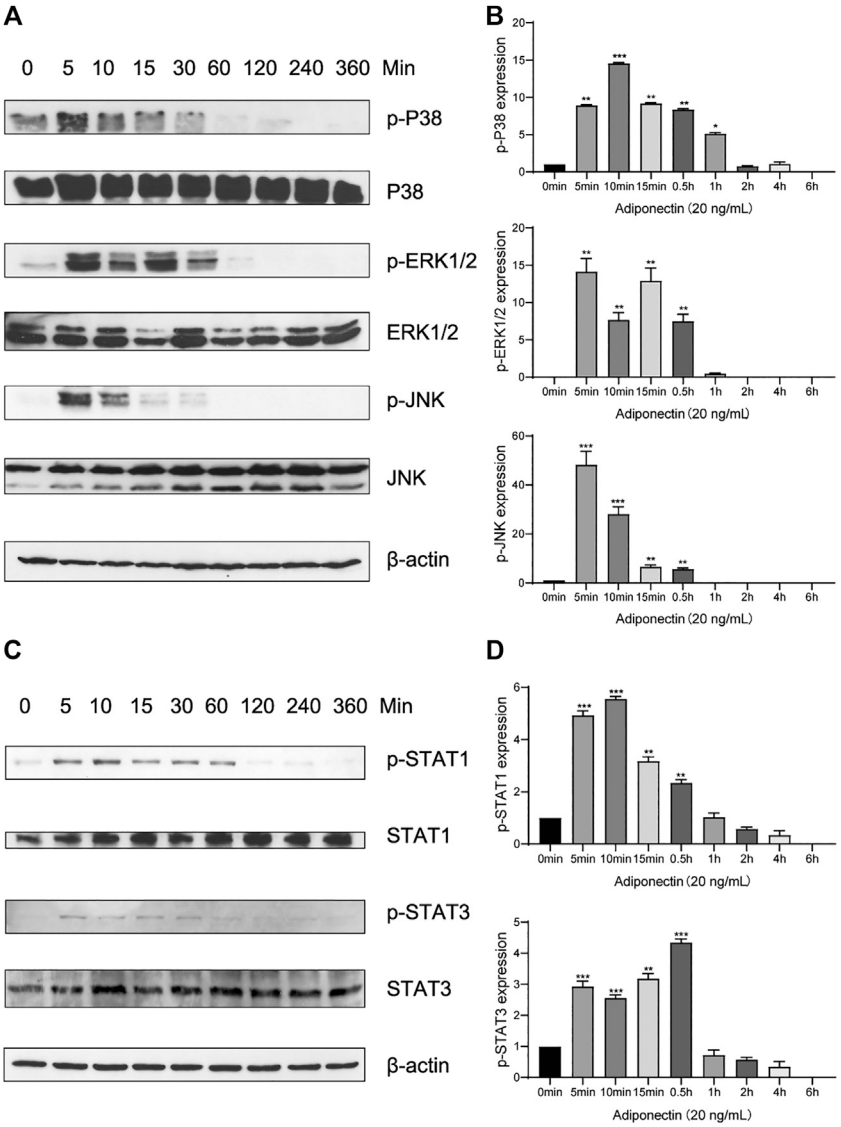

FIGURE 4 | Adiponectin promotes JNK, ERK1/2 and P38 phosphorylation on OCCM-30 cells. **(A,B)** The expression of JNK (46 and 54 kDa), ERK1/2 (42 and 44 kDa) and P38 (42 kDa) expression as well as their phosphorylated forms after Adiponectin (20 ng/ml) stimulation were analyzed by Western Blots. β-actin served as a loading control. Graphics show the relative expression of p-JNK, p-ERK1/2 and p-P38 compared to cells at time point 0 min. **(C,D)** Adiponectin (20 ng/ml) promotes STAT1 (98 KDa) and STAT3 (85 KDa) phosphorylation during a period of 30 min. Graphics show the relative expression of p-STAT1 and p-STAT3 compared to cells at time point 0 min. Values are expressed as means ± SD: Ns (not significant), $*p < 0.05$; $**p < 0.01$; $***p < 0.001$.

14 days in the absence of Adiponectin (100 ng/ml) microscopically exhibited increased mineralization. In the presence of Adiponectin (100 ng/ml), such effect was slightly but significantly decreased (**Figures 6A,B**). On the contrary, the sustained blockade of JNK did not alter mineralized matrix production on OCCM-30 cells despite Adiponectin addition.

DISCUSSION

In the present *in vitro* study, we demonstrated that OCCM-30 cementoblasts express Adiponectin receptor 1 and 2 and that its activation facilitates cell migration, proliferation and mineralization. These effects are partially orchestrated via activation of the MAPK signaling pathway.

Clinical studies have shown that the normal salivary Adiponectin levels are around 10.92 (3.22–28.71) ng/ml and the normal serum levels are around 12.27 (8.15–14.70) μg/ml (Mamali et al., 2012). These values drastically decrease in case of obesity (Carbone et al., 2012). Reduced levels of Adiponectin as well as AdipoRs are also present in patients with severe periodontitis, a fact that suggests impaired Adiponectin function to be associated with disease severity (Saito et al., 2008; Yamaguchi et al., 2010). In our experiment, we focused

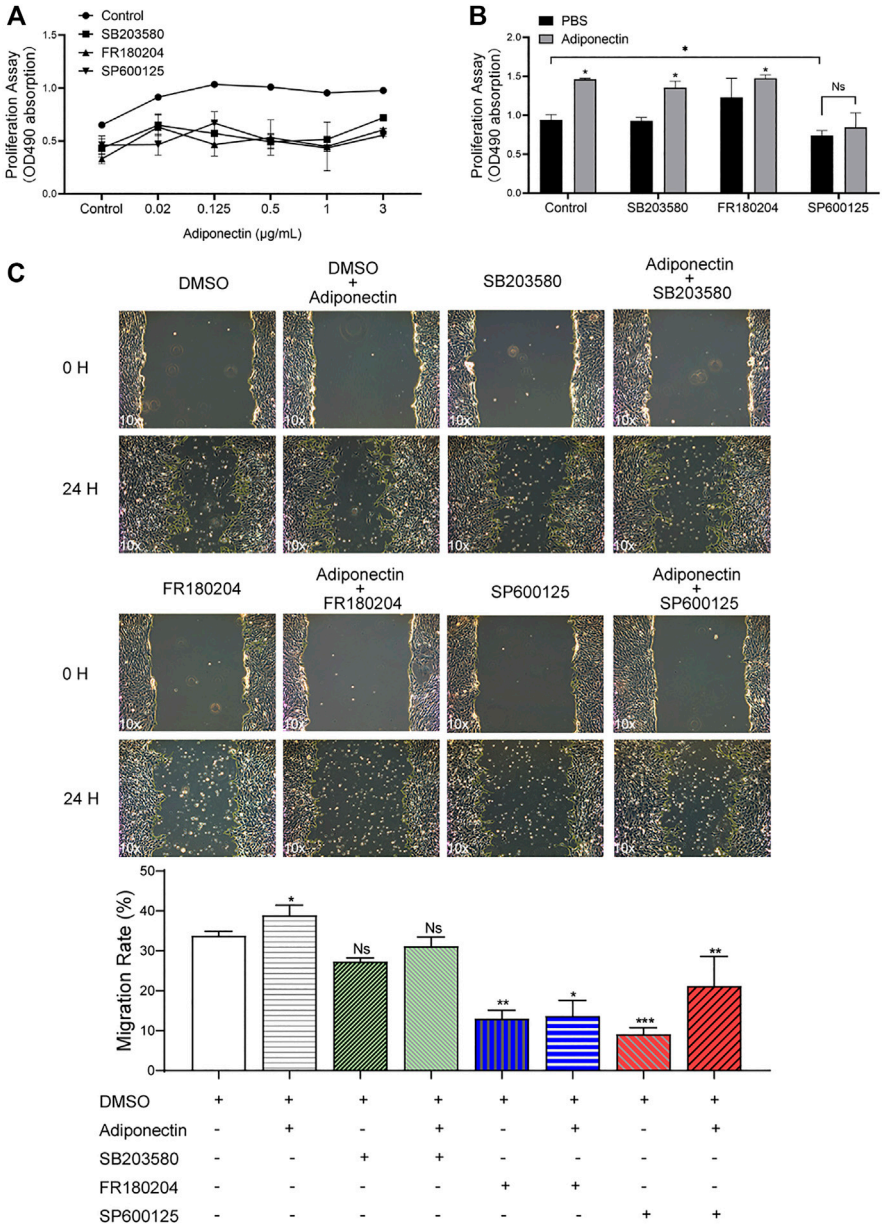

FIGURE 5 | The MAP kinase pathway is involved in Adiponectin-induced migration and proliferation of OCCM-30 cementoblasts. **(A,B)** Cells were treated with the MAP kinase inhibitors: SB203580 (InvivoGen), FR180204 (Calbiochem) and SP600125 (InvivoGen) for 1 h and afterwards stimulated with Adiponectin during 24 h. As result, MAP kinase inhibition impairs cell proliferation (MTS assay). This effect was rescued after Adiponectin (100 ng/ml) stimulation. **(C)** Images of cell migration were captured prior to stimulation (0 h) and after 24 h. The recovered areas were calculated by ImageJ software comparing the scratched areas. Blockade of ERK1/2 (FR180204) and JNK (SP600125) over a period of 24 h significantly decreases cell migration whereas P38 inhibition did not significantly influence the migration rate. Values are expressed as means ± SD of three independent results: Ns (not significant), $*p < 0.05$; $**p < 0.01$; $***p < 0.001$.

on the Adiponectin effects resembling normal salivary levels (20 ng/ml) and higher Adiponectin concentrations exert *in vitro* on OCCM-30 cementoblasts.

Previous reports have shown the favorable effects Adiponectin exerts *in vitro* on the proliferation of human osteoblasts via the MAPK signaling pathway (Luo et al., 2005). In the present study, we observed over a period of 24 h, that the number of viable cementoblasts was significantly increased in presence of higher concentration of Adiponectin compared to unstimulated cells. Similar results were also obtained by Berner et al. (2004) showing that a supplementation of cell culture medium with recombinant Adiponectin enhances the proliferation of murine osteoblasts (Berner et al., 2004). In contrast to the study performed by Kanazawa et al. (2007) reporting that even low concentrations of Adiponectin stimulate the proliferation of the MC3T3-E1 osteoblast cell line (Kanazawa et al., 2007), we observed that

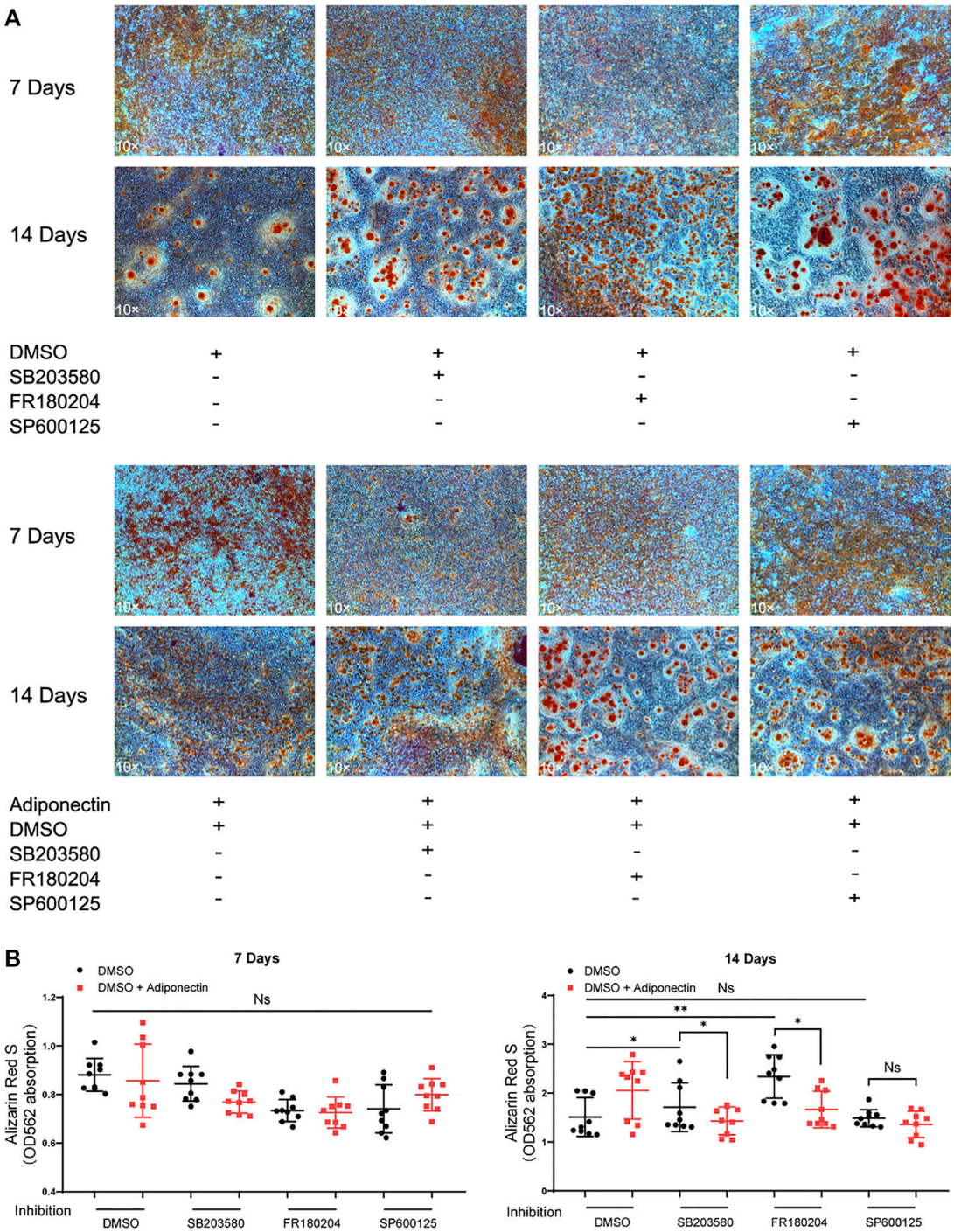

FIGURE 6 | Inhibition of MAP kinases alter Adiponectin-induced cementogenesis. **(A)** Cells were treated with MAP kinase inhibitors in the presence or absence of Adiponectin (100 ng/ml) for 7 and 14 days, respectively. **(B)** Graphic shows the absorbance (OD_{562}) of Alizarin Red S dilution after induction of mineralization for 7 and 14 days. Mineralization grade does not differ significantly among the groups after 7 days induction. However, after 14 days induction, the sustained blockade of P38 (SB203580) and ERK1/2 (FR180204) facilitate mineralized nodule formation, effect that was partially counteracted by Adiponectin. This effect was not observed in the groups cultivated with the JNK inhibitor (SP600125) in the presence or absence of Adiponectin. Values are expressed as means ± SD: Ns (not significant), $^{*}p < 0.05$; $^{**}p < 0.01$; $^{***}p < 0.001$.

lower concentrations of Adiponectin did not significantly stimulate cementoblast proliferation.

In our experiment we demonstrated that the expression of *Runx-2*, an essential transcription factor for osteoblast differentiation, mineralization and migration (Bosshardt, 2005; Liu and Lee, 2013) as well as for cementogenesis (Hakki et al., 2018) was strongly up-regulated in OCCM-30 cells in response to high concentrations of Adiponectin. Adiponectin-induced *Runx-2* upregulation in cementoblasts may be interpreted in the circumstances of wound healing and cementum repair and regeneration, because the regulatory role that *Runx-2* exerts in cementum formation (Kimura et al., 2018). *F-Spondin*, a cementoblast specific gene that orchestrate cementoblast differentiation (Kitagawa et al., 2012), was also up-regulated by Adiponectin. Likewise, the OCCM-30 cells presented up-regulated mRNA expression of *AP*, *BSP*, *OCN* and *OPG* after adipokine stimulation.

Alkaline phosphatase (*AP*) is essential for osteoblast (Koh et al., 1997) and cementoblasts (Hakki et al., 2018) function and is up-regulated during mineralization, thus, it is generally considered as an early marker for osteoblasts as well as for cementoblasts (Carvalho et al., 2012). It is well known that *AP* regulates the formation of cementum and is involved more in the formation of acellular than cellular cementum (Saygin et al., 2000). Here we could observe that Adiponectin strongly increases mRNA *AP* as well as AP enzymatic activity in cementoblasts.

Osteocalcin (OCN) is a non-collagenous protein that plays a regulatory role during the mineralization process (Tokiyasu et al., 2000; Thomson et al., 2003). Its expression is restricted to cells with mineralizing capacity, including osteoblasts, odontoblasts as well as cementoblasts (McKee and Nanci, 1996; Saygin et al., 2000). In our results, the up-regulation of *OCN* after Adiponectin stimulation clearly indicates that this adipokine favorably induces cementogenesis. Our *in vitro* results are consistent with previous data supporting the fact that Adiponectin can enhance the osteogenic differentiation of osteoblasts (Lee et al., 2009) as well as promote osteoblastogenesis of HPDL cells (Iwayama et al., 2012).

We could observe that Adiponectin strongly promotes mineralization in OCCM-30 cells. In concordance with these results, Wang et al. (2017) demonstrated the osteogenic capacity of Adiponectin *in vitro* using rat mesenchymal stem cells (Wang et al., 2017). Another study showed that Adiponectin enhanced the mRNA expression of *AP* and the mineralization of osteoblasts (Oshima et al., 2006). Iwayama et al. (2012) also observed that Adiponectin promotes *AP* and *Runx-2* mRNA expression as well as up-regulate the AP enzymatic activity of HPDL cells (Iwayama et al., 2012). However, in the latter study, extremely high concentrations (5–10 μg/ml) of Adiponectin were used to observe these effects (Iwayama et al., 2012). In our experiment, we used ranges of Adiponectin concentrations of among 100 ng/ml, demonstrating that murine cementoblasts require lower concentrations of this adipokine to achieve the same results. However, these concentrations still exceed the biologic concentrations of Adiponectin in saliva or in crevicular fluids (Mamali et al., 2012). In the presence of biological concentrations of Adiponectin, we could observe a moderate but not statistically significant increase of *AP*, *BSP*, *OCN* and *OPG* (Data not shown).

Our results indicate that in OCCM-30 cells, Adiponectin signals act through activation of ERK1/2, JNK as well as P38. Moreover, our present results show that activation of MAPK pathway is essential for Adiponectin-stimulated OCCM-30 proliferation and migration as these effects were partially counteracted when SB203580, FR180204 and SP600125, three highly selective inhibitors of the MAP kinase cascade, were applied. On the contrary, we observe that the sustained inhibition of P38 and ERK1/2 significantly enhances the mineralization rate of cementoblasts, effect that was partially counteracted by Adiponectin addition. These results accord with previous studies showing that long-term inhibition of the MAPK signaling pathway promotes early mineralization as well as the increase of AP activity in preosteoblastic cells (Higuchi et al., 2002).

Several *in vitro* studies have shown that Adiponectin plays a role as regulator of the MAP kinase pathways in cell homeostasis (Luo et al., 2005; Miyazaki et al., 2005; Junker et al., 2017). (Miyazaki et al., 2005) shown that Adiponectin activates the P38 and JNK pathways in myocytes (Miyazaki et al., 2005). In osteoarthritis, Adiponectin induces P38-MAPK to promote osteophyte formation (Junker et al., 2017). Interesting, Luo et al. (2005) showed that Adiponectin can activate P38 and JNK but not ERK1/2 on primary osteoblasts and that suppression of AdipoR1 abolished Adiponectin induced cell proliferation, suggesting that cell proliferation is regulated by AdipoR/JNK signaling whereas differentiation is mediated via the AdipoR/P38 cascade (Luo et al., 2005).

In a previous study, we have shown that blockade of ERK1/2 impairs leptin-induced Caspase 3 and Caspase 9 expression on OCCM-30 cells (Ruiz-Heiland et al., 2020). (Kadowaki et al., 2006) observed that Adiponectin induces osteogenesis via P38 through AdipoR1, but not AdipoR2 on C3H10/T2 cells up-regulating the expression of *Runx-2* (Kadowaki et al., 2006). However, the relation between Adiponectin and P38 stimulation may generate different outputs depending on the cell type (Kadowaki et al., 2006). For example, in calcifying vascular smooth muscle cells, the Adiponectin-P38 interactions impair osteoblastic differentiation (Luo et al., 2009). The blockade of P38 caused significant down-regulated AP activity, mineralization, and osteogenic markers such as *BSP* in odontoblast-like cells (Tang and Saito, 2018). Activity of ERKs regulates the transcription of Runx-2 during the extracellular matrices induced osteoblastogenesis of mouse pre-osteoblast cell (Xiao et al., 2002). Likewise, activation of ERKs enhances AP expression in murine osteoblastic cells (Takeuchi et al., 1997). Suzuki et al., (1999) reported that the ERK pathway promotes proliferation in osteoblastic cells, whereas the P38 MAPK pathway regulates AP activity (Suzuki et al., 1999).

CONCLUSION

Our findings show that Adiponectin influences *in vitro* the migration, proliferation and cementogenesis of OCCM-30 cells partly through the MAPK signaling pathway.

DATA AVAILABILITY STATEMENT

The raw data supporting the conclusions of this article will be made available by the authors, without undue reservation, to any qualified researcher.

AUTHOR CONTRIBUTIONS

JY acquired and analyzed the data. JY, GR-H, and JB interpreted the data and wrote the manuscript. JY, GR-H, SR conceived, designed, and supervised the study.

ACKNOWLEDGMENTS

We sincerely thank J. Deschner and M. Nokhbehsaim, Department of Periodontology, University of Bonn, Germany to facilitate the sending of OCCM-30 cells. We also thank to the China Scholarship Council (CSC) for Ph.D. financial support.

REFERENCES

Arzate, H., Zeichner-David, M., and Mercado-Celis, G. (2015). Cementum proteins: role in cementogenesis, biomineralization, periodontium formation and regeneration. *Periodontol. 2000* 67 (1), 211–233. doi:10.1111/prd.12062

Benedix, F., Westphal, S., Patschke, R., Granowski, D., Luley, C., Lippert, H., et al. (2011). Weight loss and changes in salivary ghrelin and adiponectin: comparison between sleeve gastrectomy and Roux-en-Y gastric bypass and gastric banding. *Obes. Surg* 21 (5), 616–624. doi:10.1007/s11695-011-0374-5

Berner, H. S., Lyngstadaas, S. P., Spahr, A., Monjo, M., Thommesen, L., Drevon, C. A., et al. (2004). Adiponectin and its receptors are expressed in bone-forming cells. *Bone* 35 (4), 842–849. doi:10.1016/j.bone.2004.06.008

Bosshardt, D. D. (2005). Are cementoblasts a subpopulation of osteoblasts or a unique phenotype? *J. Dent. Res* 84 (5), 390–406. doi:10.1177/154405910508400501

Buechler, C., Wanninger, J., and Neumeier, M. (2010). Adiponectin receptor binding proteins–recent advances in elucidating adiponectin signalling pathways. *FEBS Lett* 584 (20), 4280–4286. doi:10.1016/j.febslet.2010.09.035

Cao, Z., Li, J., Luo, L., Li, X., Liu, M., Gao, M., et al. (2015). Molecular cloning and expression analysis of adiponectin and its receptors (AdipoR1 and AdipoR2) in the hypothalamus of the Huoyan goose during different stages of the egg-laying cycle. *Reprod. Biol. Endocrinol* 13, 87. doi:10.1186/s12958-015-0085-1

Carbone, F., La Rocca, C., and Matarese, G. (2012). Immunological functions of leptin and adiponectin. *Biochimie* 94 (10), 2082–2088. doi:10.1016/j.biochi.2012.05.018

Carvalho, S. M., Oliveira, A. A., Jardim, C. A., Melo, C. B., Gomes, D. A., de Fátima Leite, M., et al. (2012). Characterization and induction of cementoblast cell proliferation by bioactive glass nanoparticles. *J. Tissue Eng. Regen. Med* 6 (10), 813–821. doi:10.1002/term.488

Caverzasio, J., and Manen, D. (2007). Essential role of Wnt3a-mediated activation of mitogen-activated protein kinase p38 for the stimulation of alkaline phosphatase activity and matrix mineralization in C3H10T1/2 mesenchymal cells. *Endocrinology* 148 (11), 5323–5330. doi:10.1210/en.2007-0520

Chen, X., Lu, J., Bao, J., Guo, J., Shi, J., and Wang, Y. (2013). Adiponectin: a biomarker for rheumatoid arthritis? *Cytokine Growth Factor Rev* 24 (1), 83–89. doi:10.1016/j.cytogfr.2012.07.004

D'Errico, J. A., Berry, J. E., Ouyang, H., Strayhorn, C. L., Windle, J. J., and Somerman, M. J. (2000). Employing a transgenic animal model to obtain cementoblasts *in vitro*. *J. Periodontol* 71 (1), 63–72. doi:10.1902/jop.2000.71.1.63

de Carvalho, P. M., Gavião, M. B., and Carpenter, G. H. (2017). Altered autophagy and sympathetic innervation in salivary glands from high-fat diet mice. *Arch. Oral Biol* 75, 107–113. doi:10.1016/j.archoralbio.2016.10.033

Ding, Q., Wang, Z., and Chen, Y. (2009). Endocytosis of adiponectin receptor 1 through a clathrin- and Rab5-dependent pathway. *Cell Res* 19 (3), 317–327. doi:10.1038/cr.2008.299

Funahashi, T., Nakamura, T., Shimomura, I., Maeda, K., Kuriyama, H., Takahashi, M., et al. (1999). Role of adipocytokines on the pathogenesis of atherosclerosis in visceral obesity. *Intern. Med* 38 (2), 202–206. doi:10.2169/internalmedicine.38.202

Hakki, S. S., Bozkurt, S. B., Türkay, E., Dard, M., Purali, N., and Götz, W. (2018). Recombinant amelogenin regulates the bioactivity of mouse cementoblasts *in vitro*. *Int. J. Oral Sci* 10 (2), 15. doi:10.1038/s41368-018-0010-5

Haugen, S., Aasarød, K. M., Stunes, A. K., Mosti, M. P., Franzen, T., Vandevska-Radunovic, V., et al. (2017). Adiponectin prevents orthodontic tooth movement in rats. *Arch. Oral Biol* 83, 304–311. doi:10.1016/j.archoralbio.2017.08.009

Higuchi, C., Myoui, A., Hashimoto, N., Kuriyama, K., Yoshioka, K., Yoshikawa, H., et al. (2002). Continuous inhibition of MAPK signaling promotes the early osteoblastic differentiation and mineralization of the extracellular matrix. *J. Bone Miner. Res* 17 (10), 1785–1794. doi:10.1359/jbmr.2002.17.10.1785

Iwayama, T., Yanagita, M., Mori, K., Sawada, K., Ozasa, M., Kubota, M., et al. (2012). Adiponectin regulates functions of gingival fibroblasts and periodontal ligament cells. *J. Periodontal. Res* 47 (5), 563–571. doi:10.1111/j.1600-0765.2012.01467.x

Junker, S., Frommer, K. W., Krumbholz, G., Tsiklauri, L., Gerstberger, R., Rehart, S., et al. (2017). Expression of adipokines in osteoarthritis osteophytes and their effect on osteoblasts. *Matrix Biol* 62, 75–91. doi:10.1016/j.matbio.2016.11.005

Kadowaki, T., Yamauchi, T., Kubota, N., Hara, K., Ueki, K., and Tobe, K. (2006). Adiponectin and adiponectin receptors in insulin resistance, diabetes, and the metabolic syndrome. *J. Clin. Invest* 116 (7), 1784–1792. doi:10.1172/JCI29126

Kanazawa, I., Yamaguchi, T., Yano, S., Yamauchi, M., Yamamoto, M., and Sugimoto, T. (2007). Adiponectin and AMP kinase activator stimulate proliferation, differentiation, and mineralization of osteoblastic MC3T3-E1 cells. *BMC Cell Biol* 8, 51. doi:10.1186/1471-2121-8-51

Katsiougiannis, S., Kapsogeorgou, E. K., Manoussakis, M. N., and Skopouli, F. N. (2006). Salivary gland epithelial cells: a new source of the immunoregulatory hormone adiponectin. *Arthritis Rheum* 54 (7), 2295–2299. doi:10.1002/art.21944

Kimura, A., Kunimatsu, R., Yoshimi, Y., Tsuka, Y., Awada, T., Horie, K., et al. (2018). Baicalin promotes osteogenic differentiation of human cementoblast lineage cells via the wnt/β catenin signaling pathway. *Curr. Pharm. Des* 24 (33), 3980–3987. doi:10.2174/1381612824666181116103514

Kitagawa, M., Ao, M., Miyauchi, M., Abiko, Y., and Takata, T. (2012). F-spondin regulates the differentiation of human cementoblast-like (HCEM) cells via BMP7 expression. *Biochem. Biophys. Res. Commun* 418 (2), 229–233. doi:10.1016/j.bbrc.2011.12.155

Koh, E. T., Torabinejad, M., Pitt Ford, T. R., Brady, K., and McDonald, F. (1997). Mineral trioxide aggregate stimulates a biological response in human osteoblasts. *J. Biomed. Mater. Res* 37 (3), 432–439. doi:10.1002/(sici)1097-4636(19971205)37:3<432::aid-jbm14>3.0.co;2-d

Lee, H. W., Kim, S. Y., Kim, A. Y., Lee, E. J., Choi, J. Y., and Kim, J. B. (2009). Adiponectin stimulates osteoblast differentiation through induction of COX2 in mesenchymal progenitor cells. *Stem Cells* 27 (9), 2254–2262. doi:10.1002/stem.144

Liu, T. M., and Lee, E. H. (2013). Transcriptional regulatory cascades in Runx2-dependent bone development. *Tissue Eng. B Rev* 19 (3), 254–263. doi:10.1089/ten.TEB.2012.0527

Luo, X. H., Guo, L. J., Yuan, L. Q., Xie, H., Zhou, H. D., Wu, X. P., et al. (2005). Adiponectin stimulates human osteoblasts proliferation and differentiation via the MAPK signaling pathway. *Exp. Cell Res* 309 (1), 99–109. doi:10.1016/j.yexcr.2005.05.021

Luo, X. H., Zhao, L. L., Yuan, L. Q., Wang, M., Xie, H., and Liao, E. Y. (2009). Development of arterial calcification in adiponectin-deficient mice: adiponectin regulates arterial calcification. *J. Bone Miner. Res* 24 (8), 1461–1468. doi:10.1359/jbmr.090227

Mamali, I., Roupas, N. D., Armeni, A. K., Theodoropoulou, A., Markou, K. B., and Georgopoulos, N. A. (2012). Measurement of salivary resistin, visfatin and adiponectin levels. *Peptides* 33 (1), 120–124. doi:10.1016/j.peptides.2011.11.007

McKee, M. D., and Nanci, A. (1996). Osteopontin at mineralized tissue interfaces in bone, teeth, and osseointegrated implants: ultrastructural distribution and implications for mineralized tissue formation, turnover, and repair. *Microsc. Res. Tech* 33 (2), 141–164. doi:10.1002/(SICI)1097-0029(19960201)33:2<141::AID-JEMT5>3.0.CO;2-W

Miyazaki, T., Bub, J. D., Uzuki, M., and Iwamoto, Y. (2005). Adiponectin activates c-Jun NH2-terminal kinase and inhibits signal transducer and activator of transcription 3. *Biochem. Biophys. Res. Commun* 333 (1), 79–87. doi:10.1016/j.bbrc.2005.05.076

Nanci, A., and Bosshardt, D. D. (2006). Structure of periodontal tissues in health and disease. *Periodontol. 2000* 40, 11–28. doi:10.1111/j.1600-0757.2005.00141.x

Nigro, E., Piombino, P., Scudiero, O., Monaco, M. L., Schettino, P., Chambery, A., et al. (2015). Evaluation of salivary adiponectin profile in obese patients. *Peptides* 63, 150–155. doi:10.1016/j.peptides.2014.11.007

Oshima, K., Nampei, A., Matsuda, M., Iwaki, M., Fukuhara, A., Hashimoto, J., et al. (2006). Adiponectin increases bone mass by suppressing osteoclast and activating osteoblast. *Biochem. Biophys. Res. Commun* 331 (2), 520–526. doi:10.1016/j.bbrc.2005.03.210

Park, C. H., Oh, J. H., Jung, H. M., Choi, Y., Rahman, S. U., Kim, S., et al. (2017). Effects of the incorporation of ε-aminocaproic acid/chitosan particles to fibrin on cementoblast differentiation and cementum regeneration. *Acta Biomater* 61, 134–143. doi:10.1016/j.actbio.2017.07.039

Ruiz-Heiland, G., Yong, J. W., von Bremen, J., and Ruf, S. (2020). Leptin reduces *in vitro* cementoblast mineralization and survival as well as induces PGE2 release by ERK1/2 commitment. *Clin. Oral Invest* [Epub ahead of print]. doi:10.1007/s00784-020-03501-3

Saito, T., Yamaguchi, N., Shimazaki, Y., Hayashida, H., Yonemoto, K., Doi, Y., et al. (2008). Serum levels of resistin and adiponectin in women with periodontitis: the Hisayama study. *J. Dent. Res* 87 (4), 319–322. doi:10.1177/154405910808700416

Saygin, N. E., Giannobile, W. V., and Somerman, M. J. (2000). Molecular and cell biology of cementum. *Periodontol. 2000* 24, 73–98. doi:10.1034/j.1600-0757.2000.2240105.x

Seo, B. M., Miura, M., Gronthos, S., Bartold, P. M., Batouli, S., Brahim, J., et al. (2004). Investigation of multipotent postnatal stem cells from human periodontal ligament. *Lancet* 364 (9429), 149–155. doi:10.1016/S0140-6736(04)16627-0

Suzuki, A., Palmer, G., Bonjour, J. P., and Caverzasio, J. (1999). Regulation of alkaline phosphatase activity by p38 MAP kinase in response to activation of Gi protein-coupled receptors by epinephrine in osteoblast-like cells. *Endocrinology* 140 (7), 3177–3182. doi:10.1210/endo.140.7.6857

Swarbrick, M. M., and Havel, P. J. (2008). Physiological, pharmacological, and nutritional regulation of circulating adiponectin concentrations in humans. *Metab. Syndr. Relat. Disord* 6 (2), 87–102. doi:10.1089/met.2007.0029

Takeuchi, Y., Suzawa, M., Kikuchi, T., Nishida, E., Fujita, T., and Matsumoto, T. (1997). Differentiation and transforming growth factor-β receptor down-regulation by collagen-α2β1 integrin interaction is mediated by focal adhesion kinase and its downstream signals in murine osteoblastic cells. *J. Biol. Chem* 272 (46), 29309–29316. doi:10.1074/jbc.272.46.29309

Tang, J., and Saito, T. (2018). Elucidation on predominant pathways involved in the differentiation and mineralization of odontoblast-like cells by selective blockade of mitogen-activated protein kinases. *BioMed Res. Int* 2018, 2370438. doi:10.1155/2018/2370438

Thomson, T. S., Berry, J. E., Somerman, M. J., and Kirkwood, K. L. (2003). Cementoblasts maintain expression of osteocalcin in the presence of mineral trioxide aggregate. *J. Endod* 29 (6), 407–412. doi:10.1097/00004770-200306000-00007

Tokiyasu, Y., Takata, T., Saygin, E., and Somerman, M. (2000). Enamel factors regulate expression of genes associated with cementoblasts. *J. Periodontol* 71 (12), 1829–1839. doi:10.1902/jop.2000.71.12.1829

Wang, Y., Zhang, X., Shao, J., Liu, H., Liu, X., and Luo, E. (2017). Adiponectin regulates BMSC osteogenic differentiation and osteogenesis through the Wnt/β-catenin pathway. *Sci. Rep* 7 (1), 3652. doi:10.1038/s41598-017-03899-z

Xiao, G., Gopalakrishnan, R., Jiang, D., Reith, E., Benson, M. D., and Franceschi, R. T. (2002). Bone morphogenetic proteins, extracellular matrix, and mitogen-activated protein kinase signaling pathways are required for osteoblast-specific gene expression and differentiation in MC3T3-E1 cells. *J. Bone Miner. Res* 17 (1), 101–110. doi:10.1359/jbmr.2002.17.1.101

Yamaguchi, N., Hamachi, T., Kamio, N., Akifusa, S., Masuda, K., Nakamura, Y., et al. (2010). Expression levels of adiponectin receptors and periodontitis. *J. Periodontal. Res* 45 (2), 296–300. doi:10.1111/j.1600-0765.2009.01222.x

Yamauchi, N., Takazawa, Y., Maeda, D., Hibiya, T., Tanaka, M., Iwabu, M., et al. (2012). Expression levels of adiponectin receptors are decreased in human endometrial adenocarcinoma tissues. *Int. J. Gynecol. Pathol* 31 (4), 352–357. doi:10.1097/PGP.0b013e3182469583

Yamauchi, T., Kamon, J., Ito, Y., Tsuchida, A., Yokomizo, T., Kita, S., et al. (2003a). Cloning of adiponectin receptors that mediate antidiabetic metabolic effects. *Nature* 423 (6941), 762–769. doi:10.1038/nature01705

Yamauchi, T., Kamon, J., Terauchi, Y., Froguel, P., Tobe, K., Nagai, R., et al. (2003b). Cloning of receptors for adiponectin that mediates anti-diabetic and anti-atherogenic effects. *Circulation* 108 (17 Suppl.), 4–113. doi:10.1038/nature01705

Conflict of Interest: The authors declare that the research was conducted in the absence of any commercial or financial relationships that could be construed as a potential conflict of interest.

frontiers in Pharmacology

ORIGINAL RESEARCH
published: 21 January 2021
doi: 10.3389/fphar.2020.606514

4-Hydroxyisoleucine Alleviates Macrophage-Related Chronic Inflammation and Metabolic Syndrome in Mice Fed a High-Fat Diet

*Jiali Yang[1], Yunhui Ran[2], Yonghui Yang[2], Shuyi Song[2], Yahong Wu[2], Yuanming Qi[2], Yanfeng Gao[2,3] and Guodong Li[2]**

[1]School of Pharmaceutical Sciences, Zhengzhou University, Zhengzhou, China, [2]School of Life Sciences, Zhengzhou University, Zhengzhou, China, [3]School of Pharmaceutical Sciences (Shenzhen), Sun Yat-sen University, Guangzhou, China

In obesity, macrophages and other immune cells accumulate in organs affected by insulin, leading to chronic inflammation and insulin resistance. 4-Hydroxyisoleucine (4-HIL) is a non-protein amino acid found in fenugreek seeds. 4-HIL enhances insulin sensitivity, but its mechanism is still unclear. In this study, 4-HIL intervention reduced weight gain, liver steatosis, and dyslipidemia; moreover, it increased systemic insulin sensitivity and improved insulin resistance in mice. Importantly, after administration, the accumulation of M1 like CD11c$^+$ macrophages and inflammation in the liver and adipose tissue were reduced in the mice. 4-HIL also reduced the proportion of CD11c$^+$ macrophages among bone marrow-derived macrophages, which were induced *in vitro*. These observations demonstrate a new role of 4-HIL in insulin resistance in hepatocytes and adipocytes. 4-HIL inhibits obesity-related insulin resistance by reducing inflammation and regulating the state of M1/M2 macrophages.

Keywords: 4-hydroxyisoleucine, insulin resistance, obesity, macrophages, inflammation

OPEN ACCESS

Edited by:
David E. Stec, University of Mississippi Medical Center, United States

Reviewed by:
Erin Taylor, University of Mississippi Medical Center, United States
Barbara Wegiel, Beth Israel Deaconess Medical Center and Harvard Medical School, United States

****Correspondence:***
Guodong Li
ligd@zzu.edu.cn

Specialty section:
This article was submitted to Experimental Pharmacology and Drug Discovery, a section of the journal Frontiers in Pharmacology

Received: *15 September 2020*
Accepted: *25 November 2020*
Published: *21 January 2021*

Citation:
Yang J, Ran Y, Yang Y, Song S, Wu Y, Qi Y, Gao Y and Li G (2021) 4-Hydroxyisoleucine Alleviates Macrophage-Related Chronic Inflammation and Metabolic Syndrome in Mice Fed a High-Fat Diet. Front. Pharmacol. 11:606514. doi: 10.3389/fphar.2020.606514

INTRODUCTION

Insulin resistance is a key part of the etiology of type 2 diabetes, and obesity is clearly the most common cause of insulin resistance in humans (Moller and Kaufman, 2005). As a result of the ongoing global obesity epidemic, the prevalence of related metabolic diseases has increased (Jastreboff et al., 2019). One of the hallmarks of obesity in humans and rodents is chronic inflammation of adipose tissue, and liver and skeletal muscle (Haiyan et al., 2003; Weisberg et al., 2003; Nicolas et al., 2010; Pillon et al., 2013). In this obesity-induced tissue inflammatory response, the accumulation of proinflammatory macrophages significantly increases, especially in adipose tissue and the liver (Pingping et al., 2010; Lackey and Olefsky, 2016).

Studies have shown that anti-inflammatory treatment and the disruption of important genes in proinflammatory response can improve insulin sensitivity in obese animals (Kim et al., 2001; Yuan et al., 2001). The dominant immune cell type causing inflammation in obese and T2DM islets is the macrophage (Ying et al., 2020). Macrophage recruitment and polarization are key to obesity-induced inflammation and insulin resistance. Many previous studies have shown that macrophage accumulation is increased in adipose tissue, liver tissue, and muscle tissue in obese individuals, particularly with a large increase in pro-inflammatory M-1-like Cd11c$^+$ macrophages (Lumeng et al., 2007; Olefsky and Glass, 2010; Bijnen et al., 2018). Removing CD11c$^+$ cells *in vivo* can improve

obesity-related insulin resistance, suggesting that chronic tissue inflammation plays an important role in obesity-related insulin resistance (Patsouris et al., 2008). Studies have shown that the accumulation of adipose tissue macrophages is positively correlated with the degree of obesity in mice and humans (Weisberg et al., 2003). However, treatment options for immune cells aimed at preventing the development of insulin resistance and type 2 diabetes remain limited. There is an urgent need for new and promising treatments for obesity-related metabolic diseases in order to control and possibly reverse the progression of the disease.

Chinese traditional medicine has a long history in Asian countries (Stone, 2008). 4-HIL is a special amino acid that does not exist in mammalian tissues, but only in some plants, especially fenugreek (Fowden et al., 1973; Sauvaire et al., 1984). Fenugreek, a leguminous plant, has been used as part of traditional medicine for the treatment of diabetes, and 4-HIL has been proven to be one of the active components of fenugreek (Sharma, 1986; Broca et al., 2000). Fenugreek has anti-hyperglycemia and anti-dyslipidemia effects in a diabetic animal model (Narender et al., 2006; Singh et al., 2010; Rawat et al., 2014). Sauvaire et al. studied the structure of 4-HIL (Broca et al., 2000). The authors described that the molecule with three chiral centers existed in fenugreek seeds in the form of two dienantiomers. The main non-enantiomers with the 2S, 3R, and 4S accounted for approximately 90% of the total 4-HIL in seeds, followed by 2R, 3R, and 4S. The main 4-HIL isomers (2S, 3R, 4S) extracted from fenugreek seeds were the most effective insulin sensitizers among the 12 structure-related amino acids tested (Broca et al., 2000). In addition, 4-hydroxyisoleucine potentiates insulin secretion in a glucose-dependent manner. (Broca et al., 1999), although the mechanism needs to be further studied. In this paper, 4-HIL is a drug with the (2S, 3R, 4S) configuration obtained by microbial enzyme transformation. The purity of the product was 98.3%, the stability was good, and the oral bioavailability was high. In this study, we evaluated the therapeutic effect of 4-HIL on obesity and metabolic disorders, and explored the potential mechanism of this effect.

MATERIALS AND METHODS

Source of 4-Hydroxyisoleucine

4-HIL was provided by Julong Biological Engineering Co. Ltd., Henan, China.

Animals and Diets

Male C57BL/6 mice 6–8 weeks of age were purchased from Charles River (Beijing, China). The mice were maintained using a 12 h light/dark cycle in a specific pathogen free facility with free access to food and water throughout the experiment. Animals were fed a standard laboratory chow diet (12.8% fat, 21.6% protein, 65.6% carbohydrate; HFK Bioscience, Beijing, China) or a high-fat diet (HFD, 60% fat, 26.2% protein, 26.3% carbohydrate; HFK Bioscience). The mice were randomly divided into 5 groups with eight mice in each group. One group was given standard laboratory chow diet (CHOW), and the remaining mice were given high-fat diet (HFD). After 8 weeks, the HFD group was randomly divided into HFD normal saline, HFD 4-HIL 50 mg/kg, HFD 4-HIL 100 mg/kg and HFD 4-HIL 200 mg/kg, CHOW group, which was also given normal saline. Each group was administered once a day by gavage in a volume of 0.1 ml/10 g of mouse body weight for 8 weeks. 4-HIL was dissolved into different concentrations by saline. We recorded weekly changes in body weight and blood glucose for each mouse, also the changes in water intake and food intake for each cage of mice. Animal welfare and experimental procedures were carried out in accordance with the ethical provisions on the care and use of experimental animals at Zhengzhou University and were approved by the university's Animal Experimental Committee.

Acute Toxicity

Twenty C57BL/6 mice with a body weight of 18–25 g, each half male and female, were adaptively fed for one week. The mice were randomly divided into a normal control group and an administration group; after fasting for 12 h, they were given normal saline by intragastric administration, Or 4-HIL (2 g/kg); 4 h after the end of the administration, freely drink and eat for 1 week, and record the weight of the mice during the breeding period to observe whether there is poisoning or death; one week later, the mice are dissected. Observe whether the main organs such as heart, liver, spleen, lung and kidney are abnormal.

MTT

The cells were inoculated on a flat-bottomed 96-well plate at a density of 4,000 cells/well. After the cells were grown overnight, the cells were treated with serum-free medium for 12 h, and the plates were tested after 24, 48 and 72 h. 20 μL MTT was added 4 h before each detection time point to avoid light. The supernatant of the medium was discarded, 150 μL DMSO was added, and the absorbance was measured at 490 nm. The absorption values of 4-HIL at 490 nm were determined by a microplate analyzer at different concentrations of 1 μM, 10 M, 100 μM and 1,000 μM at different time points for 24, 48 and 72 h.

Immunohistochemical Staining

Hematoxylin and eosin (HE) stain, immunohistochemistry materials, and Oil Red O stain used to examine animal tissues were all provided by Wuhan Servicebio Technology Co. Ltd. (Wuhan, China).

Insulin Tolerance Test and Glucose Tolerance Test

To perform GTTs, the weight of each mouse in each group was measured and recorded. Each mouse was intraperitoneally injected with glucose solution (2 g/kg) and blood glucose was measured using a blood glucose meter at 0, 15, 30, 60, 90, and 120 min. The results were used to construct a curve and the area under the curve was calculated.

To perform ITTs, each mouse was intraperitoneally injected with insulin solution (0.75 U/kg) and the blood glucose of mice was measured using a blood glucose meter at 0, 15, 30, 60, 90, and

120 min. A curve was constructed and the AUC calculated. Tail blood glucose levels were monitored using a glucometer (Roche Diagnostics, Basel, Switzerland).

Blood Serum Indices

Blood serum triglyceride (TG), total cholesterol (TC), high density lipoprotein cholesterol (HDL-C), low density lipoprotein cholesterol (LDL-C), aspartate aminotransferase (AST), and alanine aminotransferase (ALT) were determined using commercial kits (Jiancheng, Nanjing, China).

Extraction of RNA and Quantitative Real-Time Polymerase Chain Reaction

According to the trade description, total RNA was extracted from mouse tissues using TRIZol reagent (Thermo Fisher Scientific, Waltham, MA, United States) and reverse transcribed with RT2 first chain kit (Thermo Fisher Scientific). PCR was performed using a LightCycler480 real-time PCR system (Roche Diagnostics). The $2^{\Delta\Delta Ct}$ method was used to calculate the multiple changes of gene expression. Objective gene and internal reference gene 36B4 primers were synthesized by Jin Weizhi Biotechnology Co., Ltd. (Beijing, China). The primer sequences used in this experiment are summarized in **Supplementary Table S1**.

Western Blot Analysis

Antibodies against IkB-α (nuclear factor of kappa light polypeptide gene enhancer in B cells inhibitor alpha; 1:1,000), JNK (c-Jun N-terminal), phosphorylated JNK (1:1,000), β-actin (1:1,000) and TLR4 (1:1,000) were purchased from Cell Signaling Technology (United States). Total protein of liver and adipose tissue was extracted by adding lytic buffer to each ice-cold sample. Proteins were isolated by sodium dodecyl sulfate-polyacrylamide gel electrophoresis (SDS-PAGE) and transferred to a polyvinylidene difluoride membrane (Millikon). Each membrane was sealed in the presence of Tris buffered saline containing Tween (TBST) containing 5% skimmed milk powder at room temperature for 1 h. Then, a defined concentration of diluted antibody was added as described by the manufacturer. The blot was incubated overnight in a flip shaking bed at 4 °C and washed six times for 5 min each time using TBST. TBST containing 5% skimmed milk powder a 1:8,000 dilution of mouse anti-rabbit antibody labeled with horseradish peroxidase (HRP) and incubated at room temperature for 2 h. The blot was washed six times for 5 min each time. An enhanced chemiluminescence (ECL) detection kit (Applygen Technologies, Beijing, China) was used to display protein bands. The protein bands were analyzed by ImageJ image analysis software (NIH, Bethesda, MD, United States).

Flow Cytometry

Mice were killed and the liver and epididymal adipose tissues were isolated. The tissues were each ground into single cell suspension and filtered through a 70 μm cell screen. After the red blood cells were lyzed, the cells were blocked using 10% rat serum in PBS for 10 min. The M1 macrophage maker was $CD45^+F4/80^+CD11b^+CD11c^+$ and M2 macrophage maker was $CD45^+F4/80^+CD11b^+CD206^+$. Representative flow cytometry plots showing the gating scheme for adipose tissue or liver macrophages. Cells from mouse were gated on forward-and side-scatter-area (FSC-A and SSC-A, respectively). immune cells were further selected by CD45 staining. $CD45^+F4/80^+$ATMs were selected and plotted to show $CD11b^+$ and $CD11c^+$ (M1)/$CD206^+$(M2)fluorescence. Anti-mouse CD11b-APC(1:100; eBioscience), Anti-mouse CD11c-PE (1:100; eBioscience), Anti-mouse CD206-PE (1:100; eBioscience); Anti-mouse CD45-FITC (1:100; eBioscience); Anti-mouse F4/80 PerCP-Cyanine5.5 (1:100; eBioscience); Anti-mouse F4/80 FITC(1:100; eBioscience); Anti-mouse CD11b-PE (1:100; eBioscience), Anti-mouse CD11c-APC(1:100; eBioscience), Anti-mouse CD206-APC (1:100; eBioscience); Armenian hamster IgG-PE (1:100; eBioscience); Rat IgG2α kappa -FITC (1:100; eBioscience); Rat IgG2b kappa-APC (1:100; eBioscience); Rat IgG2α kappa -APC (1:100; eBioscience); Rat IgG2α kappa -PE (1:100; eBioscience); Rat IgG2α kappa PerCP-Cyanine5.5 (1:100; eBioscience) antibodies were also used. The streaming data was obtained by using a FACS Calibur device (BD Biosciences, Santa Clara, CA, United States) and analyzed and processed by FlowJo software.

Preparation of Mouse Bone Marrow-Derived Macrophages

Bone marrow cells were isolated from 8 to 12-week-old mice. The hind limb bones were isolated in the biosafety cabinet after the mice were killed. DMEM medium was aspirated using a 1 ml syringe to flush out the bone marrow. The single-cell suspension was collected and filtered with a sieve. The bone marrow cells were centrifuged, and 5 ml red blood cell lysate was added for lysis at room temperature for 5–8 min. After washing with PBS twice, red blood cells were removed to obtain bone marrow cells, which were used to induce macrophages. To generate M0 or M1 macrophages, sorted monocytes or bone marrow cells were treated for 7 days with 20 ng/ml of either recombinant human or mouse granulocyte macrophage colony-stimulating factor (GM-CSF). M1 polarization was achieved on Day 5 by stimulation with 20 ng/ml of interferon gamma (IFN-γ) for 1 h, followed by 100 ng/ml lipopolysaccharide (LPS) for 48 h. To generate M2 macrophages, cells were cultured in the presence of M-CSF (20 ng/ml) for 7 days, at the 6 and 7 days IL-13 (20 ng/ml), IL4 (20 ng/ml) were add. The cells were inoculated into wells of a 6-well plate at the density of 2×10^5/well in a 6-well plate. The cells were incubated overnight (12 h) in serum-free DMEM. After this period of synchronization, 4-HIL was added to the culture for 24 h. Control cells were not treated. Both groups of macrophages were examined by flow cytometry.

Statistical Analysis

The data are shown as means ± s.e.m. Data sets that involved more than two groups were assessed by one-way ANOVA followed by Newman–Keuls post hoc tests. Next generation sequencing analysis was assessed using Tukey's honest significant difference post hoc tests. In the figures, the data

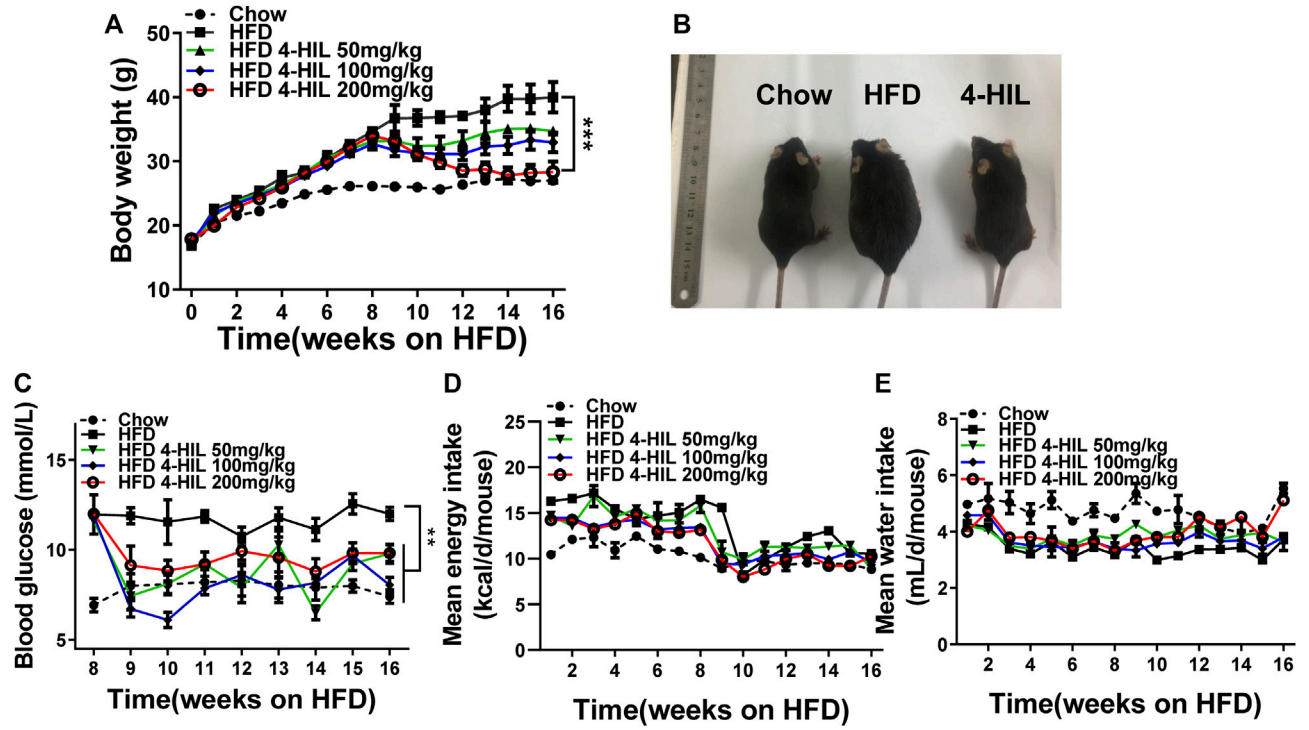

FIGURE 1 | 4-HIL therapy reverses HFD-induced obesity and hyperglycemia. Mice were fed with HFD for 16 weeks and body weight **(A)**, diet consumption **(D)**, and drinking water consumption **(E)** were recorded every week. 4-HIL intervention was given every day from week 9 and the change of blood glucose was detected every week after administration **(C)**. **(B)** Representative photographs of mice in the CHOW group **(left)**, HFD group **(middle)**, and 4-HIL (200 mg/kg) group **(right)**. *, $0.01 < p < 0.05$; **, $0.001 < p < 0.01$; ***, $p < 0.001$ ($n = 8$ for each group).

with *are different based on post hoc ANOVA statistical analysis. SPSS version 20.0 was used. The statistical analysis diagram is completed by software GraphPad Prism8. *$p < 0.05$; ** $0.001 < p < 0.01$; or ***$p < 0.001$.

RESULTS

4-Hydroxyisoleucine Decreases Body Weight and Hyperglycemia of Obese Mice Induced by High-Fat Diet

C57BL/6 mice were fed the HFD for 8 weeks, and then fed HFD supplemented with 4-HIL (50, 100, or 200 mg/kg) for another 8 weeks. Mice fed HFD 16 weeks became obese and developed hepatic steatosis, hyperlipidemia, and insulin resistance. The body weight, diet, and drinking water consumption of each mouse was measured and recorded weekly. Blood sugar was monitored weekly after drug intervention. 4-HIL lessened body weight and diet-related obesity. The 8-weeks treatment with the different doses of 4-HIL significantly decreases the body weights of mice in a dose-dependent manner. Use of 200 mg/kg 4-HIL lowered body weight of mice to almost the same weight as the control mice (**Figures 1A,B**). The intervention of 4-HIL had no effect on the diet consumption and water intake of mice (**Figures 1D,E**), indicating that the weight loss of mice after administration was not caused by the reduced consumption of food or drinking water. Monitoring of blood glucose levels in mice after administration of 4-HIL revealed reduced blood glucose levels (**Figure 1C**).

4-Hydroxyisoleucine Markedly Improves Insulin Sensitivity and Reverses Insulin Resistance

To verify the effect of the drug on insulin resistance, the GTT was used to detect glucose tolerance in mice. Due to the long-term intake of high glucose and high-fat, the blood glucose of the HFD group increased sharply after injection of glucose and did not recover within 2 h. Mice in the HFD group had abnormal glucose metabolism and glucose intolerance (**Figures 2A,B**). The glucose tolerance in the 4-HIL treatment group was significantly improved compared with the HFD control group, and the area under the curve was significantly different from that in the model control group ($p < 0.05$). The ITT results showed that the model control group was insensitive to insulin and the hypoglycemic ability decreased after injection of insulin. The hypoglycemic ability of 4-HIL group was significantly higher than that of HFD group, and decreased significantly below the curve ($p < 0.001$), indicating that 4-HIL increased insulin sensitivity mi the mice (**Figures 2C,D**). After 8 weeks of administration, blood samples were collected from the tail tip of each mouse to measure blood

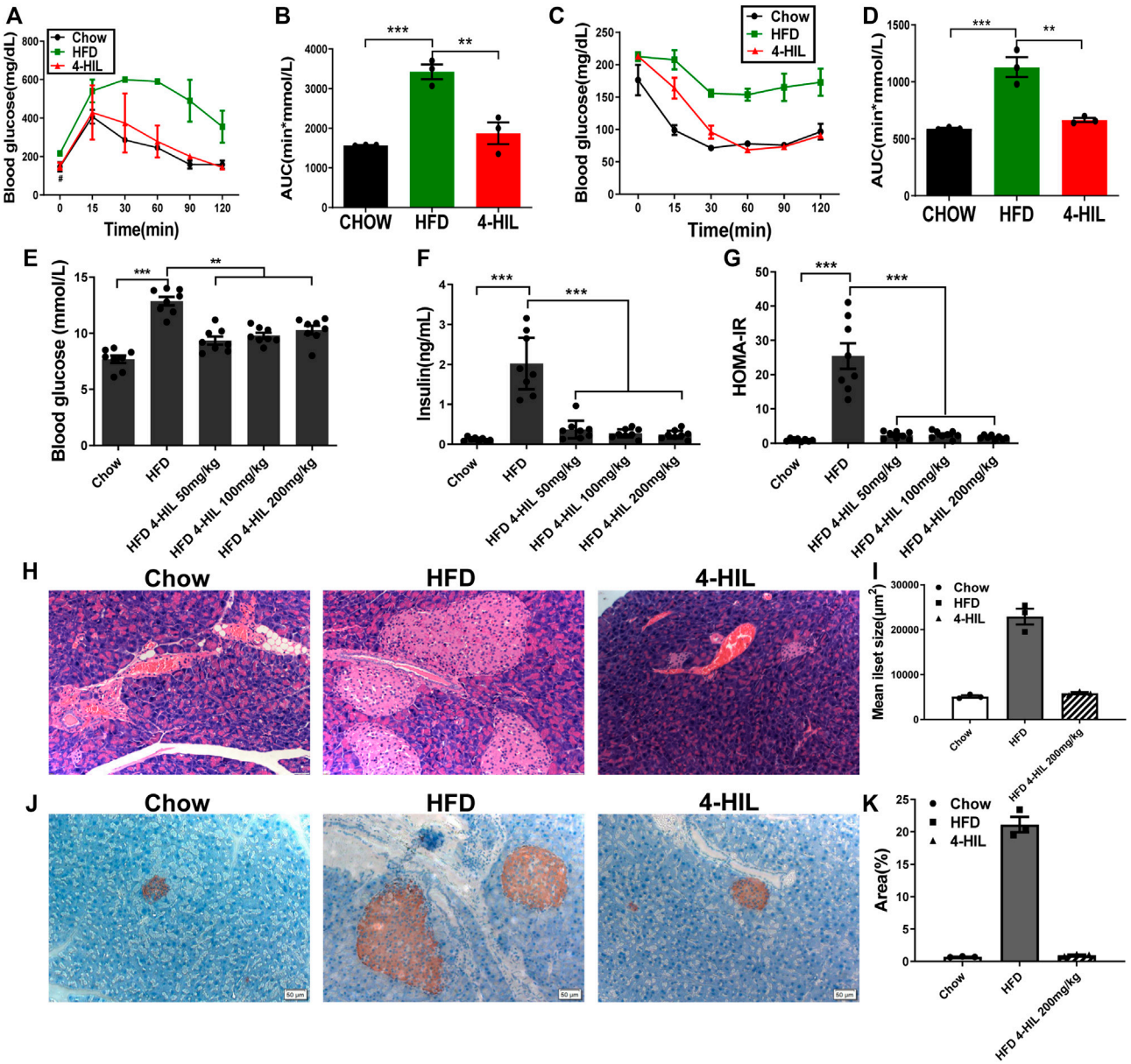

FIGURE 2 | 4-HIL improves insulin sensitivity. After 4-HIL administration, the mice in CHOW, HFD, and 4-HIL (200 mg/kg) were fasted for 8 h prior to glucose tolerance test **(A)** and insulin tolerance test **(C)**. The area under the curve **(B)**, **(D)** was calculated. After fasting for 8 h, blood samples of mice were taken from the tail tip to measure blood glucose using a blood glucose meter **(E)**, and the concentration of insulin in the sample was measured by ELISA **(F)**. The insulin resistance index **(G)** was calculated according to the formula provided in the text. At the end of administration, the isolated pancreatic tissues of mice were used for HE staining **(H)** and insulin antibody immunohistochemical staining **(J)**. The mean islet area **(I)** and insulin positive **(K)** were analyzed and quantified using ImageJ software. *, $0.01 < p < 0.05$; **, $0.001 < p < 0.01$; ***, $p < 0.001$ ($n = 8$ for each group).

glucose, blood samples were taken from the orbit of the eye to obtain plasma, and plasma insulin concentration was measured by the double antibody sandwich ELISA method. Compared with the CHOW group, the fasting plasma insulin content in the HFD group was significantly higher than that in the 4-HIL group ($p < 0.01$), and the 4-HIL intervention group significantly reversed the increase in fasting plasma insulin content in mice (**Figures 2E,F**). In the model control group, due to the intake of high-sugar and HFD, the increase of blood glucose led to the compensatory increase of insulin secretion, which led to the compensatory increase of fasting plasma insulin content in the mice. The 4-HIL treatment group displayed significant improvement that was dose-dependent. We calculated the insulin resistance index (fasting blood glucose level (mmol/L) × fasting insulin level (mIU/L)/22.5). Treatment of 4-HIL significantly decreased the insulin resistance index ($p < 0.05$, **Figure 2G**).

Insulin is the only hormone in the body that lowers blood sugar. In the early stage, we found that the insulin sensitivity

TABLE 1 | Body and organ weights at the end of treatment.

	CHOW	HFD	4-HIL		
			50 mg/kg	100 mg/kg	200 mg/kg
Liver weight (g)	0.90 ± 0.03	1.29 ± 0.22	1.08 ± 0.03	0.99 ± 0.06	0.99 ± 0.12*
Kidney weight (g)	0.30 ± 0.01	0.39 ± 0.03	0.38 ± 0.02	0.36 ± 0.03	0.33 ± 0.04
Fat pad (g)	0.61 ± 0.08	7.36 ± 0.99	3.52 ± 0.5	3.14 ± 0.73	1.51 ± 0.47*
Liver index (%)	3.38 ± 0.08	3.00 ± 0.35	3.18 ± 0.06	3.18 ± 0.24	3.42 ± 0.20
Kidney index (%)	1.13 ± 0.02	0.91 ± 0.02	1.12 ± 0.03	1.13 ± 0.03	1.15 ± 0.06
Index of fat (%)	2.28 ± 0.28	17.10 ± 1.25	10.12 ± 1.2	9.14 ± 1.84	5.13 ± 1.32**

Data were analyzed using one-way ANOVA. Values (mean ± SEM; n = *8) were taken at the end of the treatment day.*

was improved after 4-HIL treatment. Furthermore, the effect of 4-HIL on insulin-secreting pancreatic tissue was verified by HE staining, and the average islet area was calculated by ImageJ software. The islet area increased significantly in the model control group, but decreased significantly in the 4-HIL group (**Figures 2H,I**). Insulin antibody was used to detect islet β cells, and the results were analyzed and quantified by ImageJ software. A large proportion of the cytoplasm in the islet cells were positive, but there was no obvious positive reaction in the extra islet acinar cells, and the positive rate in the model control group was significantly higher than that in the normal control group (**Figures 2J,K**). These results confirmed our hypothesis that, due to the decreased insulin sensitivity in the model control group, the intake of high-sugar and HFD stimulates the compensatory secretion of insulin by islet β cells to regulate blood glucose, resulting in compensatory proliferation of islet β cells. The intervention of 4-HIL significantly inhibited the compensatory proliferation of islet β cells, which further indicated that insulin sensitivity was improved after administration of 4-HIL.

4-Hydroxyisoleucine Improves Dyslipidemia and Reduces Lipid Ectopic Accumulation in Model Mice

After 16 weeks of the HFD, the liver weight and especially fat accumulation of mice had increased significantly. The liver weight and fat accumulation were significantly lower in the 4-HIL treatment group as compared with the HFD group. The decrease was related to the 4-HIL dose and had no significant effect on the kidney (**Table 1**). In order to explore the effect of 4-HIL on blood lipids in the HFD-related obese mice, we used the isolated plasma to determine the four contents of blood lipids. Dyslipidemia occurred in the HFD group, with reduced levels of blood lipid evident in the 4-HIL treatment group (**Figures 3A–D**). HE staining of liver tissue showed that after induction by high glucose and high-fat, mouse liver cells contained many fat vacuoles in mouse liver cells, mainly small and medium-sized vacuoles, accompanied by inflammatory cell infiltration, consistent with reports in the literature (Gregor and Hotamisligil, 2011; Saltiel and Olefsky, 2017). In the 4-HIL group, the degree of vesicular degeneration and steatosis of liver cells was significantly reduced, and the number of fat vacuoles was significantly reduced (**Figure 3I**). After Oil Red O staining, the number and volume of fat droplets in liver cells of mice in the 4-HIL group were significantly lower than those in HFD group (**Figures 3G,H**). HE staining of epididymal adipose tissue revealed that the adipocytes in the model control group were significantly hypertrophic and the inflammatory infiltration of the crown-like structure was obvious, consistent with reports in the literature (Han and Levings, 2013; Lee et al., 2013; Tanaka et al., 2014). The volume of adipocytes and inflammatory infiltrating cells decreased significantly in the 4-HIL group, which indicated that 4-HIL could inhibit adipocyte hypertrophy and reduce inflammatory infiltration (**Figure 3J**). The long-term intake of the high-sugar and HFD damaged liver function, as evident by the significant increases in plasma AST and ALT. 4-HIL significantly reduced the increase plasma AST and ALT caused by HFD (**Figures 3E,F**).

4-Hydroxyisoleucine Reduces Expression of Proinflammatory Cytokines

In order to further study the effect of 4-HIL on obesity-related chronic inflammation, we measured the levels of inflammatory gene mRNA in liver and adipose tissue (**Figures 4A–F**). The expression levels of tumor necrosis factor-alpha (TNF-α), IL-1 β, IL-6, plasminogen activator inhibitor-1 (PAI-1), monocyte chemoattractant protein-1 (MCP-1), and NF- κ B in liver and adipose tissue of the model control group were significantly increased as compared with the values reported in the literature (Chawla et al., 2011). However, the expression of inflammatory gene mRNA decreased significantly after 4-HIL intervention. The Toll-like receptor 4 (TLR4) signaling pathway induces the production of proinflammatory cytokines by regulating the activities of c-Jun N-terminal kinase (JNK) and NF-κB, and leads to chronic inflammation and insulin resistance. TLR4 knockout mice fed with a high-sugar and HFD did not develop obesity and insulin resistance (Shi et al., 2006; Jia et al., 2014; Wada and Makino, 2016). We detected TLR4-related signaling pathways in liver and adipose tissue by western blot. Compared with HFD group, 4-HIL reduced the expression

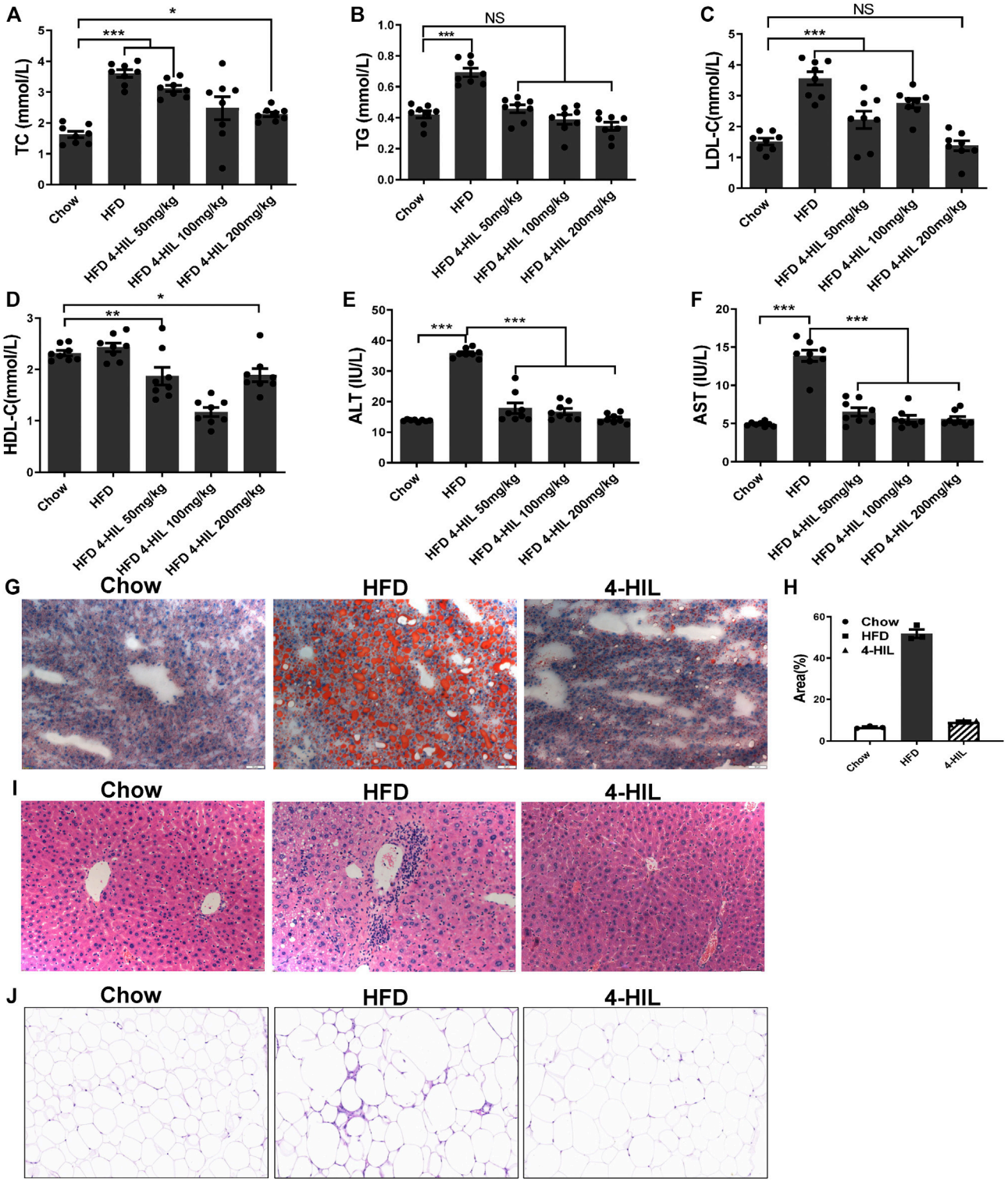

FIGURE 3 | 4-HIL reduces dyslipidemia. After 4-HIL administration, blood samples were taken from the orbit of mice after fasting for 8 h, and the contents of TC **(A)**, TG **(B)**, LDL-C **(C)**, HDL-C **(D)**, ALT **(E)**, and AST **(F)** in plasma were measured according to the instructions of the kits. Oil Red O staining of liver tissue (200×) **(G)**, HE staining of liver tissue (200×) **(I)**, and HE staining of adipose tissue (200×) **(J)** are presented. *, $0.01 < p < 0.05$; **, $0.001 < p < 0.01$; ***, $p < 0.001$ ($n = 8$ for each group).

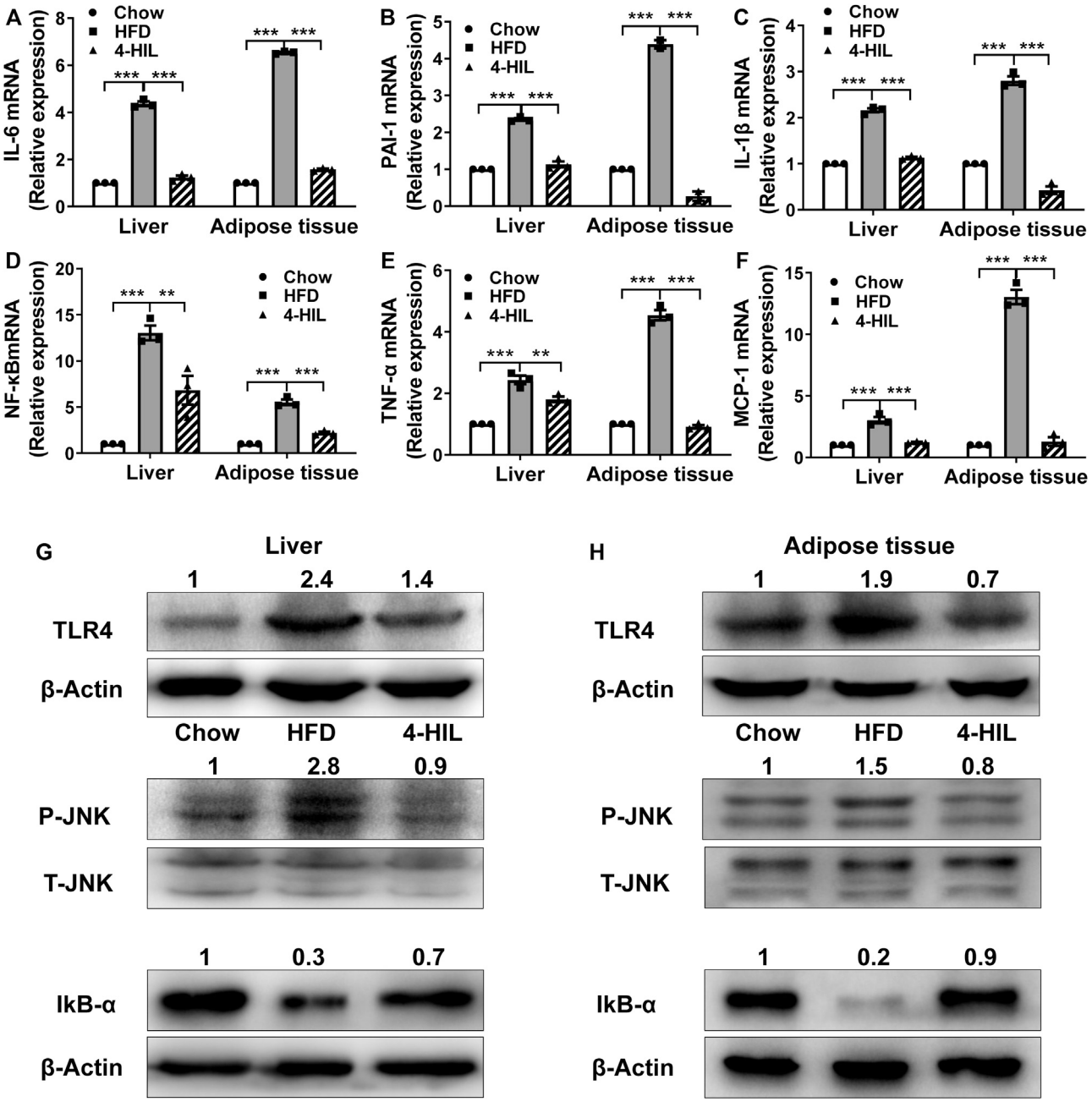

FIGURE 4 | 4-HIL decreases proinflammatory cytokine expression. After 8 weeks of 4-HIL (200 mg/kg)administration, the mRNA expression levels of IL-6 **(A)**, PAI-1 **(B)**, IL-1β **(C)**, NF-κB **(D)**, TNF-α **(E)**, and MCP-1 **(F)** in mouse liver and adipose tissues were detected by qRT-PCR. The relative level of mRNA was determined by comparing the relative expression of mRNA with that of the CHOW group by the Ct method. Effect of 4-HIL (200 mg/kg) on TLR4 related signaling pathway **(G)–(H)**. Representative immunoblotting of target proteins was used to detect the effects of 4-HIL treatment on TLR4 protein production, JNK phosphorylation and IkB-α production in liver and epididymal adipose tissues. *, $0.01 < p < 0.05$; **, $0.001 < p < 0.01$; ***, $p < 0.001$ ($n = 3$ for each group).

of TLR4 protein and inhibited JNK phosphorylation in liver and adipose tissue of HFD mice. Increasing the production of nuclear factor of kappa light polypeptide gene enhancer in B-cells inhibitor, alpha (IκB-α) in NF-κ B interaction can prevent the translocation and activation of NF-κ B. The 4-HIL intervention decreased the expression of TLR4, inhibited the phosphorylation of JNK, and increased the production of IκB-α (**Figures 4G,H**).

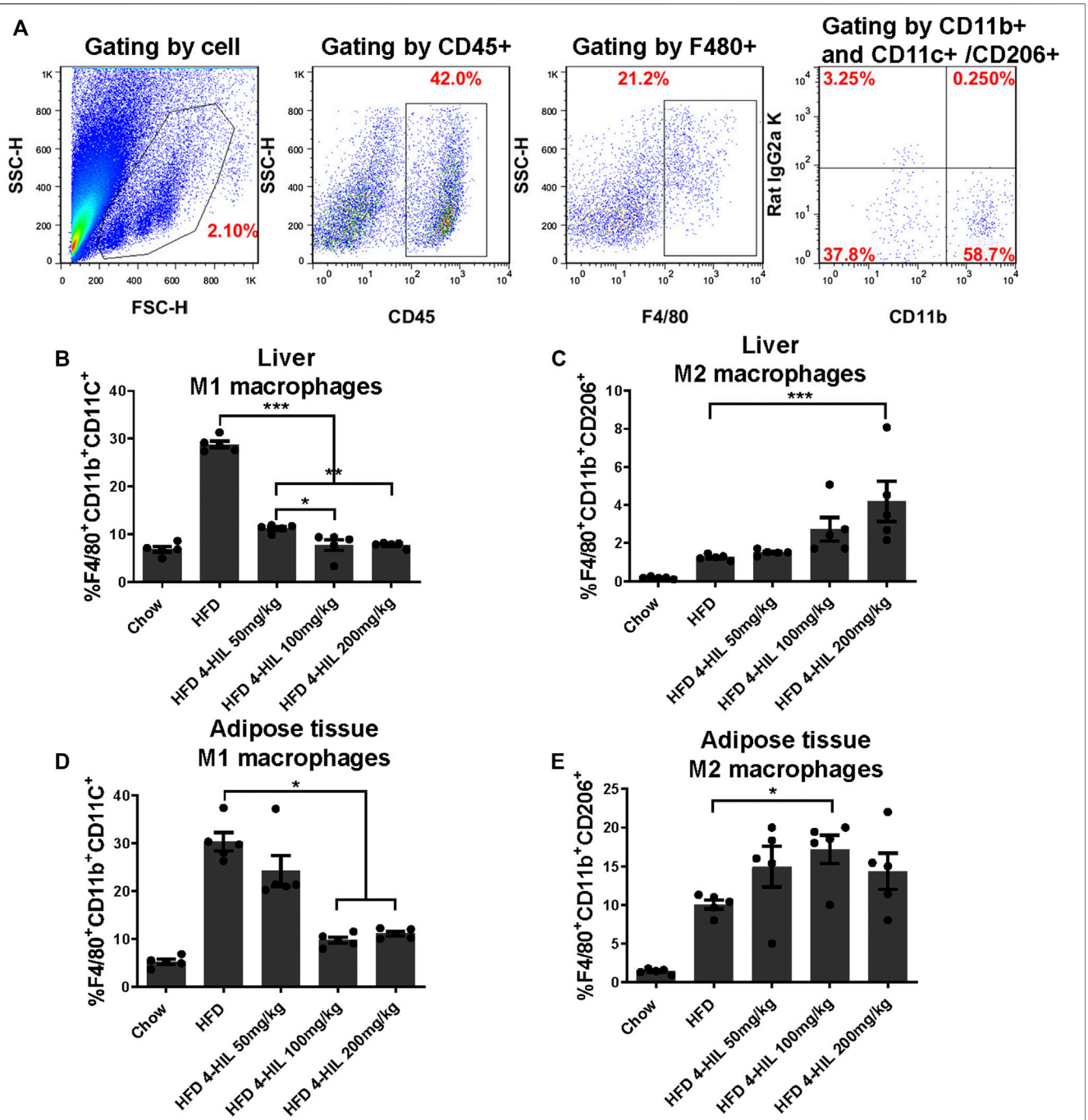

FIGURE 5 | Proinflammatory M-1-like CD11c$^+$ macrophages from HFD-fed mice are inhibited by 4-HIL *in vivo*. After the end of the period of 4-HIL administration, the liver and adipose tissue were obtained and the tissues was processed to single cell suspensions. The antibody was added and incubated in the dark, and the effect of the 4-HIL administration on the macrophage was detected by flow cytometry. Typical flow cytometry shows the gating scheme of macrophages **(A)**. Fluorescence-activated cell sorting gating results of macrophage flow cytometry are shown in **(B)**–**(E)**.

4-Hydroxyisoleucine Reduces the Proportion of Proinflammatory M1 Macrophages

Macrophage recruitment and polarization play key roles in obesity-related chronic inflammation. In order to study the effect of 4-HIL on macrophages in liver and adipose tissue, the proportion of macrophages in liver tissue and adipose tissue was analyzed by fluorescence-activated cell sorting. The proportion of M1 macrophages in liver tissue and adipose tissue of mice in the HFD group was higher than that in normal control group. The level of proinflammatory macrophages in mice treated with 4-HIL decreased in a dose-dependent manner. The 4-HIL treatment reduced the number of M1 macrophages in the liver

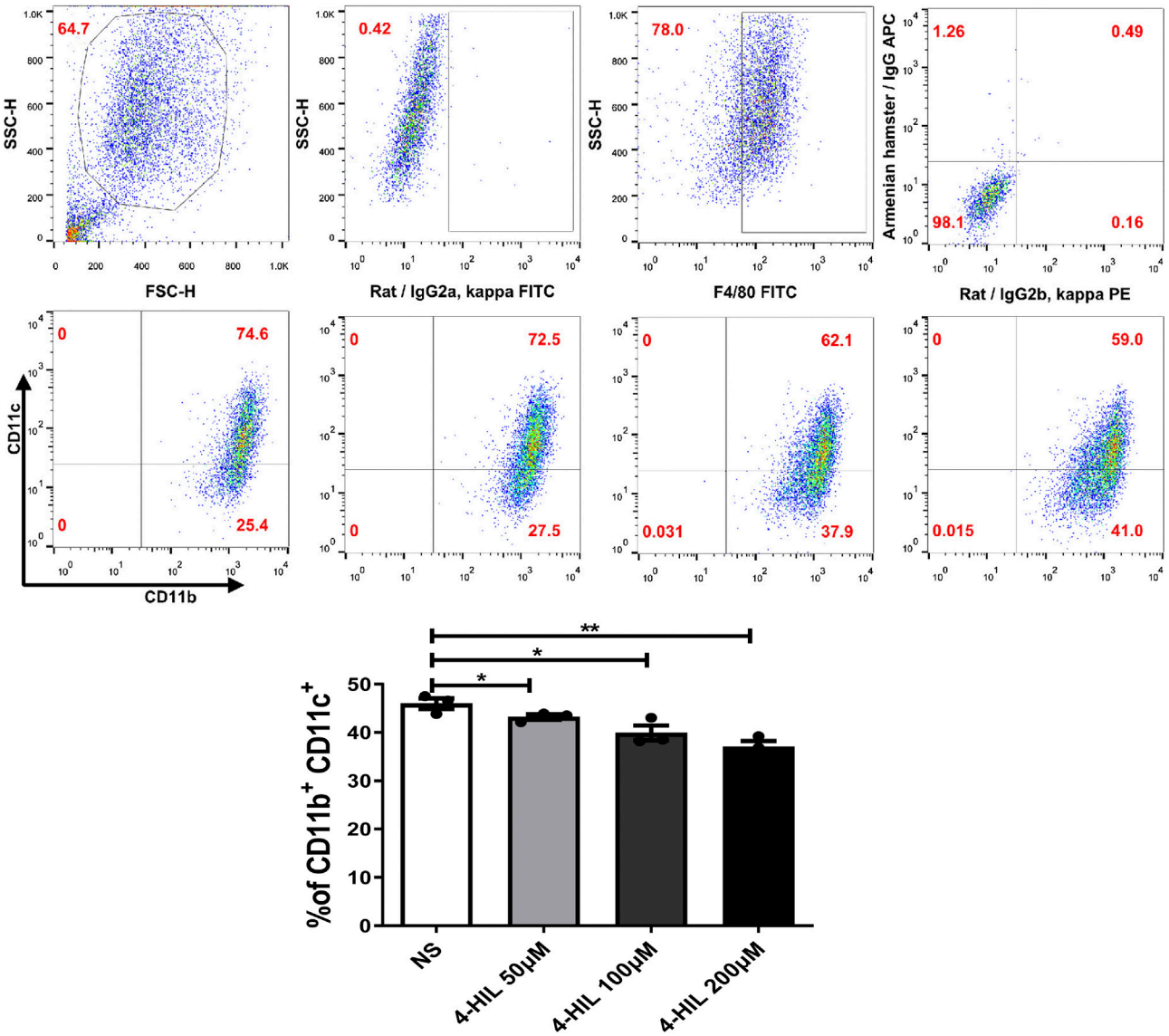

FIGURE 6 | Effect of 4-HIL on macrophages *in vitro*. Bone marrow-derived cells were cultured with GM-CSF (20 ng/ml) for 7 days. INF- γ (20 ng/ml) and LPS (100 ng/ml) was added on the day 6 and 7, respectively. After removing the non-adherent cells, the adherent cells were exposed to 4-HIL for 24 h. The proportion of macrophages was analyzed by flow cytometry.

and adipose tissue of HFD mice, and significantly reduced the increase of M1-ATM and the decrease of M2-ATM induced by HFD (**Figures 5A–E**). These findings suggested that the inflammatory state was reduced, consistent with the observed decrease in the expression of a variety of proinflammatory genes in adipose tissue and liver tissue after 4-HIL administration. Flow cytometry analysis revealed that 4-HIL administration reduced the proportion of M1 macrophages in liver and adipose tissue, and also reduced the high expression of MCP-1 induced by HFD at the mRNA level. We further explored whether 4-HIL could directly affect the polarization of macrophages and thus, reduce inflammation and improve metabolism-related diseases. We induced mouse BMDM *in vitro* to observe whether 4-HIL can directly affect M1 macrophages. After macrophages induced *in vitro* were treated with 4-HIL for 24 h, the proportion of M1 macrophages was detected by flow cytometry. Administration of 4-HIL in the macrophage model *in vitro* could still reduce the proportion of M1 macrophages. However, there was no difference in the proportion of M2 macrophages (**Figures 6A–C**).

DISCUSSION

One of the important findings of this study is that 4-HIL intervention can led to significantly weight reduction. In particular, even if the HFD was continued for 8 weeks, the

concurrent use of 4-HIL delayed obesity, steatosis, hyperglycemia and insulin resistance in the obese mice. There was no significant difference in daily food intake between HFD and 4-HIL groups, suggesting that 4-HIL attenuated HFD-induced obesity through metabolic regulation. The findings demonstrate that 4-HIL improves metabolic disorders and reduces obesity-related inflammation in HFD mice by reducing the proportion of M1 macrophages and inhibiting the function of M1 macrophages, thereby inhibiting chronic inflammation in adipose and liver tissues. Furthermore, 4-HIL significantly increased insulin sensitivity of and improved the dysfunctions in glucose and lipid metabolism in the model mice.

According to the literature, 4-HIL can stimulate the insulin secretion of isolated rat pancreas (Sergent et al., 2008). Our experimental results showed that the regulation of blood glucose level by 4-HIL occurred mainly through the increase of insulin sensitivity, but not increased insulin secretion. In order to verify whether 4-HIL increased insulin secretion *in vivo*, GTT was performed in normal C57BL/6 mice to evaluate whether the drug stimulated insulin secretion. The blood glucose level in mice administered 4-HIL at 200 mg/kg for 15 min group was significantly lower than that in the vehicle group, and other time points had no significant effect on blood glucose value and AUC value (**Supplementary Figure S1**). We also applied 4-HIL to epinephrine-induced hyperglycemia mice and observed that 4-HIL had no significant hypoglycemic effect on subacute epinephrine hyperglycemia model (**Supplementary Figure S2**). However, in the HFD model, 4-HIL could significantly reduce the blood glucose value and AUC value, the serum insulin content in the 4-HIL treatment group was significantly lower than that in the HFD group, and the Homeostatic Model Assessment of Insulin Resistance value showed that the insulin resistance in the treatment group was significantly decreased. The results of HE staining and insulin antibody immunohistochemistry showed that the area of insulin area (β cell dense area) in the HFD group was significantly increased because high glucose and high lipid intake induced insulin resistance and led to compensatory proliferation of islet β cells. Islet β cells secrete a large amount of insulin in a compensatory response to regulate blood glucose. The significant reduction in the islet area of the 4-HIL intervention group further proved that the insulin content of mice in the treatment group was decreased.

Obese mice produce high levels of proinflammatory cytokines, including TNF- α, IL-1 β, IL-6, and PAI-1, in liver and adipose tissue, and obesity is characterized by infiltration and activation of immune cells in liver and adipose tissues (Chawla et al., 2011; Bu et al., 2018). The expressions of inflammatory gene mRNAs in the 4-HIL treatment group were significantly decreased, indicating that 4-HIL can reduce the level of inflammatory factors in insulin target organs of HFD model mice. TLR4 signal leads to the production of proinflammatory cytokines in the target tissue of HFD mice and leads to chronic inflammation and insulin resistance (Shi et al., 2006; Cani et al., 2008). The intervention of 4-HIL decreased the expression of TLR4, inhibited the phosphorylation of JNK, and increased the production of IκB-α. These results indicated that the administration of 4-HIL could significantly improve the state of chronic inflammation in the body. 4-HIL can reduce the ratio of M1/M2 in liver and adipose tissues of HDF mice, affect the polarization of macrophages, and improve the chronic inflammatory response. Flow cytometry examination of liver and adipose tissues of HDF mice after 4-HIL administration revealed the accumulation of a large number of proinflammatory macrophages, consistent with prior observations in the literature (Pal et al., 2012). The level of proinflammatory macrophages in 4-HIL treatment group decreased in a dose-dependent manner. We further explored *in vitro* whether 4-HIL directly affects the polarization of macrophages, and observe the direct effect of 4-HIL on macrophages by inducing mouse BMDM. 4-HIL could still reduce the proportion of M1 macrophages *in vitro*, and similar results were found in both BMDM and M1 macrophage models *in vitro*. At the same time, we also studied the effect of 4-HIL on BMDM induced in TLR4 deficient mice. The proportion of M1 macrophages in these mice was still reduced, indicating that the effect of 4-HIL does not depend on TLR4.

Obesity, especially the increase of visceral fat content, will lead to the occurrence and development of metabolism-related diseases (Moller and Kaufman, 2005). The increase of free fatty acids and lipid accumulation in liver and other organs are the main causes of insulin resistance. Studies in humans and mice have shown that the size of adipocytes is a powerful predictor of the proportion of macrophages in adipose tissue (Weisberg et al., 2003). Adipocyte volume is closely associated with systemic insulin resistance, dyslipidemia, and the risk of type 2 diabetes, and weight loss is accompanied by a decrease in adipocyte volume. The liver is an important site of lipid metabolism. In the HFD group, the liver was light yellow and had a tight capsule, blunt edge, slightly soft texture, and greasy touch. Oil Red O staining revealed the pronounced accumulation of lipids, accompanied by a significant increase in plasma AST and ALT levels. This is consistent with literature reports. As the site of crosstalk between adipocytes and macrophages, there is a unique structure in obese adipose tissue called crown-like structure (CLS), where macrophages are considered to scavenge the residual lipid droplets of dead adipocytes (Cinti et al., 2005; Lumeng et al., 2007). Histologically, proinflammatory M1 macrophages aggregate to constitute CLS in obese adipose tissue of humans and rodents. On the other hand, M2 macrophages are scattered in the interstitial spaces between adipocytes. Notably, the number of CLS is positively correlated with systemic insulin resistance in obese subjects (Apovian et al., 2008; Bremer et al., 2011), suggesting the pathophysiologic role of CLS in adipose tissue inflammation and systemic energy metabolism (Tanaka et al., 2014). In the 4-HIL group, the amount of fat accumulation was significantly decreased, and serum AST and ALT were significantly decreased. Tissue sections showed that the number of adipocytes decreased, the cell volume significantly decreased, and the infiltration of inflammatory cells decreased, indicating that 4-HIL can improve the disorder

of lipid metabolism caused by high-fat. Weisberg et al. reported that the size of adipocytes is related to the number of macrophages in adipose tissue (Weisberg et al., 2003), and the regulation of adipose metabolism by 4-HIL is closely related to macrophages.

These results were derived from a diet-induced obesity model in mice. Whether 4-HIL has a similar effect on insulin resistance in patients with type 2 diabetes remains to be studied. The activation characteristics of mouse macrophages and human macrophages are different (Mantovani et al., 2004). For example, the activity of inducible nitric oxide synthase in macrophages is different between mouse and human inflammatory models (Zhang et al., 1996; Schneemann and Schoedon, 2002). However, for many inflammatory markers, obese human and mouse adipose tissue macrophage (ATM) are similar, so mice are still useful models for testing the biology of ATM (Weisberg et al., 2003; Xu et al., 2003; Cancello et al., 2005). Future studies will focus on the importance of identified genes for ATM function and the development of type 2 diabetes. In addition, we found that 4-HIL significantly reduced fat accumulation in obese model animals, but had no significant effect on diet. These findings need to be assessed in more depth. Whether 4-HIL can produce heat by blocking the function of the RCAN1 gene or whether it promotes the conversion of white fat into brown fat, individuals can maintain low body fat levels without the need to reduce food intake or increase exercise (Bal et al., 2012). Alternately, as reported by Eichmann et al., by reducing fat absorption, excess fat in the intestinal cavity with fecal excretion may occur (Zhang et al., 2018). These aspects still need to be investigated.

CONCLUSION

In conclusion, 4-HIL significantly improved glucose and lipid metabolic dysfunctions in HFD mice. 4-HIL reduced the proportion of M1 macrophages in liver and adipose tissues of mice. By inhibiting the aggregation of M1 macrophages and inhibiting the chronic inflammation of adipose tissue and liver mediated by inflammation, metabolic disorders and chronic inflammation could be improved, and the insulin sensitivity could be increased. 4-HIL displayed no obvious toxic and side effects *in vitro* and *in vivo*. 4-HIL is a potential drug for the treatment of obesity-related metabolic diseases.

DATA AVAILABILITY STATEMENT

The raw data supporting the conclusions of this article will be made available by the authors, without undue reservation, to any qualified researcher.

ETHICS STATEMENT

The animal study was reviewed and approved by Animal Experimental Committee of Zhengzhou University.

AUTHOR CONTRIBUTIONS

GL conceived and designed the experiments. JY performed the experiments. PZ, YR and YY helped to perform the experiments. GL, JY, YQ and YG analyzed and interpreted the results. JY, SS, YW, GL, YQ and YG wrote the manuscript with inputs from all authors. GL is the guarantor of this work, so he has full access to all the data in the study and is responsible for the completeness of the data and the accuracy of the data analysis. All authors discussed the results and gave final approval of the manuscript.

FUNDING

Support for the studies described here was provided by the Natural Science Foundation of China (81571547, 81601448) and the Henan Province and the Key Scientific Research Projects of Henan Higher Education Institutions (19A180007).

ACKNOWLEDGMENTS

Thanks to the lab members for their suggestions and help. Due to limited space, it is not possible to discuss all the important contributions made in this regard.

SUPPLEMENTARY MATERIAL

The Supplementary Material for this article can be found online at: https://www.frontiersin.org/articles/10.3389/fphar.2020.606514/full#supplementary-material.

REFERENCES

Apovian, C. M., Bigornia, S., Mott, M., Meyers, M. R., Ulloor, J., Gagua, M., et al. (2008). Adipose macrophage infiltration is associated with insulin resistance and vascular endothelial dysfunction in obese subjects. *Arterioscler. Thromb. Vasc. Biol.* 28, 1654–1659. doi:10.1161/ATVBAHA.108.170316

Bal, N. C., Maurya, S. K., Sopariwala, D. H., Sahoo, S. K., Gupta, S. C., Shaikh, S. A., et al. (2012). Sarcolipin is a newly identified regulator of muscle-based thermogenesis in mammals. *Nat. Med.* 18, 1575–1579. doi:10.1038/nm.2897

Bijnen, M., Josefs, T., Cuijpers, I., Maalsen, C. J., Van De Gaar, J., Vroomen, M., et al. (2018). Adipose tissue macrophages induce hepatic neutrophil recruitment and macrophage accumulation in mice. *Gut.* 67, 1317–1327. doi:10.1136/gutjnl-2016-313654

Bremer, A. A., Devaraj, S., Afify, A., and Jialal, I. (2011). Adipose tissue dysregulation in patients with metabolic syndrome. *J. Clin. Endocrinol. Metab.* 96, E1782–E1788. doi:10.1210/jc.2011-1577

Broca, C., Gross, R., Petit, P., Sauvaire, Y., Manteghetti, M., Tournier, M., et al. (1999). 4-Hydroxyisoleucine: experimental evidence of its insulinotropic and antidiabetic properties. *Am. J. Physiol.* 277, E617–E623. doi:10.1152/ajpendo.1999.277.4.E617

Broca, C., Manteghetti, M., Gross, R., Baissac, Y., Jacob, M., Petit, P., et al. (2000). 4-Hydroxyisoleucine: effects of synthetic and natural analogues on insulin secretion. *Eur. J. Pharmacol.* 390, 339–345. doi:10.1016/s0014-2999(00)00030-3

Bu, Y., Okunishi, K., Yogosawa, S., Mizuno, K., Irudayam, M. J., Brown, C. W., et al. (2018). Insulin regulates lipolysis and fat mass by upregulating growth/differentiation factor 3 in adipose tissue macrophages. *Diabetes* 67, 1761–1772. doi:10.2337/db17-1201

Cancello, R., Henegar, C., Viguerie, N., Taleb, S., Poitou, C., Rouault, C., et al. (2005). Reduction of macrophage infiltration and chemoattractant gene expression changes in white adipose tissue of morbidly obese subjects after surgery-induced weight loss. *Diabetes* 54, 2277–2286. doi:10.2337/diabetes.54.8.2277

Cani, P. D., Bibiloni, R., Knauf, C., Waget, A., Neyrinck, A. M., Delzenne, N. M., et al. (2008). Changes in gut microbiota control metabolic endotoxemia-induced inflammation in high-fat diet-induced obesity and diabetes in mice. *Diabetes* 57, 1470–1481. doi:10.2337/db07-1403

Chawla, A., Nguyen, K. D., and Goh, Y. P. (2011). Macrophage-mediated inflammation in metabolic disease. *Nat. Rev. Immunol.* 11, 738–749. doi:10.1038/nri3071

Cinti, S., Mitchell, G., Barbatelli, G., Murano, I., Ceresi, E., Faloia, E., et al. (2005). Adipocyte death defines macrophage localization and function in adipose tissue of obese mice and humans. *J. Lipid Res.* 46, 2347–2355. doi:10.1194/jlr.M500294-JLR200

Fowden, L., Pratt, H. M., and Smith, A. (1973). 4-Hydroxyisoleucine from seed of *Trigonella foenum-graecum*. *Phytochemistry* 12, 1707–1711. doi:10.1016/0031-9422(73)80391-7

Gregor, M. F., and Hotamisligil, G. S. (2011). Inflammatory mechanisms in obesity. *Annu. Rev. Immunol.* 29, 415–445. doi:10.1146/annurev-immunol-031210-101322

Haiyan, X., Barnes, G. T., Qing, Y., Guo, T., Daseng, Y., Chou, C. J., et al. (2003). Chronic inflammation in fat plays a crucial role in the development of obesity-related insulin resistance. *J. Clin. Invest.* 112 (12), 1821–1830. doi:10.1172/JCI19451

Han, J. M., and Levings, M. K. (2013). Immune regulation in obesity-associated adipose inflammation. *J. Immunol.* 191, 527–532. doi:10.4049/jimmunol.1301035

Jastreboff, A. M., Kotz, C. M., Kahan, S., Kelly, A. S., and Heymsfield, S. B. (2019). Obesity as a disease: the obesity society 2018 position statement. *Obesity* 27, 7–9. doi:10.1002/oby.22378

Jia, L., Vianna, C. R., Fukuda, M., Berglund, E. D., Liu, C., Tao, C., et al. (2014). Hepatocyte toll-like receptor 4 regulates obesity-induced inflammation and insulin resistance. *Nat. Commun.* 5, 3878. doi:10.1038/ncomms4878

Kim, J. K., Kim, Y. J., Fillmore, J. J., Chen, Y., Moore, I., Lee, J., et al. (2001). Prevention of fat-induced insulin resistance by salicylate. *J. Clin. Invest.* 108, 437–446. doi:10.1172/JCI11559

Lackey, D. E., and Olefsky, J. M. (2016). Regulation of metabolism by the innate immune system. *Nat. Rev. Endocrinol.* 12, 15–28. doi:10.1038/nrendo.2015.189

Lee, Y. H., Petkova, A. P., and Granneman, J. G. (2013). Identification of an adipogenic niche for adipose tissue remodeling and restoration. *Cell Metabol.* 18, 355–367. doi:10.1016/j.cmet.2013.08.003

Lumeng, C. N., Bodzin, J. L., and Saltiel, A. R. (2007). Obesity induces a phenotypic switch in adipose tissue macrophage polarization. *J. Clin. Invest.* 117, 175–184. doi:10.1172/JCI29881

Mantovani, A., Sica, A., Sozzani, S., Allavena, P., Vecchi, A., and Locati, M. (2004). The chemokine system in diverse forms of macrophage activation and polarization. *Trends Immunol.* 25, 677–686. doi:10.1016/j.it.2004.09.015

Moller, D. E., and Kaufman, K. D. (2005). Metabolic syndrome: a clinical and molecular perspective. *Annu. Rev. Med.* 56, 45–62. doi:10.1146/annurev.med.56.082103.104751

Narender, T., Puri, A., Shweta, T., Saxena, R., Bhatia, G., et al. (2006). 4-hydroxyisoleucine an unusual amino acid as antidyslipidemic and antihyperglycemic agent. *Bioorg. Med. Chem. Lett.* 16, 293–296. doi:10.1016/j.bmcl.2005.10.003

Nicolas, L., Olivier, M. C., Yves, H., Nico, V. R., Cani, P. D., and Leclercq, I. A. (2010). Kupffer cell activation is a causal factor for hepatic insulin resistance. *Am. J. Physiol. Gastrointest. Liver Physiol.* 298, G107–G116. doi:10.1152/ajpgi.00391.2009

Olefsky, J. M., and Glass, C. K. (2010). Macrophages, inflammation, and insulin resistance. *Annu. Rev. Physiol.* 72, 219–246. doi:10.1146/annurev-physiol-021909-135846

Pal, D., Dasgupta, S., Kundu, R., Maitra, S., Das, G., Mukhopadhyay, S., et al. (2012). Fetuin-A acts as an endogenous ligand of TLR4 to promote lipid-induced insulin resistance. *Nat. Med.* 18, 1279–1285. doi:10.1038/nm.2851

Patsouris, D., Li, P. P., Thapar, D., Chapman, J., Olefsky, J. M., and Neels, J. G. (2008). Ablation of CD11c-positive cells normalizes insulin sensitivity in obese insulin resistant animals. *Cell Metabol.* 8, 301–309. doi:10.1016/j.cmet.2008.08.015

Pillon, N. J., Bilan, P. J., Fink, L. N., and Klip, A. (2013). Cross-talk between skeletal muscle and immune cells: muscle-derived mediators and metabolic implications. *Am. J. Physiol. Endocrinol. Metab.* 304, E453–E465. doi:10.1152/ajpendo.00553.2012

Pingping, L., Min, L., Nguyen, M. T. A., Eun Ju, B., Justin, C., Daorong, F., et al. (2010). Functional heterogeneity of CD11c-positive adipose tissue macrophages in diet-induced obese mice. *J. Biol. Chem.* 285, 15333–15345. doi:10.1074/jbc.M110.10026

Rawat, A. K., Korthikunta, V., Gautam, S., Pal, S., Tadigoppula, N., Tamrakar, A. K., et al. (2014). 4-Hydroxyisoleucine improves insulin resistance by promoting mitochondrial biogenesis and act through AMPK and Akt dependent pathway. *Fitoterapia*. 99, 307–317. doi:10.1016/j.fitote.2014.10.006

Saltiel, A. R., and Olefsky, J. M. (2017). Inflammatory mechanisms linking obesity and metabolic disease. *J. Clin. Invest.* 127, 1–4. doi:10.1172/JCI92035

Sauvaire, Y., Girardon, P., Baccou, J. C., and Ristérucci, A. M. (1984). Changes in growth, proteins and free amino acids of developing seed and pod of fenugreek. *Phytochemistry* 23, 479–486. doi:10.1016/S0031-9422(00)80363-5

Schneemann, M., and Schoedon, G. (2002). Species differences in macrophage NO production are important. *Nat. Immunol.* 3, 102. doi:10.1038/ni0202-102a

Sergent, D., Wang, Q., Sasaki, N. A., and Ouazzani, J. (2008). Synthesis of hydantoin analogues of (2S,3R,4S)-4-hydroxyisoleucine with insulinotropic properties. *Bioorg. Med. Chem. Lett.* 18, 4332–4335. doi:10.1016/j.bmcl.2008.06.081

Sharma, R. D. (1986). Effect of fenugreek seeds and leaves on blood glucose and serum insulin responses in human subjects. *Nutr. Res.* 6, 1353–1364. doi:10.1016/S0271-5317(86)80020-3

Shi, H., Kokoeva, M. V., Inouye, K., Tzameli, I., Yin, H., and Flier, J. S. (2006). TLR4 links innate immunity and fatty acid-induced insulin resistance. *J. Clin. Invest.* 116, 3015–3025. doi:10.1172/JCI28898

Singh, A. B., Tamarkar, A. K., Narender, T., and Srivastava, A. K. (2010). Antihyperglycaemic effect of an unusual amino acid (4-hydroxyisoleucine) in C57BL/KsJ-db/db mice. *Nat. Prod. Res.* 24, 258–265. doi:10.1080/14786410902836693

Stone, R. (2008). Biochemistry. Lifting the veil on traditional Chinese medicine. *Science* 319, 709–710. doi:10.1126/science.319.5864.709

Tanaka, M., Ikeda, K., Suganami, T., Komiya, C., Ochi, K., Shirakawa, I., et al. (2014). Macrophage-inducible C-type lectin underlies obesity-induced adipose tissue fibrosis. *Nat. Commun.* 5, 4982. doi:10.1038/ncomms5982

Wada, J., and Makino, H. (2016). Innate immunity in diabetes and diabetic nephropathy. *Nat. Rev. Nephrol.* 12, 13–26. doi:10.1038/nrneph.2015.175

Weisberg, S. P., Mccann, D., Desai, M., Rosenbaum, M., Leibel, R. L., and Ferrante, A. W., Jr. (2003). Obesity is associated with macrophage accumulation in adipose tissue. *J. Clin. Invest.* 112, 1796–1808. doi:10.1172/JCI19246

Xu, H., Barnes, G. T., Yang, Q., Tan, G., Yang, D., Chou, C. J., et al. (2003). Chronic inflammation in fat plays a crucial role in the development of obesity-related insulin resistance. *J. Clin. Invest.* 112, 1821–1830. doi:10.1172/JCI19451

Ying, W., Fu, W., Lee, Y. S., and Olefsky, J. M. (2020). The role oThe role of macrophages in obesity-associated islet inflammation and β-cell abnormalities. *Nat. Rev. Endocrinol.* 16, 81–90. doi:10.1038/s41574-019-0286-3

Yuan, M., Konstantopoulos, N., Lee, J., Hansen, L., Li, Z. W., Karin, M., et al. (2001). Reversal of obesity- and diet-induced insulin resistance with salicylates or targeted disruption of Ikkbeta. *Science* 293, 1673–1677. doi:10.1126/science.1061620

Zhang, X., Laubach, V. E., Alley, E. W., Edwards, K. A., Sherman, P. A., Russell, S. W., et al. (1996). Transcriptional basis for hyporesponsiveness of the human inducible nitric oxide synthase gene to lipopolysaccharide/interferon-gamma. *J. Leukoc. Biol.* 59, 575–585. doi:10.1002/jlb.59.4.575

Zhang, F., Zarkada, G., Han, J., Li, J., Dubrac, A., Ola, R., et al. (2018). Lacteal junction zippering protects against diet-induced obesity. *Science* 361, 599–603. doi:10.1126/science.aap9331

Conflict of Interest: The authors declare that the research was conducted in the absence of any commercial or financial relationships that could be construed as a potential conflict of interest.

frontiers in Pharmacology

ORIGINAL RESEARCH
published: 25 January 2021
doi: 10.3389/fphar.2020.636533

Inhibition of Lipid Accumulation in Skeletal Muscle and Liver Cells: A Protective Mechanism of Bilirubin Against Diabetes Mellitus Type 2

Claudia A. Hana[1], Eva-Maria Klebermass[2], Theresa Balber[2,3], Markus Mitterhauser[2,3], Ruth Quint[1], Yvonne Hirtl[1], Antonia Klimpke[1], Sophie Somloi[1], Juliana Hutz[1], Elisabeth Sperr[1], Paulina Eder[1], Jana Jašprová[4], Petra Valášková[4], Libor Vítek[4,5], Elke Heiss[6] and Karl-Heinz Wagner[1]*

[1]Department of Nutritional Sciences, Faculty of Life Sciences, University of Vienna, Vienna, Austria, [2]Department of Biomedical Imaging and Image-guided Therapy, Division of Nuclear Medicine, Medical University of Vienna, Vienna, Austria, [3]Ludwig Boltzmann Institute Applied Diagnostics, Vienna, Austria, [4]Institute of Medical Biochemistry and Laboratory Diagnostics, University General Hospital and 1st Faculty of Medicine, Charles University, Prague, Czechia, [5]4th Department of Internal Medicine, University General Hospital and 1st Faculty of Medicine, Charles University, Prague, Czechia, [6]Department of Pharmacognosy, University of Vienna, Vienna, Austria

OPEN ACCESS

Edited by:
David E. Stec, University of Mississippi Medical Center, United States

Reviewed by:
Terry D. Hinds Jr., University of Kentucky, United States
Peter Hosick, Montclair State University, United States

***Correspondence:**
Claudia A. Hana
claudia.hana@univie.ac.at

Specialty section:
This article was submitted to Experimental Pharmacology and Drug Discovery, a section of the journal Frontiers in Pharmacology

Received: 01 December 2020
Accepted: 11 December 2020
Published: 25 January 2021

Citation:
Hana CA, Klebermass E-M, Balber T, Mitterhauser M, Quint R, Hirtl Y, Klimpke A, Somloi S, Hutz J, Sperr E, Eder P, Jašprová J, Valášková P, Vítek L, Heiss E and Wagner K-H (2021) Inhibition of Lipid Accumulation in Skeletal Muscle and Liver Cells: A Protective Mechanism of Bilirubin Against Diabetes Mellitus Type 2. Front. Pharmacol. 11:636533. doi: 10.3389/fphar.2020.636533

Ectopic lipid accumulation in skeletal muscle and liver drives the pathogenesis of diabetes mellitus type 2 (DMT2). Mild hyperbilirubinaemia has been repeatedly suggested to play a role in the prevention of DMT2 and is known for its capacity to shape an improved lipid phenotype in humans and in animals. To date, the effect of bilirubin on lipid accumulation in tissues that are prone to ectopic lipid deposition is unclear. Therefore, we analyzed the effect of bilirubin on lipid accumulation in skeletal muscle and liver cell lines. C2C12 skeletal mouse muscle and HepG2 human liver cells were treated with physiological concentrations of free fatty acids (FFA) (0.5 mM and 1 mM) and unconjugated bilirubin (UCB) (17.1 and 55 μM). The intracellular presence of UCB upon exogenous UCB administration was confirmed by HPLC and the lipid accumulation was assessed by using Nile red. Exposure of both cell lines to UCB significantly reduced lipid accumulation by up to 23% ($p \leq 0.001$) in HepG2 and by up to 17% ($p \leq 0.01$) in C2C12 cells at 0.5 and 5 h under hypoglycaemic conditions. Simultaneously, UCB slightly increased FFA uptake in HepG2 cells after 0.5 and 5 h and in C2C12 cells after 12 h as confirmed by gas chromatographic analyses of the remaining FFA content in the incubation media. The effects of UCB on lipid accumulation and uptake were abolished in the presence of higher glucose concentrations. Monitoring the uptake of a radiolabeled glucose analogue [18F]FDG: (2-deoxy-2-[^{18}F]fluoro-D-glucose) into both cell types further indicated higher glucose consumption in the presence of UCB. In conclusion, our findings show that UCB considerably decreases lipid accumulation in skeletal muscle and liver cells within a short incubation time of max. 5 h which suggests that mildly elevated bilirubin levels could lower ectopic lipid deposition, a major key element in the pathogenesis of DMT2.

Keywords: bilirubin, mild hyperbilirubinaemia, ectopic lipid accumulation, C2C12 skeletal muscle cells, HepG2 cells, [^{18}F]FDG uptake, insulin resistance, lipid accumulation

Abbreviations: DMT2, diabetes mellitus type 2; [^{18}F]FDG, 2-deoxy-2-[^{18}F]fluoro-D-glucose; FFA, free fatty acids; GS, Gilbert's syndrome; LA, linoleic acid; NR, Nile red; OA, oleic acid; PA, palmitic acid; UCB, unconjugated bilirubin.

INTRODUCTION

Globally, the increase in diabetes mellitus type 2 (DMT2) is emerging with 463 million cases worldwide, a prevalence that tripled over the last 20 years and is projected to rise to 700 million cases in 2045 (International Diabetes Federation, 2019). Obesity and an increased fat mass are major contributors to the development of insulin resistance and DMT2. Many studies have shown that the distribution of body fat and particularly the deposition of lipids within non-adipose tissues drive insulin resistance. Indeed, ectopic lipid accumulation in tissues such as skeletal muscle and liver that are responsible for the majority of insulin stimulated glucose disposal drive the pathogenesis and progression of DMT2 (Shulman 2000; Moore et al., 2003; Goodpaster and Wolf 2004).

Prospective and retrospective human studies repeatedly found a protective role of mildly elevated blood bilirubin levels in DMT2 and a Mendelian Randomization study observed a causal risk reduction for DMT2 by mild hyperbilirubinaemia (Vítek 2012; Abbasi et al., 2015; Nano et al., 2016; Yang et al., 2019). Further, subjects with Gilbert´s syndrome (GS), an existing human model with constant mildly increased unconjugated blood bilirubin (UCB) levels have repeatedly been linked to a reduced fat mass, BMI and blood lipids (Wallner et al., 2013) and also exhibited a health beneficial glucose metabolic phenotype including a reduction in fasting glucose, insulin, C-peptide and insulin resistance (Mölzer et al., 2016; Khoei et al., 2018). This might suggest that mild hyperbilirubinaemia reduces the risk of DMT2 by protecting from disadvantageous, diabetes related changes in lipid metabolism. To date, data about bilirubin and its relation to ectopic lipid accumulation is scarce and limited to the liver, showing a decreased hepatic lipid content in mildly hyperbilirubinaemic mice (Hinds et al., 2017). However, experimental studies on lipid accumulation in skeletal muscle cells and hepatocytes, tissues that are prone to ectopic lipid deposition and simultaneously responsible for the majority of the insulin-stimulated glucose disposal are lacking. Therefore, this study aims for the first time to investigate the effect of UCB on intracellular lipid accumulation in C2C12 skeletal mouse muscle cells and HepG2 hepatoblastoma-derived cells.

MATERIALS AND METHODS

Cell Culture and Treatment

C2C12, murine myoblast (ATCC Cat# CRL-1772, RRID: CVCL_0188) and HepG2, human hepatoblastoma cells (ATCC Cat# HB-8065, RRID:CVCL_0027) purchased from LGC Standards GmbH were routinely cultured in high glucose (25 mM) containing DMEM (D1145, Sigma-Aldrich, US) with 10% FBS (10270-098, Gibco, Thermo Fisher, US), 4 mM L-glutamine (G7513, Sigma-Aldrich, US) and 1% penicillin/streptomycin (P0781, Sigma-Aldrich, US) at 37°C, 5% CO_2 under subconfluent conditions. Prior to experiments, HepG2 cells were grown to confluence for 2 days and confluent C2C12 cells were supplemented for another 6 days with 2% horse serum (10500-056, Gibco, Thermo Fisher, US) to allow differentiation into multinucleated myotubes. Cells were then treated with 0.5 mM or 1 mM BSA-coupled free fatty acids (FFA) (Svedberg et al., 1990) using palmitic acid (PA, P9767, Sigma-Aldrich, US), oleic acid (OA, O7501, Sigma-Aldrich, US) and linoleic acid (LA, L8134, Sigma-Aldrich, US) at a ratio of 2:1:2 which is consistent with the physiological FFA concentration and composition in human blood (Hodson et al., 2008). Simultaneously cells were exposed to 17.1 µM UCB (B412, Sigma-Aldrich, US), the threshold of the UCB blood concentration that characterizes GS (Wagner et al., 2018). In addition, 55 µM UCB was used for the principal lipid-based experiments to reflect the higher UCB concentrations in the liver compared to other tissues such as muscle (Zelenka et al., 2008) using an upper UCB concentration seen in sera of GS subjects. UCB was dissolved in DMSO (0.275% final DMSO concentration in all treatments) and then added to the BSA-containing media by shaking. Prior to the experiments, the solubility of UCB was routinely checked for possible UCB microprecipitate formation under the microscope. All experiments were performed in a darkened room. The control and reference for all treatments consisted of DMEM supplemented with 4 mM L-glutamine, 0.45 mM BSA and 0.275% DMSO. Cytotoxicity of the treatments was tested by MTT assay with 1×10^4 C2C12 and 0.5×10^5 HepG2 in 96 well plates. Formazan crystals were formed with 1 mg/ml MTT (M2128-1G, Sigma-Aldrich, US) in DMEM (37°C, 5% CO_2, 4 h), dissolved in 200 µL DMSO (37°C, 5% CO_2, 1 h) and measured at 485 nm using a plate reader (Fluorostar Optima, BMG Labtech, Germany).

Cellular Unconjugated Bilirubin Uptake

The cellular UCB uptake and the remaining UCB concentration in the incubation media were analyzed by HPLC. Briefly, 4×10^5 C2C12 and 4.5×10^6 HepG2 cells were seeded into 100 × 20 mm cell culture dishes for treatment (10 ml). After exposure to UCB for 0.5 and 5 h, the supernatant was immediately frozen at −80°C. The cells were put on ice, washed with 10 ml PBS (4°C), collected using a cell scraper (5 ml PBS 4°C) and centrifuged at 179 g, 4°C for 5min. The cell pellet was stored in 1 ml PBS (4°C) at −80°C after adding N_2.

The sample solutions for HPLC analysis consisted of 500 µL of UCB-non-treated media, 50 µL of UCB-treated media or 450 µL of cellular homogenate, disintegrated by ultrasound on ice as well as 50 µL of internal standard (5 mM mesobilirubin, Frontier Scientific, US) and the trace of BHT (antioxidant) (Sigma-Aldrich, US). UCB was extracted into 6 ml of methanol/chloroform/hexane (10/5/1 v/v/v) and concentrated into a small droplet of carbonate buffer (100 mM, pH 10) which was injected (50 µL) onto HPLC Agilent 1200 (CA, US) equipped with a diode-array detector. Bilirubin was then separated on the Luna C8 column (4.6 mm × 150 mm, 3 mM/100A, Phenomenex, CA, US). The mobile phase for the analysis contained methanol (450 g), water (300 g) and tetrabutylammonium hydroxide (7.5 ml) and its pH was adjusted by phosphoric acid (9–9.3). The signal was detected at 440 nm with 550 nm as the reference wavelength (Zelenka et al., 2008). The final amount of bilirubin in

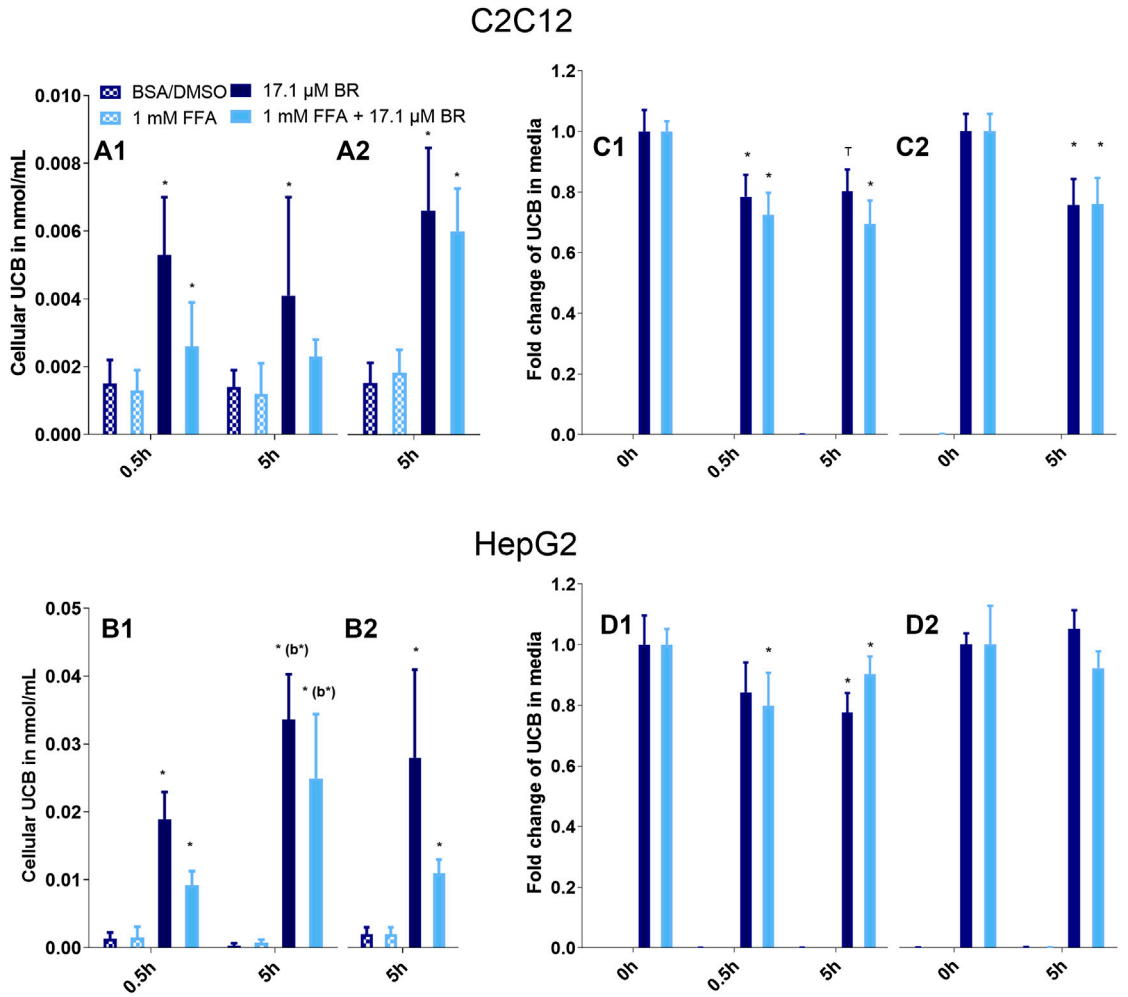

FIGURE 1 | UCB significantly increased the cellular UCB content of **(A)** C2C12 and **(B)** HepG2 cells and UCB concentration in the incubation media of **(C)** C2C12 and **(D)** HepG2 cells dropped significantly after 0.5 and 5 h. Cells were incubated under (**1**) hypoglycaemic conditions or (**2**) with glucose. Data are mean ± SD of four independent replicates, *$p \leq 0.05$ and T $p \leq 0.1$ compared to cells treated without UCB, compared to media prior incubation or compared to *b* = the preceding incubation time.

the medium was calculated as nmoL of UCB per mL of sample. The amount of protein in the cellular homogenate was measured by Bio-Rad Protein Assay (Bio-Rad, CA, US) using the microplate reader (Sunrise, Tecan, Austria). Concentration of bilirubin in cells was calculated as pmol of UCB per mg of protein.

Lipid Accumulation and Uptake

Lipid accumulation was measured by the Nile red (NR) assay that selectively stains intracellular lipids. Therefore, 1×10^4 C2C12 and 0.5×10^5 HepG2 cells were seeded into a black 96 well µclear plate (Greiner, Austria) for treatment (final volume 200 µL). Then cells were fixed with 3% paraformaldehyde (F1635, Sigma-Aldrich, US) (24°C, 20min), stained with NR (3.3 µg/ml in PBS, 37°C, 5% CO2, 2 h) and rinsed with 100 µL PBS. NR fluorescence was measured from the bottom of the plate at ex: 485 nm and em: 590 nm, the background fluorescence was subtracted prior staining and NR fluorescence was adjusted by Bradford protein content (B6916, Sigma-Aldrich, US). Images of intracellular lipids were obtained with the confocal microscope Leica TCS SPE including the inverse microscope DMi8 and analyzed using the LAS X 2.0.014332 software from Leica.

Lipid accumulation at a single cell level was measured using flow cytometry after NR staining. C2C12 (0.2×10^6) and HepG2 (0.6×10^6) cells were seeded into a six well plate (Greiner, Austria) with 2 ml treatment solution. Cells were harvested with accutase (A6964, Sigma-Aldrich, US), collected in a 5 ml Polystyrene Round-Bottom Tube (352058, Corning, US), centrifuged (179 g, 5 min), washed with 1 ml PBS (37°C) and incubated in the dark for 15 min with 1 ml 0.75 µg/ml NR in PBS. Cells were centrifuged and analyzed in 400 µL NR solution. 50.000 cells were measured in FL2 excluding cell debris using a four-channel FACS CaliburTM flow cytometer (BD, Europe).

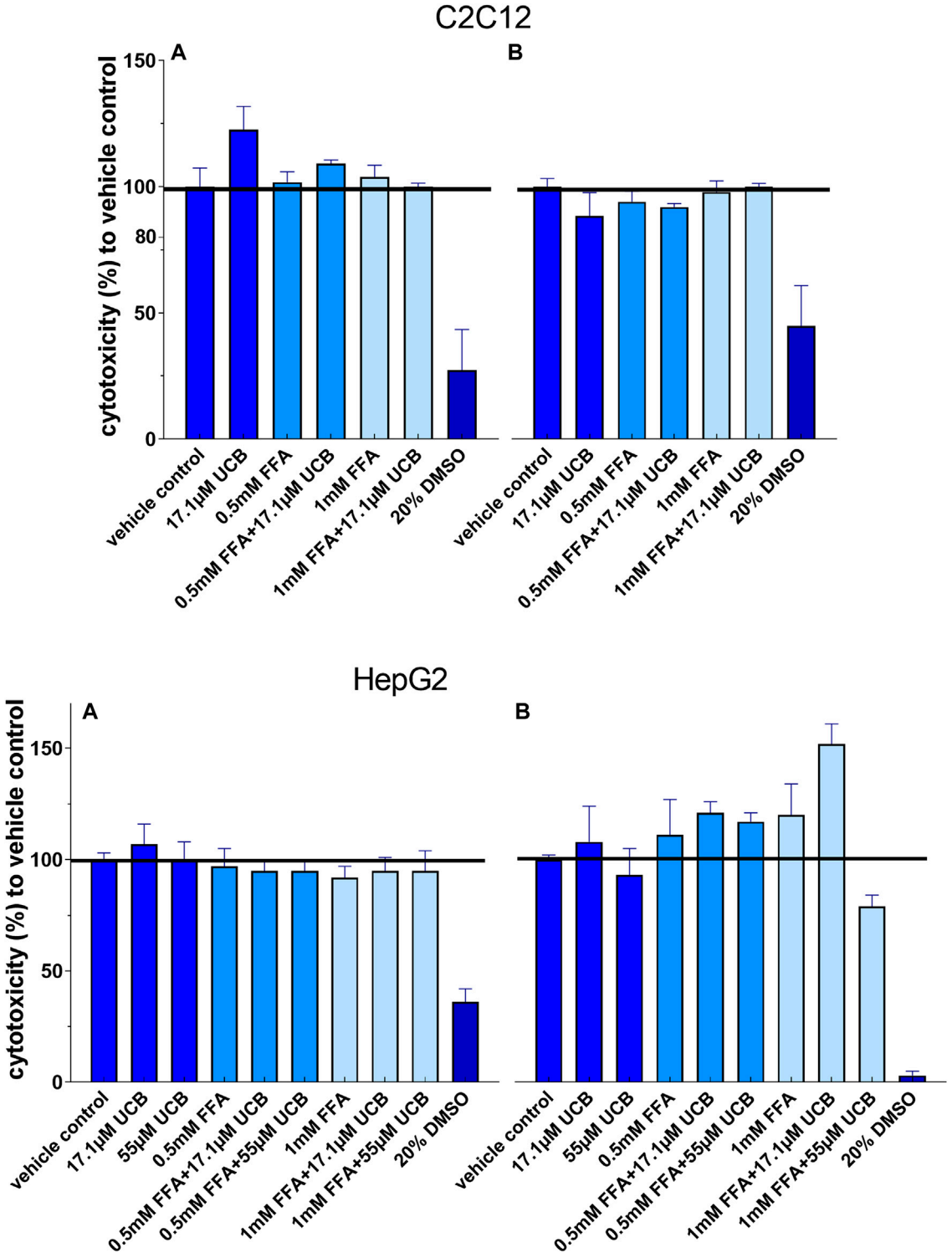

FIGURE 2 | None of the treatments was cytotoxic to C2C12 and HepG2 cells: Cells were incubated **(A)** at hypoglycaemic conditions for 12 h (C2C12) and 5 h (HepG2) or **(B)** with glucose for 24 h. Absorbance 485 nm, data are mean ± SD of at least n = 2 (each in sextuplicate).

The cellular lipid uptake was analyzed indirectly by measuring the remaining FFA concentrations from the incubation media by gas chromatography. The lipid extraction was performed according to modified protocols from Folch and Metcalfe (Folch et al., 1957; Metcalfe et al., 1966). First, the sample solution consisting of 2 ml incubation media and 100 µL of internal standard (2 mM stearic acid

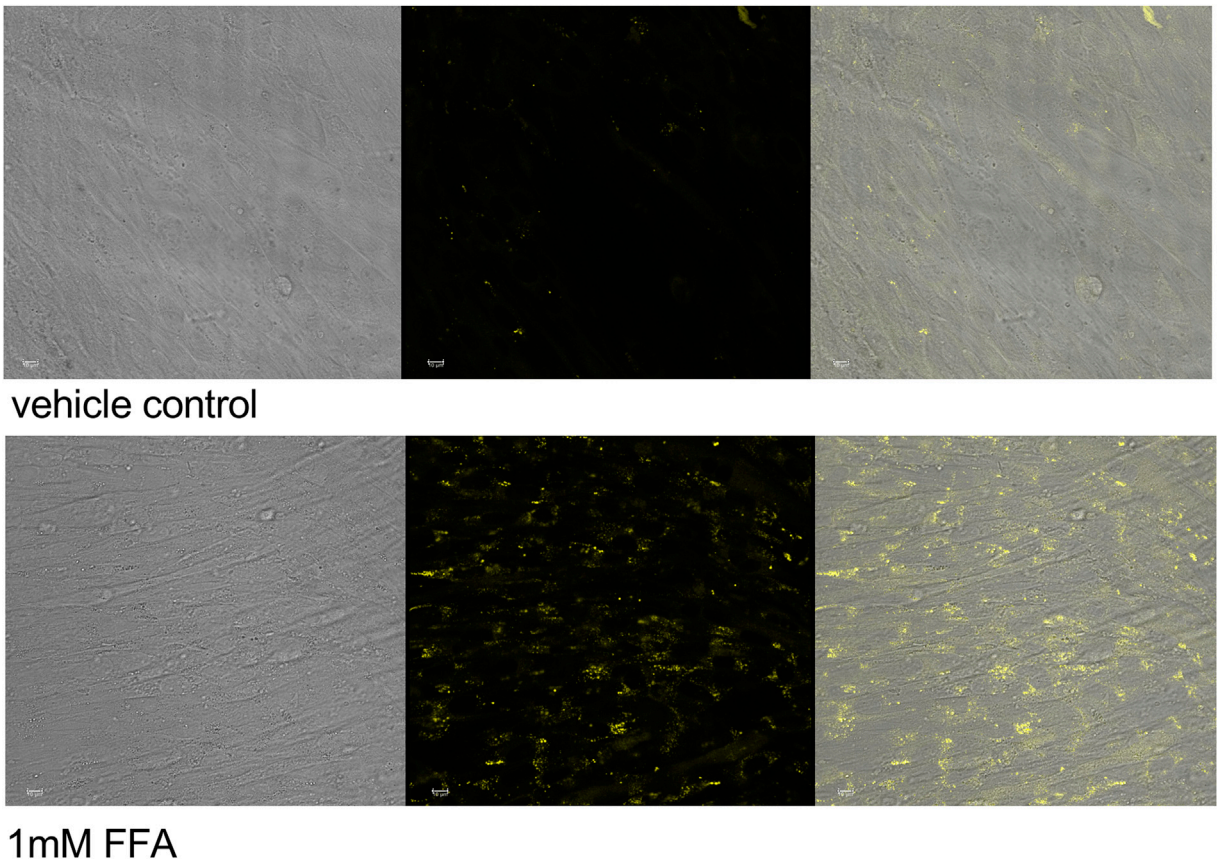

FIGURE 3 | Lipid accumulation and lipid droplet formation in C2C12 myotubes Cells were incubated for 5 h, stained with NR and viewed by fluorescence confocal microscopy. Transmission **(left)**, fluorescence **(center)** images and overlay **(right)**, ex: 488 nm, em: 509–560 nm, no adjustment of gain.

in isopropanol) was extracted twice using 10ml/5 ml chloroform/methanol (2:1) for 20 min on ice while vortexing twice for 0.5 min. The lipophilic phases were collected (2,000 g for 10 min), pooled and evaporated with N_2 (37°C). Then, saponification and methylation were performed using 1 ml methanolic NaOH (0.5 M NaOH and 0.27 mM BHT) and 1 ml BF3 (14% in methanol) respectively at 100°C for 5 min. The samples were immediately cooled on ice for 10 min and fatty acid methyl esters (FAMES) were collected twice in 2 and 1.5 ml hexane by shaking for 20 min. The hexane phases were pooled, evaporated with N_2 (37°C) and dissolved in 200 ml hexane. Samples were analyzed with an auto system gas chromatograph (Perkin Elmer Clarus 500, US), a Rtx-2330 30 m × 0.25 mm i.d. silica column, a flame ionization detector (270°C) and helium as a carrier gas. FAMES, 1 µL per sample were injected at an initial injector temperature of 250°C. The initial oven temperature was set to 90°C and was increased 3 times. First to 150°C by 13.0°C/min, then to 180°C by 2.9°C/min with an isothermal period of 5 min and finally to 230°C by 4.0°C/min and an isothermal period of 7 min. FFAs were quantified based on a six point calibration curve (200µg/ml-800 µg/ml) using a five component FAMES Mix Standard ME28 (8691.1, Carl Roth, Germany). The concentration of the FFAs was adjusted according to recovery of the internal standard.

Glucose Uptake Using [^{18}F]FDG

We analyzed the cellular uptake of 2-deoxy-2-[^{18}F]fluoro-D-glucose ([^{18}F]FDG), a radiolabeled glucose analogue, which allows to mimic glucose uptake. [^{18}F]FDG is GLUT-dependently transported into cells mainly via GLUT1 (Wiebe 2001) which is predominantly expressed in C2C12 (Calderhead et al., 1990) and HepG2 cells (Takanaga et al., 2008) and allows to monitor basal glucose uptake. [^{18}F]FDG uptake was investigated at a single time point and by real-time kinetic measurements over 60 min using LigandTracer® Yellow (Ridgeview Instruments, Sweden) (Balber et al., 2019). Briefly, C2C12 (0.16×10^6) and HepG2 (1.2×10^6) cells were seeded into a six well plate and incubated with 4 ml UCB treatment solution for 5 and 24 h followed by 2 h glucose starving in the presence of UCB. 150kBq of [^{18}F]FDG were added to the cells for 1 h at 37°C, subsequently, supernatant and cells (accutase) were collected and measured with a gamma counter (Wizard^2 ™ 3", PerkinElmer, USA) for 30 s. Results were expressed relative to a reference adding [^{18}F]FDG to PBS instead of treatment and cells. For the real-time kinetic [^{18}F]FDG measurements, 0.8×10^6 C2C12 and HepG2 cells were seeded onto one half of a 100 × 20 mm cell culture dish, the opposite side was used as a reference. Cells were treated analogue to the six well assay and cell associated radioactivity

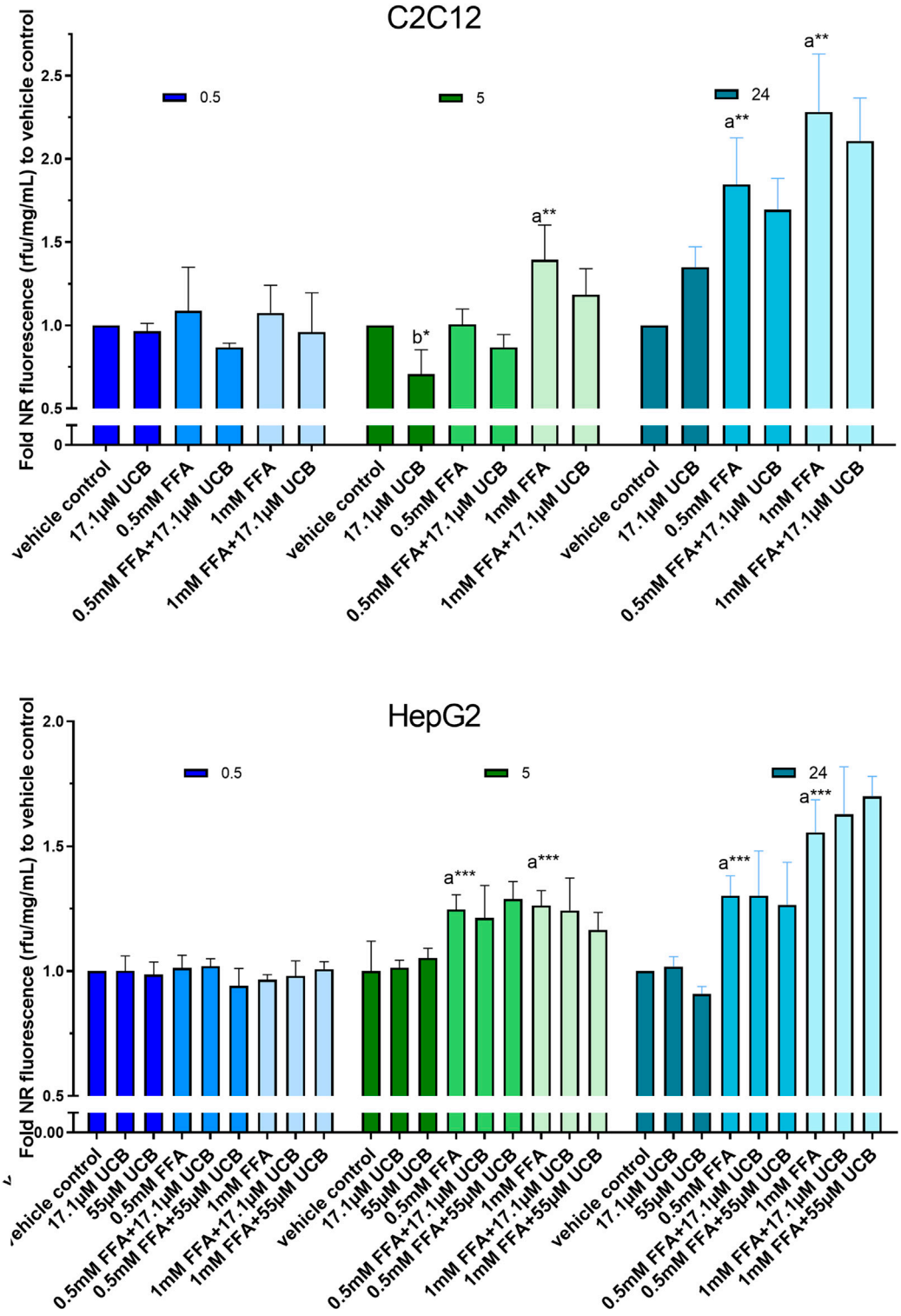

FIGURE 4 | UCB had no significant effect on lipid accumulation in C2C12 and HepG2 cells in the presence of glucose. Cells were exposed to treatments for 0.5, 5 and 24 h. NR fluorescence was adjusted by protein content (rfu/mg/mL) and compared to vehicle control. Data are mean ± SD of n = 3 (each in triplicate). Significant differences according to Bonferroni (***$p \leq 0.001$, **$p \leq 0.01$, *$p \leq 0.05$) of a = compared to vehicle control and b = UCB treated vs. untreated cells.

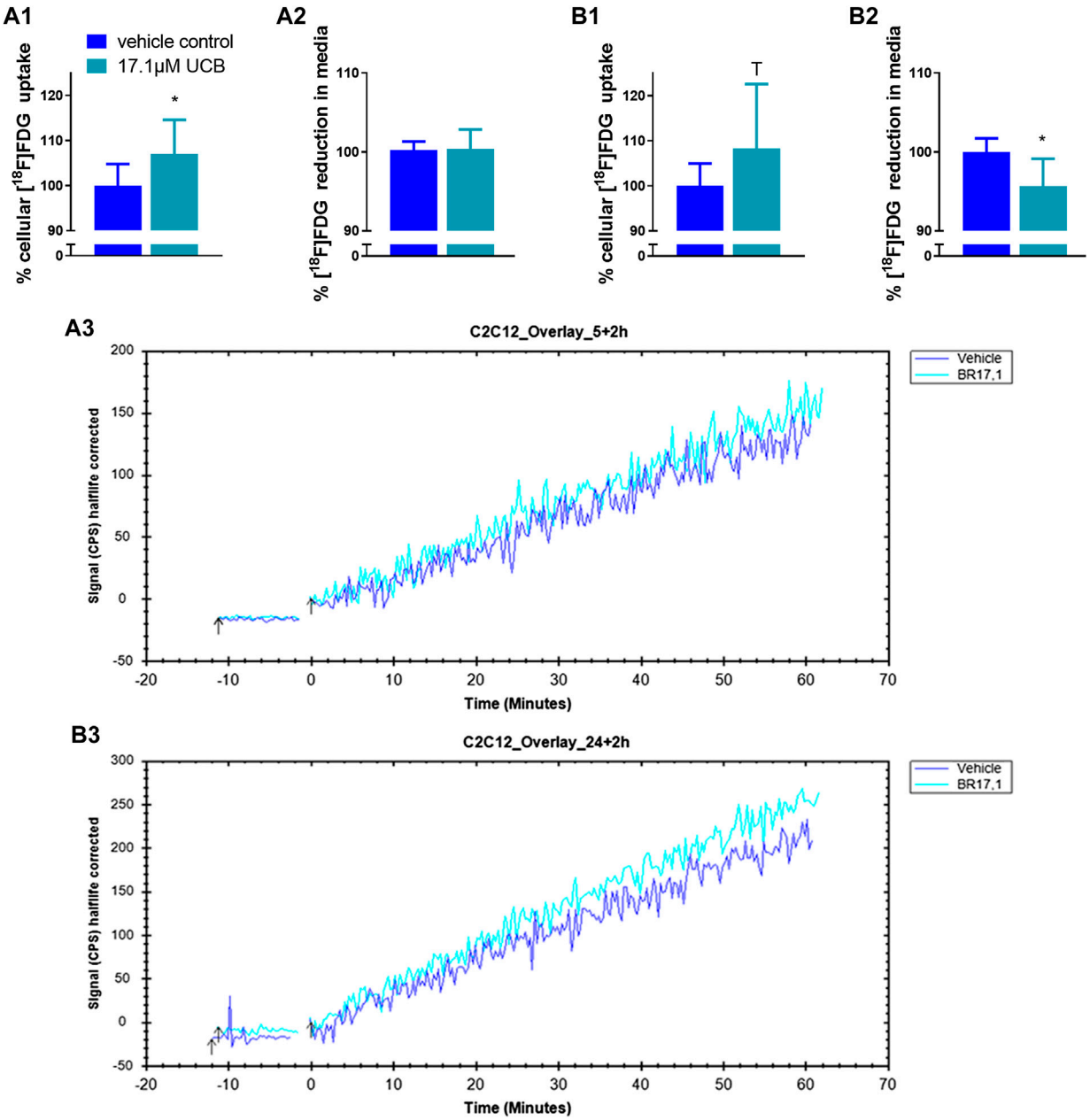

FIGURE 5 | UCB changed [^{18}F]FDG uptake in C2C12 cells. (**1**) Cellular uptake (%) of [^{18}F]FDG and (**2**) reduction (%) of [^{18}F]FDG in the supernatant determined by gamma counting after UCB incubation compared to vehicle control (100%) at **(A)** 5 h and **(B)** 24 h. Data are mean ± SD of n = 3 (each in triplicate). *$p \leq 0.05$, T $p \leq 0.1$. **(3)** Representative [^{18}F]FDG kinetics (0–60min) after UCB/vehicle treatment.

was measured starting directly after addition of [^{18}F]FDG for 60 min.

Statistical Analysis

Statistical analysis and calculations were completed using IBM SPSS 24 (IBM SPSS Statistics, RRID: SCR_019096). Data distribution was checked based on histograms and box plots. For parametric data One-Way ANOVA and for non-parametric data Kruskal-Wallis test were performed. Alpha was set at $p \leq 0.05$ according to Bonferroni.

RESULTS

Exogenous Administration of Unconjugated Bilirubin Increased the Intracellular Unconjugated Bilirubin Content and Was Not Cytotoxic

The exposure of C2C12 and HepG2 cells to 17.1 µM UCB significantly increased the intracellular UCB concentration after 0.5 and 5 h (**Figures 1A, B**). Consistently, the UCB concentration in the

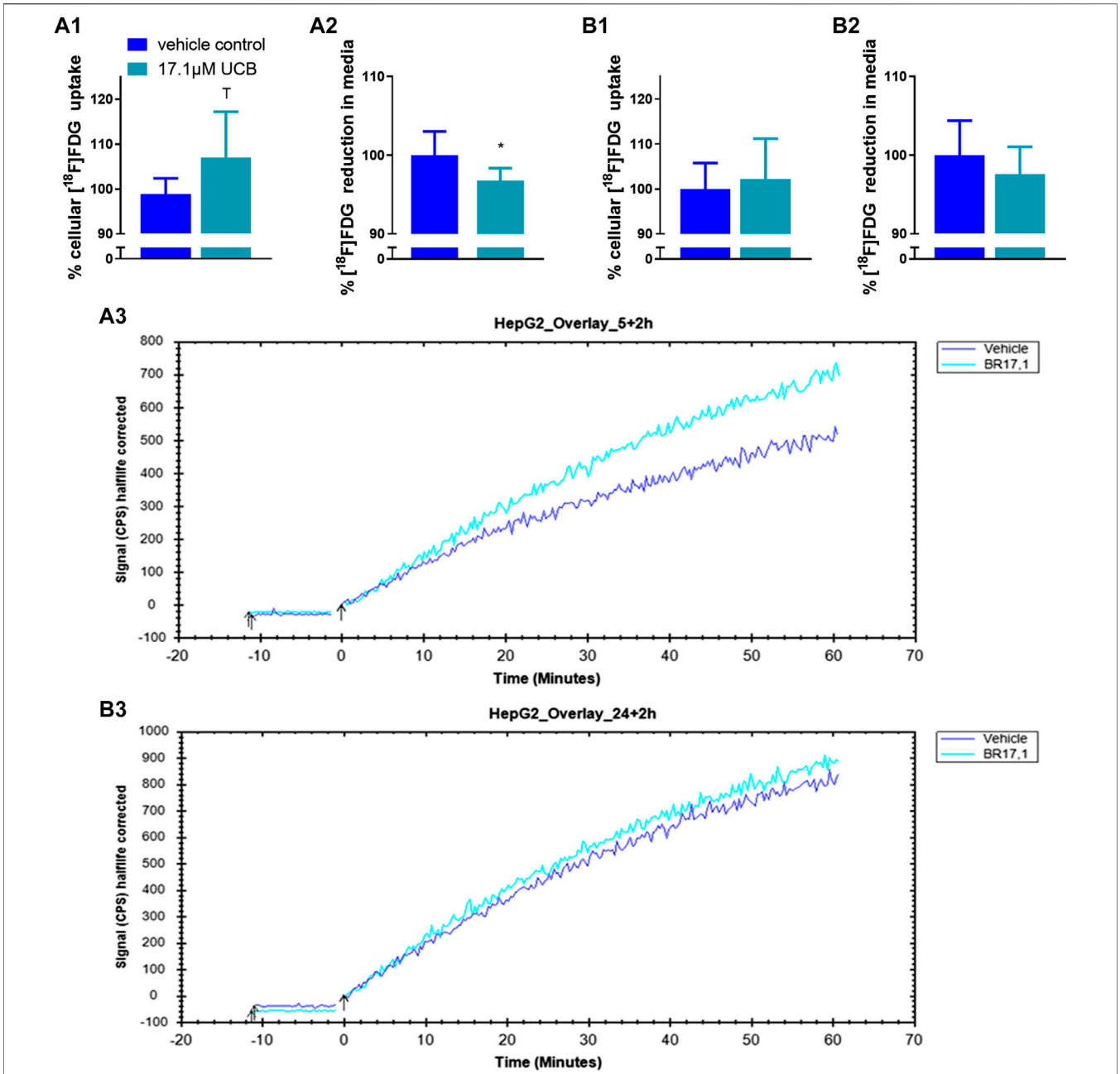

FIGURE 6 | UCB changed [^{18}F]FDG uptake in HepG2 cells. (**1**) Cellular uptake (%) of [^{18}F]FDG and (**2**) reduction (%) of [^{18}F]FDG in the supernatant determined by gamma counting after UCB incubation compared to vehicle control (100%) at **(A)** 5 h and **(B)** 24 h. Data are mean ± SD of n = 3 (each in triplicate). *$p \leq 0.05$, T $p \leq 0.1$. **(3)** Representative [^{18}F]FDG kinetics (0–60 min) after UCB/vehicle treatment.

incubation media of both cell lines decreased significantly after 0.5 and 5 h (**Figures 1C, D**). None of the treatments was cytotoxic to C2C12 or HepG2 cells compared to the vehicle control (**Figure 2**).

Unconjugated Bilirubin did Not Change Lipid Accumulation in C2C12 and HepG2 Cells in the Presence of Glucose

First, intracellular lipids and lipid droplet formation upon FFA incubation for 5 h were confirmed via confocal microscopy (**Figure 3**). In a second step, lipid accumulation was quantified via NR assay. C2C12 and HepG2 cells were exposed to 0.5mM and 1 mM FFAs which significantly increased the content of intracellular lipids in both cell lines compared to vehicle control after 5 and 24 h of incubation. However, the treatment with UCB did not significantly change the basal or the FFA-driven lipid accumulation in C2C12 and HepG2 cells. We only observed a reproducible but non-significant slight reduction in lipid accumulation in all FFA treatments in C2C12 cells (**Figure 4**). This was somewhat unexpected, however, the treatments were

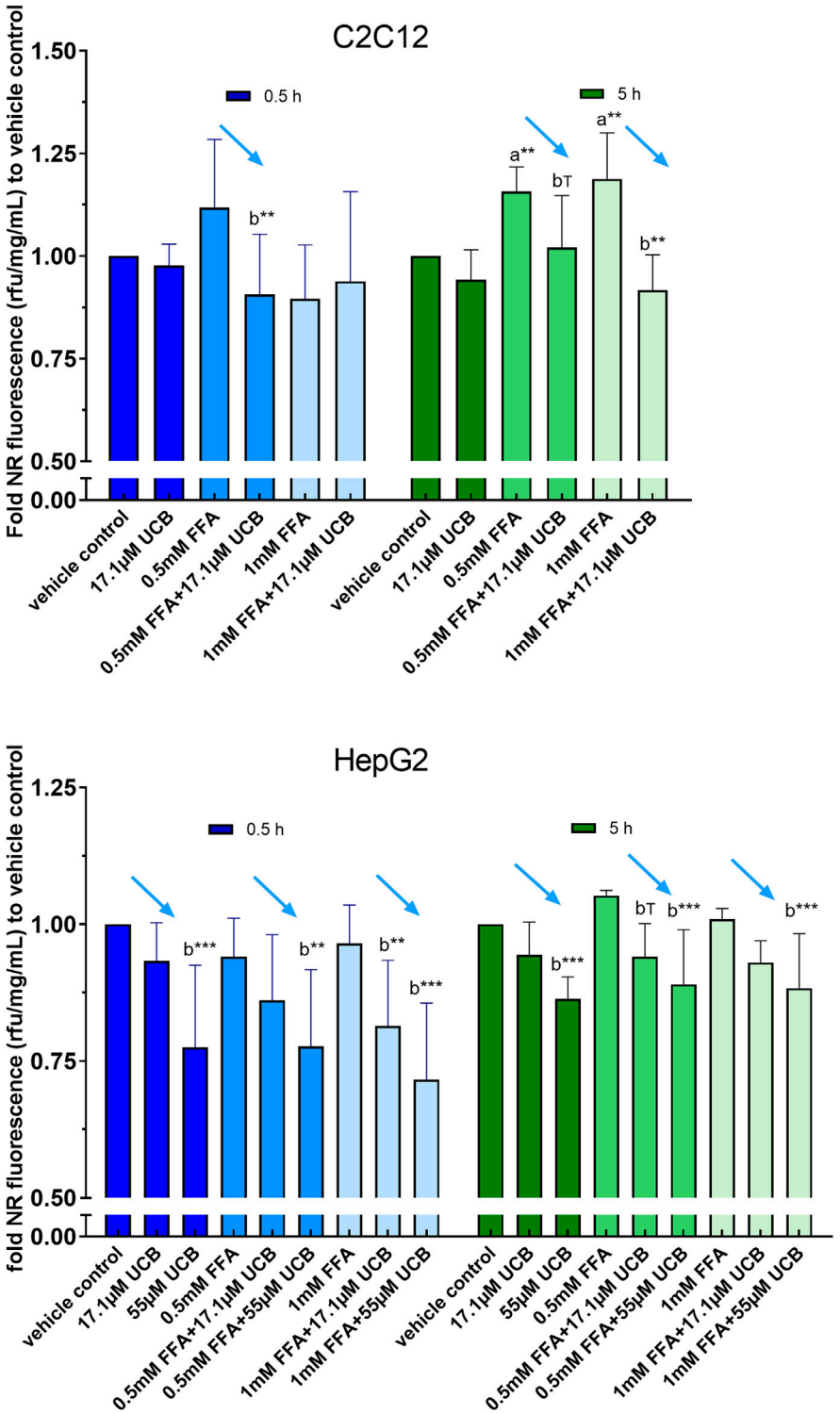

FIGURE 7 | UCB significantly decreased lipid accumulation in C2C12 and HepG2 cells at hypoglycaemic conditions. Cells were exposed to treatments for 0.5 and 5 h. NR fluorescence was adjusted by protein content (rfu/mg/mL) and compared to vehicle control. Data are mean ± SD of n = 3 (each in quadruplicate). ***$p \leq 0.001$, **$p \leq 0.01$, T $p \leq 0.1$ of *a* = compared to vehicle control and *b* = compared to UCB treated vs. untreated cells according to Bonferroni.

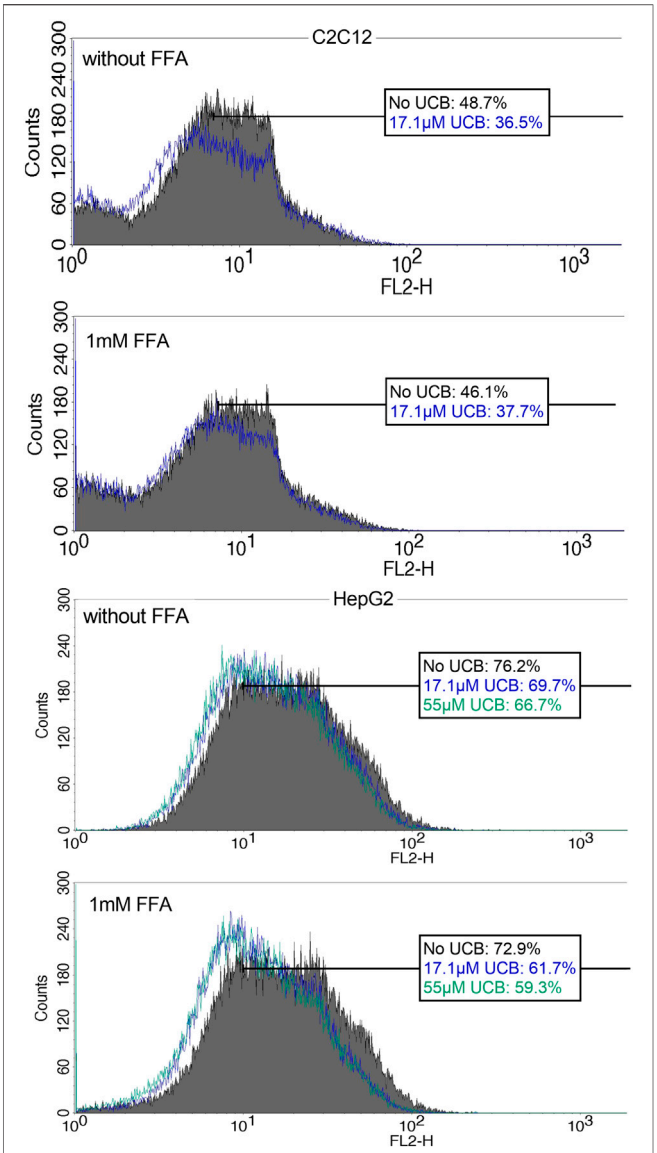

FIGURE 8 | NR fluorescence indicates a decreased lipid accumulation in C2C12 and HepG2 cells upon UCB exposure. Cells were exposed to the respective treatments for 5 h at hypoglycaemic conditions. Cell associated fluorescence was analyzed by flow cytometry (FL2). The blue (17.1 µM UCB) and green (55 µM UCB) histograms show a shift to the left toward decreased NR fluorescence intensity in comparison to the gray histogram (without UCB). The boxes show the % of cells with a higher NR fluorescence *intensity* after incubation without UCB, with 17.1 µM or 55 µM UCB. Representative histogram of **Supplementary Tables S2** of 50,000 cells.

performed in presence of glucose. It is known that skeletal muscle and liver preferentially rely on glucose as energy source upon sufficient glucose availability but switch from glucose toward lipids at hypoglycaemic conditions. Further, people with GS beside having health beneficial lipid blood and anthropometric biomarkers (Wallner et al., 2013; Wagner et al., 2015), also exhibited beneficial changes in glucose metabolism (decreased fasting glucose, insulin and C-peptide) in a more recent study (Mölzer et al., 2016). This could suggest that UCB has effects on the glycaemic response of our cell model masking or overriding changes in lipid metabolism. Therefore, we assessed in a next step basal glucose uptake into C2C12 and HepG2 cells upon UCB treatment by using the radiolabeled glucose analogue [^{18}F]FDG.

Unconjugated Bilirubin Mildly Increased Cellular [^{18}F]FDG Uptake in C2C12 and HepG2 Cells

In C2C12 cells, UCB significantly increased the intracellular [^{18}F]FDG content by 7% after 5 h and by 8% after 24 h (**Figures 5A1,B1**). Simultaneously, UCB lowered the [^{18}F]FDG concentration in the incubation media significantly by 4% after 24 h (**Figure 5B2**). Consistent with these observations, cell associated radioactivity derived from [^{18}F]FDG decay was slightly higher in real-time kinetic measurements after exposure of C2C12 cells to UCB for 5 and 24 h (**Figure 5A3,B3**). In HepG2 cells, UCB increased the intracellular [^{18}F]FDG content by trend by 8% and significantly reduced the [^{18}F]FDG concentration in the media by 7% only after 5 h of incubation (**Figure 6A1,A2**). In real-time kinetic measurements, cell associated radioactivity derived from [^{18}F]FDG decay was again higher after exposure to UCB for 5 and 24 h (**Figure 6A3,B3**).

Unconjugated Bilirubin Decreases Lipid Accumulation in C2C12 and HepG2 Cells at Hypoglycaemic Conditions

In a second batch of experiments the effect of UCB on lipid accumulation was investigated in the absence of glucose with incubation times up to 5 h. We decided to remove glucose 1) due to the effects of UCB on [^{18}F]FDG uptake in our cell model and 2) to challenge lipid catabolism since glucose deprived conditions stimulate the oxidative metabolism as shown in HepG2 cells (Weber et al., 2002). Prior to the lipid accumulation experiment, we confirmed that the UCB uptake was largely unaltered in the absence of glucose compared to glucose conditions and that the treatments were not cytotoxic to the cells (**Figures 1A1,B1,C1,D1,2A**).

C2C12 cells exposed to 17.1 µM UCB significantly decreased the intracellular lipid accumulation by up to 17% ($p \leq 0.01$) compared to vehicle controls at 0.5 and 5 h. In HepG2 cells, UCB significantly decreased lipid accumulation in all treatments after 0.5 and 5 h by up to 23% ($p \leq 0.001$), whereas 55 µM UCB further decreased the lipid accumulation compared to 17.1 µM UCB, indicating a dose dependency (**Figure 7**). Lipid accumulation was also decreased after UCB treatment in C2C12 and HepG2 cells using flow cytometry at hypoglycaemic conditions, in contrast to treatments with glucose (**Figures 7, 8**, **Supplementary Tables S1, S2**).

Unconjugated Bilirubin Slightly Increased Cellular Lipid Uptake

To exclude a decreased lipid uptake as a reason for the decreased lipid accumulation upon UCB treatment, we analyzed the remaining FFA concentrations in the incubation media by gas chromatography. UCB did not change the concentration of PA and OA in the treatments of C2C12 cells, which indicates that UCB did not change the cellular FFA uptake after 0.5 and 5 h under

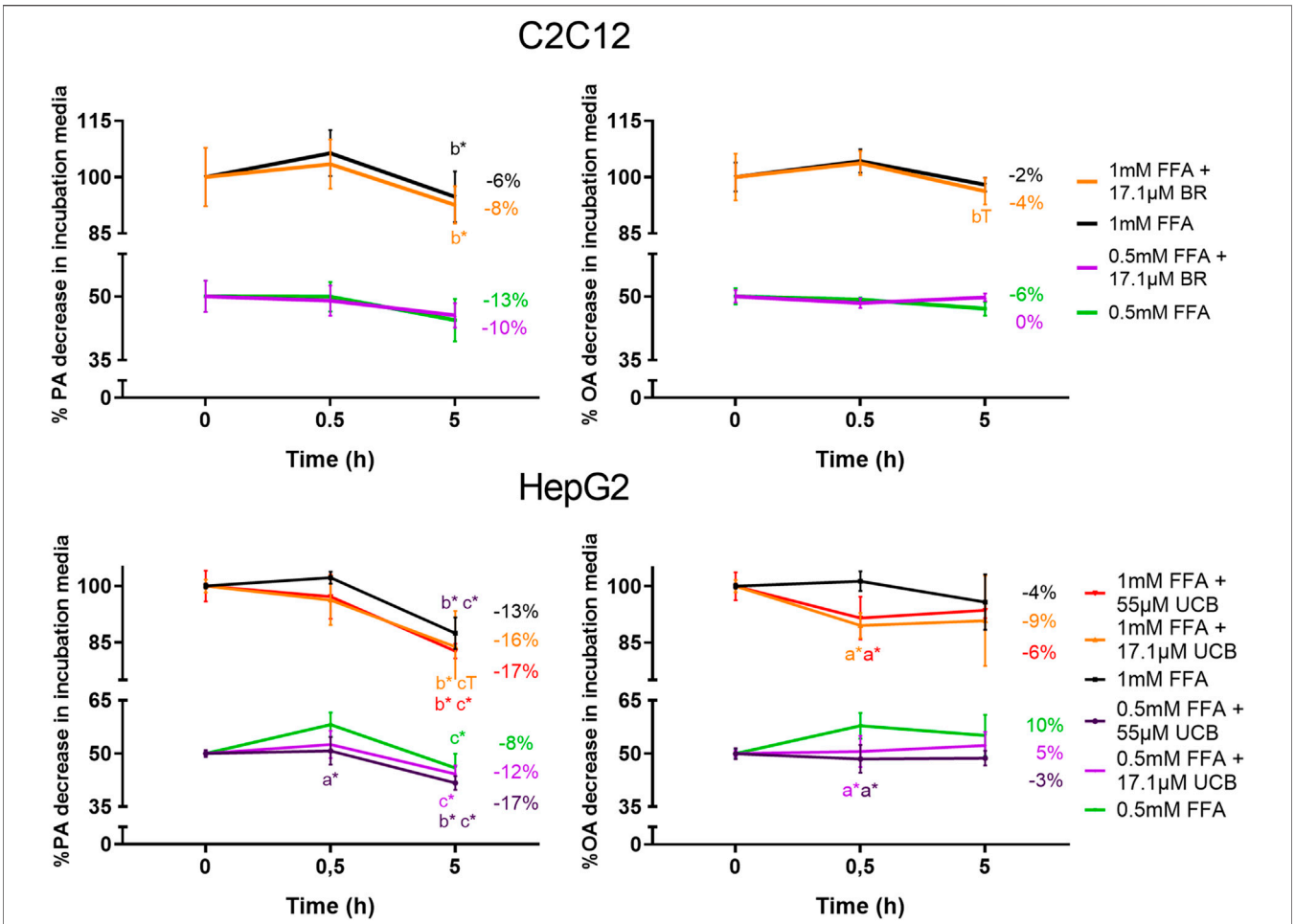

FIGURE 9 | UCB slightly increased the FFA uptake of HepG2 cells and did not significantly change the FFA uptake of C2C12 cells. Cells were exposed to the respective treatments for 0.5 and 5 h at hypoglycaemic conditions. The FFA uptake was assessed indirectly by measuring the PA and OA concentrations in the supernatant of both cell lines by gas chromatography. Data are mean ± SD of n = 3 (each in triplicate). *$p \leq 0.05$, T $p \leq 0.1$ of *a* = compared to UCB treated vs. untreated cells, of *b* = compared to the preceding incubation time and of *c* = compared to the initial concentration of the incubation media.

hypoglycaemic conditions (**Figure 9**). Further investigations of FFA uptake up to 12 h showed that UCB slightly reduced the FFA concentrations by approximately 5% in the incubation media of C2C12 cells at hypoglycaemic conditions in contrast to treatments with glucose (**Supplementary Figures S1, S2**). In detail, PA dropped by 22% and OA by 10% significantly in the presence of UCB and 1 mM FFA, whereas the drop of PA by 17% and OA by 6% was not significant in the absence of UCB (**Supplementary Figure S1**). In HepG2 cells, PA and OA concentrations were consistently lower ($\bar{x} \approx 8\%$) in the presence of UCB over all treatments and incubation times which was significant at 0.5 h. Thus, this data not only excludes that UCB decreases lipid uptake, it also indicates that UCB slightly increases FFA uptake in both cell lines.

DISCUSSION

Over the last decade, accumulating evidence has been suggesting a role of mildly elevated systemic bilirubin concentrations in the prevention of metabolic diseases and particularly in DMT2. Epidemiologic studies repeatedly showed a protection against DMT2 at mildly increased blood bilirubin levels (Abbasi et al., 2015; Nano et al., 2016). In case control studies, GS individuals with constant mild hyperbilirubinaemia revealed a reduced fat mass, BMI and blood lipids next to improved insulin resistance, fasting glucose, insulin and C-peptide levels (Wallner et al., 2013; Mölzer et al., 2016). Mice with diet induced obesity displayed an improved insulin sensitivity and reduced body weight and fat mass when treated with bilirubin (Dong et al., 2014; Liu et al., 2015; Gordon et al., 2020). Genetically modified mice with mild hyperbilirubinaemia are resistant to high fat diet induced hepatic steatosis, obesity, hypertriglyceridaemia, glucose intolerance, hyperglycaemia and hyperinsulinaemia due to an increased PPARα activity (Hinds et al., 2017). This evidence indicates that mildly elevated bilirubin levels have a strong DMT2-preventive potential via shaping an improved lipid phenotype. However, the mechanisms of this lipid based diabetes-protective capacity of UCB remain unclear.

The pathogenesis of DMT2 involves ectopic lipid accumulation in tissues that account for most of the insulin-dependent glucose disposal. Studies about the effects of UCB on ectopic lipids are rare, only focused on the liver and show a reduced diet induced hepatic lipid content in the presence of mild hyperbilirubinaemia in mice (Hinds et al., 2017). However, to date there are no experimental studies about the effect of UCB on ectopic lipid deposition in skeletal muscle cells and hepatocytes, cell types that are responsible for the majority of the whole-body glucose uptake. Thus, this study focused on the UCB driven changes of lipid accumulation in C2C12 skeletal muscle cells and HepG2 hepatocytes.

Mild hyperbilirubinaemic conditions (17.1 μM UCB) significantly decreased the intracellular lipid accumulation by up to 17% ($p \leq 0.01$) in C2C12 skeletal mouse muscle cells after 0.5 and 5 h. In HepG2 cells, exposure to mildly elevated UCB concentrations in the medium (17.1 and 55 μM) significantly reduced the lipid accumulation by up to 23% ($p \leq 0.001$) dose dependently and consistently in all FFA treatments at 0.5 and 5 h of incubation (**Figure 7**). Simultaneously, a slightly decreased PA and OA concentration in the UCB containing incubation media indicated that UCB slightly increased FFA uptake in both cell lines (**Figure 9**, **Supplementary Figure S1**). This confirms that the lipid content in the presence of UCB is reduced not based on a decrease in lipid uptake but rather due to a reduction of intracellular lipids. This strong UCB-induced reduction in lipid accumulation by up to 23% within a short incubation period of max. 5 h suggests that mild hyperbilirubinaemia might considerably lower ectopic lipid accumulation.

In contrast to these experiments that were performed with hypoglycaemic media, UCB had no effect on lipid accumulation or uptake in both cell lines when using glucose at a concentration recommended for both cell lines (**Figure 4**, **Supplementary Figure S2, Table S1**). Under hypoglycaemic fasting conditions PPARα and AMPK are activated to upregulate the cellular lipid oxidative metabolism and lipid uptake (Kersten et al., 1999; Towler and Hardie 2007). Thus while in the presence of glucose, our cell model might preferentially metabolize glucose for energy production, the hypoglycaemia activates PPARα and AMPK and forces the cells into the oxidative lipid metabolism. We and other groups showed that the beneficial metabolic profile in mild hyperbilirubinaemia might be PPARα and AMPK dependent (Mölzer et al., 2016; Gordon et al., 2020) and UCB was shown to be an activator of PPARα (Stec et al., 2016). This might explain the differences of lipid accumulation and lipid uptake at varying glucose concentrations (**Figures 4**, **7**, **9**, **Supplementary Figures S1, S2**) and suggests an increased lipid oxidation as a reason for the UCB-induced reduction of lipid accumulation in muscle and liver cells.

Mild hyperbilirubinaemia has been associated with beneficial changes in the blood glucose profile in humans and in mice (Liu et al., 2015, Mölzer et al., 2016, Hinds et al., 2017). Hence, it is possible that UCB increased the glycaemic response of our cell model in the presence of glucose masking or overriding changes in lipid metabolism. UCB had indeed effects on the [^{18}F]FDG uptake in both cell lines which was one of the main reasons why we continued our experiments under hypoglycaemic conditions. These experiments showed a slightly increased [^{18}F]FDG uptake in C2C12 and HepG2 cells, indicating a rise of mainly GLUT1-dependent glucose uptake (**Figures 5, 6**). To our knowledge there is no other data to date about the effects of UCB on glucose uptake. However, there is one study that observed a significantly increased GLUT4 expression in the muscle cell membrane of bilirubin-treated mice (Dong et al., 2014).

This is the first study that reports a UCB driven decrease in lipid accumulation in skeletal muscle and liver cells, types of tissues that are most affected by ectopic lipid deposition. Lipid accumulation was investigated at varying physiological FFA concentrations considering the level of glucose and was simultaneously compared to the lipid uptake. Another strength of this study was that the uptake and the intracellular presence of UCB was confirmed by HPLC (**Figure 1**). For future experiments it is necessary to explore the effect of UCB on ectopic lipid deposition in animals or humans to further support our results.

CONCLUSION

Our findings show that UCB considerably decreases lipid accumulation in skeletal muscle and liver cells by up to 23% within a short incubation time of max. 5 h. This suggests that mild hyperbilirubinaemia could lower ectopic lipid deposition, a major key element in the pathogenesis of DMT2. Thus, the reduced ectopic lipid accumulation in skeletal muscle and liver cells could indeed, at least partly explain the reduced insulin resistance in GS and the protective role of mild hyperbilirubinaemia in DMT2.

DATA AVAILABILITY STATEMENT

The raw data supporting the conclusion of this article will be made available by the authors, without undue reservation.

AUTHOR CONTRIBUTIONS

CAH designed the project and the experiments, performed experiments and statistical analysis and wrote the manuscript. K-HW. conceived the original idea, designed and supervised the project and revised the manuscript. E-MK and TB designed and performed glucose uptake experiments and revised manuscript. MM contributed his radiopharmaceutical expertize, supervised radioactive uptake experiments and revised the manuscript. RQ, YH, AK, JH, SS, PE, ES, JJ, and PV performed experiments. LV contributed the UCB uptake method and revised the manuscript. EH provided support with cell culture expertize and revised the manuscript. All authors provided final approval of the manuscript.

FUNDING

This project was funded by the Austrian Hochschuljubiläumsstiftung der Stadt Wien, the FWF Stand-Alone Project P 29608 and RVO VFN64165/2020 from the Czech Ministry of Health.

ACKNOWLEDGMENTS

We are grateful to Dr. Lukas Nics and Dr. Chrysoula Vraka for initiating the radiopharmaceutical project cooperation with the Department of Biomedical Imaging and Image-guided Therapy. We are also greatful to Daniel Schachner for his technical support with the confocal microscope and to George Mare for his technical support with the fatty acid extractions.

SUPPLEMENTARY MATERIAL

The Supplementary Material for this article can be found online at: https://www.frontiersin.org/articles/10.3389/fphar.2020.636533/full#supplementary-material.

REFERENCES

Abbasi, A., Deetman, P. E., Corpeleijn, E., Gansevoort, R. T., Gans, R. O., Hillege, H. L., et al. (2015). Bilirubin as a potential causal factor in type 2 diabetes risk: a Mendelian randomization study. *Diabetes.* 64 (4), 1459–1469. doi:10.2337/db14-0228

Balber, T., Benčurová, K., Kiefer, F. W., Kulterer, O. C., Klebermass, E. M., Egger, G., et al. (2019). *In vitro* radiopharmaceutical evidence for MCHR1 binding sites in murine Brown adipocytes. *Front. Endocrinol.* 10 (324), 324. doi:10.3389/fendo.2019.00324

Calderhead, D. M., Kitagawa, K., Lienhard, G. E., and Gould, G. W. (1990). Translocation of the brain-type glucose transporter largely accounts for insulin stimulation of glucose transport in BC3H-1 myocytes. *Biochem. J.* 269 (3), 597–601. doi:10.1042/bj2690597

Dong, H., Huang, H., Yun, X., Kim, D. S., Yue, Y., Wu, H., et al. 2014). Bilirubin increases insulin sensitivity in leptin-receptor deficient and diet-induced obese mice through suppression of ER stress and chronic inflammation. *Endocrinology*. 155 (3), 818–828. doi:10.1210/en.2013-1667

Folch, J., Lees, M., and Sloane Stanley, G. (1957). A simple method for the isolation and purification of total lipides from animal tissues. *J. Biol. Chem*. 226 (1), 497–509.

Goodpaster, B. H., and Wolf, D. (2004). Skeletal muscle lipid accumulation in obesity, insulin resistance, and type 2 diabetes. *Pediatr. Diabetes*. 5 (4), 219–226. doi:10.1111/j.1399-543X.2004.00071.x

Gordon, D. M., Neifer, K. L., Hamoud, A.-R. A., Hawk, C. F., Nestor-Kalinoski, A. L., Miruzzi, S. A., et al. (2020). Bilirubin remodels murine white adipose tissue by reshaping mitochondrial activity and the coregulator profile of peroxisome proliferator-activated receptor α. *J. Biol. Chem*. 295 (29), 9804–9822. doi:10.1074/jbc.RA120.013700

Hinds, T. D., Jr, Hosick, P. A., Chen, S., Tukey, R. H., Hankins, M. W., Nestor-Kalinoski, A., et al. (2017). Mice with hyperbilirubinemia due to Gilbert's syndrome polymorphism are resistant to hepatic steatosis by decreased serine 73 phosphorylation of PPARα. *Am. J. Physiol. Endocrinol. Metab*. 312 (4), E244–E252. doi:10.1152/ajpendo.00396.2016

Hodson, L., Skeaff, C. M., and Fielding, B. A. (2008). Fatty acid composition of adipose tissue and blood in humans and its use as a biomarker of dietary intake. *Prog. Lipid Res*. 47 (5), 348–380. doi:10.1016/j.plipres.2008.03.003

International Diabetes Federation (2019). *IDF diabetes atlas*. 9th Edn. Available at: https://www.diabetesatlas.org/en/resources/ (Accessed October 10, 2020).

Kersten, S., Seydoux, J., Peters, J. M., Gonzalez, F. J., Desvergne, B., and Wahli, W. (1999). Peroxisome proliferator-activated receptor alpha mediates the adaptive response to fasting. *J. Clin. Invest*. 103 (11), 1489–1498. doi:10.1172/JCI6223

Khoei, N. S., Grindel, A., Wallner, M., Mölzer, C., Doberer, D., Marculescu, R., et al. (2018). Mild hyperbilirubinaemia as an endogenous mitigator of overweight and obesity: implications for improved metabolic health. *Atherosclerosis*. 269, 306–311. doi:10.1016/j.atherosclerosis.2017.12.021

Liu, J., Dong, H., Zhang, Y., Cao, M., Song, L., Pan, Q., et al. (2015). Bilirubin increases insulin sensitivity by regulating cholesterol metabolism, adipokines and PPARγ levels. *Sci. Rep*. 5 (1), 9886. doi:10.1038/srep09886

Metcalfe, L., Schmitz, A., and Pelka, J. (1966). Rapid preparation of fatty acid esters from lipids for gas chromatographic analysis. *Anal. Chem*. 38 (3), 514–515. doi:10.1021/ac60235a044

Mölzer, C., Wallner, M., Kern, C., Tosevska, A., Schwarz, U., Zadnikar, R., et al. (2016). Features of an altered AMPK metabolic pathway in Gilbert's Syndrome, and its role in metabolic health. *Sci. Rep*. 6, 30051. doi:10.1038/srep30051

Moore, M. C., Cherrington, A. D., and Wasserman, D. H. (2003). Regulation of hepatic and peripheral glucose disposal. *Best Pract. Res. Clin. Endocrinol. Metabol*. 17 (3), 343–364. doi:10.1016/s1521-690x(03)00036-8

Nano, J., Muka, T., Cepeda, M., Voortman, T., Dhana, K., Brahimaj, A., et al. (2016). Association of circulating total bilirubin with the metabolic syndrome and type 2 diabetes: a systematic review and meta-analysis of observational evidence. *Diabetes Metab*. 42 (6), 389–397. doi:10.1016/j.diabet.2016.06.002

Shulman, G. I. (2000). Cellular mechanisms of insulin resistance. *J. Clin. Invest*. 106 (2), 171–176. doi:10.1172/JCI10583

Stec, D. E., John, K., Trabbic, C. J., Luniwal, A., Hankins, M. W., Baum, J., et al. (2016). Bilirubin binding to PPARα inhibits lipid accumulation. *PLoS One*. 11 (4), e0153427. doi:10.1371/journal.pone.0153427

Svedberg, J., Björntorp, P., Smith, U., and Lönnroth, P. (1990). Free-fatty acid inhibition of insulin binding, degradation, and action in isolated rat hepatocytes. *Diabetes*. 39 (5), 570–574. doi:10.2337/diab.39.5.570

Takanaga, H., Chaudhuri, B., and Frommer, W. B. (2008). GLUT1 and GLUT9 as major contributors to glucose influx in HepG2 cells identified by a high sensitivity intramolecular FRET glucose sensor. *Biochim. Biophys. Acta*. 1778 (4), 1091–1099. doi:10.1016/j.bbamem.2007.11.015

Towler, M. C., and Hardie, D. G. (2007). AMP-activated protein kinase in metabolic control and insulin signaling. *Circ. Res*. 100 (3), 328–341. doi:10.1161/01.RES.0000256090.42690.05

Vítek, L. (2012). The role of bilirubin in diabetes, metabolic syndrome, and cardiovascular diseases. *Front. Pharmacol*. 3, 55. doi:10.3389/fphar.2012.00055

Wagner, K. H., Shiels, R. G., Lang, C. A., Seyed Khoei, N., and Bulmer, A. C. (2018). Diagnostic criteria and contributors to Gilbert's syndrome, *Crit. Rev. Clin. Lab Sci*. 55 (2), 129–139. doi:10.1080/10408363.2018.1428526

Wagner, K. H., Wallner, M., Mölzer, C., Gazzin, S., Bulmer, A. C., Tiribelli, C., et al. (2015). Looking to the horizon: the role of bilirubin in the development and prevention of age-related chronic diseases. *Clin. Sci.* 129 (1), 1–25. doi:10.1042/CS20140566

Wallner, M., Marculescu, R., Doberer, D., Wolzt, M., Wagner, O., Vitek, L., et al. (2013). Protection from age-related increase in lipid biomarkers and inflammation contributes to cardiovascular protection in Gilbert's syndrome. *Clin. Sci.* 125 (5), 257–264. doi:10.1042/CS20120661

Weber, K., Ridderskamp, D., Alfert, M., Hoyer, S., and Wiesner, R. J. (2002). Cultivation in glucose-deprived medium stimulates mitochondrial biogenesis and oxidative metabolism in HepG2 hepatoma cells. *Biol. Chem*. 383 (2), 283–290. doi:10.1515/BC.2002.030

Wiebe, L. I. (2001). FDG metabolism: quaecumque sunt vera. *J. Nucl. Med*. 42 (11), 1679–1681.

Yang, M., Ni, C., Chang, B., Jiang, Z., Zhu, Y., Tang, Y., et al. (2019). Association between serum total bilirubin levels and the risk of type 2 diabetes mellitus. *Diabetes Res. Clin. Pract*. 152, 23–28. doi:10.1016/j.diabres.2019.04.033

Zelenka, J., Lenícek, M., Muchová, L., Jirsa, M., Kudla, M., Balaž, P., et al. (2008). Highly sensitive method for quantitative determination of bilirubin in biological fluids and tissues. *J. Chromatogr. B.* 867 (1), 37–42. doi:10.1016/j.jchromb.2008.03.005

Conflict of Interest: The authors declare that the research was conducted in the absence of any commercial or financial relationships that could be construed as a potential conflict of interest.

frontiers in Pharmacology

ORIGINAL RESEARCH
published: 08 March 2021
doi: 10.3389/fphar.2021.586715

Mitochondrial Function, Fatty Acid Metabolism, and Body Composition in the Hyperbilirubinemic Gunn Rat

*Josif Vidimce[1], Johara Pillay[1], Nirajan Shrestha[1], Lan-feng Dong[1], Jiri Neuzil[1,2], Karl-Heinz Wagner[3], Olivia Jane Holland[1] and Andrew Cameron Bulmer[1]**

[1]School of Medical Science, Griffith University, Gold Coast, QLD, Australia, [2]Institute of Biotechnology, Czech Academy of Sciences, Prague, Czechia, [3]Department of Nutritional Sciences and Research Platform Active Ageing, University of Vienna, Vienna, Austria

Background: Circulating bilirubin is associated with reduced adiposity in human and animal studies. A possible explanation is provided by *in vitro* data that demonstrates that bilirubin inhibits mitochondrial function and decreases efficient energy production. However, it remains unclear whether hyperbilirubinemic animals have similar perturbed mitochondrial function and whether this is important for regulation of energy homeostasis.

Aim: To investigate the impact of unconjugated hyperbilirubinemia on body composition, and mitochondrial function in hepatic tissue and skeletal muscle.

Materials and Methods: 1) Food intake and bodyweight gain of 14-week old hyperbilirubinemic Gunn (n = 19) and normobilirubinemic littermate (control; n = 19) rats were measured over a 17-day period. 2) Body composition was determined using dual-energy X-ray absorptiometry and by measuring organ and skeletal muscle masses. 3) Mitochondrial function was assessed using high-resolution respirometry of homogenized liver and intact permeabilized extensor digitorum longus and soleus fibers. 4) Liver tissue was flash frozen for later gene (qPCR), protein (Western Blot and citrate synthase activity) and lipid analysis.

Results: Female hyperbilirubinemic rats had significantly reduced fat mass (Gunn: 9.94 ± 5.35 vs. Control: 16.6 ± 6.90 g, $p < 0.05$) and hepatic triglyceride concentration (Gunn: 2.39 ± 0.92 vs. Control: 4.65 ± 1.67 mg g^{-1}, $p < 0.01$) compared to normobilirubinemic controls. Furthermore, hyperbilirubinemic rats consumed fewer calories daily ($p < 0.01$) and were less energetically efficient (Gunn: 8.09 ± 5.75 vs. Control: 14.9 ± 5.10 g bodyweight $kcal^{-1}$, $p < 0.05$). Hepatic mitochondria of hyperbilirubinemic rats demonstrated increased flux control ratio (FCR) via complex I and II (CI+II) (Gunn: 0.78 ± 0.16 vs. Control: 0.62 ± 0.09, $p < 0.05$). Similarly, exogenous addition of 31.3 or 62.5 μM unconjugated bilirubin to control liver homogenates significantly increased CI+II FCR ($p < 0.05$). Hepatic *PGC-1α* gene expression was significantly increased in hyperbilirubinemic females while *FGF21* and *ACOX1* was significantly greater in male hyperbilirubinemic rats ($p < 0.05$). Finally, hepatic mitochondrial complex IV subunit 1 protein expression was significantly increased in female hyperbilirubinemic rats ($p < 0.01$).

OPEN ACCESS

Edited by:
Barbara Wegiel,
Beth Israel Deaconess Medical Center and Harvard Medical School, United States

Reviewed by:
Eugenio Barone,
Sapienza University of Rome, Italy
Enzo Nisoli,
University of Milan, Italy

***Correspondence:**
Andrew Cameron Bulmer
a.bulmer@griffith.edu.au

Specialty section:
This article was submitted to Experimental Pharmacology and Drug Discovery, a section of the journal Frontiers in Pharmacology

Received: 23 July 2020
Accepted: 11 January 2021
Published: 08 March 2021

Citation:
Vidimce J, Pillay J, Shrestha N, Dong L, Neuzil J, Wagner K-H, Holland OJ and Bulmer AC (2021) Mitochondrial Function, Fatty Acid Metabolism, and Body Composition in the Hyperbilirubinemic Gunn Rat. Front. Pharmacol. 12:586715. doi: 10.3389/fphar.2021.586715

Conclusions: This is the first study to comprehensively assess body composition, fat metabolism, and mitochondrial function in hyperbilirubinemic rats. Our findings show that hyperbilirubinemia is associated with reduced fat mass, and increased hepatic mitochondrial biogenesis, specifically in female animals, suggesting a dual role of elevated bilirubin and reduced UGT1A1 function on adiposity and body composition.

Keywords: lipids, respiration, metabolism, mitochondria, Gunn rat, triglycerides, unconjugated bilirubin (UCB), hyperbilirubinemia

INTRODUCTION

Bilirubin is a breakdown product of heme catabolism and it is used clinically to assist in diagnosis of liver dysfunction and blood disorders (Fevery, 2008). A central dogma asserts that unconjugated bilirubin (UCB) is toxic due to its potential to accumulate in specific regions of the brain, and induce oxidative stress, mitochondrial dysfunction, and apoptosis (Rodrigues et al., 2002a; Watchko and Tiribelli, 2013). At physiological pH, UCB has strong intramolecular hydrogen bonding that renders it hydrophobic, consequently, in the circulation UCB is solubilized by strong binding to albumin (Rolf and Stern, 1980; Fevery, 2008). Unbound UCB has low aqueous solubility (<70 nM) (Ostrow et al., 2004) and accumulates within hydrophobic regions of lipid membranes, including the mitochondria (Mustafa and King, 1970; Ostrow et al., 2004).

UCB affects mitochondria by increasing permeability, oxidative damage, and uncoupling of the mitochondrial membrane potential (Ostrow et al., 2004; Watchko and Tiribelli, 2013). Rodrigues et al., (2000) demonstrated that incubation of primary rat neurons with UCB induced mitochondrial swelling and membrane permeability, release of cytochrome c, and apoptosis. Spin-labelling investigations have reported that UCB-induced mitochondrial membrane permeability and lipid peroxidation is related to superficial association of UCB to phospholipid bilayers of the inner mitochondrial membrane (Zucker et al., 1992; Rodrigues et al., 2002b). Together, these findings corroborate the prevailing notion that UCB perturbs membrane dynamics by interacting with lipids (Zucker et al., 1992; Rodrigues et al., 2002b).

Skeletal muscle and liver are the major determinants of basal metabolic rate (BMR) contributing to more than 50% of total BMR in rodents (Kummitha et al., 2014). Under physiological conditions, dietary substrates are oxidized primarily by the mitochondrial electron transport chain (ETC) to produce energy in the form of ATP. However, a fraction of this energy produces heat instead of ATP due to a benign rate of proton leak across the inner mitochondrial membrane, known as (unregulated) mitochondrial uncoupling (Divakaruni and Brand, 2011). Therefore, severe uncoupling of the mitochondrial membrane inhibits ATP synthesis and leads to cell death (Busiello et al., 2015). Interestingly, mild uncoupling induced experimentally does not affect ATP synthesis and may help with weight loss and prevention of chronic diseases such as Type 2 Diabetes Mellitus (T2DM) (Busiello et al., 2015). Transgenic mice overexpressing uncoupling proteins such as UCP1 and UCP3 are resistant against obesity and show improved insulin sensitivity when fed a high fat diet (HFD) (Costford et al., 2006; Keipert et al., 2013; Ost et al., 2014).

At high concentrations, UCB uncouples the mitochondrial membrane (Ostrow et al., 2004; Watchko and Tiribelli, 2013). However, whether mildly elevated concentrations of UCB affect mitochondrial function remains unknown and could provide a rational explanation for improved body composition and reduced risk of metabolic syndrome in individuals with increased UCB concentrations (Vitek and Ostrow, 2009; Vaz et al., 2010; Vítek, 2012; Pennell et al., 2019). Interestingly, individuals with Gilbert's syndrome (GS) who have mildly elevated UCB concentrations (17–80 μM) are protected against cardiovascular diseases (CVDs) and have reduced body mass index (BMI) compared to individuals with normal UCB levels (<17 μM serum UCB) (Bulmer et al., 2013; Bulmer et al., 2018). Generally, the protection of GS individuals from chronic disease is attributed to the antioxidant properties of UCB (Stocker et al., 1987; Neuzil and Stocker, 1994; Bakrania et al., 2016; Bulmer et al., 2018; Shiels et al., 2019). However, few studies have explored the impact of mildly elevated concentrations of UCB on body composition and fewer still have investigated its effect on cellular and mitochondrial metabolism *in vivo* (Liu et al., 2015; Stec et al., 2016; Zelenka et al., 2016; Seyed Khoei et al., 2018).

Gunn rats have a congenital unconjugated hyperbilirubinemia in the upper range of GS due to the absence of functional UDP-glucuronosyltransferase 1A1 (UGT1A1), which leads to impaired conjugation and elimination of UCB. Therefore, these animals serve as a relevant model to study the effects of unconjugated hyperbilirubinemia on body composition and metabolism. In the present study, we investigated whether Gunn rats had reduced bodyweight, altered body composition, and impaired skeletal muscle and hepatic mitochondrial function compared to normobilirubinemic littermate rats.

MATERIALS AND METHODS

Materials

All consumables were obtained from Sigma-Aldrich (Australia) unless otherwise stated. Chemicals for high-resolution respirometry were obtained from manufacturers as recommended by Oroboros Instruments (Fontana-Ayoub et al., 2016).

Synthesis of Sodium Bilirubinate

Sodium bilirubinate was synthesized in order to make UCB soluble in respiration buffer (Mir06: 280 U mL^{-1} catalase,

0.5 mM EGTA, 3 mM $MgCl_2{\cdot}6H_2O$, 60 mM K-lactobionate, 20 mM taurine, 10 mM KH_2PO_4, 20 mM HEPES, 110 mM sucrose, and 1 g L^{-1} bovine serum albumin (BSA), pH 7.1). 2.1 M equivalents of NaOH solution (1.5 mg ml^{-1} in ethanol) was added to UCB. The mixture was vortexed vigorously and diluted 10-fold with ethanol and evaporated in the dark under vacuum in a rotary evaporator (Maxivac; Labogene, Australia) at 21°C for 4 h. The UCB content of the powder was determined to be >99% of the commercially supplied standard, using high-performance liquid chromatography photodiode array (HPLC: PDA) as previously published (Bulmer et al., 2011).

Animals

Breeding pairs of heterozygote and homozygote Gunn rats on a Wistar background were imported from the Rat Research and Resource Centre (Columbia, MO, United States) and bred to produce both hyperbilirubinemic (homozygote) and normobilirubinemic (heterozygote) Gunn rats. The Gunn rat phenotype was determined based on the presence of jaundice in the first 3 days after birth. Jaundiced Gunn rats were tagged, and their phenotype was confirmed by measuring TBIL concentrations. From herein, animals expressing hyperbilirubinemia are phenotypically defined as "Gunn" rats while littermates with normal bilirubin levels are termed as "normobilirubinemic controls". Animals were housed in the G26 animal house facility at Griffith University (Gold Coast, Australia) at constant temperature (20°C) and humidity (60%), with a 12 h light: dark cycle. All animals were provided a standard rodent diet (18% Protein Rodent Diet, 18% protein, 6.2% fat; TEKLAD Standard Global, United States) and water *ad libitum*. All procedures were approved by the Griffith University Animal Ethics Research Committee (MSC/02/17/AEC) prior to experimentation.

Experimental Protocol

Thirty six age-matched rats (~10 weeks of age; Cohort 1) were separated into four groups based on sex and phenotype: Gunn female (n = 10), Control female (n = 9), Gunn male (n = 9), Control male (n = 8). Gunn animals were hyperbilirubinemic and were compared to normobilirubinemic controls of the same sex. These animals were gradually acclimatized in metabolic cages for 2, 5, then 24 h before entering the protocol. Acclimatized animals entered a 17-days protocol (Day 0–16) and were housed in metabolic cages three times for a period of 24 h at a time, at Day 0, 11, and 15 (11–13 weeks of age) of the protocol. In the metabolic cages, food and water remained available *ad libitum* and was weighed before and after the animal was housed to determine daily energy intake. Bodyweight was recorded every 2 days from Day 0 in addition to before and after each metabolic cage day. To control for future therapeutic interventions additional procedures (i.p. saline and p.o. water) were conducted as described in **Supplementary Material** (see *Additional procedures*). Energy efficiency was calculated by subtracting the final bodyweight at Day 16 from the initial bodyweight at Day 0 and this value was then divided by the calories (kcal) consumed daily $\left(Energy\ efficiency = \frac{weight\ gained\ per\ day\ (g)}{\text{calories consumed per day (kcal)}}\right)$. Daily calories consumed were calculated from the average food intake across 3 metabolic cage days.

A second cohort (Cohort 2) of rats (Gunn female (n = 11), Control female (n = 11), Gunn male (n = 8), Control male (n = 7)) were bred to similar age (13–14 weeks old) and anesthetized after an overnight fast using 50 mg kg^{-1} sodium pentobarbitone (Pharmachem, Australia) via an i.p. injection. While anesthetized the animals were placed in a prone position and total body length of each animal was measured using a tape measurer from tip of the nose to the last sacral vertebrae. Anesthetized animals were euthanized by removal of the heart. Blood collected from the chest cavity was centrifuged (2000 g, 10 min, 21°C) and the serum was flash frozen and stored at −80°C for later analysis. Organs and skeletal muscle [soleus and extensor digitorum longus (EDL)] were dissected free from fat and washed in ice cold dPBS (Gibco®, United Kingdom), then patted dry, and weighed on a calibrated balance. Immediately after, a section of liver tissue was flash frozen and stored at −80°C for later analysis. Likewise, a piece of liver, EDL, and soleus were stored in Mir06 (liver) or BIOPS (muscle; 2.77 mM CaK_2EGTA, 7.23 mM K_2EGTA, 20 mM imidazole, 20 mM taurine, 50 mM MES hydrate, 0.5 mM dithiothreitol, 6.56 mM $MgCl_2$ $6H_2O$, 5.77 mM Na_2ATP, 15 mM Na_2phosphocreatine, pH 7.1) as described in "*High-resolution respirometry*".

Additionally, a third cohort (Cohort 3) of rats (Gunn female (n = 9), Control female (n = 10), Gunn male (n = 7), Control male (n = 17)) were bred to similar age (13–14 weeks old) and scanned using dual-energy X-ray absorptiometry (DEXA) as described in "*DEXA scan*".

Finally, a fourth cohort (Cohort 4) of juvenile (3–4 weeks of age) female control rats (n = 5) was euthanized using 50 mg kg^{-1} sodium pentobarbitone i.p. following an overnight fast and a piece of liver tissue was stored in Mir06 as described in "*High-resolution respirometry*".

Analysis of Serum Biochemistry

Serum samples were thawed and analyzed using the COBAS Integra® 400+ (Roche Diagnostics, Australia) for direct reacting bilirubin (BILD2), TBIL (BILT3) and albumin (ALB). All assays were calibrated with appropriate standards (CFAS) and accuracy was checked with appropriate quality controls [precinorm clinchem multi 1 (PCCC1), precinorm clinchem multi 2 (PCCC2)]. All analyses were conducted in duplicate and the average of each parameter reported.

Lipid Extraction

Frozen liver tissue (~100 mg) was homogenized frozen (with liquid N_2) using a mortar and pestle. Lipids were extracted with isopropyl-alcohol at a 50:1 mg: mL ratio of tissue to isopropyl-alcohol as previously published (Hsun-Wei Huang et al., 2006). Homogenates were vortexed vigorously and sonicated for 10 min and then centrifuged (43,000 g, 10 min, 21°C). The supernatant was collected in a separate tube and evaporated using a rotary evaporator at 35°C. Dry pellets were reconstituted in 250 µL of isopropanol and triglycerides were analyzed spectrophotometrically (TRIGL, Roche Diagnostics) on the COBAS Integra 400+ following manufacturer's instruction.

High-Resolution Respirometry

Liver Homogenate

A small section of liver tissue was dissected from the left lateral lobe and added directly to ice-cold Mir06 buffer. Two to three pieces weighing 8–16 mg of wet-weight (Wd) of dissected liver tissue were transferred (SHREDDER Tube, Pressure BioSciences, United States) and homogenized using a PBI shredder (Shredder SG3 Kit, Pressure BioSciences, MA, United States) as previously published (Larsen et al., 2014). Using the strongest force (position 3) the tissue was shredded for 5 s, followed by medium force (position 2) for 3 s. The homogenate was then diluted into ice-cold Mir06 to a final concentration of 1.3 mg tissue mL^{-1} and transferred into Oxygraph chambers (Oxygraph-2k; Oroboros Instruments, Austria). After O_2 flux stabilized, the substrate-uncoupler-inhibitor titration (SUIT) protocol was utilized to evaluate mitochondrial function described under "*Measurement of mitochondrial respiration*".

Permeabilization of Skeletal Muscle Fibers

Mechanical and chemical permeabilization of skeletal muscle was conducted as previously published (Liu et al., 2015). Briefly, after dissection, soleus and EDL were added to BIOPS buffer. 5–7 mg pieces of muscle tissue were used for mechanical isolation of muscle fibers using sharp round-end tweezers. After mechanical isolation, muscle fibers were permeabilized by adding saponin (final concentration 50 μg ml^{-1}) to the BIOPS buffer followed by gentle agitation on an orbital shaker for 30 min on ice. Tissue was then washed in Mir06 for 10 min with gentle agitation on ice. Permeabilized muscle fibers (0.7–1.5 mg Wd) were added to each Oxygraph chamber, with analysis performed in duplicates. Samples were analyzed using two different conditions: first batch of animals (3 per group) were analyzed at air saturation (~180 μM O_2) while the remaining animals were super-oxygenated to 400 μM O_2 concentration initially, and oxygen (O_2) concentration was maintained above 250 μM using H_2O_2 and catalase throughout measurement (Doerrier et al., 2018). Respiration parameters did not differ between methods, therefore, all results were combined for the final analysis.

Measurement of Mitochondrial Respiration

Mitochondrial respiration measurements were conducted within 2 h of sample collection at 37°C using three Oxygraph units in parallel containing 2 ml of Mir06 buffer in each chamber. Data acquisition and analysis was conducted using 7.0 DatLab software (Oroboros Instruments). Standard carbohydrate SUIT protocol as previously published (Gnaiger, 2014) was utilized to measure the contribution of carbohydrates to the rate of mitochondrial O_2 consumption (O_2 flux: pmol s^{-1}) in liver tissue and skeletal muscle of adult female and male rats (see *Cohort 2* within "*Experimental protocol*"). Additionally, the effect of UCB on hepatic mitochondrial function was determined by adding exogenous UCB (31.3, 62.5, and 125 μM) or vehicle (H_2O; control) to Oxygraph chambers containing liver homogenate from female control juvenile rats (see *Cohort 4* within "*Experimental protocol*"). All concentrations are represented as final concentrations. The O_2 flux of intrinsic uncoupled respiration (LEAK) was measured in the presence of 5 mM pyruvate, 1 mM malate and 10 mM glutamate (PMG). The maximal O_2 flux of oxidative phosphorylation (OXPHOS) through complex I (CI OXPHOS) was measured by step-wise titration with 1 mM ADP in the presence of PMG. Lack of increase in O_2 flux (<10%) after the addition of cytochrome c confirmed the integrity of the outer mitochondrial membrane. To assess CI+II convergent OXPHOS (CI+II OXPHOS), 10 mM succinate was added in the presence of PMG, cytochrome c, and saturating levels of ADP. The maximum O_2 flux of the electron transfer system (ETS) was measured by uncoupling CI+II O_2 flux from ATP synthesis (noncoupled state) by step-wise titration with 0.5 μM carbonyl cyanide p-trifluoromethoxyphenylhydrazone (FCCP; an extrinsic uncoupler). Noncoupled maximal respiration of complex II (CII ETS) was measured by inhibiting complex I with rotenone (0.5 μM) and residual O_2 flux (ROX) was measured by inhibiting mitochondrial respiration with 2.5 mM antimycin (AMA). All O_2 flux measurements were corrected for ROX and tissue mass (pmol mg^{-1} s^{-1}) or citrate synthase (pmol s^{-1} ng^{-1} CS). Flux control ratios (FCRs) were calculated by normalizing the O_2 flux of the electron pathways (i.e. LEAK, OXPHOS and CII ETS) to a common reference state (OXPHOS or ETS).

DEXA Scan

Dual-energy X-ray absorptiometry (DEXA) (XR-36 Quickscan densitometer 4.2.4/2.3.1, software version 2.5.3a; Norland Medical Systems, Inc. United States) was conducted on a subgroup of adult Gunn and normobilirubinemic control rats (15 weeks of age). Animals were anesthetized using ketamine (50 mg kg^{-1}) and xylazine (3 mg kg^{-1}) mixture in a 50:30 ratio via i. p. injection and placed in a prone position in the DEXA machine. Bone mineral density (BMD), total mass, lean mass, and fat mass was collected for each animal and all scans were performed at 1.5 × 1.5 mm resolution at 60 mm s^{-1} in small animal mode.

Citrate Synthase

Citrate synthase (CS) activity was measured as previously published (Eigentler et al., 2015). Briefly, hepatic tissue collected from Oxygraph chambers, hepatic homogenates (see Western blot analysis), or CS standard (#C3260) were mixed with 5,5′-dithiobis(2-nitrobenzoic acid) (DTNB; #D8130), acetyl CoA (#A2181) and oxaloacetic acid (#O4126) in a 96-well plate, and the reaction was monitored at 412 nm over 30 min in a spectrophotometer (ThermoFisher Scientific, Australia). All samples were analyzed in duplicate and the average absorbance was used to calculate CS activity or the amount of CS protein using the specific activity equation #6 as previously published (Eigentler et al., 2015).

Real-Time Quantitative Polymerase Chain Reaction (qPCR)

RNA extraction, cDNA synthesis, and qPCR were conducted according to the Minimum Information for Publication of Quantitative Real-Time PCR Experiments (MIQE) guidelines (Bustin et al., 2009). Briefly, liver samples (~10 mg) stored in RNAlater (Invitrogen, Australia) were homogenized and RNA was extracted using a RNAeasy mini kit (Qiagen, Australia)

TABLE 1 | TBIL concentrations and body composition of hyperbilirubinemic and normobilirubinemic rats. Bold values represent statistically significant *p*-values (< 0.05). The non-bold values are non-significant *p*-values (i.e. > 0.05).

Variable	Phenotype		*P* value
	Control	Gunn	
Serum TBIL (μmol L^{-1})			
Males	2.76 (0.66)	99.8 (15.9)	<**0.001**
Females	2.33 (1.20)	79.3 (20.6)	<**0.001**
Body length (cm)			
Males	25.2 (1.10)	23.9 (1.15)	0.09
Females	21.2 (0.65)	19.7 (0.58)	<**0.001**
Bodyweight (g)			
Males	309 (17.7)	261 (37.4)	<**0.001**
Females	176 (16.5)	150 (9.57)	<**0.001**
Lean mass (g)			
Males	256 (18.4)	215 (32.1)	<**0.001**
Females	160 (16.0)	140 (12.1)	<**0.01**
Fat mass (g)			
Males	53.0 (17.7)	46.8 (19.3)	0.46
Females	16.1 (6.65)	9.94 (5.35)	<**0.05**
Liver triglycerides (mg g^{-1})			
Males	9.99 (3.16)	9.45 (4.38)	0.78
Females	4.65 (1.67)	2.39 (0.92)	<**0.01**
Lean mass (% of bodyweight)			
Males	83.0 (5.34)	82.3 (6.82)	0.79
Females	90.9 (3.81)	93.3 (3.83)	0.18
Fat mass (% of bodyweight)			
Males	17.0 (5.34)	17.7 (6.82)	0.79
Females	9.13 (3.81)	6.70 (3.83)	0.18
Soleus (mg)			
Males	175 (38.1)	134 (24.2)	<**0.05**
Females	104 (18.1)	76.3 (11.0)	<**0.001**
EDL (mg)			
Males	147 (20.5)	120 (10.1)	<**0.01**
Females	89.7 (7.80)	64.0 (9.72)	<**0.001**

Two different cohorts of animals were used for the parameters analyzed. DEXA analysis (bodyweight, lean mass, and fat mass) was conducted on animals from Cohort 3 constituting 27 control and 16 Gunn rats. All other parameters were measured on animals from Cohort 2 constituting 18 control and 19 Gunn rats. Control group represents normobilirubinemic heterozygote littermates. Gunn group represents hyperbilirubinemic homozygote littermates. TBIL, total bilirubin; EDL, extensor digitorum longus. Values are represented as mean (standard deviation). All comparisons are made between phenotype within the same sex.

TABLE 2 | Organ weights of hyperbilirubinemic and normobilirubinemic rats. Bold values represent statistically significant *p*-values (< 0.05). The non-bold values are non-significant *p*-values (i.e. > 0.05).

Variable	Phenotype		*P* value
	Control (*n* = 18)	Gunn (*n* = 19)	
Liver (g)			
Males	14.8 (3.01)	13.8 (2.79)	0.52
Females	8.84 (1.23)	8.74 (0.91)	0.82
Heart (g)			
Males	1.19 (0.11)	1.07 (0.13)	0.07
Females	0.82 (0.06)	0.67 (0.06)	<**0.001**
Lungs (g)			
Males	1.54 (0.23)	1.37 (0.19)	0.14
Females	1.15 (0.12)	0.95 (0.08)	<**0.001**
Kidney (g)			
Males	1.62 (0.23)	1.53 (0.22)	0.48
Females	0.98 (0.06)	0.77 (0.04)	<**0.001**
Spleen (g)			
Males	1.17 (0.12)	1.03 (0.13)	**0.05**
Females	0.80 (0.10)	0.73 (0.12)	0.15
Testes (g)			
Males	1.89 (0.20)	1.75 (0.13)	0.24

Control group represents normobilirubinemic heterozygote littermates. Gunn group represents hyperbilirubinemic homozygote littermates. Values are represented as mean (standard deviation). All comparisons are made between phenotype within the same sex.

according to manufacturer's guidelines. The RNA concentration and quality (260/280 and 260/230 nm) were measured using a Nanodrop 1,000 spectrophotometer (ThermoFisher Scientific). Complementary DNA (cDNA) was synthesized from RNA using iScript gDNA clear cDNA synthesis kit (Bio-Rad, Australia) following manufacturer's protocol and stored at −20°C for later analysis. qPCR was conducted using KiCqStart™ predesigned primers (Sigma-Aldrich) and QuantiNova SYBR® green master mix (Qiagen) on StepOne™ real-time PCR systems (Applied Biosystems, Australia) following manufacturer's instruction (PCR initial heat activation: 2 min at 95°C; Denaturation: 40 cycles of 95°C for 5 s per cycle; Combined annealing/extension: 40 cycles of 60°C for 10 s per cycle). All data acquisition was conducted with StepOnePlus™ (v2.3). Gene expression was calculated according to the $2^{-\Delta\Delta Cq}$ method. *β-2-microglobulin* was stable across group and was used as the reference gene for normalizing gene expression. The list of primers is provided in the **Supplementary Table S1**.

Western Blot Analysis

Frozen liver samples were homogenized by shearing tissue through 18, 21 and then 23G needles in CelLytic MT Cell Lysis buffer (2.5: 50 mg/μL; #C3228) in the presence of protease inhibitor (#P8340) and phosphatase inhibitor (#ab201114, Abcam, Australia) as per manufacturer's protocol. Tissue supernatant was generated by centrifugation (4,000 g, 10 min, 4°C) and standardized based on protein concentration using the Pierce BCA Protein Assay Kit (ThermoFisher Scientific) as per manufacturer's protocol. Samples were prepared in Laemmli 2X buffer (#S3401) at 1:1 ratio and were heated for 30 min at 37°C (mitochondrial protein targets) or 5 min at 95°C (AMPK), prior to loading. Proteins (10–25 μg) were separated on 12% SDS-PAGE using TGX™ FastCast™ gels (#1610175, Bio-Rad). Following electrophoresis, proteins were transferred onto 0.45 μm polyvinylidene fluoride membranes (PVDF; #IPFL0010, Millipore, Australia) for 1–2 h on ice in Towbin buffer (25 mM Tris, 192 mM glycine, and 20% (v/v) methanol) for AMPK proteins or CAPS buffer (10 mM CAPS and 10% (v/v) methanol, pH 11) for mitochondrial protein targets. Following transfer, membranes were blocked with Odyssey Blocking Buffer (Millenium Science, Australia) and incubated with primary antibodies (subunits of mitochondrial respiratory complexes, #ab110413 (Abcam); p-AMPK, #ab133448 (Abcam); AMPK, #ab80039 (Abcam); GAPDH, #14C10 (Cell Signaling, Australia)) with gentle agitation overnight at 4°C. Finally, membranes were incubated with secondary antibodies (#IRDye 680 or #IRDye 800CW, LI-COR, Australia) for 1 h with gentle agitation at room temperature and visualized using Odyssey CLX (LI-COR). Densitometry analysis of mitochondrial respiratory complexes was normalized to GAPDH while p-AMPK

TABLE 3 | Multiple linear regression of the effect of bodyweight and the hyperbilirubinemic phenotype on organ weights and skeletal muscle. Bold values represent statistically significant *p*-values (< 0.05). The non-bold values are non-significant *p*-values (i.e. > 0.05).

	Independent variables		R^2	*P* value
	Bodyweight[a] B_1 (95% CI)	Phenotype[b] B_2 (95% CI)		
Dependent variables				
Liver (mg)				
Males (*n* = 14)	40.7 (32.0, 49.3)	1,070 (–156, 2,300)	0.91	<**0.001**[a], 0.08[b]
Females (*n* = 22)	35.6 (21.0, 50.2)	2,440 (1,220, 3,670)	0.58	<**0.001**[a], <**0.001**[b]
Combined (*n* = 36)	32.0 (28.7, 35.3)	1,550 (873, 2,230)	0.92	<**0.001**[a], <**0.001**[b]
Heart (mg)				
Males (*n* = 14)	1.69 (1.20, 2.18)	–31.8 (–101, 37.6)	0.87	<**0.001**[a], 0.33[b]
Females (*n* = 20)	0.90 (–0.39, 2.20)	–77.5 (–185, 29.9)	0.64	0.16[a], 0.15[b]
Combined (n = 34)	1.99 (1.78, 2.20)	–4.21 (–47.3, 38.8)	0.93	<**0.001**[a], 0.84[b]
Lungs (mg)				
Males (*n* = 14)	2.78 (1.88, 3.68)	–34.9 (–162, 92.6)	0.84	<**0.001**[a], 0.56[b]
Females (*n* = 21)	1.63 (–0.38, 3.63)	–80.6 (–253, 91.7)	0.58	0.11[a], 0.34[b]
Combined (*n* = 35)	2.31 (1.98, 2.64)	–43.5 (–112, 24.8)	0.88	<**0.001**[a], 0.20[b]
Kidney (mg)				
Males (*n* = 14)	2.86 (1.78, 3.94)	49.9 (–104, 203)	0.77	<**0.001**[a], 0.49[b]
Females (*n* = 22)	0.82 (–0.12, 1.76)	–147 (–226, –67.6)	0.85	0.08[a], <**0.01**[b]
Combined (*n* = 36)	3.62 (3.27, 3.96)	71.1 (0.29, 142)	0.93	<**0.001**[a], <**0.05**[b]
Spleen (mg)				
Males (*n* = 14)	1.37 (0.50, 2.23)	–56.7 (–180, 66.4)	0.63	<**0.01**[a], 0.33[b]
Females (*n* = 22)	1.67 (–0.45, 3.79)	49.6 (–128, 228)	0.21	0.12[a], 0.57[b]
Combined (*n* = 36)	1.70 (1.36, 2.04)	18.4 (–52.3, 89.1)	0.76	<**0.001**[a], 0.60[b]
Soleus (mg)				
Males (*n* = 14)	0.44 (0.33, 0.54)	–15.9 (–31.1, –0.66)	0.92	<**0.001**[a], <**0.05**[b]
Females (*n* = 22)	0.46 (0.24, 0.68)	5.10 (–13.3, 23.5)	0.74	<**0.001**[a], 0.57[b]
Combined (*n* = 36)	0.36 (0.32, 0.40)	–9.22 (–17.9, –0.57)	0.91	<**0.001**[a], <**0.05**[b]
EDL (mg)				
Males (*n* = 14)	0.19 (0.10, 0.27)	–14.9 (–27.3, –2.46)	0.81	<**0.001**[a], <**0.05**[b]
Females (*n* = 22)	0.21 (0.05, 0.36)	–11.1 (–24.0, 1.85)	0.79	<**0.05**[a], 0.09[b]
Combined (*n* = 36)	0.28 (0.25, 0.31)	–6.89 (–13.5, –0.33)	0.92	<**0.001**[a], <**0.05**[b]

Phenotype was entered as a dummy variable with normobilirubinemic phenotype used as the reference group to which the hyperbilirubinemic phenotype was compared. B_{1-2} represent the un-standardized regression coefficients for bodyweight and phenotype, respectively. The "B coefficient" estimates the change in mass (mg) of the dependent variables per unit of increase in bodyweight (g) or in the presence of the hyperbilirubinemic phenotype. CI, Confidence Interval; EDL, extensor digitorum longus.

[a]*Statistical significance of bodyweight as an independent predictor of organ weight* p < *0.05.*

[b]*Statistical significance of phenotype as an independent predictor of organ weight* p < *0.05.*

was normalized as a ratio to total AMPK (Image Studio Lite version 5.2; LI-COR).

Statistical Analysis

All values are expressed as mean ± (standard deviation), while multiple linear regression data are presented as un-standardized regression coefficients and 95% confidence intervals. Multicollinearity in multiple linear regression was ruled out by a variance inflation factor (VIF) of less than 5. Data was tested for normality and homogeneity of variance with Kolmogorov-Smirnov and Spearman tests, respectively. Comparisons were performed between phenotypes from the same sex using unpaired t-tests. When data failed normality or equality of variance, nonparametric Mann–Whitney test and Welch's correction were used, respectively. The dose-dependent effect of UCB on mitochondrial respiration was compared using repeated measures two-way ANOVA with Bonferroni's post-hoc test comparing the effect of UCB treatment to control (vehicle) on each respiratory state (e.g. CI OXPHOS and CI+II OXPHOS). Statistical analysis was performed in GraphPad PRISM (v8.2) and $p < 0.05$ was considered significant.

RESULTS

Phenotype

Breeding pairs produced similar distribution of heterozygote controls (normobilirubinemic) and homozygote Gunn (hyperbilirubinemic) rats over 7 litters (**Supplementary Table S2**; NS). Serum TBIL concentrations were significantly greater in Gunn rats compared to controls ($p < 0.001$, **Table 1**).

Body Composition

A total of 16 homozygote Gunn and 27 heterozygote controls were scanned using DEXA to determine body composition (**Table 1**). Both male and female Gunn rats had significantly lower bodyweight ($p < 0.001$) and lean mass ($p < 0.01$) when compared to controls (**Table 1**). Female Gunn rats had significantly lower body length ($p < 0.001$), fat mass ($p < 0.05$), and liver triglyceride concentration ($p < 0.01$) compared to female controls (**Table 1**). Male and female Gunn rats had significantly lower soleus and EDL muscle mass compared to littermate controls ($p < 0.01$; **Table 1**).

Organ Weights

There were no significant differences in liver mass between groups (**Table 2**). Heart and lung mass were only significantly reduced ($p < 0.001$) in female Gunn rats when compared to controls, with a trend toward reduced heart ($p = 0.07$) and lung ($p = 0.14$) mass in male Gunn rats (**Table 2**). Only female Gunn rats had significantly reduced kidney mass ($p < 0.001$), however, all Gunn rats presented a trend toward a reduced spleen mass ($p = 0.15$ and $p = 0.05$, respectively) compared to controls (**Table 2**). Additional organ masses are presented in **Table 2**. Organ masses expressed relative to bodyweight are provided in **Supplementary Table S3**.

Multiple Linear Regression of Organ Weights

In order to differentiate the effects of the hyperbilirubinemic phenotype (condition) from bodyweight on organ mass, multiple linear regression was conducted with organ mass as a dependent variable while bodyweight and the presence/absence of hyperbilirubinemia were used as independent variables. In male rats, bodyweight significantly and positively predicted all organ and skeletal muscle weights ($p < 0.01$) while the hyperbilirubinemic phenotype was a significant negative predictor of soleus and EDL mass ($p < 0.05$, **Table 3**). In females, bodyweight and the hyperbilirubinemic phenotype significantly and positively predicted liver mass ($p < 0.001$), however, only the hyperbilirubinemic phenotype was a significant negative predictor of kidney mass ($p < 0.01$, **Table 3**). Additionally, bodyweight was a significant positive predictor of soleus and EDL mass in females ($p < 0.05$. **Table 3**). In the second analysis, data from both sexes were combined, which demonstrated that bodyweight was a significant positive predictor for all organ and skeletal muscle masses ($p < 0.001$, **Table 3**). Conversely, the hyperbilirubinemic phenotype was a significant positive predictor for liver and kidney mass ($p < 0.001$), and a negative predictor for soleus and EDL mass ($p < 0.05$, **Table 3**).

Energy Balance

Body mass and food intake were measured over a 17-day period. Female Gunn rats gained significantly less bodyweight and consumed significantly fewer energy daily compared to controls ($p < 0.01$, **Table 4**). In contrast, there was no difference in bodyweight gain and food intake in male Gunn rats compared to controls (**Table 4**). Bodyweight gain relative to energy intake (energetic efficiency) was significantly reduced in female Gunn rats compared to controls ($p < 0.05$), however, no difference existed in males (**Table 4**).

TABLE 4 | Food intake, bodyweight gain, and energy efficiency of hyperbilirubinemic rats and their normobilirubinemic littermates. Bold values represent statistically significant *p*-values (< 0.05). The non-bold values are non-significant *p*-values (i.e. > 0.05).

Variable	Phenotype		*P* value
	Control	Gunn	
Food intake (kcal day^{-1})			
Males	83.5 (14.1)	82.4 (6.78)	0.85
Females	63.3 (6.95)	54.1 (6.38)	**<0.01**
Bodyweight gain (Day 16–Day 0) (g)			
Males	22.1 (4.78)	21.1 (14.1)	0.84
Females	15.2 (5.29)	6.60 (6.10)	**<0.01**
Energy efficiency (mg kcal^{-1})			
Males	15.6 (2.70)	17.0 (7.60)	0.65
Females	14.9 (5.10)	8.09 (5.75)	**<0.05**

Control and Gunn groups represent normobilirubinemic heterozygote and hyperbilirubinemic homozygote littermates, respectively. Values are represented as mean (standard deviation). Statistical comparisons are made between phenotypes within the same sex.

Liver and Skeletal Muscle Mitochondrial Function

Given that reduced energetic efficiency was reported in female Gunn rats (**Table 4**), the effect of acute UCB on mitochondrial function was investigated *in vitro*. Exogenous UCB was added to female control (normobilirubinemic) liver tissue and the dose-dependent effect of UCB on mitochondrial function was assessed (**Figure 1**). At the highest concentration (125 μM), UCB significantly inhibited LEAK, CI and CI+II OXPHOS respiration when compared to control ($p < 0.001$ and $p < 0.05$, respectively; **Figure 1A**). Furthermore, 31.3 and 125 μM UCB significantly inhibited CI+II ETS and CII ETS compared to control ($p < 0.01$ and $p < 0.001$, respectively; **Figure 1A**). The flux control ratio (FCR) of CI+II OXPHOS was significantly reduced by 31.3 and 62.5 μM UCB compared to control ($p < 0.05$ and $p < 0.01$, respectively; **Figure 1C**). O_2 flux following cytochrome c addition was significantly increased with 125 μM UCB compared to control ($p < 0.05$; **Figure 1D**).

To assess whether similar effects observed *in vitro* with exogenous UCB were recapitulated in adult hyperbilirubinemic Gunn rats, mitochondrial function was assessed in fresh liver tissue. No significant change in O_2 flux (LEAK, OXPHOS, or ETS) was found between Gunn rats and controls, when normalized to liver mass or citrate synthase activity (**Figures 2**, **3**). However, CI+II OXPHOS FCR was significantly increased in female Gunn rats compared to controls ($p < 0.05$; **Figure 2B**).

There was no difference in O_2 flux (LEAK, OXPHOS, or ETS) between Gunn and control rats for soleus or EDL (**Figures 4**, **5**). Since CI+II OXPHOS represented the maximum O_2 flux (greater than ETS) in skeletal muscle, CI+II OXPHOS instead of ETS was used as a reference state to calculate FCRs. FCRs were not significantly different across groups in soleus or EDL (**Figures 4**, **5**). Gunn rats did not significantly differ in O_2 flux after addition of cytochrome c compared to controls in liver or skeletal muscle (data not shown).

Gene Expression Related to Fatty Acid Metabolism and PPARα Activity

Genes related to mitochondrial β-oxidation [Acyl-CoA dehydrogenase, very long chain (*ACADVL*) and hydroxyacyl-CoA dehydrogenase trifunctional multienzyme complex subunit alpha (*HADHA*)], fatty acid transport [carnitine palmitoyltransferase 1A (*CPT1a*)], fatty acid synthesis [fatty acid synthase (*FASN*)] and peroxisome proliferator-activated

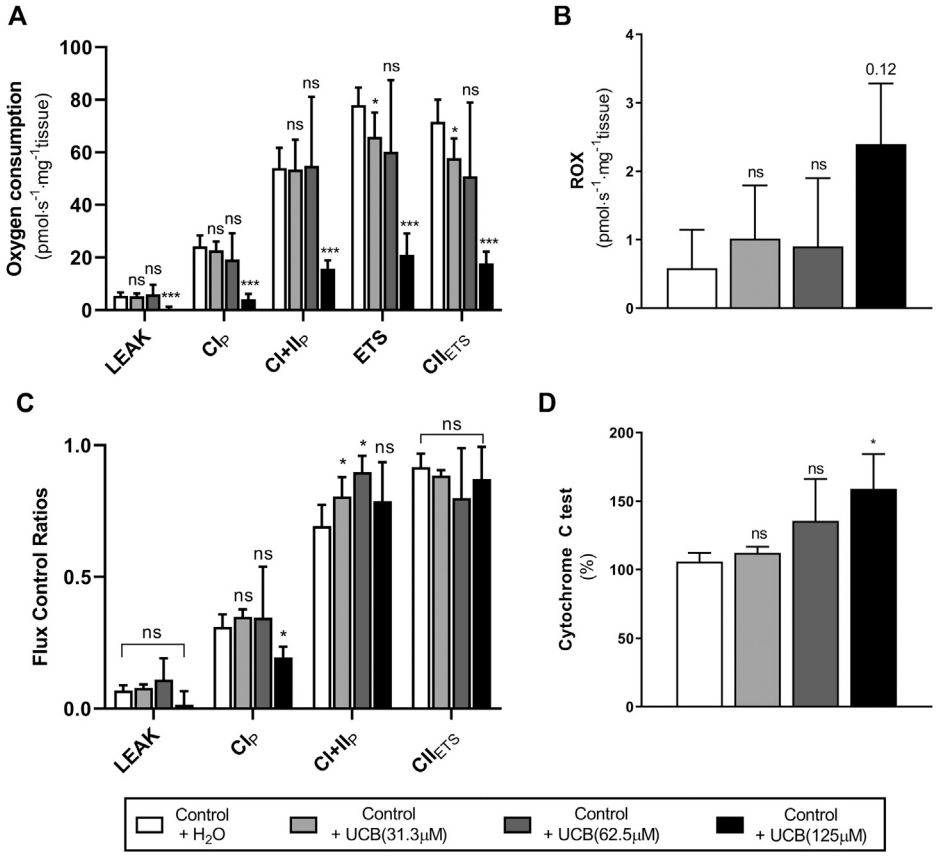

FIGURE 1 | Effect of exogenous UCB on mitochondrial function in juvenile control (normobilirubinemic) liver tissue (n = 5). Mitochondrial respiratory states are identified as intrinsic uncoupling measured in the absence of ADP (LEAK), OXPHOS capacity measured at saturating levels of ADP via CI (CI_P) or CI+CII ($CI+II_P$) and noncoupled respiratory capacity (ETS and CII_{ETS}). **(A, B)** The rate of respiratory states evaluated based on O_2 consumption per mass of tissue at varying UCB concentrations. **(C)** Respiratory states expressed relative to a common reference state (ETS). **(D)** Evaluating mitochondrial outer membrane integrity by the addition of cytochrome c, represented as % change in O_2 consumption relative to before cytochrome c addition. CI, CII, mitochondrial respiratory chain Complex I and Complex II, respectively; ETS, electron transfer system; ROX, residual O_2 consumption; UCB, unconjugated bilirubin. $p < 0.05$*, <0.01**, <0.001*** compared to control+H_2O. ns: non-significant.

receptor alpha (*PPARα*) activity [fibroblast growth factor 21 (*FGF21*) and acyl-CoA oxidase 1 (*ACOX1*)] were measured using qPCR in hepatic tissue. *ACADVL* and *HADHA* showed a non-significant ($p = 0.06$ and $p = 0.15$, respectively; **Figures 6B,C**) trend toward increased expression in female Gunn compared to control rats. There was no difference in gene expression related to fatty acid metabolism between male Gunn and control rats (**Figures 6A–D**). *ACOX1* expression tended to increase ($p = 0.05$) while *FGF21* was not different in female Gunn vs. control rats (**Figures 6E,F**). In contrast, expression of *FGF21* and *ACOX1* were significantly greater in male Gunn compared to control rats ($p < 0.05$; **Figures 6E,F**).

Gene Expression Related to Mitochondrial Biogenesis

Genes that regulate mitochondrial biogenesis were measured using qPCR in hepatic tissue. Peroxisome proliferative activated receptor gamma coactivator 1 alpha (*PGC-1α*) expression was significantly ($p < 0.01$; **Figure 7A**) increased with nuclear respiratory factor 1 (*NRF1*) tending to increase ($p = 0.09$; **Figure 7B**) in female Gunn vs. control rats. In comparison, *PGC-1α* tended to increase ($p = 0.11$; **Figure 7A**) with no change in *NRF1* (**Figure 7B**) in male Gunn compared to control rats.

Expression of Subunits Specific to Hepatic Mitochondrial Respiratory Complexes

Finally, hepatic mitochondrial quantity and quality were evaluated by measuring the relative expression of subunits specific to mitochondrial respiratory complexes (complex I (CI) subunit NDUFB8, complex II (CII) subunit SDHB, complex III (CIII) core protein 2, complex IV (CIV) subunit 1, complex V (CV) subunit alpha) using western blot. There was significantly greater expression of CIV subunit 1 in female Gunn rats when compared to controls ($p < 0.01$; **Figure 8D**). No significant differences in the expression of subunits specific to mitochondrial complexes were observed in male Gunn vs. control rats (**Figure 8**).

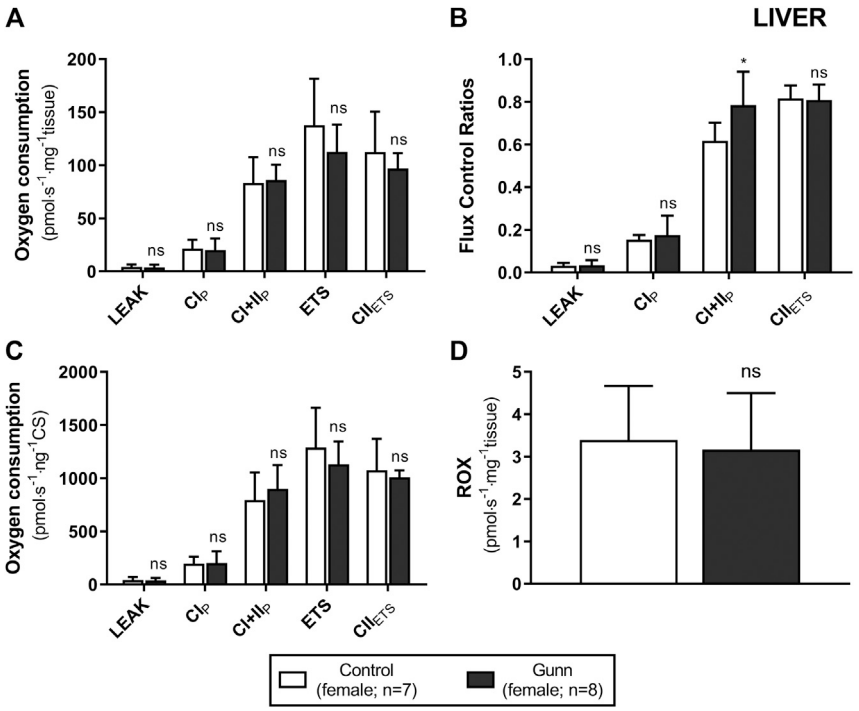

FIGURE 2 | Mitochondrial function in adult female Gunn (hyperbilirubinemic) and control (normobilirubinemic) liver tissue. Mitochondrial respiratory states are identified as intrinsic uncoupling measured in the absence of ADP (LEAK), OXPHOS capacity measured at saturating levels of ADP via CI (CI_P) or CI+CII ($CI+II_P$) and noncoupled respiratory capacity (ETS and CII_{ETS}). **(A, D)** The rate of respiratory states evaluated based on O_2 consumption per mass of tissue. **(B)** Respiratory states expressed relative to a common reference state (ETS). **(C)** The rate of respiratory states evaluated based on O_2 consumption per protein of citrate synthase. CI, CII, mitochondrial respiratory chain Complex I and Complex II, respectively; ETS, electron transfer system; ROX, residual O_2 consumption. $p < 0.05$*, <0.01**, <0.001*** compared to control. ns: non-significant.

Hepatic Citrate Synthase Activity and AMPK Expression

Citrate synthase activity was measured as a crude indicator of mitochondrial density in liver homogenates of adult Gunn and control rats. There were no differences in citrate synthase activity between groups (**Figure 9A**). Phosphorylated AMP-activated protein kinase (pAMPK) relative to total AMPK was measured as an indirect marker of the AMP to ATP ratios and the energetic state of liver tissue. Ratios of pAMPK:AMPK were unchanged across groups (**Figure 9B**).

DISCUSSION

This study presents the first comprehensive evaluation of body composition and mitochondrial function in an animal model of UGT1A1 mutation and unconjugated hyperbilirubinemia. Greater hepatic CI+II OXPHOS FCR, increased *PGC-1α* and CIV subunit 1 expression were observed in female Gunn rats, suggesting an increase in mitochondrial biogenesis. These findings were associated with lower fat mass and a trend toward increased hepatic mitochondrial β-oxidation gene expression in female Gunn rats. In contrast, exogenous addition of UCB inhibited mitochondrial function, thus, the lack of mitochondrial dysfunction in female Gunn rats may reflect the differences in bilirubin: albumin molar ratios between the two conditions and/or a compensatory mechanism to UCB inhibition. Female Gunn rats had physiological changes at both the whole body (e.g. fat mass) and subcellular (e.g. increased mitochondrial biogenesis) levels; in contrast, we did not observe many of these changes in male Gunn rats, suggesting that reduced UGT1A1 function leads to sexually dimorphic effects on metabolism.

Although previous papers have reported reduced bodyweight in hyperbilirubinemic Gunn rats compared to normobilirubinemic littermates, none have characterized the body composition of these animals (Fu et al., 2010; Boon et al., 2012; Wallner et al., 2013). Significant decrease in lean mass was observed in male and female Gunn rats compared to normobilirubinemic littermates (controls). However, significantly lower total fat mass and body length were only observed in female Gunn rats. Excess body fat relative to bodyweight [fat mass (%)] increases the risk of CVD (Zeng et al., 2012), with female Gunn rats demonstrating a notable non-significant, 26% reduction in fat mass (%) compared to controls (**Table 1**). Therefore, the change in female Gunn rats may be protective against CVD and this is consistent with epidemiological evidence that reports reduced risk from CVD

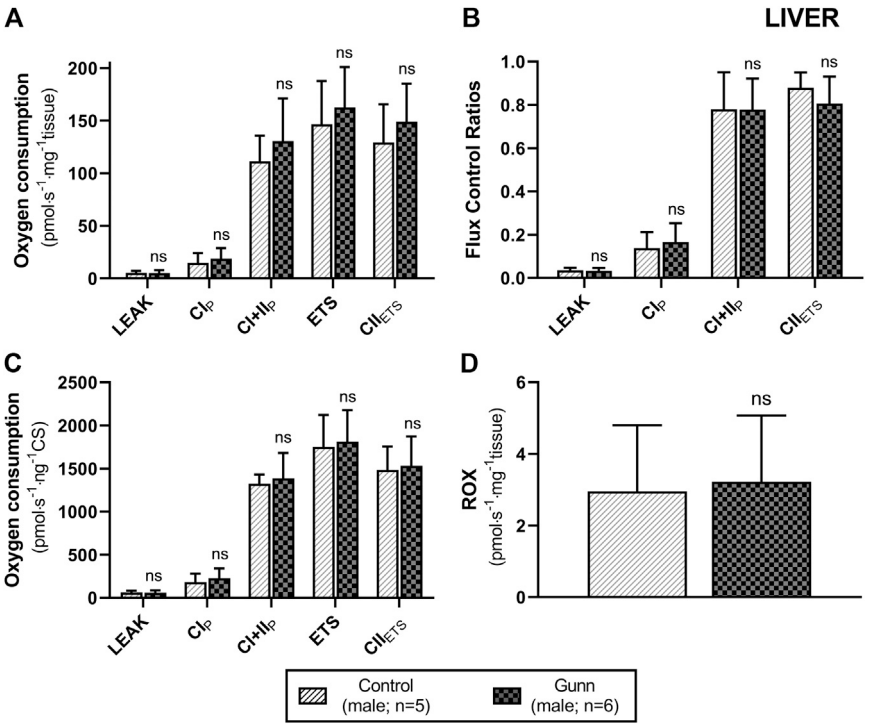

FIGURE 3 | Mitochondrial function in adult male Gunn (hyperbilirubinemic) and control (normobilirubinemic) liver tissue. Mitochondrial respiratory states are identified as intrinsic uncoupling measured in the absence of ADP (LEAK), OXPHOS capacity measured at saturating levels of ADP via CI (CI_P) or CI+CII ($CI+II_P$) and noncoupled respiratory capacity (ETS and CII_{ETS}). **(A, D)** Respiratory states evaluated based on O_2 consumption per mass of tissue. **(B)** The rate of respiratory states expressed relative to a common reference state (ETS). **(C)** The rate of respiratory states evaluated based on O_2 consumption per protein of citrate synthase. CI, CII, mitochondrial respiratory chain Complex I and Complex II, respectively; ETS, electron transfer system; ROX, residual O_2 consumption. $p < 0.05$*, <0.01**, <0.001*** compared to control. ns: non-significant.

in individuals with mildly elevated circulating UCB concentrations (Bulmer et al., 2018).

Considering that female Gunn rats had reduced fat mass we investigated whether there were changes to hepatic gene expression related to fatty acid metabolism. Interestingly, there was a notable trend toward increased expression in *ACADVL* and *HADHA* ($p < 0.15$; **Figure 6**) in female Gunn rats. These data suggest that mitochondrial β-oxidation could be upregulated in female Gunn rats leading to increased fat breakdown (Nguyen et al., 2008). Collectively, increased mitochondrial β-oxidation may account for the reduced energetic efficiency and decreased fat mass in female Gunn rats (Nguyen et al., 2008). On the contrary, there was no change in genes associated with fatty acid metabolism in male Gunn rats which is consistent with the lack of difference in adiposity when compared to male normobilirubinemic controls.

Stec et al. reported that a week of UCB treatment in male normobilirubinemic mice fed a HFD resulted in reduced bodyweight and fat mass (%), with increased lean mass (%) (Stec et al., 2016). Similarly, male mice with chronic hyperbilirubinemia consuming a HFD demonstrated reduced bodyweight, fat mass (%), and liver triglycerides, with increased β-oxidation gene expression when compared to normobilirubinemic controls (Hinds et al., 2017). Interestingly, these studies reported that UCB is an endogenous agonist of PPARα with the lipid-reducing effects of UCB being mediated through this nuclear receptor (Stec et al., 2016; Hinds et al., 2017). Therefore, these studies suggest that UCB is an endogenous regulator of fat metabolism and support the present results of reduced fat mass and elevated β-oxidation gene expression in a rat model of hyperbilirubinemia.

To determine whether PPARα activity was also increased in Gunn rats we investigated the expression of downstream gene targets *ACOX1* and *FGF21* (Rakhshandehroo et al., 2010). Although *ACOX1* expression was non-significantly ($p = 0.05$; **Figure 6**) three-fold greater in female Gunn rats there was no change in *FGF21* expression. In comparison, *ACOX1* and *FGF21* gene expression were significantly upregulated in male Gunn rats (**Figure 6**). These data suggest that PPARα activity is potentially increased in male but not in female Gunn rats. It is unknown whether Stec and colleagues (Stec et al., 2016; Hinds et al., 2017) found similar sexual dimorphism in PPARα activation in hyperbilirubinemic animals because their findings were reported in male mice. However, studies investigating the effectiveness of PPARα agonists such as fenofibrate demonstrated diminished activity of this receptor in ovary intact and ovariectomized mice treated with estrogen. These mice also demonstrated decreased *ACOX1* expression and attenuated fatty acid oxidation compared to estrogen poor ovariectomized mice (Yoon et al., 2002; Jeong and Yoon,

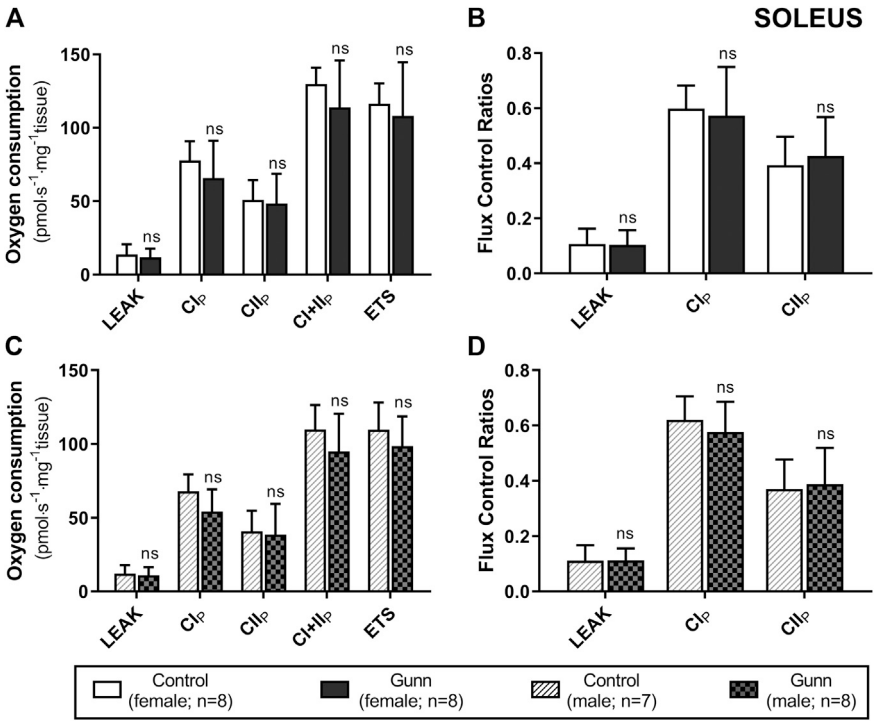

FIGURE 4 | Mitochondrial function in adult female **(A, B)** and male **(C, D)** Gunn (hyperbilirubinemic) and control (normobilirubinemic) permeabilized soleus fibers. Mitochondrial respiratory states are identified as intrinsic uncoupling measured in the absence of ADP (LEAK), OXPHOS capacity measured at saturating levels of ADP via CI (CI_P), CII (CII_P), and CI+II ($CI+II_P$), and noncoupled respiratory capacity (ETS). **(A, C)** The rate of respiratory states evaluated based on O_2 consumption per mass of tissue. **(B, D)** Respiratory states expressed relative to a common reference state ($CI+II_P$). CI, CII, mitochondrial respiratory chain Complex I and Complex II, respectively; ETS, electron transfer system; $p < 0.05$*, <0.01**, <0.001*** compared to control. ns: non-significant.

2007). Therefore, discrepancy in PPARα activity between male and female Gunn rats could potentially be determined by sexual dimorphism in the function of this receptor.

BMR contributes ~65% of daily energy expenditure, which is proportional to lean mass and its composition (Dulloo et al., 2010). Although organs constitute a small fraction of lean mass, they determine the majority of BMR (70–90% organs vs 13–20% skeletal muscle) (Holliday et al., 1967; Even et al., 2001; Kummitha et al., 2014). In mice, the liver alone accounts for 50% of BMR while constituting only 6.2% of bodyweight (Kummitha et al., 2014). Intriguingly, organs from female Gunn rats were generally lighter than controls, however, when corrected for bodyweight were significantly heavier (**Table 2** and **Supplementary Table S3**). Toxicity studies show that the relationship of organ mass to bodyweight is nonlinear for some organs, thus, correction for bodyweight can introduce error and misrepresent the effect of the condition/treatment on organ masses (Bailey et al., 2004). To avoid this limitation, we applied multiple linear regression to separate the effects of bodyweight from phenotype on organ masses. This analysis revealed that on average the liver mass was heavier by 2.44 g while kidney mass was lighter by 0.15 g in female Gunn rats independent of bodyweight (**Table 3**). This is the first study to demonstrate an association of hyperbilirubinemia/UGT1A1 impairment with organ masses. Considering that organs are more metabolically active than other forms of lean mass, larger liver mass in female Gunn rats may indicate greater BMR in these animals which would in turn explain their reduced energetic efficiency and decreased bodyweight (**Table 1** and **4**) (Holliday et al., 1967; Even et al., 2001; Kummitha et al., 2014). Interestingly, Hinds et al. reported that the daily rate of O_2 consumption (VO_2) was not different in male hyperbilirubinemic mice compared to controls, however, it remains to be investigated in female hyperbilirubinemic animals (Hinds et al., 2017). Higher voluntary physical activity is another possible reason for the leaner phenotype in Gunn rats. This conclusion is supported by data showing that 3–4 month old male Gunn rats had reduced bodyweight and traveled 23–160% more distance compared to normobilirubinemic littermates (Stanford et al., 2015). However, a lack of measurements on the energy expenditure in Gunn rats precludes the ability to determine the cause of reduced bodyweight in these animals.

To explore the possibility of greater BMR we investigated mitochondrial function in several tissues. UCB has traditionally been described as toxic to mitochondria because it uncouples oxidative phosphorylation and induces membrane permeabilisation (Noir et al., 1972; Zucker et al., 1992; Rodrigues et al., 2000, Rodrigues et al., 2002b; Jiang and Wang, 2004). For instance, 20–40 μM of UCB reduced state 3 (submaximal oxidative phosphorylation) respiration by 50% with a corresponding increase in the rate of LEAK respiration (uncoupled mitochondrial respiration) via CI and CII in

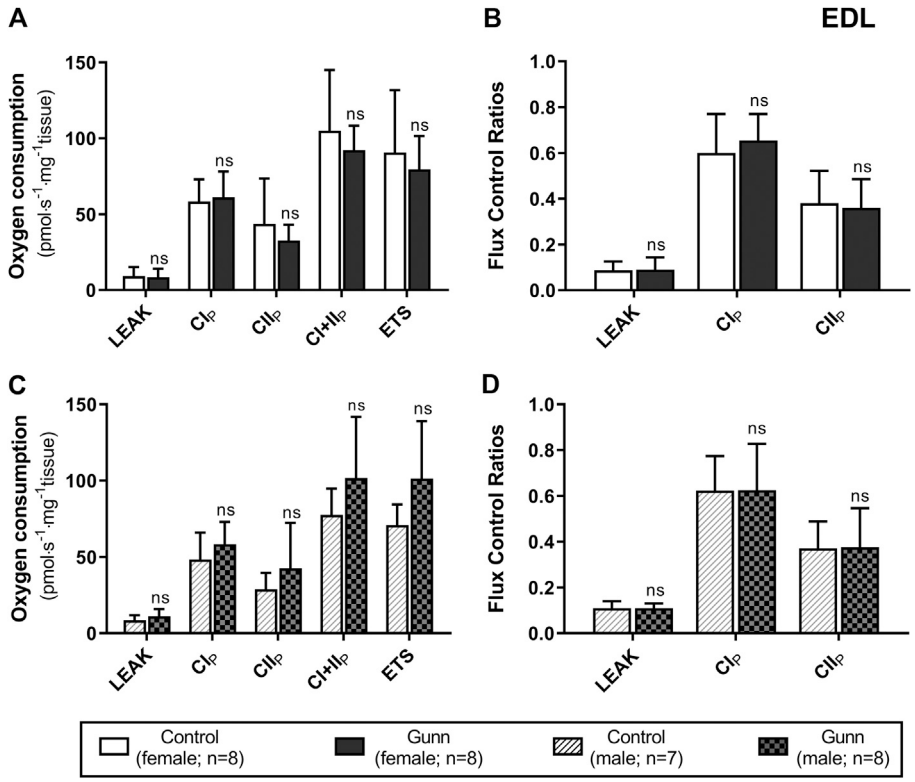

FIGURE 5 | Mitochondrial function in adult female **(A, B)** and male **(C, D)** Gunn (hyperbilirubinemic) and control (normobilirubinemic) permeabilized EDL fibers. Mitochondrial respiratory states are identified as intrinsic uncoupling measured in the absence of ADP (LEAK), OXPHOS capacity measured at saturating levels of ADP via CI (CI_P), CII (CII_P), and CI+II ($CI+II_P$), and noncoupled respiratory capacity (ETS). **(A, C)** The rate of respiratory states evaluated based on O_2 consumption per mass of tissue. **(B, D)** Respiratory states expressed relative to a common reference state ($CI+II_P$). CI, CII, mitochondrial respiratory chain Complex I and Complex II, respectively; ETS, electron transfer system; EDL, Extensor digitorum longus. $p < 0.05$*, <0.01**, <0.001*** compared to control. ns: non-significant.

isolated rat mitochondria (Noir et al., 1972). In the present study, exogenous UCB addition to control liver tissue induced dose-dependent inhibition of ETS, and inhibited OXPHOS at concentrations of 125 μM UCB (see **Figure 1A**) which is above the reference range and potentially toxic in humans (Jansen, 1999). Furthermore, 125 μM UCB affected the membrane integrity of mitochondria, as demonstrated by a 59% increase in O_2 flux with cytochrome c addition (**Figure 1D**) and may indicate that UCB induces apoptosis at this concentration through the mitochondrial pathway. This is consistent with previous studies that show that UCB increases mitochondrial membrane permeability and induces release of cytochrome c/apoptosis (Rodrigues et al., 2000; Rodrigues et al., 2002b; Naveenkumar et al., 2015).

Surprisingly, the rate of LEAK respiration was not affected by UCB, nor was OXPHOS inhibited at concentrations less than 125 μM (**Figure 1A**). This is contrary to previous studies that demonstrate an uncoupling effect of UCB on respiration and inhibition of oxidative phosphorylation in the presence of 10–100 μM UCB (Mustafa et al., 1969; Noir et al., 1972). This inconsistency may be explained by the concentration of albumin used in experimental models, as albumin avidly binds UCB and limits its diffusion into mitochondria (Vitek and Ostrow, 2009). For example, in the absence of albumin, free UCB induces mitochondrial uncoupling, however, it has no effect on mitochondrial function at 1:1 UCB: albumin molar ratios (Mustafa et al., 1969; Noir et al., 1972). This study used a final albumin concentration of 15 μM (1 g L^{-1}) with UCB: albumin molar ratios that are greater than 1, indicating that significant mitochondrial dysfunction was induced above a 8:1 UCB: albumin ratio (125 μM UCB). These molar ratios are higher than that found *in vivo* in the circulation of Gunn rats and would likely lead to greater UCB transfer and accumulation into the tissue (Odell, 1966). Understanding the physiological importance of this finding remains an important research question requiring further investigation of variable tissue UCB concentrations.

The impact of UCB on mitochondrial function has been investigated extensively *in vitro*. However, few studies have evaluated mitochondrial function in hyperbilirubinemic animals, and these investigations report inconsistent results (Fritz-Niggli, 1968; Celier et al., 1992; Zelenka et al., 2016). Celier et al., (1992) showed that isolated hepatic mitochondria from male Gunn and wild type control rats (8 weeks of age) have comparable state 3 O_2 flux and respiratory control ratios (RCRs). Conversely, Fritz-Niggli (1968) reported reductions in P/O ratios in male and female Gunn rats compared to Sprague–Dawley controls in isolated hepatic mitochondria indicating that Gunn

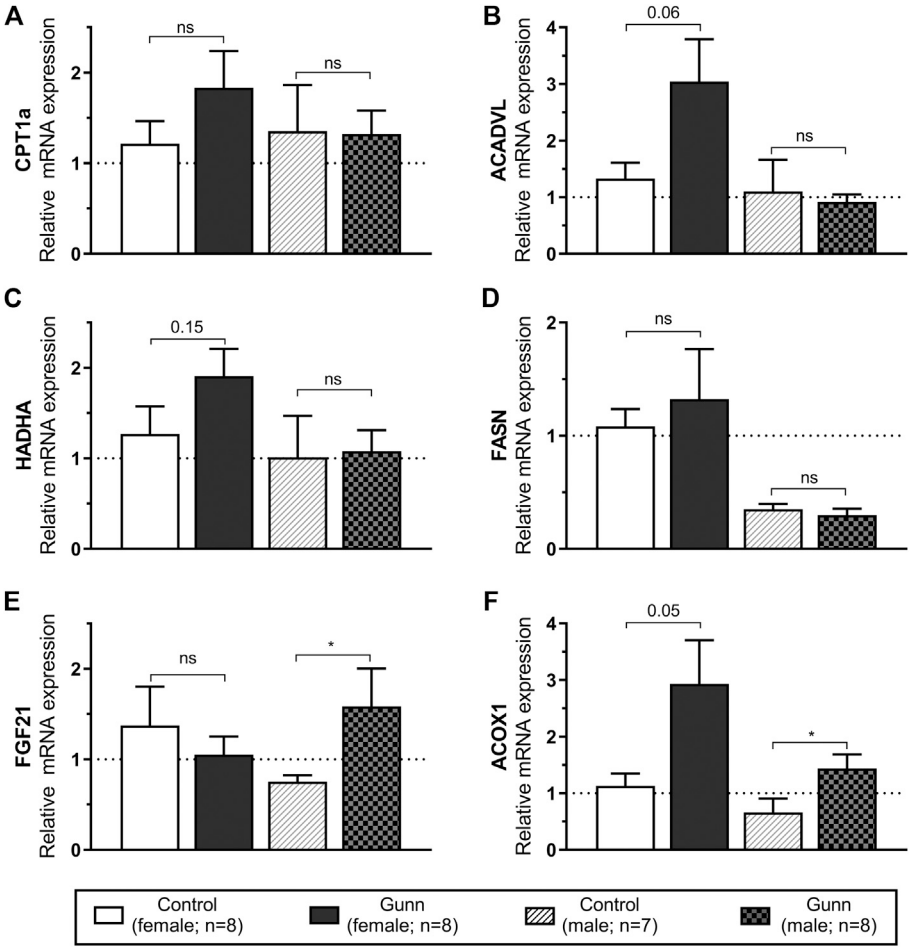

FIGURE 6 | Hepatic gene expression related to fatty acid metabolism and PPARα activity in adult Gunn (hyperbilirubinemic) and control (normobilirubinemic) rats. Data are presented as mean ± standard error of the mean (SEM). *CPT1a*, carnitine palmitoyltransferase 1A; *ACADVL*, acyl-CoA dehydrogenase, very long chain; *HADHA*, hydroxyacyl-CoA dehydrogenase trifunctional multienzyme complex subunit alpha; *FASN*, fatty acid synthase; *FGF21*, fibroblast growth factor 21; *ACOX1*, acyl-CoA oxidase 1. $p < 0.05$*, <0.01**, <0.001*** compared to control. ns: non-significant.

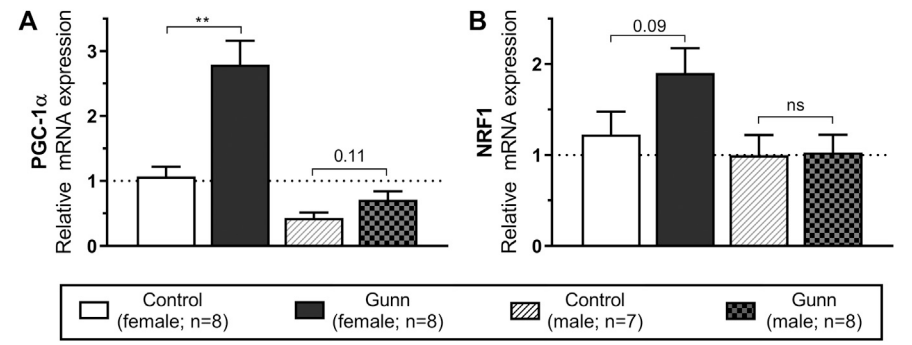

FIGURE 7 | Hepatic gene expression related to mitochondrial biogenesis in adult Gunn (hyperbilirubinemic) and control (normobilirubinemic) rats. Data are presented as mean ± standard error of the mean (SEM). *PGC-1α*, peroxisome proliferative activated receptor gamma coactivator 1 alpha; *NRF1*, nuclear respiratory factor 1. $p < 0.05$*, <0.01**, <0.001*** compared to control. ns: non-significant.

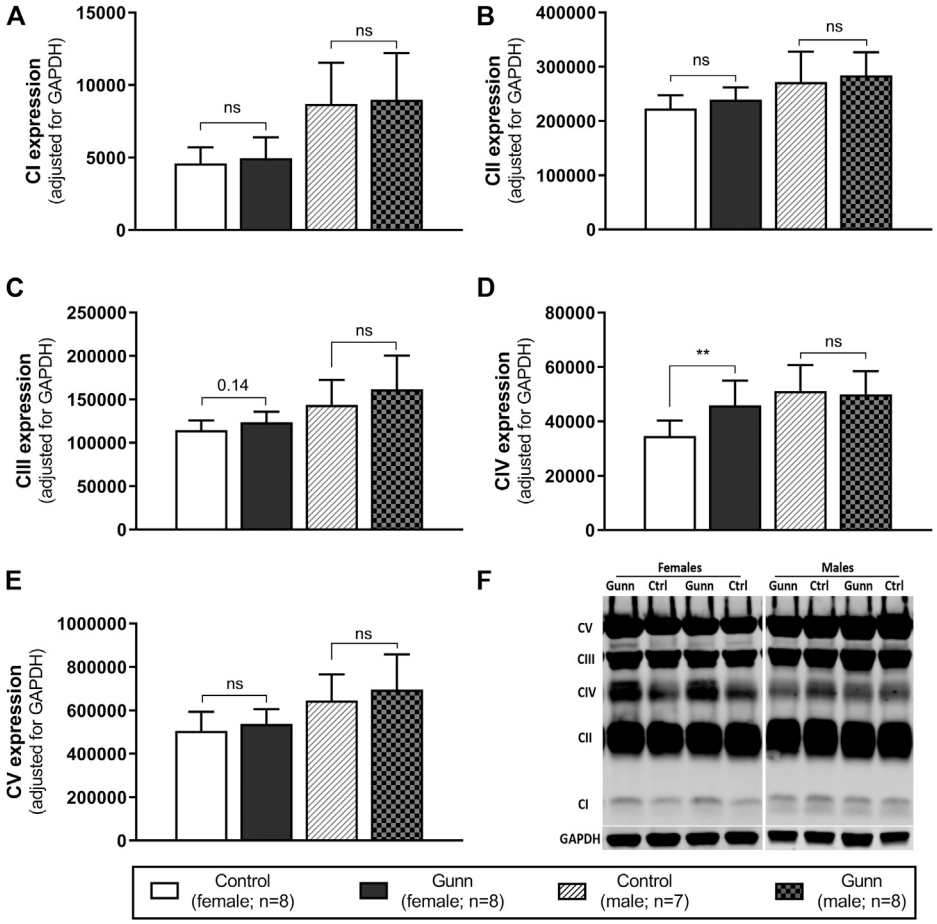

FIGURE 8 | Mitochondrial quality and density assessed by western blot in adult Gunn (hyperbilirubinemic) and control (normobilirubinemic) liver tissue. **(A–E)** Protein extracts from liver tissue were investigated for protein expression of subunits representing mitochondrial respiratory complexes (CI-V) adjusted for a loading control (GAPDH). **(F)** Example western blot analysis of subunits of mitochondrial complexes. CI, complex I subunit NDUFB8; CII, complex II subunit SDHB; CIII, complex III core protein 2; CIV, complex IV subunit 1; CV, complex V subunit alpha. $p < 0.05$*, <0.01**, <0.001*** compared to control. ns: non-significant.

rats have reduced capacity for oxidative phosphorylation. It is important to note that the serum bilirubin concentrations of the Gunn rats from Fritz-Niggli (1968) ranged between 115–240 μM, whilst those within this study approximated 80–100 μM (**Table 1**). These bilirubin concentrations are more likely to affect mitochondrial function and may contribute to the discrepancies between studies (Rossi et al., 2005). Unlike the other two studies that report no change or a decline in mitochondrial function, Zelenka et al., (2016) demonstrated that O_2 flux of isolated hepatic mitochondria from aged (12–18 months old) Gunn rats was greater when compared to normobilirubinemic siblings. In the present study we did not report any changes to mitochondrial O_2 flux (relative to tissue mass or citrate synthase activity) in hepatic tissue or skeletal muscle between adult (~3.5 months old) hyperbilirubinemic Gunn and normobilirubinemic littermates which is in agreement with Celier et al., (1992). Inconsistent findings between studies could be caused by differences in the degree of hyperbilirubinemia—although this cannot be confirmed because bilirubin concentrations were not reported outside of Fritz-Niggli (1968)—methods employed, and the age of the animals studied. Considering that this is the first study of hyperbilirubinemic rats to measure mitochondrial function in additional tissue (i.e. skeletal muscle) beyond the liver, it gives us confidence that the degree of hyperbilirubinemia reported in this model does not influence mitochondrial O_2 flux.

Conversely, CI+II OXPHOS relative to ETS (CI+II OXPHOS FCR) was significantly greater in hepatic tissue of female Gunn rats (**Figure 2B**) and this was also observed when liver tissue of normobilirubinemic female rats was treated with 31 or 62.5 μM exogenous UCB (**Figure 1C**). O_2 flux is affected by mitochondrial density and mitochondrial quality (i.e. function per individual mitochondria). Therefore, FCRs such as OXPHOS: ETS ratios, eliminate the influence of mitochondrial density allowing the study of qualitative changes in the electron transfer pathways involved in the electron transfer system (Gnaiger, 2014). Increased CI+II OXPHOS FCR indicates that hepatic mitochondria in female Gunn rats are working closer to their maximal oxidative capacity and may indicate greater mitochondrial energy efficiency (Gnaiger, 2014; Holland et al.,

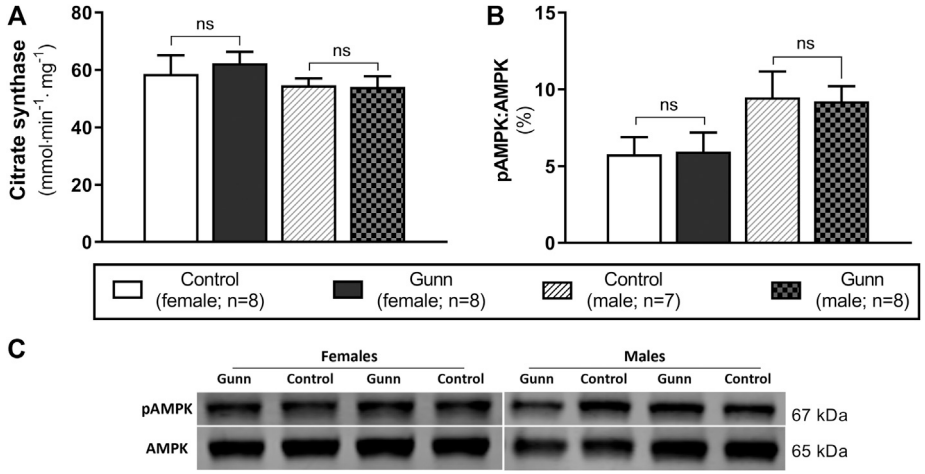

FIGURE 9 | Hepatic mitochondrial density measured by citrate synthase activity and energetic state assessed using pAMPK:AMPK ratios in adult Gunn (hyperbilirubinemic) and control (normobilirubinemic) liver tissue. **(A)** Citrate synthase activity measured in protein extracts from liver tissue standardized for total protein. **(B)** Phosphorylated AMPK expression over total AMPK measured using Western blot. AMPK, AMP-activated protein kinase; pAMPK, phosphorylated AMPK. $p < 0.05$*, <0.01**, <0.001*** compared to control. ns: non-significant.

2018). Increased OXPHOS respiration, without a change in ETS, reflects greater coupling of mitochondrial respiration to ATP synthesis (i.e. greater mitochondrial efficiency) and causes a reduction in reserve oxidative capacity (Lemieux et al., 2011; Gnaiger, 2014; Greggio et al., 2017; Holland et al., 2018). Conversely, enzymatic defects in mitochondrial respiratory complexes (CI-IV), independent of ATP synthesis, limits ETS respiration and reduces reserve oxidative capacity (Lemieux et al., 2011; Gnaiger, 2014). Female Gunn rats demonstrated a small non-significant increase in CI+II OXPHOS and a decrease in ETS (**Figure 2**). Therefore, these results suggest that the reason of increased hepatic CI+II OXPHOS FCR in female Gunn rats was due to a combination of improved mitochondrial efficiency and enzymatic dysfunction.

Although, a similar effect was reported when control liver tissue was treated with exogenous UCB (31 or 62.5 μM), reduction in reserve oxidative capacity in this instance was likely caused by UCB-mediated inhibition of mitochondrial respiratory complexes. Exogenous UCB treatment dose-dependently inhibited ETS causing an increase in CI+II OXPHOS FCR (**Figure 1A**). Therefore, reduction in ETS respiration suggests that UCB inhibits activity of one or more of the mitochondrial complexes (Lemieux et al., 2011; Gnaiger, 2014). This conclusion is supported by a study showing that UCB inhibits CIV activity by 18–20% in liver tissue at 1:2 UCB: albumin molar ratios (Malik et al., 2010). Since this study employed UCB: albumin molar ratios greater than 1:2, exogenous UCB treatment likely inhibited CIV activity in liver tissue causing a reduction in ETS capacity.

To explore further potential mechanisms that could explain the reduced adiposity in female Gunn rats, we measured hepatic gene expression related to mitochondrial biogenesis. PGC-1α is a co-activator that interacts with transcription factors to modulate gene expression of mitochondrial biogenesis and fatty acid metabolism (Scarpulla, 2011). For instance, PGC-1a induces NRF1 gene expression and interacts with NRF1 protein to induce mitochondrial biogenesis (Wu et al., 1999). *PGC-1α* expression was significantly increased in female Gunn rats with a similar trend ($p = 0.11$) in male Gunn rats compared to controls (**Figure 7**). Furthermore, we found a near two-fold (non-significant, $p = 0.09$) increase in *NRF1* expression in female Gunn rats which is consistent with elevated *PGC-1α* expression (**Figure 7**). Therefore, elevated *PGC-1α* and *NRF1* gene expression suggests that there is increased hepatic mitochondrial biogenesis in female Gunn rats (Scarpulla, 2011).

To evaluate the possibility of increased mitochondrial biogenesis in Gunn rats, we measured citrate synthase activity and the protein expression of subunits representative of mitochondrial respiratory complexes in liver tissue. Although there was no change in citrate synthase activity, there was a significant increase in CIV subunit 1 expression in female Gunn rats. Elevated CIV subunit 1 expression is consistent with greater *PGC-1α* and *NRF1* expression indicating that there may be increased hepatic mitochondrial biogenesis in female Gunn rats. Considering that UCB can inhibit CIV activity, greater CIV subunit 1 expression in female Gunn rats could represent a compensatory mechanism to UCB-mediated inhibition (Vaz et al., 2010; Malik et al., 2010). Surprisingly, a similar effect was not observed in male Gunn rats suggesting that changes to CIV subunit 1 expression could be caused by other factors. In addition to UCB, UGT1A1 is an important enzyme for 17β-estradiol conjugation and excretion through the hepatobiliary route (Zhou et al., 2011; Sambasivarao, 2013). Consequently, UGT1A1 impairment in female Gunn rats potentially increases estrogen concentrations, however, this remains to be determined. Galmés-Pascual et al., (2017) demonstrated that 17β-estradiol administration in ovariectomized rats increased hepatic CIV activity and protein expression. Furthermore, incubating HepG2 cells with 17β-estradiol increases CIV expression and ATP levels compared to non-treated cells (Galmés-Pascual et al.,

2017). Although pAMPK:AMPK ratios were not different, CIV subunit 1 expression was increased in female Gunn rats, indicating that 17β-estradiol levels may be elevated in this animal model, and requires assessment in future studies.

CONCLUSION

Hyperbilirubinemic Gunn rats displayed a strong sexually dimorphic effect on body composition, fatty acid metabolism, and hepatic mitochondrial biogenesis. While all Gunn rats demonstrated reduced bodyweight and lean mass compared to normobilirubinemic controls, only females had reduced fat mass and hepatic triglyceride concentrations with a trend toward increased β-oxidation gene expression. Reduced fat mass could potentially be explained by elevated hepatic β-oxidation, reduced food intake, differences in lean mass constitution, or increase in hepatic mitochondrial biogenesis. Female Gunn rats demonstrated increased hepatic CI+II OXPHOS FCR and this was associated with elevated *PGC-1α* and greater CIV subunit 1 expression which could have developed as an adaptive response to UCB-mediated inhibition. The absence of significant effects in male Gunn rats suggests an interaction with reproductive hormones including estrogen and warrants further investigation.

DATA AVAILABILITY STATEMENT

The raw data supporting the conclusion of this article will be made available by the authors, without undue reservation, to any qualified researcher.

ETHICS STATEMENT

The animal study was reviewed and approved by Animal Ethics Research Committee of Griffith University, Queensland, Australia.

AUTHOR CONTRIBUTIONS

JV designed and performed the research, analyzed the data, and wrote the manuscript. AB conducted DEXA scan measurements, assisted in method development and study design, provided general guidance and supervision, and had primary role in revision of manuscript. AB and JP assisted in tissue collection surgeries. JP conducted AMPK analysis and measured hepatic triglyceride levels. JV and NS conducted PCR analysis. LD and OH were involved in training and guidance of mitochondrial respiration experiments. OH contributed to study design and interpretation of results. JP, NS, JN, LD, and KW contributed to interpretation of results. All authors contributed to the critical revision of the manuscript. All authors approved the final version and submission of this manuscript.

FUNDING

All funding for this research was provided by the School of Medical Science, Griffith University, Gold Coast, Queensland, Australia.

ACKNOWLEDGMENTS

The authors thank Mr Ryan Shiels and Mr Evan Pennell for input in ideas and general help in the laboratory. The authors also thank Professor John Headrick for his critical revision of the manuscript.

SUPPLEMENTARY MATERIAL

The Supplementary Material for this article can be found online at: https://www.frontiersin.org/articles/10.3389/fphar.2021.586715/full#supplementary-material.

REFERENCES

Bailey, S. A., Zidell, R. H., and Perry, R. W. (2004). Relationships between organ weight and body/brain weight in the rat: what is the best analytical endpoint? *Toxicol. Pathol.* 32, 448–466. doi:10.1080/01926230490465874

Bakrania, B., Du Toit, E. F., Wagner, K. H., Headrick, J. P., and Bulmer, A. C. (2016). Pre- or post-ischemic bilirubin ditaurate treatment reduces oxidative tissue damage and improves cardiac function. *Int. J. Cardiol.* 202, 27–33. doi:10.1016/j.ijcard.2015.08.192

Boon, A. C., Hawkins, C. L., Bisht, K., Coombes, J. S., Bakrania, B., Wagner, K. H., et al. (2012). Reduced circulating oxidized LDL is associated with hypocholesterolemia and enhanced thiol status in Gilbert syndrome. *Free Radic. Biol. Med.* 52, 2120–2127. doi:10.1016/j.freeradbiomed.2012.03.002

Bulmer, A. C., Coombes, J. S., Blanchfield, J. T., Toth, I., Fassett, R. G., and Taylor, S. M. (2011). Bile pigment pharmacokinetics and absorption in the rat: therapeutic potential for enteral administration. *Br. J. Pharmacol.* 164, 1857–1870. doi:10.1111/j.1476-5381.2011.01413.x

Bulmer, A. C., Verkade, H. J., and Wagner, K. H. (2013). Bilirubin and beyond: a review of lipid status in Gilbert's syndrome and its relevance to cardiovascular disease protection. *Prog. Lipid Res.* 52, 193–205. doi:10.1016/j.plipres.2012.11.001

Bulmer, A. C., Bakrania, B., Du Toit, E. F., Boon, A.-C., Clark, P. J., Powell, L. W., et al. (2018). Bilirubin acts as a multipotent guardian of cardiovascular integrity: more than just a radical idea. *Am. J. Physiol. Heart Circul. Physiol.* 315, H429–H447. doi:10.1152/ajpheart.00417.2017

Busiello, R. A., Savarese, S., and Lombardi, A. (2015). Mitochondrial uncoupling proteins and energy metabolism. *Front. Physiol.* 6, 36. doi:10.3389/fphys.2015.00036

Bustin, S. A., Benes, V., Garson, J. A., Hellemans, J., Huggett, J., Kubista, M., et al. (2009). The MIQE guidelines: Minimum information for publication of quantitative real-time PCR experiments. *Clin. Chem.* 55, 611–622. doi:10.1373/clinchem.2008.112797

Celier, C., Francois, D., Marsac, C., and Cresteil, T. (1992). Impairment of mitochondrial 5-aminolevulinic acid synthase activity in Gunn rat liver. *Biochem. Pharmacol.* 44, 1465–1467. doi:10.1016/0006-2952(92)90550-3

Costford, S. R., Chaudhry, S. N., Salkhordeh, M., and Harper, M. E. (2006). Effects of the presence, absence, and overexpression of uncoupling protein-3 on adiposity and fuel metabolism in congenic mice. *Am. J. Physiol. Endocrinol. Metab.* 290, E1304–E1312. doi:10.1152/ajpendo.00401.2005

Divakaruni, A. S., and Brand, M. D. (2011). The regulation and physiology of mitochondrial proton leak. *Physiology* 26, 192–205. doi:10.1152/physiol.00046.2010

Doerrier, C., Garcia-Souza, L. F., Krumschnabel, G., Wohlfarter, Y., Mészáros, A. T., and Gnaiger, E. (2018). High-resolution FluoRespirometry and OXPHOS protocols for human cells, permeabilized fibers from small biopsies of muscle, and isolated mitochondria. *Methods Mol. Biol.* 1782, 31–70. doi:10.1007/978-1-4939-7831-1_3

Dulloo, A. G., Jacquet, J., Solinas, G., Montani, J. P., and Schutz, Y. (2010). Body composition phenotypes in pathways to obesity and the metabolic syndrome. *Int. J. Obes.* 34 Suppl 2, S4–S17. doi:10.1038/ijo.2010.234

Eigentler, A., Draxl, A., and Wiethüchter, A. (2015). Laboratory protocol: citrate synthase a mitochondrial marker enzyme. *Mitochondr. Physiol. Netw.* 04, 1–11.

Even, P. C., Rolland, V., Roseau, S., Bouthegourd, J. C., and Tomé, D. (2001). Prediction of basal metabolism from organ size in the rat: relationship to strain, feeding, age, and obesity. *Am. J. Physiol. Regul. Integr. Comp. Physiol.* 280, R1887–R1896. doi:10.1152/ajpregu.2001.280.6.r1887

Fevery, J. (2008). Bilirubin in clinical practice: a review. *Liver Int.* 28, 592–605. doi:10.1111/j.1478-3231.2008.01716.x

Fontana-Ayoub, M., Fasching, M., and Gnaiger, E. (2016). Selected media and chemicals for respirometry with mitochondrial preparations. *Mitochondr. Physiol. Netw.* 02, 1–10.

Fritz-Niggli, H. (1968). Inhibited oxidative phosphorylation in rat liver mitochondria of congenitally jaundiced Gunn rats and the protective action of hydroxyethylrutosides against bilirubin-induced uncoupling. *Med. Exp. Int. J. Exp. Med.* 18, 239–246. doi:10.1159/000137160

Fu, Y. Y., Kang, K. J., Ahn, J. M., Kim, H. R., Na, K. Y., Chae, D. W., et al. (2010). Hyperbilirubinemia reduces the streptozotocin-induced pancreatic damage through attenuating the oxidative stress in the Gunn rat. *Tohoku J. Exp. Med.* 222, 265–273. doi:10.1620/tjem.222.265

Galmés-Pascual, B. M., Nadal-Casellas, A., Bauza-Thorbrügge, M., Sbert-Roig, M., García-Palmer, F. J., Proenza, A. M., et al. (2017). 17β-estradiol improves hepatic mitochondrial biogenesis and function through PGC1B. *J. Endocrinol.* 232, 297–308. doi:10.1530/JOE-16-0350

Gnaiger, E. (2014). *Mitochondrial pathways and respiratory control an introduction to OXPHOS analysis*.

Greggio, C., Jha, P., Kulkarni, S. S., Lagarrigue, S., Broskey, N. T., Boutant, M., et al. (2017). Enhanced respiratory chain supercomplex formation in response to exercise in human skeletal muscle. *Cell Metab.* 25, 301–311. doi:10.1016/j.cmet.2016.11.004

Hinds, T. D., Hosick, P. A., Chen, S., Tukey, R. H., Hankins, M. W., Nestor-Kalinoski, A., et al. (2017). Mice with hyperbilirubinemia due to Gilbert's syndrome polymorphism are resistant to hepatic steatosis by decreased serine 73 phosphorylation of PPARα. *Am. J. Physiol. Endocrinol. Metab.* 312, E244–E252. doi:10.1152/ajpendo.00396.2016

Holland, O. J., Cuffe, J. S. M., Dekker Nitert, M., Callaway, L., Kwan Cheung, K. A., Radenkovic, F., et al. (2018). Placental mitochondrial adaptations in preeclampsia associated with progression to term delivery. *Cell Death Dis* 9, 1150. doi:10.1038/s41419-018-1190-9

Holliday, M. A., Potter, D., Jarrah, A., and Bearg, S. (1967). The relation of metabolic rate to body weight and organ size. *Pediatr. Res.* 1, 185–195. doi:10.1203/00006450-196705000-00005

Huang, T., Peng, G., Li, G., Yamahara, J., Roufogalis, B. D., and Li, Y. (2006). Salacia oblonga root improves postprandial hyperlipidemia and hepatic steatosis in Zucker diabetic fatty rats: activation of PPAR-alpha. *Toxicol. Appl. Pharmacol.* 210, 225–235. doi:10.1016/j.taap.2005.05.003

Jansen, P. L. M. (1999). Diagnosis and management of Crigler-Najjar syndrome. *Eur. J. Pediatr.* 158 Suppl 2, S89–S94. doi:10.1007/PL00014330

Jeong, S., and Yoon, M. (2007). Inhibition of the actions of peroxisome proliferator-activated receptor alpha on obesity by estrogen. *Obesity (Silver Spring)* 15, 1430–1440. doi:10.1038/oby.2007.171

Jiang, X., and Wang, X. (2004). Cytochrome C-mediated apoptosis. *Annu. Rev. Biochem.* 73, 87–106. doi:10.1146/annurev.biochem.73.011303.073706

Keipert, S., Ost, M., Chadt, A., Voigt, A., Ayala, V., Portero-Otin, M., et al. (2013). Skeletal muscle uncoupling-induced longevity in mice is linked to increased substrate metabolism and induction of the endogenous antioxidant defense system. *Am. J. Physiol. Endocrinol. Metab.* 304, E495–E506. doi:10.1152/ajpendo.00518.2012

Kummitha, C. M., Kalhan, S. C., Saidel, G. M., and Lai, N. (2014). Relating tissue/organ energy expenditure to metabolic fluxes in mouse and human: experimental data integrated with mathematical modeling. *Physiol. Rep.* 2, 1–20. doi:10.14814/phy2.12159

Larsen, S., Kraunsøe, R., Gram, M., Gnaiger, E., Helge, J. W., and Dela, F. (2014). The best approach: homogenization or manual permeabilization of human skeletal muscle fibers for respirometry? *Anal. Biochem.* 446, 64–68. doi:10.1016/j.ab.2013.10.023

Lemieux, H., Semsroth, S., Antretter, H., Höfer, D., and Gnaiger, E. (2011). Mitochondrial respiratory control and early defects of oxidative phosphorylation in the failing human heart. *Int. J. Biochem. Cell Biol.* 43, 1729–1738. doi:10.1016/j.biocel.2011.08.008

Liu, J., Dong, H., Zhang, Y., Cao, M., Song, L., Pan, Q., et al. (2015). Bilirubin increases insulin sensitivity by regulating cholesterol metabolism, adipokines and PPARγ levels. *Sci. Rep.* 5, 9886. doi:10.1038/srep09886

Malik, S. G., Irwanto, K. A., Ostrow, J. D., and Tiribelli, C. (2010). Effect of bilirubin on cytochrome c oxidase activity of mitochondria from mouse brain and liver. *BMC Res. Notes* 3, 162. doi:10.1186/1756-0500-3-162

Mustafa, M. G., Cowger, M. L., and King, T. E. (1969). Effects of bilirubin on mitochondrial reactions. *J. Biol. Chem.* 244, 6403–6414. doi:10.1016/s0021-9258(18)63479-9

Mustafa, M. G., and King, T. E. (1970). Binding of bilirubin with lipid. A possible mechanism of its toxic reactions in mitochondria. *J. Biol. Chem.* 245, 1084–1089. doi:10.1016/s0021-9258(18)63292-2

Naveenkumar, S. K., Thushara, R. M., Sundaram, M. S., Hemshekhar, M., Paul, M., Thirunavukkarasu, C., et al. (2015). Unconjugated bilirubin exerts pro-apoptotic effect on platelets via p38-MAPK activation. *Sci. Rep.* 5, 1–16. doi:10.1038/srep15045

Neuzil, J., and Stocker, R. (1994). Free and albumin-bound bilirubin are efficient co-antioxidants for alpha-tocopherol, inhibiting plasma and low density lipoprotein lipid peroxidation. *J. Biol. Chem.* 269, 16712–16719. doi:10.1016/s0021-9258(19)89449-8

Nguyen, P., Leray, V., Diez, M., Serisier, S., Le Bloch, J. B., and Dumon, H (2008). Liver lipid metabolism. *J. Anim. Physiol. Anim. Nutr. (Berl)* 92, 272–283. doi:10.1111/j.1439-0396.2007.00752.x

Odell, G. B. (1966). The distribution of bilirubin between albumin and mitochondria. *J. Pediatr.* 68, 164–180. doi:10.1016/S0022-3476(66)80147-6

Ost, M., Werner, F., Dokas, J., Klaus, S., and Voigt, A. (2014). Activation of AMPKα2 is not crucial for mitochondrial uncoupling-induced metabolic effects but required to maintain skeletal muscle integrity. *PLoS One* 9, e94689. doi:10.1371/journal.pone.0094689

Ostrow, J. D., Pascolo, L., Brites, D., and Tiribelli, C. (2004). Molecular basis of bilirubin-induced neurotoxicity. *Trends Mol. Med.* 10, 65–70. doi:10.1016/j.molmed.2003.12.003

Pennell, E. N., Shiels, R., Vidimce, J., Wagner, K.-H., Shibeeb, S., and Bulmer, A. C. (2019). The impact of bilirubin ditaurate on platelet quality during storage. *Platelets* 31, 884–813. doi:10.1080/09537104.2019.1693038

Rakhshandehroo, M., Knoch, B., Müller, M., and Kersten, S. (2010). Peroxisome proliferator-activated receptor alpha target genes. *PPAR Res.* 2010, 1–20. doi:10.1155/2010/612089

Rodrigues, C. M., Solá, S., and Brites, D. (2002a). Bilirubin induces apoptosis via the mitochondrial pathway in developing rat brain neurons. *Hepatology* 35, 1186–1195. doi:10.1053/jhep.2002.32967

Rodrigues, C. M., Solá, S., Brito, M. A., Brites, D., and Moura, J. J. (2002b). Bilirubin directly disrupts membrane lipid polarity and fluidity, protein order, and redox status in rat mitochondria. *J. Hepatol.* 36, 335–341. doi:10.1016/S0168-8278(01)00279-3

Rodrigues, C. M., Solá, S., Silva, R., and Brites, D. (2000). Bilirubin and amyloid-beta peptide induce cytochrome c release through mitochondrial membrane permeabilization. *Mol. Med.* 6, 936–946. doi:10.1007/bf03401828

Rolf, B., and Stern, L. (1980). Introduction: bilirubin encephalopathy - the preventive role of bilirubin binding to albumin. *Crit. Rev. Clin. Lab. Sci.* 11, 307–399.

Rossi, F., Francese, M., Iodice, R. M., Falcone, E., Vetrella, S., Punzo, F., et al. (2005). [Inherited disorders of bilirubin metabolism]. *Minerva Pediatr.* 57, 53–63. doi:10.1016/S0168-8278(02)00359-8

Sambasivarao, S. V. (2013). Glucuronidation of the steroid enantiomers ent-17β-estradiol ent-androsterone and ent-etiocholanolone by the human UDP-glucuronosyltransferases. 18, 1199–1216. doi:10.1016/j.micinf.2011.07.011.Innate

Scarpulla, R. C. (2011). Metabolic control of mitochondrial biogenesis through the PGC-1 family regulatory network. *Biochim. Biophys. Acta* 1813, 1269–1278. doi:10.1016/j.bbamcr.2010.09.019

Seyed Khoei, N., Grindel, A., Wallner, M., Mölzer, C., Doberer, D., Marculescu, R., et al. (2018). Mild hyperbilirubinaemia as an endogenous mitigator of overweight and obesity: implications for improved metabolic health. *Atherosclerosis* 269, 306–311. doi:10.1016/j.atherosclerosis.2017.12.021

Shiels, R. G., Vidimce, J., Pearson, A. G., Matthews, B., Wagner, K. H., Battle, A. R., et al. (2019). Unprecedented microbial conversion of biliverdin into bilirubin-10-sulfonate. *Sci. Rep.* 9, 1–10. doi:10.1038/s41598-019-39548-w

Siliart, B. A., Boveris, A., Garaza Pereira, A. M., and Stoppani, A. O. (1972). Bilirubin: a multi-site inhibitor of mitochondrial respiration. *FEBS Lett.* 27, 270. doi:10.1016/0014-5793(72)80638-0

Stanford, J. A., Shuler, J. M., Fowler, S. C., Stanford, K. G., Ma, D., Bittel, D. C., et al. (2015). Hyperactivity in the Gunn rat model of neonatal jaundice: age-related attenuation and emergence of gait deficits. *Pediatr. Res.* 77, 434–439. doi:10.1038/pr.2014.199

Stec, D. E., John, K., Trabbic, C. J., Luniwal, A., Hankins, M. W., Baum, J., et al. (2016). Bilirubin binding to PPARα inhibits lipid accumulation. *PLoS One* 11, e0153427. doi:10.1371/journal.pone.0153427

Stocker, R., Yamamoto, Y., McDonagh, A. F., Glazer, A. N., and Ames, B. N. (1987). Bilirubin is an antioxidant of possible physiological importance. *Science* 235, 1043–1046. doi:10.1126/science.3029864

Vaz, A. R., Delgado-Esteban, M., Brito, M. A., Bolaños, J. P., Brites, D., and Almeida, A. (2010). Bilirubin selectively inhibits cytochrome c oxidase activity and induces apoptosis in immature cortical neurons: assessment of the protective effects of glycoursodeoxycholic acid. *J. Neurochem.* 112, 56–65. doi:10.1111/j.1471-4159.2009.06429.x

Vítek, L., and Ostrow, J. (2009). Bilirubin chemistry and metabolism; harmful and protective aspects. *Curr. Pharm. Des.* 15, 2869–2883. doi:10.2174/138161209789058237

Vítek, L. (2012). The role of bilirubin in diabetes, metabolic syndrome, and cardiovascular diseases. *Front. Pharmacol.* 3, 1–7. doi:10.3389/fphar.2012.00055

Wallner, M., Marculescu, R., Doberer, D., Wolzt, M., Wagner, O., Vitek, L., et al. (2013). Protection from age-related increase in lipid biomarkers and inflammation contributes to cardiovascular protection in Gilbert's syndrome. *Clin. Sci.* 125, 257–264. doi:10.1042/Cs20120661

Watchko, J. F., and Tiribelli, C. (2013). Bilirubin-induced neurologic damage--mechanisms and management approaches. *N. Engl. J. Med.* 369, 2021–2030. doi:10.1056/NEJMra1308124

Wu, Z., Puigserver, P., Andersson, U., Zhang, C., Adelmant, G., Mootha, V., et al. (1999). Mechanisms controlling mitochondrial biogenesis and respiration through the thermogenic coactivator PGC-1. *Cell* 98, 115–124. doi:10.1016/S0092-8674(00)80611-X

Yoon, M., Jeong, S., Nicol, C. J., Lee, H., Han, M., Kim, J. J., et al. (2002). Fenofibrate regulates obesity and lipid metabolism with sexual dimorphism. *Exp. Mol. Med.* 34, 481–488. doi:10.1038/emm.2002.67

Zelenka, J., Dvořák, A., Alán, L., Zadinová, M., Haluzík, M., and Vítek, L. (2016). Hyperbilirubinemia protects against aging-associated inflammation and metabolic deterioration. *Oxid. Med. Cell. Longev.* 26, 6190609. doi:10.1155/2016/6190609

Zeng, Q., Dong, S. Y., Sun, X. N., Xie, J., and Cui, Y. (2012). Percent body fat is a better predictor of cardiovascular risk factors than body mass index. *Braz. J. Med. Biol. Res.* 45, 591–600. doi:10.1590/S0100-879X2012007500059

Zhou, J., Tracy, T. S., and Remmel, R. P. (2011). Correlation between bilirubin glucuronidation and estradiol-3-gluronidation in the presence of model UDP-glucuronosyltransferase 1A1 substrates/inhibitors. *Drug Metab. Dispos.* 39, 322–329. doi:10.1124/dmd.110.035030

Zucker, S. D., Storch, J., Zeidel, M. L., and Gollan, J. L. (1992). Mechanism of the spontaneous transfer of unconjugated bilirubin between small unilamellar phosphatidylcholine vesicles. *Biochemistry* 31, 3184–3192. doi:10.1021/bi00127a020

Conflict of Interest: The authors declare that the research was conducted in the absence of any commercial or financial relationships that could be construed as a potential conflict of interest.

The handling editor declared a past co-authorship with one of the authors AB.

frontiers in Pharmacology

ORIGINAL RESEARCH
published: 12 March 2021
doi: 10.3389/fphar.2021.646953

Life-Long Hyperbilirubinemia Exposure and Bilirubin Priming Prevent *In Vitro* Metabolic Damage

Annalisa Bianco[1,2], *Serena Pinci*[1,2], *Claudio Tiribelli*[1] *and Cristina Bellarosa*[1]*

[1]*Italian Liver Foundation (FIF), Trieste, Italy,* [2]*Department of Life Sciences, University of Trieste, Trieste, Italy*

Background: Unconjugated bilirubin (UCB) is more than the final product of heme catabolism. Mildly elevated systemic bilirubin concentrations, such as in Gilbert syndrome (GS), protect against various oxidative stress-mediated and metabolic diseases, including cardiovascular disease, type 2 diabetes mellitus, metabolic syndrome, cancer, and age-related disease. The Gunn rat is an animal model of hereditary hyperbilirubinemia widely used in assessing the effect of high serum bilirubin concentration in various organs. The present work aims to understand if life-long hyperbilirubinemia and bilirubin-priming might contribute to protection against atherosclerosis and diabetic nephropathy (DN) at the cellular level.

Methods: Primary aortic endothelial cells and podocytes obtained from hyperbilirubinemic homozygous jj and normobilirubinemic heterozygous Nj Gunn rats were exposed to Palmitic Acid (PA) and Angiotensin II (Ang II), respectively, and the effects on cell viability and the activation of damage-related metabolic pathways evaluated. Results were validated on immortalized H5V and HK2 cells exposed to damage after UCB pretreatment.

Results: In both primary cell models, cells obtained from jj Gunn rats showed as significantly higher than Nj Gunn rats at any dose of the toxic agent. Reduction in CHOP expression and IL-6 release was observed in jj primary aortic endothelial cells exposed to PA compared to Nj cells. The same occurred on H5V pretreated with Unconjugated bilirubin. Upon Ang II treatment, primary podocytes from jj Gunn rats showed lower DNA fragmentation, cleaved caspase-3, and cleaved PARP induction than primary podocytes from Nj Gunn rats. In HK2 cells, the induction by Ang II of HIF-1α and LOXl2 was significantly reduced by UCB pretreatment.

Conclusion: Our data suggest that in models of atherosclerosis and DN life–long hyperbilirubinemia exposure or bilirubin-priming significantly contribute to decrease the injury by enhancing thecellular defensive response,

Keywords: Bilirubin, life-long hyperbilirubinemia, metabolic damage, apoptosis, inflammation, fibrosis, ER-stress

OPEN ACCESS

Edited by:
Terry D Hinds,
University of Kentucky, United States

Reviewed by:
David E. Stec,
University of Mississippi Medical Center, United States
Andrew Bulmer,
Griffith University, Australia

***Correspondence:**
Cristina Bellarosa
cristina.bellarosa@fegato.it

Specialty section:
This article was submitted to Experimental Pharmacology and Drug Discovery, a section of the journal Frontiers in Pharmacology

Received: *28 December 2020*
Accepted: *15 February 2021*
Published: *12 March 2021*

Citation:
Bianco A, Pinci S, Tiribelli C and Bellarosa C (2021) Life-Long Hyperbilirubinemia Exposure and Bilirubin Priming Prevent In Vitro *Metabolic Damage. Front. Pharmacol. 12:646953. doi: 10.3389/fphar.2021.646953*

INTRODUCTION

Unconjugated bilirubin (UCB) is the final product of the heme catabolic pathway in the intravascular compartment. UCB is transported in the blood tightly bound to serum albumin before being taken up by the hepatocytes, where it is conjugated. The UCB fraction unbound to albumin (so-called free bilirubin, Bf) represents less than 0.1% and determines the biological properties of this pigment (Ahlfors et al., 2009). Bilirubin behavior in a human body has two faces, similar to the Janus Bifrons, a Roman god (Bianco et al., 2020). Elevated serum UCB concentration, and in particular the Bf fraction, exposes newborns to the risk of neurotoxicity (Watchko and Tiribelli, 2013). Conversely, mildly elevated systemic bilirubin concentrations, such as in Gilbert syndrome (GS) (Bosma et al., 1995), protect against various oxidative stress-mediated and metabolic disorders including cardiovascular disease, type 2 diabetes mellitus, metabolic syndrome, cancer, and age-related disease (Wagner et al., 2015; Vitek et al., 2018). These broad metabolic effects depend on the potent antioxidant activities, anti-inflammatory and immunomodulatory effects (Gazzin et al., 2016), and the recently described endocrine activity of UCB (Hinds Terry and Stec David, 2018; Hinds and Stec, 2019; Creeden et al., 2020; Vítek, 2020).

The partial deficiency of hepatic bilirubin UDP glucuronosyl transferase (UGT1A1) enzyme described in Gilbert patients, increases the unconjugated bilirubin level from 10μM (0.6mg/dl) to 20–70μM (1–5mg/dl) without any sign of liver damage (Vítek and Ostrow, 2009; Wagner et al., 2015). The Gunn rat is a model of hereditary hyperbilirubinemia widely used in assessing the effect of high serum bilirubin concentration in various organs. UCB concentration in hyperbilirubinemic homozygous jj Gunn rats (jj) serum (approximately from 2.42 to 7.36mg/dl) (Boon et al., 2012; Vianello et al., 2018) overlaps with elevated bilirubin concentrations seen in Gilbert subjects (Vítek et al., 2002; Bulmer et al., 2008; Boon et al., 2012). The UCB concentration in various organs and tissues of adult jj Gunn rats is higher than the normobilirubinemic heterozygous Nj Gunn rats (Nj) littermates. The UCB tissue content differs 131 fold in the myocardium (12.3ng/mg of tissue in jj vs. 0.093ng/mg of tissue in Nj) and 144 fold in the kidney (19.3ng/mg of tissue in jj vs. 0.134ng/mg of tissue in Nj) (Zelenka et al., 2008). The hyperbilirubinemia shown by jj Gunn rat is associated with marked anti-inflammatory (Wang et al., 2004), antiproliferative (Ollinger et al., 2005), antihypertensive (Pflueger et al., 2005), blood lipid-modulating properties (Wallner et al., 2013) and with fewer signs of cellular senescence (Zelenka et al., 2016). Moderate hyperbilirubinemia was demonstrated to lower (Ang II)–dependent hypertension by a mechanism that is partially dependent on the inhibition of superoxide production *in vivo* (Stec et al., 2013).

Atherosclerosis represents the major cause of cardiovascular diseases and it is caused by a combination of immune and inflammatory conditions leading to arterial wall injury (Zhang and Kaufman, 2008; Kang et al., 2014). The accumulation of cholesterol and free fatty acids (FFAs) in the ER membranes of macrophages causes calcium release, UPR activation, and CHOP-induced apoptosis (Feng et al., 2003). Palmitic acid (PA) plays an important role in the development of atherosclerosis (Wu et al., 2014) due to its abundance as saturated fatty acid in FFAs (Lambertucci et al., 2008). The accumulation of PA in macrophages activates different transcriptional factors such as NF-κB, thereby inducing the expression of genes encoding inflammatory cytokines including TNF-α and IL-6 (Zhang and Kaufman, 2008; Mazzone et al., 2009).

Diabetic nephropathy (DN) is a complication of diabetes mellitus and it is the leading cause of end-stage renal disease. The final effects of DN involve endothelial injury, tubulointerstitial fibrosis, and podocyte detachment and apoptosis (Maezawa et al., 2015). Angiotensin II (Ang II) has been commonly used in *in vitro* modeling of DN as a pathophysiological mediator that mimics the disease (Slyne et al., 2015). HIF-1α was recently identified as a promoter of kidney fibrosis (Haase, 2012) and has been demonstrated that its activation stimulates collagen accumulation and inflammatory cell recruitment in experimental model of CKD (Higgins et al., 2007; Kimura et al., 2008; Wang et al., 2011). While hypoxia is the main stimulus for HIF activation, Ang II have also been shown to activate HIF-1α (Patten et al., 2010). LOXl2 is considered an element of pro-fibrotic HIF-1α pathway contributing to tubulointerstitial fibrosis development (Schietke et al., 2010). The early pathological changes of DN include podocyte apoptosis (Kume and Koya, 2015). Cleavage of PARP by caspase-3 is considered a hallmark of apoptosis (Jagtap and Szabó, 2005).

The present work aimed to understand if life-long hyperbilirubinemia and bilirubin-priming might have a protective effect in *in vitro models* of atherosclerosis and DN. The use of cellular models might help us to unravel the mechanisms associated with protection from renal injury and metabolic syndrome. Cells obtained from hyperbilirubinemic jj and normobilirubinemic Nj Gunn rats were exposed to damage in the absence of UCB. ER-stress and inflammation activation were evaluated on primary aortic endothelial cells exposed to PA to mimic atherosclerosis. Cell death by apoptosis was studied on primary podocytes exposed to Ang II to mimic diabetic nephropathy. Results were also validated on immortalized cell lines pretreated with UCB (bilirubin-priming) and then exposed to damage.

MATERIALS AND METHODS

Primary Cultures of Rat Podocytes and Aortic Endothelial Cells

Rats used in the project were born in the animal facility of the University of Trieste and animal handling was approved by the Ethics Committee for Animal Experimentation (OPBA) of the University of Trieste (NO1487BEL19) in compliance with the Italian regulation (D.L.vo 26/2014) and the Directive 2010/63/EU of the European Parliament. Hyperbilirubinemic jj and normobilirubinemic Nj Gunn rats were obtained by breeding a male homozygote (jj) with a female heterozygote (Nj). Rats were anesthetized by intraperitoneal injection of Zoletin (60mg/Kg)

and Xylazine (40mg/Kg) and successively sacrificed through decapitation. 90% of rats used were male, but we did not distinguish between males and females, Rats were sacrificed when reached a weight around 200gr, corresponding to 8weeks for males and 10weeks for females..

The kidneys were extracted and conserved in D-glucose (5.5mM) Dulbecco's Modified Eagle's Medium (DMEM) and Ham's F12 medium (Euroclone S. p.A., Milano, Italy) in the ratio 1:1 on ice; Bowman's capsule was removed by pliers (Rush et al., 2018) and the cortical region of the organ was cut into thin strips. Glomeruli were collected in 50ml DMEM/F12 solution using filters with different sizes (80, 100, and 300 meshes) (Sigma-Aldrich, St. Louis MO, United States) and a pestle. They were then centrifuged at 136g for 5minat room temperature. The pellet was seeded in the 25cm^2 culture flasks pre-coated with collagen type IV (Sigma-Aldrich, St. Louis MO, United States). Glomeruli were left in the incubator at 37°C in 5% CO_2 humidified atmosphere in a medium composed by DMEM low glucose and Ham's F12 media (1:1) supplemented with a final concentration of decomplemented 10% (v/v) FBS, 1% penicillin/streptomycin solution (penicillin G (100U/mL), streptomycin (100mg/ml)), L-glutamine (2mmol/L), bovine insulin (5mg/ml), 5μg/ml holo-transferrin (5mg/ml), sodium selenite (5ng/ml) and hydrocortisone (5ng/ml) (Sigma-Aldrich, St. Louis MO, United States) (Zennaro et al., 2014). After 4/5days of incubation podocytes began to emerge and grow out from the glomeruli and, once reached 70–80% of confluence, they were detached using trypsin-EDTA (Euroclone S.p.A., Milano, Italy) and scraper, and collected using a 40-mesh filter. Finally, they were seeded in the 25cm^2 culture flasks pre-coated with collagen type IV (Sigma-Aldrich, St. Louis MO, United States).

The aorta was extracted and conserved in Human Endothelial serum-free medium GIBCO (Life Technologies, Monza, Italy). The aorta (approximately 2cm long) was cleaned from fat tissue, cut into two halves longitudinally, and digested by collagenase type II (2mg/ml) (Worthington Industries, OH, United States). After collagenase treatment, endothelial cells removed from the aorta were collected by centrifugation and suspended in 10ml of Human Endothelial medium GIBCO (Life Technologies, Monza, Italy) supplemented with a final concentration of 10% FBS, EGF (10ng/ml), bFGF 20ng/ml, and 1% penicillin/streptomycin solution (penicillin G (100U/mL) in 5 wells (2ml/well) of 6-multiwell coated with gelatin. After 1h of incubation at 37°C, the supernatant containing endothelial cells was re-seeded in another well. Then aortic endothelial cells were isolated and characterized by magnetic beads coated with CD31 (BD Biosciences, San Jose, CA), a characteristic marker for endothelial cells (Liu et al., 2008).

Immortalized Cell Culture

HK2, an immortalized human proximal tubular epithelial cell line (kindly provided by Prof. R. Bulla, Department of Life Sciences, University of Trieste), was cultured in DMEM low glucose and Ham's F12 media (1:1) supplemented with a final concentration of decomplemented 5% (v/v) FBS, 1% penicillin/streptomycin solution (penicillin G (100U/mL), streptomycin (100mg/ml)), L-glutamine (2mmol/L), bovine insulin (5mg/ml), holo-transferrin (5mg/ml), sodium selenite (5ng/ml), hydrocortisone (5ng/ml), EGF (10ng/ml), T3 (5pg/ml), and PGE (15pg/ml).

H5V, murine heart endothelial cells transformed by polyomavirus middle T-antigen (kindly provided by Istituto Mario Negri, Milan, Italy) were grown in DMEM low glucose containing a final concentration of 10% (v/v) FBS, 1% penicillin/streptomycin solution (penicillin G (100U/mL), streptomycin (100mg/ml)), and L-glutamine (2mmol/L).

Once reached 80% of confluence, both the cell lines were employed for the experimental studies as described below.

Treatments

UCB Treatment

UCB (Sigma-Aldrich, St. Louis MO, United States) was purified as previously described (McDonagh and Assisi, 1972) and dissolved in DMSO to reach a final concentration of 6mM. To reach the final concentrations desired, UCB was serially diluted with DMSO and then with a growth medium. All UCB treatments were performed in the presence of BSA 30μM. The solvent was always 0.1% (v/v) in all bilirubin concentrations used. DMSO 0.1% was used to treat control cells. H5V and HK2 UCB pretreatment were performed in cell culture medium in the presence of BSA 30μM with total UCB concentrations of 1.25 and 2.5μM. According to Roca et al. (2006), these concentration correspond to a Bf < 15nM and = 15nM, respectively. These concentrations of Bf were chosen since they are similar to the plasma Bf levels found in humans with mild unconjugated hyperbilirubinemia (Jacobsen and Wennberg, 1974; Nelson et al., 1974).

Angiotensin II Treatment

Human Angiotensin II (Sigma-Aldrich, St. Louis MO, United States) was reconstituted with phosphate-buffered saline (PBS) at the concentration of 1mg/ml. The range of angiotensin II concentration used in the experiments ranged from 0.01μM up to 10μM and all treatments required 24h (Chen et al., 2017).

Palmitic Acid Preparation and Treatment

Palmitic acid (PA) 0.1M stock solutions were prepared by dissolving fatty acid-free (FFAs) in DMSO. The cells were exposed for 24h. Since albumin played a crucial role in determining the FFAs available concentration, the BSA concentration was kept fixed at 75μM. The FFAs were complexed with bovine serum albumin at a different molar ratio. The medium containing BSA 75μM was aliquoted to set up various BSA/PA ratios (1:1, 1:2, 1:3, 1:4, 1:5, 1:6). DMSO solution was used as control and its final concentration never exceeded 0.1%.

Cytotoxicity Test (PI) and Metabolic Activity Test (MTT)

Both the cytotoxicity test and metabolic activity test were performed in black 96-well plates. Propidium iodide (PI) (Sigma-Aldrich, St. Louis MO, United States) was solubilized in PBS to a final concentration of 50μg/ml. After 60min of

incubation at 37°C, the initial fluorescence intensity due to the dead cells was measured using a multiplate reader (EnSpire 2300, PerkinElmer, MA, United States). The excitation and the emission wavelengths were 530 and 620nm, respectively. After the measurement, Triton X-100at a final concentration of 0.6% was added to each well to permeabilize the cells and let PI label cell nuclei. After 30min of incubation on ice, fluorescence intensity was re-measured to obtain a value corresponding to the total cells. The percentage of dead cells was calculated as the proportion of fluorescence intensity of dead cells to that of total cells.

Metabolic activity was determined by assessing the reduction of 3 (4,5-dimethyl thiazolyl-2)-2,5 diphenyl tetrazolium (MTT, Sigma-Aldrich, St. Louis MO, United States) to formazan by succinate dehydrogenase, a mitochondrial enzyme. In brief, a stock solution of MTT was prepared in PBS (5mg/ml) and then diluted to 0.5mg/ml in the cell medium. Cells were incubated with the cell medium containing MTT for 1hat 37°C. At the end of the incubation time, the insoluble formazan crystals were dissolved in 100μL of DMSO. Absorbance was determined at 562nm by using a multiplate reader (EnSpire 2300, PerkinElmer). The results were expressed as the percentage of control cells not exposed to UCB, which were considered as being 100% viable. It is important to note that MTT test is a quantitative colorimetric assay to detect the survival and proliferation rate of living cells (Mosmann, 1983).

Total Protein Extractions, Quantification, and Western Blot Analysis

Cells were treated when they reached a confluence of approximately 80%. Total proteins were extracted by lysing the cells in an ice-cold cell lysis buffer (Cell Signaling Technology, MA, United States). The protein concentration was determined by the bicinchoninic acid protein assay (BCA) according to manufacturer's instructions. Equal amounts of protein were separated by SDS-polyacrylamide gel electrophoresis (SDS-PAGE) and transferred to PVDF membranes (Bio-Rad Laboratories, CA, United States). Membranes were blocked in 4% milk or 4% BSA in T-TBS (0.2% Tween 20, 20 mMTris–HCl (pH 7.5) and 500 mMNaCl) and incubated overnight at 4°C with the primary antibodies: Anti-HIF-1α antibody (GeneTex, CA, United States), Anti-LOXl2 antibody (CUSABIO Technology LLC, TX, United States), Anti-PARP antibody (Cell Signaling Technology, MA, United States), Anti-CHOP antibody (Invitrogen, Carlsbad, United States) Anti-Caspase-3antibody (Pro and Cleaved forms) (Thermo Fisher Scientific, MA, United States) and antiα-Actin (Sigma-Aldrich, St. Louis MO, United States). Membranes were then incubated with anti-rabbit or anti-mouse secondary antibodies (Dako Laboratories, CA, United States). Protein bands were detected by peroxide reaction using ECL Plus Western Blot detection system solutions (ECL Plus Western Blot detection reagents, GE-Healthcare Bio-Sciences). The relative intensity of protein bands was scanned and analyzed using the C-DiGit® Blot Scanner—LI-COR (Biosciences). The optical density of the bands of interest was normalized to α-Actin and represented as relative to DMSO-treated cells.

Immunofluorescence

Podocytes were seeded onto appropriate glass coverslips pre-coated with poly-L-lysine (Sigma Aldrich, United States) and fixed with 4% paraformaldehyde. A permeabilization step was performed using 0.5% Triton X-100 for 5min. After being blocked with 5% bovine serum albumin (BSA) in PBS-T + 0.1% Tween 20 for 60minat room temperature, the coverslips were incubated with the primary antibody rabbit anti-nephrin (Sigma-Aldrich, St. Louis MO, United States) or anti-Cleaved Caspase-3 antibody (Elabscience, TX, United States) overnight at 4°C. The coverslips were washed thoroughly in PBS and incubated with Alexa Fluor 546 goat anti-rabbit (Invitrogen, Carlsbad, CA, United States) in the dark for 1hat room temperature. After appropriate washes, cell nuclei were stained with Hoechst 33,328 (Sigma-Aldrich, St. Louis MO, United States) at room temperature. Cells were mounted with Fluorescent Mounting Media (Calbiochem, San Diego, CA, United States) and images were acquired using a Leica DM 2000 microscope equipped with an appropriate filter to cover both the excitation and emission wavelengths of Alexa Fluor 546 and Hoechst 33,328. In each experimental setting, images were captured with identical light exposure parameters and aperture settings.

TUNEL Assay

For *in situ* detection of DNA fragmentation, the Click-iT ™ Plus TUNEL Assay was used following the manufacturer's protocol (Thermo Fisher Scientific, MA, United States).

IL-6 ELISA

The supernatants of H5V and Aortic endothelial primary cells were collected and subjected to ELISA analysis using Mouse IL-6 ELISA KIT (Diaclone, Besançon, Francia) and Rat IL-6 ELISA KIT (Thermo Fisher Scientific, MA, United States) respectively, following the manufacturer's instructions.

Statistical Analysis

GraphPad Prism 5 software (GraphPad, San Diego, CA, United States) was used to perform statistical analysis. A statistically significant difference between two data sets was assessed by unpaired two-tailed Student's t-test. Data were obtained from at least three independent experiments and were expressed as mean ± SD. Significance was graphically indicated as follows: $*p < 0.05$, $**p < 0.01$, $***p < 0.001$.

RESULTS

PA and Angiotensin II Impact on Cell Viability in Nj and jj Primary Cells

Aortic endothelial cells harvested from Nj and jj Gunn rats were treated for 24h with increasing doses of PA ranging from 75μM up to 450μM in the presence of 75μM BSA. As shown in **Figure 1A**, upon 75μMPA Nj cells showed a 30% reduction of their viability of as compared to 15–20% jj cells '. A significantly higher ($*p < 0.05$, $***p < 0.001$) viability of jj-derived was found at any PA concentration.

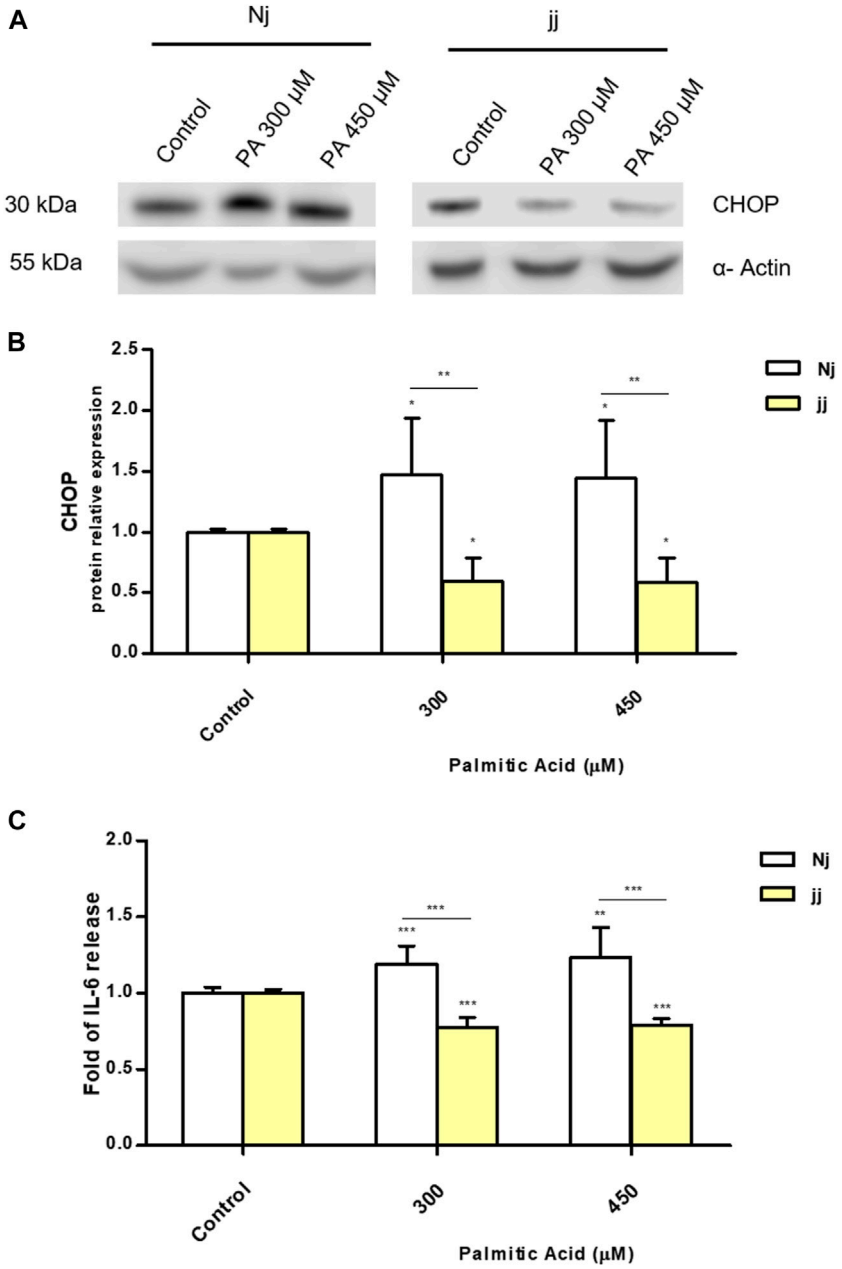

FIGURE 1 | Effect of PA and Ang II treatments on cell viability (MTT test) in normobilirubinemic (Nj) and hyperbiliruninemic (jj) primary cells. **(A)** Aortic endothelial primary cells were exposed to increasing PA concentrations (from 75 to 450μM in the presence of 75μM BSA) for 24h. Cells treated with complete growth medium were considered 100% of viability. Data were expressed as mean ± SD of six independent experiments. **(B)** Primary podocytes were exposed to the Ang II 0.01, 0.1, and 1μM for 24h. Cells treated with complete growth medium were considered 100% of viability. Data were expressed as mean ± SD of three independent experiments. $^{*}p < 0.05$, $^{**}p < 0.01$, $^{***}p < 0.001$.

Primary podocyte characterization by immunofluorescence indicated a highly elevated level of nephrin protein with a plasma membrane and perinuclear co-localization (**Supplementary Figure S1**). The viability of primary podocytes exposed to Ang II 0.01, 0.1, and 1μM for 24h (**Figure 1B**) was significantly ($^{**}p < 0.01$, $^{***}p < 0.001$) reduced at any Ang II concentration (20–25% vs. 10–15% in Nj and jj podocytes.)

The effect of bilirubin priming on cell viability was also evaluated on immortalized cell lines. Heart endothelial cells (H5V) were first exposed to 1.25 or 2.5μM UCB for 16h and then exposed to increasing doses of PA for 24h. As shown in **Figure2** panel A and B, while PA treatment reduced cell viability by approximately 50% and increased cell death up to 20%, UCB pretreatment increased cell viability and reduced the cell death rate. Immortalized human proximal tubular epithelial cells (HK-

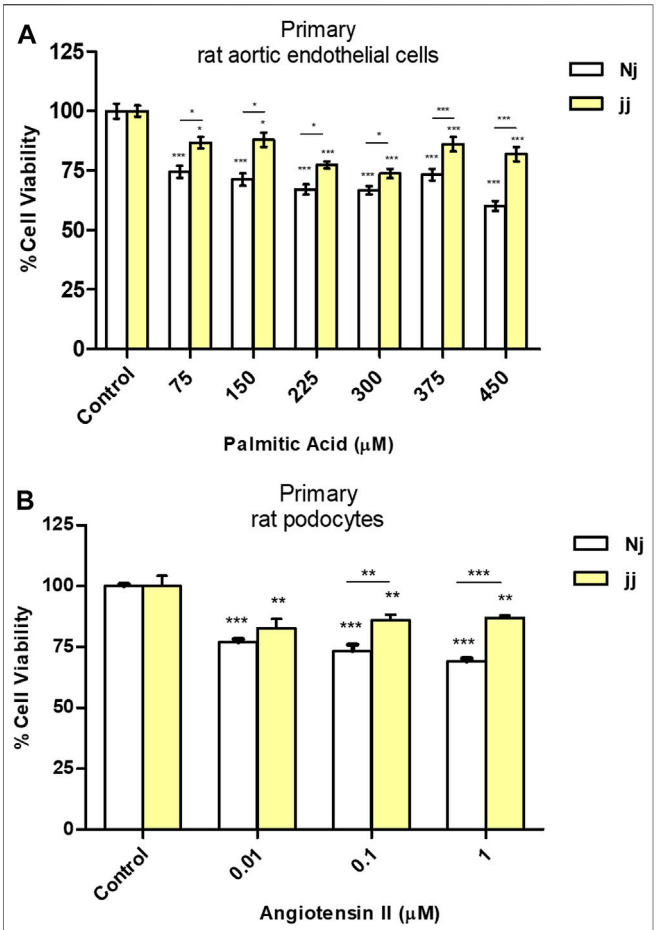

FIGURE 2 | The effect of UCB pretreatment in PA-induced damage on immortalized H5Vcells. H5Vcells were pre-incubated with UCB 1.25 or 2.5μM or DMSO 0.1% (as control) in the presence of BSA 30μM for 16h. At the end of incubation, UCB was removed and H5Vcells were treated with PA 300μM for 24h. **(A)** UCB effect on cell viability was measured by MTT. The viability of control cells was considered 100%. **(B)** UCB effect on cell death detected by PI assay. The percentage of dead cells was calculated as the proportion of fluorescence intensity of dead cells to that of total cells. **(C)** Representative Western Blot for CHOP and α-Actin. **(D)** The optical density of each band was normalized to α-Actin and represented as relative to control cells. **(E)** ELISA quantification of IL-6 release in the cell medium. Results were expressed as relative to control cells release, considered as one. Data were expressed as mean ± SD of at least three independent experiments. $^{*}p < 0.05$, $^{**}p < 0.01$, $^{***}p < 0.001$.

2) were exposed to increasing Ang II concentration (0.01–10μM for 24h). Even if Ang II treatment affected podocytes cell viability, as expected (Baker and Kumar, 2006), there was no change on HK2 cell viability or cell mortality compared to control, when exposed to Ang II (**Supplementary Figures S2A** and **S2B**).

PA Impact on CHOP Activation and IL-6 Release in Nj and jj Aortic Endothelial Primary Cells

We investigated the metabolic pathways involved in aortic endothelial cell viability focusing on ER stress and inflammation. Primary endothelial Nj and jj cells were treated with PA 300 and 450μM for 24h. A significant up-regulation of CHOP protein was observed after 24h of incubation with PA 300 and 450μM only in Nj aortic endothelial cells ($p < 0.05$). Conversely, the same treatment on jj showed a significant decrease in CHOP protein level ($p < 0.05$) (**Figures 3A,B**). A boost in IL-6 production upon PA 300μM and PA 450μM treatments was observed only in Nj cells, while cells from jj rats showed a significant decrease in IL-6 release ($p < 0.001$). The IL-6 release in the cell medium by jj cells was significantly lower than that released by cells from Nj rats ($p < 0.001$) (**Figure 3C**).

Similar results were observed in H5Vcells. Cells were first treated with UCB1.25 or 2.5μM for 16h and then exposed to PA 300μM for 24h. 300μMPA treatment significantly increased the expression level of CHOP protein ($p < 0.01$) while UCB pretreatment restores it to the control level (**Figures 2C,D**). Similarly, UCB pretreatment significantly ($p < 0.05$) reduced PA 300μM increase of IL-6 release (**Figure 2E**).

Angiotensin II Impact on Apoptosis Activation in Nj and jj Podocyte Primary Cells

Treatment with Ang II 0.01, 0.1, and 1μM for 24h showed a significant increase in the number of apoptotic podocytes in both genotypes, as detected by TUNEL assay (**Figure 4A**). However, the extent of Ang II-induced apoptosis was greater in podocytes harvested from Nj rats compared to the podocytes of jj rats at each Ang II concentration tested (**Figure 4B**). In normobilirubinemic podocytes, Ang II treatment induced a dose-dependent increase in cleaved caspase-3 expression assessed by immunofluorescence. Conversely, only 1μM Ang II significantly increased the expression of cleaved caspase-3 in jj podocytes ($p < 0.001$). Caspase-3 activation significantly ($p < 0.01$) differed between the two genotypes upon all Ang II treatments (**Figures 5A,B**). Due to the limited yield of total protein obtained from primary podocyte cultures, WB analysis was performed only on Ang II 0.01 and 0.1μM treatments for cleaved PARP and cleaved caspase-3 (**Figure 5C**). Both treatments induced an almost two-fold increase in the protein level of activated caspase-3 only in cells from Nj rats, while the expression remained similar to control levels in podocytes from jj rats (**Figure 5D**). The cleaved PARP expression was slightly induced in podocytes from Nj rats, while its expression is reduced compared to control cells in podocytes from jj rats (**Figure 5E**).

Impact of UCB on Fibrosis Induced by Angiotensin II in Proximal Tubular Epithelial Cells

Ang II is known to induce fibrosis in tubular epithelial cells. A dose-dependent increase of HIF-1α and LOXl2 protein expression was detected on immortalized human proximal tubular epithelial cells (HK-2) exposed to increasing concentration of Ang II for 24h. Treatment with Ang II concentrations 0.5 and 1μM showed a significant ($p < 0.05$)

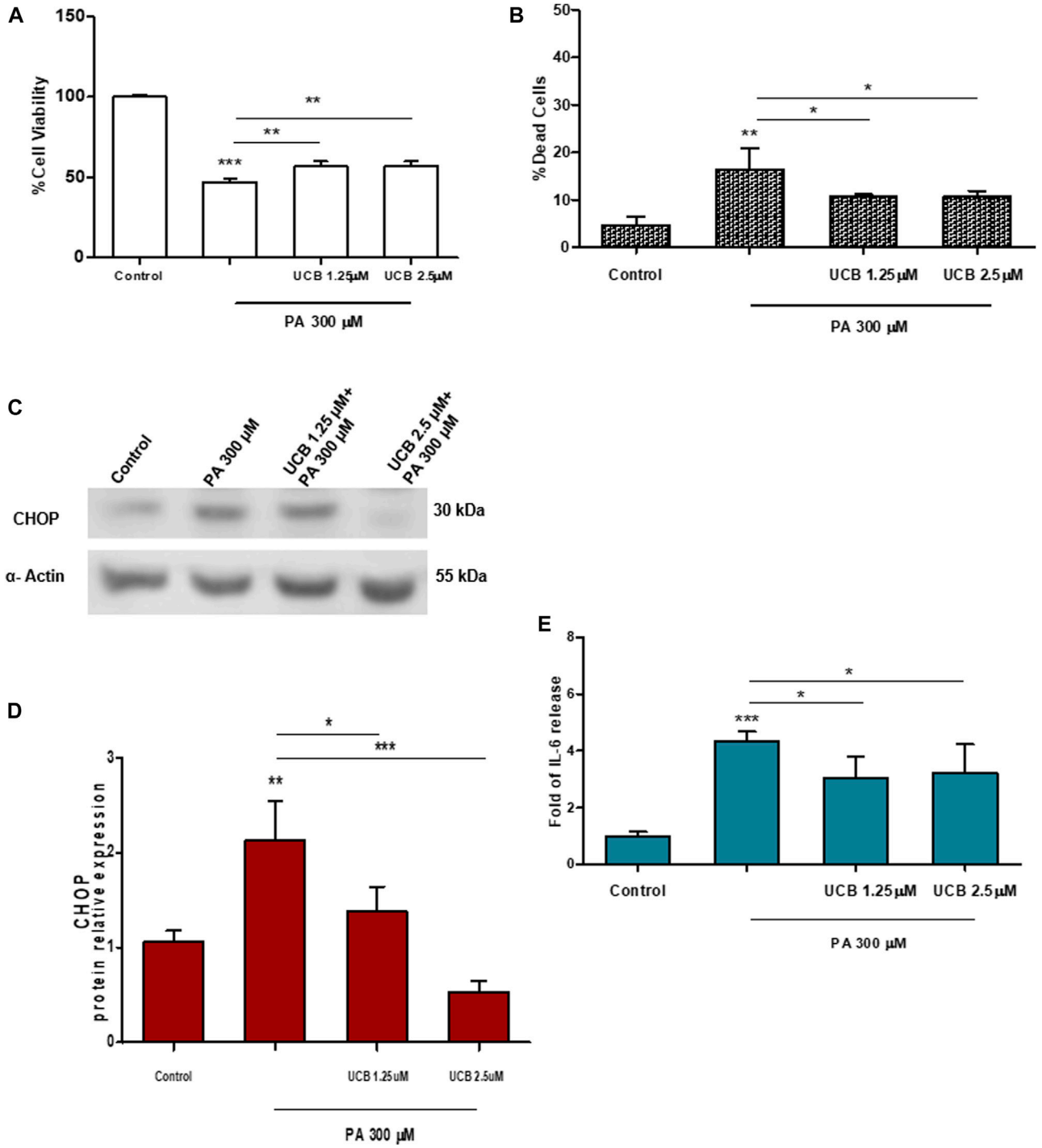

FIGURE 3 | PA impact on CHOP activation and IL-6 release in normobilirubinemic (Nj) and hyperbiliruninemic (jj) aortic endothelial primary cells. Aortic endothelial cells were treated with PA 300 or 450μM or DMSO (as control) in the presence of BSA 75μM for 24h. **(A)** Representative Western Blot for CHOP and α-Actin. **(B)** The optical density of each band was normalized to α-Actin and represented as relative to control cells. **(C)** ELISA quantification of IL-6 release in the cell medium. Results were expressed as relative to control cells release, considered as one. Data were expressed as mean ± SD of at least three independent experiments. Significativity was calculated compared to the control or between samples indicated with bars at each sampling concentration point. $^{*}p < 0.05$, $^{**}p < 0.01$, $^{***}p < 0.001$.

up-regulation of HIF-1α protein expression while LOXl2 protein expression was significantly ($p < 0.05$) up-regulated by AngII 0.05μM (**Figures 6A,B**). Moreover, the effects of Ang II on HIF-1α mRNA expression did not show any variation compared to controls (data not shown). Considering the induction o fHIF-1α and LOXl2 protein by Ang II, we investigated whether UCB

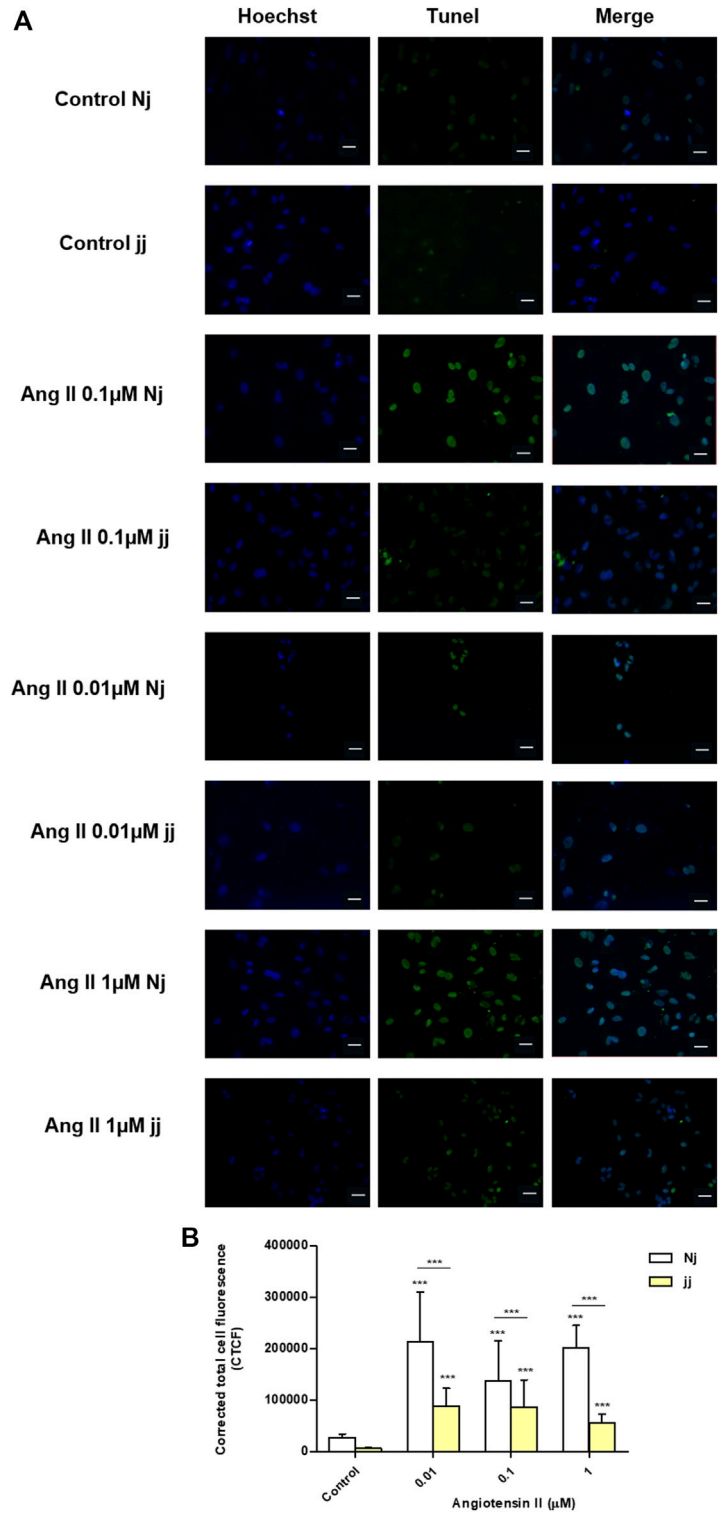

FIGURE 4 | TUNEL staining of normobilirubinemic (Nj) and hyperbiliruninemic (jj) Gunn rat primary podocytes exposed to Ang II treatments. Primary podocytes were exposed to Ang II 0.01, 0.1, and 1μM for 24h. Cells treated with complete growth medium were considered as control. **(A)** Apoptotic cells were detected by TUNEL assay. Green fluorescence indicated TUNEL-positive and blue indicated Hoechst nuclear dye. Magnification ×40. Scale bar 50μm. **(B)** Quantification of fluorescence intensity. The fluorescence intensity was quantified using ImageJ and displayed as corrected total cell fluorescence (CTCF). Results shown represented the mean ± SD of three independent experiments. Significativity was calculated compared to the control or between samples indicated with bars at each sampling concentration point. $^{*}p < 0.05$, $^{**}p < 0.01$, $^{***}p < 0.001$.

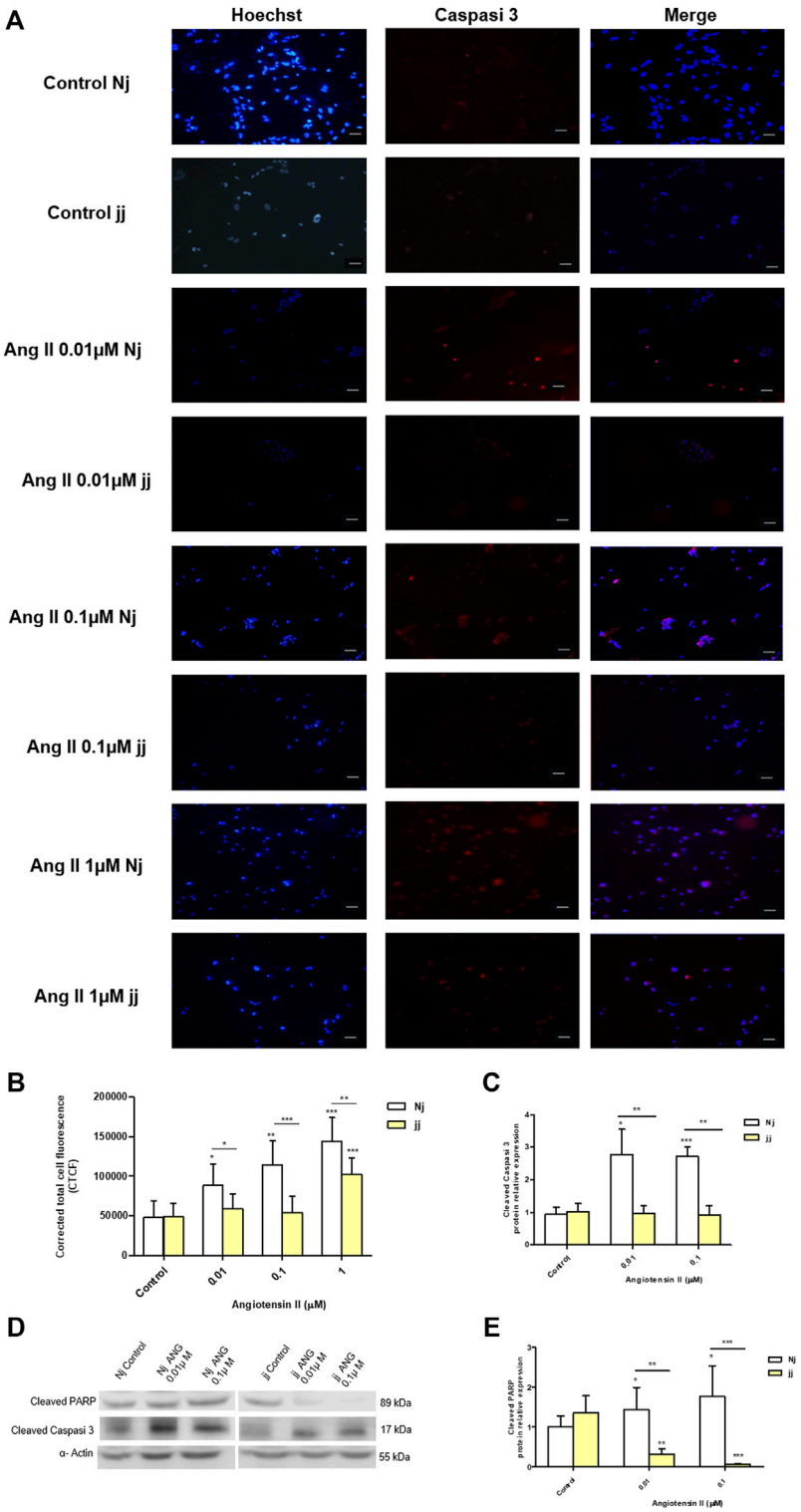

FIGURE 5 | Activation of apoptosis signaling by Ang II in normobilirubinemic (Nj) and hyperbiliruninemic (jj) podocytes primary cells. Primary podocytes were exposed to Ang II 0.01, 0.1, and 1μM for 24h. Cells treated with complete growth medium were considered as control. **(A)** Representative immunofluorescence ($n = 3$) images showing immunostaining for cleaved Caspase-3 (red) and Hoechst (blue) for nuclei. Magnification ×20. Scale bar 50μm. **(B)** Quantification of Cleaved Caspase-3 fluorescence intensity. The fluorescence intensity was quantified using ImageJ and displayed in corrected total cell fluorescence (CTCF). **(C)** Representative Western blot analysis of cleaved PARP, cleaved caspase-3 and α-Actin expression in total cell lysates. **(D)** The optical density of cleaved caspase-3 protein from three independent experiments was normalized to α-Actin and represented as relative to untreated cells. **(E)** The optical density of cleaved PARP protein from three independent experiments was normalized to α-Actin and represented as relative to untreated cells. Significativity was calculated compared to the control or between samples indicated with bars at each sampling concentration point. $^{*}p < 0.05$, $^{**}p < 0.01$, $^{***}p < 0.001$.

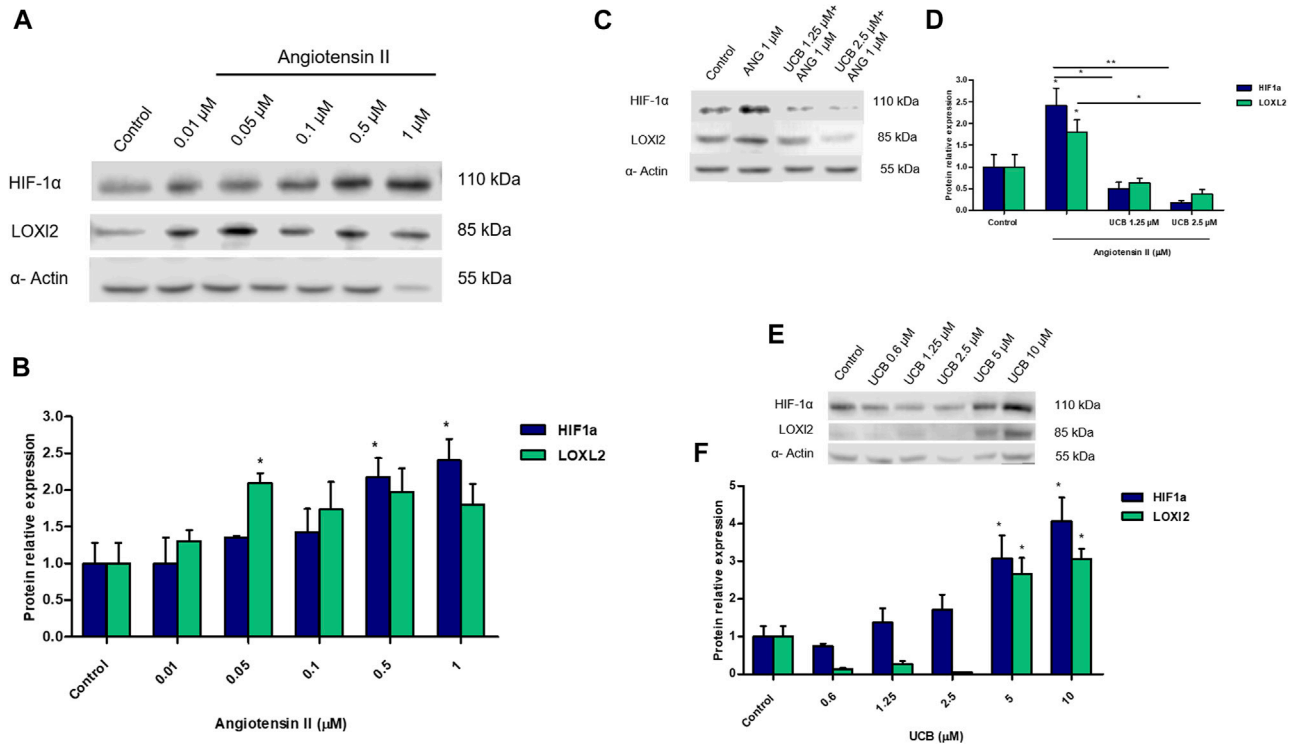

FIGURE 6 | The impact of UCB on proximal tubular epithelial cells fibrosis induced by Ang II. **(A)** Representative Western blot analysis of HIF-1a, LOXl2 and α-Actin expression in HK2 cells treated with increasing doses of Ang II for 24h. **(B)** Theoptical density of each band was normalized to α-Actin and represented as relative to control cells. **(C)** Representative Western blot analysis of HIF-1α, LOXl2 and α-Actin expression in HK2. Cells were pre-incubated with UCB 1.25 or 2.5µM or DMSO 0.1% in the presence of BSA 30µM for 16h. At the end of incubation, UCB was removed and cells treated with Ang II 1µM for 24h. **(D)** The optical density of each band was normalized to α-Actin and represented as relative to control cells. **(E)** Representative Western blot analysis of HIF-1α, LOXl2 and α-Actin expression in HK2 cells treated with increasing doses of UCB for 24h. **(F)** The optical density of each band was normalized to α-Actin and represented as relative to control cells. Data were expressed as mean ± SD of three independent experiments. Significativity was calculated compared to the control or between samples indicated with bars at each sampling concentration point. $^{**}p < 0.05$, $^{**}p < 0.01$, $^{***}p < 0.001$.

pretreatment may influence its expression. Pretreatment with 1.25µM or 2.5 UCB significantly reduced HIF-1α protein induction by AngII in a dose-dependent manner ($p < 0.05$, $p < 0.01$). UCB also significantly ($p < 0.05$) reduced LOXl2 protein to 0.5-fold of control cells (**Figures 6C,D**). The effect of UCB alone on HIF-1α and LOXl2 protein expression was evaluated by exposing for 24h HK2 cells to a dose-dependent UCB treatment (from 0.6 to 10µM). HIF-1α and LOXl2 expression was reduced by UCB treatment up to 2.5µM, while higher concentration induced their expression (**Figures 6E,F**).

DISCUSSION

Several studies showed the protective effect of bilirubin against oxidative-stress based disease. In the present work, we assessed if life-long hyperbilirubinemia and bilirubin-priming might significantly contribute to the protection against metabolic insult *in vitro*. To this goal, we used primary cells obtained from hyperbilirubinemic jj and normobilirubinemic Nj Gunn rats exposed to damaging agents. Primary cells from jj Gunn rats were more viable and less prone to damage compared to cells from Nj Gunn rats, suggesting a modulating activity on cellular signaling of a life-long hyperbilirubinemia. This conclusion was further supported by data obtained in immortalized cell lines pretreated with UCB (bilirubin-priming) and then exposed to damage.

Studies comparing the response to damage between primed and not primed UCB cells are scant. Recently Valaskova et al. showed that the cell viability of primary hepatocytes from jj Gunn rats exposed to TNF-α 100ng/ml was significantly higher than that of primary hepatocytes from Nj Gunn rats ($p < 0.05$) (Valaskova et al., 2019). Our results expand this observation as we assayed the viability of other primary cell types (podocytes and primary aortic endothelial cells) exposed to increasing concentration of a damaging stimulus (PA and Ang II, respectively). In both cell models and at any toxic agent concentration, the viability of cells derived from jj Gunn rats was significantly higher than that of Nj cells. In line with this, UCB pretreatment in H5V cells exposed to PA reduced the percentage of dead cells and increased cell viability compared to DMSO pretreated cells. Bilirubin activates various nuclear and cytoplasmic receptors, resembling the endocrine activities of hormonal substances. This is true both for the "classic" hepatic nuclear receptors, and for some lesser-explored receptors or other

signaling molecules (Vítek, 2020). We previously showed that 24h of bilirubin-priming modulates the glutathione levels in neuroblastoma cells through the induction of the System Xc-, and this renders the cell less prone to oxidative damage (Giraudi et al., 2011).

Bilirubin exerts potent anti-inflammatory and immunomodulatory activities (Jangi et al., 2013) and the interrelation between UCB, ER-Stress, inflammation, and associated cascade of events has been demonstrated (Barateiro et al., 2012). An increasing body of evidence suggests that mildly elevated bilirubin level could control inflammation, both *in vitro* and *in vivo*, through the mechanisms involved in NF-κB signaling pathway inhibition as well as the activation of inflammasomes (Li et al., 2020) suppressing the production of pro-inflammatory cytokines (Liu et al., 2008; Adin et al., 2017). We observed a reduced CHOP expression and IL-6 release in jj aortic endothelial primary cells exposed to PA compared to cells from Nj rats. Besides, in immortalized H5V cell line pretreatment with UCB significantly reduced CHOP expression and IL-6 release induced by PA treatment. Of notice, the TNF-α-stimulated nuclear translocation of NF-kβ was inhibited by UCB in H5V cells (Mazzone et al., 2009). Co-treatment with UCB resulted in reducing ER-stress and the subsequent inflammatory response also in *in vitro* model of gut inflammation (Gundamaraju et al., 2019). The anti-inflammatory and anti-oxidative effects may likely contribute to the protective role of bilirubin on vascular damage (Inoguchi et al., 2016).

Diabetic nephropathy (DN) is a complication of diabetes mellitus and is the leading cause of end-stage renal disease. The final effects of diabetic nephropathy involve endothelial injury, tubule-interstitial fibrosis, and podocytes detachment and apoptosis (Maezawa et al., 2015). Bilirubin provided a nephroprotective effect in different *in vivo* models as showed by the finding that jj Gunn rats showed significantly lower creatinine compared with Wistar rats at day 5 in a cisplatin nephrotoxicity model (Barabas et al., 2008). In streptozotocin-induced diabetic damage, jj Gunn rats exhibited significantly less urinary albumin excretion, did not develop renal mesangial expansion, and expressed lower levels of TGF-β and fibronectin than diabetic Nj Gunn rats (Fujii et al., 2010). We found that, upon Ang II treatment, primary podocytes from jj Gunn rats showed lower DNA fragmentation, cleaved caspase-3, and cleaved PARP induction than primary podocytes from Nj Gunn rats. Also, on the cyclosporine (CsA)-induced nephropathy rat model, a significantly lower number of apoptotic cells was observed in the bilirubin-treated rat kidneys compared to controls, confirming the bilirubin anti-apoptotic effect (Oh et al., 2013).

Recent studies have proposed for HIF-1α downstream function of a pro-fibrotic signaling cascade stimulated by angiotensin II, leading to epithelial-mesenchymal transition and excessive collagen apposition (Wang et al., 2011). We found that Ang II acts as a pro-fibrotic marker inducing HIF-1α and LOXl2 protein expression in a dose-dependent manner. Expanding the previous evidence (Kim et al., 2014), we showed that bilirubin modulated the expression of the pro-fibrotic marker with double-side behavior. UCB treatment up to 2.5μM decreased HIF-1α and LOXl2 expression compared to control, while higher UCB concentration induced their expression This is due to the extent of intracellular UCB concentration which determines the UCB anti-or pro-oxidant effect (Bianco et al., 2020). HIF-1α and LOXl2 protein induction by Ang II was significantly reduced by UCB pretreatment of 1.25 or 2.5μM corresponding to an antioxidant intracellular UCB concentration (Bianco et al., 2020). Bilirubin has been shown to have an anti-fibrotic effect on cyclosporine (CsA)-induced nephropathy *in vivo*, given that bilirubin pretreatment significantly improved afferent arteriolopathy, tubulointerstitial fibrosis, and tubular injury compared to the CsA-only treated rats (Oh et al., 2013).

Our data suggest that life–long hyperbilirubinemia exposure and bilirubin-priming significantly contribute to increase cell viability and enhance responses to damage in *in vitro* models of atherosclerosis and DN. Collectively these findings further support the beneficial effect of bilirubin on different organs.

DATA AVAILABILITY STATEMENT

The original contributions presented in the study are included in the article/**Supplementary Material**, further inquiries can be directed to the corresponding author.

ETHICS STATEMENT

The animal study was reviewed and approved by the Ethics Committee for Animal Experimentation (OPBA), University of Trieste.

AUTHOR CONTRIBUTIONS

AB and CB designed the study. AB, SP, and CB performed experiments and data analysis. AB, SP, CT, and CB interpreted the findings, prepared, and completed the manuscript. CT revised the final version. All authors contributed to the article and approved the submitted version.

FUNDING

This work has been supported in part by Beneficentia Stiftung, Banca d'Italia, and FIF internal grants.

ACKNOWLEDGMENTS

The authors want to thank Deborah Bonazza e Cristina Bottin for IHC of rat aorta and kidney; Cristina Zennaro for teaching how to prepare primary rat podocytes; Fluer Bossi for helping in the setup or rat aortic endothelial isolation.

SUPPLEMENTARY MATERIAL

The Supplementary Material for this article can be found online at: https://www.frontiersin.org/articles/10.3389/fphar.2021.646953/full#supplementary-material.

REFERENCES

Adin, C. A., VanGundy, Z. C., Papenfuss, T. L., Xu, F., Ghanem, M., Lakey, J., et al. (2017). Physiologic doses of bilirubin contribute to tolerance of islet transplants by suppressing the innate immune response. *Cell Transpl.* 26, 11–21. doi:10.3727/096368916X692096

Ahlfors, C. E., Wennberg, R. P., Ostrow, J. D., and Tiribelli, C. (2009). Unbound (free) bilirubin: improving the paradigm for evaluating neonatal jaundice. *Clin. Chem.* 55, 1288–1299. doi:10.1373/clinchem.2008.121269

Baker, K. M., and Kumar, R. (2006). Intracellular angiotensin II induces cell proliferation independent of AT1 receptor. *Am. J. Physiol. Cell Physiol.* 291, C995–C1001. doi:10.1152/ajpcell.00238.2006

Barabas, K., Milner, R., Farese, J., Baylis, C., Croker, B., Archer, L., et al. (2008). Hyperbilirubinemia's protective effect against cisplatin nephrotoxicity in the Gunn rat. *Anticancer Drugs* 19, 495–502. doi:10.1097/CAD.0b013e3282fdc391

Barateiro, A., Vaz, A. R., Silva, S. L., Fernandes, A., and Brites, D. (2012). ER stress, mitochondrial dysfunction and calpain/JNK activation are involved in oligodendrocyte precursor cell death by unconjugated bilirubin. *Neuromolecul. Med.* 14, 285–302. doi:10.1007/s12017-012-8187-9

Bianco, A., Dvořák, A., Capková, N., Gironde, C., Tiribelli, C., Furger, C., et al. (2020). The extent of intracellular accumulation of bilirubin determines its anti- or pro-oxidant effect. *Int. J. Mol. Sci.* 21. doi:10.3390/ijms21218101

Boon, A.-C., Hawkins, C. L., Bisht, K., Coombes, J. S., Bakrania, B., Wagner, K.-H., et al. (2012). Reduced circulating oxidized LDL is associated with hypocholesterolemia and enhanced thiol status in Gilbert syndrome. *Free Radic. Biol. Med.* 52, 2120–2127. doi:10.1016/j.freeradbiomed.2012.03.002

Bosma, P. J., Chowdhury, J. R., Bakker, C., Gantla, S., de Boer, A., Oostra, B. A., et al. (1995). The genetic basis of the reduced expression of bilirubin UDP-glucuronosyltransferase 1 in Gilbert's syndrome. *N. Engl. J. Med.* 333, 1171–1175. doi:10.1056/NEJM199511023331802

Bulmer, A. C., Blanchfield, J. T., Toth, I., Fassett, R. G., and Coombes, J. S. (2008). Improved resistance to serum oxidation in Gilbert's syndrome: a mechanism for cardiovascular protection. *Atherosclerosis* 199, 390–396. doi:10.1016/j.atherosclerosis.2007.11.022

Chen, L., Chen, D.-Q., Wang, M., Liu, D., Chen, H., Dou, F., et al. (2017). Role of RAS/Wnt/β-catenin axis activation in the pathogenesis of podocyte injury and tubulo-interstitial nephropathy. *Chem. Biol. Interact.* 273, 56–72. doi:10.1016/j.cbi.2017.05.025

Creeden, J. F., Gordon, D. M., Stec, D. E., and Hinds, T. D. (2020). Bilirubin as a metabolic hormone: the physiological relevance of low levels. *Am. J. Physiol. Endocrinol. Metab.* doi:10.1152/ajpendo.00405.2020

Feng, B., Yao, P. M., Li, Y., Devlin, C. M., Zhang, D., Harding, H. P., et al. (2003). The endoplasmic reticulum is the site of cholesterol-induced cytotoxicity in macrophages. *Nat. Cell Biol.* 5, 781–792. doi:10.1038/ncb1035

Fujii, M., Inoguchi, T., Sasaki, S., Maeda, Y., Zheng, J., Kobayashi, K., et al. (2010). Bilirubin and biliverdin protect rodents against diabetic nephropathy by downregulating NAD(P)H oxidase. *Kidney Int.* 78, 905–919. doi:10.1038/ki.2010.265

Gazzin, S., Vitek, L., Watchko, J., Shapiro, S. M., and Tiribelli, C. (2016). A novel perspective on the biology of bilirubin in health and disease. *Trends Mol. Med.* 22, 758–768. doi:10.1016/j.molmed.2016.07.004

Giraudi, P. J., Bellarosa, C., Coda-Zabetta, C. D., Peruzzo, P., and Tiribelli, C. (2011). Functional induction of the cystine-glutamate exchanger system Xc(-) activity in SH-SY5Y cells by unconjugated bilirubin. *PloS One* 6, e29078. doi:10.1371/journal.pone.0029078

Gundamaraju, R., Vemuri, R., Chong, W. C., Bulmer, A. C., and Eri, R. (2019). Bilirubin attenuates ER stress-mediated inflammation, escalates apoptosis and reduces proliferation in the LS174T colonic epithelial cell line. *Int. J. Med. Sci.* 16, 135–144. doi:10.7150/ijms.29134

Haase, V. H. (2012). Hypoxia-inducible factor signaling in the development of kidney fibrosis. *Fibrogenesis Tissue Rep.* 5, S16. doi:10.1186/1755-1536-5-S1-S16

Higgins, D. F., Kimura, K., Bernhardt, W. M., Shrimanker, N., Akai, Y., Hohenstein, B., et al. (2007). Hypoxia promotes fibrogenesis *in vivo* via HIF-1 stimulation of epithelial-to-mesenchymal transition. *J. Clin. Invest.* 117, 3810–3820. doi:10.1172/JCI30487

Hinds, T. D., and Stec, D. E. (2019). Bilirubin safeguards cardiorenal and metabolic diseases: a protective role in health. *Curr. Hypertens. Rep.* 21, 87. doi:10.1007/s11906-019-0994-z

Hinds Terry, D., and Stec David, E. (2018). Bilirubin, a cardiometabolic signaling molecule. *Hypertension* 72, 788–795. doi:10.1161/HYPERTENSIONAHA.118.11130

Inoguchi, T., Sonoda, N., and Maeda, Y. (2016). Bilirubin as an important physiological modulator of oxidative stress and chronic inflammation in metabolic syndrome and diabetes: a new aspect on old molecule. *Diabetol. Int.* 7, 338–341. doi:10.1007/s13340-016-0288-5

Jacobsen, J., and Wennberg, R. P. (1974). Determination of unbound bilirubin in the serum of newborns. *Clin. Chem.* 20, 783.

Jagtap, P., and Szabó, C. (2005). Poly(ADP-ribose) polymerase and the therapeutic effects of its inhibitors. *Nat. Rev. Drug Discov.* 4, 421–440. doi:10.1038/nrd1718

Jangi, S., Otterbein, L., and Robson, S. (2013). The molecular basis for the immunomodulatory activities of unconjugated bilirubin. *Int. J. Biochem. Cell Biol.* 45, 2843–2851. doi:10.1016/j.biocel.2013.09.014

Kang, S. J., Lee, C., and Kruzliak, P. (2014). Effects of serum bilirubin on atherosclerotic processes. *Ann. Med.* 46, 138–147. doi:10.3109/07853890.2014.895588

Kim, S. G., Ahn, S.-Y., Lee, E. S., Kim, S., Na, K. Y., Chae, D.-W., et al. (2014). Bilirubin activates transcription of HIF-1α in human proximal tubular cells cultured in the physiologic oxygen content. *J. Korean Med. Sci.* 29 (Suppl. 2), S146–S154. doi:10.3346/jkms.2014.29.S2.S146

Kimura, K., Iwano, M., Higgins, D. F., Yamaguchi, Y., Nakatani, K., Harada, K., et al. (2008). Stable expression of HIF-1α in tubular epithelial cells promotes interstitial fibrosis. *Am. J. Physiol. Ren. Physiol.* 295, F1023–F1029. doi:10.1152/ajprenal.90209.2008

Kume, S., and Koya, D. (2015). Autophagy: a novel therapeutic target for diabetic nephropathy. *Diabetes Metab. J.* 39, 451–460. doi:10.4093/dmj.2015.39.6.451

Lambertucci, R. H., Hirabara, S. M., Silveira, L. D. R., Levada-Pires, A. C., Curi, R., and Pithon-Curi, T. C. (2008). Palmitate increases superoxide production through mitochondrial electron transport chain and NADPH oxidase activity in skeletal muscle cells. *J. Cell. Physiol.* 216, 796–804. doi:10.1002/jcp.21463

Li, Y., Huang, B., Ye, T., Wang, Y., Xia, D., and Qian, J. (2020). Physiological concentrations of bilirubin control inflammatory response by inhibiting NF-κB and inflammasome activation. *Int. Immunopharmacol.* 84, 106520. doi:10.1016/j.intimp.2020.106520

Liu, Y., Li, P., Lu, J., Xiong, W., Oger, J., Tetzlaff, W., et al. (2008). Bilirubin possesses powerful immunomodulatory activity and suppresses experimental autoimmune encephalomyelitis. *J. Immunol. Baltim.* 181, 1887–1897. doi:10.4049/jimmunol.181.3.1887

Maezawa, Y., Takemoto, M., and Yokote, K. (2015). Cell biology of diabetic nephropathy: roles of endothelial cells, tubulointerstitial cells and podocytes. *J. Diabetes Investig.* 6, 3–15. doi:10.1111/jdi.12255

Mazzone, G. L., Rigato, I., Ostrow, J. D., and Tiribelli, C. (2009). Bilirubin effect on endothelial adhesion molecules expression is mediated by the NF-kappaB signaling pathway. *Biosci. Trends* 3, 151–157.

McDonagh, A. F., and Assisi, F. (1972). The ready isomerization of bilirubin IX- in aqueous solution. *Biochem. J.* 129, 797–800.

Mosmann, T. (1983). Rapid colorimetric assay for cellular growth and survival: application to proliferation and cytotoxicity assays. *J. Immunol. Methods* 65, 55–63.

Nelson, T., Jacobsen, J., and Wennberg, R. P. (1974). Effect of pH on the interaction of bilirubin with albumin and tissue culture cells. *Pediatr. Res.* 8, 963–967. doi:10.1203/00006450-197412000-00010

Oh, S. W., Lee, E. S., Kim, S., Na, K. Y., Chae, D. W., Kim, S., et al. (2013). Bilirubin attenuates the renal tubular injury by inhibition of oxidative stress and apoptosis. *BMC Nephrol.* 14, 105. doi:10.1186/1471-2369-14-105

Ollinger, R., Bilban, M., Erat, A., Froio, A., McDaid, J., Tyagi, S., et al. (2005). Bilirubin: a natural inhibitor of vascular smooth muscle cell proliferation. *Circulation* 112, 1030–1039. doi:10.1161/CIRCULATIONAHA.104.528802

Patten, D. A., Lafleur, V. N., Robitaille, G. A., Chan, D. A., Giaccia, A. J., and Richard, D. E. (2010). Hypoxia-inducible factor-1 activation in nonhypoxic conditions: the essential role of mitochondrial-derived reactive oxygen species. *Mol. Biol. Cell* 21, 3247–3257. doi:10.1091/mbc.E10-01-0025

Pflueger, A., Croatt, A. J., Peterson, T. E., Smith, L. A., d'Uscio, L. V., Katusic, Z. S., et al. (2005). The hyperbilirubinemic Gunn rat is resistant to the pressor effects of angiotensin II. *Am. J. Physiol. Ren. Physiol.* 288, F552–F558. doi:10.1152/ajprenal.00278.2004

Roca, L., Calligaris, S., Wennberg, R. P., Ahlfors, C. E., Malik, S. G., Ostrow, J. D., et al. (2006). Factors affecting the binding of bilirubin to serum albumins: validation and application of the peroxidase method. *Pediatr. Res.* 60, 724–728. doi:10.1203/01.pdr.0000245992.89965.94

Rush, B. M., Small, S. A., Stolz, D. B., and Tan, R. J. (2018). An efficient sieving method to isolate intact glomeruli from adult rat Kidney. *J. Vis. Exp. JoVE.* doi:10.3791/58162

Schietke, R., Warnecke, C., Wacker, I., Schödel, J., Mole, D. R., Campean, V., et al. (2010). The Lysyl oxidases LOX and LOXL2 are necessary and sufficient to repress E-cadherin in hypoxia. *J. Biol. Chem.* 285, 6658–6669. doi:10.1074/jbc.M109.042424

Slyne, J., Slattery, C., McMorrow, T., and Ryan, M. P. (2015). New developments concerning the proximal tubule in diabetic nephropathy: *in vitro* models and mechanisms. *Nephrol. Dial. Transpl. Off. Publ. Eur. Dial. Transpl. Assoc. Eur. Ren. Assoc.* 30 (Suppl. 4), iv60–iv67. doi:10.1093/ndt/gfv264

Stec, D. E., Storm, M. V., Pruett, B. E., and Gousset, M. U. (2013). Antihypertensive actions of moderate hyperbilirubinemia: role of superoxide inhibition. *Am. J. Hypertens.* 26, 918–923. doi:10.1093/ajh/hpt038

Valaskova, P., Dvorak, A., Lenicek, M., Zizalova, K., Kutinova-Canova, N., Zelenka, J., et al. (2019). Hyperbilirubinemia in Gunn rats is associated with decreased inflammatory response in LPS-mediated systemic inflammation. *Int. J. Mol. Sci.* 20, 306. doi:10.3390/ijms20092306

Vianello, E., Zampieri, S., Marcuzzo, T., Tordini, F., Bottin, C., Dardis, A., et al. (2018). Histone acetylation as a new mechanism for bilirubin-induced encephalopathy in the Gunn rat. *Sci. Rep.* 8, 13690. doi:10.1038/s41598-018-32106-w

Vitek, L., Bellarosa, C., and Tiribelli, C. (2018). Induction of mild hyperbilirubinemia: hype or real therapeutic opportunity?. *Clin. Pharmacol. Ther.* 13, 41. doi:10.1002/cpt.1341

Vítek, L. (2020). Bilirubin as a signaling molecule. *Med. Res. Rev.* 21, 660. doi:10.1002/med.21660

Vítek, L., Jirsa, M., Brodanová, M., Kalab, M., Marecek, Z., Danzig, V., et al. (2002). Gilbert syndrome and ischemic heart disease: a protective effect of elevated bilirubin levels. *Atherosclerosis* 160, 449–456. doi:10.1016/s0021-9150(01)00601-3

Vítek, L., and Ostrow, J. D. (2009). Bilirubin chemistry and metabolism; harmful and protective aspects. *Curr. Pharm. Des.* 15, 2869–2883. doi:10.2174/138161209789058237

Wagner, K.-H., Wallner, M., Mölzer, C., Gazzin, S., Bulmer, A. C., Tiribelli, C., et al. (2015). Looking to the horizon: the role of bilirubin in the development and prevention of age-related chronic diseases. *Clin. Sci. Lond. Engl.* 129, 1–25. doi:10.1042/CS20140566

Wallner, M., Marculescu, R., Doberer, D., Wolzt, M., Wagner, O., Vitek, L., et al. (2013). Protection from age-related increase in lipid biomarkers and inflammation contributes to cardiovascular protection in Gilbert's syndrome. *Clin. Sci. Lond. Engl.* 125, 257–264. doi:10.1042/CS20120661

Wang, W. W., Smith, D. L. H., and Zucker, S. D. (2004). Bilirubin inhibits iNOS expression and NO production in response to endotoxin in rats. *Hepatol. Baltim. Md.* 40, 424–433. doi:10.1002/hep.20334

Wang, Z., Tang, L., Zhu, Q., Yi, F., Zhang, F., Li, P.-L., et al. (2011). Contribution of hypoxia inducible factor-1α to the profibrotic action of angiotensin II in cultured renal medullary interstitial cells. *Kidney Int.* 79, 300–310. doi:10.1038/ki.2010.326

Watchko, J. F., and Tiribelli, C. (2013). Bilirubin-induced neurologic damage--mechanisms and management approaches. *N. Engl. J. Med.* 369, 2021–2030. doi:10.1056/NEJMra1308124

Wu, D., Liu, J., Pang, X., Wang, S., Zhao, J., Zhang, X., et al. (2014). Palmitic acid exerts pro-inflammatory effects on vascular smooth muscle cells by inducing the expression of C-reactive protein, inducible nitric oxide synthase and tumor necrosis factor-α. *Int. J. Mol. Med.* 34, 1706–1712. doi:10.3892/ijmm.2014.1942

Zelenka, J., Dvořák, A., Alán, L., Zadinová, M., Haluzík, M., and Vítek, L. (2016). Hyperbilirubinemia protects against aging-associated inflammation and metabolic deterioration. *Oxid. Med. Cell. Longev.* 60, 6190609. doi:10.1155/2016/6190609

Zelenka, J., Lenícek, M., Muchová, L., Jirsa, M., Kudla, M., Balaz, P., et al. (2008). Highly sensitive method for quantitative determination of bilirubin in biological fluids and tissues. *J. Chromatogr. B Analyt. Technol. Biomed. Life Sci.* 867, 37–42. doi:10.1016/j.jchromb.2008.03.005

Zennaro, C., Mariotti, M., Carraro, M., Pasqualetti, S., Corbelli, A., Armelloni, S., et al. (2014). Podocyte developmental defects caused by adriamycin in zebrafish embryos and larvae: a novel model of glomerular damage. *PloS One* 9, e98131. doi:10.1371/journal.pone.0098131

Zhang, K., and Kaufman, R. J. (2008). From endoplasmic-reticulum stress to the inflammatory response. *Nature* 454, 455–462. doi:10.1038/nature07203

Conflict of Interest: The authors declare that the research was conducted in the absence of any commercial or financial relationships that could be construed as a potential conflict of interest.

frontiers in Pharmacology

REVIEW
published: 04 May 2021
doi: 10.3389/fphar.2021.670076

Coordinated Contribution of NADPH Oxidase- and Mitochondria-Derived Reactive Oxygen Species in Metabolic Syndrome and Its Implication in Renal Dysfunction

Hewang Lee[1] *and Pedro A Jose*[1,2]*

[1]Department of Medicine, The George Washington University School of Medicine and Health Sciences, Washington, DC, United States, [2]Department of Pharmacology and Physiology, The George Washington University School of Medicine and Health Sciences, Washington, DC, United States

OPEN ACCESS

Edited by:
David E. Stec,
University of Mississippi Medical Center, United States

Reviewed by:
Patrick Pagano,
University of Pittsburgh, United States
Sean P. Didion,
University of Mississippi Medical Center, United States

***Correspondence:**
Pedro A. Jose
pjose@mfa.gwu.edu

Specialty section:
This article was submitted to Experimental Pharmacology and Drug Discovery, a section of the journal Frontiers in Pharmacology

Received: 20 February 2021
Accepted: 14 April 2021
Published: 04 May 2021

Citation:
Lee H and Jose PA (2021) Coordinated Contribution of NADPH Oxidase- and Mitochondria-Derived Reactive Oxygen Species in Metabolic Syndrome and Its Implication in Renal Dysfunction. Front. Pharmacol. 12:670076. doi: 10.3389/fphar.2021.670076

Metabolic syndrome (MetS), a complex of interrelated risk factors for cardiovascular disease and diabetes, is comprised of central obesity (increased waist circumference), hyperglycemia, dyslipidemia (high triglyceride blood levels, low high-density lipoprotein blood levels), and increased blood pressure. Oxidative stress, caused by the imbalance between pro-oxidant and endogenous antioxidant systems, is the primary pathological basis of MetS. The major sources of reactive oxygen species (ROS) associated with MetS are nicotinamide-adenine dinucleotide phosphate (NADPH) oxidases and mitochondria. In this review, we summarize the current knowledge regarding the generation of ROS from NADPH oxidases and mitochondria, discuss the NADPH oxidase- and mitochondria-derived ROS signaling and pathophysiological effects, and the interplay between these two major sources of ROS, which leads to chronic inflammation, adipocyte proliferation, insulin resistance, and other metabolic abnormalities. The mechanisms linking MetS and chronic kidney disease are not well known. The role of NADPH oxidases and mitochondria in renal injury in the setting of MetS, particularly the influence of the pyruvate dehydrogenase complex in oxidative stress, inflammation, and subsequent renal injury, is highlighted. Understanding the molecular mechanism(s) underlying MetS may lead to novel therapeutic approaches by targeting the pyruvate dehydrogenase complex in MetS and prevent its sequelae of chronic cardiovascular and renal diseases.

Keywords: metabolic syndrome, mitochondria, nicotinamide-adenine dinucleotide phosphate oxidase, NLRP3, oxidative stress, reactive oxygen species, pyruvate dehydrogenase complex, renal dysfunction

Abbreviations: CoQ10, coenzyme Q10; ETC, electron transport chain; HOMA-B, homeostasis model of assessment β-cell function; HOMA-IR, homeostasis model of assessment insulin resistance; NA, not applicable; NCT, National Clinical Trial, ND, not determined; ROS, reactive oxygen species.

INTRODUCTION

Metabolic syndrome (MetS), a complex of interrelated risk factors for cardiovascular disease and diabetes, is comprised of central obesity (increased waist circumference), hyperglycemia, dyslipidemia (high triglyceride blood levels, low high-density lipoprotein blood levels), and increased blood pressure (Alberti et al., 2009; Nilsson et al., 2019). The presence of three of the five criteria qualifies a diagnosis of MetS: waist circumference ≥102 cm for males and ≥88 cm for females (≥90 cm and ≥80 cm for Asians, respectively); fasting blood glucose ≥5.6 mmol/L or drug treatment for elevated blood glucose; blood triglycerides ≥1.7 mmol/L or drug treatment for elevated blood triglycerides; reduced blood high-density lipoprotein cholesterol (<1.0 mmol/L for females and <1.4 mmol/L for males) or drug treatment for reduced blood high-density lipoprotein cholesterol; and systolic blood pressure ≥130 mmHg and/or diastolic blood pressure ≥85 mmHg or antihypertensive drug treatment in a patient with a history of hypertension (Alberti et al., 2009, Nillson et al., 2019). MetS is characterized by systemic oxidative stress, chronic inflammation, and insulin resistance (Furukawa et al., 2004; Grundy, 2016).

Oxidative stress, the principal pathological basis for MetS (Spahis et al., 2017), is a state of an imbalance of the production and degradation of reactive oxygen and nitrogen species, resulting in an increase in reactive oxygen and nitrogen species (Egea et al., 2017). Reactive oxygen species (ROS) and nitrogen species are reactive derivatives of oxygen metabolism. Excessive ROS damage lipids, proteins, nucleic acids, and carbohydrates, resulting in a chronic increase in the production of proinflammatory cytokines and cellular inflammation (Touyz et al., 2020). Experimental and clinical evidence suggests that oxidative stress increases leptin secretion by adipocytes, induces β-cell dysfunction, and impairs insulin signaling and glucose tolerance, leading to the development of insulin resistance (Newsholme et al., 2019).

Oxidative stress occurs when energy supply exceeds energy expenditure and as a consequence, adipocytes undergo proliferation and hypertrophy, leading to visceral obesity (Jia et al., 2016; Masschelin et al., 2020; Prasun, 2020). There is a direct correlation between the plasma level of malondialdehyde (MDA), a biomarker of lipid peroxidation and total oxidant status, and the body mass index in subjects with MetS (Furukawa et al., 2004; Maslov et al., 2019). Oxidative stress activates a series of stress pathways, modulates transcription factors, increases the generation of adipokines and cytokines, and causes derangements in metabolism, including impaired glucose tolerance, dyslipidemia, ectopic lipid accumulation, gut microbiota dysbiosis, and hypertension, ultimately leading to MetS (Rani et al., 2016; Vona et al., 2019). MetS markedly increases the risk of the occurrence and progression of chronic cardiovascular and renal diseases (Zhang and Lerman, 2017; Senoner and Dichtl, 2019; Podkowińska and Formanowicz, 2020).

Knowledge of the sources of ROS, the amount and type of reactive species produced, the cellular signaling involved, and the affected targets, is critical in understanding the initiation and progression of MetS. In this review, we discuss the generation of ROS from two major sources (NADPH oxidases and mitochondria), downstream signaling pathways, pathophysiological processes, and progression of MetS.

REACTIVE OXYGEN SPECIES GENERATION BY NICOTINAMIDE-ADENINE DINUCLEOTIDE PHOSPHATE OXIDASES AND MITOCHONDRIA

ROS can be free radicals and non-free radicals (Zeng et al., 2009; Gutteridge and Halliwell, 2018; Zhang et al., 2019) (**Table 1**). A free radical contains one unpaired reactive electron in the outer orbit, such as superoxide anion (O_2-), hydroxyl radical (OH), nitric oxide (NO), carbonate radical anion (CO_3-), nitrogen dioxide (NO_2), and alkoxyl/alkyl peroxyl (RO/ROO). A non-free radical does not contain unpaired electron, such as hydrogen peroxide (H_2O_2), hypochlorous acid (HOCl), and peroxynitrite (ONOO-) (Zeng et al., 2009).

Superoxide anion (O_2-), designated as the primary ROS, is derived from O_2 after receiving an electron from oxidases or the mitochondrial electron transport chain (ETC) (Gutteridge and Halliwell, 2018). O_2- is then dismutated spontaneously or by superoxide dismutase (SOD) into H_2O_2, which is then converted to water by glutathione peroxidase or catalase. O_2- reacts with nitric oxide (NO) to form ONOO-. Hydroxyl radical (OH) is derived from ONOOH by homolytic fission or from H_2O_2 through the Haber-Weiss reaction in the presence of transition metals, such as Fe^{2+}, or through HOCl by myeloperoxidase in reaction with O_2. The formation of lipid radical (L) (not listed in **Table 1**) is usually initiated by OH^-, abstracting an allylic hydrogen from unsaturated lipid, which then reacts with O_2 to form a lipid peroxyl radical (LOO); the abstraction of one H^+, from an unsaturated lipid, forms lipid hydroperoxide (LOOH) (Zhang et al., 2019). ROS are cleared by antioxidant systems. As aforementioned, O_2- can be dismutated to H_2O_2; H_2O_2 can be further decomposed by catalase, glutathione redox cycle, and thioredoxin redox cycle. ROS can be removed by some non-enzymatic compounds, such as vitamins C and E, carotenoids, glutathione, nicotinamide, and flavonoids (Tan et al., 2018).

ROS are generated by specific oxidase enzymes, such as the nicotinamide-adenine dinucleotide phosphate (NADPH) oxidases, xanthine oxidases, arachidonic acid monooxygenases, nitric oxide synthases, cyclooxygenases, cytochrome P450 enzymes, and lipoxygenases, as well as cell organelles, such as mitochondria, peroxisomes, and endoplasmic reticula (Zeng et al., 2009; Jia et al., 2016; Prasun, 2020). The major sources of ROS associated with MetS pathogenesis are NADPH oxidases (DeVallance et al., 2019) and mitochondria (Prasun, 2020).

NADPH oxidase, a major source of O_2- and H_2O_2 (Bedard and Krause, 2007), is comprised of seven structurally similar members, NOX1 to NOX5, and Duox1 and Duox2 (**Figure 1**). All NADPH oxidase members have two heme groups, six transmembrane domains, and flavin adenine dinucleotide (FAD) and NADPH binding sites (Groemping and Rittinger,

TABLE 1 | Characteristics of some major ROS generated by NADPH oxidases and mitochondria[6,7,16–18].

ROS	Free radical	Lifetime	Major targets	Possible candidate as second messenger	Scavengers
Superoxide anion ($O_2^{\bullet-}$)	Yes	~50 ms	Fe-S cluster NO	No	SOD
Hydrogen peroxide (H_2O_2)	No	~1 ms	Thiols Metals	Yes	Catalase GPX PRDX Bilirubin
Hydroxyl radical (OH•)	Yes	~10^{-9}s	Any macromolecule	No	Uric acid Vitamin E
Nitric oxide (NO•)	Yes	~1s	Metals	Yes	NA
Nitrogen dioxide (NO_2•)	Yes	NA	Thiols	ND	GPX PRDX
Hypochlorous acid (HOCl)	No	NA	Amino Thiols	No	Uric acid
Peroxynitrite (ONOO–/ONOOH)	No	~15°µs	CO2 Cysteine Tryptophan Tyrosine Metals	No	GPX PRDX Bilirubin
Carbonate radical anion (CO_3•-)	Yes	~10^{-6}s	Thiols Guanine	No	ND
Alkoxyl/Peroxyl radical (RO/ROO•)	Yes	NA	Organic compounds	ND	GPX PRDX

Fe-S, iron (II) sulfide; GPX, glutathione peroxidase; PRDX, peroxiredoxin; SOD, superoxide dismutase; NA, not available; ND, not determined.

2005). The cytosolic FAD domain receives two electrons from NADPH that are sequentially transferred along the two heme domains which reduce O_2 to O_2- (DeVallance et al., 2019). Activation of NOX1, NOX2, and NOX3 requires the assembly of membrane and cytosolic subunits, similar to the classical NADPH oxidase, NOX2 (membrane subunit, $p22^{phox}$, and cytosolic subunits, $p47^{phox}$, $p67^{phox}$, and $p40^{phox}$) to produce O_2- (Nauseef, 2014). Activation of NOX4 (heterodimerized with $p22^{phox}$) which does not require classical cytosolic subunits or their homologs, produces mainly H_2O_2 (Lyle et al., 2009). Activation of NOX5 and Duoxs 1 and 2 does not require cytosolic subunits either, but rather by the binding of calcium to their intracellular EF-hand motifs, resulting in the production of O_2- and/or H_2O_2 (Banfi et al., 2004).

The mitochondrion, the other major source of ROS, in addition to NADPH oxidases, within the cell (Murphy, 2009), continuously metabolizes oxygen which generates ROS (Bhatti et al., 2017). During the process of oxidative phosphorylation, electrons leak from the ETC to oxygen and produce ROS: single electron leak generates O_2- while two-electron leak generates H_2O_2 (Brand, 2016). In general, increasing electron flux through the ETC decreases the probability of unpaired electron leakage to form ROS (Hoffman and Brookes, 2009); ROS production is increased at high ETC rates when ROS scavenging pathways are overwhelmed (Sharaf et al., 2017). However, ROS are also produced during low ETC activity when electron flux is inhibited (Murphy, 2009), because the electron spends more time at reductive centers, increasing the chances of its transfer to oxygen (Gnaiger et al., 1998). The increase in ROS production in both low and high ETC fluxes is evidence of the complicated nature of ROS production in mitochondria under different conditions (Murphy, 2009; Berry et al., 2018). ETC Complex I is believed to be a major source of mitochondrial ROS (Murphy, 2009). In ETC Complex I, electrons enter the NADH/NAD^+ pool through NAD-linked dehydrogenases, and ROS can be produced from multiple sites (Brand, 2016), when the NADH/NAD^+ ratio is high in cells (Kussmaul and Hirst, 2006), particularly at the site of dihydrolipoamide dehydrogenase subunit (Bazil et al., 2014). Electrons from NADH flow into the flavin-containing sites to the ETC Complex I quinone-binding site and then to the next isopotential pool ETC Complex II (Brand, 2016). ROS are also produced by the flavin in ETC Complex I, under the condition of reverse electron transport (Chouchani et al., 2014), when the protonmotive force (pmf, including $\Delta\psi m$ and ΔpH) is increased (Scialò et al., 2017). In ETC Complex III, electrons are transferred from QH2 to the outer Q-binding site of ETC Complex III (site III Qo), then through cytochrome b566 to ETC Complex III Qi in the Q-cycle, and subsequently down through cytochrome C, and ETC Complex IV to oxygen (Brand, 2016). ROS production is dependent on kinetics and redox status during the Q cycle (Dröse and Brandt, 2012); high ΔpH component of the pmf leads to an increase in ROS production from ETC Complex III (Wong et al., 2017). When the electrons are transferred from ETC Complexes I, III, and IV, the isopotential drops, the protons are pumped across the inner mitochondrial membrane, and energy is conserved as the pmf, which is driven for ATP synthesis (Brand, 2016). In addition to the ETCs, ROS in the mitochondria can also be produced by enzymes, such as pyruvate dehydrogenases which transfer electrons to oxygen (Quinlan et al., 2014; Ambrus et al., 2015).

The concentration of ROS within cells is the net balance of ROS producing and antioxidant systems. Endogenous

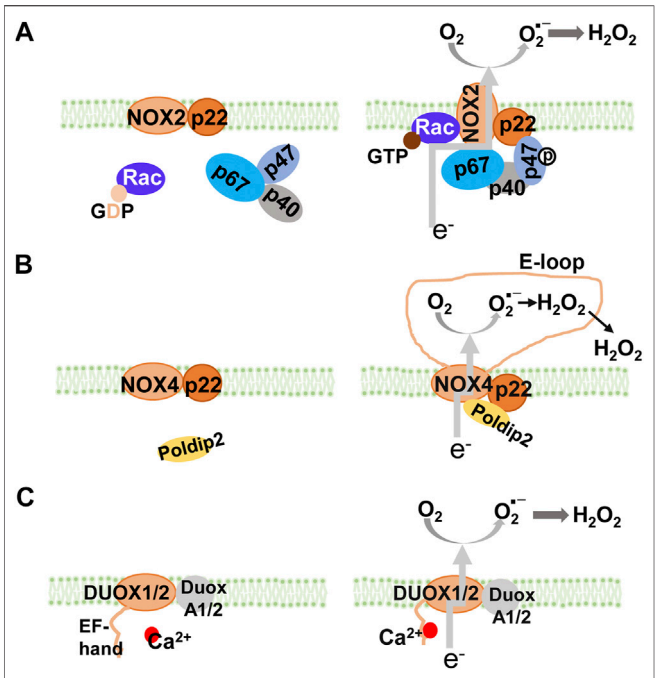

FIGURE 1 | NADPH oxidase isoforms and their assembly. All NOX isoforms have membrane-spanning catalytic subunit that transfers electrons from NADPH through their NADPH and FAD-binding sites and heme groups to reduce O_2 into superoxide anion **(A)** NOX1, NOX2, and NOX3 are cytosolic activators-dependent with the stabilizing $p22^{phox}$ membrane subunit. Activation of NOX2 requires assembly with cytosolic $p47^{phox}$ (equivalent to NoxO1 in NOX1 and NOX3), $p67^{phox}$ (equivalent to NoxA1 in NOX1 and NOX3), and $p40^{phox}$. In resting cells **(left panel)**, NOX2 and $p22^{phox}$ are associated, co-stabilizing each other. Upon activation **(right panel)**, GDP is exchanged for GTP on Rac. The phosphorylation of $p47^{phox}$ subunit leads to a conformational change, which brings with $p67^{phox}$ and $p40^{phox}$, to form the active NOX2 enzyme complex (NOX1 and NOX3 are not shown) **(B)** NOX4 is constitutively active with the stabilizing $p22^{phox}$ membrane subunit. Its activity can be modulated by Poldip2. Inside the E-loop (3rd extracellular loop), superoxide is rapidly dismutated into H_2O_2 **(C)** NOX5, DUOX1, and DUOX2 are Ca^{2+} dependent with EF-hand domains. DUOX1 and DUOX2 (as well as NOX5, not shown) have Ca^{2+} binding domains that undergo conformational change in response to an increase in intracellular Ca^{2+}. It is speculated that activation of DUOX1, DUOX2, and NOX5, is through intramolecular protein-protein interaction between the Ca^{2+}-binding domain and the C-terminal catalytic domain. GDP, guanosine diphosphate; GTP, guanosine-5′-triphosphate; NADPH, nicotinamide adenine dinucleotide phosphate; NOX, NADPH oxidase.

antioxidants consist of enzymatic and non-enzymatic scavengers (Ahmadinejad et al., 2017). Enzymatic scavengers include superoxide dismutases (SODs), catalases, and various peroxidases, and non-enzymatic antioxidants include vitamin C and E, carotenoids, glutathione, lipoic acid and transition-metal ions (Moldogazieva et al., 2018). The three isoforms of SODs in mammals, SOD1 in the cytoplasm and the mitochondrial intermembrane space, SOD2 in the mitochondrial matrix, and SOD3 in the extracellular space, scavenge superoxide into H_2O_2 and inhibit the formation of $ONOO^-$ from NO (Ahmadinejad et al., 2017). Catalases and peroxidases catalyze the conversion of H_2O_2 into water (Moldogazieva et al., 2018). However, it is more dependent on rates of ROS production than on the rates of antioxidant scavenging (Munro and Treberg, 2017). For simplicity, this review does not discuss other cellular producers of ROS and enzymatic or non-enzymatic antioxidants.

CROSSTALK BETWEEN NICOTINAMIDE-ADENINE DINUCLEOTIDE PHOSPHATE OXIDASES AND MITOCHONDRIA-DERIVED REACTIVE OXYGEN SPECIES

ROS-induced ROS release is a self-amplified phenomenon initially observed in mitochondrial ROS (Mito-ROS) generation triggered by ROS released from dysfunctional mitochondria (Zorov et al., 2006). This positive feedback cycle is also observed later in the ROS generation between the activation of NADPH oxidases and mitochondria, which becomes a vicious cycle (Daiber, 2010; Zinkevich and Gutterman, 2011). The crosstalk between the two major sources of ROS augments oxidative stress (Daiber, 2010; Dikalov, 2011). ROS derived from NADPH oxidases promote Mito-ROS production and vice versa, such that Mito-ROS activate NADPH oxidases to generate more ROS (Daiber et al., 2017; Egea et al., 2017; Dikalov and Dikalova, 2019).

The phenomenon that ROS derived from NADPH oxidases promote Mito-ROS production is well described in the activation of NADPH oxidases by the renin-angiotensin (Ang II)-aldosterone system (RAAS) (Kimura et al., 2005). Activation of NADPH oxidases located in both the plasma and cytosolic membranes generates O_2-. Its dismutation into H_2O_2 activates PKC-ε and induces phosphorylation-dependent mitochondrial K_{ATP} channel (Mito-K_{ATP}) opening (Costa and Garlid, 2008a). This increases K^+ influx, decreases mitochondrial membrane potential ($\Delta\Psi m$), and induces mitochondrial O_2- production by reverse electron transfer, which is released by the opening of mitochondrial permeability transition pore (Dikalov and Dikalova, 2019). The matrix alkalinization following K^+ influx due to Mito-K_{ATP} opening results in an increase in H_2O_2 formation (Daiber et al., 2020). The O_2- production can be blocked by the specific Mito-K_{ATP} inhibitor 5-hydroxydecanoate (Daiber et al., 2020). In preadipocytes and adipocytes (Baret et al., 2017), endothelial cells (Coughlan et al., 2009), and renal mesangial cells (Xie et al., 2012), activation of NADPH oxidases by advanced glycation end-products (AGEs) enhances mitochondrial biogenesis, decreases mitochondrial electron transport, and overproduction of Mito-ROS. The increase in the production of Mito-ROS is attenuated by knockdown of NADPH oxidase subunits or NOX inhibitors (Ahmed et al., 2012; Daiber et al., 2017; Dikalov and Dikalova, 2019), supporting the existence of ROS crosstalk from NADPH oxidases to the mitochondria.

Mito-ROS can also activate NADPH oxidases to produce ROS. O_2- generated in the mitochondria is mainly dismutated into H_2O_2. Mito-ROS (mainly O_2- and H_2O_2) are released to the cytosol via mitochondrial permeability transition pore (mPTP), inner membrane anion channel (IMAC), voltage-dependent anion

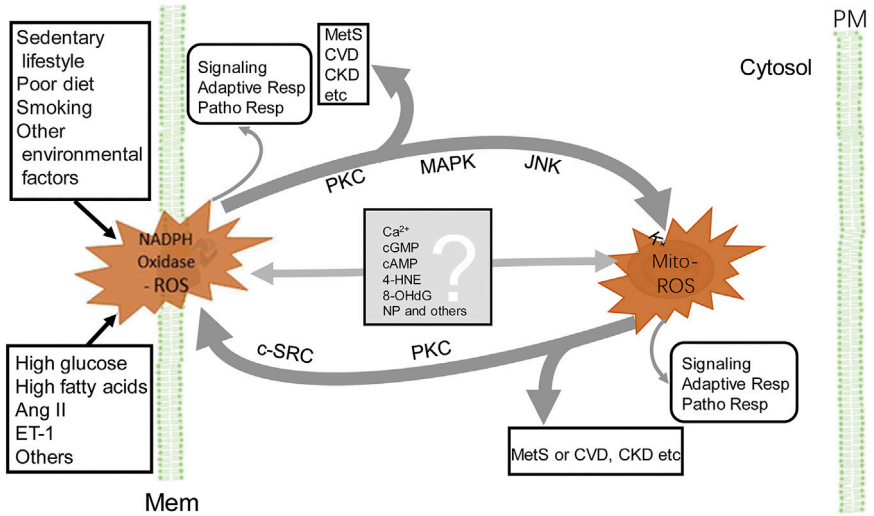

FIGURE 2 | Crosstalk between NADPH oxidase and mitochondria-derived ROS. NADPH oxidase activation, by endogenous and exogenous stimulation (for example Ang II), produces ROS, which stimulate PKC, MAPK, and JNK, leading to the increase in Mito-ROS production (see the text). ROS, released from mitochondria, activate redox-sensitive PKC and c-SRC, which phosphorylate NADPH oxidases and increase ROS production by NADPH oxidases. The Mito-ROS trigger NADPH oxidases activation and generation of ROS and vice versa, resulting in a vicious circle (thick gray lines). The converged increase in ROS contributes to the pathogenesis of MetS, CVD, and CKD, among others. In addition to PKC, other potential molecules (listed in the gray box) relay the signaling between NADPH oxidase and mitochondria. ROS generated by either NADPH oxidase or mitochondria exert their individual actions, such as signaling, adaptive responses, and pathophysiological responses (very thin gray line arrows). 4-HNE, 4-hydroxynonenal; 8-OHdG, 8-hydroxy-20-deoxyguanosine; Adaptive Resp, adaptive responses; CKD, chronic kidney disease; c-SRC, proto-oncogene tyrosine-protein kinase; CVD, cardiovascular disease; MAPK, mitogen-activated protein kinase; PM, plasma membrane and other cellular membranes (Mem), such as in endoplasmic reticula, endosomes etc; MetS, metabolic syndrome; Mito-ROS, ROS generated from mitochondria (right side); NADPH Oxidase-ROS, ROS generated from NADPH oxidases (left side); NP, nanoparticles or microparticles; Patho Resp, pathological responses; PKC, protein kinase C. For simplicity, other ROS-generating sources and enzymatic and non-enzymatic antioxidants are not shown.

channel, and aquaporins, or via diffusion due to increased mitochondrial permeability under proinflammatory conditions (Daiber, 2010; Dikalov, 2011; Brand, 2016; Daiber et al., 2017). The cytosolic H_2O_2 derived from the mitochondria activates redox-sensitive tyrosine kinases (c-SRCs) and protein kinases (PKCs), which subsequently phosphorylate NADPH oxidases, facilitating the assembly of NADPH oxidase subunits in the membranes, which amplifies the ROS production (Dikalov, 2011; Kröller-Schön et al., 2014; Zhang et al., 2014; Daiber et al., 2017; Daiber et al., 2020). Inhibition of Mito-ROS by Mito-TEMPO effectively suppresses the activities of NADPH oxidases and ROS production (Park et al., 2015; Ni et al., 2016). Depletion of mitochondrial SOD2 increases both basal and Ang II-stimulated NADPH oxidase activity, whereas overexpression of SOD2 attenuates ROS production from NADPH oxidases by scavenging mito-ROS (Dikalov, 2011; Egea et al., 2017). The regulation of NADPH oxidases by Mito-ROS is observed *in vivo,* as well (Tran et al., 2017). All of these studies show the existence of ROS crosstalk from mitochondria to NADPH oxidases.

The crosstalk between NADPH oxidase and mitochondrial ROS provides a network of intracellular redox regulation (**Figure 2**). Each ROS source has so-called "redox switches" that confer activation upon oxidation (Egea et al., 2017). The on/off of the redox switches results in activation or inactivation of effector proteins and transcription factors that function in a wide array of cellular physiological and pathophysiological responses (Daiber et al., 2017). For example, in endothelial cells, ROS activate PKC and protein tyrosine kinase 2-dependent phosphorylation and uncoupling of endothelial NO synthase, desensitization of soluble guanylate cyclase, nitration of prostacyclin and increase in cyclooxygenase activity, and augmentation of vasoconstriction and resulting hypertension induced by endothelin-1 (Li et al., 2003; Chen et al., 2012; Wu et al., 2014; Daiber et al., 2017). The crosstalk produces increased levels of ROS (Egea et al., 2017), resulting in a vicious cycle (Daiber, 2010; Dikalov, 2011; Daiber et al., 2020). Because ROS lifetime is short (**Table 1**), there must be some mediators to carry out the crosstalk from NADPH oxidases to mitochondria and vice versa (**Figure 2**). It is speculated that calcium (Görlach et al., 2015), cGMP (Costa et al., 2008b), cAMP (Palmeira et al., 2019), 4-hydroxy-2-nonenal (Xiao L. et al., 2017), 8-hydroxy-20-deoxyguanosine (Termini, 2000), and microparticles (Uusitalo and Hempel, 2012), among others, are the candidates that relay the signal from one to another. This synergistic regulation may not necessarily represent a general mechanism, depending on the highly dynamic spatiotemporal relationship between these two major ROS sources. The mitochondrion, itself, is a very dynamic organelle, which can be physically associated with NADPH oxidases through the contact sites between the mitochondria and ER, endosomes, or the plasma membrane. The NADPH oxidase isoform, NOX4, which directly produces H_2O_2, is expressed in the mitochondria (Hirschhäuser et al., 2015). As aforementioned, the crosstalk between mitochondria- and NADPH oxidase-generated ROS can result in the vicious cycle

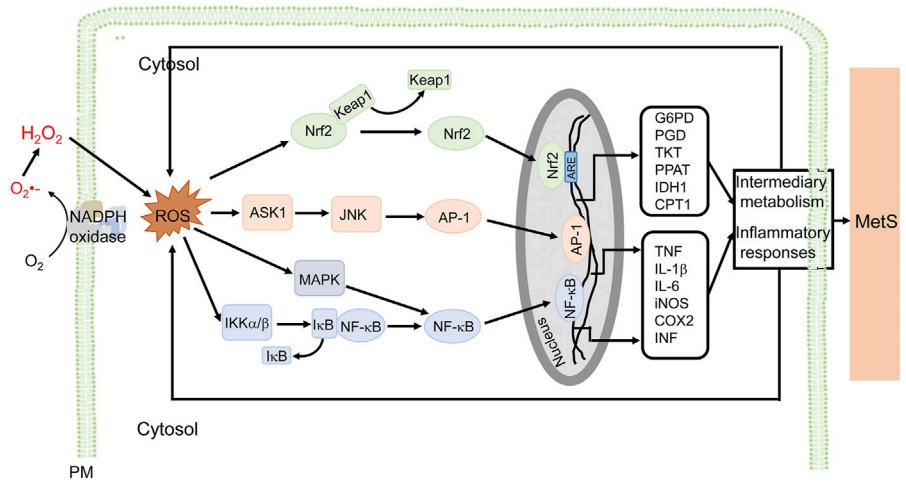

FIGURE 3 | NADPH oxidase-derived ROS signaling and cellular effects in MetS. ROS derived from NADPH oxidases are involved in the inflammatory responses associated with MetS, in macrophages, for example. ROS stimulate NF-κB, via MAPK and IKKα/β, and AP-1, via ASK1 and JNK, which promote the transcription of proinflammatory genes (e.g., TNF, IL-1β, IL-6, iNOS, COX2, and INF), resulting in inflammatory responses associated with MetS. ROS also activate Nrf2 to induce genes that regulate intermediary metabolism (e.g., G6PD, PGD, TKT, PPAT, IDH1, and CPT1) (only some genes are listed). The antioxidant effect and modulation of metabolism are adaptive responses to ROS-induced proinflammatory responses and altered metabolism. ROS exert a wide range of effects such as inflammation, insulin resistance, adipocyte proliferation, altered metabolism, among others in diverse cells, including macrophages, endothelial cells, vascular cells, adipocytes, preadipocytes, and epithelial cells. The ROS-mediated signaling and cellular efforts are cell type-specific that are overlapping. For simplicity and clarity, only part of signaling and cellular effects in macrophages are illustrated. AP-1, activator protein 1; ASK1, apoptosis signal-regulating kinase 1; COX2, cyclooxygenase-2; CPT1, carnitine palmitoyltransferase 1; G6PD, glucose-6-phosphate dehydrogenase; IDH1, isocitrate dehydrogenase 1; IL, interleukin; iNOS, inducible nitric oxide synthase; JNK, c-Jun N-terminal kinases; Keap1, Kelch-like ECH-associated protein 1; IKK, IκB kinase; MAPK, mitogen-activated protein kinase; MetS, metabolic syndrome; PM, plasma membrane and other cellular membranes; NF-κB, nuclear factor kappa-light-chain-enhancer of activated B cells; Nrf2, nuclear factor-erythroid 2 p45-related factor 2; PGD, 6-phosphogluconate dehydrogenase; PPAT, phosphoribosyl pyrophosphate aminotransferase; TKT, transketolase.

of ROS formation, resulting in oxidative stress, which contributes to the development and progression of pathological conditions, including MetS (**Figure 2**).

NICOTINAMIDE-ADENINE DINUCLEOTIDE PHOSPHATE OXIDASE-REACTIVE OXYGEN SPECIES SIGNALING AND PATHOPHYSIOLOGICAL EFFECTS IN METABOLIC SYNDROME

In response to extracellular and intracellular metabolic alterations or damage, ROS, generated by NADPH oxidases located in plasma or cytosolic membranes, trigger a series of physiological, adaptive, and subsequently pathological responses (Yang et al., 2021). These regulate transcriptional factors and gene expression, resulting in metabolic reprogramming, that results in the initiation and progression of MetS (Perez-Martinez et al., 2012; Purkayastha and Cai, 2013). NADPH oxidases are widely expressed in various cells: NOX2 in macrophage and neutrophils; NOX2, NOX4, with some NOX1 and NOX5 in endothelial cells (DeVallance et al., 2019); NOX4 and NOX1 in vascular smooth muscle cells (VSMCs) (Akoumianakis and Antoniades, 2019); NOX4 in adipocytes (DeVallance et al., 2019); and NOX2, NOX4, and NOX5 in renal epithelial cells (Yang et al., 2020; Yang et al., 2021), all playing critical roles in the pathogenesis of MetS.

ROS derived from NADPH oxidases are important in the inflammation associated with MetS (**Figure 3**). In immune cells, ROS (mainly O_2-) activate the MAP kinase signaling pathway and induce the translocation of nuclear factor kappa B (NF-κB) from the cytosol to the nucleus, where it promotes the synthesis of tumor necrosis factor (TNF), interleukin-6 (IL-6), and inducible nitric oxide synthase (iNOS), leading to proinflammatory responses (Maslov et al., 2019; Touyz et al., 2020; Verzola et al., 2020). In endothelial cells, the increase in NOX activity activates NK-κB and activator protein-1 (AP-1) transcription factors, and upregulates P-selectin and fractalkine, causing the adhesion of monocytes to the endothelium (Manduteanu et al., 2010). In addition, ROS promote AGEs formation, activate c-Jun N-terminal kinases (JNKs), induce expression of heat shock factor 1(HSF1), plasminogen activator inhibitor-1 (PAI-1), and monocyte chemoattractant protein-1 (MCP-1), increase vascular permeability, and recruit immune cells into the sites of inflammation (Sangle et al., 2010). The atypical PKCζ activates NOX2 through phosphoinositide 3-kinase (PI3K)γ by TNF in endothelial cells (Frey et al., 2006). In adipocytes, H_2O_2 generated mainly by NOX4, promotes the activation of anti-apoptotic kinase (Akt), Janus kinases (JAKs), and extracellular signal-regulated kinase (ERK1/2), followed simultaneously by the activation of transcription factor, signal transducer and activator of transcription (STAT), resulting in an increase in MCP-1, TNF, and IL-6 production (Maslov et al., 2019). In VSMCs, ROS activate NF-κB, AP-1 and induce gene expression responsible for migration and proliferation of

VSMCs (Akoumianakis and Antoniades, 2019). In human aortic VSMCs, transcription factors AP-1 and STAT1/STAT3 interact with the NOX5 promoter; depletion or inhibition of NF-B, AP-1, or STAT1/3 reduces the interferon-induced Ca^{2+}-dependent NOX activation and NOX5 expression (Manea et al., 2012). In addition to the increase in the activity of NOX and associated mediators, the aforementioned transcription factors increase NOX activity and ROS production, contributing to the "vicious cycle" in the development of MetS (Manea et al., 2015). NADPH oxidase inhibitors reduce proinflammatory cytokines and decrease hyperlipidemia (Furukawa et al., 2004) in high-glucose diet-fed mice which are hyperglycemic and have oxidative stress and inflammation (McCracken et al., 2018). High-fat diet in mice overexpressing $p22^{phox}$ induces an inflammatory state and MetS phenotype (Youn et al., 2014). Plasma levels of proinflammatory cytokines and adipocytokines are higher in MetS patients than normal subjects (Kim et al., 2016).

Oxidative stress can trigger obesity. NADPH oxidase overexpression, particularly NOX4, increases ROS production, promotes preadipocyte differentiation into adipocytes (Schröder et al., 2009), and induces adipocyte proliferation (Macleod, 2008) and differentiation from adipose-derived stem cells (Kanda et al., 2011). ROS, by stimulation of protein phosphatase 2A and inhibition of cyclin-dependent kinases (Magenta et al., 2008; Burhans and Heintz, 2009), induce dephosphorylation of retinoblastoma protein and activate the transcription factor E2F, a critical regulator of cell proliferation genes. E2F accelerates the re-entry of preadipocytes and adipocytes into the cell cycle (Macleod, 2008). In addition, ROS activation of cyclins D and E allows resting cells to enter into the cell cycle; c-Myc, through ERK, activates cyclin A which promotes proliferation of adipocytes and VSMCs (Macleod, 2008). Subsequently, the expression of p21 and p27, which are cyclin-dependent kinase inhibitors, is increased, facilitating adipocyte differentiation (Macleod, 2008; Rani et al., 2016). Furthermore, in mouse embryonic fibroblasts and adipocytes, ROS also activate C/enhancer-binding protein β and increase peroxisome proliferator-activated receptor (PPAR) γ, promoting adipogenesis and lipogenesis (Shin et al., 2020).

NADPH oxidases are critical in the development of insulin resistance and abnormal glucose and lipid metabolism associated with MetS. NOX4 is required for the physiological actions of insulin. ROS oxidize cysteine residues of protein tyrosine phosphatase (PTP) 1B, facilitate the tyrosine phosphorylation of insulin receptor substrate (IRS)1, and glucose uptake (Guichard et al., 2008). However, excessive ROS interfere with insulin signaling, increasing JNK1-mediated IRS1 phosphorylation and proteasomal degradation, impairing insulin-stimulated IRS1 redistribution and PI3K activity, and reducing Akt/PKB phosphorylation (Guichard et al., 2008). JNK1 and MAP kinases activate AP-1, which increases the transcription of inflammatory genes and eventually produces insulin resistance (Bedi et al., 2019). Oxidative stress in pancreatic islets induces β-cell apoptosis through the Bcl-2/Bax pathway (Liang et al., 2017). β-cell dysfunction decreases insulin secretion, resulting in hyperglycemia and more hyperlipidemia (Guichard et al., 2008). In skeletal muscle cells, pigment epithelium-derived factor, a multifunctional serpin implicated in insulin resistance, induces NADPH oxidase-dependent ROS production, enhances phospholipase A2 activity, resulting in lipolysis to produce free fatty acids and stimulation of glycolysis (Carnagarin et al., 2016).

ROS, through vasoactive and renal sodium transport inhibitors or enhancers, such as dopamine, angiotensin II, endothelin 1, and urotensin I, regulate blood pressure by actions in the vasculature and kidney, among others (Touyz et al., 2020; Yang N et al., 2020; Yang S et al., 2021). In the kidney, excessive ROS production increases afferent arteriolar tone and tubular sodium reabsorption and impairs tubuloglomerular feedback (Yang et al., 2020), all of which are involved in the regulation of blood pressure. The overall effect of ROS on renal sodium transport is nephron-segment specific and time- and concentration-dependent (Cuevas et al., 2013; Gonzales-Vicente et al., 2019; Yang et al., 2020). In the renal proximal tubule, NOX2, NOX4, and NOX5 play important roles in the regulation of sodium transport; an increase in ROS production increases sodium transport and subsequently, blood pressure (Han et al., 2008; Li et al., 2009; Yu et al., 2014; Yang et al., 2021). In the vasculature, ROS activate ERK1/2, p38MAPK, and JNK, promoting VSMC proliferation, migration, and inflammation. ROS also activate tyrosine kinases, including c-Src, PI3K/Akt, FAK, and receptor tyrosine kinases, stimulating NFκB activity, STAT1, AP-1, and hypoxia-inducible factor 1 (HIF-1]), leading to an increase in the expression of proinflammatory genes, production of chemokines and cytokines, and recruitment and activation of immune cells that promote vascular inflammation, proliferation, and contraction. The endothelial dysfunction and vascular remodeling result in hypertension and vascular damage (DeVallance et al., 2019; Touyz et al., 2019; Guerby et al., 2021).

Taken together, NADPH oxidases in macrophages and other immune cells, adipocytes, endothelial cells, VSMCs, and renal epithelial cells play important roles in the initiation and progression of MetS by inducing inflammatory responses, adipogenesis and lipogenesis, insulin resistance, metabolic derangements, and increase in renal sodium transport and blood pressure. However, the activation of the transcriptional factor, nuclear factor-erythroid 2 p45-related factor 2 (Nrf2), may also combat the inflammation and altered metabolism (Hayes and Dinkova-Kostova, 2014; He et al., 2020). Activation of Nrf2 upregulates antioxidant and detoxification genes to repair and degrade the damaged macromolecules (Hayes and Dinkova-Kostova, 2014; Saha et al., 2020). Nrf2 also facilitates NADPH regeneration through pentose phosphate pathway and increases β-oxidation of fatty acids (Hayes and Dinkova-Kostova, 2014; Dinkova-Kostova and Abramov, 2015). It is speculated that if adaptive responses cannot resolve the damage caused by inflammation, insulin resistance, and metabolic abnormalities, the pathological processes eventually result in MetS.

MITOCHONDRIA-DERIVED REACTIVE OXYGEN SPECIES SIGNALING AND PATHOPHYSIOLOGICAL EFFECTS IN METABOLIC SYNDROME

As an inevitable byproduct, mitochondrial ROS must be maintained in a certain range for normal mitochondrial

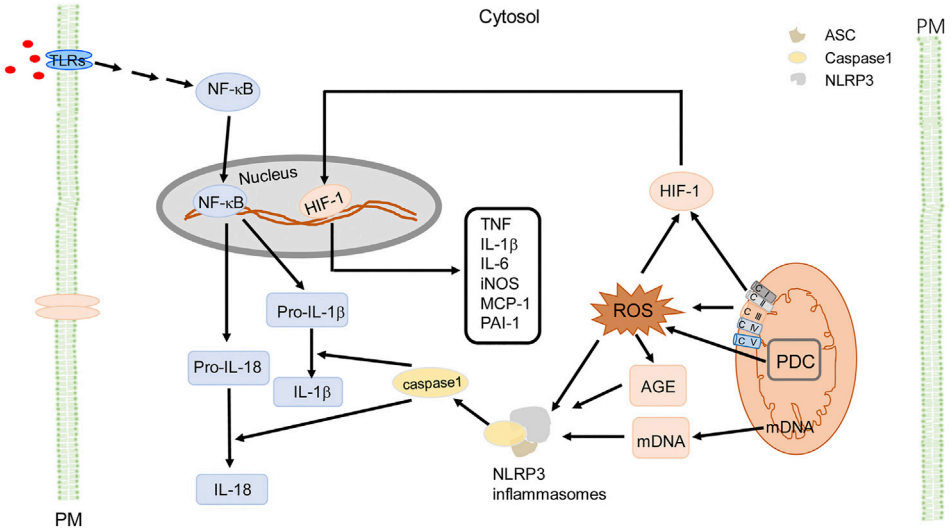

FIGURE 4 | Mito-ROS signaling and cellular effects in MetS. Mito-ROS, produced mainly by ETC (mainly C I and C III) during oxidative phosphorylation and enzymes like pyruvate dehydrogenase complex (PDC), provide the signaling to trigger NLRP3 inflammasome oligomerization with adaptor protein ASC and pro-caspase-1. NLRP3 activation can be primed by TLRs (step 1) to activate NF-κB or a non-NF-κB pathway to produce pro- IL-1β and pro-IL-18. Step 2 occurs when active caspase-1 cleaves pro-IL-1β and pro-IL-18 to produce mature cytokines IL-1β and IL-18. Mito-ROS also induce the formation of AGE, as a DAMP to activate NLRP3; mDNA also activates NLRP3 inflammasomes as a DAMP. Additionally, Mito-ROS trigger responses to hypoxia, activating HIF-1, and upregulate proinflammatory genes like TNF, IL-1β, IL-6, iNOS, MCP-1, and PAI-1. These cytokines activate the insulin signaling pathway and induce local and systemic insulin resistance (not shown). PDC is an important source of mitochondrial ROS, resulting in activation of NLRP3 inflammasomes as a DAMP. For simplicity and clarity, only part of signaling and cellular effects in macrophages are illustrated. AGE, advanced glycation end-products; ASC (apoptosis-associated speck-like protein containing a CARD), CI, ETC complex I; CII, ETC complex II; CIII, ETC complex III; CIV, ETC complex IV; CV, ETC complex V; ETC, electron transport chain; IL, interleukin; iNOS, inducible nitric oxide synthase; PM, plasma membrane; NF-κB, nuclear factor kappa-light-chain-enhancer of activated B cells; PAI-1, plasminogen activator inhibitor 1; PDC, pyruvate dehydrogenase complex; TNF, tumor necrosis factor; TLR, Toll-like receptor.

metabolism that involves mPTP and IMAC (Brady et al., 2006). Reversible opening of mPTP and IMAC apparently responds to the inter- and intra-mitochondrial ROS level to release ROS from the mitochondria. This process can play a physiological role to remove unwanted or damaged proteins, organelles (including mitochondria) and cells or cause pathological effects that damage essential proteins, lipids, and nucleic acids, and even eliminate vital and functional mitochondria and cells (Zorov et al., 2014). Therefore, mito-ROS can serve as one of damage-associated molecular patterns (DAMPs). NLRP3 inflammasomes can sense the DAMP-associated danger signals (Schroder and Tschopp, 2010; Abderrazak et al., 2015) and contribute to metabolic reprogramming that leads to the initiation and progression of MetS (Mastrocola et al., 2018).

Excessive Mito-ROS drive inflammation through activation of NLRP3 inflammasomes (**Figure 4**) that can lead into insulin resistance and hypertension. Mito-ROS provide signaling to trigger NLRP3 inflammasome oligomerization or its relocation in proximity to the mitochondria (Misawa et al., 2013; Mastrocola et al., 2018). The NLRP3 inflammasome is a cytoplasmic multi-protein complex which is comprised of a sensor protein, an adaptor protein apoptosis-associated speck-like protein containing a caspase recruitment domain (ASC), and pro-caspase-1, a cysteine protease (Schroder and Tschopp, 2010). NLRP3 activation can be primed by toll-like receptors (TLRs) (step 1), which activates NF-κB or a non-NF-κB pathway to produce pro- IL-1β and pro-IL-18; step 2 involves the oligomerization of NLRP3 and recruitment of the adaptor protein ASC and pro-caspase-1 (Lee et al., 2020). Active caspase-1 or caspase-11 then cleaves pro-IL-1β and pro-IL-18 to produce mature cytokines IL-1β and IL-18 (Lee et al., 2020). IL-1β and IL-18 are among the most potent pro-inflammatory cytokines and are important in macrophage M1 (pro-inflammatory) polarization (Lee et al., 2020). Of note, increased ROS activate mediators of inflammation ultimately contributing to oxidative stress-induced metabolic diseases. There is increasing evidence that TLRs activate inflammation, which increases ROS production, leading to the vicious cycle of ROS and inflammation, and subsequent development and progression of chronic inflammatory diseases (Liang et al., 2013; Jha et al., 2018). Mito-ROS also induce the formation of AGEs, which function as a damage-associated molecular pattern (DAMP) or interact with its receptor, RAGE (receptor for advanced glycation end products) to activate NLRP3 (Misawa et al., 2013). The activation of NLRP3 contributes to the progression of several diseases, including MetS (Yu and Lee, 2016). Increased Mito-ROS production activates the NLRP3 inflammasome and the scavenging of Mito-ROS suppresses activation of the NLRP3 inflammasome (Yu and Lee, 2016). Pro-inflammatory cytokines, particularly IL-1β, act in an autocrine and paracrine manner to interfere with insulin signaling in adipose tissue, liver, skeletal muscle, and pancreas or induce β-cell dysfunction which leads to insulin deficiency and insulin resistance (Esser et al., 2014; Mastrocola et al., 2018).

AGEs and other endogenous ligands interact with RAGE (Mastrocola et al., 2018), leading to the dysregulation of adipokines and cytokines, which results in insulin resistance and reinforces the already existing inflammatory responses (Gaens et al., 2014; Garay-Sevilla et al., 2021). In addition, Mito-ROS trigger responses to hypoxia, activating HIF-1 (Waypa et al., 2016), which induces inflammatory responses, via overexpression of inflammatory genes such as MCP-1, PAI-1, macrophage migration inhibition factor (MIF), TNF, IL-1β, IL-6, iNOS, and matrix metalloproteinases (Kim et al., 2014). These cytokines activate the insulin signaling pathway and local and systemic insulin resistance (Kim et al., 2014). Mito-ROS also suppress the expression of peroxisome proliferator-activated receptor gamma coactivator 1-α (PGC-1α), a co-activator of nuclear transcription factors, including nuclear respiratory factor (NRF)-1, PPARα, and PPARγ, that contribute to insulin resistance in MetS (Aroor et al., 2012). In mesenchymal stem cells of adipose tissue, ROS also activate transcription factor E2F, which activates PPARγ, stimulating adipocyte differentiation (Wang et al., 2015), indicating a role of Mito-ROS in regulating the cell cycle that induces adipogenesis and subsequently obesity (Rani et al., 2016). Mito-ROS also contribute to sustained vascular dysfunction and development of hypertension (Togliatto et al., 2017), which can be attenuated by inhibition of cyclophilin D, a regulatory subunit of the mitochondrial permeability transition pore, confirming a critical role of Mito-ROS in the development of hypertension (Itani et al., 2016).

Pyruvate dehydrogenase complex (PDC), an enzyme complex in mitochondria that converts pyruvate into acetyl-CoA, is an important source of ROS in the mitochondria (Holness and Sugden, 2003). PDC can be inactivated by phosphorylation with pyruvate dehydrogenase kinase (PDK)1-4 and activated by dephosphorylation with pyruvate dehydrogenase phosphatase (PDP)1–2 (Holness et al., 2003). In the brain, cardiac, liver, and skeletal muscle mitochondria, PDC produces ~4 times more ROS than ETC Complex I (Quinlan et al., 2014; Brand, 2016). PDC activation in many cells increases aerobic respiration and ROS production (Yang et al., 2018; Huang et al., 2021). Patients with metabolic diseases have higher PDC activity. For example, PDC activity and protein expression in platelets are higher in diabetic patients than healthy volunteers (Michno et al., 2020).

Emerging evidence shows that sustained PDC activity induces chronic inflammation. In hepatic tissue, sterile inflammation leads to a 2.5–fold increase in the proportion of active, dephosphorylated form of PDC (Vary et al., 1986). PDC-induced inflammation occurs through activation of NLRP3 inflammasomes (Han et al., 2020), which, in turn, can be activated by increased ATP or ROS, as a DAMP, due to the increase in aerobic respiration induced by PDC (Yang et al., 2018; Huang et al., 2021). In mouse macrophages, inhibition of pyruvate flux decreases citrate, itaconate, and succinate levels and represses Tnf, iNos, Irg1, and Il1b gene expression (Meiser et al., 2016), indicating that PDC activation, indeed, promotes macrophage pro-inflammatory responses due to an increase in pyruvate influx. The chronic low-grade inflammation, in adipose tissue, liver, skeletal muscle, and vasculature of obese subjects, induces insulin resistance (Wu and Ballantyne, 2020). Mice lacking PDK2 and PDK4 have constitutively activated PDC, which increases glucose oxidation, reduces insulin-stimulated muscle glucose uptake, and decreases fatty acid oxidation. These result in increased re-esterification of acyl-CoA into diacylglycerol and triacylglycerol, with subsequent activation of PKC-θ and inhibition of insulin signaling and development of insulin resistance (Rahimi et al., 2014). However, a role of PDC in inflammation and insulin resistance is not accepted by everyone (Constantin-Teodosiu et al., 2015; Petersen et al., 2015), indicating the complicated nature of its role in the pathogenesis of MetS and warrants further investigation.

RENAL DYSFUNCTION IN METABOLIC SYNDROME

In addition to cardiovascular diseases and diabetes (Alberti et al., 2009; Nilsson et al., 2019), MetS also increases the risk of kidney injury and chronic kidney disease (Locatelli et al., 2006). The pathophysiologic mechanisms underlying MetS, such as oxidative stress, chronic inflammation, insulin resistance, hyperglycemia, dyslipidemia, and increased activity of the RAAS could all contribute to the renal dysfunction and pathogenesis of chronic kidney disease (CKD) (Zhang and Lerman, 2017; Lakkis and Weir, 2018), with oxidative stress playing a fundamental role (Ravarotto et al., 2018). CKD patients have oxidative stress, as shown by increased levels of oxidative stress markers, such as MDA and F2-isoprostanes, which further worsen the renal dysfunction (Tbahriti et al., 2013). The major sources of ROS in the kidney are also NADPH oxidases (Gill and Wilcox, 2006; Wan et al., 2016; Qaddumi and Jose, 2021) and mitochondria (Plotnikov et al., 2007; Lindblom et al., 2015).

NADPH oxidases, NOX1, NOX2, NOX4, and NOX5, are predominantly expressed in renal epithelial, tubulointerstitial, mesangial, and glomerular epithelial cells (Gill and Wilcox, 2006; Zeng et al., 2009; Qaddumi and Jose, 2021; Yang et al., 2021). Metabolic (hyperglycemia, dyslipidemia, ox-LDL, etc.) and non-metabolic stimuli (Ang II, aldosterone, vascular endothelial growth factor, etc.) activate the expression and activity of NADPH oxidases (Gill and Wilcox, 2006; Yang et al., 2020), resulting in ROS overproduction, which is involved in vascular, glomerular, renal tubular, and endothelial dysfunction, mesangial proliferation, and increase in renal sodium reabsorption, eventually resulting in hypertension and CKD (Wan et al., 2016; Ravarotto et al., 2018). A high glucose environment upregulates NOX4 expression, inactivates AMP-activated protein kinase, and promotes podocyte apoptosis via p53-and PUMA (p53 upregulated modulator of apoptosis)-dependent pathway (Eid et al., 2010), leading to podocyte injury, a critical early event of glomerulosclerosis. In high-fat diet fed mice, upregulation of NOX2, $p47^{phox}$, and $p67^{phox}$ expression induces hyperlipidemia-associated glomerular injury (Wan et al., 2016). Under MetS conditions, glomerular mesangial and vascular endothelial cells have decreased level of arginine or tetrahydrobiopterin, which promotes the electron transfer to

oxygen, decreasing NO bioavailability, leading to endothelial dysfunction and mesangial expansion (Lee et al., 2013). NADPH oxidase activation, caused by Ang II and/or aldosterone, increases renal sodium transport, decreases NO bioavailability, and increases the proliferation of VSMCs and mesangial cells (Gill and Wilcox, 2006; Fazeli et al., 2012; Lee et al., 2013). Activation of NOX5 not only increases sodium transport in the renal proximal tubule (Yu et al., 2014; Yang et al., 2021) but also increases MCP-1 expression, macrophage infiltration, and secretion of proinflammatory chemokines and cytokines, and accelerates mesangial expansion and extracellular matrix protein accumulation, leading to glomerulosclerosis (Jha et al., 2017).

The genetic deletion or overexpression of NOX4, a major NADPH oxidase isoform in the kidney, does not affect the pathogenesis of CKD *in vivo* (Rajaram et al., 2019; Thallas-Bonke et al., 2020), indicating that other sources of ROS or additional yet unknown mechanism(s) are involved in the pathogenesis of renal dysfunction. The kidney utilizes a lot of energy with continuous oxidative phosphorylation within the mitochondria and as aforementioned, mitochondria and NADPH oxidases, are the major ROS sources in the cell (Murphy, 2009; Brand, 2016).

The abundance of mitochondria in the kidney produces the high energy demanded in the reabsorption and secretion of ions. However, an overly increase in Mito-ROS production causes mitochondrial dysfunction and mitochondrial damage that are involved in the pathogenesis of MetS (Zhang and Lerman, 2017; Podkowińska and Formanowicz, 2020). MetS affects renal mitochondrial structure and function through several different pathways (Zhang and Lerman, 2017; Podkowińska and Formanowicz, 2020). Metabolomics analysis demonstrated that the suppression of mitochondrial metabolism and activity in patients with MetS is associated with lower gene expression of PGC1α (a master regulator of mitochondrial biogenesis) and less mitochondria DNA and protein content in the kidney (Sharma et al., 2013). These findings are consistent with a recent observation that MetS patients with CKD (Jiang et al., 2019) have increased apoptosis and impaired $\Delta\Psi m$ in renal tubules but not podocytes (Jiang et al., 2019). Furthermore, oxidative stress-mediated perturbance of glycolysis and tricarboxylic acid cycle contributes to the tubular injury in MetS (Jiang et al., 2019). The injury in human renal proximal tubule cells caused by high-glucose in the medium is reversed by the mitochondria-targeted antioxidant, MitoQ (Xiao M. et al., 2017), that is related to the restoration of the Nrf2 expression, inhibition of the expression of Kelch-like ECH-associated protein (Keap1), and the interaction between Nrf2 and Keap1 (Xiao L et al., 2017). The high glucose-mediated injury of mouse renal mesangial cells can be attenuated by the tetrapeptide, SS-31, a mitochondria-targeted ROS scavenger (Hou et al., 2016). In these mouse mesangial cells exposed to high glucose, SS-31 decreased Mito-ROS generation, associated with a decrease in the expression of transforming growth factor β1, thioredoxin-interacting protein (TXNIP), BCL-2, apoptosis regulator (BAX), and cleaved caspase-3, and activation of p38 MAP kinase and cAMP-response element binding protein (CREB) (Hou et al., 2016).

Oxidative stress activates NLRP3 inflammasomes and quenching of Mito-ROS reverses NLRP3 activation (Yu and Lee, 2016). In MetS, the expression and activity of NLRP3 inflammasomes are increased in podocytes, glomerular endothelial cells, and tubular interstitial epithelial cells (Mastrocola, et al., 2018). Genetic deletion of NLRP3 ameliorates renal injury by preventing the early infiltration of immune cells, decreasing IL-1β and IL-18 expression and secretion, and proteinuria (Shahzad et al., 2015). NLRP3 inflammasomes are also involved in the disturbance of lipid metabolism in renal disease (Mastrocola, et al., 2018). NLRP3 activates sterol regulatory-element binding proteins (SREBPs) in lipotoxicity-driven inflammation and induces AGEs production. In Western diet-fed mice, the germline deletion of NLRP3 inactivates SREBPs, prevents renal lipid accumulation, and attenuates glomerular damage and proteinuria (Bakker et al., 2014). Hyperglycemia also promotes ROS through the enhanced glycolytic flux in mitochondria, induces AGEs production and TXNIP accumulation, which play a crucial role in NLRP3 inflammasome activation and increase in glomerular inflammatory injury (Tan et al., 2015).

Oxidative stress is also involved in the increased renal vascular resistance in the hypertension in MetS (Zeng et al., 2009; Ando and Fujita, 2012; Qaddumi and Jose, 2021). Induction of ROS generation in the renal medulla and cortex promotes hypertension (Cowley et al., 2015; Yang et al., 2020). Both NOX- and Mito-ROS, among others, contribute to the renal pathophysiology of hypertension (Zeng et al., 2009; Araujo and Wilcox, 2014; Loperena and Harrison, 2017; Yang et al., 2020; Yang et al., 2021). As mentioned previously, Ang II and aldosterone may be causal of the excessive ROS production in MetS. The chronic administration of Ang II type I receptor (AT_1R) blocker decreases ROS production and vascular resistance (Gill and Wilcox, 2006; Daenen et al., 2019). Both blockade of AT_1R and stimulation of dopamine receptors are reno-protective against oxidative stress by decreasing NADPH oxidase expression and activity (Cuevas et al., 2019; Daenen et al., 2019; Qaddumi and Jose, 2021; Yang et al., 2021). D_1R activation increases the expression of the antioxidant, paraoxonase 2, in both lipid and non-lipid rafts in renal proximal tubule cells (Yang et al., 2015), D_2R decreases ROS production through upregulation of paraoxonase 2 (Yang et al., 2012), DJ-1 (Cuevas et al., 2012), and another antioxidant, sestrin2 (Yang et al., 2014) in the kidney. In renal proximal tubule cells, D_5R activation increases paraoxonase 2 (Yang et al., 2015), HO-1 (Lu et al., 2013), and Nrf2 (Jiang et al., 2018) protein expression. The involvement of Mito-ROS in the pathogenesis of hypertension is most likely caused by oxidative phosphorylation. Recently, Lee et al., in our laboratory, reported that PDC activity and expression are increased in both renal proximal tubule cells and cortical homogenates from spontaneously hypertensive rats compared with normotensive Wistar-Kyoto rats (Lee et al., 2014). This activation may be involved in the increase in the expression of sodium transporters and channels in nephron segments, including the renal proximal tubule (Knepper and

Brooks, 2001; Wang et al., 2009; Maxwell et al., 2020; Pitzer et al., 2020).

REACTIVE OXYGEN SPECIES-TARGETED THERAPEUTIC IMPLICATIONS

Because oxidative stress plays a fundamental role in the pathogenesis and progression of MetS, and the overproduction of ROS damages cellular macromolecules, there is increasing interest in developing therapeutic approaches targeting NADPH oxidases and mitochondria, or both to reduce ROS levels. Currently, the clinical approaches to reduce ROS in the treatment of MetS mainly involve changes in lifestyle, pharmacological drug therapy, and bariatric surgery (Murphy and Hartley, 2018; Bozi et al., 2020; Tun et al., 2020).

Decades of endeavors have targeted NADPH oxidases to lower ROS production (Araujo and Wilcox, 2014; DeVallance et al., 2019). The first generation of NADPH oxidase inhibitors are diphenyleneiodonium (DPI) and apocynin, which are not isoform-specific (Gill and Wilcox, 2006). Due to their broad profile of inhibition and side effects, more specific NADPH oxidase inhibitors have been developed, specifically GenKyoTex compounds, such as GKT137831 and GKT-136901 (Teixeira et al., 2017), triazolo pyrimidine compounds, such as VAS2870 and VAS3947 (Schramm et al., 2012), and the synthetic organoselenium ebselen, along with its congeners (DeVallance et al., 2019). Ebselen inhibits NOX1, NOX2, and NOX5, reduces vascular dysfunction, and improves insulin signaling in obese and diabetic rodents (Chen et al., 2009; DeVallance et al., 2019). NADPH oxidase isoform-specific inhibitors have been developed recently, specifically NOX1 inhibitors, such as ML171 and NoxA1ds, that block the interaction of NoxA1 with NOX1, reducing vascular resistance, improving endothelial function, and decreasing fat differentiation and migratory potential in MetS (Sela et al., 2015; Camargo et al., 2018). Nox2ds-tat, a peptide inhibitor of NOX2, interferes with p47phox docking to NOX2, causing the inhibition of ROS production (Csányi et al., 2011), reversal of vascular pathology, and restoration of insulin signaling (Sukumar et al., 2013; Quesada et al., 2015). Similar to the Nox2ds-tat, CPP11G and CPP11H, interfere with the translocation of p47phox to NOX2 in the plasma membrane, abolish ROS production, and attenuate endothelial cell inflammation and vascular dysfunction in an acute inflammatory mouse model (Li et al., 2019). All of these NADPH oxidase inhibitors are expected to be useful in the treatment of MetS.

Mitochondria-targeted antioxidants are reported to ameliorate MetS in experimental animals and humans (Bhatti et al., 2017; Murphy and Hartley, 2018; Bozi et al., 2020). Antioxidant compounds incorporated with ubiquinone or vitamin E, and the resulting compounds, MitoQ and MitoVit E, can specifically target the mitochondria to reduce oxidative injury and reverse mitochondrial dysfunction (Mao et al., 2011; Feillet-Coudray et al., 2014). The lipophilic triphenylphosphonium cation enables MitoQ to cross phospholipid bilayers, which leads to its accumulation within the mitochondria and reduction of mitochondrial ROS. MitoQ has been shown to reverse partially glucose intolerance, improve lipid metabolism, and restore mitochondrial activity in high-fat diet-fed Sprague-Dawley rats (Coudray et al., 2016), effects that were associated with a decrease in adipose tissue, and liver and body weights. In high-fat diet-fed mice, MitoVitE, another mitochondria-targeted antioxidant, protected the mitochondria against oxidative damage, improved subsarcolemmal mitochondrial density, and decreased systemic oxidative stress, manifested by an increase in plasma SOD activity and a decrease in urinary isoprostanes (Mao et al., 2011). Metformin, a drug widely used in the treatment of diabetes because of its ability to decrease the intestinal absorption of glucose and improve insulin sensitivity, decreases mitochondrial ROS, increases ADP:ATP ratio, induces AMPK activation, which then inhibits hepatic gluconeogenesis (Madiraju et al., 2018).

Antioxidants targeting both NADPH oxidases and mitochondria have been tested in clinical trials (**Table 2**). Although the role of ROS in the pathogenesis of MetS has been established in preclinical studies, the results in clinical studies have not been encouraging. Considering that high concentrations of ROS are harmful, reducing ROS levels should be beneficial. However, the degree of reduction of ROS to be beneficial is not known. The normal range more than likely varies in different cells at different times. Therefore, specific NADPH oxidase isoform or mitochondria-site antioxidants with cell- or tissue-specific drug delivery at a specific time is a promising therapeutic approach (Casas et al., 2020).

CONCLUSION AND PERSPECTIVES

MetS, which is a complex tangled web of oxidative stress with unhealthy states, including visceral obesity, hyperglycemia, dyslipidemia, and hypertension, occurs concomitantly in patients with elevated risk for cardiovascular diseases and chronic kidney diseases. As discussed in this review, the exact mechanisms underlying MetS are not clear. Oxidative stress, with inflammation, insulin resistance, and vascular endothelial damage, creates a pathophysiological condition that promotes the initiation and progression of MetS. Oxidative stress, the fundamental pathological basis for MetS, occurs because cellular anti-oxidative responses cannot counteract pro-oxidative effects. NADPH oxidases and mitochondria are the two major cellular sources for ROS production. ROS generated by NADPH oxidases may induce Mito-ROS generation, and vice versa, resulting in a vicious cycle. ROS, generated by NADPH oxidases and mitochondria, by themselves or by their interaction, in response to various exogenous and endogenous stimuli and metabolic alterations, trigger a series of adaptive and pathological responses, including the regulation of transcriptional factors and gene expression, and metabolic reprogramming. It is believed that low levels of ROS function as signaling molecules for physiological cellular functions whereas high levels of ROS are harmful to proteins, lipids, and nucleic acids. However, the boundary between the physiological signaling and pathological effects is unknown.

TABLE 2 | Clinical trials of antioxidants in the therapy of metabolic syndrome or associated cardiovascular and chronic renal diseases.

Target	Antioxidant	NCT number	Subject recruitment status	Therapeutics	Main findings in clinical trials	Reference(s)
NADPH oxidases	Ebselen	NCT 00762671	Completed	Inhibitor	Anti-inflammatory No inhibition of ROS	Beckman et al., (2016), Garland et al., (2020)
	GKT137831	NCT 02010242	Completed	Inhibitor	ND	NA
	Apocynin	NCT 03680638	Completed	Scavenger	ND	NA
		NCT 03680404 NCT 03680573	Completed		ND	NA
		NCT 04087655	Not yet recruiting		ND	NA
Both NADPH oxidases and Mitochondria	Tempol	NCT 03680638; NCT 03680404	Completed	Scavenger	ND	NA
Mitochondria	CoQ10	NCT 02407548	Completed	Inhibitor (cofactor of ETC)	CoQ10 increases TAC, reduces triglyceride, LDL-C, insulin resistance index, and blood pressure.	Zhang et al., (2018)
		IRCT2016011125949N1	Completed		CoQ10 decreases HOMA-IR, TC, LDL-C and increases HDL-C in diabetic patients.	Gholami et al., (2019)
		IRCT201502245623N35	Completed		CoQ10 has beneficial effects on serum insulin levels, HOMA-IR, HOMA-B and TAC in MetS patients.	Raygan et al., (2016)
		NCT 01412476	Completed		ND	NA
	Armolipid Plus (CoQ10)	NCT 01087632 NCT 01562080	Completed		Inhibition of Mito-ROS reduces blood glucose, cholesterol and triglycerides, and improves endothelial function and insulin resistance.	Solà et al., (2014) and Cicero et al., (2021)
	Armolipid Prev (CoQ10)	NCT 01293162	Completed		CoQ10 has anti-hypertensive, anti-dyslipidemic effects, reduces plasma homocysteine levels.	Izzo et al., (2010)
	MitoQ	NCT03586414	Suspended	Inhibitor	ND	NA
		NCT04334135	Recruiting		ND	NA
		NCT02364648	Recruiting		ND	NA

ROS, as DAMPs, activate NLRP3 inflammasomes, and therefore, mitochondria (and perhaps NADPH oxidases) can be considered as an integral component of the innate immune system to respond to intracellular and extracellular metabolic changes and stresses. It is assumed that ROS, generated from mitochondria, not only can cause the signaling and effects discussed above, but may also shape the metabolism and adaptive response of the immune system, including T and B cells. Further investigation is needed, not only on the mechanism underlying MetS but also the effects of cellular immunometabolism, to provide new paths for the therapeutic targeting for MetS.

Mito-ROS is usually linked to oxidative phosphorylation along the ETC. Recent evidence has demonstrated many sites that generate ROS in the mitochondria. For example, PDC produces more ROS than ETC Complex I. Consistent with the notion that oxidative stress is associated with the metabolic abnormality in MetS, renal proximal tubule cells from SHRs have higher PDC protein expression and activity than normotensive WKY rats; blood pressure also increases with the increase in PDC activity. PDC activity contributes to oxidative stress, but whether or not PDC activity increases sodium transport in the renal proximal tubule and other nephron segments warrants further investigation in patients and animals with MetS. The potential roles of PDC and the associated oxidative stress on inflammation, insulin resistance, alteration of glucose and lipid metabolism, adipocyte proliferation, endothelial dysfunction, and vascular resistance are largely unknown. The association of increased PDC activity with hyperglycemia, dyslipidemia, and even gut dysbiosis in the pathogenesis of MetS needs further investigation.

AUTHOR CONTRIBUTIONS

HL and PAJ wrote the manuscript; HL and PAJ prepared the figures and tables. HL and PAJ edited and revised the manuscript and PAJ approved its final version.

FUNDING

The work was funded by grants from the US National Institutes of Health R01DK119652, R37HL023081, R01DK039308, R01HL092196, R01DK090918, P01HL068686, P01HL074940 and U01GM074492.

REFERENCES

Abderrazak, A., Syrovets, T., Couchie, D., El Hadri, K., Friguet, B., Simmet, T., et al. (2015). NLRP3 Inflammasome: from a Danger Signal Sensor to a Regulatory Node of Oxidative Stress and Inflammatory Diseases. *Redox Biol.* 4, 296–307. doi:10.1016/j.redox.2015.01.008

Ahmadinejad, F., Geir Møller, S., Hashemzadeh-Chaleshtori, M., Bidkhori, G., and Jami, M. S. (2017). Molecular Mechanisms behind Free Radical Scavengers Function against Oxidative Stress. *Antioxidants* 6, 51. doi:10.3390/antiox6030051

Ahmed, K. A., Sawa, T., Ihara, H., Kasamatsu, S., Yoshitake, J., Rahaman, M. M., et al. (2012). Regulation by Mitochondrial Superoxide and NADPH Oxidase of Cellular Formation of Nitrated Cyclic GMP: Potential Implications for ROS Signalling. *Biochem. J.* 441, 719–730. doi:10.1042/BJ20111130

Akoumianakis, I., and Antoniades, C. (2019). Impaired Vascular Redox Signaling in the Vascular Complications of Obesity and Diabetes Mellitus. *Antioxid. Redox Signaling* 30, 333–353. doi:10.1089/ars.2017.7421

Alberti, K. G. M. M., Eckel, R. H., Grundy, S. M., Zimmet, P. Z., Cleeman, J. I., Donato, K. A., et al. (2009). Harmonizing the Metabolic Syndrome: a Joint Interim Statement of the International Diabetes Federation Task Force on Epidemiology and Prevention; National Heart, Lung, and Blood Institute; American Heart Association; World Heart Federation; International Atherosclerosis Society; and International Association for the Study of Obesity. *Circulation* 120, 1640–1645. doi:10.1161/CIRCULATIONAHA.109.192644

Ambrus, A., Nemeria, N. S., Torocsik, B., Tretter, L., Nilsson, M., Jordan, F., et al. (2015). Formation of Reactive Oxygen Species by Human and Bacterial Pyruvate and 2-oxoglutarate Dehydrogenase Multienzyme Complexes Reconstituted from Recombinant Components. *Free Radic. Biol. Med.* 89, 642–650. doi:10.1016/j.freeradbiomed.2015.10.001

Ando, K., and Fujita, M. (2012). Reactive Oxygen Species and the Central Nervous System in Salt-Sensitive Hypertension: Possible Relationship with Obesity-Induced Hypertension. *Clin. Exp. Pharmacol. Physiol.* 39, 111–116. doi:10.1111/j.1440-1681.2011.05510.x

Araujo, M., and Wilcox, C. S. (2014). Oxidative Stress in Hypertension: Role of the Kidney. *Antioxid. Redox Signaling* 20, 74–101. doi:10.1089/ars.2013.5259

Aroor, A. R., Mandavia, C., Ren, J., Sowers, J. R., and Pulakat, L. (2012). Mitochondria and Oxidative Stress in the Cardiorenal Metabolic Syndrome. *Cardiorenal Med.* 2, 87–109. doi:10.1159/000335675

Bakker, P. J., Butter, L. M., Kors, L., Teske, G. J. D., Aten, J., Sutterwala, F. S., et al. (2014). Nlrp3 Is a Key Modulator of Diet-Induced Nephropathy and Renal Cholesterol Accumulation. *Kidney Int.* 85, 1112–1122. doi:10.1038/ki.2013.503

Bánfi, B., Tirone, F., Durussel, I., Knisz, J., Moskwa, P., Molnár, G. Z., et al. (2004). Mechanism of Ca2+ Activation of the NADPH Oxidase 5 (NOX5). *J. Biol. Chem.* 279, 18583–18591. doi:10.1074/jbc.M310268200

Baret, P., Le Sage, F., Planesse, C., Meilhac, O., Devin, A., Bourdon, E., et al. (2017). Glycated Human Albumin Alters Mitochondrial Respiration in Preadipocyte 3T3-L1 Cells. *Biofactors* 43, 577–592. doi:10.1002/biof.1367

Bazil, J. N., Pannala, V. R., Dash, R. K., and Beard, D. A. (2014). Determining the Origins of Superoxide and Hydrogen Peroxide in the Mammalian NADH: ubiquinone Oxidoreductase. *Free Radic. Biol. Med.* 77, 121–129. doi:10.1016/j.freeradbiomed.2014.08.023

Beckman, J. A., Goldfine, A. B., Leopold, J. A., and Creager, M. A. (2016). Ebselen Does Not Improve Oxidative Stress and Vascular Function in Patients with Diabetes: a Randomized, Crossover Trial. *Am. J. Physiology-Heart Circulatory Physiol.* 311, H1431–H1436. doi:10.1152/ajpheart.00504.2016

Bedard, K., and Krause, K.-H. (2007). The NOX Family of ROS-Generating NADPH Oxidases: Physiology and Pathophysiology. *Physiol. Rev.* 87, 245–313. doi:10.1152/physrev.00044.2005

Bedi, O., Aggarwal, S., Trehanpati, N., Ramakrishna, G., and Krishan, P. (2019). Molecular and Pathological Events Involved in the Pathogenesis of Diabetes-Associated Nonalcoholic Fatty Liver Disease. *J. Clin. Exp. Hepatol.* 9, 607–618. doi:10.1016/j.jceh.2018.10.004

Berry, B. J., Trewin, A. J., Amitrano, A. M., Kim, M., and Wojtovich, A. P. (2018). Use the Protonmotive Force: Mitochondrial Uncoupling and Reactive Oxygen Species. *J. Mol. Biol.* 430, 3873–3891. doi:10.1016/j.jmb.2018.03.025

Bhatti, J. S., Bhatti, G. K., and Reddy, P. H. (2017). Mitochondrial Dysfunction and Oxidative Stress in Metabolic Disorders - A Step towards Mitochondria Based Therapeutic Strategies. *Biochim. Biophys. Acta (Bba) - Mol. Basis Dis.* 1863, 1066–1077. doi:10.1016/j.bbadis.2016.11.010

Bozi, L. H. M., Campos, J. C., Zambelli, V. O., Ferreira, N. D., and Ferreira, J. C. B. (2020). Mitochondrially-targeted Treatment Strategies. *Mol. Aspects Med.* 71, 100836. doi:10.1016/j.mam.2019.100836

Brady, N. R., Hamacher-Brady, A., Westerhoff, H. V., and Gottlieb, R. A. (2006). A Wave of Reactive Oxygen Species (ROS)-induced ROS Release in a Sea of Excitable Mitochondria. *Antioxid. Redox Signaling* 8, 1651–1665. doi:10.1089/ars.2006.8.1651

Brand, M. D. (2016). Mitochondrial Generation of Superoxide and Hydrogen Peroxide as the Source of Mitochondrial Redox Signaling. *Free Radic. Biol. Med.* 100, 14–31. doi:10.1016/j.freeradbiomed.2016.04.001

Burhans, W. C., and Heintz, N. H. (2009). The Cell Cycle Is a Redox Cycle: Linking Phase-specific Targets to Cell Fate. *Free Radic. Biol. Med.* 47, 1282–1293. doi:10.1016/j.freeradbiomed.2009.05.026

Camargo, L. L., Harvey, A. P., Rios, F. J., Tsiropoulou, S., Da Silva, R. d. N. O., Cao, Z., et al. (2018). Vascular Nox (NADPH Oxidase) Compartmentalization, Protein Hyperoxidation, and Endoplasmic Reticulum Stress Response in Hypertension. *Hypertension* 72, 235–246. doi:10.1161/HYPERTENSIONAHA.118.10824

Carnagarin, R., Carlessi, R., Newsholme, P., Dharmarajan, A. M., and Dass, C. R. (2016). Pigment Epithelium-Derived Factor Stimulates Skeletal Muscle Glycolytic Activity through NADPH Oxidase-dependent Reactive Oxygen Species Production. *Int. J. Biochem. Cel Biol.* 78, 229–236. doi:10.1016/j.biocel.2016.06.013

Casas, A. I., Nogales, C., Mucke, H. A. M., Petraina, A., Cuadrado, A., Rojo, A. I., et al. (2020). On the Clinical Pharmacology of Reactive Oxygen Species. *Pharmacol. Rev.* 72, 801–828. doi:10.1124/pr.120.019422

Chen, D.-D., Dong, Y.-G., Yuan, H., and Chen, A. F. (2012). Endothelin 1 Activation of Endothelin A receptor/NADPH Oxidase Pathway and Diminished Antioxidants Critically Contribute to Endothelial Progenitor Cell Reduction and Dysfunction in Salt-Sensitive Hypertension. *Hypertension* 59, 1037–1043. doi:10.1161/HYPERTENSIONAHA.111.183368

Chen, J., Li, H., Addabbo, F., Zhang, F., Pelger, E., Patschan, D., et al. (2009). Adoptive Transfer of Syngeneic Bone Marrow-Derived Cells in Mice with Obesity-Induced Diabetes. *Am. J. Pathol.* 174, 701–711. doi:10.2353/ajpath.2009.080606

Chouchani, E. T., Pell, V. R., Gaude, E., Aksentijević, D., Sundier, S. Y., Robb, E. L., et al. (2014). Ischaemic Accumulation of Succinate Controls Reperfusion Injury through Mitochondrial ROS. *Nature* 515, 431–435. doi:10.1038/nature13909

Cicero, A. F. G., Kennedy, C., Knežević, T., Bove, M., Georges, C. M. G., Šatrauskienė, A., et al. (2021). Efficacy and Safety of Armolipid Plus: An Updated PRISMA Compliant Systematic Review and Meta-Analysis of Randomized Controlled Clinical Trials. *Nutrients* 13, 638. doi:10.3390/nu13020638

Constantin-Teodosiu, D., Stephens, F. B., and Greenhaff, P. L. (2015). Perpetual Muscle PDH Activation in PDH Kinase Knockout Mice Protects against High-Fat Feeding-Induced Muscle Insulin Resistance. *Proc. Natl. Acad. Sci. USA* 112, E824. doi:10.1073/pnas.1422929112

Costa, A. D. T., and Garlid, K. D. (2008a). Intramitochondrial Signaling: Interactions Among mitoKATP, PKCε, ROS, and MPT. *Am. J. Physiology-Heart Circulatory Physiol.* 295, H874–H882. doi:10.1152/ajpheart.00858.201210.1152/ajpheart.01189.2007

Costa, A. D. T., Pierre, S. V., Cohen, M. V., Downey, J. M., and Garlid, K. D. (2008b). cGMP Signalling in Pre- and Post-conditioning: the Role of Mitochondria. *Cardiovasc. Res.* 77, 344–352. doi:10.1093/cvr/cvm050

Coudray, C., Fouret, G., Lambert, K., Ferreri, C., Rieusset, J., Blachnio-Zabielska, A., et al. (2016). A Mitochondrial-Targeted Ubiquinone Modulates Muscle Lipid Profile and Improves Mitochondrial Respiration in Obesogenic Diet-Fed Rats. *Br. J. Nutr.* 115, 1155–1166. doi:10.1017/S0007114515005528

Coughlan, M. T., Thorburn, D. R., Penfold, S. A., Laskowski, A., Harcourt, B. E., Sourris, K. C., et al. (2009). RAGE-induced Cytosolic ROS Promote Mitochondrial Superoxide Generation in Diabetes. *Jasn* 20, 742–752. doi:10.1681/ASN.2008050514

Cowley, A. W., Jr, Abe, M., Mori, T., O'Connor, P. M., Ohsaki, Y., and Zheleznova, N. N. (2015). Reactive Oxygen Species as Important Determinants of Medullary

Flow, Sodium Excretion, and Hypertension. *Am. J. Physiology-Renal Physiol.* 308, F179–F197. doi:10.1152/ajprenal.00455.2014

Csányi, G., Cifuentes-Pagano, E., Al Ghouleh, I., Ranayhossaini, D. J., Egaña, L., Lopes, L. R., et al. (2011). Nox2 B-Loop Peptide, Nox2ds, Specifically Inhibits the NADPH Oxidase Nox2. *Free Radic. Biol. Med.* 51, 1116–1125. doi:10.1016/j.freeradbiomed.2011.04.025

Cuevas, S., Villar, V. A. M., and Jose, P. A. (2019). Genetic Polymorphisms Associated with Reactive Oxygen Species and Blood Pressure Regulation. *Pharmacogenomics J.* 19, 315–336. doi:10.1038/s41397-019-0082-4

Cuevas, S., Villar, V., Jose, P., and Armando, I. (2013). Renal Dopamine Receptors, Oxidative Stress, and Hypertension. *Ijms* 14, 17553–17572. doi:10.3390/ijms140917553

Cuevas, S., Zhang, Y., Yang, Y., Escano, C., Asico, L., Jones, J. E., et al. (2012). Role of Renal DJ-1 in the Pathogenesis of Hypertension Associated with Increased Reactive Oxygen Species Production. *Hypertension* 59, 446–452. doi:10.1161/HYPERTENSIONAHA.111.185744

Daenen, K., Andries, A., Mekahli, D., Van Schepdael, A., Jouret, F., and Bammens, B. (2019). Oxidative Stress in Chronic Kidney Disease. *Pediatr. Nephrol.* 34, 975–991. doi:10.1007/s00467-018-4005-4

Daiber, A., Di Lisa, F., Oelze, M., Kröller-Schön, S., Steven, S., Schulz, E., et al. (2017). Crosstalk of Mitochondria with NADPH Oxidase via Reactive Oxygen and Nitrogen Species Signalling and its Role for Vascular Function. *Br. J. Pharmacol.* 174, 1670–1689. doi:10.1111/bph.13403

Daiber, A. (2010). Redox Signaling (Cross-talk) from and to Mitochondria Involves Mitochondrial Pores and Reactive Oxygen Species. *Biochim. Biophys. Acta* 1797, 897–906. doi:10.1016/j.bbabio.2010.01.032

Daiber, A., Steven, S., Vujacic-Mirski, K., Kalinovic, S., Oelze, M., Di Lisa, F., et al. (2020). Regulation of Vascular Function and Inflammation via Cross Talk of Reactive Oxygen and Nitrogen Species from Mitochondria or NADPH Oxidase-Implications for Diabetes Progression. *Int. J. Mol. Sci.* 21, 3405. doi:10.3390/ijms21103405

DeVallance, E., Li, Y., Jurczak, M. J., Cifuentes-Pagano, E., and Pagano, P. J. (2019). The Role of NADPH Oxidases in the Etiology of Obesity and Metabolic Syndrome: Contribution of Individual Isoforms and Cell Biology. *Antioxid. Redox Signaling* 31, 687–709. doi:10.1089/ars.2018.7674

Dikalov, S. (2011). Cross Talk between Mitochondria and NADPH Oxidases. *Free Radic. Biol. Med.* 51, 1289–1301. doi:10.1016/j.freeradbiomed.2011.06.033

Dikalov, S. I., and Dikalova, A. E. (2019). Crosstalk between Mitochondrial Hyperacetylation and Oxidative Stress in Vascular Dysfunction and Hypertension. *Antioxid. Redox Signaling* 31, 710–721. doi:10.1089/ars.2018.7632

Dinkova-Kostova, A. T., and Abramov, A. Y. (2015). The Emerging Role of Nrf2 in Mitochondrial Function. *Free Radic. Biol. Med.* 88, 179–188. doi:10.1016/j.freeradbiomed.2015.04.036

Dröse, S., and Brandt, U. (2012). Molecular Mechanisms of Superoxide Production by the Mitochondrial Respiratory Chain. *Adv. Exp. Med. Biol.* 748, 145–169. doi:10.1007/978-1-4614-3573-0_6

Egea, J., Fabregat, I., Frapart, Y. M., Ghezzi, P., Görlach, A., Kietzmann, T., et al. (2017). European Contribution to the Study of ROS: a Summary of the Findings and Prospects for the Future from the COST Action BM1203 (EU-ROS). *Redox Biol.* 13, 94–162. doi:10.1016/j.redox.2017.05.007

Eid, A. A., Ford, B. M., Block, K., Kasinath, B. S., Gorin, Y., Ghosh-Choudhury, G., et al. (2010). AMP-activated Protein Kinase (AMPK) Negatively Regulates Nox4-dependent Activation of P53 and Epithelial Cell Apoptosis in Diabetes*. *J. Biol. Chem.* 285, 37503–37512. doi:10.1074/jbc.M110.136796

Esser, N., Legrand-Poels, S., Piette, J., Scheen, A. J., and Paquot, N. (2014). Inflammation as a Link between Obesity, Metabolic Syndrome and Type 2 Diabetes. *Diabetes Res. Clin. Pract.* 105, 141–150. doi:10.1016/j.diabres.2014.04.006

Fazeli, G., Stopper, H., Schinzel, R., Ni, C.-W., Jo, H., and Schupp, N. (2012). Angiotensin II Induces DNA Damage via AT1 Receptor and NADPH Oxidase Isoform Nox4. *Mutagenesis* 27, 673–681. doi:10.1093/mutage/ges033

Feillet-Coudray, C., Fouret, G., Ebabe Elle, R., Rieusset, J., Bonafos, B., Chabi, B., et al. (2014). The Mitochondrial-targeted Antioxidant MitoQ Ameliorates Metabolic Syndrome Features in Obesogenic Diet-fed Rats Better than Apocynin or Allopurinol. *Free Radic. Res.* 48, 1232–1246.

Frey, R. S., Gao, X., Javaid, K., Siddiqui, S. S., Rahman, A., and Malik, A. B. (2006). Phosphatidylinositol 3-Kinase γ Signaling through Protein Kinase Cζ Induces NADPH Oxidase-Mediated Oxidant Generation and NF-Kb Activation in Endothelial Cells. *J. Biol. Chem.* 281, 16128–16138. doi:10.1074/jbc.M508810200

Furukawa, S., Fujita, T., Shimabukuro, M., Iwaki, M., Yamada, Y., Nakajima, Y., et al. (2004). Increased Oxidative Stress in Obesity and its Impact on Metabolic Syndrome. *J. Clin. Invest.* 114, 1752–1761. doi:10.1172/JCI21625

Gaens, K. H. J., Goossens, G. H., Niessen, P. M., van Greevenbroek, M. M., van der Kallen, C. J. H., Niessen, H. W., et al. (2014). N ε -(Carboxymethyl)lysine-Receptor for Advanced Glycation End Product Axis Is a Key Modulator of Obesity-Induced Dysregulation of Adipokine Expression and Insulin Resistance. *Arterioscler Thromb. Vasc. Biol.* 34, 1199–1208. doi:10.1161/ATVBAHA.113.302281

Garay-Sevilla, M. E., Gomez-Ojeda, A., González, I., Luévano-Contreras, C., and Rojas, A. (2021). Contribution of RAGE axis Activation to the Association between Metabolic Syndrome and Cancer. *Mol. Cel Biochem.* 476, 1555–1573. Epub ahead of print. doi:10.1007/s11010-020-04022-z

Garland, M., Hryckowian, A. J., Tholen, M., Oresic Bender, K., Van Treuren, W. W., Loscher, S., et al. (2020). The Clinical Drug Ebselen Attenuates Inflammation and Promotes Microbiome Recovery in Mice after Antibiotic Treatment for CDI. *Cel Rep. Med.* 1, 100005. doi:10.1016/j.xcrm.2020.100005

Gholami, M., Rezvanfar, M., Delavar, M., Abdollahi, M., and Khosrowbeygi, A. (2019). Effects of Coenzyme Q10 Supplementation on Serum Values of Gamma-Glutamyl Transferase, Pseudocholinesterase, Bilirubin, Ferritin, and High-Sensitivity C-Reactive Protein in Women with Type 2 Diabetes. *Exp. Clin. Endocrinol. Diabetes* 127, 311–319. doi:10.1055/s-0043-124183

Gill, P. S., and Wilcox, C. S. (2006). NADPH Oxidases in the Kidney. *Antioxid. Redox Signaling* 8, 1597–1607. doi:10.1089/ars.2006.8.1597

Gnaiger, E., Lassnig, B., Kuznetsov, A., Rieger, G., and Margreiter, R. (1998). Mitochondrial Oxygen Affinity, Respiratory Flux Control and Excess Capacity of Cytochrome C Oxidase. *J. Exp. Biol.* 201, 1129–1139.

Gonzales-Vicente, A., Hong, N., and Garvin, J. L. (2019). Effects of Reactive Oxygen Species on Renal Tubular Transport. *Am. J. Physiol. Ren. Physiol.* 317, F444–F455. doi:10.1152/ajprenal.00604.2018

Görlach, A., Bertram, K., Hudecova, S., and Krizanova, O. (2015). Calcium and ROS: A Mutual Interplay. *Redox Biol.* 6, 260–271. doi:10.1016/j.redox.2015.08.010

Groemping, Y., and Rittinger, K. (2005). Activation and Assembly of the NADPH Oxidase: a Structural Perspective. *Biochem. J.* 386, 401–416. doi:10.1042/BJ20041835

Grundy, S. M. (2016). Metabolic Syndrome Update. *Trends Cardiovasc. Med.* 26, 364–373. doi:10.1016/j.tcm.2015.10.004

Guerby, P., Tasta, O., Swiader, A., Pont, F., Bujold, E., Parant, O., et al. (2021). Role of Oxidative Stress in the Dysfunction of the Placental Endothelial Nitric Oxide Synthase in Preeclampsia. *Redox Biol.* 40, 101861. doi:10.1016/j.redox.2021.101861

Guichard, C., Moreau, R., Pessayre, D., Epperson, T. K., and Krause, K.-H. (2008). NOX Family NADPH Oxidases in Liver and in Pancreatic Islets: a Role in the Metabolic Syndrome and Diabetes? *Biochem. Soc. Trans.* 36, 920–929. doi:10.1042/BST0360920

Gutteridge, J. M. C., and Halliwell, B. (2018). Mini-Review: Oxidative Stress, Redox Stress or Redox Success? *Biochem. Biophysical Res. Commun.* 502, 183–186. doi:10.1016/j.bbrc.2018.05.045

Han, W., Li, H., Villar, V. A. M., Pascua, A. M., Dajani, M. I., Wang, X., et al. (2008). Lipid Rafts Keep NADPH Oxidase in the Inactive State in Human Renal Proximal Tubule Cells. *Hypertension* 51, 481–487. doi:10.1161/HYPERTENSIONAHA.107.103275

Han, Y., Sun, W., Ren, D., Zhang, J., He, Z., Fedorova, J., et al. (2020). SIRT1 Agonism Modulates Cardiac NLRP3 Inflammasome through Pyruvate Dehydrogenase during Ischemia and Reperfusion. *Redox Biol.* 34, 101538. doi:10.1016/j.redox.2020.101538

Hayes, J. D., and Dinkova-Kostova, A. T. (2014). The Nrf2 Regulatory Network Provides an Interface between Redox and Intermediary Metabolism. *Trends Biochem. Sci.* 39, 199–218. doi:10.1016/j.tibs.2014.02.002

He, F., Ru, X., and Wen, T. (2020). NRF2, a Transcription Factor for Stress Response and beyond. *Ijms* 21, 4777. doi:10.3390/ijms21134777

Hirschhäuser, C., Bornbaum, J., Reis, A., Böhme, S., Kaludercic, N., Menabò, R., et al. (2015). NOX4 in Mitochondria: Yeast Two-Hybrid-Based Interaction with Complex I without Relevance for Basal Reactive

Oxygen Species? *Antioxid. Redox Signaling* 23, 1106–1112. doi:10.1089/ars.2014.6238

Hoffman, D. L., and Brookes, P. S. (2009). Oxygen Sensitivity of Mitochondrial Reactive Oxygen Species Generation Depends on Metabolic Conditions. *J. Biol. Chem.* 284, 16236–16245. doi:10.1074/jbc.M809512200

Holness, M. J., and Sugden, M. C. (2003). Regulation of Pyruvate Dehydrogenase Complex Activity by Reversible Phosphorylation. *Biochem. Soc. Trans.* 31, 1143–1151. doi:10.1042/bst0311143

Hou, Y., Li, S., Wu, M., Wei, J., Ren, Y., Du, C., et al. (2016). Mitochondria-targeted Peptide SS-31 Attenuates Renal Injury via an Antioxidant Effect in Diabetic Nephropathy. *Am. J. Physiology-Renal Physiol.* 310, F547–F559. doi:10.1152/ajprenal.00574.2014

Huang, C.-R., Chang, T.-W., Lee, C.-T., Shen, C.-J., Chang, W.-C., and Chen, B.-K. (2021). ARNT Deficiency Represses Pyruvate Dehydrogenase Kinase 1 to Trigger ROS Production and Melanoma Metastasis. *Oncogenesis* 10, 11. doi:10.1038/s41389-020-00299-3

Itani, H. A., Dikalova, A. E., McMaster, W. G., Nazarewicz, R. R., Bikineyeva, A. T., Harrison, D. G., et al. (2016). Mitochondrial Cyclophilin D in Vascular Oxidative Stress and Hypertension. *Hypertension* 67, 1218–1227. doi:10.1161/HYPERTENSIONAHA.115.07085

Izzo, R., de Simone, G., Giudice, R., Chinali, M., Trimarco, V., De Luca, N., et al. (2010). Effects of Nutraceuticals on Prevalence of Metabolic Syndrome and on Calculated Framingham Risk Score in Individuals with Dyslipidemia. *J. Hypertens.* 28, 1482–1487. doi:10.1097/HJH.0b013e3283395208

Jha, J. C., Banal, C., Okabe, J., Gray, S. P., Hettige, T., Chow, B. S. M., et al. (2017). NADPH Oxidase Nox5 Accelerates Renal Injury in Diabetic Nephropathy. *Diabetes* 66, 2691–2703. doi:10.2337/db16-1585

Jha, J. C., Ho, F., Dan, C., and Jandeleit-Dahm, K. (2018). A Causal Link between Oxidative Stress and Inflammation in Cardiovascular and Renal Complications of Diabetes. *Clin. Sci.* 132, 1811–1836. doi:10.1042/CS20171459

Jia, G., Jia, Y., and Sowers, J. R. (2016). Contribution of Maladaptive Adipose Tissue Expansion to Development of Cardiovascular Disease. *Compr. Physiol.* 7, 253–262. doi:10.1002/cphy.c160014

Jiang, H., Shao, X., Jia, S., Qu, L., Weng, C., Shen, X., et al. (2019). The Mitochondria-Targeted Metabolic Tubular Injury in Diabetic Kidney Disease. *Cell Physiol. Biochem.* 52, 156–171. doi:10.33594/000000011

Jiang, X., Liu, Y., Liu, X., Wang, W., Wang, Z., Hu, Y., et al. (2018). Over-expression of a Cardiac-specific Human Dopamine D5 Receptor Mutation in Mice Causes a Dilated Cardiomyopathy through ROS Over-generation by NADPH Oxidase Activation and Nrf2 Degradation. *Redox Biol.* 19, 134–146. doi:10.1016/j.redox.2018.07.008

Kanda, Y., Hinata, T., Kang, S. W., and Watanabe, Y. (2011). Reactive Oxygen Species Mediate Adipocyte Differentiation in Mesenchymal Stem Cells. *Life Sci.* 89, 250–258. doi:10.1016/j.lfs.2011.06.007

Kim, M., Neinast, M. D., Frank, A. P., Sun, K., Park, J., Zehr, J. A., et al. (2014). ERα Upregulates Phd3 to Ameliorate HIF-1 Induced Fibrosis and Inflammation in Adipose Tissue. *Mol. Metab.* 3, 642–651. doi:10.1016/j.molmet.2014.05.007

Kim, S.-H., Chung, J.-h., Song, S.-W., Jung, W. S., Lee, Y.-A., and Kim, H.-N. (2016). Relationship between Deep Subcutaneous Abdominal Adipose Tissue and Metabolic Syndrome: a Case Control Study. *Diabetol. Metab. Syndr.* 8, 10. doi:10.1186/s13098-016-0127-7

Kimura, S., Zhang, G.-X., Nishiyama, A., Shokoji, T., Yao, L., Fan, Y.-Y., et al. (2005). Role of NAD(P)H Oxidase- and Mitochondria-Derived Reactive Oxygen Species in Cardioprotection of Ischemic Reperfusion Injury by Angiotensin II. *Hypertension* 45, 860–866. doi:10.1161/01.HYP.0000163462.98381.7f

Knepper, M. A., and Brooks, H. L. (2001). Regulation of the Sodium Transporters NHE3, NKCC2 and NCC in the Kidney. *Curr. Opin. Nephrol. Hypertens.* 10, 655–659. doi:10.1097/00041552-200109000-00017

Kröller-Schön, S., Steven, S., Kossmann, S., Scholz, A., Daub, S., Oelze, M., et al. (2014). Molecular Mechanisms of the Crosstalk between Mitochondria and NADPH Oxidase through Reactive Oxygen Species-Studies in White Blood Cells and in Animal Models. *Antioxid. Redox Signaling* 20, 247–266. doi:10.1089/ars.2012.4953

Kussmaul, L., and Hirst, J. (2006). The Mechanism of Superoxide Production by NADH:ubiquinone Oxidoreductase (Complex I) from Bovine Heart Mitochondria. *Proc. Natl. Acad. Sci.* 103, 7607–7612. doi:10.1073/pnas.0510977103

Lakkis, J. I., and Weir, M. R. (2018). Obesity and Kidney Disease. *Prog. Cardiovasc. Dis.* 61, 157–167. doi:10.1016/j.pcad.2018.07.005

Lee, D.-Y., Wauquier, F., Eid, A. A., Roman, L. J., Ghosh-Choudhury, G., Khazim, K., et al. (2013). Nox4 NADPH Oxidase Mediates Peroxynitrite-dependent Uncoupling of Endothelial Nitric-Oxide Synthase and Fibronectin Expression in Response to Angiotensin II. *J. Biol. Chem.* 288, 28668–28686. doi:10.1074/jbc.M113.470971

Lee, H., Abe, Y., Lee, I., Shrivastav, S., Crusan, A. P., Hüttemann, M., et al. (2014). Increased Mitochondrial Activity in Renal Proximal Tubule Cells from Young Spontaneously Hypertensive Rats. *Kidney Int.* 85, 561–569. doi:10.1038/ki.2013.397

Lee, H., Fessler, M. B., Qu, P., Heymann, J., and Kopp, J. B. (2020). Macrophage Polarization in Innate Immune Responses Contributing to Pathogenesis of Chronic Kidney Disease. *BMC Nephrol.* 21, 270. doi:10.1186/s12882-020-01921-7

Li, H., Han, W., Villar, V. A. M., Keever, L. B., Lu, Q., Hopfer, U., et al. (2009). D1-like Receptors Regulate NADPH Oxidase Activity and Subunit Expression in Lipid Raft Microdomains of Renal Proximal Tubule Cells. *Hypertension* 53, 1054–1061. doi:10.1161/HYPERTENSIONAHA.108.120642

Li, L., Watts, S. W., Banes, A. K., Galligan, J. J., Fink, G. D., and Chen, A. F. (2003). NADPH Oxidase-Derived Superoxide Augments Endothelin-1-Induced Venoconstriction in Mineralocorticoid Hypertension. *Hypertension* 42, 316–321. doi:10.1161/01.HYP.0000084853.47326.F2

Li, Y., Cifuentes-Pagano, E., DeVallance, E. R., de Jesus, D. S., Sahoo, S., Meijles, D. N., et al. (2019). NADPH Oxidase 2 Inhibitors CPP11G and CPP11H Attenuate Endothelial Cell Inflammation & Vessel Dysfunction and Restore Mouse Hind-Limb Flow. *Redox Biol.* 22, 101143. doi:10.1016/j.redox.2019.101143

Liang, L., Tan, X., Zhou, Q., Zhu, Y., Tian, Y., Yu, H., et al. (2013). IL-1β Triggered by Peptidoglycan and Lipopolysaccharide through TLR2/4 and ROS-NLRP3 Inflammasome-dependent Pathways Is Involved in Ocular Behçet's Disease. *Invest. Ophthalmol. Vis. Sci.* 54, 402–414. doi:10.1167/iovs.12-11047

Liang, M., Li, A., Lou, A., Zhang, X., Chen, Y., Yang, L., et al. (2017). Advanced Oxidation Protein Products Promote NADPH Oxidase-dependent β-cell Destruction and Dysfunction through the Bcl-2/Bax Apoptotic Pathway. *Lab. Invest.* 97, 792–805. doi:10.1038/labinvest.2017.24

Lindblom, R., Higgins, G., Coughlan, M., and de Haan, J. B. (2015). Targeting Mitochondria and Reactive Oxygen Species-Driven Pathogenesis in Diabetic Nephropathy. *Rev. Diabet. Stud.* 12, 134–156. doi:10.1900/RDS.2015.12.134

Locatelli, F., Pozzoni, P., and Del Vecchio, L. (2006). Renal Manifestations in the Metabolic Syndrome: Table 1. *Jasn* 17 (4 Suppl. 2), S81–S85. doi:10.1681/ASN.2005121332

Loperena, R., and Harrison, D. G. (2017). Oxidative Stress and Hypertensive Diseases. *Med. Clin. North America* 101, 169–193. doi:10.1016/j.mcna.2016.08.004

Lu, Q., Yang, Y., Villar, V. A., Asico, L., Jones, J. E., Yu, P., et al. (2013). D5 Dopamine Receptor Decreases NADPH Oxidase, Reactive Oxygen Species and Blood Pressure via Heme Oxygenase-1. *Hypertens. Res.* 36, 684–690. doi:10.1038/hr.2013.9

Lyle, A. N., Deshpande, N. N., Taniyama, Y., Seidel-Rogol, B., Pounkova, L., Du, P., et al. (2009). Poldip2, a Novel Regulator of Nox4 and Cytoskeletal Integrity in Vascular Smooth Muscle Cells. *Circ. Res.* 105, 249–259. doi:10.1161/CIRCRESAHA.109.193722

Macleod, K. F. (2008). The Role of the RB Tumour Suppressor Pathway in Oxidative Stress Responses in the Haematopoietic System. *Nat. Rev. Cancer* 8, 769–781. doi:10.1038/nrc2504

Madiraju, A. K., Qiu, Y., Perry, R. J., Rahimi, Y., Zhang, X.-M., Zhang, D., et al. (2018). Metformin Inhibits Gluconeogenesis via a Redox-dependent Mechanism In Vivo. *Nat. Med.* 24, 1384–1394. doi:10.1038/s41591-018-0125-4

Magenta, A., Fasanaro, P., Romani, S., Di Stefano, V., Capogrossi, M. C., and Martelli, F. (2008). Protein Phosphatase 2A Subunit PR70 Interacts with pRb and Mediates its Dephosphorylation. *Mcb* 28, 873–882. doi:10.1128/MCB.00480-07

Manduteanu, I., Pirvulescu, M., Gan, A. M., Stan, D., Simion, V., Dragomir, E., et al. (2010). Similar Effects of Resistin and High Glucose on P-Selectin and Fractalkine Expression and Monocyte Adhesion in Human Endothelial Cells. *Biochem. Biophysical Res. Commun.* 391, 1443–1448. doi:10.1016/j.bbrc.2009.12.089

Manea, A., Manea, S. A., Florea, I. C., Luca, C. M., and Raicu, M. (2012). Positive Regulation of NADPH Oxidase 5 by Proinflammatory-Related Mechanisms in Human Aortic Smooth Muscle Cells. *Free Radic. Biol. Med.* 52, 1497–1507. doi:10.1016/j.freeradbiomed.2012.02.018

Manea, S.-A., Constantin, A., Manda, G., Sasson, S., and Manea, A. (2015). Regulation of Nox Enzymes Expression in Vascular Pathophysiology: Focusing on Transcription Factors and Epigenetic Mechanisms. *Redox Biol.* 5, 358–366. doi:10.1016/j.redox.2015.06.012

Mao, G., Kraus, G. A., Kim, I., Spurlock, M. E., Bailey, T. B., and Beitz, D. C. (2011). Effect of a Mitochondria-Targeted Vitamin E Derivative on Mitochondrial Alteration and Systemic Oxidative Stress in Mice. *Br. J. Nutr.* 106, 87–95. doi:10.1017/S0007114510005830

Maslov, L. N., Naryzhnaya, N. V., Boshchenko, A. A., Popov, S. V., Ivanov, V. V., and Oeltgen, P. R. (2019). Is Oxidative Stress of Adipocytes a Cause or a Consequence of the Metabolic Syndrome? *J. Clin. Transl. Endocrinol.* 15, 1–5. doi:10.1016/j.jcte.2018.11.001

Masschelin, P. M., Cox, A. R., Chernis, N., and Hartig, S. M. (2020). The Impact of Oxidative Stress on Adipose Tissue Energy Balance. *Front. Physiol.* 10, 1638. doi:10.3389/fphys.2019.01638

Mastrocola, R., Aragno, M., Alloatti, G., Collino, M., Penna, C., and Pagliaro, P. (2018). Metaflammation: Tissue-specific Alterations of the NLRP3 Inflammasome Platform in Metabolic Syndrome. *Cmc* 25, 1294–1310. doi:10.2174/0929867324666170407123522

Maxwell, K. D., Chuang, J., Chaudhry, M., Nie, Y., Bai, F., Sodhi, K., et al. (2021). The Potential Role of Na-K-ATPase and its Signaling in the Development of Anemia in Chronic Kidney Disease. *Am. J. Physiology-Renal Physiol.* 320, F234–F242. [Epub ahead of print]. doi:10.1152/ajprenal.00244.2020

McCracken, E., Monaghan, M., and Sreenivasan, S. (2018). Pathophysiology of the Metabolic Syndrome. *Clin. Dermatol.* 36, 14–20. doi:10.1016/j.clindermatol.2017.09.004

Meiser, J., Krämer, L., Sapcariu, S. C., Battello, N., Ghelfi, J., D'Herouel, A. F., et al. (2016). Pro-inflammatory Macrophages Sustain Pyruvate Oxidation through Pyruvate Dehydrogenase for the Synthesis of Itaconate and to Enable Cytokine Expression. *J. Biol. Chem.* 291, 3932–3946. doi:10.1074/jbc.M115.676817

Michno, A., Grużewska, K., Bielarczyk, H., Zyśk, M., and Szutowicz, A. (2020). Inhibition of Pyruvate Dehydrogenase Complex Activity by 3-bromopyruvate Affects Blood Platelets Responses in Type 2 Diabetes. *Pharmacol. Rep.* 72, 225–237. doi:10.1007/s43440-019-00005-0

Misawa, T., Takahama, M., Kozaki, T., Lee, H., Zou, J., Saitoh, T., et al. (2013). Microtubule-driven Spatial Arrangement of Mitochondria Promotes Activation of the NLRP3 Inflammasome. *Nat. Immunol.* 14, 454–460. doi:10.1038/ni.2550

Moldogazieva, N. T., Mokhosoev, I. M., Feldman, N. B., and Lutsenko, S. V. (2018). ROS and RNS Signalling: Adaptive Redox Switches through Oxidative/nitrosative Protein Modifications. *Free Radic. Res.* 52, 507–543. doi:10.1080/10715762.2018.1457217

Munro, D., and Treberg, J. R. (2017). A Radical Shift in Perspective: Mitochondria as Regulators of Reactive Oxygen Species. *J. Exp. Biol.* 220, 1170–1180. doi:10.1242/jeb.132142

Murphy, M. P., and Hartley, R. C. (2018). Mitochondria as a Therapeutic Target for Common Pathologies. *Nat. Rev. Drug Discov.* 17, 865–886. doi:10.1038/nrd.2018.174

Murphy, M. P. (2009). How Mitochondria Produce Reactive Oxygen Species. *Biochem. J.* 417, 1–13. doi:10.1042/BJ20081386

Nauseef, W. M. (2014). Detection of Superoxide Anion and Hydrogen Peroxide Production by Cellular NADPH Oxidases. *Biochim. Biophys. Acta (Bba) - Gen. Subjects* 1840, 757–767. doi:10.1016/j.bbagen.2013.04.040

Newsholme, P., Keane, K. N., Carlessi, R., and Cruzat, V. (2019). Oxidative Stress Pathways in Pancreatic β-cells and Insulin-Sensitive Cells and Tissues: Importance to Cell Metabolism, Function, and Dysfunction. *Am. J. Physiology-Cell Physiol.* 317, C420–C433. doi:10.1152/ajpcell.00141.2019

Ni, R., Cao, T., Xiong, S., Ma, J., Fan, G.-C., Lacefield, J. C., et al. (2016). Therapeutic Inhibition of Mitochondrial Reactive Oxygen Species with Mito-TEMPO Reduces Diabetic Cardiomyopathy. *Free Radic. Biol. Med.* 90, 12–23. doi:10.1016/j.freeradbiomed.2015.11.013

Nilsson, P. M., Tuomilehto, J., and Rydén, L. (2019). The Metabolic Syndrome - what Is it and How Should it Be Managed? *Eur. J. Prev. Cardiol.* 26 (Suppl. 2), 33–46. doi:10.1177/2047487319886404

Palmeira, C. M., Teodoro, J. S., Amorim, J. A., Steegborn, C., Sinclair, D. A., and Rolo, A. P. (2019). Mitohormesis and Metabolic Health: The Interplay between ROS, cAMP and Sirtuins. *Free Radic. Biol. Med.* 141, 483–491. doi:10.1016/j.freeradbiomed.2019.07.017

Park, J., Min, J.-S., Kim, B., Chae, U.-B., Yun, J. W., Choi, M.-S., et al. (2015). Mitochondrial ROS Govern the LPS-Induced Pro-inflammatory Response in Microglia Cells by Regulating MAPK and NF-Kb Pathways. *Neurosci. Lett.* 584, 191–196. doi:10.1016/j.neulet.2014.10.016

Perez-Martinez, P., Garcia-Rios, A., Delgado-Lista, J., Perez-Jimenez, F., Lopez-Miranda, J., et al. (2012). Metabolic Syndrome: Evidences for a Personalized Nutrition. *Mol. Nutr. Food Res.* 56, 67–76. doi:10.1002/mnfr.201100531

Petersen, M. C., Rahimi, Y., Camporez, J.-P. G., Pesta, D., Perry, R. J., Jurczak, M. J., et al. (2015). Reply to Constantin-Teodosiu et al.: Mice with genetic PDH activation are Not protected from high-fat diet-induced muscle insulin resistance. *Proc. Natl. Acad. Sci. USA* 112, E825. doi:10.1073/pnas.1423574112

Pitzer, A. L., Van Beusecum, J. P., Kleyman, T. R., and Kirabo, A. (2020). ENaC in Salt-Sensitive Hypertension: Kidney and beyond. *Curr. Hypertens. Rep.* 22, 69. doi:10.1007/s11906-020-01067-9

Plotnikov, E. Y., Kazachenko, A. V., Vyssokikh, M. Y., Vasileva, A. K., Tcvirkun, D. V., Isaev, N. K., et al. (2007). The Role of Mitochondria in Oxidative and Nitrosative Stress during Ischemia/reperfusion in the Rat Kidney. *Kidney Int.* 72, 1493–1502. doi:10.1038/sj.ki.5002568

Podkowińska, A., and Formanowicz, D. (2020). Chronic Kidney Disease as Oxidative Stress- and Inflammatory-Mediated Cardiovascular Disease. *Antioxidants* 9, 752. doi:10.3390/antiox9080752

Prasun, P. (2020). Mitochondrial Dysfunction in Metabolic Syndrome. *Biochim. Biophys. Acta (Bba) - Mol. Basis Dis.* 1866, 165838. doi:10.1016/j.bbadis.2020.165838

Purkayastha, S., and Cai, D. (2013). Neuroinflammatory Basis of Metabolic Syndrome. *Mol. Metab.* 2, 356–363. doi:10.1016/j.molmet.2013.09.005

Qaddumi, W. N., and Jose, P. A. (2021). The Role of the Renal Dopaminergic System and Oxidative Stress in the Pathogenesis of Hypertension. *Biomedicines* 9, 139. doi:10.3390/biomedicines9020139

Quesada, I. M., Lucero, A., Amaya, C., Meijles, D. N., Cifuentes, M. E., Pagano, P. J., et al. (2015). Selective Inactivation of NADPH Oxidase 2 Causes Regression of Vascularization and the Size and Stability of Atherosclerotic Plaques. *Atherosclerosis* 242, 469–475. doi:10.1016/j.atherosclerosis.2015.08.011

Quinlan, C. L., Goncalves, R. L. S., Hey-Mogensen, M., Yadava, N., Bunik, V. I., and Brand, M. D. (2014). The 2-oxoacid Dehydrogenase Complexes in Mitochondria Can Produce Superoxide/hydrogen Peroxide at Much Higher Rates Than Complex I. *J. Biol. Chem.* 289, 8312–8325. doi:10.1074/jbc.M113.545301

Rahimi, Y., Camporez, J.-P. G., Petersen, M. C., Pesta, D., Perry, R. J., Jurczak, M. J., et al. (2014). Genetic Activation of Pyruvate Dehydrogenase Alters Oxidative Substrate Selection to Induce Skeletal Muscle Insulin Resistance. *Proc. Natl. Acad. Sci. USA* 111, 16508–16513. doi:10.1073/pnas.1419104111

Rajaram, R. D., Dissard, R., Faivre, A., Ino, F., Delitsikou, V., Jaquet, V., et al. (2019). Tubular NOX4 Expression Decreases in Chronic Kidney Disease but Does Not Modify Fibrosis Evolution. *Redox Biol.* 26, 101234. doi:10.1016/j.redox.2019.101234

Rani, V., Deep, G., Singh, R. K., Palle, K., and Yadav, U. C. S. (2016). Oxidative Stress and Metabolic Disorders: Pathogenesis and Therapeutic Strategies. *Life Sci.* 148, 183–193. doi:10.1016/j.lfs.2016.02.002

Ravarotto, V., Simioni, F., Pagnin, E., Davis, P. A., and Calò, L. A. (2018). Oxidative Stress - Chronic Kidney Disease - Cardiovascular Disease: A Vicious Circle. *Life Sci.* 210, 125–131. doi:10.1016/j.lfs.2018.08.067

Raygan, F., Rezavandi, Z., Dadkhah Tehrani, S., Farrokhian, A., and Asemi, Z. (2016). The Effects of Coenzyme Q10 Administration on Glucose Homeostasis Parameters, Lipid Profiles, Biomarkers of Inflammation and Oxidative Stress in Patients with Metabolic Syndrome. *Eur. J. Nutr.* 55, 2357–2364. doi:10.1007/s00394-015-1042-7

Saha, S., Buttari, B., Panieri, E., Profumo, E., and Saso, L. (2020). An Overview of Nrf2 Signaling Pathway and its Role in Inflammation. *Molecules* 25, 5474. doi:10.3390/molecules25225474

Sangle, G. V., Zhao, R., Mizuno, T. M., and Shen, G. X. (2010). Involvement of RAGE, NADPH Oxidase, and Ras/Raf-1 Pathway in Glycated LDL-Induced Expression of Heat Shock Factor-1 and Plasminogen Activator Inhibitor-1 in

Vascular Endothelial Cells. *Endocrinology* 151, 4455–4466. doi:10.1210/en.2010-0323

Schramm, A., Matusik, P., Osmenda, G., and Guzik, T. J. (2012). Targeting NADPH Oxidases in Vascular Pharmacology. *Vasc. Pharmacol.* 56, 216–231. doi:10.1016/j.vph.2012.02.012

Schroder, K., and Tschopp, J. (2010). The Inflammasomes. *Cell* 140, 821–832. doi:10.1016/j.cell.2010.01.040

Schröder, K., Wandzioch, K., Helmcke, I., and Brandes, R. P. (2009). Nox4 Acts as a Switch between Differentiation and Proliferation in Preadipocytes. *Arterioscler. Thromb. Vasc. Biol.* 29, 239–245. doi:10.1161/ATVBAHA.108.174219

Scialò, F., Fernández-Ayala, D. J., and Sanz, A. (2017). Role of Mitochondrial Reverse Electron Transport in ROS Signaling: Potential Roles in Health and Disease. *Front. Physiol.* 8, 428. doi:10.3389/fphys.2017.00428

Sela, M., Tirza, G., Ravid, O., Volovitz, I., Solodeev, I., Friedman, O., et al. (2015). NOX1-induced Accumulation of Reactive Oxygen Species in Abdominal Fat-Derived Mesenchymal Stromal Cells Impinges on Long-Term Proliferation. *Cell Death Dis* 6, e1728. doi:10.1038/cddis.2015.84

Senoner, T., and Dichtl, W. (2019). Oxidative Stress in Cardiovascular Diseases: Still a Therapeutic Target? *Nutrients* 11, 2090. doi:10.3390/nu11092090

Shahzad, K., Bock, F., Dong, W., Wang, H., Kopf, S., Kohli, S., et al. (2015). Nlrp3-inflammasome Activation in Non-myeloid-derived Cells Aggravates Diabetic Nephropathy. *Kidney Int.* 87, 74–84. doi:10.1038/ki.2014.271

Sharaf, M. S., Stevens, D., and Kamunde, C. (2017). Mitochondrial Transition ROS Spike (mTRS) Results from Coordinated Activities of Complex I and Nicotinamide Nucleotide Transhydrogenase. *Biochim. Biophys. Acta (Bba) - Bioenerg.* 1858, 955–965. doi:10.1016/j.bbabio.2017.08.012

Sharma, K., Karl, B., Mathew, A. V., Gangoiti, J. A., Wassel, C. L., Saito, R., et al. (2013). Metabolomics Reveals Signature of Mitochondrial Dysfunction in Diabetic Kidney Disease. *Jasn* 24, 1901–1912. doi:10.1681/ASN.2013020126

Shin, S.-K., Cho, H.-W., Song, S.-E., Im, S.-S., Bae, J.-H., and Song, D.-K. (2020). Oxidative Stress Resulting from the Removal of Endogenous Catalase Induces Obesity by Promoting Hyperplasia and Hypertrophy of White Adipocytes. *Redox Biol.* 37, 101749. doi:10.1016/j.redox.2020.101749

Solà, R., Valls, R.-M., Puzo, J., Calabuig, J.-R., Brea, A., Pedret, A., et al. (2014). Effects of Poly-Bioactive Compounds on Lipid Profile and Body Weight in a Moderately Hypercholesterolemic Population with Low Cardiovascular Disease Risk: a Multicenter Randomized Trial. *PLoS One* 9, e101978. doi:10.1371/journal.pone.0101978

Spahis, S., Borys, J.-M., and Levy, E. (2017). Metabolic Syndrome as a Multifaceted Risk Factor for Oxidative Stress. *Antioxid. Redox Signaling* 26, 445–461. doi:10.1089/ars.2016.6756

Sukumar, P., Viswambharan, H., Imrie, H., Cubbon, R. M., Yuldasheva, N., Gage, M., et al. (2013). Nox2 NADPH Oxidase Has a Critical Role in Insulin Resistance-Related Endothelial Cell Dysfunction. *Diabetes* 62, 2130–2134. doi:10.2337/db12-1294

Tan, B. L., Norhaizan, M. E., Liew, W.-P. -P., and Sulaiman Rahman, H. (2018). Antioxidant and Oxidative Stress: a Mutual Interplay in Age-Related Diseases. *Front. Pharmacol.* 9, 1162. doi:10.3389/fphar.2018.01162

Tan, C. Y. R., Weier, Q., Zhang, Y., Cox, A. J., Kelly, D. J., and Langham, R. G. (2015). Thioredoxin-interacting Protein: a Potential Therapeutic Target for Treatment of Progressive Fibrosis in Diabetic Nephropathy. *Nephron* 129, 109–127. doi:10.1159/000368238

Tbahriti, H. F., Kaddous, A., Bouchenak, M., and Mekki, K. (2013). Effect of Different Stages of Chronic Kidney Disease and Renal Replacement Therapies on Oxidant-Antioxidant Balance in Uremic Patients. *Biochem. Res. Int.* 2013, 358985. doi:10.1155/2013/358985

Teixeira, G., Szyndralewiez, C., Molango, S., Carnesecchi, S., Heitz, F., Wiesel, P., et al. (2017). Therapeutic Potential of NADPH Oxidase 1/4 Inhibitors. *Br. J. Pharmacol.* 174, 1647–1669. doi:10.1111/bph.13532

Termini, J. (2000). Hydroperoxide-induced DNA Damage and Mutations. *Mutat. Research/Fundamental Mol. Mech. Mutagenesis* 450, 107–124. doi:10.1016/s0027-5107(00)00019-1

Thallas-Bonke, V., Tan, S. M., Lindblom, R. S., Snelson, M., Granata, C., Jha, J. C., et al. (2020). Targeted Deletion of Nicotinamide Adenine Dinucleotide Phosphate Oxidase 4 from Proximal Tubules Is Dispensable for Diabetic Kidney Disease Development. *Nephrol. Dial. Transpl.*, gfaa376. doi:10.1093/ndt/gfaa376[Epub ahead of print.]

Togliatto, G., Lombardo, G., and Brizzi, M. F. (2017). The Future Challenge of Reactive Oxygen Species (ROS) in Hypertension: from Bench to Bed Side. *Ijms* 18, 1988. doi:10.3390/ijms18091988

Touyz, R. M., Anagnostopoulou, A., Camargo, L. L., Rios, F. J., and Montezano, A. C. (2019). Vascular Biology of Superoxide-Generating NADPH Oxidase 5-implications in Hypertension and Cardiovascular Disease. *Antioxid. Redox Signaling* 30, 1027–1040. doi:10.1089/ars.2018.7583

Touyz, R. M., Rios, F. J., Alves-Lopes, R., Neves, K. B., Camargo, L. L., and Montezano, A. C. (2020). Oxidative Stress: a Unifying Paradigm in Hypertension. *Can. J. Cardiol.* 36, 659–670. doi:10.1016/j.cjca.2020.02.081

Tran, T.-V., Shin, E.-J., Dang, D.-K., Ko, S. K., Jeong, J. H., Nah, S.-Y., et al. (2017). Ginsenoside Re Protects against Phencyclidine-Induced Behavioral Changes and Mitochondrial Dysfunction via Interactive Modulation of Glutathione Peroxidase-1 and NADPH Oxidase in the Dorsolateral Cortex of Mice. *Food Chem. Toxicol.* 110, 300–315. doi:10.1016/j.fct.2017.10.019

Tun, S., Spainhower, C. J., Cottrill, C. L., Lakhani, H. V., Pillai, S. S., Dilip, A., et al. (2020). Therapeutic Efficacy of Antioxidants in Ameliorating Obesity Phenotype and Associated Comorbidities. *Front. Pharmacol.* 11, 1234. doi:10.3389/fphar.2020.01234

Uusitalo, L. M., and Hempel, N. (2012). Recent Advances in Intracellular and In Vivo ROS Sensing: Focus on Nanoparticle and Nanotube Applications. *Ijms* 13, 10660–10679. doi:10.3390/ijms130910660

Vary, T. C., Siegel, J. H., Nakatani, T., Sato, T., and Aoyama, H. (1986). Regulation of Glucose Metabolism by Altered Pyruvate Dehydrogenase Activity. I. Potential Site of Insulin Resistance in Sepsis. *JPEN. J. Parenter. Enteral Nutr.* 10, 351–355. doi:10.1177/0148607186010004351

Verzola, D., Milanesi, S., Viazzi, F., Ansaldo, F., Saio, M., Garibaldi, S., et al. (2020). Enhanced Myostatin Expression and Signalling Promote Tubulointerstitial Inflammation in Diabetic Nephropathy. *Sci. Rep.* 10, 6343. doi:10.1038/s41598-020-62875-2

Vona, R., Gambardella, L., Cittadini, C., Straface, E., and Pietraforte, D. (2019). Biomarkers of Oxidative Stress in Metabolic Syndrome and Associated Diseases. *Oxidative Med. Cell Longevity* 2019, 8267234. doi:10.1155/2019/8267234

Wan, C., Su, H., and Zhang, C. (2016). Role of NADPH Oxidase in Metabolic Disease-Related Renal Injury: An Update. *Oxidative Med. Cell Longevity* 2016, 7813072. doi:10.1155/2016/7813072

Wang, W., Zhang, Y., Lu, W., and Liu, K. (2015). Mitochondrial Reactive Oxygen Species Regulate Adipocyte Differentiation of Mesenchymal Stem Cells in Hematopoietic Stress Induced by Arabinosylcytosine. *PLoS One* 10, e0120629. doi:10.1371/journal.pone.0120629

Wang, X., Armando, I., Upadhyay, K., Pascua, A., and Jose, P. A. (2009). The Regulation of Proximal Tubular Salt Transport in Hypertension: an Update. *Curr. Opin. Nephrol. Hypertens.* 18, 412–420. doi:10.1097/MNH.0b013e32832f5775

Waypa, G. B., Smith, K. A., and Schumacker, P. T. (2016). O 2 Sensing, Mitochondria and ROS Signaling: The Fog Is Lifting. *Mol. Aspects Med.* 47-48, 76–89. doi:10.1016/j.mam.2016.01.002

Wong, H.-S., Dighe, P. A., Mezera, V., Monternier, P.-A., and Brand, M. D. (2017). Production of Superoxide and Hydrogen Peroxide from Specific Mitochondrial Sites under Different Bioenergetic Conditions. *J. Biol. Chem.* 292, 16804–16809. doi:10.1074/jbc.R117.789271

Wu, H., and Ballantyne, C. M. (2020). Metabolic Inflammation and Insulin Resistance in Obesity. *Circ. Res.* 126, 1549–1564. doi:10.1161/CIRCRESAHA.119.315896

Wu, K. L. H., Chao, Y.-M., Tsay, S.-J., Chen, C. H., Chan, S. H. H., Dovinova, I., et al. (2014). Role of Nitric Oxide Synthase Uncoupling at Rostral Ventrolateral Medulla in Redox-Sensitive Hypertension Associated with Metabolic Syndrome. *Hypertension* 64, 815–824. doi:10.1161/HYPERTENSIONAHA.114.03777

Xiao, L., Xu, X., Zhang, F., Wang, M., Xu, Y., Tang, D., et al. (2017a). The Mitochondria-Targeted Antioxidant MitoQ Ameliorated Tubular Injury Mediated by Mitophagy in Diabetic Kidney Disease via Nrf2/PINK1. *Redox Biol.* 11, 297–311. doi:10.1016/j.redox.2016.12.022

Xiao, M., Zhong, H., Xia, L., Tao, Y., and Yin, H. (2017b). Pathophysiology of Mitochondrial Lipid Oxidation: Role of 4-hydroxynonenal (4-HNE) and Other Bioactive Lipids in Mitochondria. *Free Radic. Biol. Med.* 111, 316–327. doi:10.1016/j.freeradbiomed.2017.04.363

Xie, X., Zhao, R., and Shen, G. (2012). Impact of Cyanidin-3-Glucoside on Glycated LDL-Induced NADPH Oxidase Activation, Mitochondrial Dysfunction and Cell Viability in Cultured Vascular Endothelial Cells. *Ijms* 13, 15867–15880. doi:10.3390/ijms131215867

Yang, J., Villar, V. A. M., Jose, P. A., and Zeng, C. (2021). Renal Dopamine Receptors and Oxidative Stress: Role in Hypertension. *Antioxid. Redox Signaling* 34, 716–735. doi:10.1089/ars.2020.8106

Yang, N., Gonzalez-Vicente, A., and Garvin, J. L. (2020). Angiotensin II-Induced Superoxide and Decreased Glutathione in Proximal Tubules: Effect of Dietary Fructose. *Am. J. Physiology-Renal Physiol.* 318, F183–F192. doi:10.1152/ajprenal.00462.2019

Yang, S., Yang, Y., Yu, P., Yang, J., Jiang, X., Villar, V. A. M., et al. (2015). Dopamine D1and D5receptors Differentially Regulate Oxidative Stress through Paraoxonase 2 in Kidney Cells. *Free Radic. Res.* 49, 397–410. doi:10.3109/10715762.2015.1006215

Yang, Y., Cuevas, S., Yang, S., Villar, V. A., Escano, C., Asico, L., et al. (2014). Sestrin2 Decreases Renal Oxidative Stress, Lowers Blood Pressure, and Mediates Dopamine D 2 Receptor-Induced Inhibition of Reactive Oxygen Species Production. *Hypertension* 64, 825–832. doi:10.1161/HYPERTENSIONAHA.114.03840

Yang, Y., Zhang, Y., Cuevas, S., Villar, V. A., Escano, C., D. Asico, L., et al. (2012). Paraoxonase 2 Decreases Renal Reactive Oxygen Species Production, Lowers Blood Pressure, and Mediates Dopamine D2 Receptor-Induced Inhibition of NADPH Oxidase. *Free Radic. Biol. Med.* 53, 437–446. doi:10.1016/j.freeradbiomed.2012.05.015

Yang, Z., Wang, Y., Zhang, Y., He, X., Zhong, C.-Q., Ni, H., et al. (2018). RIP3 Targets Pyruvate Dehydrogenase Complex to Increase Aerobic Respiration in TNF-Induced Necroptosis. *Nat. Cel Biol.* 20, 186–197. doi:10.1038/s41556-017-0022-y

Youn, J.-Y., Siu, K. L., Lob, H. E., Itani, H., Harrison, D. G., and Cai, H. (2014). Role of Vascular Oxidative Stress in Obesity and Metabolic Syndrome. *Diabetes* 63, 2344–2355. doi:10.2337/db13-0719

Yu, J.-W., and Lee, M.-S. (2016). Mitochondria and the NLRP3 Inflammasome: Physiological and Pathological Relevance. *Arch. Pharm. Res.* 39, 1503–1518. doi:10.1007/s12272-016-0827-4

Yu, P., Han, W., Villar, V. A. M., Yang, Y., Lu, Q., Lee, H., et al. (2014). Unique Role of NADPH Oxidase 5 in Oxidative Stress in Human Renal Proximal Tubule Cells. *Redox Biol.* 2, 570–579. doi:10.1016/j.redox.2014.01.020

Zeng, C., Villar, V. A. M., Yu, P., Zhou, L., and Jose, P. A. (2009). Reactive Oxygen Species and Dopamine Receptor Function in Essential Hypertension. *Clin. Exp. Hypertens.* 31, 156–178. doi:10.1080/10641960802621283

Zhang, L., Wang, X., Cueto, R., Effi, C., Zhang, Y., Tan, H., et al. (2019). Biochemical Basis and Metabolic Interplay of Redox Regulation. *Redox Biol.* 26, 101284. doi:10.1016/j.redox.2019.101284

Zhang, P., Yang, C., Guo, H., Wang, J., Lin, S., Li, H., et al. (2018). Treatment of Coenzyme Q10 for 24 Weeks Improves Lipid and Glycemic Profile in Dyslipidemic Individuals. *J. Clin. Lipidol.* 12, 417–427. doi:10.1016/j.jacl.2017.12.006

Zhang, R., Ran, H.-h., Peng, L., Xu, F., Sun, J.-f., Zhang, L.-n., et al. (2014). Mitochondrial Regulation of NADPH Oxidase in Hindlimb Unweighting Rat Cerebral Arteries. *Plos. One* 9, e95916. doi:10.1371/journal.pone.0095916

Zhang, X., and Lerman, L. O. (2017). The Metabolic Syndrome and Chronic Kidney Disease. *Translational Res.* 183, 14–25. doi:10.1016/j.trsl.2016.12.004

Zinkevich, N. S., and Gutterman, D. D. (2011). ROS-induced ROS Release in Vascular Biology: Redox-Redox Signaling. *Am. J. Physiology-Heart Circulatory Physiol.* 301, H647–H653. doi:10.1152/ajpheart.01271.2010

Zorov, D. B., Juhaszova, M., and Sollott, S. J. (2014). Mitochondrial Reactive Oxygen Species (ROS) and ROS-Induced ROS Release. *Physiol. Rev.* 94, 909–950. doi:10.1152/physrev.00026.2013

Zorov, D. B., Juhaszova, M., and Sollott, S. J. (2006). Mitochondrial ROS-Induced ROS Release: an Update and Review. *Biochim. Biophys. Acta (Bba) - Bioenerg.* 1757, 509–517. doi:10.1016/j.bbabio.2006.04.029

Conflict of Interest: The authors declare that the research was conducted in the absence of any commercial or financial relationships that could be construed as a potential conflict of interest.

frontiers in Pharmacology

ORIGINAL RESEARCH
published: 22 July 2021
doi: 10.3389/fphar.2021.704074

Anti-Obesity and Lipid Lowering Activity of Bauhiniastatin-1 is Mediated Through PPAR-γ/AMPK Expressions in Diet-Induced Obese Rat Model

Reddy Sankaran Karunakaran[1], Oruganti Lokanatha[1], Ganjayi Muni Swamy[1], Chintha Venkataramaiah[2], Muppuru Muni Kesavulu[3], Chippada Appa Rao[1], Kameswara Rao Badri[4]* and Meriga Balaji[1]**

[1]Division of Cell Culture and Molecular Biology, Department of Biochemistry, Sri Venkateswara University, Tirupati, India, [2]Division of Molecular Biology, Department of Zoology, Sri Venkateswara University, Tirupati, India, [3]Department of Basic Sciences and Humanities, Sree Vidyanikethan Engineering College, Tirupati, India, [4]Department of Pharmacology and Toxicology, Cardiovascular Research Institute, Morehouse School of Medicine, Atlanta, GA, United States

OPEN ACCESS

Edited by:
Barbara Wegiel,
Harvard Medical School,
United States

Reviewed by:
Adriano Lama,
University of Naples Federico II, Italy
Val Miranda,
Oregon State University, United States
Jung Yunu,
Kyung Hee University, South Korea

***Correspondence:**
Chippada Appa Rao
chippadar@yahoo.com
Kameswara Rao Badri
kbadri@msm.edu
Meriga Balaji
balaji.meriga@gmail.com

Specialty section:
This article was submitted to Experimental Pharmacology and Drug Discovery, a section of the journal Frontiers in Pharmacology

Received: 01 May 2021
Accepted: 08 July 2021
Published: 22 July 2021

Citation:
Karunakaran RS, Lokanatha O, Muni Swamy G, Venkataramaiah C, Muni Kesavulu M, Appa Rao C, Badri KR and Balaji M (2021) Anti-Obesity and Lipid Lowering Activity of Bauhiniastatin-1 is Mediated Through PPAR-γ/AMPK Expressions in Diet-Induced Obese Rat Model. Front. Pharmacol. 12:704074. doi: 10.3389/fphar.2021.704074

Objective: To evaluate the therapeutic efficacy and underlying molecular mechanisms of Bauhiniastatin-1 (BSTN1) to alleviate adiposity in diet-induced obese rodent model and in 3T3-L1 cells.

Methods: BSTN1 was purified and confirmed through HPLC. *In-vitro* experiments such as MTT assay, Oil Red-O (ORO) stain, cellular lipid content, glycerol release and RT-PCR analysis were performed in 3T3-L1 cells in the presence and absence of BSTN1. In animal experiments, rats were divided into Group-I: normal pellet diet-fed, Group-II: HFD-fed, Groups-III, IV and V: HFD-fed BSTN1 (1.25, 2.5, and 5 mg/kg.b.wt./day/rat)-treated and Group-VI: HFD-fed Orlistat-treated. The rats were fed either normal diet or high fat diet (HFD) for 18 weeks and water *ad-libitum*. BSTN1 was orally administered from 13th week onwards to the selected HFD-fed groups. Body composition parameters, biochemical assays, histopathology examination and western blot analysis were performed to identify the predicted targets related to obesity. Molecular docking studies threw light on the binding interactions of BSTN1 against PPAR-γ, FAS and AMPK.

Results: BSTN1 at 20 μM significantly ($p < 0.001$) inhibited adipocyte differentiation and lipid accumulation in 3T3-L1 cells. A conspicuous down-regulation in the mRNA expression levels of PPAR-γ, FAS and SREBP1 was observed but AMPK expression remained unchanged in BSTN1 treated 3T3-L1 cells. A substantial decrease in body weight gain, fat percent, total body fat, serum and liver lipid profile (except high-density lipoprotein), glucose, insulin and insulin resistance in BSTN1 treated rats was noticed in a

Abbreviations: ALT, alanine aminotransferase; AMPK, 5′ AMP-activated protein kinase; AST, aspartate transaminase; Bauhiniastatin-1, BSTN1; DMEM, Dulbecco's Modified Eagle's medium; FAS, fatty acid synthase; FBS, fetal bovine serum; HFD, High-fat diet; IBMX, 3-isobutyl-1-methyl- xanthine; MDI, differentiation medium of Induction; MTT, (3-(4,5-dimethylthiazol-2-yl)-2,5-diphenyl tetrazolium bromide); NAFLD, non-alcoholic fatty liver disease; PPAR-γ, peroxisome proliferator-activated receptor-γ; SREBP1, sterol regulatory element-binding protein 1.

dose dependent manner. In BSTN1 (5 mg/kg.b.wt.)-treated groups significantly ($p < 0.01$) elevated plasma adiponectin level but reduced leptin level as well as fall in serum AST and ALT were noticed. Further, the disturbed structural integrity and architecture of adipose and hepatic tissues due to high fat diet feeding were considerably recovered with BSTN1 treatment. Down-regulation in the protein expression level of PPAR-γ and activation of AMPK through phosphorylation was observed in BSTN1 treated rats than the untreated. Molecular docking studies revealed strong binding interactions of BSTN1 against PPAR-γ and AMPK and thus supported the experimental results.

Conclusion: Taken together, the results suggest that BSTN1 could be a promising pharmacological molecule in the treatment of obesity and dyslipidemia.

Keywords: 3T3-L1 cells, adipogenesis, AMPK, bauhiniastatin-1, diet-induced obesity, insulin resistance, molecular docking, PPAR-γ

INTRODUCTION

The epidemic of obesity has become a public health issue in both developed and developing countries as it strongly predisposes to type-2 diabetes, dyslipidemia, hypertension, cardiovascular diseases (CVDs), non-alcoholic fatty liver disease (NAFLD), sleep apnea, infertility and certain types of cancers (Hurt et al., 2010). The excess calories consumed than expended gets accumulated as fats (triglycerides) in adipocytes and leads to growth and expansion of white adipose tissue (WAT) by the process of hypertrophy and hyperplasia (Meln et al., 2019). At cellular level, adipogenesis is a complex process involving preadipocytes clonal expansion, differentiation and intracellular lipid accumulation which is tightly regulated at transcriptional level by peroxisome proliferator activated receptor-γ (PPAR-γ), members of CCAAT/enhancer binding protein (C/EBP) family and sterol regulatory element binding protein (SREBPs) (Moseti et al., 2016; Chang and Kim 2019).

White adipose tissue not only serves to store excess fats but also performs vital endocrine functions such as secretion of adipokines and release of inflammatory cytokines that play prevailing role in disturbing general energy homeostasis and insulin sensitivity resulting in various metabolic disorders (Longo et al., 2019). Similarly, due to excess accumulation of fats in hepatic tissue in conditions like hepatic steatosis, non-alcoholic steatohepatitis (NASH) and NAFLD the metabolic functions of liver are derailed (Nassir et al., 2015).

Various therapeutic approaches such as lifestyle modification, pharmacotherapy, and bariatric surgery are advocated to combat obesity ailments (Apovian et al., 2015). Although lifestyle modification is the cornerstone of weight management, it is difficult to put it in practice in day-to-day life and to sustain. On the other hand, bariatric surgery involves high risk and high cost as well. In view of this, pharmacotherapy is typically considered as an effective treatment option. Therapeutic molecules that work as lipase inhibitors, appetite suppressors, antilipidemic agents and inhibitors of adipogenesis are being intensely researched to develop effective drugs to treat obesity ailments (Balaji et al., 2016; Liu et al., 2020). Considering the growing public inclination toward natural product-based therapeutics, the present work was carried out with Bauhuniastatin-1 isolated from *Bauhinia purpurea*.

Bauhinia purpurea Linn. is a fast-growing medium sized flowering plant of Fabaceae family, widely grown in south-east Asian countries including India and China. This plant species is rich in phytochemicals like bauhiniastatins, isoquercitin, lutein, β-sitosterol, pacharin, astragalin, stigmasterol, kaempferol, lupeol etc. Its leaves, flowers and seeds are eaten along with rice in some parts of South East Asian countries (Kumar and Chandrashekar 2011). *B. purpurea* possesses anti-diabetic, anti-inflammatory, antimicrobial, analgesic and anti-neoplastic activities and has been used in traditional and folk medicine (Zakaria et al., 2007). In our previous study, we reported the anti-hyperlipidemic activity with crude extract of *B. purpurea.* (Padmaja et al., 2014).

In the present study, we isolated and purified the active principle, Bauhiniastatin-1, (BSTN1) elucidated its anti-obesity activity and underlying molecular mechanisms using diet-induced obese rat model. Adipogenic, lipogenic and lipolytic studies are complemented using the most widely used 3T3-L1 preadipocytes. In addition, molecular docking studies were carried out to understand the mechanisms of action of BSTN1.

MATERIALS AND METHODS

Chemicals and Materials

Dulbecco's Modified Eagle's Medium (DMEM), fetal bovine serum (FBS), 3-isobutyl-1-methyl-xanthine (IBMX), penicillin and streptomycin, isopropanol, insulin, and dexamethasone (DEXA) were procured from Thermo Fisher Scientific (Berkeley, MO, United States). MTT (3-(4, 5-dimethylthiazol-2-yl)-2, 5-diphenyltetrazolium bromide) and Oil-Red-O (ORO) stain were procured from Sigma Aldrich, (St Louis, MO, United States). Other solvents, chemicals and reagents utilized for the experiments were of analytical grade.

Isolation and Purification of Bauhiniastatin-1

The bark of *B. purpurea* was collected from the Seshachalam forests, spread around Tirupati, Andhra Pradesh, India. It is authenticated by taxonomist in the department of Botany, Sri Venkateswara University, Tirupati, voucher number is 136 and specimen was preserved in departmental herbarium. The bark of *B. purpurea* was powdered, extracted with ethanol and further fractionated by column chromatography using different solvents (Padmaja et al., 2014). The collected fractions were subjected to LC-MS analysis on 6520 Accurate Q-TOF (Agilent Technologies, Inc. Santa Clara, CA, United States) mass spectrometer to identify the major compounds. Bauhiniastatin-1 was purified using an HPLC system equipped with a binary gradient system, a variable UV-VIS-detector and a Rheodyne Model 7725 injector with a loop size of 20 µl, and an integrator. Reverse phase chromatographic analysis was carried out in isocratic conditions using a C-18 reverse phase column (250 × 4.6 mm id., 5 µl C-18) at 40°C. Mobile phase consisted of methanol:water (20:80 v/v) with a flow rate of 1 ml/min. The detection of compounds was performed at 220 nm. A single sharp peak at 5.942 min of retention time was identified as BSTN1 (Pettit et al., 2006).

Cell Culture and Differentiation of Adipocytes

The 3T3-L1 pre-adipocytes of American Type Culture Collection (ATCC) cells were maintained and cultured in DMEM supplemented with 10% FBS at 37°C in a humidified atmosphere with 5% CO_2. The 3T3-L1 were grown to confluence, stimulated with adipogenesis differentiation medium of induction (DMI) consisting of DMEM, 10% FBS, 0.5 mM IBMX, 1 µM DEXA and 10 µg/ml insulin for 2 days followed by treating cells with differentiation medium (DM) (DMEM with 10% FBS and 10 µg/ml insulin) for additional 8–10 days (Badri et al., 2008). All the media that we used contained 100 IU/ml penicillin and 100 mg/ml streptomycin. A volume of 0.01% DMSO was used as vehicle control for *in-vitro* experiments. For evaluating anti-adipogenic effects of BSTN1, 3T3-L1 cells cultured and adipogenesis was induced by DMI in 12 well plates and treated with different concentrations of BSTN1 (5, 10, and 20 µM) in DM. The adipocytes were stained for neutral lipids (lipid droplets) and observed under a bright field microscope or used for other studies.

Cell Viability Assay (MTT Assay)

The 3T3-L1 preadipocytes were cultured in DMEM and cell viability assays were conducted as previously described (Lee et al., 2018).

Oil Red O Staining: Determination of Lipid Content

Lipid contents in adipocytes were visualized as well as measured using Oil Red-O (ORO) staining (Nunez et al., 2019).

Lipolysis Studies

The lipolysis studies were conducted by measuring glycerol levels released into the cell culture medium, using commercial kit (Lipolysis assay kit, ab185433, Abcam, and Shanghai) following manufacturer's instructions (Shobha et al., 2017). The glycerol content was expressed as nmol/well.

RT-PCR Studies: mRNA Expression

Total RNA was isolated from 3T3-L1 cells by using tri-reagent (Sigma Aldrich, Bangalore India) according to manufacturer's protocol and reverse transcribed to obtain cDNA using cDNA synthesis kit (Applied Bio Systems, Foster City, CA, United States) (Galateanu et al., 2012). About 20 ng of cDNA was used for semi-quantitative RT-PCR (BioRad CFX96, Real-Time PCR) using SYBR green master mix and the conditions were kept as follows: 95°C for 10 min, followed by 36 cycles for 30 s at 72°C and 1 min at 60°C and followed by extension for 15 s at 72°C. Data was analyzed using ΔΔCt method and values were expressed in terms of relative fold change (RFC). PCR reactions were run in triplicate for each sample, and transcription levels of every gene were normalized to the level of β-actin. The PCR amplification was performed with transcript specific primers (**Supplementary Table 1**).

Animal Studies

Male WNIN rats (aged 5–6 weeks), normal pellet diet and high fat diet were obtained from National Institute of Nutrition (NIN), Hyderabad, India. After one-week acclimatization, rats were maintained at standard laboratory conditions (temperature: 23 ± 2°C; humidity: 40–60%), fed with either normal diet or HFD and water ad-libitum for 18 weeks as described in experimental design (Donovan et al., 2009). The composition of normal pellet diet and HFD (fat-60%) are given in supplementary files (**Supplementary Tables 2, 3**). To test for therapeutic activity, different concentrations of BSTN1 (1.25, 2.5, and 5 mg/kg b. wt.) suspended in 0.5% carboxymethylcellulose (CMC) were orally administered for 6 weeks from 13th week onwards using an intra-gastric tube. We selected these concentrations based on our initial pilot studies using solvent extracts (Padmaja et al., 2014). Guidelines of IAEC (No:55/2012/(i)/a/CPCSEA/IAEC/SVU/MBJ, dated: 8-7–2012) were followed to conduct the animal experiments.

Experimental Design

Rats initially weighing 160–180 g were randomly divided into six groups of six each (n = 6).

Group I: Normal pellet diet fed rats
Group II: HFD-fed rats (Placebo)
Group III: HFD fed + BSTN1 (1.25 mg/kg b. wt./day) treated rats
Group IV: HFD fed + BSTN1 (2.5 mg/kg b. wt./day) treated rats
Group V: HFD fed + BSTN1 (5 mg/kg b. wt./day) treated rats
Group VI: HFD fed + Orlistat (5 mg/kg b. wt./day) treated rats

Measurement of Body Composition Parameters, Food and Water Intake

Body weight, lean body mass, fat percent, fat free mass of each rat was measured by Total Body Electrical Conductivity (TOBEC) using a small animal body composition analysis system (EM-SCAN, Model SA-3000 Multi detector, Springfield, United States). Food intake, water intake and behavior was monitored every day. At the end of the experiment, animals were anesthetized using isoflurane, blood was collected by heart puncture method. Plasma and/or serum were separated by centrifugation at 2,500 rpm for 15 min. Various organs and tissues including abdominal adipose tissue and liver were dissected, and stored appropriately. For histology studies, tissues were fixed and processed as described in later sections.

Estimation of FBG, PPBG, F-Ins and HOMA-IR

After overnight fasting of experimental rats, the glycemic parameters such as fasting blood glucose (FBG) and after food intake post-prandial blood glucose (PPBG) were monitored by ACCU-Check, Glucometer. Serum fasting-insulin (F-Ins) was measured using commercially available enzyme-linked immunosorbent (ELISA) kit (Elabscience, United States) and homeostasis model assessment index for insulin resistance (HOMA-IR) was used to identify insulin resistance as follows:

HOMA-IR = [fasting glucose (mg/dl) X fasting insulin (μIU/ml)]/405.

Plasma Leptin and Adiponectin Levels

Plasma leptin and adiponectin are key adipokines secreted by adipocytes. Adipokine levels were measured in experimental rats using enzyme-linked immunosorbent assay kits (Crystal Chem, Downers Grove, IL, United States). These assays were performed in duplicates (n = 6), as per the manufacturer's guidelines and adipokine levels were expressed in ng/mL (Margoni et al., 2011).

Estimation of Serum Lipid Profile

Serum total cholesterol (TC) was estimated by CHOD-PAP method, triglycerides (TGs) and HDL-cholesterol were estimated by GPO-TOPS method, VLDL-cholesterol, LDL-cholesterol were estimated by selective inhibition method (Agappe Diagnostics Ltd., Kerala, India). The phospholipids (PLs) and free fatty acids (FFAs) were assessed by using quantification assay kits, Sigma Aldrich, Bangalore, India.

Estimation of Hepatic Lipid Levels

Lipids were extracted from the liver tissues of experimental animals (Floch et al., 1957). In brief, the tissues were rinsed with ice-cold physiological saline, homogenized in cold chloroform-methanol (2:1, v/v) and the contents were extracted for 24 h. The extraction was repeated four times. The combined filtrate was washed with 0.7% potassium chloride and the aqueous layer was discarded. The organic layer was made up to a known volume with chloroform and used for hepatic lipid analysis.

Measurement of AST and ALT Activities

Hepatic marker enzymes, aspartate transaminase (AST) and alanine transaminase (ALT) activities were estimated at the end of the experiment by using commercially available kit (Agappe Diagnostics Ltd., Kerala, India) following the manufacturer's protocol.

Western Blot Analysis

Adipose and hepatic tissue proteins were washed with sterile 1X PBS and homogenized in RIPA lysis buffer (Product No. R0278, Sigma Aldrich, Bangalore, India) containing protease inhibitors (PI) (RIPA + PI: 1 ml + 40 μl), centrifuged (14,000 rpm for 10 min at a 4°C) and the supernatant was collected. The protein concentrations were measured using the Bradford method. Forty μg of proteins were resolved on 10% SDS-PAGE gel and transferred onto a PVDF membrane. To block non-specific binding sites, blots were incubated at room temperature with 5% skimmed milk (w/v) for 1 h on shaking rocker followed by overnight incubation with specific primary antibodies of anti-PPAR-γ (Catalog No. C26H12, ILS-CST, India), anti-AMPK (Catalog No. A17290)/phospho-AMPK (Catalog No. AP0116) and mouse anti-β actin (Catalog No. AC004) (Abclonal Technology, United States) at 4°C. The immuno-reactive antigen was then recognized by incubation with HRP-conjugated secondary antibody (Abclonal Technology, United States) for 1 h at RT. After washing with 1X TBST, the membrane was treated with chemiluminescent ECL detection reagent (1:1) (Bio-Rad) and the immuno-reactive bands were visualized by ChemiScope western blot imaging system (Make: Wipro GE Healthcare) (Lira et al., 2010).

Histopathological Examination

Adipose and liver tissues were collected from both control and experimental rats and fixed in formalin solution. A small piece of tissue was cut, trimmed, processed and prepared paraffin blocks. Then the paraffin blocks were sectioned (5–8 μm) using microtome and stained using haematoxylin and eosin (H&E) following standard histology protocol (Badri et al., 2013).

Molecular Docking Studies (Accession of Target Protein)

The three-dimensional structure of FAS (6NNA), AMPK (6C9F), PPAR-γ (3WMH), and BSTN1 were downloaded from the RCSB protein Data Bank and Pub chem. The atomic coordinates of the ligand were geometrically optimized using Argus Lab 4.0.1. *In-silico* studies were carried against FAS (6NNA), AMPK (6C9F), and PPAR-γ (3WMH), with ligand (BSTN1) using the docking program Patchdock (Xiao et al., 2013). After the docking, protein–ligand complexes were studied using PyMol viewer tool (www.pymol.org)1. Protein and ligand interactions were analyzed and visualized through PyMol viewer tool (www.pymol.org)1.

Statistical Analysis

The results are expressed as the mean ± standard deviation (SD), and comparison was made by using one-way ANOVA

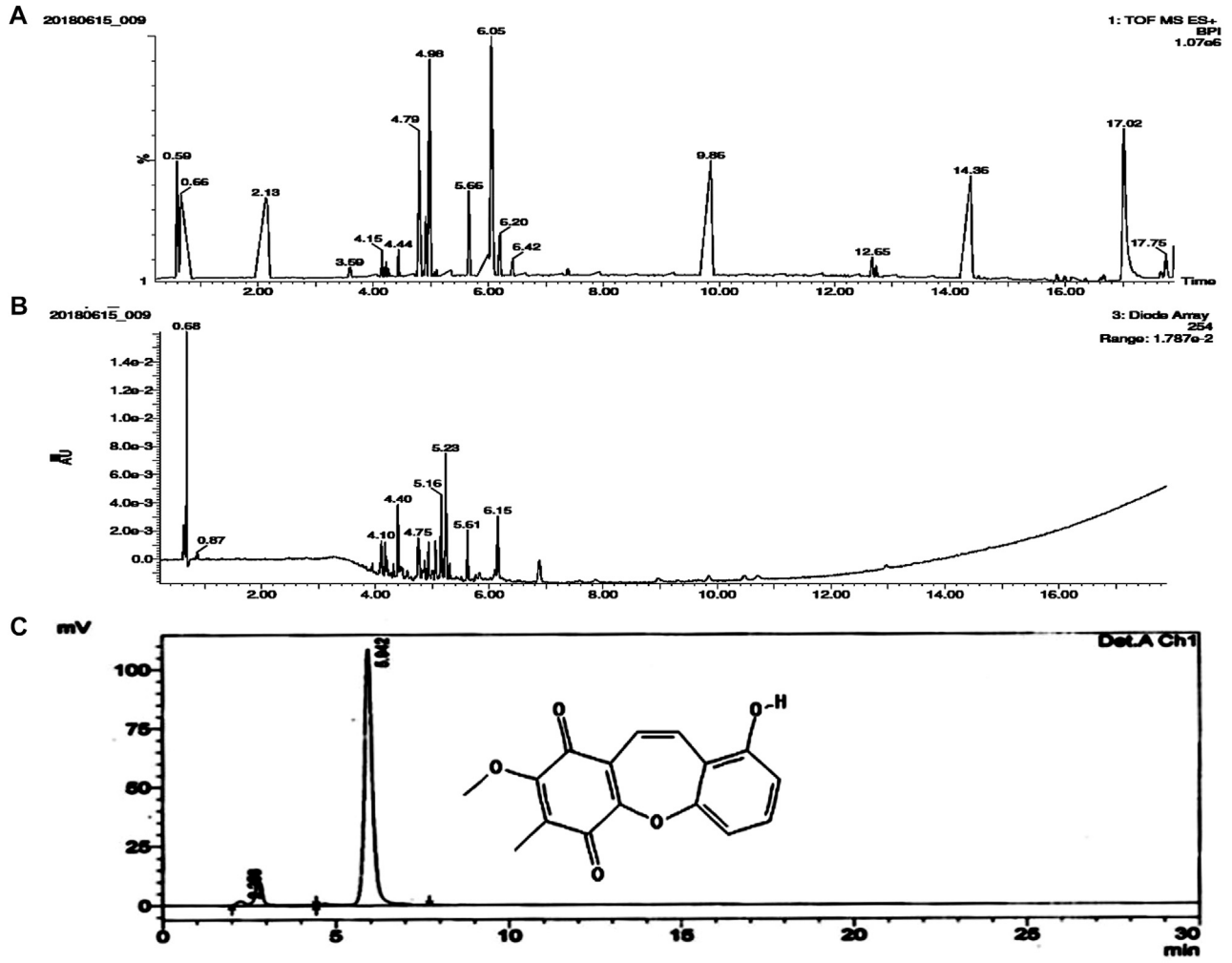

FIGURE 1 | Molecular characterization of isolated compound/s from the chloroform fraction of *B. purpurea* ethanolic extract. **(A)** and **(B)** LC-MS analysis showing TOF MS ES + BPI and Diode Array (Retention Time) **(C)** HPLC peak representing structure and retention time (5.942) of BSTN1.

program followed by Tukey's post hoc tests to study the significance level (SPSS, version 17.0; SPSS Inc., Chicago, IL, United States).

RESULTS

LC-MS and HPLC Analysis

The chloroform fraction of ethanolic extract of *B. purpurea* was subjected to LC-MS/MS analysis. Seventeen compounds were identified from which BSTN1 (m.wt.: 283.0496) was isolated, purified and confirmed by HPLC (**Figures 1A–C**).

Cell Viability Studies by MTT Assay

The effect of BSTN1 on cell viability of 3T3-L1 cells and cytotoxicity was analyzed in the dose range of 10–160 μM, at 48 h using MTT assay. The BSTN1 showed IC50 value of 118 μM (**Figure 2D**).

Effect of BSTN1 on Adipogenesis and Lipid Content

The BSTN1 at a dose of 20 μM could markedly reduce adipogenesis and intracellular lipid levels in 3T3-L1 cells, as observed by Oil-Red-O-stained images (**Figure 2A**). Furthermore, lipid content of adipocytes was measured by extracting (using isopropanol) the Oil Red O stain from 3T3-L1 adipocytes (**Figure 2B**). To complement these studies, we verified the lipolytic capacity of BSTN1 by quantifying the levels of glycerol release from treated vs. control and vehicle control 3T3-L1 adipocytes. Significantly ($p < 0.01$) high level of glycerol release was observed in adipocytes treated with BSTN1 than untreated cells and the maximum lipolytic activity was noticed at a concentration of 20 μM (**Figure 2C**).

Effect of BSTN1 on mRNA Expression

The mRNA expression levels of key adipogenic and lipogenic transcriptional factors, FAS, SREBP1, AMPK and PPAR-γ in

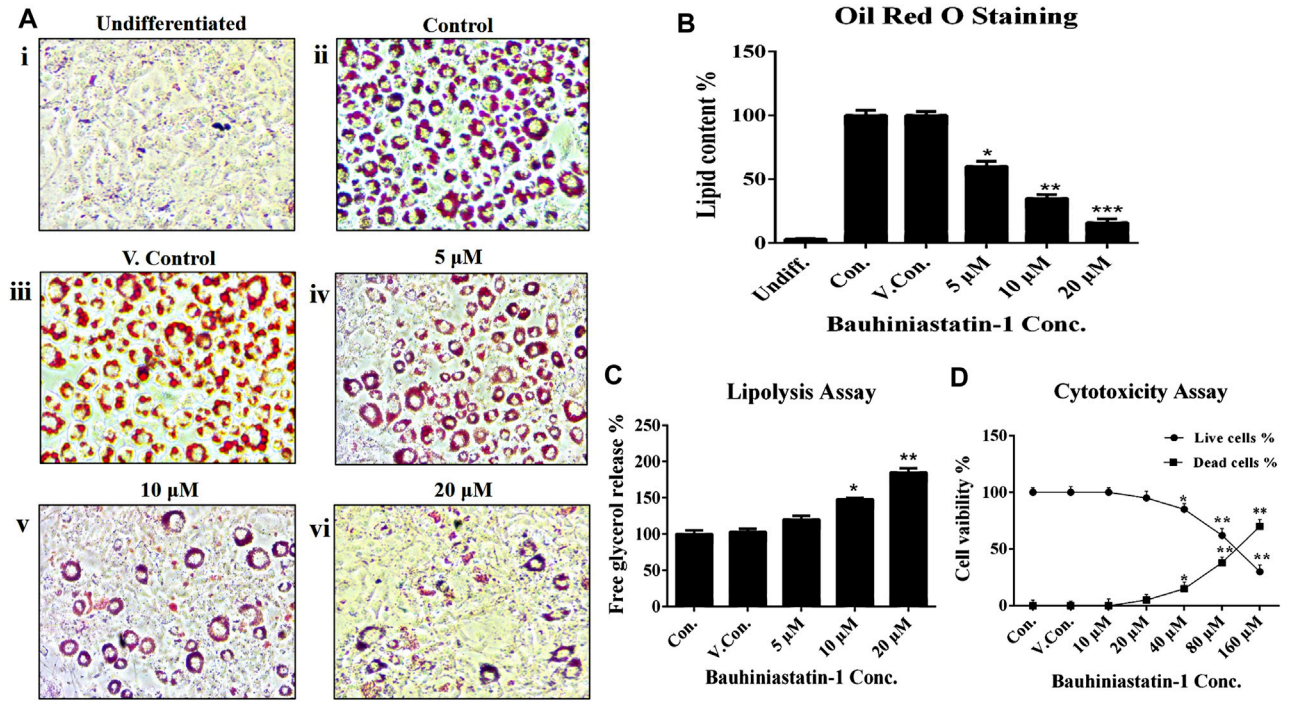

FIGURE 2 | Effect of BSTN1 on lipid levels in 3T3-L1 cells by **(A)** Oil Red O staining of 3T3-L1 cells (Magnification 40×). (i) Undifferentiated, untreated pre-adipocytes (ii) Differentiated, untreated adipocytes (control) (iii) DMSO (0.01%) treated adipocytes (vehicle control). (iv), (v), and (vi) BSTN1 treated adipocytes (5, 10, and 20 µM) showing decreased adipogenesis in dose dependent manner. **(B)** Quantification of lipid content (%) by Oil Red O stain extraction in BSTN1-treated and other groups. **(C)** Lipolysis assay indicating the amount of glycerol content released from 3T3-L1 adipocytes into the media. **(D)** Cytotoxicity assay results on the percentage of cell viability of untreated, DMSO and BSTN1 treated pre-adipocytes determined after 48 h using MTT assay. Data are presented as mean ± SD of triplicate. *, **, and *** indicate significant difference between control and treated 3T3-L1 cells at $p < 0.05$, $p < 0.01$, and $p < 0.001$ respectively.

differentiated 3T3-L1 adipocytes were estimated in the absence and presence of BSTN1 (5, 10, and 20 µM) (**Figure 3**). The expression of FAS, SREBP1, and PPAR-γ were down-regulated, while that of AMPK remained unchanged with increasing concentration of BSTN1 as represented in **Figures 3A–D**.

Effect of BSTN1 on Protein Expression

Figure 4 shows the protein expression levels of AMPK/phosphor-AMPK and PPAR-γ in hepatic and adipose tissues of obese control and obese-treated rats. BSTN1 treatment induced activation of AMPK as evident from its phosphorylation, in a dose dependent manner. However, down-regulation of PPAR-γ with increasing concentration of BSTN1 was observed in treated rats. The results indicate the efforts of BSTN1 to maintain energy homeostasis and reduce the fat accumulation in liver and adipose tissues.

Body Composition, Body Weight, Food and Water Intake of Obese Rats

Table 1 depicts the changes in body weight and fat percent of experimental rats. Consumption of HFD for 18 weeks resulted in significant rise in body weights (486 ± 9.0 g) and total body fat levels (79 ± 7.8 g) in HFD control group, compared to normal control group of rats whose body weight and total fat were 248.1 ± 6.3 g and 10.2 ± 1.4 g, respectively. Oral administration of BSTN1 considerably reduced body weight gain and body composition parameters in a dose dependent manner, with maximum reduction in body weight (320 ± 13.9 g) and total fat levels (24.9 ± 1.9 g) being noted in rats treated with 5 mg/kg b. wt. of BSTN1. However, no significant difference was observed in food and water intake (**Table 1**) of BSTN1 treated groups indicating that BSTN1 could reduce weight gain in obese rats without compromising food and water intake quantity. The behavior of all the animals was normal.

Effect of BSTN1 on Leptin and Adiponectin Levels and Adipose Tissue Architecture

Figure 5 shows the systemic levels of leptin and adiponectin in control and experimental obese rats. We observed markedly elevated levels of plasma leptin but decrease in adiponectin levels in HFD fed rats, when compared to the normal rats. Interestingly, treatment with BSTN1 has significantly ($p < 0.01$) decreased leptin levels, while the levels of adiponectin were increased. The H&E-stained adipose tissue sections of control rats showed the normal adipocyte structure (**Figure 5B**). In contrast, adipocytes of HFD-induced obese rats are significantly larger (**Figure 5C**) (hypertrophy) with

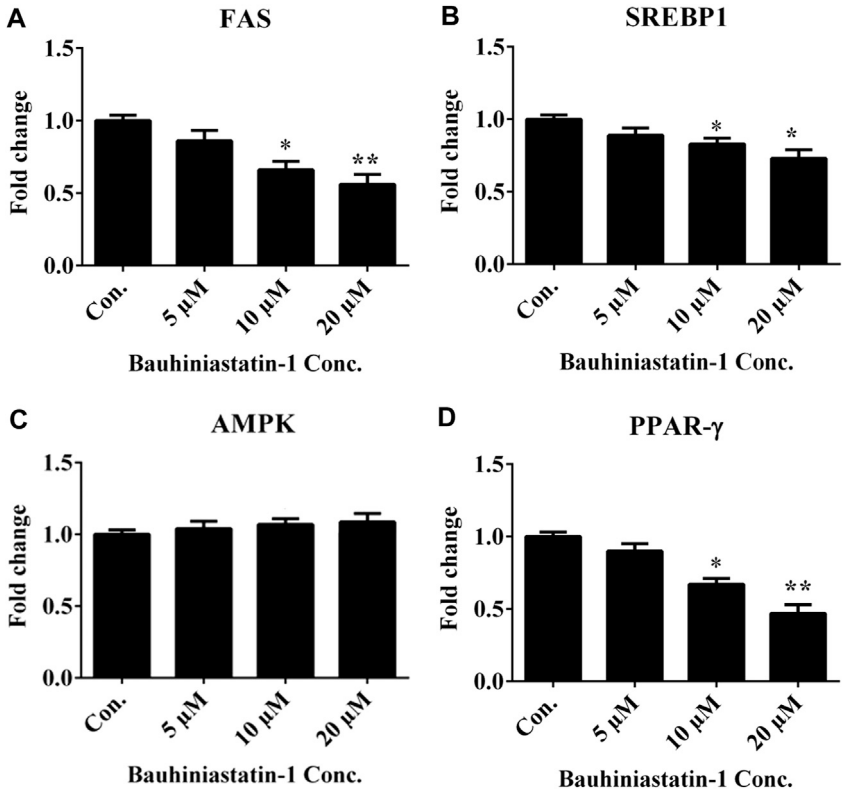

FIGURE 3 | Effect of BSTN1 on mRNA expression of target genes in 3T3-L1 cells by RT-PCR. Quantitation of fold change of key adipogenic and lipogenic markers **(A)** FAS mRNA **(B)** SREBP1 mRNA, **(C)** AMPK mRNA and **(D)** PPAR-γ mRNA. Data are presented as mean ± SD of triplicate. * and ** indicate significant difference between control and treated 3T3-L1 cells at $p < 0.05$ and $p < 0.01$, respectively. FAS, fatty acid synthase; SREBP1, sterol regulatory element-binding protein 1; AMPK, AMP-activated protein kinase and PPAR-γ, peroxisome proliferator-activated receptor-γ.

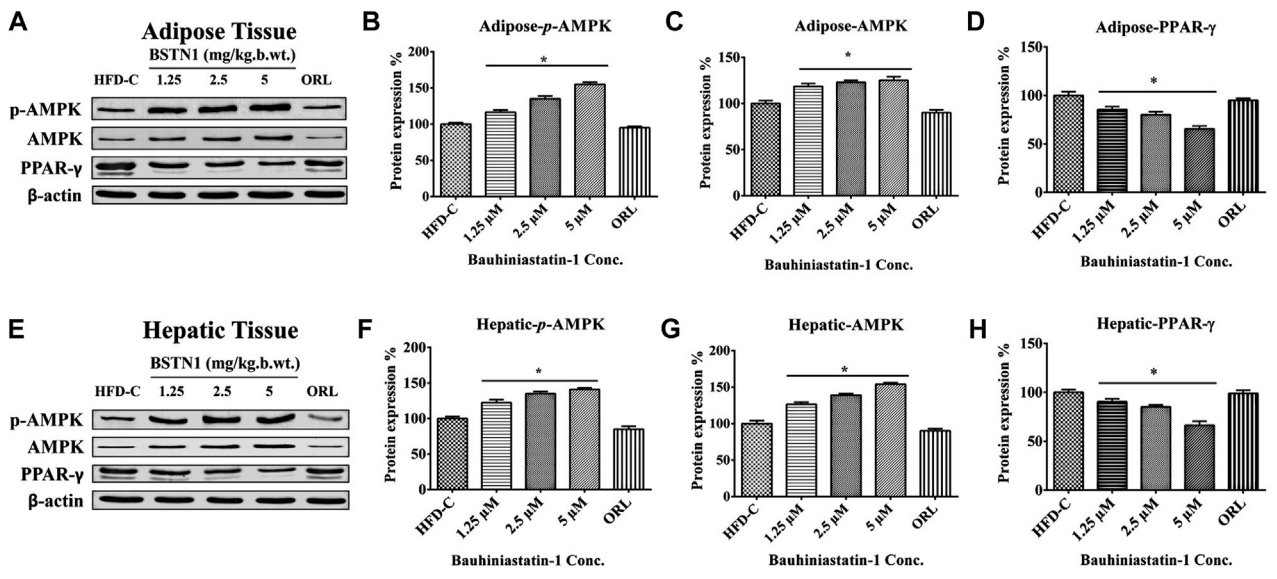

FIGURE 4 | Western blot analysis: Protein expression of control and treated rats in **(A)** adipose tissue and **(E)** liver tissue. β-actin is used as a housekeeping gene. Histograms showing quantification of expressed proteins: **(B)** Adipose-*p*-AMPK **(C)** adipose-AMPK **(D)** adipose-PPAR-γ, **(F)** Hepatic-*p*-AMPK **(G)** Hepatic-AMPK and **(H)** Hepatic-PPAR-γ. Histograms represent mean ± SD, $n = 6$. * indicates significant difference ($p < 0.01$) between HFD control and treated groups. AMPK, AMP-activated protein kinase and PPAR-γ, peroxisome proliferator-activated receptor-γ.

TABLE 1 | Effect of BSTN1 on food intake, water intake, body weight and body composition parameters of treated and untreated rats.

Parameters	Normal control	HFD control	BSTN1-1.25 mg	BSTN1-2.5 mg	BSTN1-5 mg	ORL-5 mg
Food intake (g/day/rat)	15.7 ± 0.7	14.3 ± 1.1	14.5 ± 0.8	14.7 ± 0.1	15.2 ± 0.9	15.1 ± 0.3
Water intake (mL/day/rat)	21.4 ± 1.2	26.1 ± 0.8	24.5 ± 1.0	25.7 ± 0.7	25.9 ± 1.1	24.5 ± 0.5
Initial body weight (g)	168.3 ± 7.0	182.5 ± 9.4	177.3 ± 8.4	179.3 ± 10.7	183.2 ± 8.0	180.8 ± 5.9
Final body weight (g)	248.1 ± 6.3	486.3 ± 9.0$^{\#}$	445.2 ± 11.0*	401.5 ± 12.0**	320.5 ± 13.9***	312.7 ± 7.7***
Body weight gain (g)	79.8 ± 4.6	303.8 ± 15.5$^{\#}$	267.8 ± 10.7*	222.2 ± 14.8**	137.3 ± 17.8***	131.8 ± 10.7***
Lean body mass (g)	237.9 ± 7.0	407.3 ± 7.8$^{\#}$	382.6 ± 13.6*	358.6 ± 14.2**	295.7 ± 14.4***	290.1 ± 6.5***
Total body fat (g)	10.2 ± 1.4	79 ± 7.8$^{\#}$	62.5 ± 3.8*	42.9 ± 2.4**	24.9 ± 1.9***	22.6 ± 4.6***
Body fat (%)	4.1 ± 0.6	16.2 ± 1.5$^{\#}$	14.1 ± 1.1*	10.7 ± 0.9**	7.8 ± 0.7***	7.2 ± 1.4***
Fat free mass (g)	147.1 ± 4.1	225.4 ± 5.3$^{\#}$	215.5 ± 8.3*	206.8 ± 8.5**	175.9 ± 8.3***	173.3 ± 3.9***
Total body water	620.1 ± 18.5	972.6 ± 23.9$^{\#}$	928.2 ± 37.4*	888.9 ± 38.3**	749.7 ± 37.2***	738 ± 17.4***
Total body Na+	859.4 ± 25.7	1,349 ± 33.1$^{\#}$	1,287.3 ± 52.0*	1,232.7 ± 53.2**	1,039.4 ± 51.7***	1,023.2 ± 24.2***
Total body K+	1783.1 ± 51.0	2,752.4 ± 65.6$^{\#}$	2,630.3 ± 103.0*	2,522.3 ± 105.4**	2,139.5 ± 102.3***	2,107.3 ± 48.0***

*The data is expressed as the mean ± SD, n = 6. $^{\#}p < 0.001$ indicates significant difference between HFD control (placebo) and normal control. *, ** and *** indicate significant difference between HFD control and treated groups at $p < 0.05$, $p < 0.01$, and $p < 0.001$, respectively.*

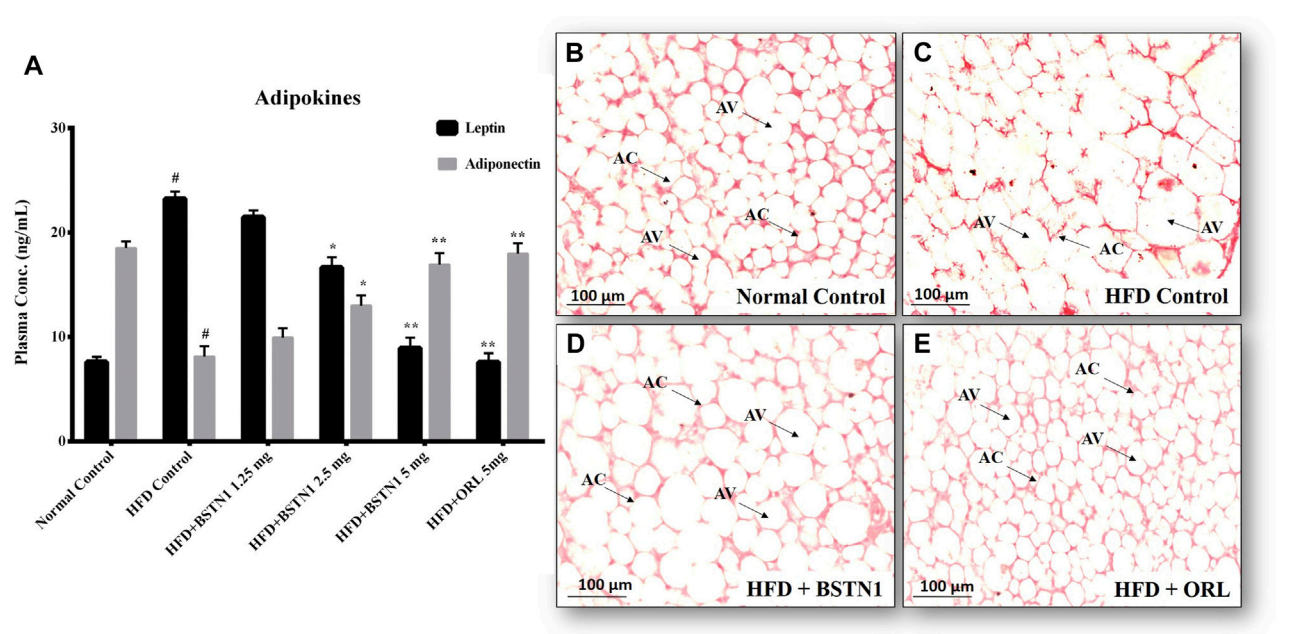

FIGURE 5 | Effect of BSTN1 on adipokines and histology of white adipose tissue (40x magnification). **(A)** Plasma adipokines levels represented as mean ± SD, $n = 6$. $^{\#}$ denotes significant ($p < 0.001$) difference between normal control and HFD control. * and ** denote significant difference between HFD control and treated groups at $p < 0.05$ and $p < 0.01$, respectively. **(B)** Histology of normal control adipose tissue **(C)** HFD-fed group showing enlarged and lipid laden adipocytes **(D)** HFD fed BSTN1 treated group showing reduction in adipocytes' size and lipid content **(E)** HFD fed orlistat treated group. AC, Adipocyte Cell and AV, Adipocyte Volume. Scale bar: 100 µm.

indistinct cell walls compared to adipocytes of control rats. Relatively smaller sized adipocytes were visualized in BSTN1 treated rats indicating reduced lipid droplets, and this effect was more significant than even orlistat treated group (**Figures 5D,E**).

Effect of BSTN1 on Hepatic Enzymes (AST and ALT) and Hepatic Tissue Architecture

Figure 6 depicts the activities of aspartate transaminase (AST) and alanine transaminase (ALT) in control and experimental obese rats. Administration of BSTN1 significantly ($p < 0.01$) reduced AST and ALT levels in dose dependent manner when compared to HFD control rats. Hepatic tissues of untreated and treated rats were sectioned, stained with H&E staining that represents normal hepatic structure made up of healthy hepatic lobules and a central vein possessing radiating strands in untreated rats (**Figure 6B**). But an accumulated lipid content around the central vein and in between the hepatocytes as well as inflated and disrupted lobules were seen in obese rats (**Figure 6C**). Interestingly, the liver sections from obese rats

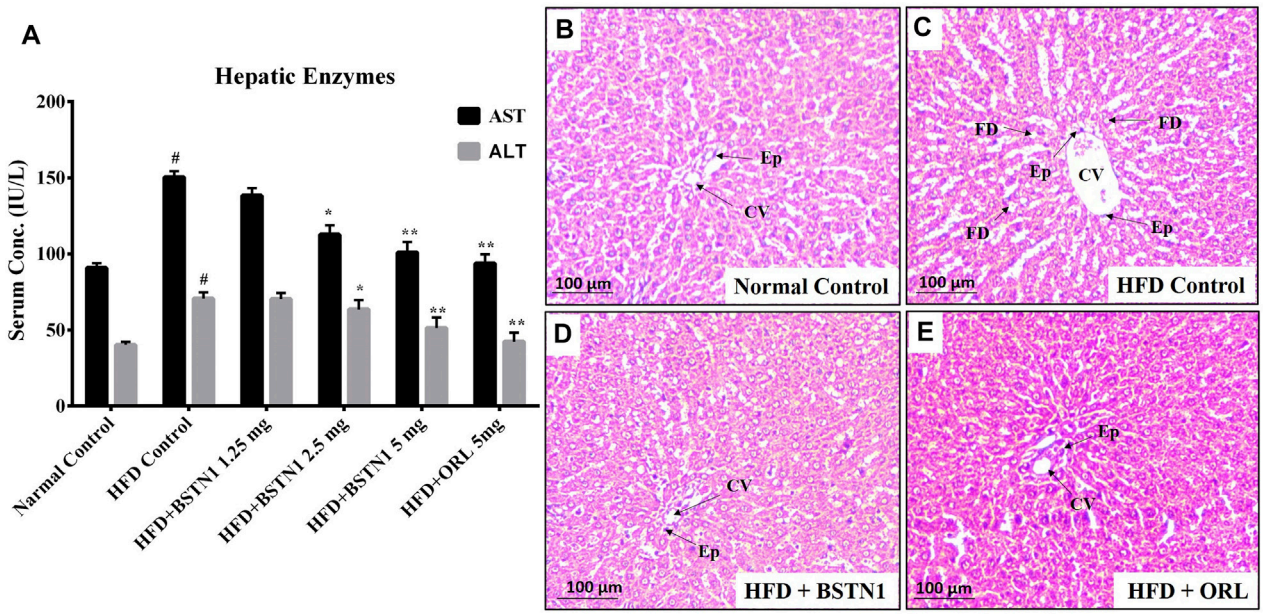

FIGURE 6 | Effect of BSTN1 on liver enzymes (AST and ALT) levels and liver tissue histology (40x magnification). **(A)** Serum AST and ALT levels represented as mean ± SD, $n = 6$. # denotes significant ($p < 0.001$) difference between normal control and HFD control. * and ** denote significant difference between HFD control and treated groups at $p < 0.05$ and $p < 0.01$, respectively. **(B)** Histology of normal control hepatic tissue **(C)** HFD fed group showing disrupted tissue structure with enlarged central vein **(D)** HFD fed BSTN1 treated group showing improvement in hepatic structure **(E)** HFD fed orlistat treated group. CV, Central Vein; FD, Fat Droplets and Ep, Epithelial cells. Scale bar: 100 µm.

TABLE 2 | Effect of BSTN1 on serum lipid profile of treated and untreated rats.

Parameters	Normal control	HFD control	BSTN1-1.25 mg	BSTN1-2.5 mg	BSTN1-5 mg	ORL-5 mg
TC (mg/dl)	84.0 ± 4.1	114.5 ± 13.2$^{\#}$	98.4 ± 9.4*	92.3 ± 9.3**	82.3 ± 14.3***	75.6 ± 15.3***
TGL (mg/dl)	148.9 ± 9.4	185.9 ± 8.7$^{\#}$	173.7 ± 6.4*	160.3 ± 6.6**	137.2 ± 8.6***	131.0 ± 9.2***
HDL (mg/dl)	45.8 ± 11.6	27.9 ± 10.5$^{\#}$	31.7 ± 12.9*	39.5 ± 13.5**	41.5 ± 10.1***	44.1 ± 13.9***
LDL (mg/dl)	62.8 ± 1.9	84.2 ± 1.7$^{\#}$	76.7 ± 1.3*	71.1 ± 1.3**	54.4 ± 1.7***	43.4 ± 1.8***
VLDL (mg/dl)	12.4 ± 15.8	29.4 ± 21.7$^{\#}$	21.0 ± 12.6*	17.8 ± 8.1**	13.4 ± 13.9***	9.0 ± 12.8***
PLs (mg/dl)	57.1 ± 3.2	112.7 ± 7.6$^{\#}$	101.4 ± 12.1*	84.3 ± 3.7**	63.4 ± 11.0**	61.7 ± 6.2**
FFA (mg/dl)	46.7 ± 2.2	96.3 ± 9.6$^{\#}$	87.4 ± 11.7*	64.1 ± 9.4**	50.5 ± 15.7***	44.7 ± 8.7***

*The data is expressed as the mean ± SD, n = 6. $^{\#}p < 0.001$ indicates significant difference between HFD control and normal control. *, ** and *** indicate significant difference between HFD control and treated groups at $p < 0.05$, $p < 0.01$, and $p < 0.001$, respectively. TC, total cholesterol; TGL, triglycerides; HDL, high-density lipoprotein; LDL, low-density lipoprotein; VLDL, very low-density lipoprotein; PLs, phospholipids and FFA, free fatty acid.*

treated with BSTN1 (**Figure 6D**) were seem to be better/equally recovered than that of Orlistat treated group (**Figure 6E**). However, central veins were found to be a little dilated in BSTN1 groups than normal but cells as such were found to be healthy.

Effect of BSTN1 on Serum and Liver Lipid Profiles

The HFD-induced obese rats exhibited significant alterations in serum and liver lipid levels (over their respective control rats). Treatment with BSTN1 (5 mg/kg b. wt.) had significantly normalized the altered levels of serum total cholesterol (TC), triglycerides (TGL), high-density lipoprotein (HDL), low-density lipoprotein (LDL), very low-density lipoproteins (VLDL), phospholipids (PLs) and free fatty acids (FFA) (**Table 2**). Similarly, the liver tissue lipids including total cholesterol (TC), triglycerides (TGL) and free fatty acids (FFA) were also markedly normalized in the presence of BSTN1 (**Table 3**).

Effect of BSTN1 on FBG, PPBG, F-Ins and HOMA-IR

Fasting blood glucose (FBG), post-prandial blood glucose (PPBG), fasting-insulin (F-Ins) and calculated HOMA-IR values were significantly diminished in BSTN1 treated rats when compared with HFD control rats in a dose dependent manner as shown in **Table 4**.

TABLE 3 | Effect of BSTN1 on hepatic lipid profile of treated and untreated rats.

Parameters	Normal control	HFD control	BSTN1-1.25 mg	BSTN1-2.5 mg	BSTN1-5 mg	ORL-5 mg
TC (mg/dl)	61.37 ± 5.3	118.2 ± 7.4$^{\#}$	111.6 ± 12.2*	91.3 ± 11.0**	67.6 ± 8.0***	62.9 ± 7.5***
TGL (mg/dl)	84.9 ± 2.7	156.1 ± 7.7$^{\#}$	127.7 ± 1.3*	97.8 ± 2.5**	79.07 ± 1.7***	81.6 ± 2.1***
FFA (mg/g)	69.34 ± 3.0	125.8 ± 2.3$^{\#}$	104.9 ± 3.0*	84.1 ± 2.3**	70.3 ± 2.7***	62.3 ± 2.1***

*The data is expressed as the mean ± SD, n = 6. $^{\#}p < 0.001$ indicates significant difference between HFD control and normal control. *, ** and*** indicate significant difference between HFD control and treated groups at $p < 0.05$, $p < 0.01$, and $p < 0.001$, respectively. TC, total cholesterol; TGL, triglycerides and FFA, free fatty acid.*

TABLE 4 | Effect of BSTN1 on FBG, PPBG, F-Ins and HOMA-IR in treated and untreated rats.

Parameters	Normal control	HFD control	BSTN1-1.25 mg	BSTN1-2.5 mg	BSTN1-5 mg	ORL-5 mg
FBG (mg/dl)	86.12 ± 4.6	159.6 ± 8.0$^{\#}$	133.0 ± 6.1*	115.1 ± 9.2**	91.2 ± 7.1***	97.3 ± 6.9***
PPBG (mg/dl)	99.6 ± 5.0	211.1 ± 9.4$^{\#}$	174.6 ± 3.7*	141.5 ± 8.7**	100.3 ± 5.7***	104.7 ± 3.9***
F-Ins (μIU/ml)	14.57 ± 1.8	18.07 ± 1.3$^{\#}$	15.33 ± 2.1*	15.09 ± 2.0**	14.72 ± 1.7***	14.94 ± 1.1***
HOMA-IR	3.1	7.1$^{\#}$	5.0*	4.3**	3.3***	3.6***

*$^{\#}p < 0.001$ indicates significant difference between HFD control and normal control. *, ** and *** indicate significant difference between HFD control and treated groups at $p < 0.05$, $p < 0.01$, and $p < 0.001$, respectively. FBG, fasting blood glucose; PPBG, post-prandial blood glucose; F-Ins, fasting insulin; HOMA-IR, homeostasis model assessment index for insulin resistance.*

TABLE 5 | Molecular docking of BSTN1 (11687814) depicting ligand-protein binding interactions.

Ligand	Proteins	Binding energy	Bond length (Å)	Bonding interaction
Bauhiniastatin-1 (BSTN1)	PPAR-γ (3WMH)	−194.0	2.3–3	H-bond interaction [–OH group of tyrosine (Tyr327), JJA—OH group of serine (Ser289), –NH group of histidine (His449)]
	AMPK (6C9F)	−148.62	3–3.3	H-bond interaction (AMP binding site—Thr86, Val127 and Pro129)
	FAS (6NNA)	−100.0	3–3.6	H-bond interaction (His1263, Asn1458, Arg1461 and Arg1462)

In-Silico Studies

The outcome of the docking studies indicated that BSTN1 interacts with FAS (6NNA) with −100 binding energy. Consequently, the results showed that BSTN1 binds to FAS at the fatty acid binding site (substrate binding cleft), at amino acid residues His1263, Asn1458, Arg1461, and Arg1462 through multiple hydrogen (H) bonds. In addition, the site at which BSTN1 binds to the enzyme is very similar to that of the binding site for NADP and ethane diol, which suggests a stronger regulatory position for BSTN1 (**Figures 7A–C**). Docking studies predict that BSTN1 binds to AMPK by H-bonds close to the adenosine monophosphate (AMP) binding site with a binding energy of −148.62 (**Figures 7D–F**). But, close to the recognized inhibitor (JAA) binding location, BSTN1 interacts strongly with PPAR-γ with a binding energy of −194.0. Three H-bond interactions (–OH group of Tyrosine, –OH group of Serine, –NH group of Histidine) were observed between PPAR-γ and Bauhiniastatin-1 (**Figures 7G–I**) (**Table 5**).

DISCUSSION

Ready availability of energy dense foods and their frequent consumption coupled with sedentary life styles results in abnormal lipid profile, weight gain and metabolic disorders. Adipocyte biology reveals that, more and more accumulation of lipid droplets (triglycerides) in adipocytes leads to growth and expansion of adipose tissue to subcutaneous and visceral parts of the body (Jo et al., 2012). Diet-induced obese rats closely resemble human physiology and biochemistry and serves as an effective model for research and drug development in addition to *in-vitro* studies using 3T3-L1 cell lines (Rodríguez-Correa et al., 2020). Modern bioinformatic tools greatly contribute to elucidate molecule-ligand interactions and enables for effective drug development. Therefore, *in-silico*, *in-vitro* and *in-vivo* studies were conducted in this study to establish the anti-obesity efficacy of BSTN-1.

Maintenance of energy homeostasis in the body involves orchestrated play of complex biochemical and molecular events. At transcriptional level members of PPARs, C/EBPs and SREBPs play decisive role in adipocyte differentiation and lipid accumulation. The expression of these transcriptional factors is in turn regulated directly or indirectly by activated/inactivated AMPK. AMPK also plays a critical role in regulating hepatic lipid metabolism, glucose transport and gluconeogenesis. Hence, identifying therapeutic agents that target these molecules can serve as precious alternatives in the quest of anti-obesity drug development (Moseti et al., 2016; Agius et al., 2020).

In the *in-vitro* cell culture experiments, BSTN1 at 20 μM showed substantial reduction in lipid accumulation and

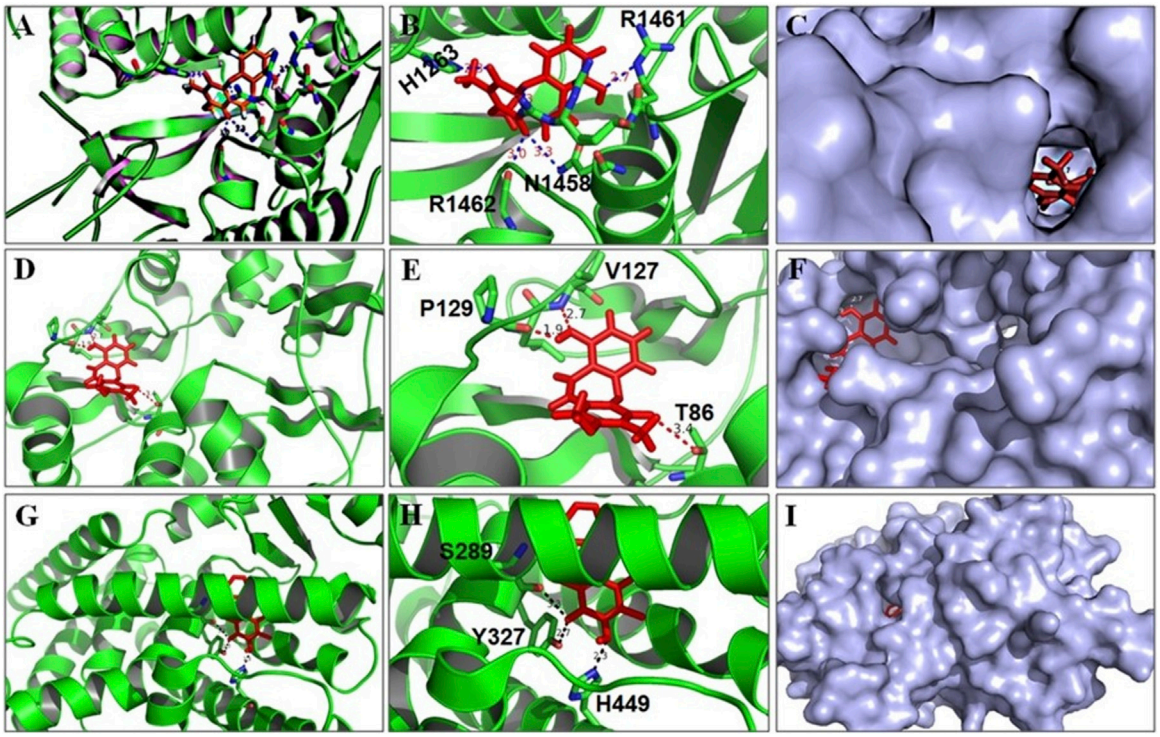

FIGURE 7 | BSTN1 docking to FAS, AMPK and PPAR-γ. **(A–C)** Computational docking of BSTN1 (red) with the FAS (6NNA). **(D–F)** Computational docking of BSTN1 (red) with the amino acids of targeting AMPK (6C9F). **(G–I)** Computational docking reveals that BSTN1 (red) strongly interacts with hydroxyl and amino groups of the tyrosine, serine and histidine residues of PPAR-γ (3WMH). FAS, fatty acid synthase; AMPK, AMP-activated protein kinase and PPAR-γ, peroxisome proliferator-activated receptor-γ.

adipogenesis in 3T3-L1 cells compared to untreated cells as evident from the Oil Red O stain and glycerol estimation assay (**Figures 2A–C**). Gene expression studies showed down-regulation of mRNA levels of PPARγ, SREBP1 and FAS in a dose dependent manner but AMPK expression remained unchanged in BSTN1 treated cells. This indicates, BSTN1 suppresses adipogenesis, lipogenesis and energy homeostasis by regulating at transcriptional level (**Figures 3A–D**). PPARγ consists of DNA binding domain, agonist-dependent and agonist-independent-activation domain expressed ubiquitously but abundantly in adipocytes. PPAR**γ**s play a central role in glucose homeostasis, fatty acid synthesis and adipogenesis (Grygiel-Gorniak, 2014). PPAR**γ** activates fatty acid uptake leading to neutral lipid accumulation in adipocytes which is sufficient for adipogenic induction making it a master regulator of adipogenesis (Shoucri et al., 2018).

In animal experiments, a substantial reduction in body weight gain and fat mass (abdominal fat), but no significant difference in food intake and water intake was noticed with BSTN1-treated rats over their HFD controls (**Table 1**). Biochemical assays of AST and ALT, serum and liver lipid profile indicate the beneficial role of BSTN1 to improve healthy lipid profile and hepatic function (**Figure 6A** and **Tables 2**, **3**). In addition, fasting blood glucose (FBG), post-prandial blood glucose (PPBG), fasting insulin (F-Ins) and homeostasis model assessment index for insulin resistance (HOMA-IR) levels were diminished in BSTN1 treated obese rats in contrast to HFD controls (**Table 4**). This confirms a potential role for BSTN1 in attenuating insulin resistance and hence to be recognised as an anti-diabetic agent also. Certain key adipokines secreted by adipose tissue such as leptin and adiponectin are involved in regulating metabolic functions related to energy homeostasis, inflammation and adiposity. In the present context, oral administration of BSTN1 decreased leptin level but increased adiponectin level (**Figure 5A**). They might promote lipolysis, fatty acid oxidation and inhibit lipogenesis in liver and adipose tissue through AMPK activation. AMPK gets activated through phosphorylation of a conserved threonine in the activation loop of kinase domain in the α subunit or binding of AMP that can be mimicked by ADP and can be antagonized by ATP. Many of the AMPK activators including plant derived therapeutics like resveratrol and berberine activate AMPK by indirectly inhibiting ATP levels through increasing AMP and/or ADP (Srivastava et al., 2012; Kim et al., 2016).

Histological examination still remains an excellent technique to elucidate the ultrastructural modification of tissues. Liver and adipose tissue micrographs of BSTN1 treated groups (**Figures 5**, **6**) evidently demonstrated their recouped architecture toward normalcy. These results support the alleviating effect of BSTN1 on serum and liver biochemical parameters mentioned above. Further, to confirm the

therapeutic effect of BSTN1, western blot analysis was performed to observe the expression levels of PPAR-γ and AMPK in adipose and in hepatic tissues, wherein PPAR-γ was down-regulated while AMPK was activated (phosphorylated) (**Figures 3**, **4**). This is in agreement with previous studies which showed activated AMPK diminishes the expression of C/EBPα, PPARγ, SREBP1 and acyl-CoA carboxylase (ACC) in adipose and hepatic tissues and thus inhibits synthesis of fatty acids and triglycerides (Ahmad et al., 2020). Some natural compounds such as capsaicin, guggulsterone, green tea extract, genistein and piperine were shown to regulate glucose homeostasis and fatty acid synthesis in liver as well as adipose tissue through PPARγ and AMPK mediated signaling to reduce fat accumulation (Feng et al., 2016). These results unambiguously emphasize the pharmacological efficiency of BSTN1 in alleviating obesity and improving hepatic function.

The molecular docking studies also suggest that BSTN1 binds AMPK at the AMP binding site through hydrogen bonding with Thr86, Val127, and Pro129. BSTN1 binding with Thr86 implicates that BSTN1 potentially activates AMPK function as well as expression through the interactions or vice versa. BSTN1 binds to PPAR-γ mediated by hydrogen bonding with amino acids Ser289, Tyr327, and His449. The observed down regulation of PPAR-γ expression could be in part due to these interactions initiating negative feedback loop. Our studies demonstrate that BSTN1 binds to AMPK near the adenosine monophosphate (AMP) binding site there by potentially mimicking AMP to activate AMPK. However, the binding of BSTN1 to the AMPK and PPAR-γ proteins seems to have positive and negative regulatory action on the transcription of AMPK and/or PPAR-γ respectively. In addition, potential binding prediction of BSTN1 with FAS indicates the inhibitory function of BSTN1 on FAS as well. BSTN1 binding at fatty acid binding site of FAS seem to be very interesting, but the lower negative energy of these interaction warrants to further investigate these enzyme substrate/inhibitor interactions (**Figure 7**). Previous studies reported that, 1w5-aminoimidazole-4-carboxamide riboside (AMPK activator) mediated activation of AMPK was shown to inhibit PPAR-γ and PPAR-α which may not be mediated through RXR or PPAR/RXR binding to DNA implicating potential multiple level regulation of BSTN1 on PPAR-γ (Sozio et al., 2011). This suggests complex agonist/antagonist binding dynamics with AMPK and PPAR-γ explaining BSTN1 binding to these two key proteins.

CONCLUSION

Considering the clearly demonstrated results of *in-vitro* and *in-vivo* studies, an emphasizing pharmacological efficiency of BSTN1 against obesity and dyslipidemia is elucidated via PPAR-γ and AMPK modulation. These evidences are further complimented and confirmed by molecular docking studies. Therefore, BSTN1 could be considered as a potential pharmacological agent in drug development to combat obesity ailments.

DATA AVAILABILITY STATEMENT

The original contributions presented in the study are included in the article/**Supplementary Material**, further inquiries can be directed to the corresponding authors.

ETHICS STATEMENT

The animal study was reviewed and approved by Sri Venkateswara University, Tirupati.

AUTHOR CONTRIBUTIONS

CA, BK, and MB conceived and developed the idea. RK and CV did isolation and purification of Bauhiniastatin-1. RK, OL, and GM conducted experiments (cell culture and animal studies). MM, BK, and CV conducted the molecular modeling studies. RK GM, OL, and MB collected the data and performed statistical analysis. RK, GM, CA, BK, and MB analyzed data and/or interpreted the results. RK, MM, BK and MB wrote and edited the manuscript.

FUNDING

This work was supported by the Indian Council of Medical Research, Govt. of India, New Delhi. (NO: 59/25/2011/BMS/TRM, dated: 23-02-2015).

ACKNOWLEDGMENTS

The authors thank and acknowledge K. Suresh Babu, Principal Scientist, Indian Institute of Chemical Technology, Hyderabad, for supporting isolation and purification of phytoconstituents; P. Suresh, N. Harishankar, K. Rajender Rao, R. Ravindar Naik, and M. Sathyavani, National Institute of Nutrition, Hyderabad, India for supporting animal research experiments.

SUPPLEMENTARY MATERIAL

The Supplementary Material for this article can be found online at: https://www.frontiersin.org/articles/10.3389/fphar.2021.704074/full#supplementary-material

REFERENCES

Agius, L., Ford, B. E., and Chachra, S. S. (2020). The Metformin Mechanism on Gluconeogenesis and AMPK Activation: The Metabolite Perspective. *Ijms* 21, 3240. doi:10.3390/ijms21093240

Ahmad, B., Serpell, C. J., Fong, I. L., and Wong, E. H. (2020). Molecular Mechanisms of Adipogenesis: The Anti-adipogenic Role of Amp-Activated Protein Kinase. *Front. Mol. Biosci.* 7, 76. doi:10.3389/fmolb.2020.00076

Apovian, C. M., Garvey, W. T., and Ryan, D. H. (2015). Challenging Obesity: Patient, Provider, and Expert Perspectives on the Roles of Available and Emerging Nonsurgical Therapies. *Obesity* 23 (Suppl. 2(0 2)), S1–S26. doi:10.1002/oby.21140

Badri, K. R., Gao, L., Hyjek, E., Schuger, N., Schuger, L., Qin, W., et al. (2013). Exonic Mutations ofTSC2/TSC1Are Common but Not Seen in All Sporadic Pulmonary Lymphangioleiomyomatosis. *Am. J. Respir. Crit. Care Med.* 187, 663–665. doi:10.1164/ajrccm.187.6.663

Badri, K. R., Zhou, Y., Dhru, U., Aramgam, S., and Schuger, L. (2008). Effects of the SANT Domain of Tension-Induced/inhibited Proteins (TIPs), Novel Partners of the Histone Acetyltransferase P300, on P300 Activity and TIP-6-Induced Adipogenesis. *Mol. Cel Biol* 28, 6358–6372. doi:10.1128/MCB.00333-08

Balaji, M., Ganjayi, M. S., Hanuma Kumar, G. E. N., Parim, B. N., Mopuri, R., and Dasari, S. (2016). A Review on Possible Therapeutic Targets to Contain Obesity: The Role of Phytochemicals. *Obes. Res. Clin. Pract.* 10, 363–380. doi:10.1016/j.orcp.2015.12.004

Chang, E., and Kim, C. (2019). Natural Products and Obesity: A Focus on the Regulation of Mitotic Clonal Expansion during Adipogenesis. *Molecules* 24, 1157. doi:10.3390/molecules24061157

Donovan, M. J., Paulino, G., and Raybould, H. E. (2009). Activation of Hindbrain Neurons in Response to Gastrointestinal Lipid Is Attenuated by High Fat, High Energy Diets in Mice Prone to Diet-Induced Obesity. *Brain Res.* 1248, 136–140. doi:10.1016/j.brainres.2008.10.042

Feng, S., Reuss, L., and Wang, Y. (2016). Potential of Natural Products in the Inhibition of Adipogenesis through Regulation of PPARγ Expression And/or its Transcriptional Activity. *Molecules* 21, 1278. doi:10.3390/molecules21101278

Floch, J., Lees, M., and Sloane Stanley, G. H. (1957). Simple Method for the Isolation and Purification of Total Lipids from Animal Tissues. *J. Biol. Chem.* 226, 497–509.

Galateanu, B., Dinescu, S., Cimpean, A., Dinischiotu, A., and Costache, M. (2012). Modulation of Adipogenic Conditions for Prospective Use of hADSCs in Adipose Tissue Engineering. *Ijms* 13, 15881–15900. doi:10.3390/ijms131215881

Grygiel-Górniak, B. (2014). Peroxisome Proliferator-Activated Receptors and Their Ligands: Nutritional and Clinical Implications - a Review. *Nutr. J.* 13, 17. doi:10.1186/1475-2891-13-17

Hurt, R. T., Kulisek, C., Buchanan, L. A., and McClave, S. A. (2010). The Obesity Epidemic: Challenges, Health Initiatives, and Implications for Gastroenterologists. *Gastroenterol. Hepatol. (N Y).* 6, 780–792.

Jo, J., Shreif, Z., and Periwal, V. (2012). Quantitative Dynamics of Adipose Cells. *Adipocyte* 1, 80–88. doi:10.4161/adip.19705

Kim, J., Yang, G., Kim, Y., Kim, J., and Ha, J. (2016). AMPK Activators: Mechanisms of Action and Physiological Activities. *Exp. Mol. Med.* 48, e224. doi:10.1038/emm.2016.16

Kumar, T., and Chandrashe, K. S. (2011). Bauhinia Purpurea Linn.: A Review of its Ethnobotany, Phytochemical and Pharmacological Profile. *Res. J. Med. Plant* 5, 420–431. doi:10.3923/rjmp.2011.420.431

Lee, H.-W., Rhee, D.-K., Kim, B.-O., and Pyo, S. (2018). Inhibitory Effect of Sinigrin on Adipocyte Differentiation in 3T3-L1 Cells: Involvement of AMPK and MAPK Pathways. *Biomed. Pharmacother.* 102, 670–680. doi:10.1016/j.biopha.2018.03.124

Lira, F. S., Rosa, J. C., Pimentel, G. D., Tarini, V. A., Arida, R. M., Faloppa, F., et al. (2010). Inflammation and Adipose Tissue: Effects of Progressive Load Training in Rats. *Lipids Health Dis.* 9, 109–110. doi:10.1186/1476-511X-9-109

Liu, T.-T., Liu, X.-T., Chen, Q.-X., and Shi, Y. (2020). Lipase Inhibitors for Obesity: A Review. *Biomed. Pharmacother.* 128, 110314–110319. doi:10.1016/j.biopha.2020.110314

Longo, M., Zatterale, F., Naderi, J., Parrillo, L., Formisano, P., Raciti, G. A., et al. (2019). Adipose Tissue Dysfunction as Determinant of Obesity-Associated Metabolic Complications. *Ijms* 20, 2358. doi:10.3390/ijms20092358

Margoni, A., Perrea, D. N., Vlachos, I., Prokopaki, G., Pantopoulou, A., Fotis, L., et al. (2011). Serum Leptin, Adiponectin and Tumor Necrosis Factor-α in Hyperlipidemic Rats With/without Concomitant Diabetes Mellitus. *Mol. Med.* 17, 36–40. doi:10.2119/molmed.2010.00167

Meln, I., Wolff, G., Gajek, T., Koddebusch, J., Lerch, S., Harbrecht, L., et al. (2019). Dietary Calories and Lipids Synergistically Shape Adipose Tissue Cellularity during Postnatal Growth. *Mol. Metab.* 24, 139–148. doi:10.1016/j.molmet.2019.03.012

Moseti, D., Regassa, A., and Kim, W.-K. (2016). Molecular Regulation of Adipogenesis and Potential Anti-adipogenic Bioactive Molecules. *Ijms* 17, 124. doi:10.3390/ijms17010124

Nassir, F., Rector, R. S., Hammoud, G. M., and Ibdah, J. A. (2015). Pathogenesis and Prevention of Hepatic Steatosis. *Gastroenterol. Hepatol. (N Y)* 11, 167–175.

Nunez, S. K., Young, C., Adebayo, O., Muppuru, K. M., and Badri, K. R. (2019). P311, a Novel Intrinsically Disordered Protein, Regulates Adipocyte Development. *Biochem. Biophysical Res. Commun.* 515, 234–240. doi:10.1016/j.bbrc.2019.05.105

Padmaja, T. K., Naidu, P. B., Hanuma Kumar, G. E. N., Ganapathy, S., and Balaji, M. (2014). Antiobesity Activity of Bauhinia Purpurea Extract: Effect on Hormones and Lipid Profile in High Calorie Diet Induced Obese Rats. *Abb* 05, 861–873. doi:10.4236/abb.2014.511101

Pettit, G. R., Numata, A., Iwamoto, C., Usami, Y., Yamada, T., Ohishi, H., et al. (2006). Antineoplastic Agents. 551. Isolation and Structures of Bauhiniastatins 1–4 fromBauhiniapurpurea⊥. *J. Nat. Prod.* 69, 323–327. doi:10.1021/np058075+

Rodríguez-Correa, E., González-Pérez, I., Clavel-Pérez, P. I., Contreras-Vargas, Y., and Carvajal, K. (2020). Biochemical and Nutritional Overview of Diet-Induced Metabolic Syndrome Models in Rats: what Is the Best Choice? *Nutr. Diabetes* 10, 1–15. doi:10.1038/s41387-020-0127-4

Shobha, C. R., Prashant, V., Akila, P., Chandini, R., Suma, M. N., and Basavanagowdappa, H. (2017). Fifty Percent Ethanolic Extract of Momordica Charantia Inhibits Adipogenesis and Promotes Adipolysis in 3T3-L1 Pre-adipocyte Cells. *Rep. Biochem. Mol. Biol.* 6 (1), 22–32.

Shoucri, B. M., Hung, V. T., Chamorro-García, R., Shioda, T., and Blumberg, B. (2018). Retinoid X Receptor Activation during Adipogenesis of Female Mesenchymal Stem Cells Programs a Dysfunctional Adipocyte. *Endocrinology* 159, 2863–2883. doi:10.1210/en.2018-00056

Sozio, M. S., Lu, C., Zeng, Y., Liangpunsakul, S., and Crabb, D. W. (2011). Activated AMPK Inhibits PPAR-α and PPAR-γ Transcriptional Activity in Hepatoma Cells. *Am. J. Physiology-Gastrointestinal Liver Physiol.* 301, G739–G747. doi:10.1152/ajpgi.00432.2010

Srivastava, R. A. K., Pinkosky, S. L., Filippov, S., Hanselman, J. C., Cramer, C. T., and Newton, R. S. (2012). AMP-activated Protein Kinase: an Emerging Drug Target to Regulate Imbalances in Lipid and Carbohydrate Metabolism to Treat Cardio-Metabolic Diseases. *J. lipid Res.* 53, 2490–2514. doi:10.1194/jlr.R025882

Xiao, B., Sanders, M. J., Carmena, D., Bright, N. J., Haire, L. F., Underwood, E., et al. (2013). Structural Basis of AMPK Regulation by Small Molecule Activators. *Nat. Commun.* 4, 3017. doi:10.1038/ncomms4017

Zakaria, Z. A., Wen, L. Y., Abdul Rahman, N. I., Abdul Ayub, A. H., Sulaiman, M. R., and Gopalan, H. K. (2007). Antinociceptive, Anti-inflammatory and Antipyretic Properties of the Aqueous Extract of *Bauhinia Purpurea* Leaves in Experimental Animals. *Med. Princ Pract.* 16, 443–449. doi:10.1159/000107749

Conflict of Interest: The authors declare that the research was conducted in the absence of any commercial or financial relationships that could be construed as a potential conflict of interest.

Advantages of publishing in Frontiers

OPEN ACCESS
Articles are free to read for greatest visibility and readership

FAST PUBLICATION
Around 90 days from submission to decision

HIGH QUALITY PEER-REVIEW
Rigorous, collaborative, and constructive peer-review

TRANSPARENT PEER-REVIEW
Editors and reviewers acknowledged by name on published articles

Frontiers
Avenue du Tribunal-Fédéral 34
1005 Lausanne | Switzerland

Visit us: www.frontiersin.org
Contact us: frontiersin.org/about/contact

REPRODUCIBILITY OF RESEARCH
Support open data and methods to enhance research reproducibility

DIGITAL PUBLISHING
Articles designed for optimal readership across devices

FOLLOW US
@frontiersin

IMPACT METRICS
Advanced article metrics track visibility across digital media

EXTENSIVE PROMOTION
Marketing and promotion of impactful research

LOOP RESEARCH NETWORK
Our network increases your article's readership